Long-term settlement behaviour in soft soil areas for stress levels below the yield stress

J. Dick

TU Delft

FUGRO

Long-term settlement behaviour in soft soil areas for stress levels below the yield stress

by

J. Dick

to obtain the degree of Master of Science
at the Delft University of Technology,
to be defended publicly on the 14th of September 2022.

Student number:	4354443	
Project duration:	November 15, 2021 – July 15, 2022	
Thesis committee:	Dr. ir. Cor Zwanenburg,	TU Delft
	Prof. dr. ir. Ramon F. Hanssen,	TU Delft
	Dr. Stefano Muraro,	TU Delft
	Ir. Flip J. M. Hoefsloot,	Fugro

TU Delft

FUGRO

Abstract

Long-term settlement is unavoidable but by good prediction accompanied risks can be reduced. Nowadays linear isotach models belong to the state of the art but result in very small strain rates when small load increments or unloading is applied. For that reason this study has focused on the validation of those predictions using InSAR. Different causes of settlement have been studied and it was found that fluctuations in groundwater do not affect the final settlement. Another influencing factor is the presence of organic matter and its degradation. This reduction of organic matter is caused by many factors and is yet to complicated to quantify and include in predicting models. In spite of the idea that predicted strain rates by linear isotach models are too small, InSAR results show that the measured displacement rates were actually smaller than predicted some years after construction for road segments of the A2 and that a new proposed model could be used to match these displacement rates better. The C+S model by Vergote et al. (2021) is an isotach model which uses non-linear isotachs which would reduce the strain rates faster than linear isotach models and viscoplastic swell is included which also reduces the total strain rate. Results on incremental loading tests show that this model captures the behaviour in unloading stages better than the linear isotach models but for conventional incremental loading tests the two models do not differ much. For field scale embankment scenarios the results show that the C+S model with non-linear isotachs and viscoplastic swell included will predict a longer swell period with more swell, lower total strain rates after the swell period with a faster decay and in the and less residual settlement.

Preface

This thesis is the final product of my study Civil Engineering at Delft University of Technology. This research has been performed at the GeoConsulting department of Fugro. The topic of this study comes from the TKI project: ”Verbetering Zettingsprognose” (Improvement of Settlement predictions), a joined research program with the following companies involved: Boskalis, Deltares, Fugro, Hasking DHV, ProRail and Wiertsema & Partners. I hereby would like to express my gratitude to all who made it possible for me to study this subject.

Since November 2021 I have been working on the project under the supervision of dr. ir. Cor Zwanenburg from the TU Delft and ir. Flip Hoefsloot from Fugro. I want to thank both for the time and effort they have put into me. Next to them I also want to thank my other committee members, prof. dr. ir. Ramon Hanssen and dr. Stefano Muraro. The expertise of all four committee members has helped me a lot during this thesis.

Finally I would like to thank my friends, family, colleagues and fellow students for their support during my time as a student. To all of them: Thank you for making it a pleasant time.

J. Dick
Delft
August 26, 2022

Summary

In many soft soil areas, settlement is an unavoidable problem. When building on soils like clay and peat the layer compresses due to applied load, when this is not well predicted it can lead to severe damage to structures. The current way of predicting settlement is by the use of isotach models, these models use a unique relation between stress, strain and strain rate. However, for small load increments, when the total applied load is smaller than the yield stress, predicted settlement and strain rates are small. This is also the case when temporary loads are applied, the predicted residual settlement over 30 years is small and the strain rate after removal is small as well. To see if this prediction is correct, and if not what can be changed, the following main question arose:

> Are long-term settlements predicted well by current prediction models and if not, what adjustments should and can be made?

To answer this question there are four parts to look at in this study:

- Settlement behaviour observation through InSAR
- Influence of organic matter
- Influence of the groundwater table
- Settlement prediction models

The settlement behaviour after pre loading will be considered for the A2 with the use of Interferometric Synthetic Aperture Radar (InSAR) images. For another highway, the N3, InSAR will be used to detect the settlement behaviour prior to construction and based on the in situ strain rate, the yield stress will be determined.

The results of the N3 project show that it is possible to determine a yield stress and OCR based on measured displacement rates as long as soil layering, soil compression parameters and topography is known. The calculated yield stress and OCR are the aged yield stress and OCR and seems high. Disadvantage is that the yield stress is determined for a merged soil layer (clay and peat merged to one soft soil layer) instead of a yield stress for both layers separately. For validation of this yield stress laboratory tests should be performed on the soil under the road embankment. If those results are smaller, the non-linear isotach model provides a possible explanation for this deviation.

Next, InSAR is used for the validation of long-term settlement behaviour at the A2 for two cross sections. During construction settlement measurements are made by settlement plates and used to fit the soil parameters, this is the starting point for the comparison with the displacement rate measured by InSAR. Both cross sections have a higher displacement rate predicted by the D-Settlement model than was actually measured by InSAR. The measured displacement rates were 2.25 ±0.39 mm/year and 2.46 ±0.6 mm/year, while the predicted displacement rates were 5.95 and 10.06 mm/year. With the use of the new proposed C+S model non-linear isotachs and viscoplastic swell was included and a similar settlement development during loading was preserved while after unloading slower displacement rates were found which are in accordance with the InSAR measurements, 2.50 mm/year and 3.41 mm/year.

Since soft soil areas are considered another factor can play a role, organic matter. When peat is considered (as is the case for the A2) the settlement behaviour can be influenced by more than compression. Therefore, the degradation of organic matter has been studied. Degradation in organic matter can be caused by many factors but the most important once for embankment situations are listed below.

- Humidity (groundwater table)
- Nutrients (available carbon and nitrogen)
- Temperature

When a degradation of the organic can be predicted this can be used to describe a change in void ratio, and with it a change in volume, but these three, among other factors, are very hard to predict over time and there precise quantitative effect is unknown. Next to the degradation of the organic matter, it was found that for an organic soil a new consolidation equation can be applied. In this equation the change of volume over time is not only given by the change in volume of water (as presented by Terzaghi) but gas and organic matter must be considered as well. For this extended consolidation equation the soil is considered as a three phase medium: gas, liquid and solids. The latter one is subdivided in organic matter and minerals, something which is not done in the old consolidation equation. With the use of Boyle's gas law and assigning a compressibility to the organic matter a time dependent equation is obtained which follows laboratory results better than the old equation. The remark to make on this new equation is that is uses much more input parameters and even though it describes the behavior more closely the final deformations and strains are comparable. When looking at the embankment problem, this new found equation would only affect the consolidation behavior and not necessarily the long-term settlement predictions.

As mentioned above, the groundwater table affects the degradation of organic matter but next to that, it also affects the effective stress of the soil. When there are fluctuations in the ground water table strain rates can change with irreversible strain as a consequence. For that reason simulations were run to see if this is the case for a constant average groundwater table but also for an increasing and decreasing groundwater table. Next to that, the amount of fluctuation has also be changed in the simulations. What was found for the linear isotach model is that the fluctuations (constant and increasing) do not affect the resulting final settlement (on average) but it does show another path. Different from these periodic fluctuations, the increase and decrease of the average groundwater table does influence the final settlement. By an increase of the groundwater table, the effective stress decreases and less settlement will be predicted and for a decrease in groundwater table, the effective stress increases with extra settlement predicted.

Finally a new isotach model is introduced, the C+S model. Different from the linear isotach models like the a,b,c-isotachenmodel and the NEN-Bjerrum models this new model is able to include viscoplastic swell behaviour besides the elastic swell and distortion of isotachs can be modelled. The first of these two features, the viscoplastic swell, enables one to use a lower reload parameter (RR / C_r) while the model would still show a steeper curve upon unloading. This is accomplished by adding the viscoplastic swell strain rate to the total strain rate. In the linear isotach models this is not the case and the strain rate consist only of the elastic and viscoplastic creep strain rate of which only the elastic strain rate can predict uplift. This viscoplastic swell strain rate is auto decaying and causes a higher viscoplastic creep strain rate but a lower total strain rate after unloading. For incremental loading tests the final predicted strain does not differ significantly as was shown in both the analysis of the Mexico Clay as in the simulations for the incremental loading tests. However the behaviour of the soil is better captured with the C+S model as was especially shown by comparing the unloading steps of the Mexico Clay analysis. The linear isotach model shows a straight line after the consolidation period while the measurements and the C+S prediction still show swell deformation. The second feature of the C+S model, the non-linearity, is for the incremental loading test simulations less important since the time to develop creep strain is limited. However, when longer tests are run the non-linearity plays a more significant role. Non-linearity causes a decay in distance between isotachs, meaning that the strain rate decays faster with smaller strain predictions as a consequence. When field situations are considered the simulations show that non-linearity in combination with viscoplastic swell lead to less predicted settlement over a lifetime of 30 years but when viscoplastic swell is included and non-linearity is not, the final predicted

settlement is comparable to the final settlement of the linear isotach model without viscoplastic swell. The difference between both predictions is that viscoplastic swell result in more deformation since there is more uplift and after the swell period has come to an end, higher strain rates are predicted. These converge over time to the same strain rates as found by the linear isotach model.

As a conclusion to the main question proposed earlier it can be stated that the current settlement predictive models do not include all possible causes of long-term settlement and that strain rates do not match with the measurements based on InSAR. A first adjustment which should be further investigated is the inclusion of viscoplastic swell and non-linear isotachs. Secondly, more detailed research should focus in the degradation of organic matter and quantify the significance. A start could be to measure organic matter contents of soil under an embankment over time to attribute not predicted settlement which did occur in the field and once it would be possible to predict the degradation, it should also be integrated in the settlement prediction models.

Contents

List of Figures

List of Tables

List of Symbols and Abbreviations

Symbol or abbreviation*	Meaning
β_2	Non-linearity parameter
β_3	Distortion parameter
$b1$	Parameter to describe secondary compression index for swell ratio to C_α
$b2$	Parameter to describe initial viscoplastic swell strain rate for an OCR of 2
$C+S\ Model$	Creep and Swell Model
C_α	secondarry compression parameter (both in terms of void ratio and strain)
$\hat{C}_\alpha$ [2]	OCR dependent sceondary compression index (in terms of void ratio)
C_c	Compression index (based on void ratio)
CH_4	Methane
CO_2	Carbon-dioxide
CR	Compression Ratio (based on strain)
C_r	Reload and unload index (based on void ratio)
CRS	Constant Rate of Strain
c_v	coefficient of consolidation
$d\ or\ \delta$	Change, considered small
Δ	Change, considered larger than d/delta
ε [1] [2]	strain
$\dot{\varepsilon}$ [1] [2]	strain rate
e [1] [2]	void ratio
$\dot{e}$ [1] [2]	strain rate (in terms of void ratio)
GH	GitHub
IL	Incremental Loading
$InSAR$	Interferometric Synthetic Aperture Radar
$m1$	Parameter to describe the OCR dependancy of the secondary compression index for swell
$m2$	Parameter to describe the OCR dependancy of the viscoplastic swell strain rate
n	porosity
OCR	Over Consolidation Ratio
OCR_{ref}	reference Over Consolidation ratio (aged OCR)
POP	Pre-Overburden Pressure
RR	Reload and unload ratio (based on strain)
σ [1]	stress
σ_p	yield stress
$\dot{\sigma}$	rate of change in stress
t [1]	time
τ [1]	intrinsic time
u_w	pore water pressure
V	Volume

[1]. can have subscript to the state e.g. 0 is intitial, ref is reference, n or t is for a specific loading step or time
[2]. can have super- or subscript refering to separate contributors e.g. el = elastic, vp = viscoplastic etc.
** Only the most frequent abbreviations and symbols are listed here, others are mentioned in the thesis.*

1

Introduction

1.1. Problem statement

Not rarely newspapers write about problems that occur due to settlement. In December 2021, an article was published by the NRC on trains in the Netherlands that can't operate on their design speed as a consequence of soft soils and their settlement due to loads and vibrations (Marée, 2021). A little longer ago in September 2020, de Volkskrant published an article about a new settlement map of the Netherlands (Bodemdalingskaart). It was stated that especially in the peat areas of the Netherlands the rate of settlement increases, having severe consequences for underground infrastructure, buildings, roads and other infrastructures. A cost estimation from 2016 of 2-6 billion euros for maintenance might not even be relevant anymore (Tieleman, 2020). In Deurne (Noord-Brabant) it was shown that settlement is not only a problem related to the applied load on the soil but also a problem related to environmental causes. After renovation of a local road, the summer had been very dry. As a result the ground water table was extremely low, which resulted in an accelerated oxidation process of the peat layer. This process is irreversible and was not accounted for in the cost estimation of the contractor. Now the municipally of Deurne needs to account for extra maintenance costs (Broers, 2021).

These three examples of the last 2 years show that the problem of settlement, even though studied for almost a century, is still an engineering issue. However, settlement is unavoidable when building but by good predictions of settlement, unexpected costs can be avoided. As mentioned in the articles above, most of the unexpected settlement problems occur in soft soil areas. These are mainly found in the western part of the Netherlands as can be seen in Figure 1.1.

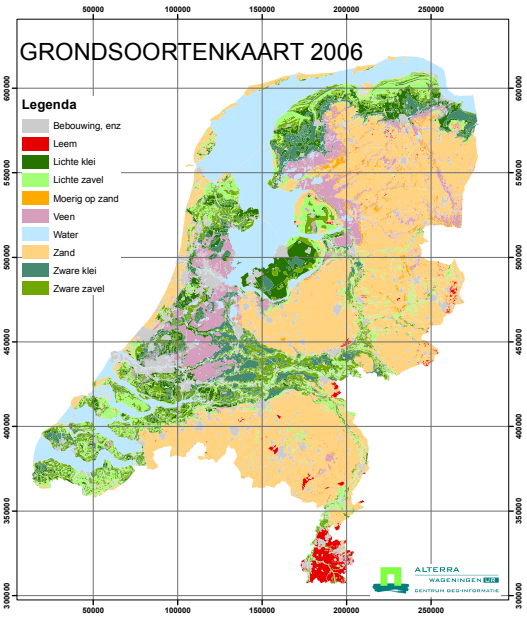

Figure 1.1: Soil map of the Netherlands (Wageningen University and Research, 2006)

Nowadays the state of the art involves modelling the settlement based on parameters derived in laboratory tests that give an indication of how the soil behaves. Models that are currently used in practise are the linear isotach models (NEN-Bjerrum or a,b,c-isotachnmodel). For large stress increments, this type of models predict the settlement quite accurately. However, for small load increments and after removal of temporary loads, as is the case for embankments and road maintenance projects, the long-term settlement differs from predicted. This problem seems to occur when stress levels are lower than the yield stress.

An extensive monitoring and laboratory research done by Deltares has shown that there is a difference in unload and reload behaviour for small load increments below a certain yield stress and after the yield (Visschedijk & Temmerman, 2009). Next to that the bias between predictions based on laboratory results and field measurements add up to 40 cm in some cases and there still remain biases after new parameter fits on settlement beacons, especially for small load increments. They conclude that the knowledge about long-term creep behaviour and the actual residual settlements for small load increments and after pre-loading is insufficient (Visschedijk & Temmerman, 2009). Therefore, it is the goal of this study to give a better insight in how soil will settle under small load increments and what causes the bias between prediction and field measurements.

1.2. Research outline

1.2.1. Objectives

To study whether the settlement predictions based on linear isotach models is accurate as well, one of the sub-questions focuses on the validation of this. Next to that, the objective of this study will be to look for other explanations that could influence settlement behaviour and to use different models than the linear isotach model. The main focus hereby will be on a different description of isotachs and the comparison with lab and field situations. Side objectives focus on including the volume decrease due to organic content in the soil (e.g. degradation of organic matter in peat), to see if transient changes in the pore water pressure give divergent results (for example induced by heavy rainfall and rise in water table or drought and lower water tables) and if the use of InSAR data could be beneficial for parameter selection for settlement prediction models. InSAR will also be used for the validation of settlement behaviour.

1.2.2. Research Questions

Main Question

Following from the objective a main question is proposed:

- Are long-term settlements predicted well by current prediction models and if not, what adjustments should and can be made?

Sub-questions

To get an answer to the main question several sub-questions are formed to look at different aspects which could be improved.

1. How can InSAR be used for settlement predictions done by isotach models?

   If the initial strain rate can be determined based on InSAR data, the yield stress can be derived from it and sample disturbances, like in conventional lab-tests, are not relevant anymore.

2. How do transient changes in pore pressures relate to extra settlement?

   When, due to longer periods of drought, the water table lowers and with it the pore water pressure, effective stresses will increase which could lead to extra settlement. If this happens every year it could contribute to the bias in predicting long-term settlements.

3. How does degradation of organic matter cause extra settlement and is it quantifiable?

   The goal is to determine how organic matter affect volume reduction and if this amount is quantifiable. If it is possible to quantify, could it be possible predict the volume loss due to organic matter and include this in settlement models.

4. How do adapted isotachs represent strain rate behaviour of soils compared to equally spaced isotachs?

   Current models use linear isotachs by which very small strains are calculated in the over consolidated stress state. New models as presented by Yuan and Whittle and by Vergote suggest non-linear and distorted isotachs with different results which could lead to higher initial strain rates and faster decrease in the normally consolidated stress state (Y. Yuan and Whittle, 2018, Vergote, 2020).

1.2.3. Approach

To answer the main research question whether it's possible to improve the prediction of long-term settlement based on a novel implementation of the isotach model, it's necessary to answer the sub-questions. An overview of how to approach these sub-questions can be found below.

Sub-Question 1:
How can InSAR be used for settlement predictions done by isotach models?
First there will be a part of literature review on the method of InSAR to get a basic understanding of the process for collecting data. Then data will be collected on the projects that will be considered. This settlement data prior to construction will be used to derive creep settlement parameters like initial strain rate and C_α, avoiding the use of yield stress determined by conventional lab-tests. These parameters will be used in the isotach model as well as parameters derived from lab-tests. Both results will be compared with settlement data from the field after construction.

Actions:

- Data collection and deriving parameters
- Comparing results from the isotach model with field data

Sub-Question 2:
How do transient changes in pore pressures relate to extra settlement?
This sub-question will be answered by programming scenarios in which over time there will be a fluctuation in the ground water table. This will be implemented in the isotach model to see if it affects the settlement prediction.

Actions:

- Write python script to simulate ground water fluctuations
- Compare results with and without fluctuations

Sub-Question 3:
How does degradation of organic matter cause extra settlement and is it quantifiable?
This sub-question will initially be answered by a literature review. The objective is to find methods that can describe the amount of organic matter that will be converted into CO_2 or CH_4. If such a method is available the next goal will be to relate it to the project areas and see if it can explain the difference between prediction and observation. If this is (partly) the case, the last goal is to implement such a model in an isotach model such that in future predictions the degradation of organic matter will be considered quantitatively.

Actions:

- Literature review

Sub-Question 4:
How do adapted isotachs represent strain rate behaviour of soils compared to equally spaced isotachs
To determine if an adapted model predicts the settlement more accurately than equally spaced isotach models it is necessary to make a python script that will predict the settlements in the current way (with the equally spaced isotachs) and to make a model that changes the isotachs. For this, a literature study will be done on the development of settlement models over the years and the current state of the art will be used as reference to compare novel models with. The model presented by Vergote (2020) will be used as the novel implementation of the isotach model and it will be compared with the model simplified linear isotach model as proposed by Hoefsloot (2022). Incremental loading tests will be used for model validation and simulations of laboratory tests and field situations will be used for the comparison of both models.

Actions:

- Implement isotach models
- Compare models with laboratory tests
- Compare laboratory simulations for both models
- Compare field simulations for both methods

1.3. Reading guide

As mentioned in the previous section, this report has 4 subjects to study (Settlement models, use of InSAR, Organic Matter and Groundwater Fluctuations). In Chapter 2 the settlement models will be explained and a theoretical background of 3 types models will be given (linear isotachs, non-linear isotachs and non-linear isotachs in combination with viscoplastic swell). In the same chapter the findings of a literature study on the organic matter can be found and a brief description of InSAR background.

Chapter 3 presents the work done on settlement models. The chapter is split up in 4 sections, a first part describes the implementation and verification of the models. The second part links the models to experimental data on Mexico Clay and compares simulations done by linear isotache model (NEN-Bjerrum) and the C+S model. The last two section make comparisons between the two models based on simulations performed on two parameter sets for a series of incremental loading tests and finally for embankment situations.

Chapter 4 shows the influence of the groundwater table on settlement predictions, based on the linear isotach model (NEN-Bjerrum). In this chapter there is a focus on seasonal fluctuation and on more permanent change of the average ground water table.

In Chapter 5 the use of InSAR for settlement predictions is presented. The first section looks at the determination of the yield stress for two locations at the N3 highway in Dordrecht. The second section in this chapter will focus on monitoring the settlement behaviour after construction for the A2 highway.

Based on the results and discussion of these chapters the conclusions for all sub-questions can be found in Chapter 6, as is the conclusion to the main question. Finally in Chapter 7 recommendations for further research and how the results of this study could be used in the field of engineering.

2 Theory

2.1. Settlement models

2.1.1. Linear isotach model

One of the first to introduce isotach behaviour was Laurits Bjerrum (Bjerrum, 1967). He described the settlement of a soil as two components.

a Instant compression, the reduction of void ratio caused by an increase in stress which will occur until there is no change in effective stress (Bjerrum, 1967).

b Delayed compression, the reduction of void ratio during a constant stress state.

These two compression parts are visualized in Figure 2.1.

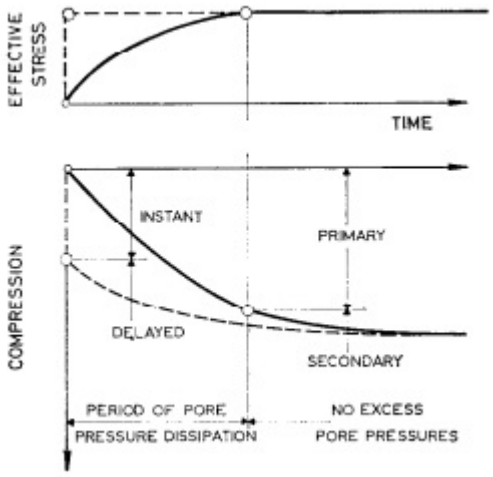

Figure 2.1: Figure 15 from Bjerrum (1967) to visualize the delayed and instant compression of a soil

Another way of visualizing this instant and delayed compression is shown in Figure 2.2. In Figure 2.2 a void ratio against the logarithm of stress is presented and a clear distinction is visible between the change in void ratio due to stress increase and the change in void ratio at a constant stress level. In the same Figure time lines can be seen, so called isochrones. These represent the time that has been passed after stress has become constant. It can be seen that the distance between two parallel lines is spaced equally with a time difference of a factor 10. Meaning that the change in void ratio between 3 and 30 years will be equal to the change in void ratio between 30 and 300 years. Furthermore, it can be seen that the change in void ratio is different depending on the load history, e.g. when a soil has aged and the stress state is less than the yield stress the soil compresses less than a soil with a stress state equal to the yield stress. What will be shown later on is that time can be rewritten as strain

rate (equation 2.6). When strain rates are shown on the parallel lines the lines are called isotachs. Which means that on one isotach the strain rate of the soil is the same and the difference between two isotachs is still a factor of 10 when creep is calculated as a logarithmic function.

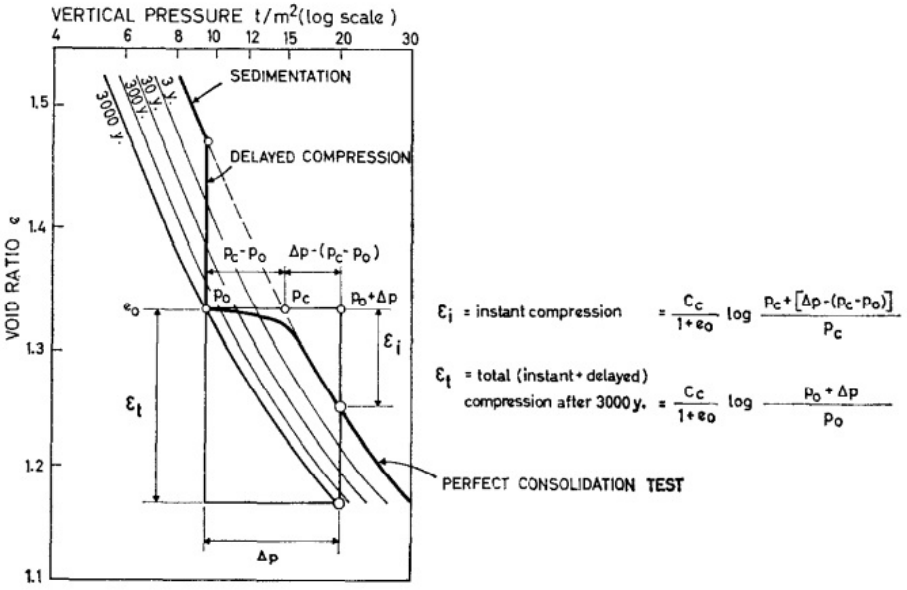

Fig. 18. Principle of settlement computation

Figure 2.2: Figure 18 from Bjerrum (1967) to visualize the delayed and instant compression of a soil

A mathematical description of the drained compression behaviour is given by equation 2.1 (Deltares, 2021). This equation also holds for the undrained compression when for σ'_n the instantaneous effective stress is taken for every time step and instead of $t - t_n + \tau_n$ the instantaneous intrinsic time for every time step is used.

$$\varepsilon(t) = RR\ log(\frac{\sigma'_p}{\sigma'_0}) + CR\ log(\frac{\sigma'_n}{\sigma'_p}) + C_\alpha\ log(\frac{t - t_n + \tau_n}{t_{ref}}) \tag{2.1}$$

Where:

RR = Reloading/Unloading Ratio
CR = Compression Ratio
C_α = Secondary creep parameter
n = load step number
σ'_p = effective yield stress
σ'_0 = effective initial stress, prior to loading
σ'_n = effective stress of load step n
t = time
t_n = time of start load step n
τ_n = intrinsic time at load step n

In equation 2.1 the first of three parts, $RR\ log(\sigma'_p/\sigma'_0)$ describes the development of strain in the stress area between the initial stress state and the yield stress by the reloading ratio (RR). The second part, $CR\ log(\sigma'_n/\sigma'_p)$, describes the strain development between the yield stress and the stress state after loading (untill some point n) by the stress state, yield stress and the compression ratio (CR). The final part of this equation, $C_\alpha\ log((t - t_n + \tau_n)/t_{ref})$, describes the time dependent strain development of the soil using the time difference between loading and the real time ($t - t_n$) and the intrinsic time of the soil representing the aging of a soil (τ_n) and lastly the secondary compression ratio (C_α). In this last part the reference time (t_{ref}) is usually set on one day since that time corresponds to the one-day compression line and by using time in days the term crosses out. In the part that is left there are 3 time variables, the first two represent the time step ($t - t_n$) and the last parameter is the intrinsic time (τ).

The intrinsic time is also measurement of time but it relates to both the time and the stress history and can be used to express stress and strain rate in each other. This time factor ($t - t_n + \tau_n$), is the updated intrinsic time for a time step. The change of this intrinsic time can be caused by either time as can be seen in equation 2.2 or change in stress (equation 2.3).

$$\tau_n = t - t_n + \tau_{n-1} \tag{2.2}$$

In equation 2.2 the subscript of n is the moment at which a load is applied. At that time t and t_n are equal to each other and τ_{n-1} is equal to the intrinsic time of the previous loading step. If the load exceeds the yield stress, the intrinsic time will be smaller than 1 day and strain rates will be high but if that load is kept constant it will end on the virgin compression line (1-day isotach) after 1 day. When a load remains constant the development of the intrinsic time will be only dependent on time t. However, when a stress increment is applied as is shown in the path A-B in Figure 2.3, the intrinsic time changes as well. This can both be by an applying a load or removing one. In equation 2.3 the change of intrinsic time is shown for a change in stress.

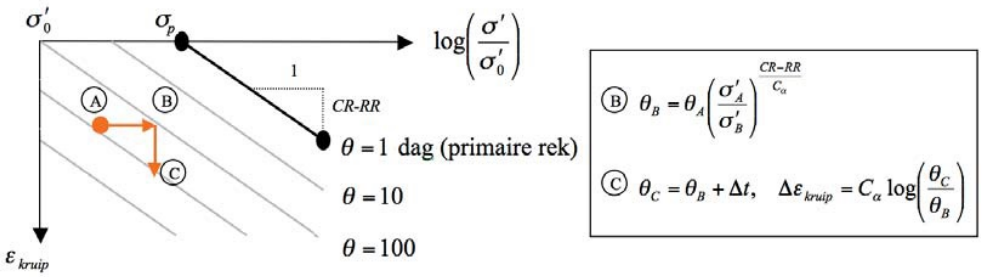

Figure 2.3: Updating the intrinsic time for a change in time (B-C) or change in stress (A-B) (Visschedijk, 2010).

$$\tau_n = \tau_{n-1}\left(\frac{\sigma'_{n-1}}{\sigma'_n}\right)^{\frac{CR-RR}{C_\alpha}} \tag{2.3}$$

When aging occurs due to both a change in time and a change in stress, e.g. the path in Figure 2.3 from A-C, both equations 2.2 and 2.3 must be used. This results in an update of the intrinsic time according to 2.4. Updating this variable ($\tau_n \rightarrow \tau_{n+1}$) depends on the time steps. This can be done by taking the previous value and adding the change of the previous step, as long as the time steps are small the changes are small and this approximation is valid. This is an example of a finite difference method to update a parameter. In equation 2.4 a central difference method is presented, an advantage of this method is that the time steps used can be larger than for backward and forward differences. However, for small time steps the results are equal. A full derivation is presented by Hoefsloot (2022).

$$\tau_n = \left(\frac{\Delta t}{2} + \tau_{n-1}\right)\left(\frac{\sigma'_{n-1}}{\sigma'_n}\right)^{\frac{CR-RR}{C_\alpha}} + \frac{\Delta t}{2} \tag{2.4}$$

$$\tau_0 = \tau_{ref}\left(\frac{\sigma'_p}{\sigma'_{v0}}\right)^{\frac{CR-RR}{C_\alpha}} \tag{2.5}$$

Where:

Δt = time step
n = time step number (different from equations 2.1-2.3 where n is load step number)
σ_n = load at time step
σ_{n-1} = load of previous time step
τ_0 = initial intrinsic time
σ'_p = yield stress
σ'_{v0} = initial stress

For determining the initial intrinsic time, corresponding to an initial stress state of a soil, the relation presented in equation 2.3 can be used. By comparing the initial stress state with the yield stress state

(σ_0' and σ_p') with a corresponding intrinsic time of the yield stress state of one day the initial intrinsic time can be calculated (see equation 2.5). Another way to derive the intrinsic time is by taking the time derivative of equation 2.1. When the applied load is constant, the only part that remains after derivation is equation 2.6.

$$\frac{d\varepsilon}{dt} = \frac{C_\alpha}{\tau \cdot ln(10)} \tag{2.6}$$

By measuring the strain rate and knowing the soil parameter C_α, the intrinsic time can be obtained without using the yield and in situ stress state. The value of τ_{ref} is especially useful for predicting strain or settlement when stress states will be changed and an initial value for τ_t must be used which should match with the in situ stress state. When the model is rewritten in incremental form, the elastic and viscoplastic parts become better distinguishable. The elastic part is the reversible deformation and is given in equation 2.7 and the viscoplastic strain, both stress and time dependent, is given in equation 2.8. By rewriting equation 2.1 in this way the change of strain can be determined for every time step. With equations 2.7 and 2.8 it is possible to describe undrained behaviour since not the load at the end of load step is used like in equations 2.1 but the effective stress at a time step. The total strain is obtained by summing the increments up.

$$d\varepsilon^{el} = RR\ log(\frac{\sigma'_{t+\Delta t}}{\sigma'_t}) \tag{2.7}$$

$$d\varepsilon^{vp} = (CR - RR)\ log(\frac{\sigma'_{t+\Delta t}}{\sigma'_t}) + C_\alpha\ log(\frac{\tau_{t+\Delta t}}{\tau_t}) \tag{2.8}$$

In these relations there are 5 soil and state parameters to determine, $RR,\ CR,\ C_\alpha,\ and\ \tau$ in which τ is dependent on $\sigma'_{v;0}\ and\ \sigma'_p$. These parameters will be discussed later.

2.1.2. Non-linear isotach models

Next to the linear isotach models in which the distance between two isotachs remains constant, there are non-linear isotach models. The base for these models lies in the finding of incremental loading tests in which a value for C_α is determined. Among others Y. Yuan (2016) found a decrease in in the secondary compression parameters (C_α) and developed a new model which takes this into account, this is the MIT-SR model. Just as linear isotach models Yuan divides strain rates in an elastic (equation 2.9) and viscoplastic part (equation 2.10) and determines the change in strain by multiplying the strain rate with the time step (equations 2.11).

$$\dot{\varepsilon}^{el} = \rho_r n \frac{\dot{\sigma}'_v}{\sigma'_v} \tag{2.9}$$

$$\dot{\varepsilon}^{vp} = R_a(\frac{\sigma'_v}{\sigma'_p}) \tag{2.10}$$

$$d\varepsilon = (\frac{d\varepsilon}{dt}) \cdot dt = (\dot{\varepsilon}^{el} + \dot{\varepsilon}^{vp}) \cdot dt \tag{2.11}$$

Where:

ρ_r = unload / reload parameter
n = porosity
$\dot{\sigma}'_v$ = rate of change in effective stress
σ'_v = effective stress
R_a = internal strain rate
σ_p = yield stress

What can be seen is that the elastic strain rate in this equation is a function of the stress, change in stress and ρ_r multiplied by the porosity while the viscoplastic strain rate is a function of the inverse of the over consolidation ratio (OCR) and a new parameter (R_a), this parameter describes the internal strain rate and develops according to equation 2.13, which makes it an auto-decaying parameter. Next to the auto-decaying process the change in internal strain rate is determined by an activation function ($f(\dot{\varepsilon})$) and a transient coefficient which describes the delayed process (m_t). Where in the linear isotach model the increase in yield stress is taken into account by updating the intrinsic time, the yield stress

for the MIT-SR model increases according to equation 2.12 when there is no increase in stress, there will be an increase in yield stress which will decrease the viscoplastic strain rate.

$$\dot{\sigma}'_p = \frac{\dot{\varepsilon}}{\rho_c n}\sigma_p \tag{2.12}$$

$$\dot{R}_a = [f(\dot{\varepsilon}) - R_a] \cdot m_t \tag{2.13}$$

Where:

$\dot{\sigma}'_p$ = rate of change in yield stress
ρ_c = Normally consolidated compression parameter
$\dot{\varepsilon}$ = strain rate
$f(\dot{\varepsilon})$ = activation function
m_t = transient coefficient

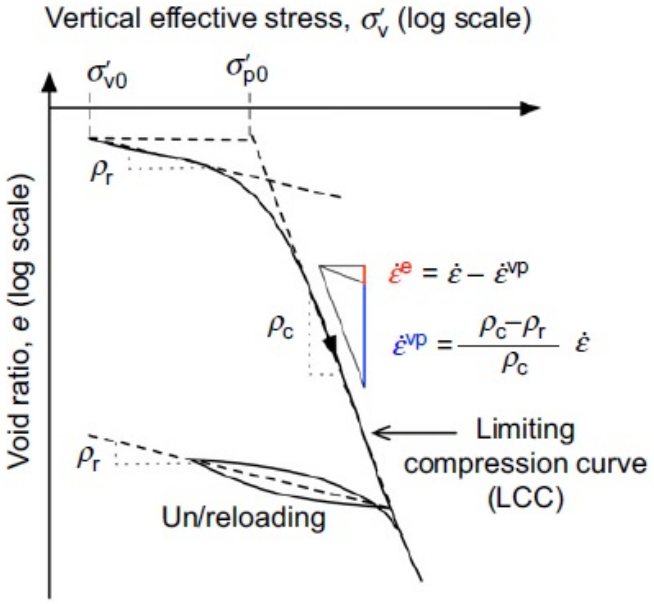

Figure 2.4: Figure 1 from Y. Yuan and Whittle (2018) showing a log(e)/log(σ'_v) graph with the unloading/reloading and compression parameters and the limiting compression curve (1-day compression curve)

As mentioned above, $\dot{R}_a$ is dependent on some activation function (equation 2.14). Since equation 2.13 is auto-decaying, it will go to a steady state that is equal to the activation function. This function can be considered as the change of strain due to external effects, e.g. applying a load or displacement to the soil. When the strain rate is equal to the reference strain rate ($\dot{\varepsilon}_{ref}$), this function represents the virgin compression curve (LCC) as can be seen in Figure 2.4.

$$f(\dot{\varepsilon}) = (\frac{\rho_c - \rho_r}{\rho_c}\dot{\varepsilon})(\frac{\dot{\varepsilon}}{\dot{\varepsilon}_{ref}})^{-\beta} \tag{2.14}$$

$$m_t = (\frac{\rho_c}{\rho_a} - 1)\frac{\dot{\varepsilon}^{vp}}{\rho_r n} + O(\dot{\varepsilon}) \tag{2.15}$$

When the strain rate goes towards a constant value, or decreases slowly, the activation function will become constant and the change in internal strain rate will be controlled by the transient coefficient. This coefficient controls the rate of change towards a steady state solution. In the formulation of the transient coefficient there is a extra term $O(\dot{\varepsilon})$ so m_t would increase even though the viscoplastic strain rate is zero. The influence of m_t, and the change of R_a towards $f(\dot{\varepsilon})$ compared to the strain rate can be seen in Figure 2.5. It can be seen that despite the change in imposed strain rate, the internal strain rate shows a delayed change.

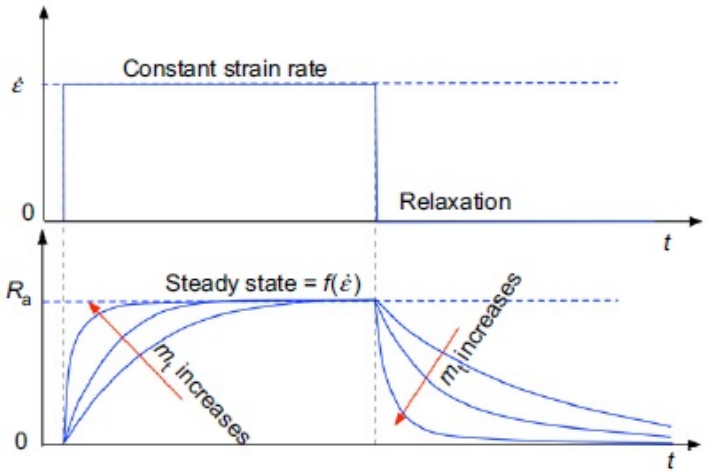

Fig. 2. Influence of m_t on the evolution of R_a during CRS compression and relaxation

Figure 2.5: Figure 2 from Y. Yuan and Whittle (2018) presenting the influence of m_t for a constant strain rate and a relaxation phase.

Based on the given equations above (2.11-2.15) the change in strain for every time step dt can be determined. By adding those up the total change in strain can be calculated and long-term strain and with that settlement can be predicted. For this model the following parameters are necessary, ρ_r, ρ_c, ρ_α, $\dot{\varepsilon}_{ref}, \beta, \sigma'_{p;0}$, $\sigma'_{v;0}$ & R_{a0}. These first 3 parameters indicated by ρ have a similar function as the compression ratios CR, RR, C_α, only these represent compression in the logarithmic void ratio against the logarithm of stress space. With the initial void ratio these parameters can be rewritten to the compression ratios. The parameter β has not been mentioned yet but is the rate dependency of the state steady behaviour. The value of β is assumed to be between a minimum of zero and a maximum of ρ_a/ρ_c. This parameter allows for non-linearity in the isotach model. Once β is larger than zero and the strain rate is smaller than the reference strain rate, the activation function (equation 2.14) will decrease faster and so will the internal strain rate R_a and as a result the viscoplastic strain rate. This means that the isotachs will lie closer together further away from the LCC. The parameter $\dot{\varepsilon}_{ref}$ is the reference strain rate which is the same as the one-day compression strain rate for virgin loading. The parameter $R_{a;0}$ is the initial internal strain rate. Since the change of internal strain rate is based on the internal strain rate itself, this parameter becomes more important when the strain rate is higher (e.g. when soil is less over consolidated). The non-linearity of the model is also described in Y. Yuan (2016), in which the conventional creep parameter (C_α) is a function of the over consolidation ratio (OCR). This is also the starting point of the next (C+S) model.

2.1.3. Non-linear distorted isotach model

Next to the non-linearity of the isotachs it has been found that there is distortion in the isotachs upon reloading, which means that instead of straight parallel lines the isotachs have some curvature. This was already found by den Haan (1996) and is illustrated in Figure 2.6.

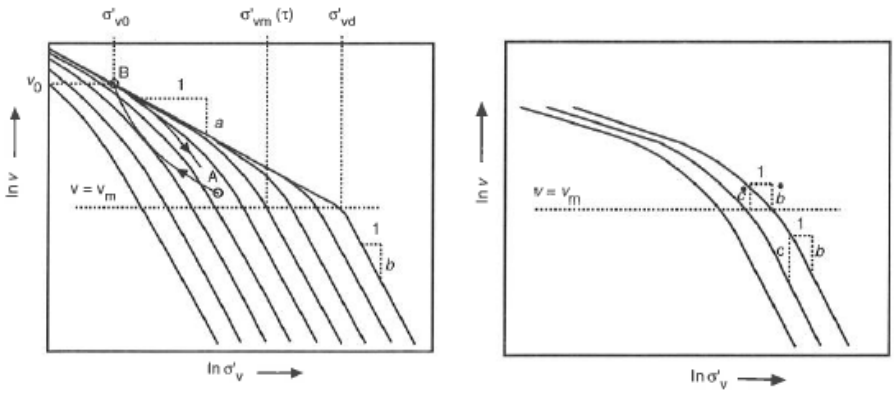

Fig. 6. Distorted reload creep isotaches above vm: (a) assumed pattern (equation (23); A, start of unloading (v_c, σ'_{vc}); B, furthest point of unloading (v_0, σ'_{v0}); (b) parallel distorted isotaches with $c^*/b^* = c/b$

Figure 2.6: Distorted reloading curves in CRS tests (den Haan, 1996)

This would imply that upon reloading the isotachs are wider spaced horizontally and that there is a smaller change in strain rate than suggested by the non distorted isotach models. An explanation for this distortion is the influence of swell. During unloading soil does not only experiences elastic swell (along the unloading / reloading line) but there is also viscoplastic swell (Vergote, 2020). This term causes extra swell and in an isotach framework the strain will become smaller, for which a higher isotach is reached with a higher strain rate as a consequence. In figure 2.7 it can be seen in Figure A how a change in strain rate develops according to non distorted isotachs and in Figure B how the higher strain rates that are measured would give a distortion in the isotachs.

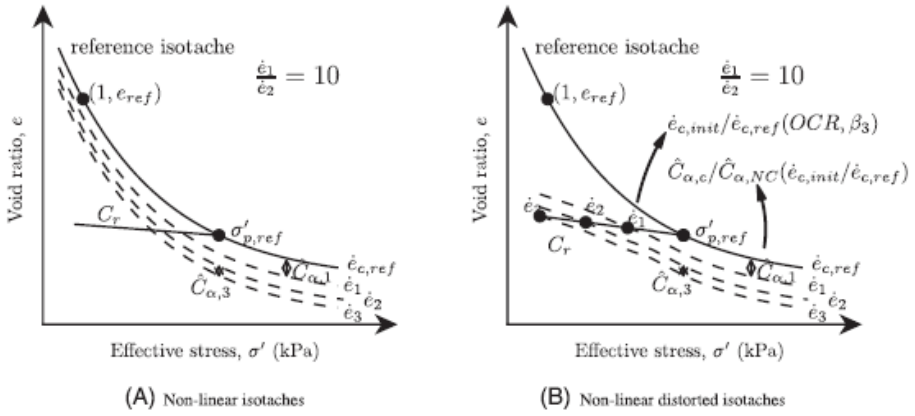

FIGURE 1 Principle of isotache system for compressive viscoplastic strains with distortion of isotaches

Figure 2.7: The distortion of isotachs according to (Vergote et al., 2021)

The C+S model is based on the previous mentioned MIT+SR model with respect to the non-linearity of the isotachs. However, the models differ in the swell term and distortion. For the description of the total strain rate Vergote expands the strain rate equation with a swell term (equation 2.16).

$$\dot{e} = \dot{e}_{el} + \dot{e}_{vp;c} - \dot{e}_s \tag{2.16}$$

With:

$$\dot{e}_{el} = \frac{C_r \cdot \dot{\sigma}'}{\sigma' \cdot ln(10)} \tag{2.17}$$

Where:

$\dot{e}_{el}$ = elastic void ratio rate
C_r = reload and unload index
$\dot{\sigma}'$ = rate of change for effective stress
σ' = effective stress

The relation given in equation 2.17 for elastic strain rate is similar to the relation purposed in the MIT-SR model by equation 2.9. For the viscoplastic strain rate there is a distinction between the strain rate in the virgin loading area and the strain rate after unloading because of the distortion. Equation 2.18 and equation 2.19 are necessary to describe the strain rate. Equation 2.18 is used for the development of strain rate as a function of the reference OCR and the factor β_2 is used to model the non-linearity of C_α in the same way as was proposed by Y. X. Yuan et al. (2015), equation 2.20. For the distortion equation 2.19 is used. The new initial strain rate is calculated as a function of the reference OCR and the reference viscoplastic strain rate and a new term β_3. In the C+S model, two different definitions of OCR are used. The OCR is defined as the maximum stress level over the stress state, e.g. $max(\sigma'_v)/\sigma'_v$, while the reference OCR represent the yield stress over the stress state, e.g. σ'_p/σ'_v. When a stress increment exceeds the yield stress the two are equal to each other but the most important difference is that the OCR does only change due to a change in stress level while the reference OCR also changes due to aging.

$$\dot{e}_{vp;c} = \dot{e}_{vp;c;ref} \cdot \left[\sqrt{1/OCR_{ref}} \cdot exp\left(\frac{1 - OCR_{ref}^{\beta_2}}{2\beta_2}\right)\right]^{C_c - C_r/C_{\alpha;NC}} \tag{2.18}$$

$$\dot{e}_{init;c} = \dot{e}_{vp;c;ref} \cdot OCR_{ref}^{-\beta_3} \tag{2.19}$$

$$\frac{\hat{C}_\alpha}{C_{\alpha NC}} = \frac{2}{OCR_{ref}^{\beta_2} + 1} \tag{2.20}$$

Where:

$\dot{e}_{vp;c}$ = viscoplastic creep strain rate
$\dot{e}_{vp;c;ref}$ = reference creep strain rate
OCR_{ref} = reference over consolidation ratio (different from OCR)
β_2 = non-linearity parameter
β_3 = distortion parameter
C_c = compression index for virgin compression
$C_{\alpha NC}$ = secondary compression index for normally consolidation
$\hat{C}_\alpha$ = OCR dependent secondary compression index

What can be seen in equations 2.18 and 2.19 is that when the reference OCR goes to a value of 1 the strain rates will be equal to the reference values despite non-linearity and distortion. Furthermore equation 2.19 is comparable to the update of the intrinsic time for linear models (equation 2.3). When a constant C_α is assumed the ratio of strain rates is equal to the ratio of intrinsic times $\dot{e}_0/\dot{e}_{ref} = \tau_{ref}/\tau_0$ as long as β_3 equals $(C_c - C_r)/C_\alpha$. Equations 2.21 - 2.25 give a step wise overview of the strain rate for linear isotachs as a function of the intrinsic time and therefor of the OCR, it can be seen in equation 2.25 that the two are equal to each other.

$$\dot{e}_0 = \frac{C_\alpha}{\tau_0 \cdot ln(10)} \tag{2.21}$$

$$\dot{e}_{ref} = \frac{C_\alpha}{\tau_{ref} \cdot ln(10)} \tag{2.22}$$

$$\frac{\dot{e}_0}{\dot{e}_{ref}} = \frac{\tau_{ref}}{\tau_0} \tag{2.23}$$

$$\frac{\tau_{ref}}{\tau_0} = \left(\frac{1}{OCR}\right)^{\frac{C_c - C_r}{C_\alpha}} \tag{2.24}$$

$$\frac{\dot{e}_0}{\dot{e}_{ref}} = OCR^{-\frac{C_c - C_r}{C_\alpha}} = OCR^{-\beta_3} \tag{2.25}$$

Finally the swell term is introduced which is considered as a non-isotach process and it develops sequentially to the creep strain rate. Swelling is described as a transient process dependent on the swell rate itself and a swell parameter $\hat{C}_{\alpha;s}$. These two parameters determine the decrease in swell rate. Just as for the creep parameter $\hat{C}_{\alpha;c}$ there is a relation with the normally consolidated reference secondary compression parameter C_α, which is dependent on the OCR and next to that there is a relation between the initial swell rate and the OCR. These two relation given by equations 2.27 and 2.28 make it possible to determine the development of the swell rate by equation 2.26. Upon unloading the OCR increases and so will the initial swell ratio which makes that the swell component will be larger than the creep rate. After some time the swell rate is decreased and the creep rate becomes dominant in equation 2.16 and an increase in (creep) strain reappears (see Figure 2.8). It can be seen from these equations that viscoplastic swell is an auto decaying process since the change in strain rate ($\ddot{e}_s$) is a function of the viscoplastic swell strain rate itself ($\dot{e}_s$) and the initial viscoplastic swell strain rate only dependents on the change in stress (OCR) and on viscoplastic swell parameters.

$$\ddot{e}_s = -\frac{\dot{e}_s^2 \cdot ln(10)}{\hat{C}_{\alpha;s}} \tag{2.26}$$

$$\frac{\hat{C}_{\alpha;s}}{C_{\alpha;NC}} = 10^{b_1}(OCR-1)^{m_1} \tag{2.27}$$

$$\dot{e}_{s;init} = 10^{b_2}(OCR-1)^{m_2} \tag{2.28}$$

Where:

$\ddot{e}_s$	= viscoplastic swell strain acceleration
$\dot{e}_s$	= viscoplastic swell strain rate
$\hat{C}_{\alpha;s}$	= viscoplastic swell creep parameter
$\dot{e}_{s;init}$	= initial viscoplastic swell rate for OCR (only dependent on stress)
b_1, b_2, m_1, m_2	= viscoplastic swell parameters

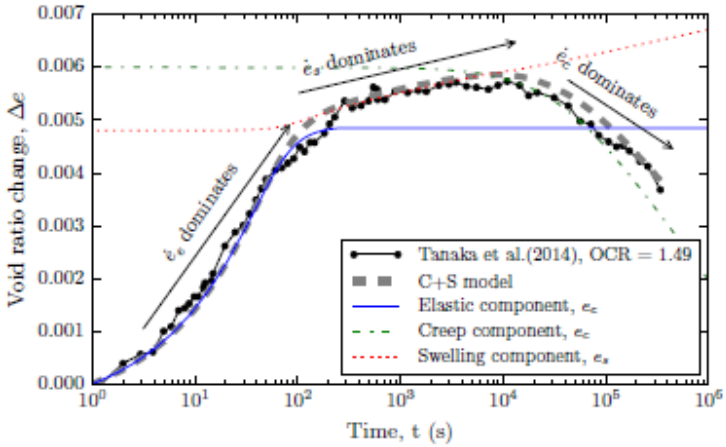

Figure 6.1: Principle of C+S model: decomposition of strain rates in an elastic, swelling and creep strain rate with sequential dominance of the three components as illustrated on a test at $OCR = 1.49$, Tanaka *et al.* (2014)

Figure 2.8: Different dominant stages of strain rate upon unloading (Vergote, 2020)

An example of how the two different types of isotachs will look like are presented in Figure 2.9. Isotachs for the same strain rates are used and it can be seen that the intersection of the reloading and virgin compression lines are equal, so the yield stress is equal and the strain rate of the one-day isotach is equal. It can be seen that the spacing for non-linear isotach becomes smaller further away from the one-day isotach and that the isotachs are curved in the area before the yield stress.

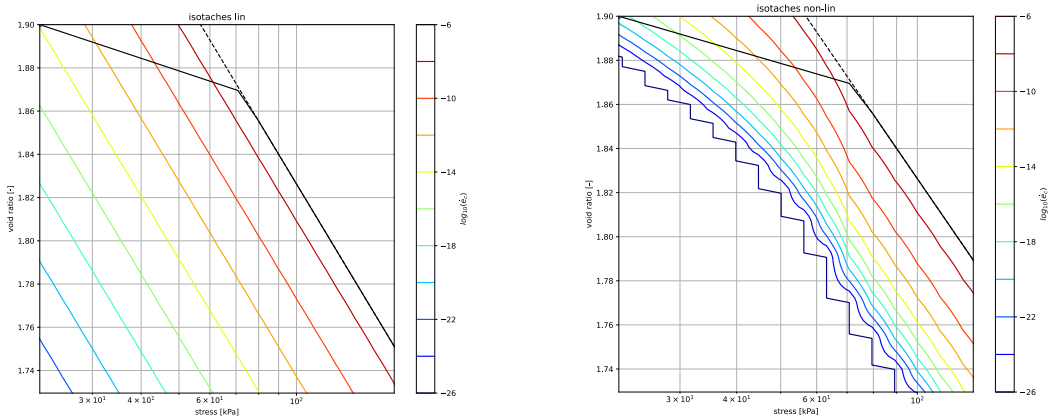

(a) Linear isotachs

(b) Non-linear isotachs

Figure 2.9: Example of linear and non-linear distorted isotachs for a yield stress of 70 kPa

2.1.4. Parameters

As mentioned in the previous two sections there are several soil and state parameters to be determined for the long-term settlement predictions.

Stress and Consolidation

Two important model parameters for both the linear and distorted non-linear models are the in situ initial stress and the yield stress. The initial stress state, also displayed as σ'_{v0}, represents the stress state of the soil prior to loading. This usually is the self weight of the soil. The in situ (total) stress can be determined by multiplying the volumetric weight of the soil by the thickness of the soil on top, when different soil layers are present, different volumetric weights must be used. For soil under the water table, the effective stress is obtained by subtracting the water pressure from the total stress, see equation 2.29. For incremental loading tests, the soil specimens are usually only 2 centimetres thick and the initial stress state can be free of choice in a small range (1-10 kPa) to fit the results (Hoefsloot, 2022).

$$\sigma'_v = \sigma_v - u_w \tag{2.29}$$

Where:

σ'_v = effective vertical stress
σ_v = total vertical stress
u_w = water pressure

Due to a load increment the total stress will change, at first this load will be carried by the water which causes excess pore water pressure. Over time excess pore water pressure will dissipate and effective stress will increase. The dissipation of the excess pore water pressure is determined by the degree consolidation. The differential equation to determine the strain caused by this change in excess pore water pressure is shown in equation 2.35. When soil is considered as an elastic material (which is in reality not the case) the relation between a change in stress and a change in strain is given by equation 2.30, since the change in effective stress for a constant load is equal to the change in excess pore water pressure equation 2.30 becomes 2.31

$$\Delta\varepsilon = -\Delta\sigma' \cdot m_v \tag{2.30}$$

$$\Delta\varepsilon = \Delta u_w \cdot m_v \tag{2.31}$$

Where:

m_v = Soil compressibility

Under the assumption that soil only deforms in a one dimensional way (z-direction for a x,y,z system), the volumetric strain is equal to the strain presented in equation 2.31. The volumetric strain is the change of volume over the total volume. The change in volume is caused by outflow of water and to a lesser extend by the compression of water, this will cause a rearrangement of soil grains. The outflow of water for a one dimensional problem is given in equation 2.32 and the water compressibility in equation 2.33. When these two are summed up divided by the total volume, the volumetric strain is obtained. For small time steps, the equations becomes equation 2.35 (Verruijt & Broere, 2011).

$$\Delta V = \frac{\delta q_z}{\delta z} V \Delta t = -\frac{k\ \delta^2 p}{\gamma_w\ \delta z^2} V \Delta t \tag{2.32}$$

$$\Delta V = -\beta n V \Delta u_w \tag{2.33}$$

$$\Delta \varepsilon = \frac{\Delta V}{V} = -n\beta \Delta p + \frac{k\ \delta^2 p}{\gamma_w\ \delta z^2} \Delta t \tag{2.34}$$

$$\frac{\delta \varepsilon_{vol}}{\delta t} = -n\beta \frac{\delta p}{\delta t} + \frac{k\ \delta^2 p}{\gamma_w\ \delta z^2} \tag{2.35}$$

Where:

ε_{vol} = volumetric strain
q_z = flow of water in z direction
p = excess pore water pressure
n = porosity
β = compressibility of water
k = permeability
γ_w = volumetric weight of water
z = vertical position

When assuming one directional compression, this volumetric strain can be equated with the strain depending on the change in stress over time, which results in equation 2.36. It is often assumed that β in equation 2.36 is equal to zero since water is assumed incompressible.

$$\frac{\delta p}{\delta t} = c_v \frac{\delta^2 p}{\delta z^2} \tag{2.36}$$

Where:

$c_v = \frac{k}{\gamma_w (m_v + n\beta)}$ = Coefficient of consolidation

$$T_v = \frac{c_v}{h^2_{drainage}} \cdot t \tag{2.37}$$

$$U(t) = \sqrt[6]{\frac{T_v^3}{0.5 + T_v^3}} \tag{2.38}$$

Where:

T_v = time factor for consolidation
c_v = consolidation coefficient
$h_{drainage}$ = maximum drainage path
t = time
U = degree of consolidation

In Verruijt and Broere (2011) an analytical and numerical solution is given which solves the pore pressure over time and place (z,t). CROW (2022) shows that the degree of consolidation can be approached with equations 2.37 and 2.38. With these equations there is no need for solving the partial differential equation 2.36 at every time step. With the degree of consolidation the excess pore pressures can be calculated by multiplying the degree of consolidation with the stress increment to calculate the effective

stress at every moment in time (see equation 2.39). In equation 2.37 the c_v is the coefficient of consolidation and is based on the stiffness of the soil, the permeability and the compressibility of the fluid or gas medium. This factor can be determined by the Cassagrande method or the Lagrange method (Verruijt & Broere, 2011). The t in this equation is the time counting from the moment the load is applied and the $h_{drainage}$ is maximum drainage path (depending on single or double drainage path, the thickness or half thickness must be used).

$$\sigma'_v(t) = \sigma'_{v0} + U(t) \cdot \Delta\sigma_v \tag{2.39}$$

The second stress state parameter is the yield stress. This stress state represents the largest stress a soil particle has experienced by loading and aging. An approximation is suggested by the Casagrande method (Figure 2.10. the yield stress is the intersection of the extended slope and the bisector slope with the smallest radius and a horizontal line in this point (e.g. point T in Figure 2.10).

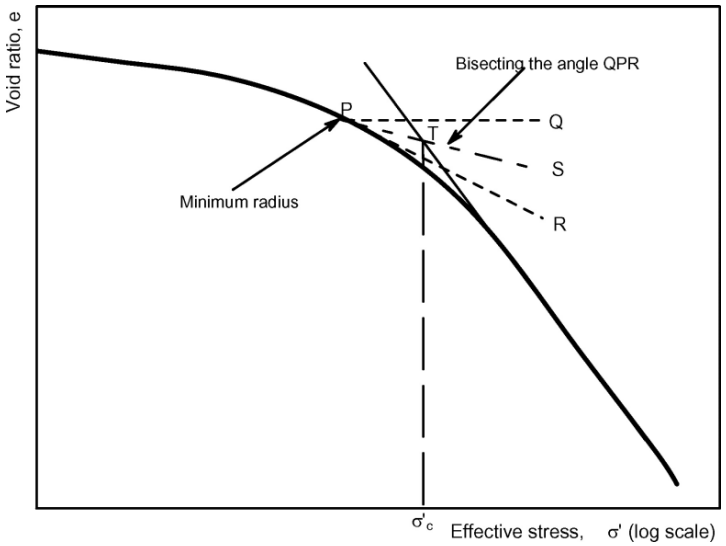

Figure 2.10: Example of how to determine the yield stress according to the Casagrande method (Çelik & Tan, 2005)

For the Casagrande method laboratory tests are required and samples are often disturbed in some way which makes such a precise determination less precise. Next to that, smooth curves as presented in Figure 2.10 will not appear for incremental loading tests. Therefore, in engineering practise the intersection of the reloading curve and the compression curve (RR and CR lines in Figure 2.11 with p_g as yield stress) is taken as the yield stress which is also used in the linear isotach model. Y. Yuan and Whittle (2018) assume the yield stress to be the stress state at which the extended limiting compression curve intersects with the initial void ratio (Figure 2.4).

Unload and reload parameter

In both the linear isotachs and the non-linear models there is a parameter that describes the behaviour of the compression when stress is decreased or increased up to the yield stress. In the linear isotachs model this is the RR and for the MIT-SR model this parameter is the ρ_r. The formal definition of the parameter RR and the approximation can be found in Table 2.1. In Figure 2.11 the approximation can be seen on data from an incremental loading test on Hazerswoude clay (den Haan et al., 2004). The RR value can be approximated by taking the slope of the stress strain curve in the region where the stress is smaller than the yield stress. One must be careful when the curve starts to bend, this happens in the transition zone close to the yield stress where the curve changes from reloading to virgin compression behaviour. A more common way to determine the RR value nowadays is to determine the slope of the unloading and reloading step, since such a step is not present in Figure 2.11 the loading step prior to the yield stress is used. The determination of the reload/unload parameter for MIT-SR is comparable. The difference is that not a change in strain but a change in void ratio is considered and instead of a linear scale, a logarithmic scale must be used on the vertical axis. The approximation of the parameter is also given in Table 2.1. Both parameters are inter changeable by there relation to the conventional

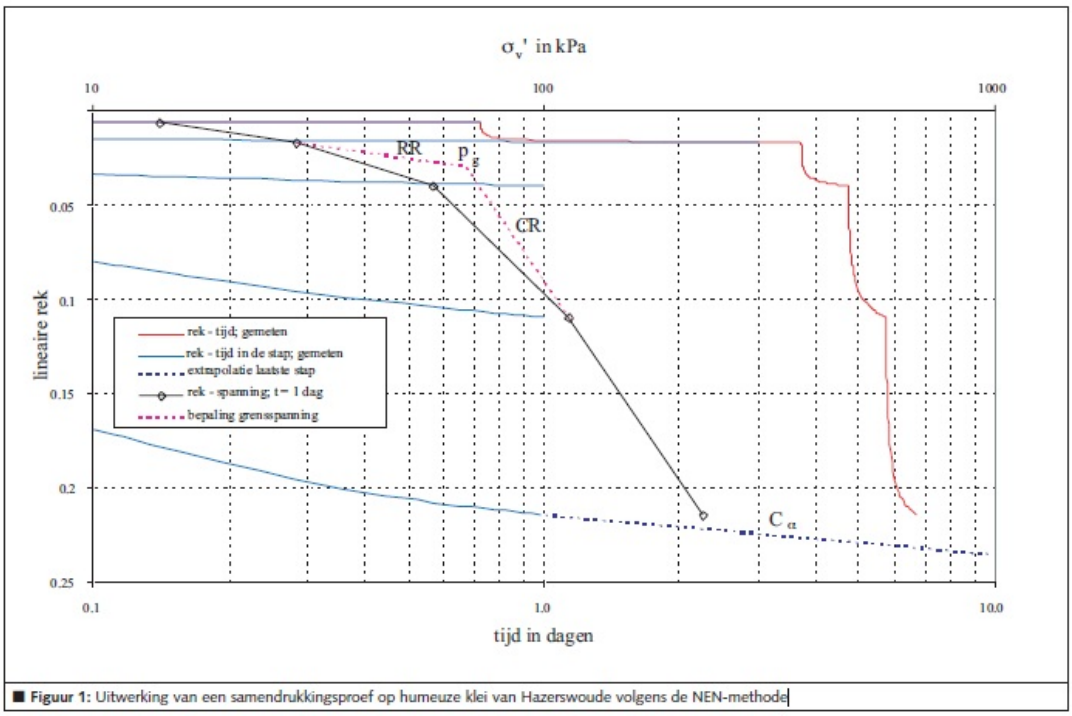

Figure 2.11: Example of a compression test on organic clay from Hazerswoude (den Haan et al., 2004).

parameter C_r given by Y. Yuan (2016) & Zwanenburg (2021), see equations 2.40 - 2.42.

$$\rho_r = \frac{C_r}{e \cdot ln(10)} \tag{2.40}$$

$$RR = \frac{C_r}{1 + e_0} \tag{2.41}$$

$$\rho_r = RR \cdot \frac{(1 + e_0)}{e \cdot ln(10)} \tag{2.42}$$

Where:

C_r = unload / reload index
RR = unload / reload ratio
e = void ratio
e_0 = initial void ratio
ρ_r = unload / reload parameter

Virgin compression parameter

Beyond the yield stress the compressibility changes and the soil behaves less stiff in normally consolidated conditions. This can be described by the virgin compression parameters CR and ρ_c. In the linear isotachs model this parameter can be obtained by taking the slope of the strains after one day when the stress level exceeds the yield stress. This part of the curve is characterized by its steepness compared to the reloading and unloading curve. Just as for the unloading and reloading parameter one should take care of using strain levels with a stress state close to the yield stress, the curve tends to bend here. The same holds when a unloading and reloading step is used. This can be avoided by using the strain level before unloading and the strain level at the end of the test (for this an extra loading step is required after reloading). The approximation of the ρ_c parameter can again be obtained from the logarithm of the void ratio against the logarithm of stress curve and the linearised slope of the steepest part of the curve for strains at one day. This is visualised in Figure 2.4. Just as for the unload and

reload parameters, the virgin compression parameters can be rewritten to one another (see equations 2.43-2.45).

$$\rho_c = \frac{C_c}{e \cdot ln(10)} \tag{2.43}$$

$$CR = \frac{C_c}{1 + e_0} \tag{2.44}$$

$$\rho_c = CR \cdot \frac{(1 + e_0)}{e \cdot ln(10)} \tag{2.45}$$

Where:

C_c = compression index
CR = compression ratio
e = void ratio
e_0 = initial void ratio
ρ_c = compression parameter

Creep parameter

The next soil parameter is the creep parameter, the C_α and ρ_α. When looking to Figure 2.11 the strain per loading step is plotted against time on a logarithmic scale. The parameter can be approached by taking the slope of this curve when the stress is constant again for the parameter of the MIT-SR model this linearised slope is taken in the logarithmic space of the void ratio against time. As a starting point in time, Hoefsloot (2022) suggests to start halfway the consolidation period. The consolidation period (time required for pore pressure to dissipate) can be approached by the use of equations 2.37 - 2.38. When the degree of consolidation $U(t)$ is set to 0.5, the time at which half the pore water pressure is dissipated can be calculated. From this point towards the end of a loading step the slope of the strain versus the logarithm of time curve can be determined, C_α. For the ρ_α the same point in time will be used only the change in void ratio should be considered. Both time and void ratio should be considered on a logarithmic scale for ρ_α. How these two parameters relate to each other can be seen in equations 2.46 - 2.48.

$$\rho_\alpha = \frac{C_{\alpha e}}{e \cdot ln(10)} \tag{2.46}$$

$$C_{\alpha\varepsilon} = \frac{C_{\alpha e}}{1 + e_0} \tag{2.47}$$

$$\rho_\alpha = C_{\alpha\varepsilon} \cdot \frac{(1 + e_0)}{e \cdot ln(10)} \tag{2.48}$$

$C_{\alpha;e}$ = secondary compression index
$C_{\alpha;\varepsilon}$ = secondary compression ratio
e = void ratio
e_0 = initial void ratio
ρ_α = secondary compression parameter

Other parameters

Above all comparable parameters for the three models are listed and what is left are additional soil and model parameters. First $\dot{\varepsilon}_{ref}$, it is the strain rate belonging to the one-day compression curve, or for the MIT-SR model the LCC. On this curve the ratio between stress state and the yield stress is 1. This value can also be obtained by equation 2.6 ($\dot{\varepsilon} = C_\alpha/\tau \cdot ln(10)$). Since the intrinsic time on this line will be equal to 1 day the strain rate will be equal to $C_\alpha/ln(10)$. The second parameter that is only used in the MIT-SR model is $R_{a;0}$ which is the initial internal strain rate. This value should be known since the change in internal strain rate is a function of the strain rate itself (see equation 2.13). Y. Yuan and Whittle (2018) state that the value of $R_{a;0}$ is more important in normally consolidated soils since it controls viscoplastic strain rate , which for over consolidated clay would be negligible small, resulting in an initial value equal to 0. When normally consolidated, the initial value for $R_{a;0}$ is equal

Table 2.1: Sum up of the soil compression parameters and their definition

Parameter	Definition
RR	$[\frac{\Delta\varepsilon}{\Delta log(\sigma'_v)}]_{\sigma'_v<\sigma'_p}$
CR	$[\frac{\Delta\varepsilon}{\Delta log(\sigma'_v)}]_{\sigma'_v>\sigma'_p}$
$C_{\alpha;\varepsilon}$	$[\frac{\Delta\varepsilon}{\Delta log(t)}]_{t>0.5\cdot T_{eop}}$
C_r	$[\frac{\Delta e}{\Delta log(\sigma'_v)}]_{\sigma'_v<\sigma'_p}$
C_c	$[\frac{\Delta e}{\Delta log(\sigma'_v)}]_{\sigma'_v>\sigma'_p}$
$C_{\alpha;e}$	$[\frac{\Delta e}{\Delta log(t)}]_{t>0.5\cdot T_{eop}}$
ρ_r	$[\frac{\Delta log(e)}{\Delta log(\sigma'_v)}]_{\sigma'_v<\sigma'_p}$
ρ_c	$[\frac{\Delta log(e)}{\Delta log(\sigma'_v)}]_{\sigma'_v>\sigma'_p}$
ρ_α	$[\frac{\Delta log(e)}{\Delta log(t)}]_{t>0.5\cdot T_{eop}}$

to the initial viscoplastic strain rate. A relation is given by Y. Yuan and Whittle (2018) to determine the initial viscoplastic strain rate based on the consolidation time as can be seen in equation 2.49, this value can be used as a starting point for $R_{a;0}$.

$$\dot{\varepsilon}_0^{vp} = \frac{\rho_\alpha n}{t_{99}} \tag{2.49}$$

In this equation the t_{99} refers to the time for which the degree of consolidation is equal to 99%. This can be calculated according to equations 2.37 and 2.38. A second suggestion for determining the initial internal strain rate by Y. Yuan et al. (2021) is to take an initial internal strain rate that would produce a straight line for a CRS simulation with a slope of ρ_c. In Figure 2.12 Y. Yuan et al. (2021) simulates different CRS tests with the MIT-SR model to illustrate that behaviour, the suggested initial strain rate would be the one corresponding to line 5', the lines represent simulations with different strain rates. This line is similar to an initial isotach with an intrinsic time of τ_0. Therefore, the initial strain rate can be picked as a first estimate of $R_{a;0}$. The disadvantage of this approach is, according to Y. Yuan and Whittle (2018), that the initial strain rate determined based on equation 2.5 and 2.6) is dependent on the yield stress. This explicitly is something Yuan and Whittle try to avoid but looking at Figure 2.12 it can be seen that only small overshoots occur when modelled with a yield stress dependent strain rate (difference between lines with a number and a number and apostrophe (e.g. 5 and 5')). A last suggested for $R_{a;0}$ is to monitor ground level movements before loading, this could provide an estimation of $\dot{\varepsilon}_0^{vp}$. Since the internal strain rate updates itself, the order of magnitude is more important than an exact value.

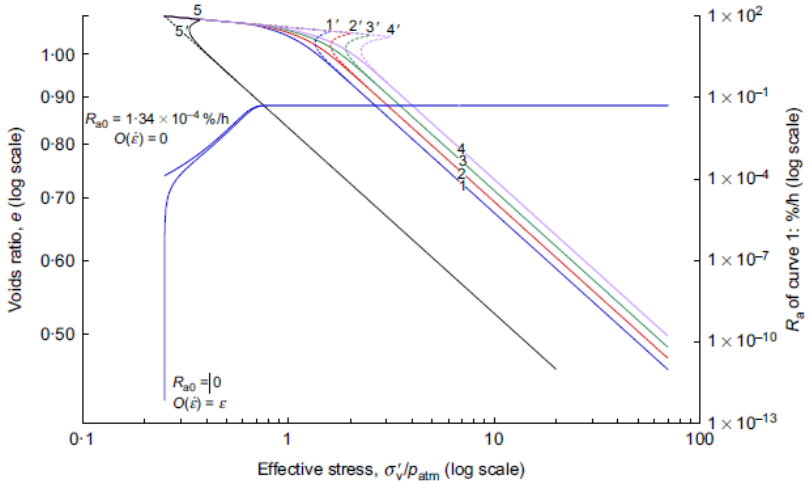

Figure 2.12: Simulated CRS tests for different strain rates (Y. Yuan et al., 2021)

The last model parameter for the MIT-SR model to discuss is β. The β parameter controls the rate dependency of the internal strain rate. The value can be determined by taking the slope of a stress against strain rate graph (on a logarithmic scale). A larger value of β ensures that the internal strain rate (and with it the viscoplastic strain rate) decays faster. The upper and lower limits for this parameter are given by $0 \leq \beta \leq \rho_\alpha/\rho_c$.

Non-linearity and distortion parameters C+S Model

In the C+S model the spacing of the isotachs is not constant, which means that the isotachs lie closer together when the OCR is increasing. The spacing of isotachs is determined by C_α. In the C+S model $\hat{C}_\alpha$ is used for this and is a function of the C_α for normally consolidated situations (similar to linear isotach model), the OCR and β_2. This relation is given by equation 2.20. The parameter β_2 controls the OCR dependency and can be obtained by considering slopes of the strain rate against change in void ratio for different OCR's (Figure 2.13). These slopes all have a different value of $\hat{C}_\alpha(OCR)$ and can be plotted against OCR (Figure 2.14). Fitting equation 2.20 trough these point will give a value for β_2.

$$\frac{\hat{C}_{\alpha;c}}{\hat{C}_{\alpha;NC}} = \frac{2}{OCR_{ref}^{\beta_2} + 1} \qquad \text{(2.20 revisited)}$$

A similar approach can be used for the determination of β_3. This parameter controls the creep strain rate due to (un)loading. In the linear isotach models this value is equal to $(C_c - C_r)/C_\alpha$ but in the C+S model this parameter is determined based on unloading tests. By taking the intersections of the strain rate against change in void ratio for a change of zero (from the moment creep is dominant) a specific strain rate is found for an OCR. By plotting these initial strain rates against the OCR will result in the right graph of Figure 2.14, by fitting equation 2.19 through it, a value for β_3 can be found.

$$\dot{e}_{init;c} = \dot{e}_{vp;c;ref} \cdot OCR_{ref}^{-\beta_3} \qquad \text{(2.19 revisited)}$$

Next are the viscoplastic swell parameters, in which the most important one is the initial viscoplastic strain rate (equation 2.28). For an OCR of 2, this initial viscoplastic swell strain rate is only dependent on b_2. By unloading to an OCR of 2 and taking the swell strain rate after consolidation this b_2 can be found. Using multiple unloading steps for different OCR's makes it possible to plot the initial viscoplastic strain rates against the OCR and also determine the OCR dependency parameter m_2.

$$\dot{e}_{s;init} = 10^{b_2}(OCR - 1)^{m_2} \qquad \text{(2.28 revisited)}$$

As mentioned earlier the viscoplastic swell strain rate is a transient, auto decaying process. The rate in which the viscoplastic swell strain rate decays is based on equation 2.26 and it can be seen that it dependent on the strain rate itself and the parameter $\hat{C}_{\alpha;s}$. This $\hat{C}_{\alpha;s}$ is the slope of the strain rate against

change in void ratio, as is the case for $\hat{C}_alpha$, but in this case for the swell period after consolidation. For different unloading steps these values van be plotted against the OCR (like in Figure 2.14 but for unloading) and the parameter b_1 is the value for an OCR of 2 and m_1 is the OCR dependency (Vergote, 2022).

$$\ddot{e}_s = -\frac{\dot{e}_s^2 \cdot ln(10)}{\hat{C}_{\alpha;s}} \qquad \text{(2.26 revisited)}$$

$$\frac{\hat{C}_{\alpha;s}}{C_{\alpha;NC}} = 10^{b_1}(OCR-1)^{m_1} \qquad \text{(2.27 revisited)}$$

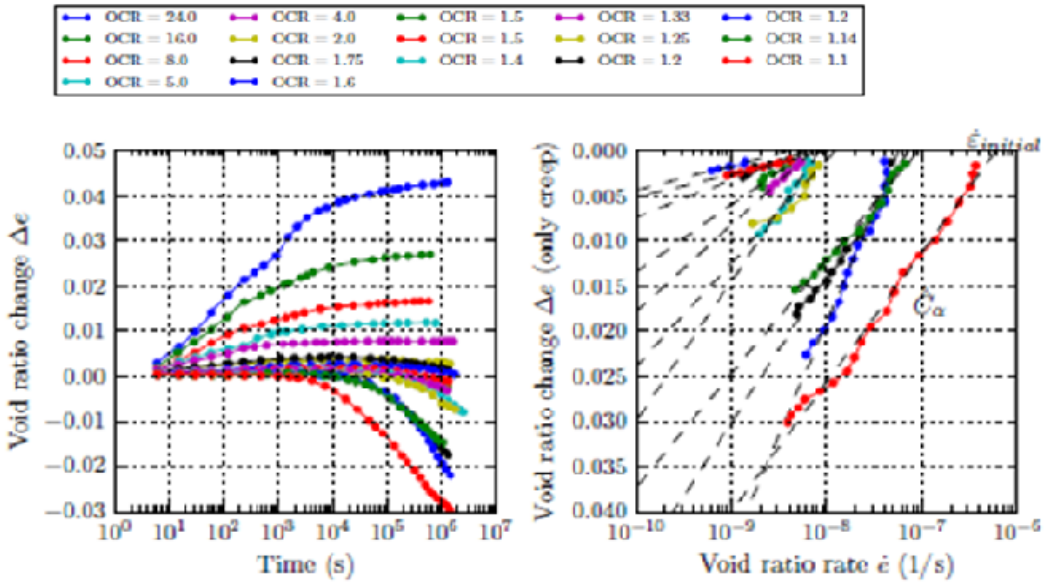

Figure 3.4: Reinterpreted results for Berthierville clay of Feng (1991)

Figure 2.13: Left: change in void ratio against the time for series of unloading steps. At some point in time creep becomes dominant from that point on the strain rate will be determined. Right: the creep strain rates against the change in void ratio to determine the (new) initial creep strain rate and the $\hat{C}_\alpha$ values for a range of OCR (Vergote, 2020)

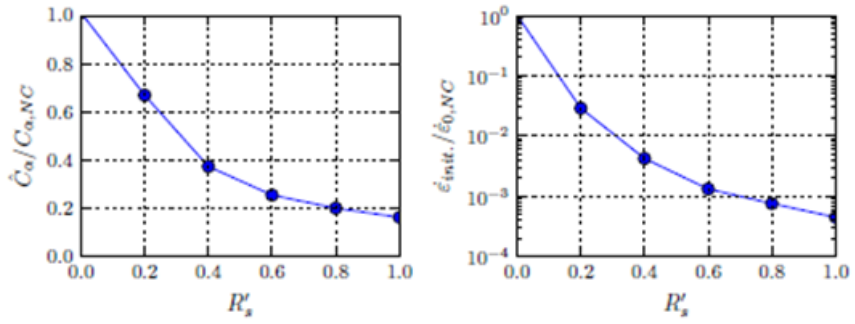

Figure 3.13: Derived semi-isotache parameters from Feng (1991)

Figure 2.14: Normalized creep parameters against the $R'_S = (OCR - 1)$ for the determination of β_2 and β_3 parameters (Vergote, 2020)

An example is made to compare linear isotach model with the C+S model in Figure 2.15. For OCR's

close to 1, creep will start earlier for the linear isotach model and higher strain rates are found when creep becomes dominant. Figures 2.15a and 2.15b show the results of simulations similar to the ones in Figure 2.13 for OCR's equal to 1.1, 1.2, 1.4 and 1.6 (for steps 3, 5, 7, 9). It can be seen that the C+S model shows similar behaviour in the change of void ratio versus time graph compared to Figure 2.13. Next to that it can be seen that the slope in the void ratio versus strain rate (Figure 2.15b) is slightly steeper for the linear isotach model where the slopes of the C+S simulations become a bit flatter.

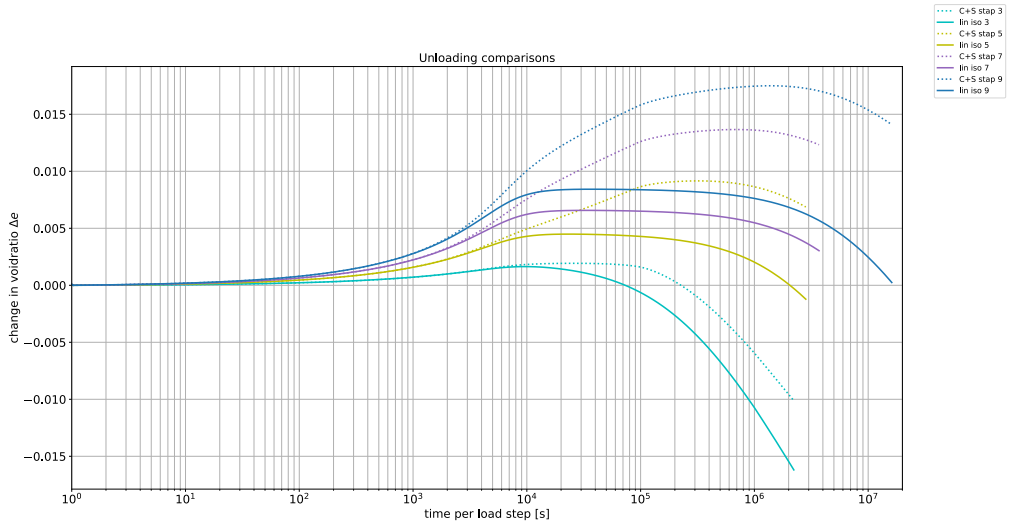

(a) Time versus change in void ratio for OCR's of 1.1, 1.2, 1.4, 1.6

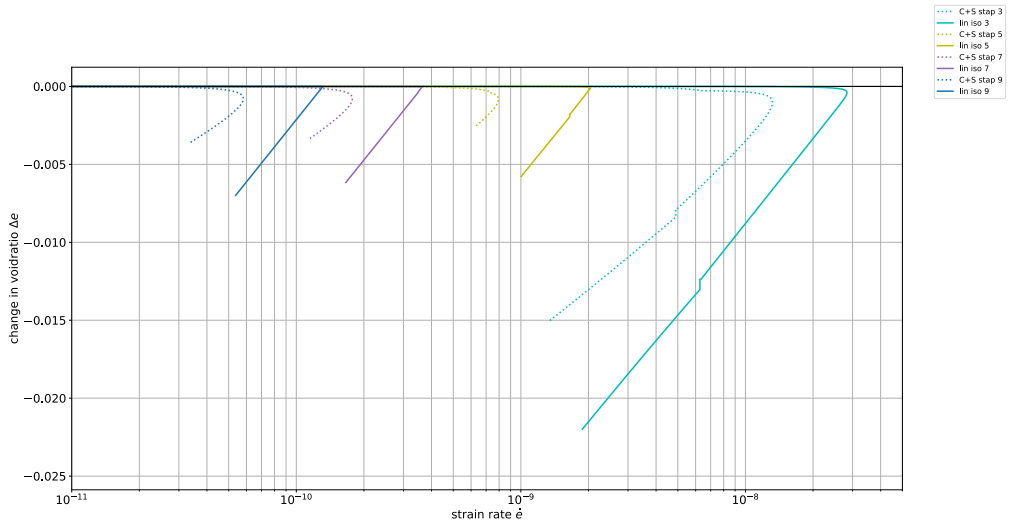

(b) Strain rate versus change in void ratio for OCR's of 1.1, 1.2, 1.4, 1.6

Figure 2.15: Simulation for C+S and linear isotach model for comparison with Figure 2.13

OCR

In the models above there are different definitions of the over consolidation ratio (OCR). The most common definition of the OCR is the yield stress divided by the current stress state. In this relation the yield stress is determined as the maximum stress that the soil has experienced. In addition to this relation aging of the soil should be considered as was shown by Polinder (2019), this means that it is not only the stress but also time that influences the yield stress and this is accounted for by the use of intrinsic time in the linear isotach model. From a point in the stress strain space the reload line should be followed toward the one-day isotach. The corresponding stress state of the intersection between

the one-day isotach and the reload line is the yield stress.

$$OCR = \frac{\sigma'_p}{\sigma'_v} \tag{2.50}$$

For the C+S model the yield stress and the OCR are defined similar. From a certain stress state a line is drawn with a slope equal to the reload index. The intersection between the reference isotach and this line is the reference yield stress. Rather than yield stress (maximum experienced stress) the C+S model uses the name reference yield stress and reference OCR. The reference stress state is equal to the one-day isotach but is defined as a straight line starting at stress state equal to 1 kPa with a corresponding reference void ratio and having a slope equal to the virgin compression index C_c. The reference void ratio is an input parameter for the numerical model and can be found by following the reload line from an initial void ratio e_0 till the reference yield stress is reached, from there on an extrapolation along the reference isotach can be constructed towards the stress level of 1 kPa. Next to the reference OCR the C+S model also uses OCR. But defines this as the maximum stress over the stress, in this way aging does not influence the OCR.

Linear and natural strain

The calculated strain in the linear isotach model are linear, or Cauchy, strains. This means that the strain is defined as the settlement compared to the initial thickness of a layer or sample. Settlement is caused by a change in volume, since minerals are considered incompressible the change in volume must come from a change in voids, the spaces in between soil particles. They can be filled with gas or water. The ratio between the volume of the voids and the volume of soil particles is called the void ratio (Verruijt & Broere, 2011). When soil is compressed gas and water is able to escape the voids and the volume of the voids decrease which causes a change in void ratio (equation 2.51).

$$e = \frac{V_{void}}{V_{soil}} \tag{2.51}$$

When a soil sample is completely saturated, the volume of the voids is assumed to be fully filled by water. The initial value for void ratio can be determined by weighting the sample followed by drying the sample at 105 °C. The sample should be weighted again so the saturated and dry masses are known. By subtracting the dry mass from the saturated mass the mass of water is known. By using the volumetric weights of water and soil the volumes can be determined. Void ratio can also be expressed in terms of porosity. Which is the ratio of void volume over total volume (instead of soil particles for the void ratio).

$$e_0 = \frac{(m_{sat} - m_{dry})/\rho_{water}}{m_{dry}/\rho_{soil}} \tag{2.52}$$

$$n = \frac{e}{1+e} \tag{2.53}$$

When one dimensional compression is considered, the area of a sample will be constant and the change in volume is proportional to the change in thickness. Therefor, the void ratio and strain can be written in term of each other (see eqation 2.54). When this equation is applied in small steps the change in strain can be determined. By choosing between the initial void ratio (e_0) in the denominator linear strains are calculated. When instead of the initial void ratio the void ratio prior to the considered step is chosen (e), natural strains will be calculated.

$$\Delta\varepsilon = -\frac{\Delta e}{1+e} \tag{2.54}$$

As mentioned the difference between linear and natural strain depends on the value in the deniminator when determining the strain. For natural (or Henky) strain changes in thickness are divided by the thickness at that moment and summed up together while for linear strain the total change in thickness is divided by the initial thickness (see equations 2.55 & 2.56 and Figure 2.16). Natural strains are used in both linear (a,b,c-isotach model) and non-linear (MIT-SR) isotach models.

$$\varepsilon_C = \frac{\Delta h}{h_0} \tag{2.55}$$

$$\varepsilon_H = \int_{h=h_0}^{h=h_0-\Delta h} \frac{dh}{h} = -ln(\frac{h_0 - \Delta h}{h_0}) = -ln(1 - \varepsilon_C) \tag{2.56}$$

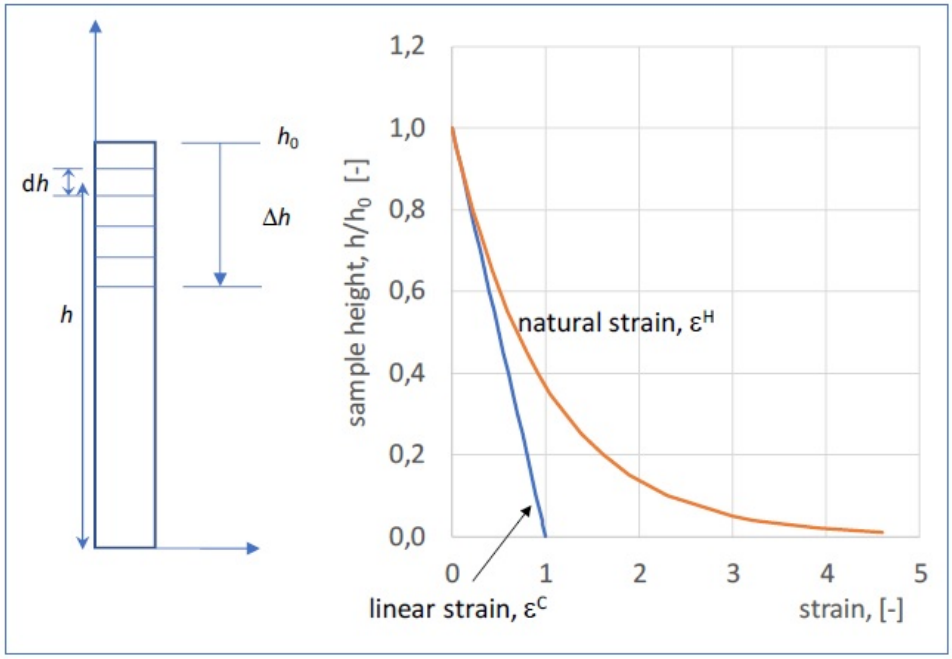

Figure 2.16: The orange graph shows the Henky strain (natural) and on the left side the incremental changes are given by dh. In blue the Cauchy strain (linear) is shown and on the left the incremental change is given by Δh (Zwanenburg, 2021).

2.1.5. Advantages and disadvantages of the models

The three different types of models discussed above are the linear isotach model, non-linear isotach model and distorted non-linear isotach model. They are listed in Tables 2.2 - 2.4.

Table 2.2: The advantages and disadvantages of the linear isotach model

Linear isotach model	
Advantages	Disadvantages
Few parameters	Strong dependency on yield stress
Good fit for NC	Bad fit for OC due to unloading
Parameters can be determined by conventional CRS and IL tests	No viscoplastic swell included

Table 2.3: The advantages and disadvantages of the non-linear isotach model

Non-linear isotach model	
Advantages	Disadvantages
Updates parameters for over consolidation	Use of internal strain rate (not measurable)
Good fit for NC	More parameters than linear isotach model
Most parameters have physical meaning	No viscoplastic swell included
Parameters can be determined by conventional CRS and IL tests	

Table 2.4: The advantages and disadvantages of the non-linear distorted isotach model

non-linear distorted isotach model	
Advantages	Disadvantages
Includes swell	Many model parameters to determine
Includes decay non-linearity of creep	Unloading tests required for parameter determination
	Not used in practice yet
	Not much suitable laboratory tests available

2.2. Organic Matter

As mentioned in Chapter 1, next to mechanical settlement that occurs in soils some organic soils as peat also consist of degradable particles which can cause volume reduction. These degradable particles consist of carbon and nitrogen from plant remains and when exposed to air they can oxidize. During oxidation of the carbon, gas will be formed. During aerobic circumstances this will be CO_2 and in an anaerobe environment it will mainly be CH_4. This results in two problems to look into, the first problem is the volume loss due to the degradation of the organic matter and secondly the gas that has been produced could affect the compressibility of the soil.

2.2.1. Volume loss by degradation of organic matter

During oxidation the percentage of organic matter will decay. The organic matter in a soil can be determined in several ways, one of them is the loss on ignition method. In this method the dry weight of a soil is compared with the weight of a soil after combustion (this can be at 500°C for the carbon content and at 1000 °C for all the organic matter) or by dissolving the organic matter with a chemical compound like hydrogen peroxide (CROW, 2010).

Den Haan has found a relation between the organic matter, effective stress and the void ratio of a soil given by equation 2.57 (Koster et al., 2018), based on empirical relations given by den Haan (1992).

$$e = (2.27 + 27.55 \cdot N) \cdot \sigma_v'^{-(0.12+0.34 \cdot N)} \tag{2.57}$$

Where:

e = void ratio
N = organic matter (percentage mass loss between 100-500 °C)
σ_v' = effective vertical stress

Koster uses this empirical relation to model the organic matter over depth of peat samples. Figure 2.17 shows that the relation gives a more or less good fit for the organic matter over depth (Koster et al., 2018). Although the study was set up for mapping the peat distribution and its organic matter, the validity of equation 2.57 can be used to predict a change in void ratio by a change in organic matter. However, to predict the change in void ratio over time the change in organic matter should be predicted.

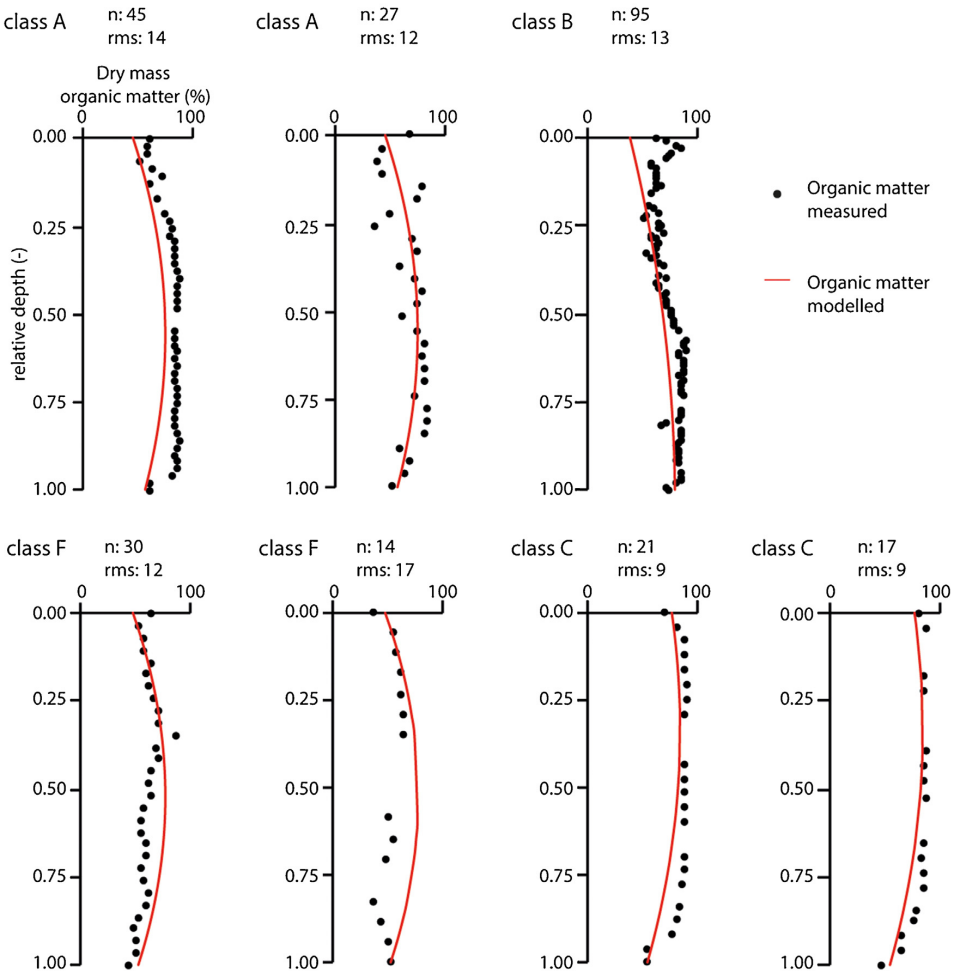

Figure 2.17: Modelled relation of organic matter versus depth by equation 2.57 with measured organic matter from laboratory results (Koster et al., 2018). In this Figure classes represent the different origins of the samples, n is the amount of samples used and rms is the root mean square.

Several publications show that the prediction of degradation of organic matter is difficult because it is influenced by many factors. Some of these factors that drive the production of greenhouse gases, which is caused by soil organic matter degradation, are listed below and explained by Oertel et al. (2016).

- Humidity
- Temperature
- Exposure and air pressure
- Vegetation fires
- Soil pH-values
- Nutrients
- Vegetation
- Land-use change

The first factor mentioned here is the humidity, which is dependent on ground water level and degree of saturation. Among others van den Akker (2017) shows the importance of the water table for oxidation and subsidence of peat and research on peatland subsidence in Venice shows that the rate of degradation is both dependent on ground water level and temperature (Zanello et al., 2011). Both these factors (humidity and temperature) also affect the microbial activities in the soil. Those microbial activities in a carbon cycle can be methanotropic (aerobic) and methanoprophs (aerobic and anaerobe). The activity of those two is strongly dependent on water levels and temperature and therefore, the gas production is as well (Stepniewska & Goraj, 2014). According to Oertel et al. (2016), exposure is mainly important because it influences the temperature and the humidity which makes it an indirect parameter and the same hold for the air pressure because the air pressure influences the ground water pressure (Reicosky et al., 2008), (Izaurralde et al., 2004). For the microorganisms to convert organic matter to gases they're in need of nutrients. An indication of this is the C/N ratio, the amount of carbon over nitrogen that is available. The production of nitrogen gases is negatively correlated to the C/N ratio while the carbon gases are positively correlated. Next to that it was found that if carbon content is not limiting, increasing content of nitrogen increase the gas production and when carbon is a limiting factor nitrogen does not play a significant role in the rate of gas production (Oertel et al., 2016). The soil pH-value on its turn also influence the microbial activity and it was found that methane production is best in a medium alkaline environment while carbon dioxide is produced best in a neutral environment (Dalal & Allen, 2008), (Cuhel et al., 2010). The other three factors mentioned by Oertel do influence the production of greenhouse gases but are not relevant for embankment projects since vegetation fires are very rare, vegetation itself is not likely to be present and the change in land-use is mainly important when forests and peatland become agricultural land.

What can be seen from above is that there are many factors that influence the degradation of organic matter and the production of greenhouse gases in soils. All these factors could cause a change in volume and therefore, extra settlement. Also, most of the mentioned parameters are not constant nor is their change. This makes it hard or even not possible yet to make accurate predictions of degradation of the organic matter.

2.2.2. Volume loss by compression

Since peat consist of soil particles, organic matter, gas and water, the compressibility of this soil type differs from other soft soils like clay which consist of mainly of soil particles and water (see Figure 2.18). A suggested approach for including those two extra properties is to expand equation 2.35. Since this equation states that the change in volume ($\delta\varepsilon_{vol}$) is a function of the water flow only it does not yet include the compressibility of gas as organic matter. A first solution would be to change the parameter β so the water/gas mixture has a compressibility. A more inclusive approach is suggested by Yang and Liu (2016) and Liu et al. (2016), by equating the change in volume to the change in volume of water, gas and organic material instead of equating the change in volume to the change in volume of water (equation 2.58) and for a short period of time (equation 2.59).

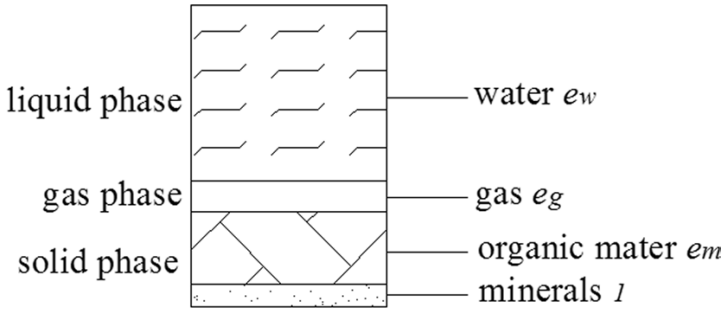

Figure 2.18: Seperation of 3 phases in a soil with associated voids (Yang & Liu, 2016)

$$\Delta V_m + \Delta V_g + \Delta V_w = \Delta V_c \tag{2.58}$$

$$\frac{dV_m}{dt} + \frac{dV_g}{dt} + \frac{dV_w}{dt} = \frac{dV_c}{dt} \tag{2.59}$$

Where:

V_m = volume of organic matter
V_g = volume of gas
V_w = volume of water
V_c = compressed volume

Regardless of what terms are included the total change in volume can still be seen as the change in void ratio. This is divided in void ratios as presented in Figure 2.18. The three components of the void ratio (organic matter, gas and water) are given a new parameter η. By substituting this in equation 2.60 and taking the time derivative of η and assuming all deformation is in vertical direction (dz), the volume change during compression over a short time is given by equation 2.63.

$$\frac{dV_c}{dt} = \frac{1}{1+e}\frac{\delta e}{\delta t}dxdydz \tag{2.60}$$

$$\frac{dV_c}{dt} = \frac{1}{1+\eta}\frac{\delta \eta}{\delta t}dz \tag{2.61}$$

$$\frac{\delta \eta}{\delta t} = \frac{\delta \eta}{\delta \sigma_v'}\frac{\delta \sigma_v'}{\delta t} = \frac{\delta \eta}{\delta \sigma_v'} \cdot \left(\frac{\delta \sigma_v}{\delta t} - \frac{\delta u_w}{\delta t}\right) \tag{2.62}$$

$$\frac{dV_c}{dt} = \frac{1}{1+\eta}\frac{\delta \eta}{\delta \sigma_v'} \cdot \left(\frac{\delta \sigma_v}{\delta t} - \frac{\delta u_w}{\delta t}\right)dz \tag{2.63}$$

Where:

e = total void ratio
η = e_g + e_m + e_w
σ_v = total stress
σ_v' = effective stress
u_w = pore water pressure

It can be seen in equation 2.59 that if organic matter and gas is neglected it is the same relation as earlier presented for the consolidation theory. However, different studies have shown that the organic solid particles in a soil are compressible compared to the incompressible inorganic solids and can not be neglected in peat (Lade & De Boer, 1997), (Moein, 2016), (Berry & Vickers, 1975). This has been taken into account in this equation and the change in organic matter is approached by a stress-strain-time formulation. With the calculated strain the change in volume, compared to an initial (total) volume can be obtained as well for a small increment in time as is shown in equations 2.64-2.66.

$$\varepsilon_m = \frac{\sigma_v}{E_m} \cdot \left(\frac{t}{t_1}\right)^{\lambda} \tag{2.64}$$

$$V_m = \alpha V_0 \cdot (1 - \varepsilon_m) \tag{2.65}$$

$$\frac{dV_m}{dt} = -\frac{\alpha}{E_m}\left(\frac{\delta\sigma_v}{\delta t}t^{\lambda} + \lambda\sigma_v t^{-1}\right)dz \tag{2.66}$$

Where:

ε_m = strain for organic matter
σ_v = total vertical stress
E_m = Stiffness of organic matter
t = time
t_1 = initial time
λ = time factor
V_m = volume organic matter
V_0 = initial total volume
dz = vertical unit length
α = initial organic matter volume ($\frac{V_{m0}}{V_0}$)

The final part is the gas compression. In the determination of the gas compression the simplification is made that dissolution and exsolution of the gas is neglected and the gas can be considered as an ideal gas which deforms by Boyle's gas law. This law states that the initial volume multiplied by the pressure should be equal to a changed pressure multiplied by a new volume. Since the gas is entrapped in water the pressure is both dependent on atmospheric, gas and water pressure. The difference between the latter two can be determined based on the surface tension between water and gas and the radius of gas bubbles that are trapped (Schuurman, 1966), (Wheeler, 1988). This results in equations 2.67. With respect to small changes in gas volume over a small change of time this equation will become like equation 2.68 (which is the time derivative of equation 2.67).

$$(P_a + \frac{2q}{r_0})V_{g0} = (P_a + \frac{2q}{r} + u_w)V_g \tag{2.67}$$

$$\frac{dV_g}{dt} = -\frac{(P_a + \frac{2q}{r_0})V_{g0}}{(P_a + \frac{2q}{r} + u_w)^2} \cdot \frac{d(\frac{2q}{r} + u_w)}{dt} \tag{2.68}$$

By substituting equations 2.66, 2.68, 2.35 (and assuming incompressibility of water so $\beta = 0$) in equation 2.59 a more general model is obtained. This resulting equation can be seen in equation 2.69 (Liu et al., 2016), (Yang & Liu, 2016).

$$\begin{aligned} &\frac{1}{1+\eta}\frac{\delta\eta}{\delta\sigma_v'}\left(\frac{\delta\sigma_v}{\delta t} - \frac{\delta u_w}{\delta t}\right) = \\ &\frac{k\ \delta^2 u_w}{\gamma_w\ \delta z^2} - \frac{(P_a + \frac{2q}{r_0})V_{g0}}{(P_a + \frac{2q}{r} + u_w)^2}\frac{d(\frac{2q}{r} + u_w)}{dt} - \frac{\alpha}{E_m}\left(\frac{\delta\sigma_v}{\delta t}t^{\lambda} + \lambda\sigma_v t^{-1}\right) \end{aligned} \tag{2.69}$$

With this new model samples of peat of two locations (north east China and Wisconsin US) have been used to compare the Terzaghi settlement prediction with equation 2.35 and new settlement predictions with equation 2.69. The results from Yang and Liu (2016) in Figure 2.19 show that this new model does give a better prediction of the settlement behaviour of peat, see Figure 2.19.

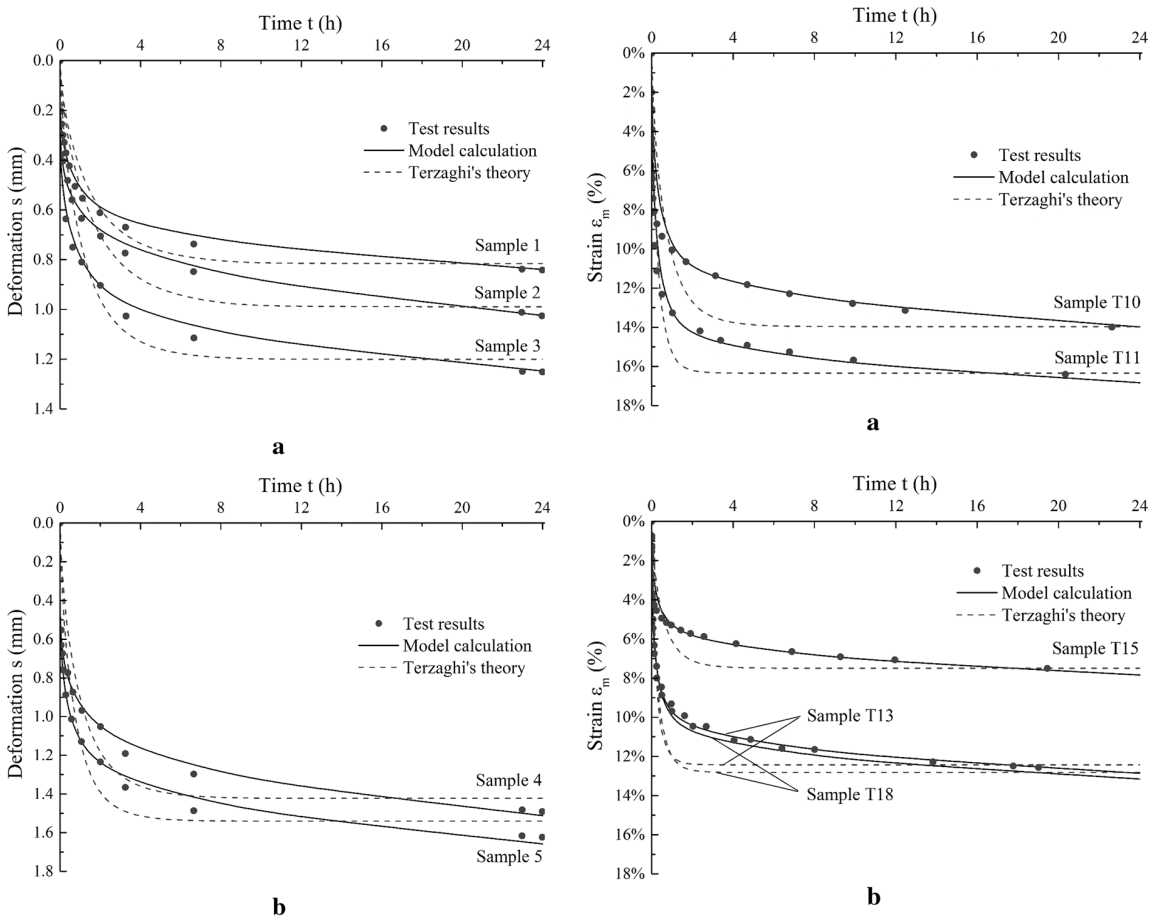

(a) Settlement over time for NO China peat (Yang & Liu, 2016)

(b) Strain over time for Wisconsin peat (Yang & Liu, 2016)

Figure 2.19: Results of the comparison between equation 2.35 and equation 2.69 based on incremental loading tests on peat

Despite the better shape of the curves it can be seen that the final deformation and strain in Figure 2.19 are close to each other but the consolidation behaviour is different.

2.3. InSAR Background

InSAR, or Interferometric Synthetic Aperture Radar, is a technique to measure differences between two (or more) images that are generated using radar technique, called SAR (Synthetic Aperture Radar). To create images from SAR, electromagnetic waves are transmitted from a radar (attached to an aircraft or satellite) and based on physical and electrical properties of the surface a portion of these signals are back scattered and received by the radar system (Moreira et al., 2013). To use SAR, the radar used must be coherent with the time span between sending and receiving, also the transmitted phase must be stored in order to compare the received signal with (Hanssen, 2001). When a signal is transmitted from the radar, the satellite (or aircraft) changes position (indicated by point 1 and 2 in Figure 2.20a). Based on the beamwidth in azimuth and range directions (β_r & β_a) and the radar pulse length τ, a radar footprint can be made (W_a in Figure 2.20a) (Hanssen, 2001). Since it takes time for the signal to travel back after transmitting, the radar produces several other chirps in the mean time, this can be seen in Figure 2.20b.

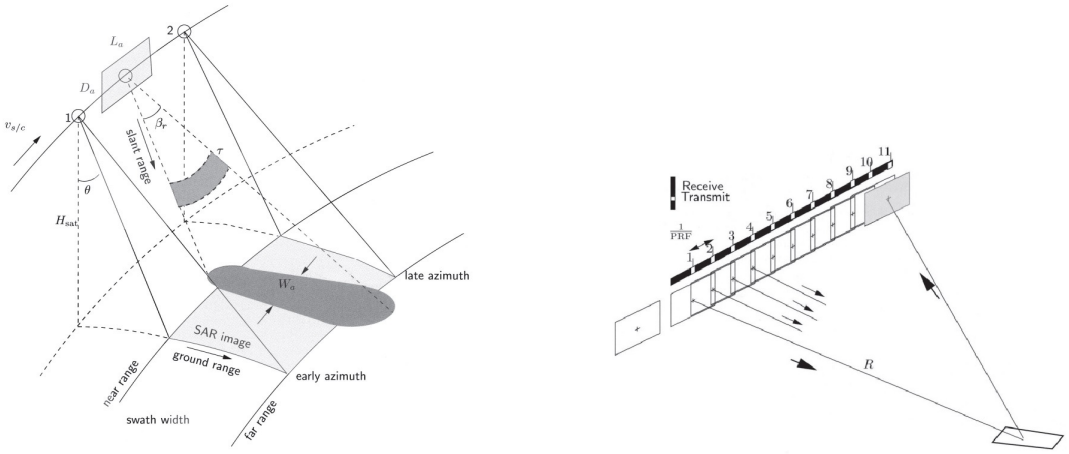

(a) Movement of the satellite and the image field of the SAR

(b) Transmitting and receiving pattern of the radar

Figure 2.20: The use of SAR (Hanssen, 2001)

Once a chirp has been received the raw data must be processed to obtain useful images. The mathematical transformation from raw data to images is outside the scoop of this study but a short overview of the steps is given in Figure 2.21. This data is not just used to project an image but based on the received signal the distance between satellite and the reflecting object can be derived.

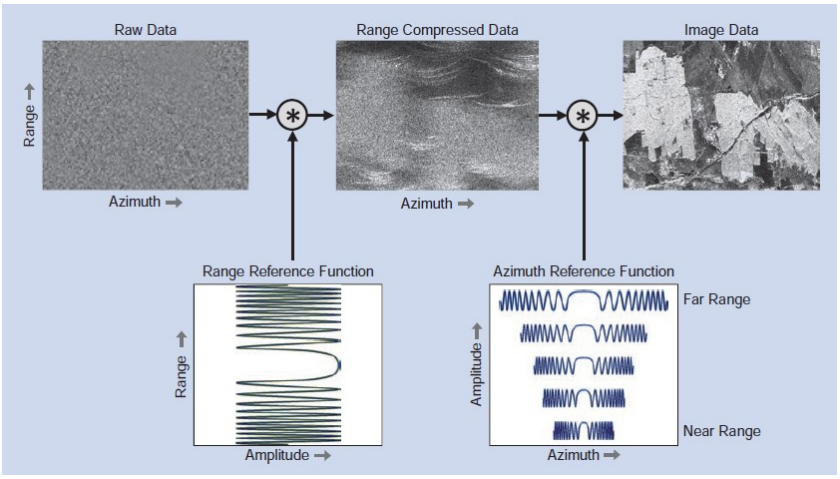

Figure 2.21: The steps taken to process raw data to a useful image of SAR (Moreira et al., 2013).

As discussed earlier, for a geotechnical project such as an embankment, settlement is an import design criteria. For the assessment of parameters in prediction models InSAR can provide an alternative approach compared to other (in situ) tests. A time series of the same spatial points could tell something about the relative deformation and the deformation rates (Reinders et al., 2022). Reinders et al. (2022) mention the benefits of the use of InSAR for geotechnical purposes per project phase and shows that even in early phases it could lead for example to detect ground movement. This could be used in infrastructure project as roads and railways. A schematic representation of the InSAR use for a rail is shown in Figure 2.22. When this is done along a trajectory settlement behaviour can be mapped, this can be done on roads when there are object that reflect the emitted electromagnetic waves, e.g. when there is pavement or asphalt but it does not reflect when a dirt road or grasslands are considered. For that reason the use of InSAR prior to construction a completely new road is limited but before maintenance and for validation of settlement behaviour InSAR could be used.

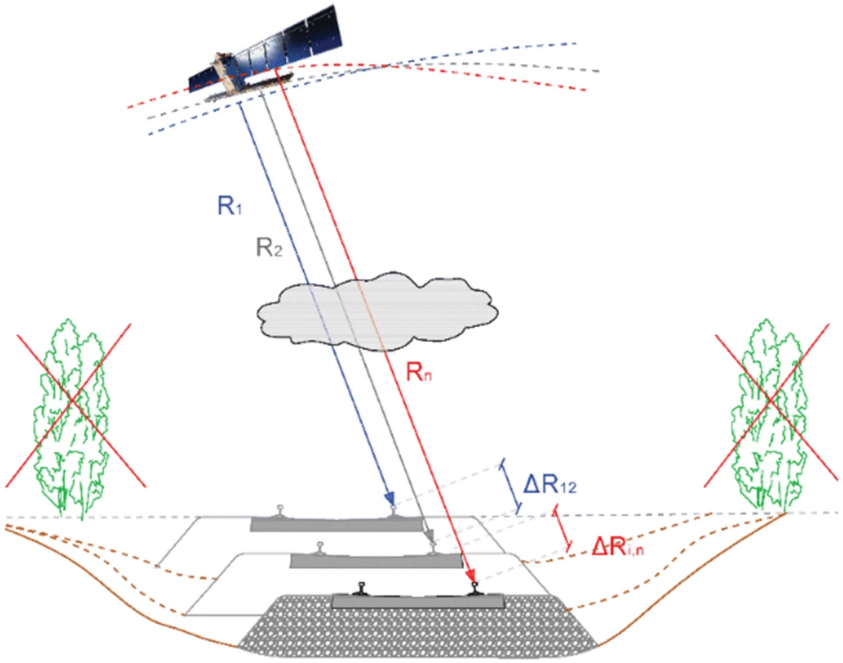

Figure 2.22: Measurements by InSAR for a rail and the detected settlement (Bianchini Ciampoli et al., 2020)

3

Implementation and application of settlement models

3.1. Implementation and Verification

3.1.1. Implementation

Linear isotach model (NEN-Bjerrum)

As described in Chapter 2 the proposed linear isotach model can calculate strain increments based on a few input parameters and a described stress path. In Algorithm 1 pseudo code is given for the implementation of the linear isotach model. The verification of this implementation is done by comparing the outcomes with the excel implementation as proposed by Hoefsloot (2022).

Algorithm 1: Pseudo-code for NEN-Bjerrum model

input : RR, CR, C_α, σ_p, σ_{v0}, Δt, t_{end}, c_v, H_0, loading scheme
output: strain, effective stress, time

begin
  calculate: $\dot{\varepsilon}_{ref}$, τ_0, $\dot{\varepsilon}_0$
  make: time array ← t_{end}, Δt
  for Δt *in time* **do**
    make: total stress ($\sigma_{v;total}$) ← σ_{v0}, time, loading scheme
    Calculate: effective stress ($\sigma_{v;eff}$) ← $\sigma_{v;total}$, `Consolidation(`c_v, *time*, H_0, $\sigma_{v;total}$`)` (eq: 2.29, 2.38, 2.37)
    Calculate: intrinsic time τ ← `Intrinsic time(`*RR, CR, Ca*, τ_0, Δt, *time*`)` (eq: 2.4)
    Calculate: Elastic strain increment $\Delta\varepsilon^{el}_{\Delta t}$ ← `Elastic(`*RR*, $\sigma_{v;eff;\Delta t}$`)` (eq: 2.7)
    Calculate: Viscoplastic strain increment $\Delta\varepsilon^{vp}_{\Delta t}$ ← `Visco-plastic(`*RR, CR*, $C\alpha$, $\tau_{\Delta t}$, $\sigma_{v;eff;\Delta t}$`)` (eq: 2.8)
    $\Delta\varepsilon_{\Delta t}$ ← $\Delta\varepsilon^{el}_{\Delta t}$ + $\Delta\varepsilon^{vp}_{\Delta t}$
    Add to total strain ε ← ε + $\Delta\varepsilon_{\Delta t}$
  end
  Plot strain vs time ($\varepsilon - time$)
  Plot strain vs stress ($\varepsilon - \sigma_{v;eff}$)
end

Non-linear distorted isotach model (C+S model)

For the C+S model the implementation as was provided by Vergote has been used. His model has been made available as open source through github (Vergote, 2021). Similar to the implementation of the linear isotach model, the change in void ratio is determined by a forward difference method for small time steps. A flowchart for every time step is given in Figure 3.1. Although in the implementation of the C+S model it is possible to include the hydro-mechanical coupling by solving the differential equation

for ground water flow, this is discouraged since it takes more computational time and the results do not differ significantly (Vergote et al., 2021, Vergote, 2022).

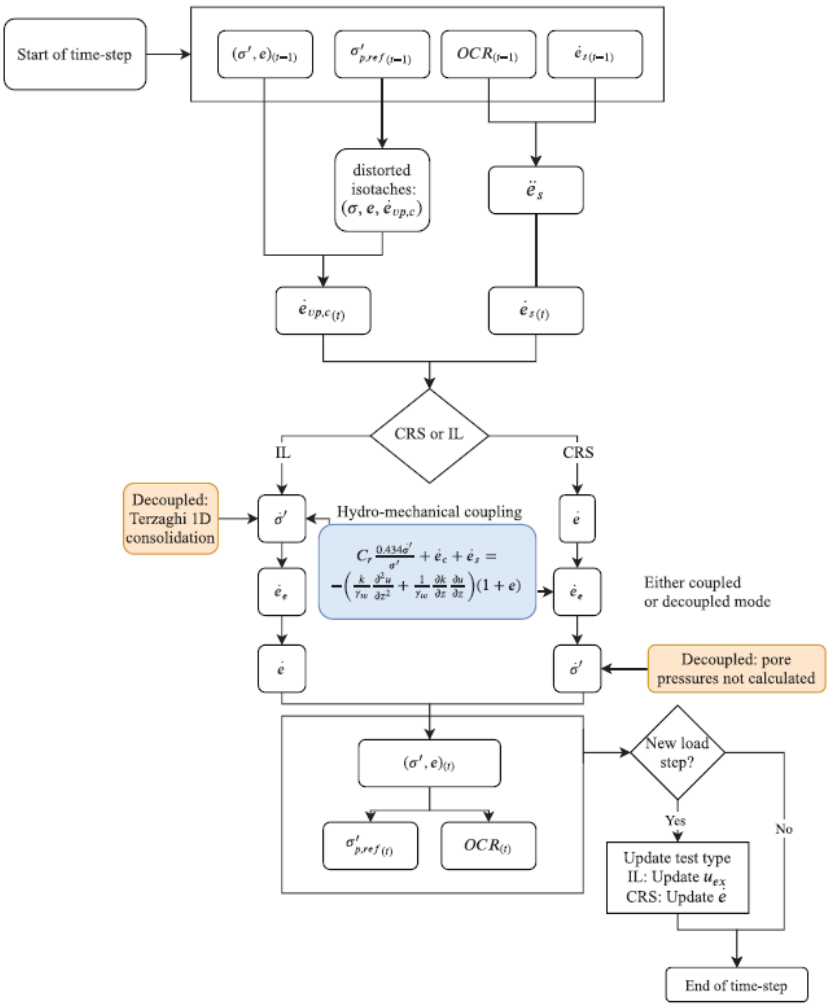

Figure 3.1: Flowchart for the C+S model (Vergote et al., 2021).

In Figure 3.1 a step wise overview of the C+S model per time step is shown. At each time step there are 5 state parameters (e, σ'_v, σ'_p, OCR, $\dot{e}_s$) from which the isotachs, viscoplastic strain rate, viscoplastic swell acceleration and strain rate are calculated. Then for an incremental loading test the change in effective stress is used to calculate the total strain rate and the total strain, for a constant rate of strain test the given strain rate is used to calculate the effective stress. These are used to calculate void ratios, stresses and OCR which are the starting point for the next time step. In Table 3.1 an overview of the used equations per time step is presented. A screenshot of the used python code for iterations is attached in Appendix A.1.

Table 3.1: Strain rates to calculate in every time step in the C+S model

Parameter	Equations
Viscoplastic creep strain rate due to (un)loading (distortion)	$\dot{e}_{vp;c} = \dot{e}_{ref}(OCR_{ref}^{-1})^{\beta_3}$
Viscoplastic creep strain rate due to aging	$\dot{e}_{vp;c} = \dot{e}_{ref}(\sqrt{OCR_{ref}^{-1}}exp(\frac{1-OCR_{ref}^{-\beta_2}}{2\beta_2}))^{\frac{C_c-C_r}{C_\alpha}}$
Viscoplastic swell strain rate due to unloading	$\dot{e}_{vp;s} = \dot{e}_{vp;s} - \frac{\dot{e}_{vp;s}^2}{ln(10)\hat{C}_{\alpha;s}}$
Elastic strain rate due to loading	$\dot{e}_{el} = C_r\frac{\dot{\sigma}_v'}{ln(10)\sigma_v'}$
Total strain rate	$\dot{e} = \dot{e}_{el} + \dot{e}_{vp;c} + \dot{e}_{vp;s}$

3.1.2. Methodology

Linear isotach model (NEN-Bjerrum)

For the verification an incremental loading test is simulated with the soil properties as listed in Table 3.2 and a loading path as presented in Table 3.3. The resulting stress path over time is shown in Figure 3.2 and the calculated strains for both the implementations in a stress strain and a time strain space are shown in Figures 3.3a - 3.4b.

Table 3.2: Soil parameters used in both the excel and python implementation for verification of the model

Input parameter	Value
H_0	0.019 [m]
RR	0.015138 [-]
CR	0.3296 [-]
C_α	0.0227 [-]
c_v	1e-7 [m^2 / s]
$Drainage\ path$	0.5 [-]
σ_p'	75 [kPa]
σ_v'	2 [kPa]
Δt	0.001 [day]
t_{end}	10 [days]
e_0	3

Table 3.3: Soil parameters used in both the excel and python implementation for verification of the model

Time [days]	Load increment [kPa]
0	15
1	15
2	30
3	60
4	-60
5	60
6	120
7	0

Non-linear isotach model (C+S Model)

For the verification of the C+S model the same parameter set as described in Tables 3.2 and 3.3 has been used. The parameters have been converted according to equations 2.41, 2.44, 2.47 and 2.54. This simulation is used to check if the results of the model under linear conditions produce the same results as the implementation of the linear isotach model. To do so, the non-linearity and the viscoplastic swell must be prevented. It can be seen in equation 2.19 that taking β_3 equal to $(Cr - Cc)/C_\alpha$ gives the same relation as in the linear isotach model and by choosing β_2 equal to 0, C_α will not be OCR dependent (see equation 2.20).

$$\dot{e}_{init;c} = \dot{e}_{vp;c;ref} \cdot OCR_{ref}^{-\beta_3} \quad \text{(2.19 revisited)}$$

$$\frac{\hat{C}_\alpha}{C_{\alpha NC}} = \frac{2}{OCR_{ref}^{\beta_2} + 1} \quad \text{(2.20 revisited)}$$

The viscoplastic swell is controlled by 4 parameters, b_1, b_2, m_1, m_2. The most important part is the initial viscoplastic swell strain rate (equation 2.28) by taking b_2 large negative, like -100, this value is already negligible small, m_2 controls the OCR dependency and is therefor set to 0. Equation 2.27 is used for the decaying equation of the viscoplastic swell strain rate and since it is an auto decaying process a small initial strain rate makes that there is not much to decay. However, a large negative value for b_1 and a value of 0 for m_1 will reduce the strain rate almost immediately.

$$\ddot{e}_s = -\frac{\dot{e}_s^2 \cdot ln(10)}{\hat{C}_{\alpha;s}} \quad \text{(2.26 revisited)}$$

$$\frac{\hat{C}_{\alpha;s}}{C_{\alpha;NC}} = 10^{b_1}(OCR - 1)^{m_1} \quad \text{(2.27 revisited)}$$

$$\dot{e}_{s;init} = 10^{b_2}(OCR - 1)^{m_2} \quad \text{(2.28 revisited)}$$

In this way non-linearity and viscoplastic swell can be avoided in the C+S model and the model responses like a linear isotach model.

3.1.3. Results

Verification linear model (NEN-Bjerrum)

Figures 3.2, 3.3, 3.4 show the results of a simulated incremental loading test as described in Section 3.1.2.

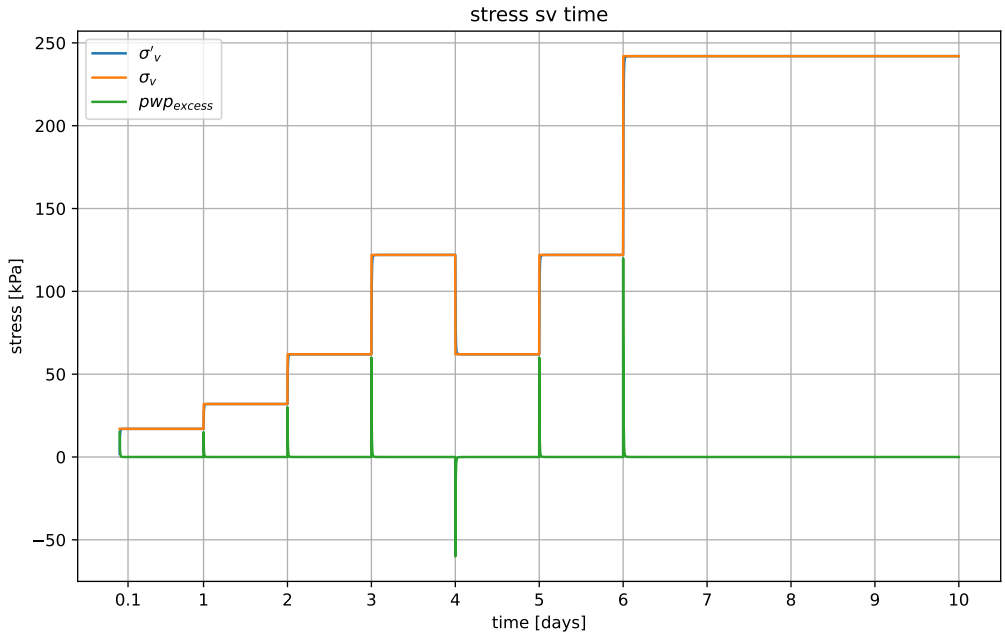

(a) The stress increments against time for python implementation

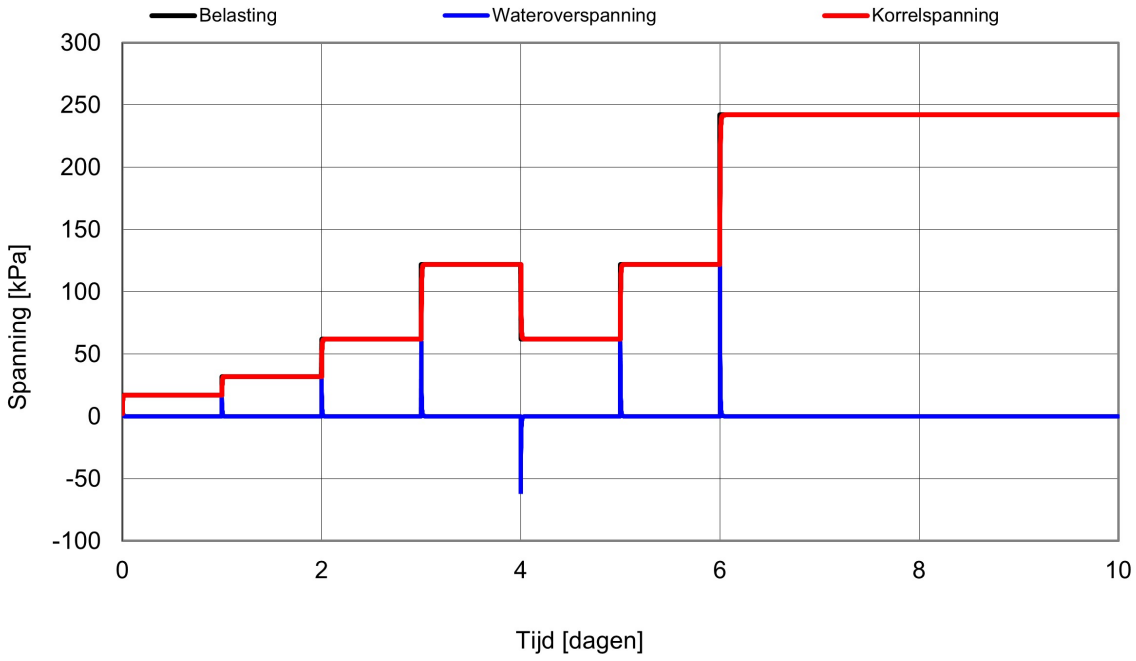

(b) The stress increments against time for excel implementation (Hoefsloot, 2022)

Figure 3.2: Stress against time for both implementations

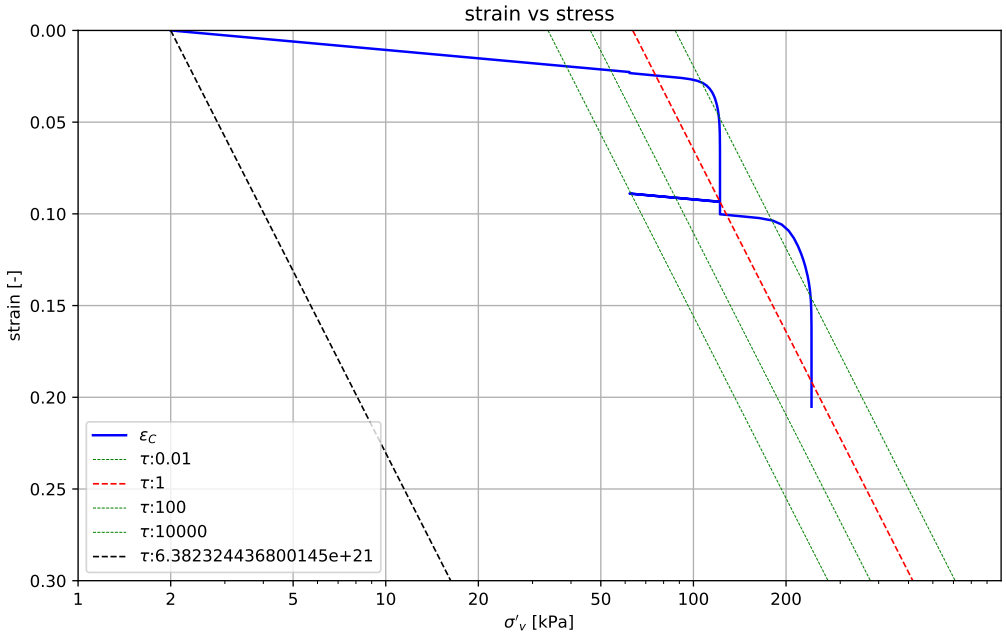

(a) The strain increments against stress for python implementation

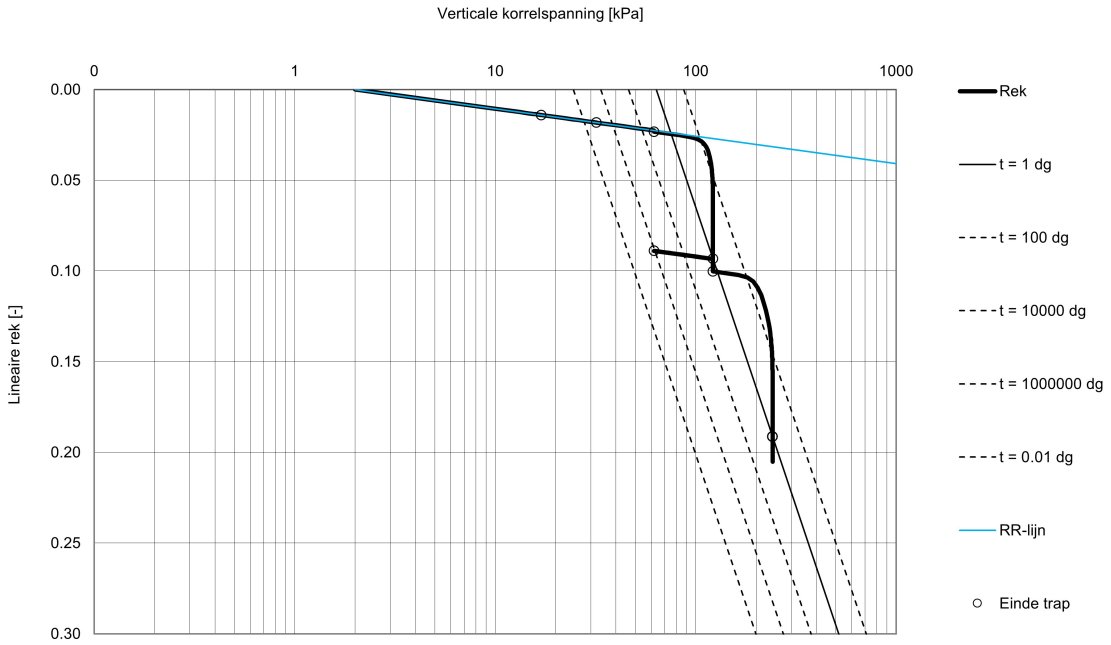

(b) The strain increments against stress for excel implementation (Hoefsloot, 2022)

Figure 3.3: Strain against stress for both implementations

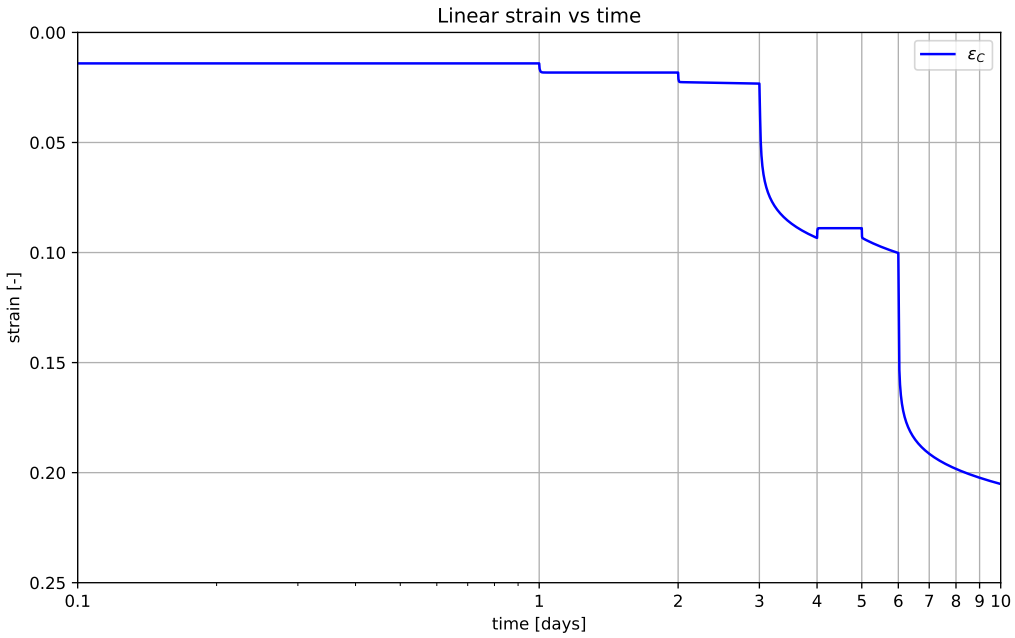

(a) Strain against time for python implementation

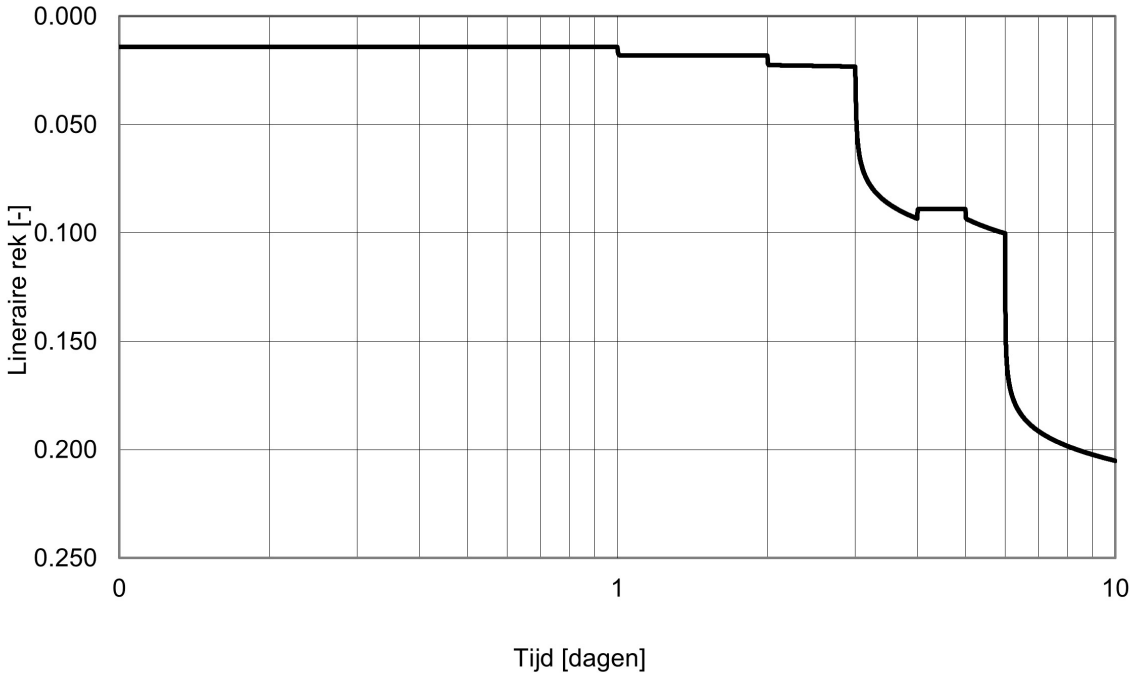

(b) The stress increments against time for excel implementation (Hoefsloot, 2022)

Figure 3.4: Strain against time for both implementations

Verification non-linear model (C+S Model)

Figures 3.5 and 3.6 show the differences in stress and strain over time for the stress calculations of the C+S model compared with the linear isotach model due to the normalisation of the degree of consolidation. Figure 3.7 and 3.8 show the results of the adjusted implementation without the normalisation of the degree of consolidation.

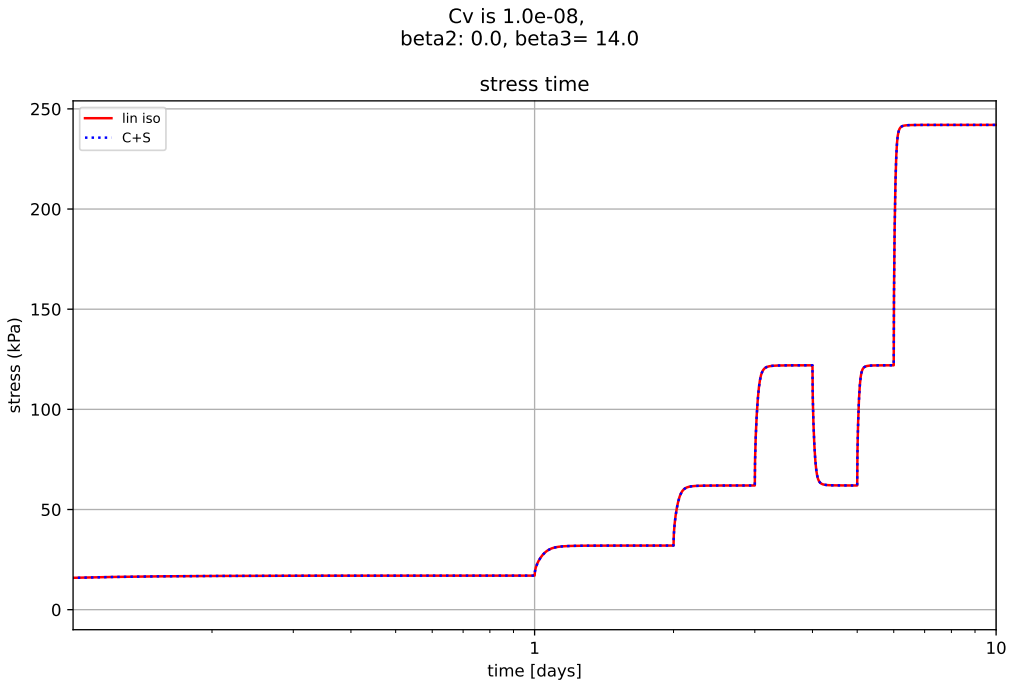

(a) Stress over time for a cv of 1e-08

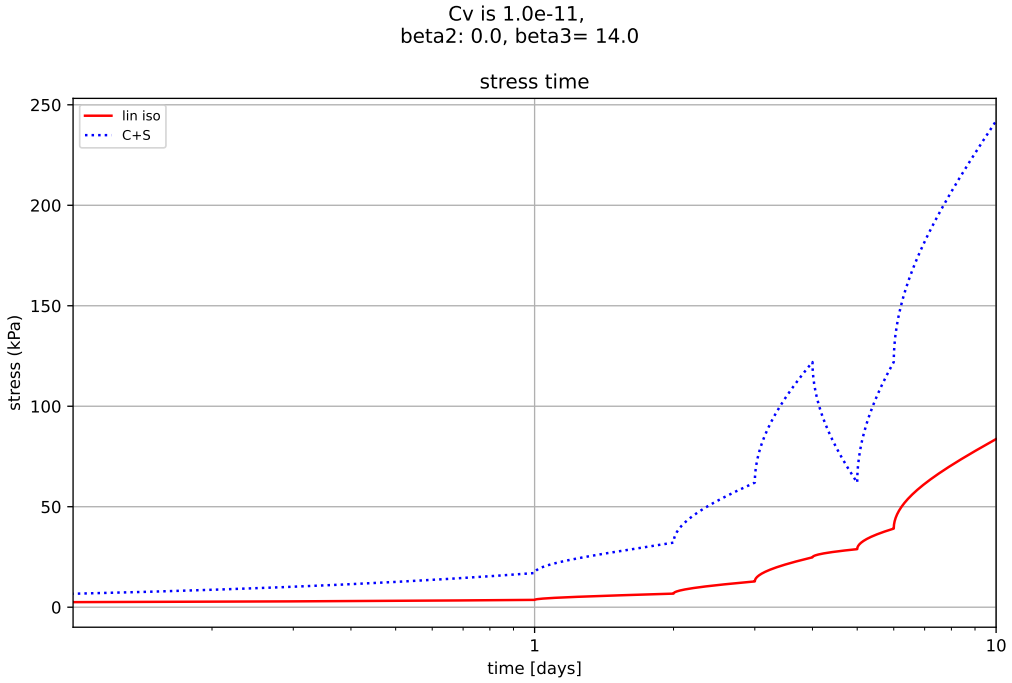

(b) Stress over time for a cv of 1e-11

Figure 3.5: Stress over time for two different values of the consolidation coefficient

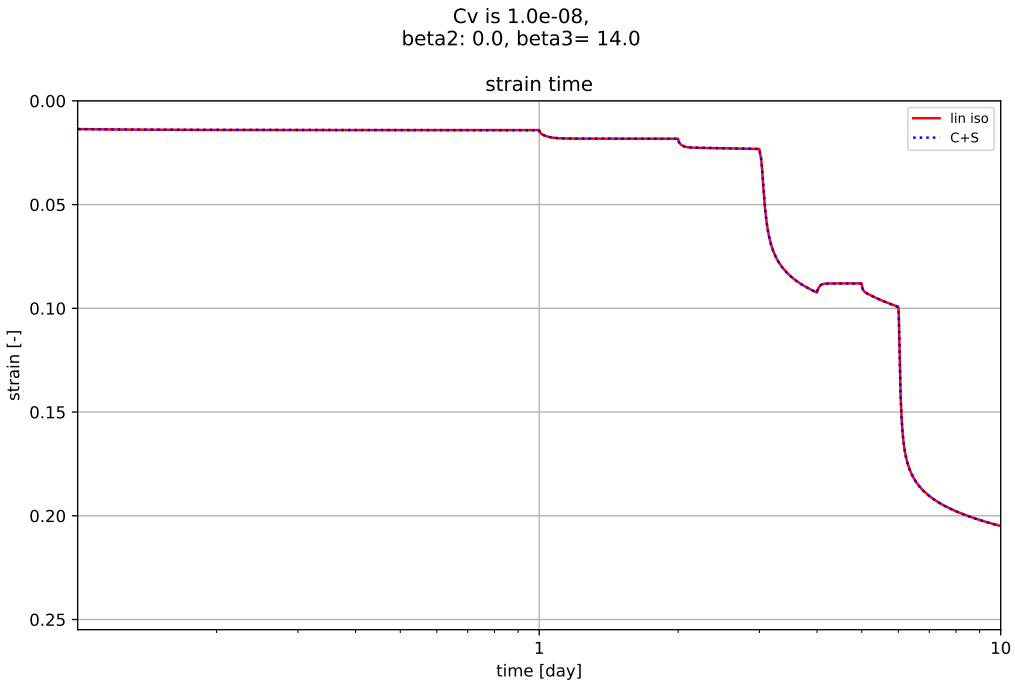

(a) Strain over time for a cv of 1e-08

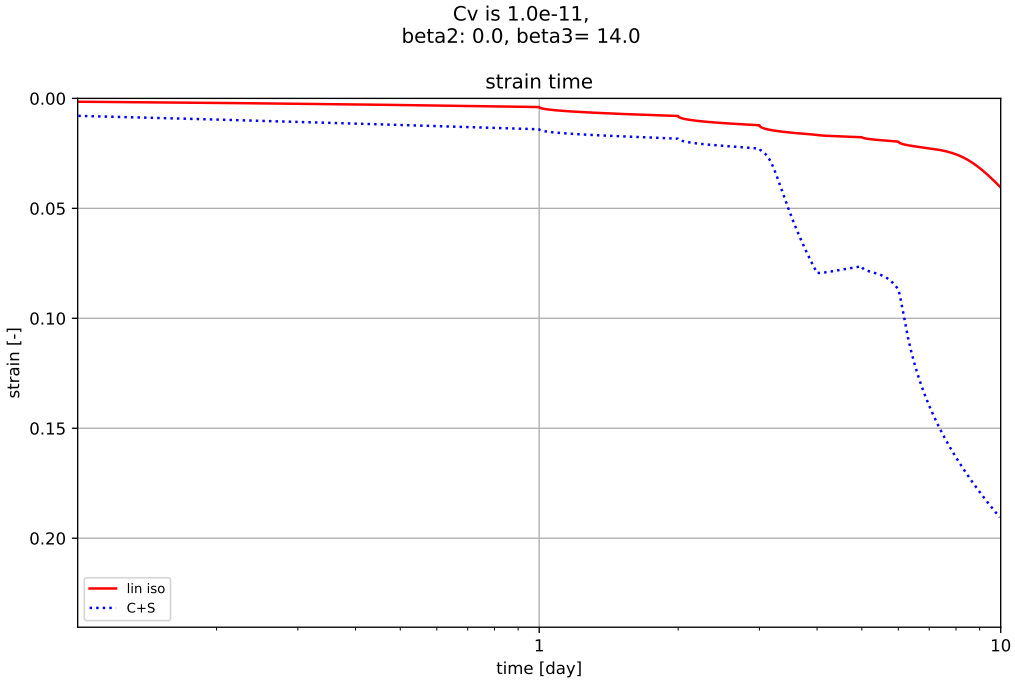

(b) Strain over time for a cv of 1e-11

Figure 3.6: Strain over time for two different values of the consolidation coefficient

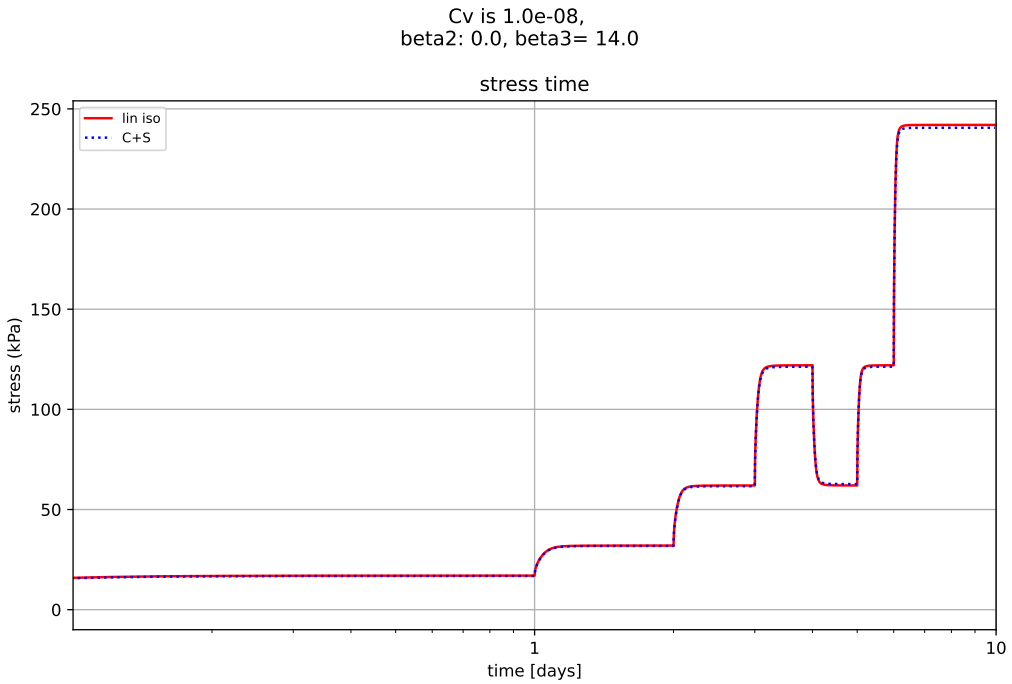

(a) Stress over time for a cv of 1e-08

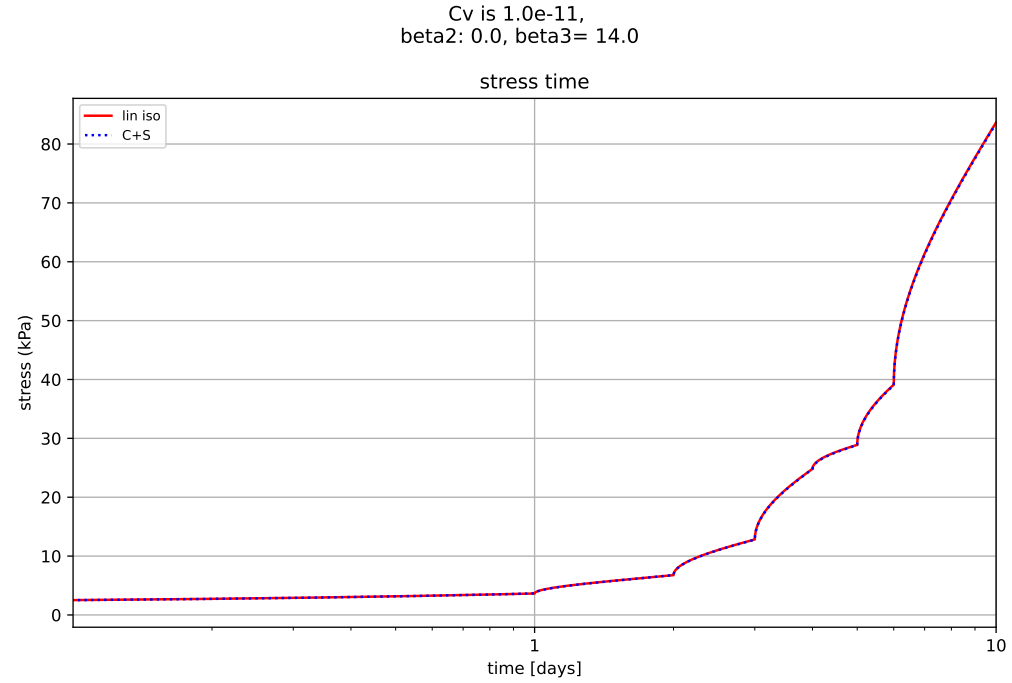

(b) Stress over time for a cv of 1e-11

Figure 3.7: Stress over time for two different values of the consolidation coefficient

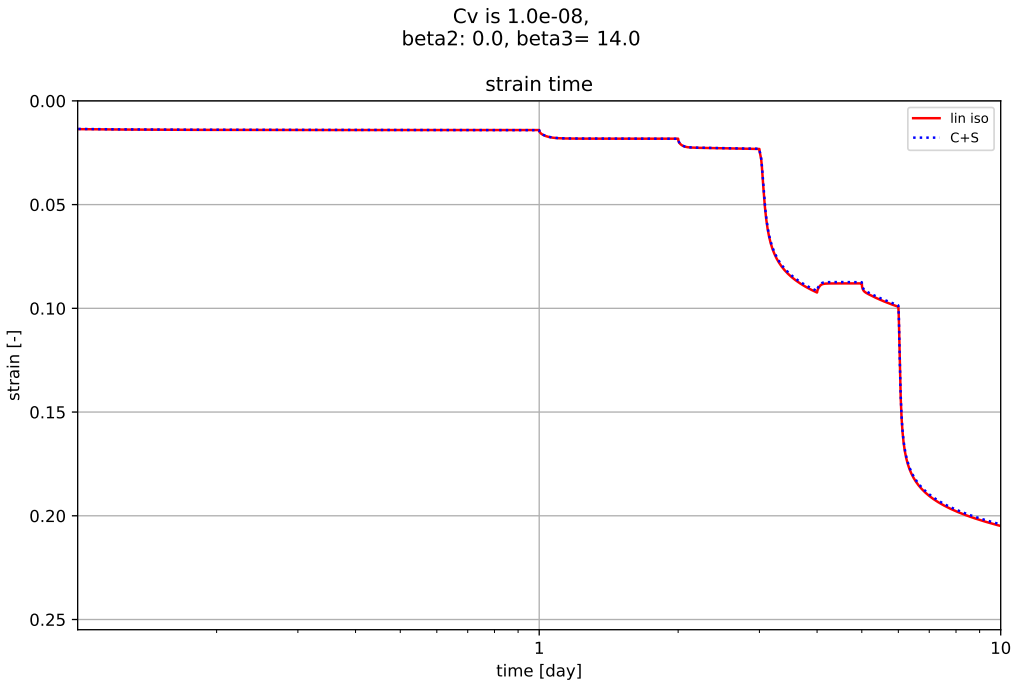

(a) Strain over time for a cv of 1e-08

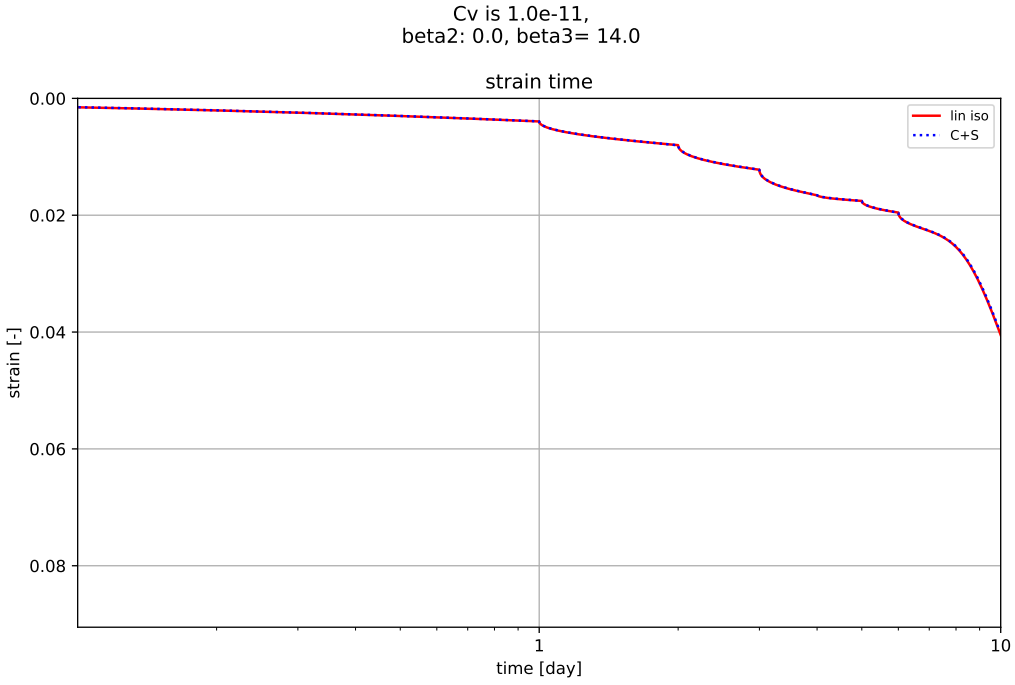

(b) Strain over time for a cv of 1e-11

Figure 3.8: Strain over time for two different values of the consolidation coefficient

3.1.4. Discussion

For the verification of the implementation the incremental loading tests have been simulated for the linear elastic model and the C+S model. With on the chosen parameter sets for the C+S model it has been shown that this model is identical to the linear isotach model behaviour after the adjustment of the consolidation as was shown in Figures 3.7-3.8. The results in figures 3.5 and 3.6 show that the outcome is the same for higher values of the consolidation coefficient. However with a smaller

coefficient of consolidation a bias occurs in the calculation of the effective stress for the C+S model. This problem is exacerbated when consolidation plays a more important role, e.g. when not all the excess pore water pressure dissipates during a loading step and the degree of consolidation will be less than 99%. According to equations 2.37 and 2.38 this is the case when the drainage path (layer thickness) increases, the duration of a loading step decreases or when the consolidation coefficient decreases. This error occurs due to a normalisation factor of the degree of consolidation, resulting in a degree of consolidation which always goes up to a 100%. In consultation with Vergote a change in the code is made and this normalisation factor has been removed. Since Vergote did not test his decoupled code for other applications than laboratory scale tests this error did not occur in his calibrations. After this modification the model output shows comparable results for the C+S model and the linear isotach model when a high and low coefficient of consolidation is used. This can be seen in figures 3.7 and 3.8.

3.2. Mexico Clay analysis

For comparison the C+S model will be used twice, one time with both distortion and swell and secondly with linear isotachs but also swell included. In this way both the influence of swell and distortion on settlement predictions can be analysed. An analysis on distortion without swell is not done, this would be comparable to the work of Yuan and Whittle (2018). But first a comparison will be made between the two models and an incremental loading test with several unloading steps performed on a clay from Mexico. In this section the term linear isotach model refers to the NEN-Bjerrum model and non-linear isotach model to the C+S Model.

3.2.1. Methodology

The sample used for this incremental loading test is conducted for Royal Haskoning DHV during ground investigation for the New International Airport of Mexico. Although the project was cancelled the very compressible clay can still be used for research purposes as the TKI project: Improvement of settlement predictions. In the test 5 loading steps are followed by 3 unloading steps. The loading and soil parameters can be found in Tables 3.4 and 3.5 (van der Linden, 2021).

Table 3.4: Parameters of Mexico clay (van der Linden, 2021).

Input parameter	Value
RR	0.0277 [-]
CR	0.718 [-]
$C_{\alpha;\varepsilon}$	0.0272 [-]
e_0	7.04
σ'_p	30.34

Table 3.5: Loading stages of Mexico clay (van der Linden, 2021).

End time of load step [days]	Load [kPa]
3.69	2.45
5.51	4.94
7.55	9.66
9.02	19.1
11.52	37.97
14.80	75.72
17.60	37.97
20.62	19.1
25.58	2.45

For these soil parameters, the C+S model will be fitted in a way that the unloading behaviour of the soil will be captured. To do so, a smaller value for C_r will be chosen, in that way the unloading and reloading line will be flatter but with swell included the unloading line will be steeper than the reloading line. The results are presented in section 3.2.2 for the measured data, simulation by the linear isotach model and the simulation of the C+S model with swell but linear isotachs. The choice to not include non-linearity is because this test has three unloading steps in which creep will not be present and only one loading step clearly exceed the yield stress and therefore deriving β_2 and β_3 is not possible. For the unloading parameters a first estimation for b_1 and b_2 is done by taking the slope of the change in void ratio over the strain rate ($\hat{C}_{\alpha;s}(OCR = 2)$) in that way b_1 can be estimated, the same is done with the initial viscoplastic swell strain rate ($\dot{e}_{s;init}(OCR = 2)$. From this starting point all 4 viscoplastic swell parameters, b_1, m_1, b_2, m_2, will be changed until the measurements and simulation curves are fit.

3.2.2. Results

In Figure 3.9 the measured change in void ratio against the strain rate is shown for the 3 unloading steps with OCR's of 2, 4 and 30. These are used for a first estimation of the viscoplastic swell parameters. It can be seen that the blue line in intersects with $\Delta e = 0$ close to $2.5 \cdot 10^{-4}$. For that reason b_2 is chosen as -4. The slope of this line $\hat{C}_{\alpha;s}$ divided by $C_{\alpha;NC}$ gives a first assumption for b_1 and is chosen as -0.9. In the same Figure, the strain rates against change in void ratio for the linear isotach model is also shown. It can be seen here that for the strain rate of a linear isotach model without viscoplastic swell included the strain rate decreases faster and less change in void ratio, so less strain is predicted.

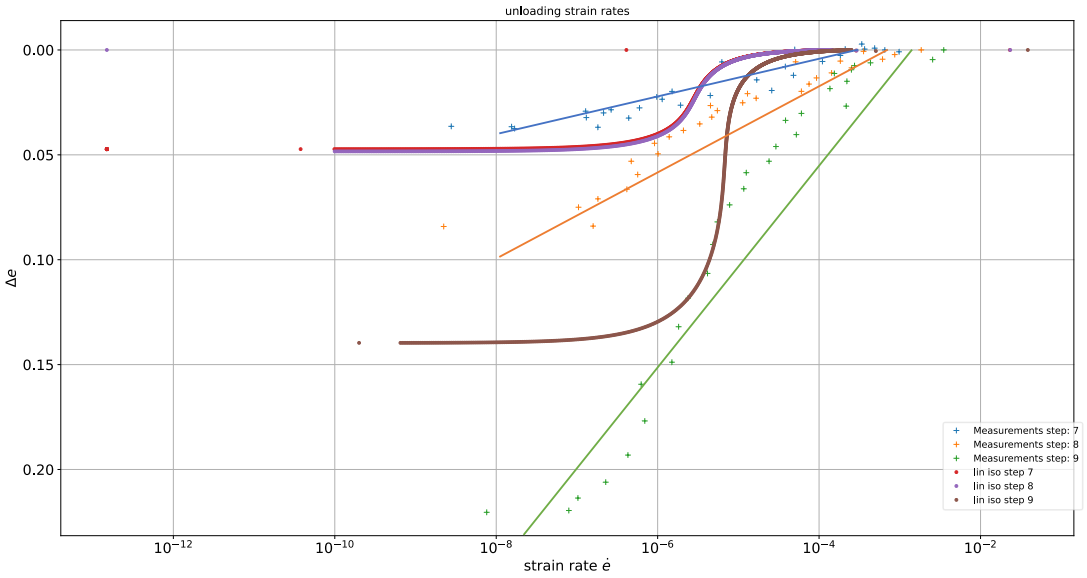

Figure 3.9: Change in void ratio of a unloading step versus the strain rate

In Figure 3.10 the resulting strain over time is presented. In Figure 3.11 the strain over stress is presented with the isotachs from the C+S model, which are slightly different than the isotachs from the linear isotach model since the value of C_α is different.

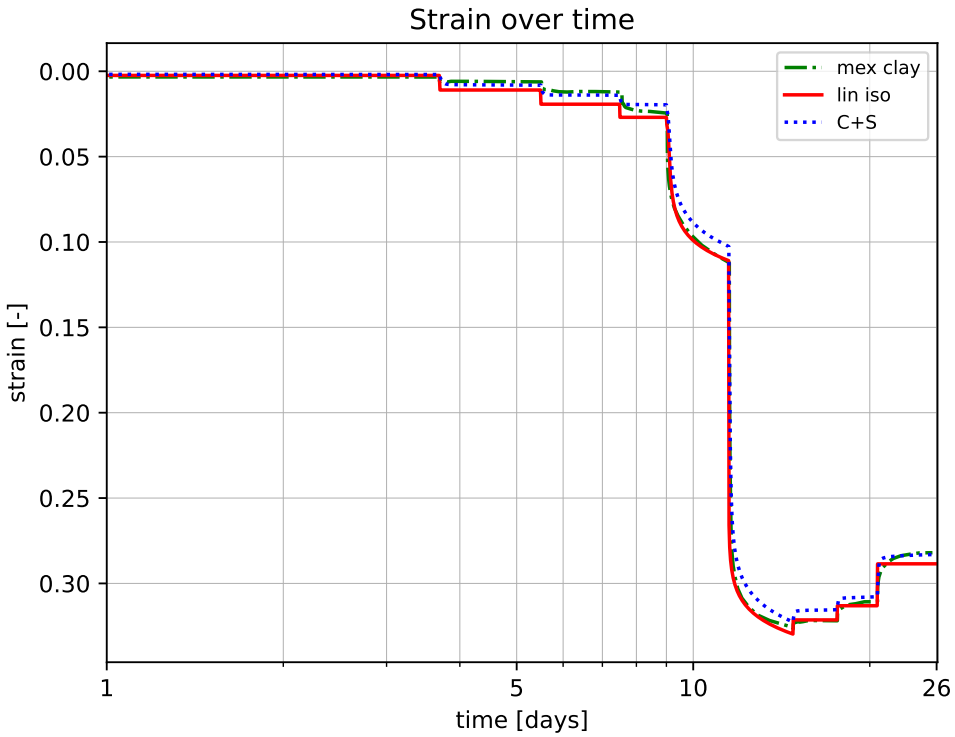

Figure 3.10: Strain over time for Mexico clay

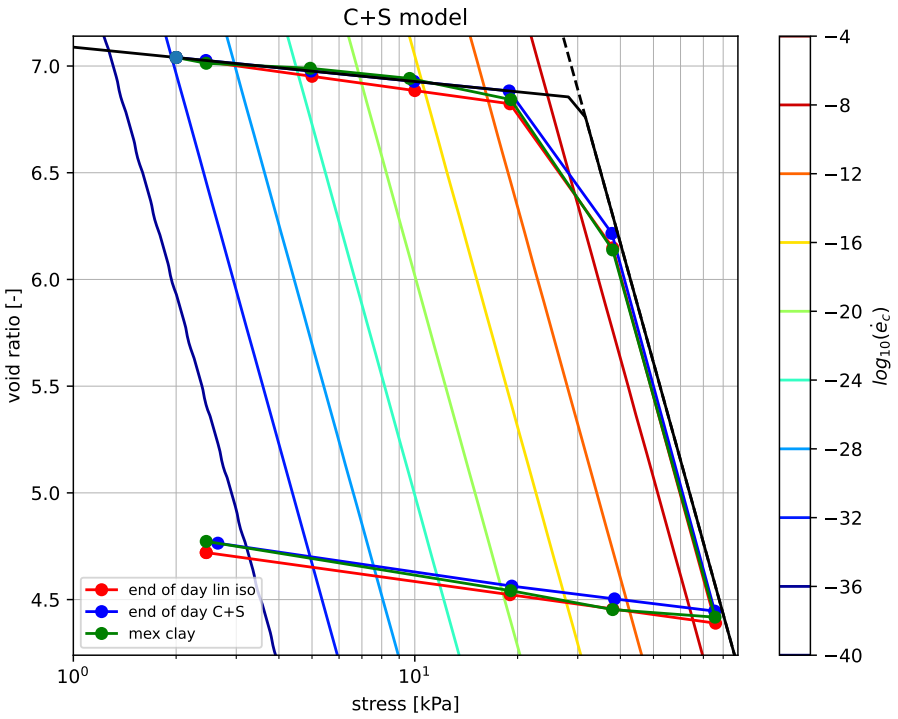

Figure 3.11: Strain over stress for Mexico clay

In Figure 3.12 the development of the stresses and strains are shown for the C+S model during unloading and in Figure 3.13 the strain development per loading step both for loading and unloading are presented for the measured data and the simulated test with the C+S model.

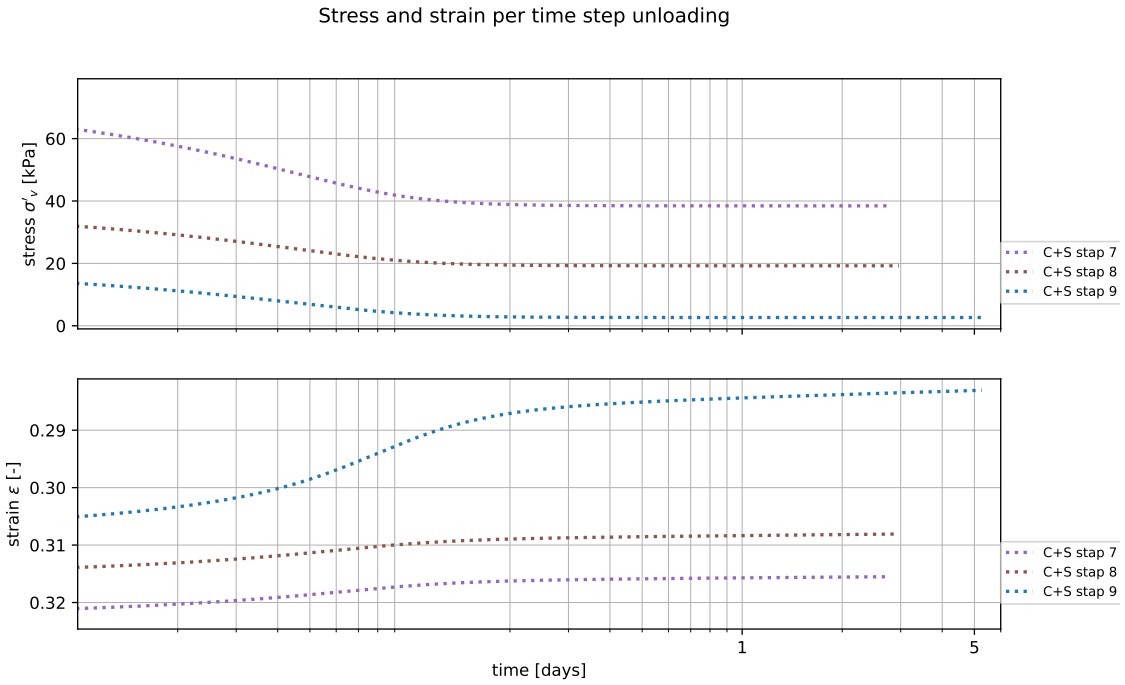

Figure 3.12: Strain development per loading step for the C+S model for both loading and unloading

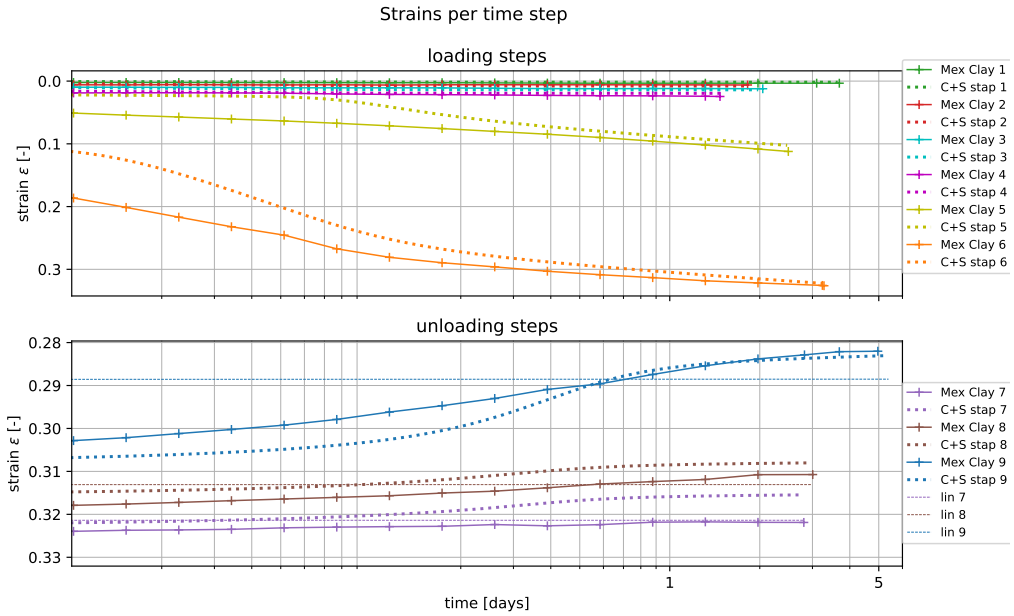

Figure 3.13: Strain development per loading step for the C+S model and Mexico clay data with a changed value of c_v upon unloading

Finally in Figure 3.14 the change in void ratio over time is shown for the unloading steps, to purely see the influence of the unloading behaviour the void ratio before unloading is taken as reference.

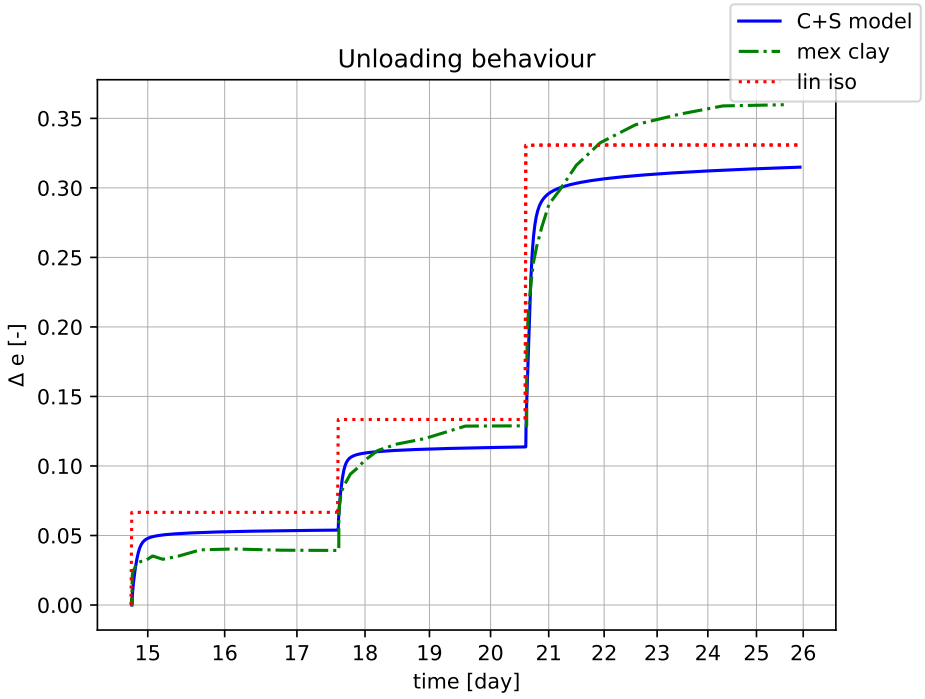

Figure 3.14: Void ratio over time only for the unloading stages on Mexico clay

To follow the unloading curve better, a smaller coefficient of consolidation is selected for the unloading steps. The coefficient of consolidation during unloading is 5 times smaller than during loading in Figure 3.15. A similar figure as Figure 3.13 but for a c_v value which is the same for loading and unloading can be found in Appendix A.2.1.

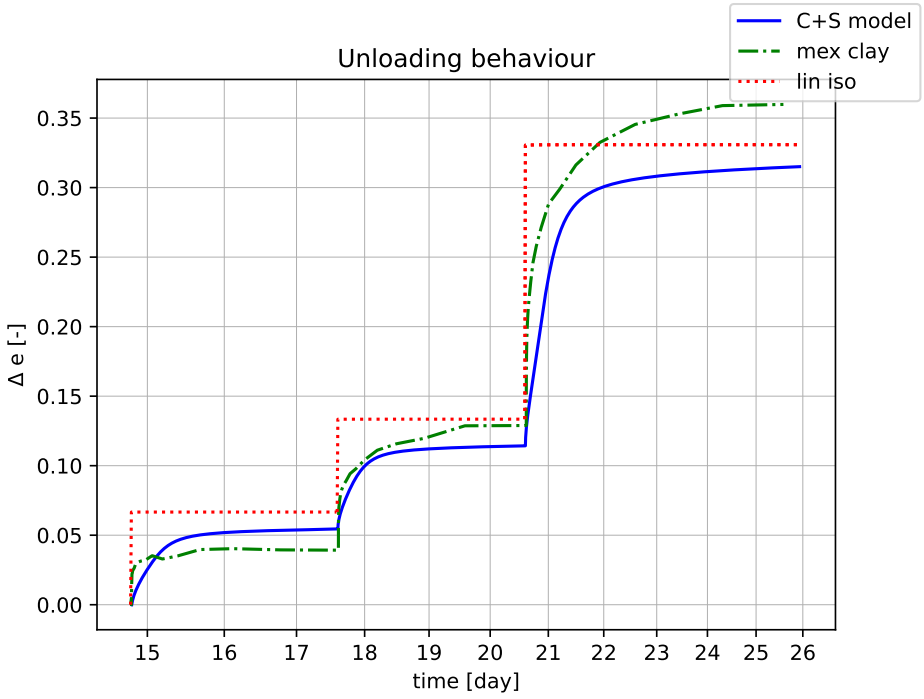

Figure 3.15: Void ratio over time only for the unloading stages on Mexico clay

3.2.3. Discussion

For the analysis of the Mexico clay, a simulation has run with the derived parameters and used as starting point to manually fit parameters for the C+S model, which are used to check if the unloading stages could be better described by the C+S model compared to linear isotachs. The RR value was derived from the unloading steps which are on average steeper than the first two reloading steps this results in a overestimation of the strain for small load increments. Furthermore, in Figures 3.10 and 3.11 it can be seen that the unloading behaviour is not linear but shows a more curved graph. As a solution for this, in the C+S model a smaller reloading parameter (C_r) is selected and viscoplastic swell is included. In this way the simulation is closer to the measurements for small load increment and it follows a more non-linear swell path which is also in accordance with the measurement data. However it must be noted that this smaller RR also ensures that the simulation of the C+S model underestimate the strain close to the yield stress.

Regarding the choice of the viscoplastic swell parameters, b_1, m_1, b_2, m_2, it can be seen in Figure 3.14 that the first two steps are close to the measurements but for a higher OCR the model underestimates the change in void ratio. What can also be seen in this figure is that the curve of the simulation is steeper than the measurements, Figure 3.15 shows that this is due to the fact a constant coefficient of consolidation is used throughout the whole first simulation and that a more curved envelope of the graph is obtained with a smaller coefficient of consolidation. Next to that it must be noted by looking at the viscoplastic swell equations 2.27 and 2.28 that the b_1 & b_2 determine the magnitudes of the initial strain rate and the swell parameter $\hat{C}_{\alpha;s}$ when the OCR is equal to 2 and the parameters m_1 & m_2 are used to regulate the influence of the OCR on the magnitude. The swell parameter set that has been used is given in Table 3.6.

Table 3.6: Viscoplastic swell parameters for Mexico clay.

Parameter	Value fit [-]	Initial assumption [-]
b_1	-2	-0.85
b_2	-5	-4
m_1	0.5	-
m_2	6	-

What can be seen from Table 3.6 is that the initial strain rate is smaller than first determined. A reason for this is that in Figure 3.9 consolidation can not be excluded and that a part of the strain rate present is due to elastic strain and should not be accounted for in the viscoplastic swell strain rate. Next to that it can be seen that the initial strain rate is strongly affected by the OCR since m_2 is 6. Regarding b_1 and m_1 it can be seen that the initial value is smaller than assumed and that in contrast to the initial viscoplastic swell strain rate the dependency on OCR is smaller but still present with a value of 0.5. It should be noted that the assumptions can be used as a starting point but due to the few data points and the influence of consolidation, it is not possible to determine the parameters from only these 3 unloading steps but it gives a starting point for fitting them.

3.3. Model comparison: Incremental Loading tests simulations

For the comparison of the models it is necessary that the input parameters which will be used in both models are the same and that the additional model parameters for the C+S model are also in accordance to the data from which the parameters are derived. Since this is not possible for conventional incremental loading test data with only one or two unloading steps, data published in Vergote, 2020, Vergote et al., 2021 and Vergote, 2021 is used as starting point. In Tables 3.7 and 3.8 the two sets of parameters are given. In the last column is indicated whether the parameter is given or assumed for the simulation. To the set in Table 3.7 will be referred to as set GitHub and the parameter set in 3.8 as set Paper. These parameter sets will both be used for IL simulations and embankment simulations.

Parameter set

Table 3.7: Model parameters as given in the GitHub example of Vergote (Vergote, 2021).

Input parameter	Value	Given or assumed
C_c	0.3 [-]	G
C_r	0.06 [-]	G
C_α	0.018 [-]	G
β_2	3	G
β_3	23	G
b_1	-0.8 [-]	G
b_2	-5 [-]	G
m_1	0.7 [-]	G
m_2	2.5 [-]	G
c_v	2.2e-7 [m^2 / s]	G
$Drainage\ path$	0.5 [-]	G
e_0	1.9	G

Table 3.8: Model parameters as given in (Vergote, 2021).

Input parameter	Value	Given or assumed
C_c	1.07 [-]	G
C_r	0.25 [-]	G
C_α	0.043 [-]	G
β_2	4	G
β_3	21.5	G
b_1	-0.84 [-]	G
b_2	-3.3 [-]	G
m_1	0.95 [-]	G
m_2	2.5 [-]	G
c_v	1e-08 [m^2 / s]	A
$Drainage\ path$	0.5 [-]	A
e_0	3.68	G

For the analysis of the C+S model with linear isotachs and swell includes the above parameters are used only the $\beta_2 = 0$ and the $\beta_3 = \frac{C_c - C_r}{C_\alpha}$.

3.3.1. Methodology

Below the model input parameters for the incremental loading tests are given. Instead of a POP a yield stress is used. All other soil parameters are equal to the sets given in Tables 3.7 and 3.8. There are two different load increment tests simulated, the first one is a more standard test in which load will exceed the yield stress followed by one unloading and reloading step and one more load step to exceed the yield stress again. All steps take one day and the last step will last for 3 days. The load increments are presented in Table 3.10. The second incremental loading test that will be simulated pays more attention to swell and creep. That is why multiple unloading steps are added which also differ in OCR. The test finishes with a small unloading step which also has a duration of multiple days so creep strain rate can become dominant over viscoplastic swell strain rate. The load steps of this test are presented in Table 3.11.

Table 3.9: Incremental loading test properties

Input parameter	Value
σ'_{v0}	1 [kPa]
$\sigma'_{p,ref}$	40
H_0	0.02 [m]

Table 3.10: The load path for the Incremental loading test simulation.

Time [days]	Total load [kPa]
0	σ'_{v0}
1	20
2	40
3	80
4	40
5	80
6	160

Table 3.11: The load path for the Incremental loading test simulation.

Time [days]	Total load [kPa]
0	σ'_{v0}
1	20
3	40
6	80
9	60
12	40
15	15
18	80
21	100
24	95

3.3.2. Results

Incremental loading test simulations for C+S model with swell and non-linear isotachs

IL GitHub parameters
In Figures 3.16 and 3.17 the results are shown for the standard incremental loading test simulation on the parameter set GitHub. In Figures 3.18 and 3.19 the results are shown for the simulated incremental loading test with multiple unloading steps on the parameter set GitHub. In this section only the strain and stress against time and the strain against stress plots are shown. Plots of the strain rate against time, stress and strain development over time per load increment can be found in Appendix A.3.1.

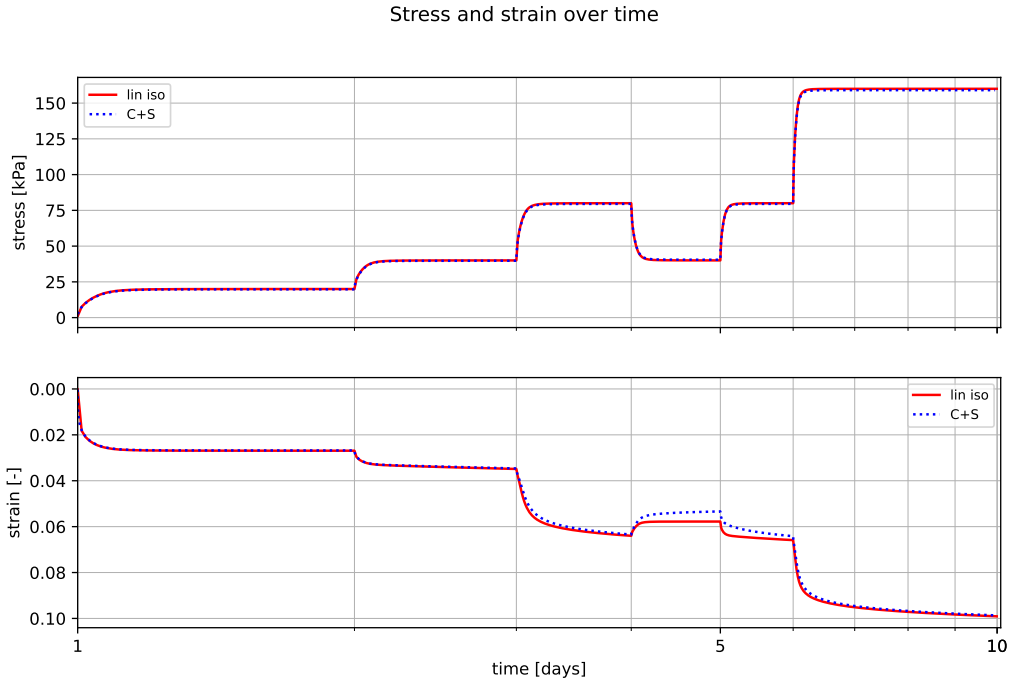

Figure 3.16: Stress and strain over time for parameter set GH in standard IL test

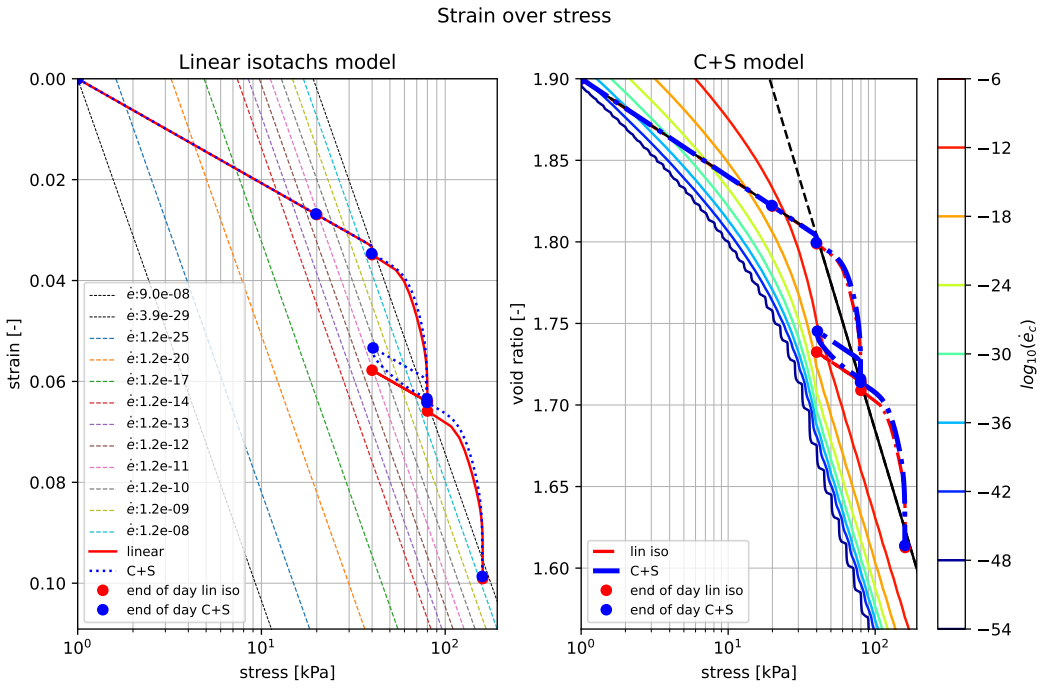

Figure 3.17: Isotachs for parameter set GH in standard IL test

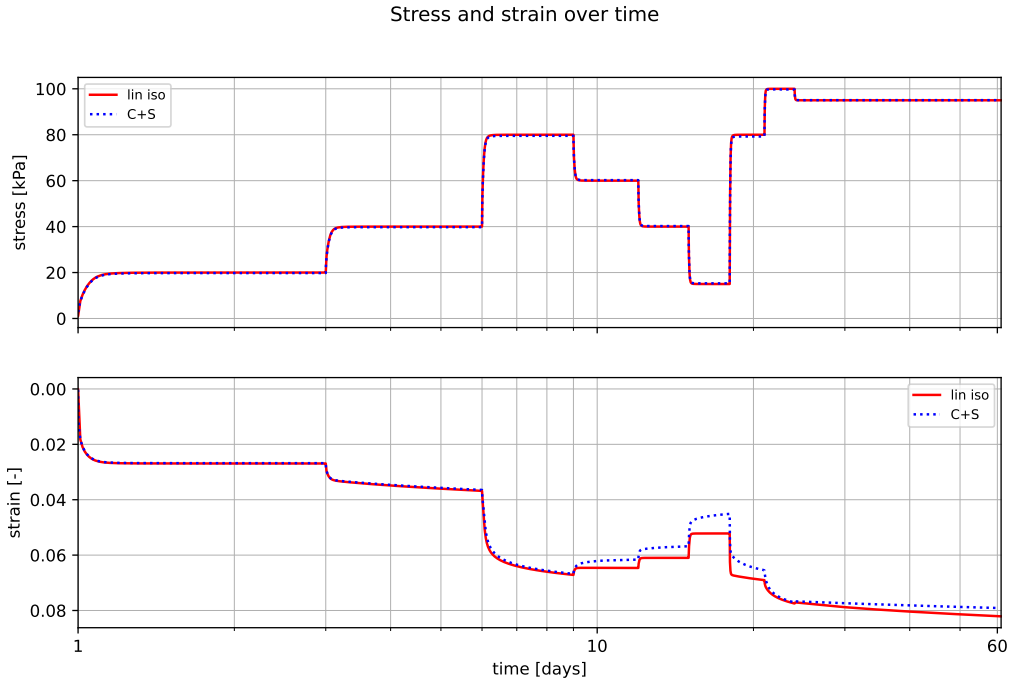

Figure 3.18: Stress and strain over time for parameter set GH in IL test with multiple unloading steps

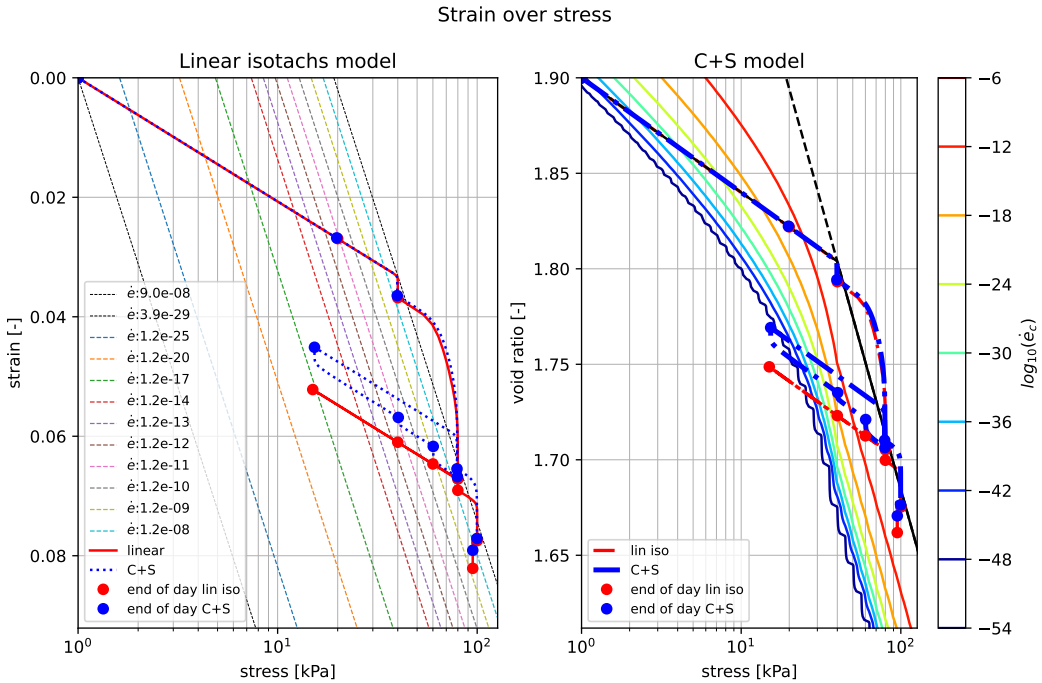

Figure 3.19: Isotachs for parameter set GH in IL test with multiple unloading steps

IL Paper parameters

In Figures 3.20 and 3.21 the results are shown for the standard incremental loading test simulation on the parameter set GitHub. In Figures 3.22 and 3.23 the results are shown for the simulated incremental loading test with multiple unloading steps on the parameter set GitHub. In this section only the strain and stress against time and the strain against stress plots are shown. Plots of the strain rate against

time, stress and strain development over time per load increment can be found in Appendix A.3.1.

Figure 3.20: Stress and strain over time for parameter set Paper in standard IL test

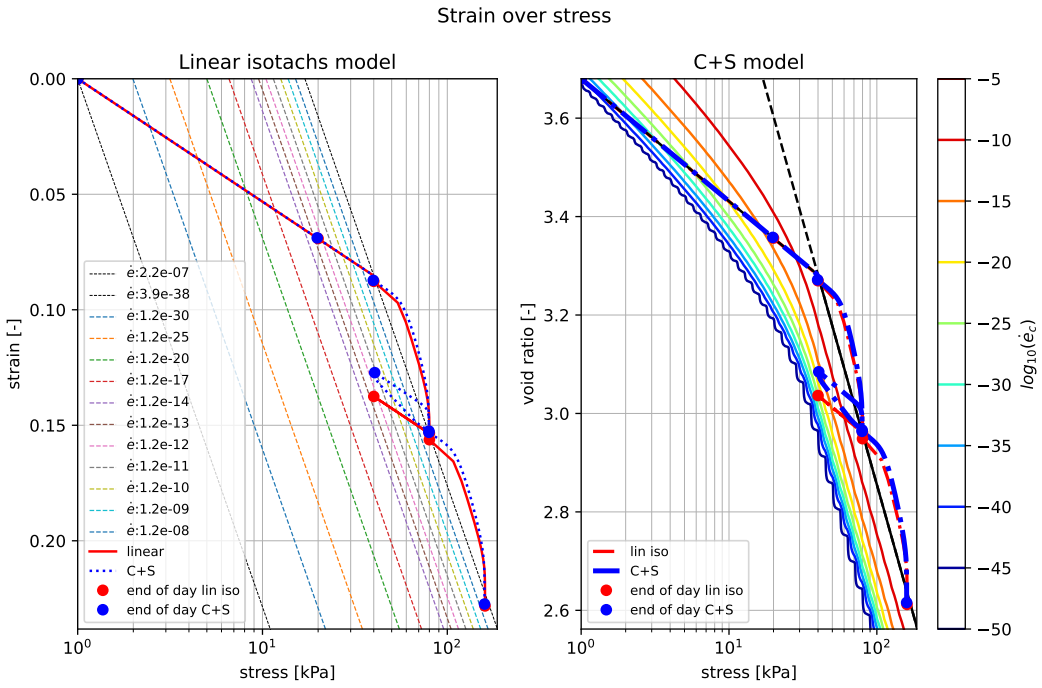

Figure 3.21: Isotachs for parameter set Paper in standard IL test

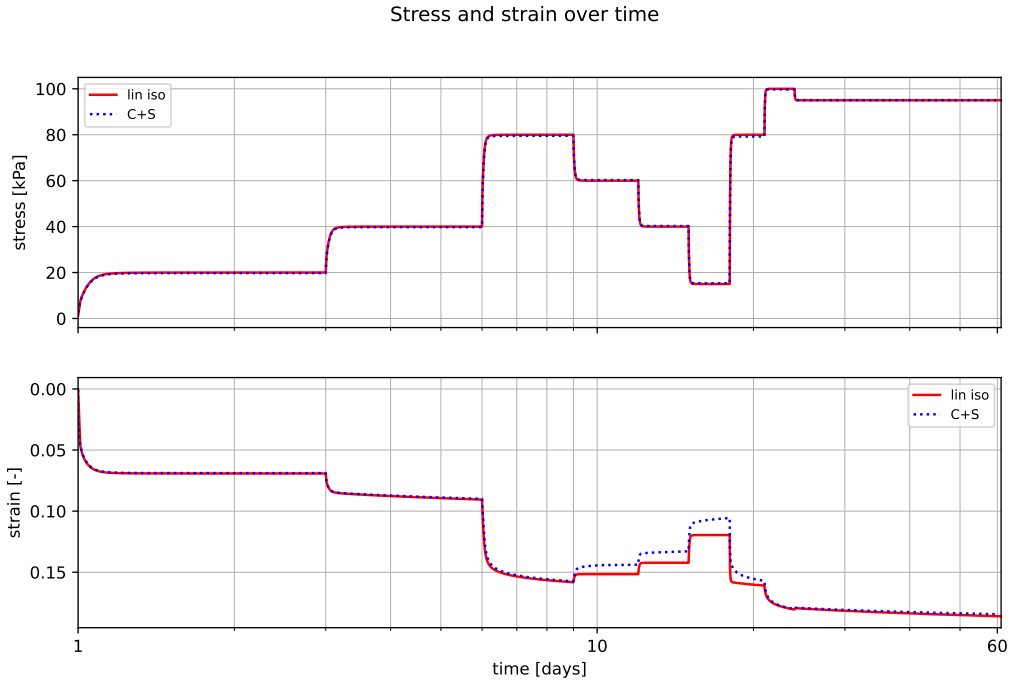

Figure 3.22: Stress and strain over time for parameter set Paper in IL test with multiple unloading steps

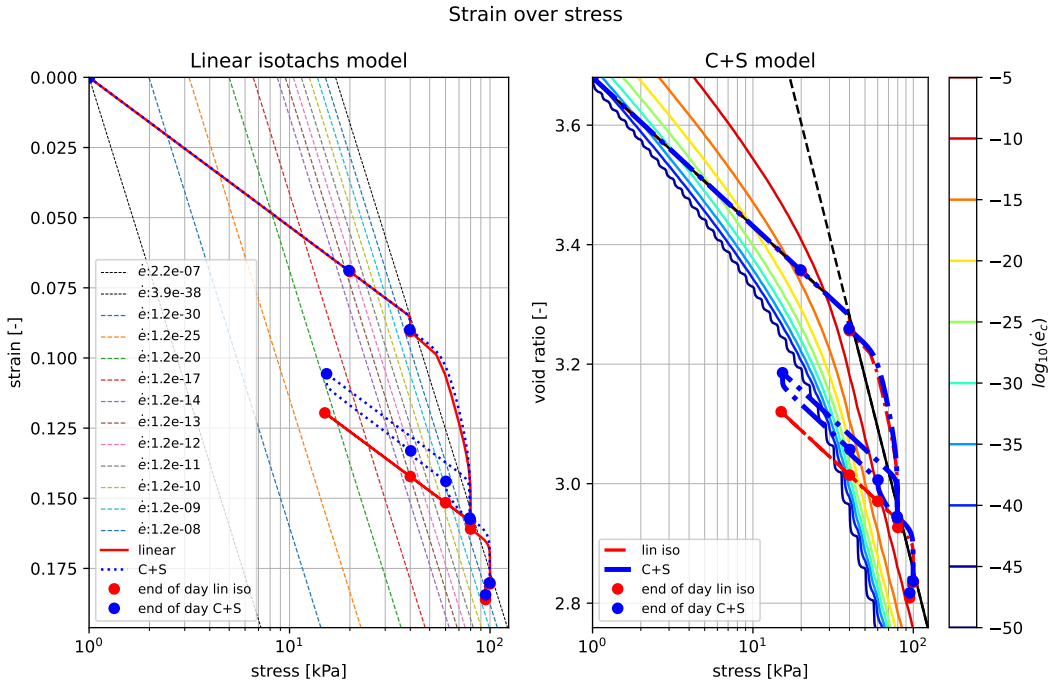

Figure 3.23: Isotachs for parameter set Paper in IL test with multiple unloading steps

Incremental loading test simulations for C+S model with swell and linear isotachs

In this section the same graphs as presented as in section 3.3.2 only here the C+S model uses linear isotachs instead. Additional graphs of strain rate against time and strain and stress development per load increment can be found in Appendix A.3.2.

IL GitHub parameters

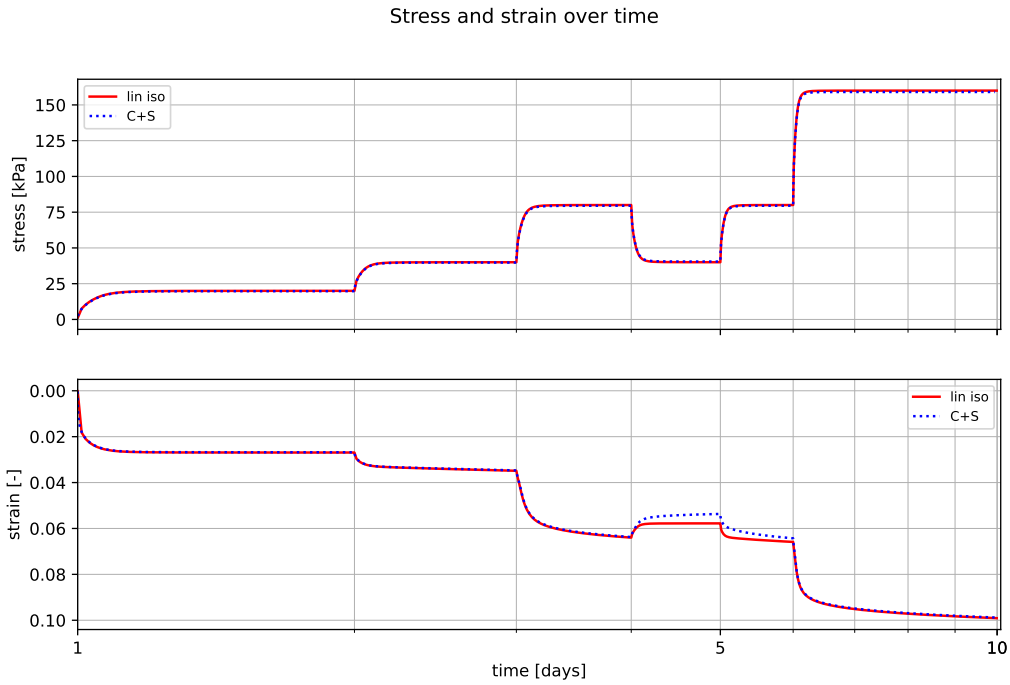

Figure 3.24: Stress and strain over time for parameter set GH in standard IL test

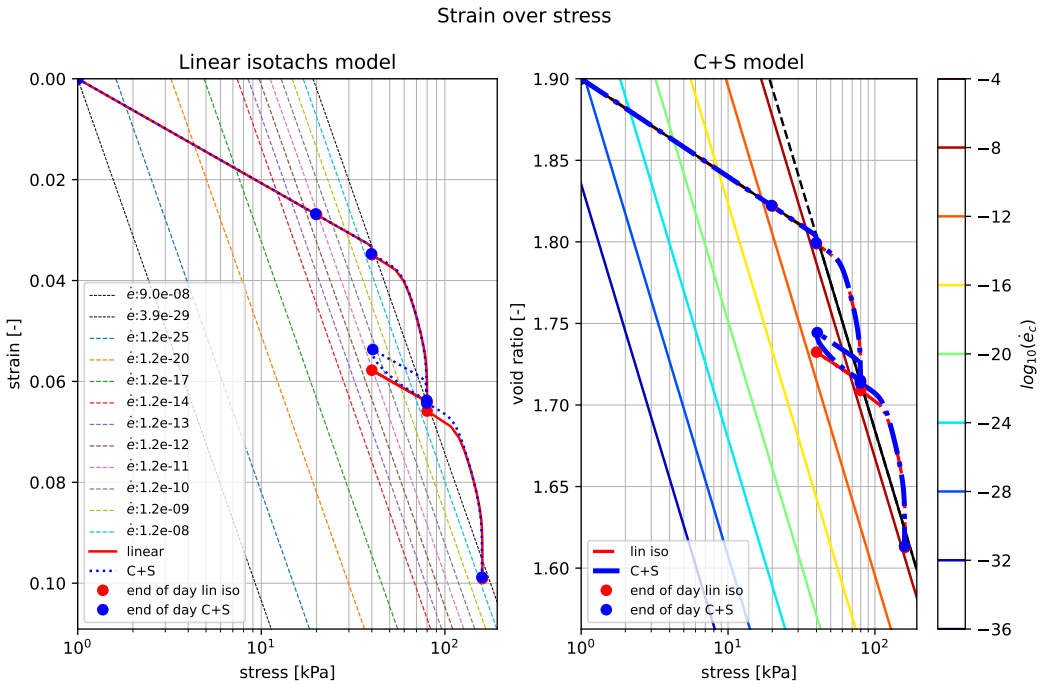

Figure 3.25: Isotachs for parameter set GH in standard IL test

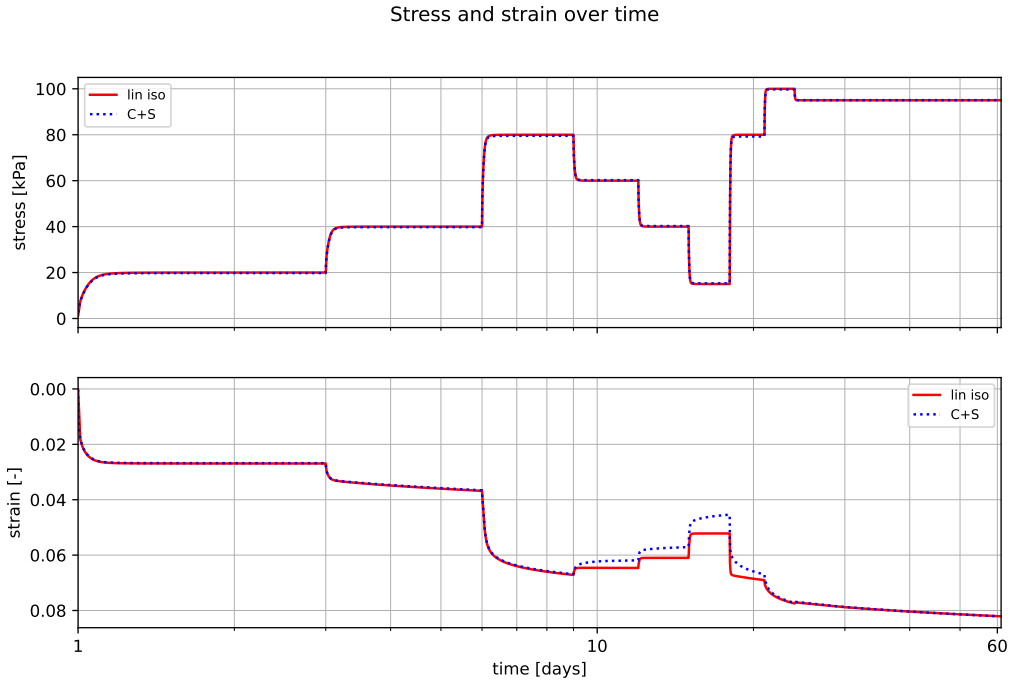

Figure 3.26: Stress and strain over time for parameter set GH in IL test with multiple unloading steps

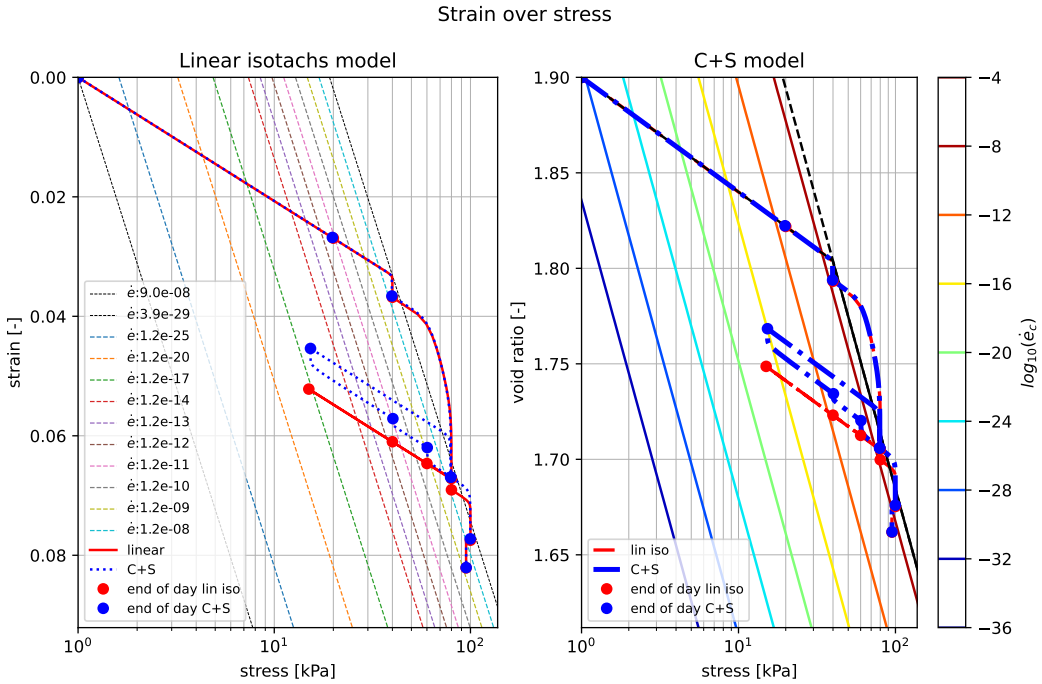

Figure 3.27: Isotachs for parameter set GH in IL test with multiple unloading steps

IL Paper parameters

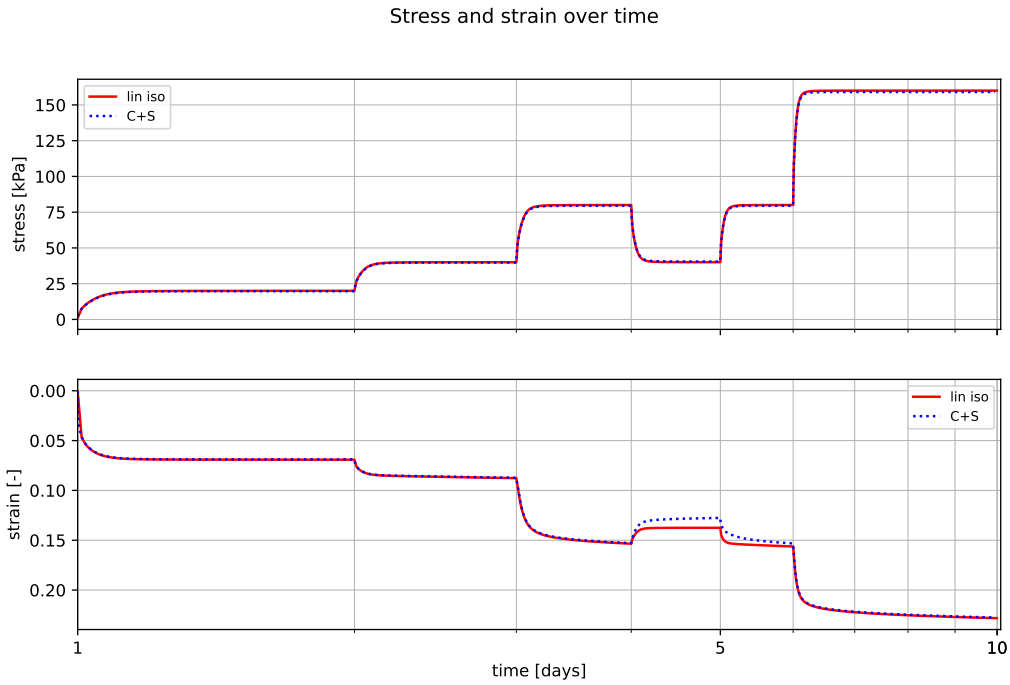

Figure 3.28: Stress and strain over time for parameter set Paper in standard IL test

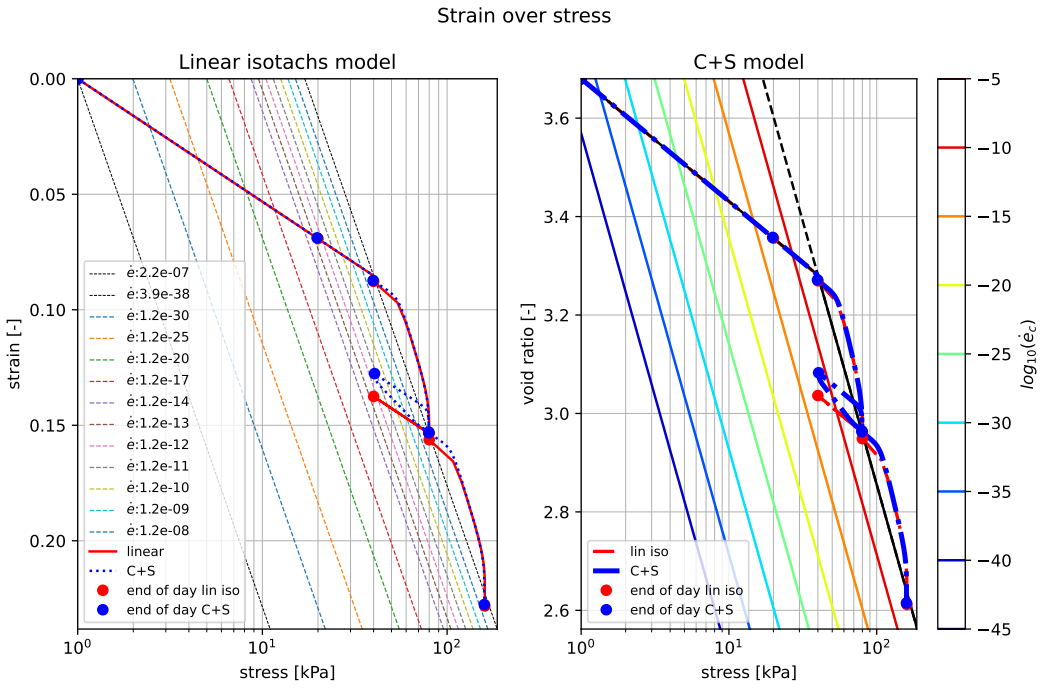

Figure 3.29: Isotachs for parameter set Paper in standard IL test

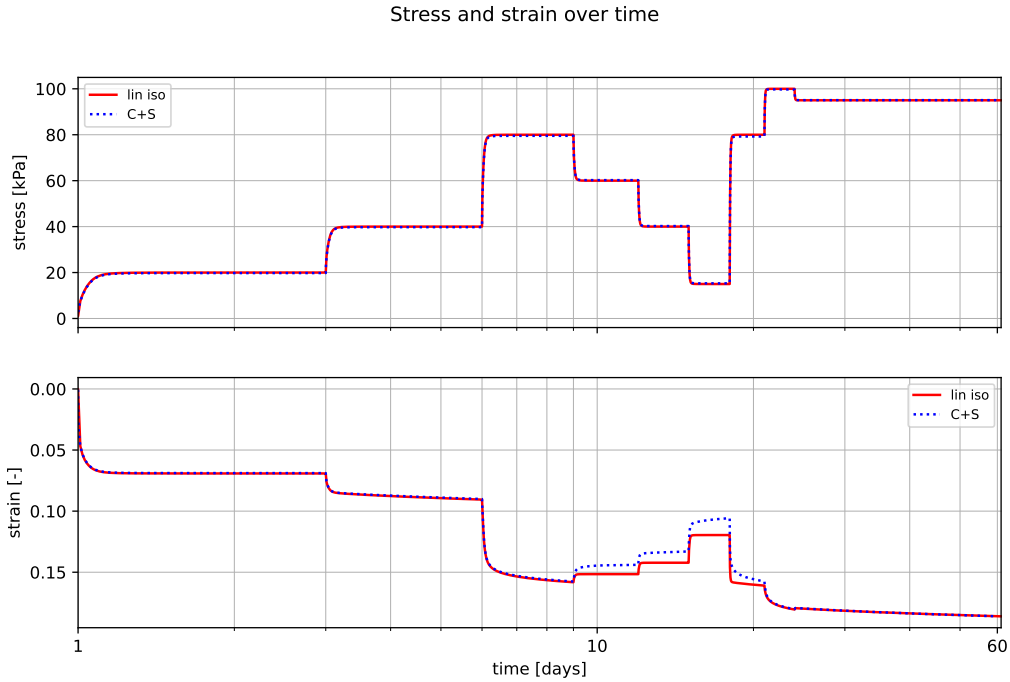

Figure 3.30: Stress and strain over time for parameter set Paper in IL test with multiple unloading steps

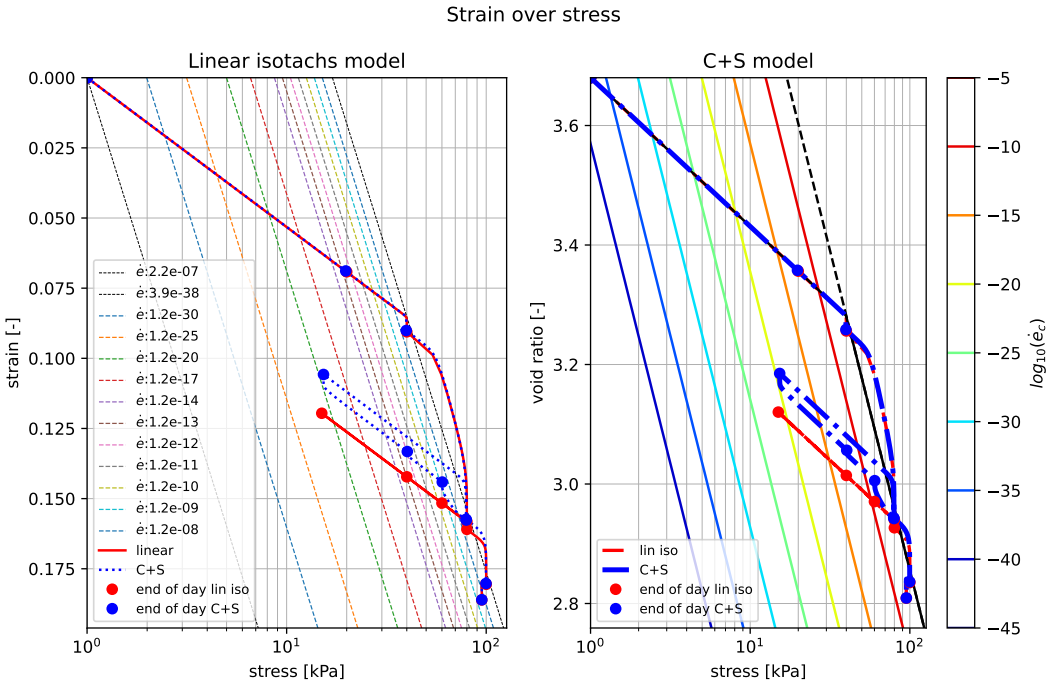

Figure 3.31: Isotachs for parameter set Paper in IL test with multiple unloading steps

3.3.3. Discussion

For the model comparison in an incremental loading test environment four different test scenarios are made. When looking at Figures 3.16 and 3.20 it can be seen that the difference between the two models is only visible in the unloading stage even though non-linearity is applied. Nevertheless the influence of the viscoplastic swell is visible in the stress strain graphs which also show that after reloading the

strains reached are smaller for the C+S model than for the linear isotach model. When a new loading step (which exceeds the yield stress) is applied this difference disappears and the strains are equal (See Figures 3.17 and 3.21). This makes that the strain development in the C+S model with and without non-linearity for a standard incremental loading test give almost identical results.

However, this does not hold for incremental loading test with multiple unloading steps and a longer creep period. These tests have been simulated and by comparing figures 3.18 and 3.22 with 3.26 and 3.30 one can see that upon unloading in both tests the C+S model predicts more swell than the linear isotach model. Different from the standard test, due to multiple unloading steps the strain after reloading (when the yield stress is exceeded) remains smaller for the C+S model than it is for the linear isotach model. This can be best seen in the GitHub parameter set but it also occurs in the paper parameter set and it happens both when the C+S model acts linear and non-linear. Another difference which can be seen by comparing the C+S model with and without linearity is the amount of creep. In the non-linear C+S simulations a clear flatting is visible in the strain against time graphs (Figures 3.18 and 3.22) due to the faster decaying strain rate by the closer spaced isotachs. This flatting is not present in the C+S model with linearity as was expected since the distance between isotachs remain constant and similar to the linear isotach model (Figures 3.26 and 3.30). Another point to mention in the comparison of the models is the development of the strain rates. In Appendix A.3.1 and A.3.2 the strain rates are plotted over time and despite the distorted isotachs it can be seen that during small load increments the strain rates are in the same order of magnitude for the C+S model with distorted isotachs as for the linear isotach model. This can be seen in all 4 tests (parameter set GitHub and Paper for both standard as unloading scenarios), this is in accordance with the drawn isotachs in Figures 3.17, 3.19, 3.21 and 3.23.

3.4. Model comparison: Embankment simulations

3.4.1. Methodology

With the two parameter sets given, different load increment simulations are set up to compare the two models. Since the goal of this study is to stress levels lower than the yield stress a scenario is simulated in which this is the case. An embankment is chosen with a pre-loading period after which the load is partly removed. In this way there is a stress level lower than the yield stress and also the influence of unloading can be studied.

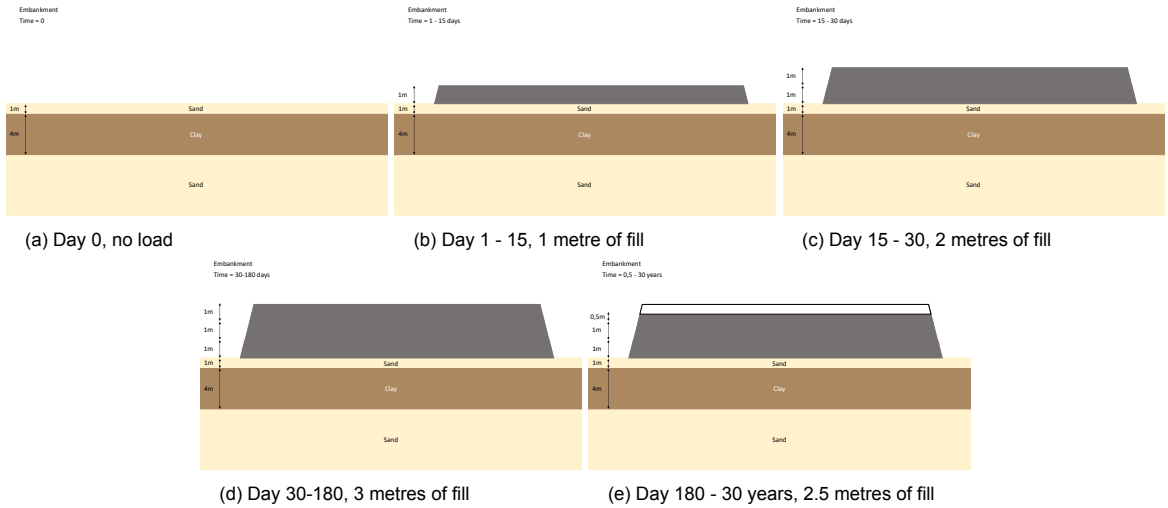

(a) Day 0, no load

(b) Day 1 - 15, 1 metre of fill

(c) Day 15 - 30, 2 metres of fill

(d) Day 30-180, 3 metres of fill

(e) Day 180 - 30 years, 2.5 metres of fill

Figure 3.32: Loading stages for the embankment simulation

For simplification only one soft layer has been chosen and the clay layer is enclosed by two permeable sand layers, in that way the drainage path is half the layer thickness. Next to that, the consolidation degree is chosen such that the time to reach 99% of consolidation is 180 days. In practice this could be achieved for example by the use of vertical drainage. The next assumption made is that the ground water table is at the surface so all the soil is fully saturated. During settlement buoyancy of the em-

bankment will be neglected. For the calculations the initial stress state for the centre of the clay layer is used, which is equal to the self weight of the soil above minus the static water pressure. For the yield stress a POP (pre overburden pressure) is added to the initial stress. Details of this simulation can be found in Table 3.12. The simulation will be done for both parameter sets given in previous section and for two different POPs for the both linear isotach model and the C+S model.

Table 3.12: Embankment properties

Input parameter	Value
γ_{sand}	20 [kPa/m]
γ_{clay}	16 [kPa/m]
γ_{water}	10 [kPa/m]
H_{clay}	4 [m]
H_{sand}	1 [m]
POP 1	20 [kPa]
POP 2	40 [kPa]

The embankment will be constructed with sand and has the same properties as the sand layer, given in Table 3.12. The values of the soil weights are based upon Table 2b of NEN 9997-1+C2 (NEN, 2017). The load increment scheme is presented in Table 3.13 and in Figure 3.32, the loads are applied at the first day mentioned in the caption of a figure.

Table 3.13: The load path for the embankment simulation. With an unloading phase as illustrated in Figure 3.32.

Time [days]	Total load [kPa]
0	σ'_{v0}
1	σ'_{v0} + 20
15	σ'_{v0} + 40
30	σ'_{v0} + 60
180	σ'_{v0} + 50

3.4.2. Results

Embankment simulations for C+S model with swell and non-linear isotachs

Comparison yield stresses

First, the stress and strain over times curves are shown for the embankment with a POP of 20 and 40 for the GitHub parameter set in Figure 3.33 and for the paper parameter set in Figure 3.34. Both simulations have swell and non-linearity. What can be seen in both figures is that the graph of the strain over time only changes in magnitude but not in shape, therefore further figures will only be shown for a POP of 20, figures for both POPs are also attached in Appendix A.4.

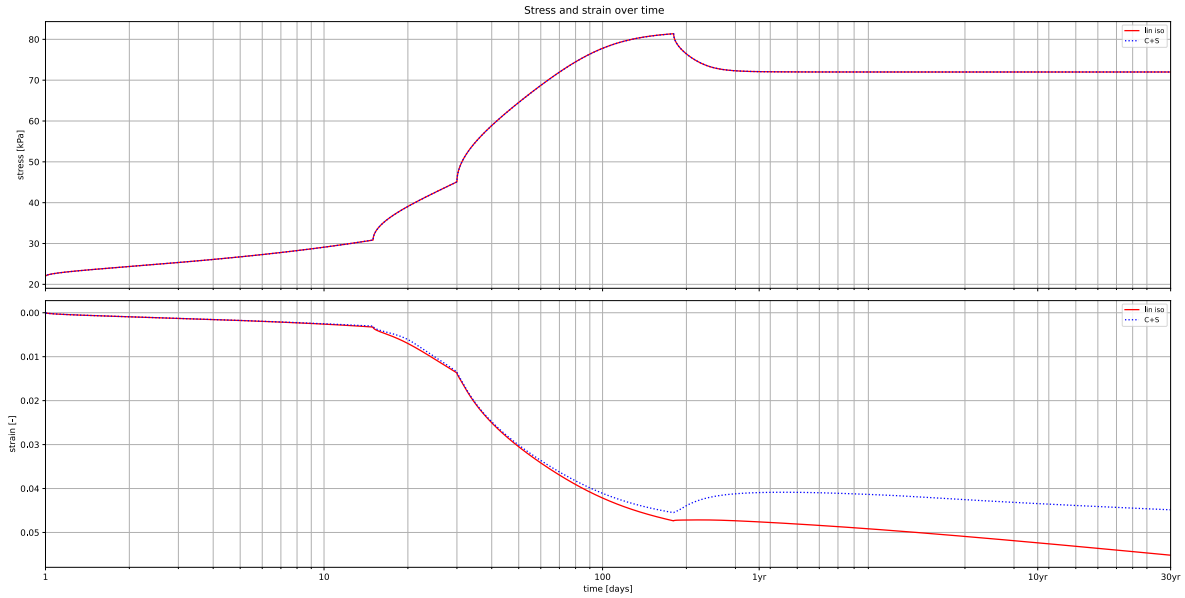

(a) POP 20 kPa

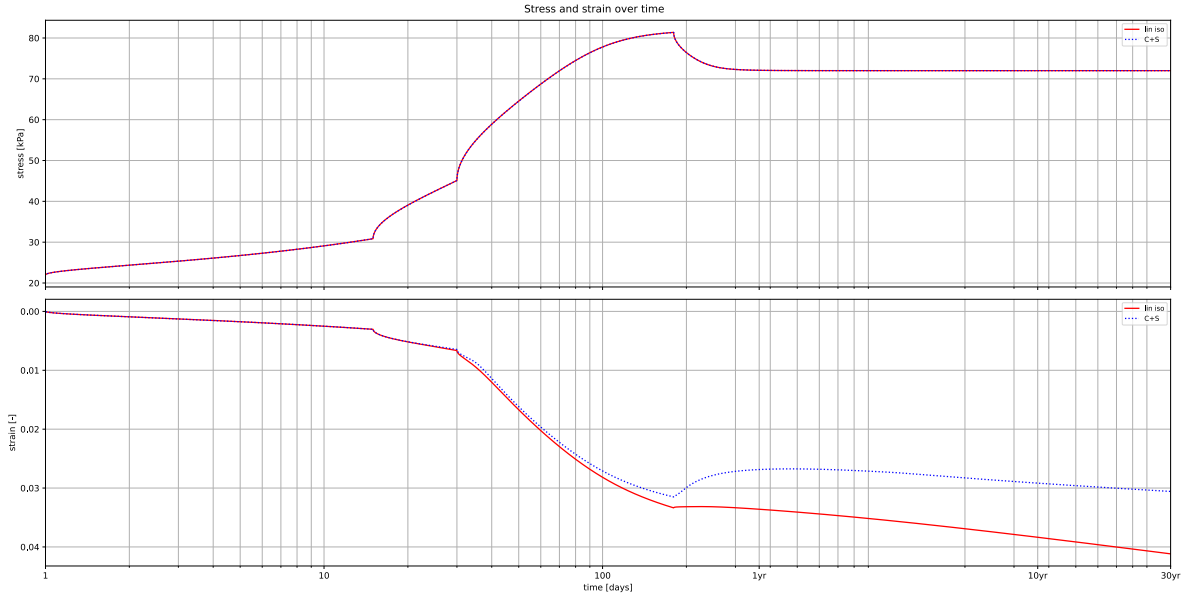

(b) POP 40 kPa

Figure 3.33: Stress and strain over time for parameter set GitHub

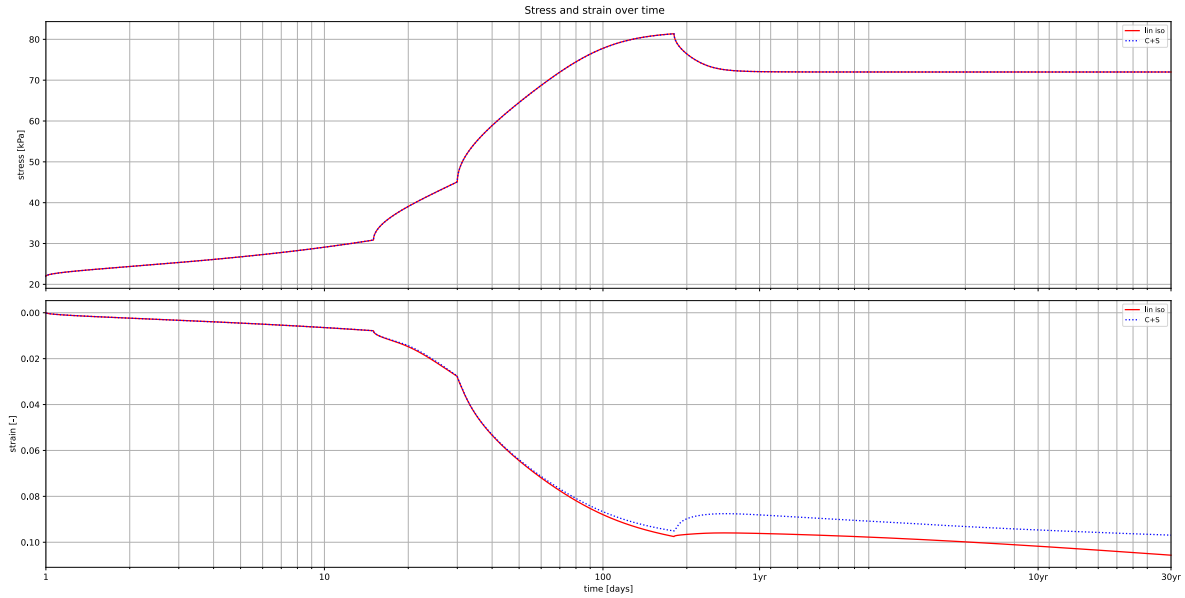

(a) POP 20 kPa

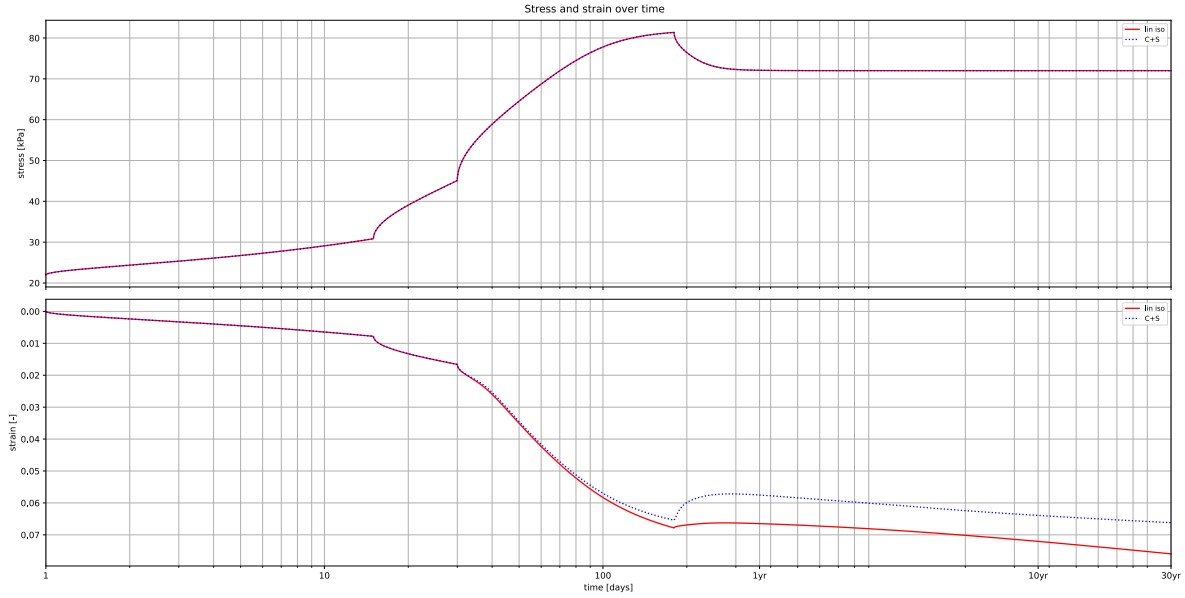

(b) POP 40 kPa

Figure 3.34: Stress and strain over time for parameter set Paper

Embankment GitHub parameters

In Figures 3.35-3.37 show the settlement over time, the strain over stress with isotachs and the stress and strain over time per load increment for the GitHub set with a POP of 20.

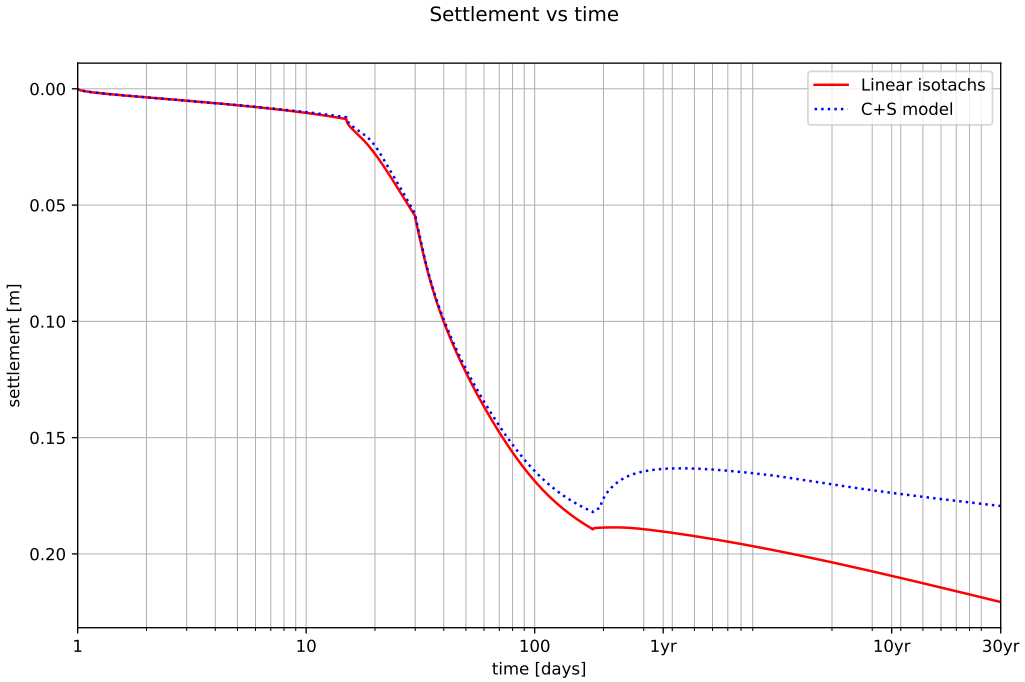

Figure 3.35: Settlement graph for GH POP 20 kPa

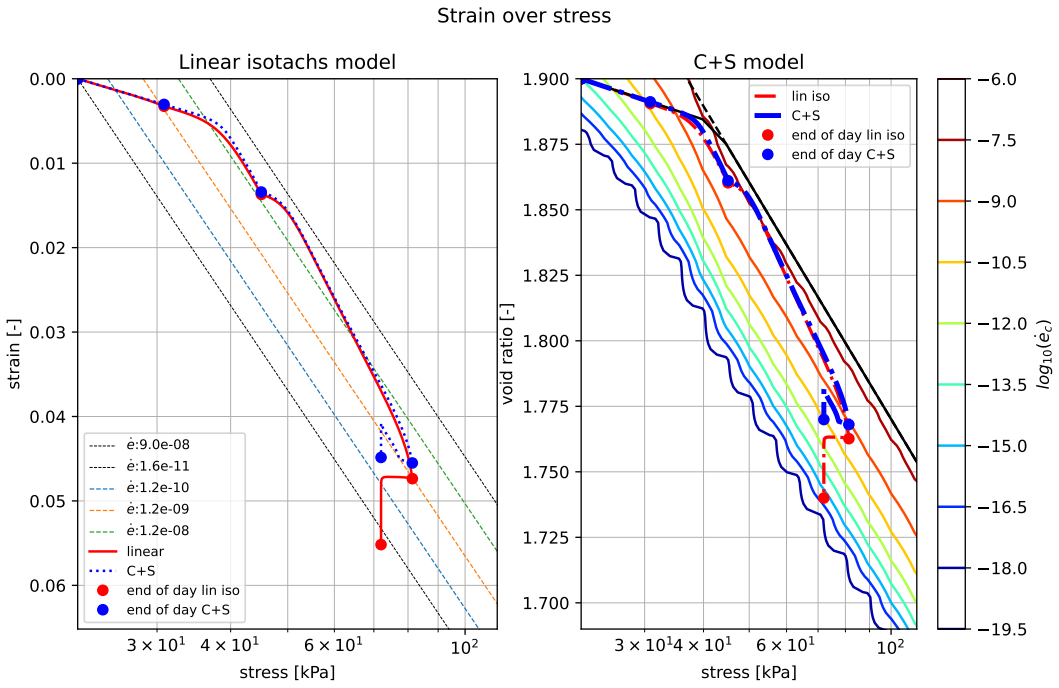

Figure 3.36: Isotachs for GH POP 20 kPa

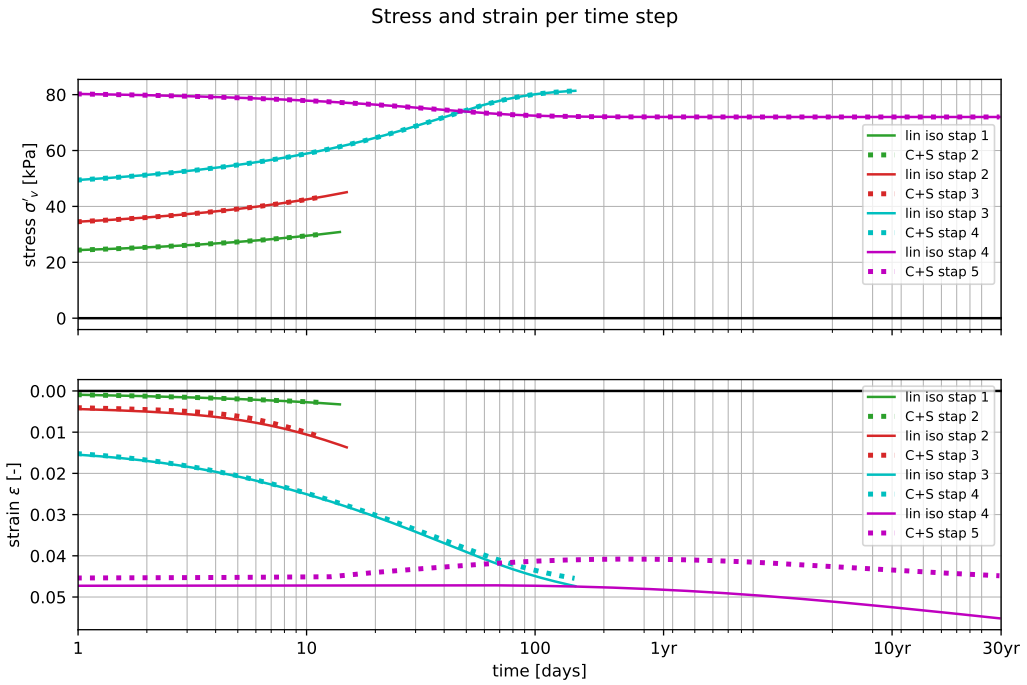

Figure 3.37: Strain and stress development per load increment for GH POP 20 kPa

In these figures it can be seen that upon loading the both models predict comparable results but when stress becomes constant the C+S model predicts less strain, this is due to the non-linearity. Next to that it can be seen that the C+S model predicts more swell. In Figure 3.38, the distorted isotachs upon unloading are presented. They should be compared with the isotachs in 3.36. In Appendix A.4.1 the development of the strain rates is shown.

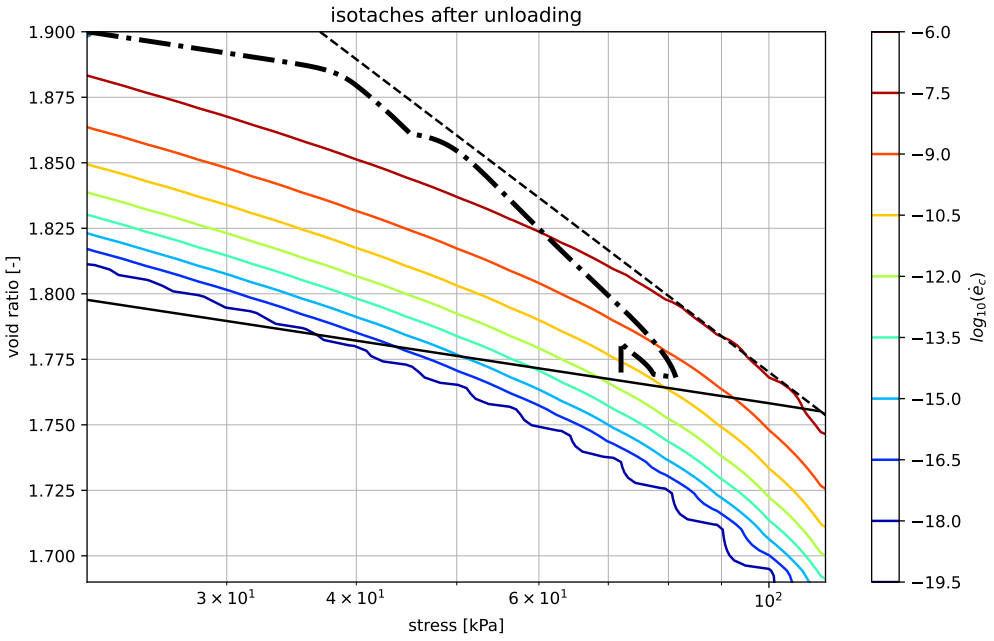

Figure 3.38: Isotachs after unloading for GH POP 20 kPa

Embankment Paper parameters

In Figures 3.39-3.41 the settlement over time graph, the strain over stress with isotachs is shown, the stress over time and the strain over time and the stress and strain over time per loading step are shown for the paper set for a POP of 20 kPa.

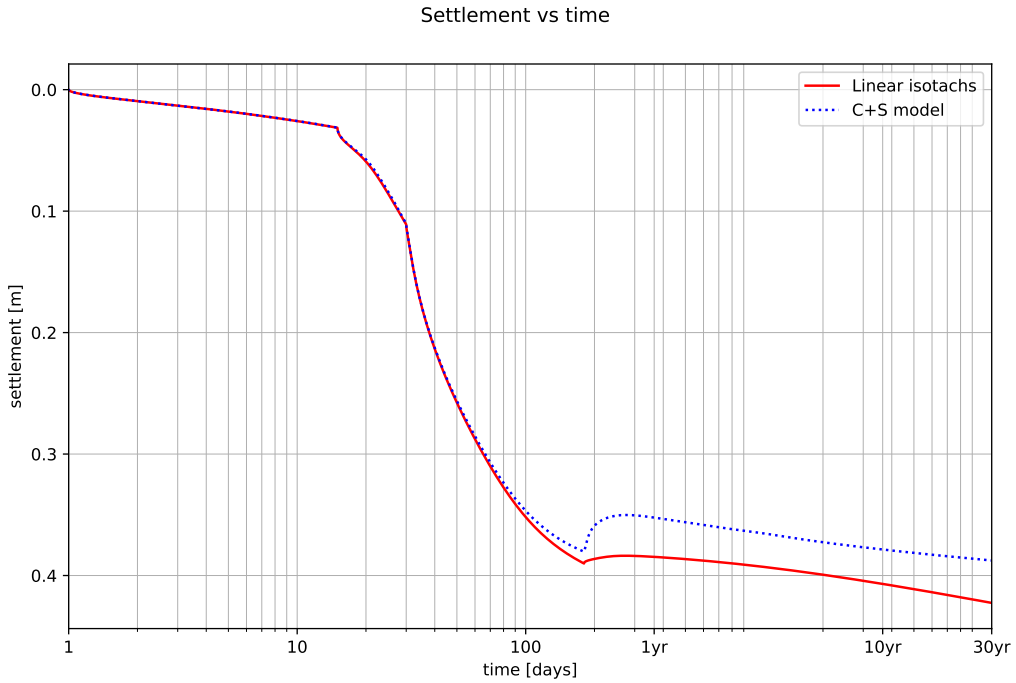

Figure 3.39: Settlement graph for paper POP 20 kPa

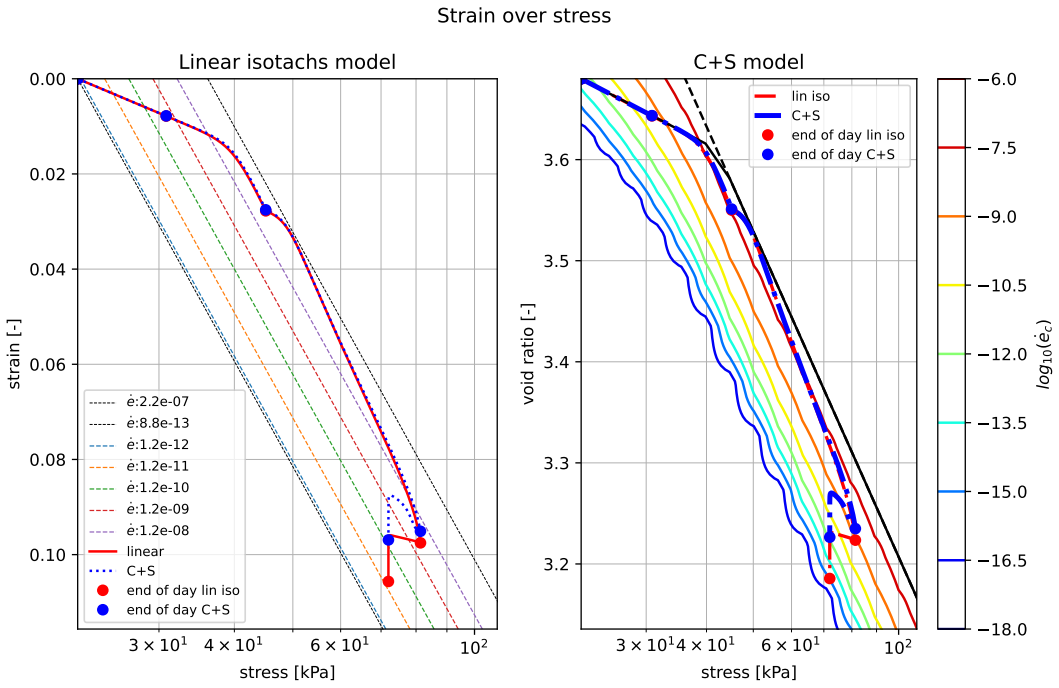

Figure 3.40: Isotachs for paper POP 20 kPa

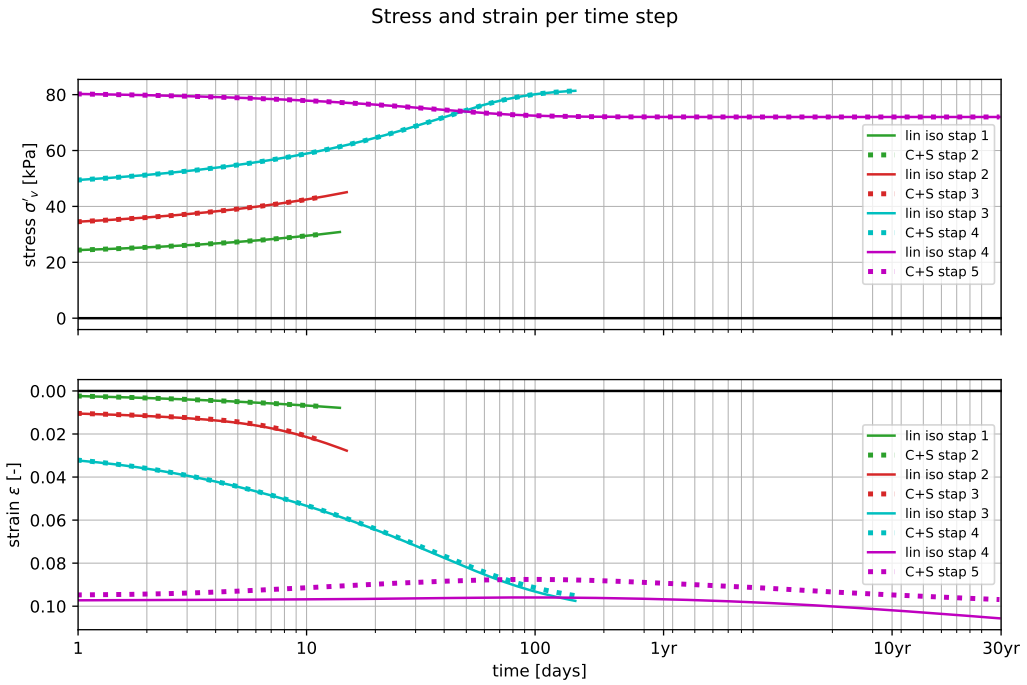

Figure 3.41: Strain and stress development per load increment for paper POP 20 kPa

In these figures it can be seen that upon loading the both models predict comparable results but when stress becomes constant the C+S model predicts less strain, this is due to the non-linearity. Next to that it can be seen that the C+S model predicts more swell. In Figure 3.42, the distortion of the isotachs upon unloading is presented. They should be compared with the isotachs in 3.40. In Appendix A.4.1 the development of the strain rates is shown.

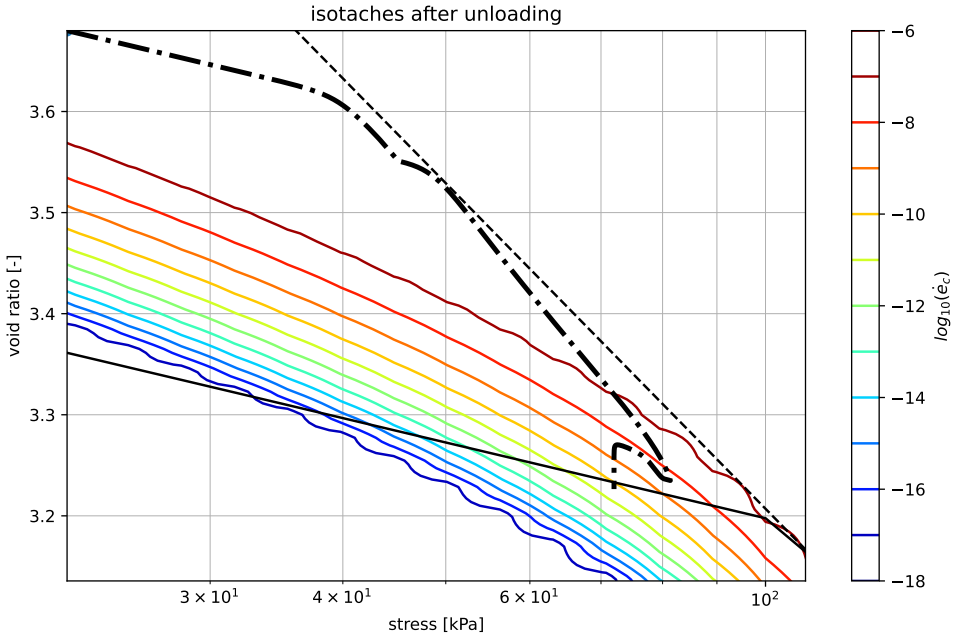

Figure 3.42: Isotachs after unloading for paper POP 20 kPa

Embankment simulations for C+S model with swell and linear isotachs

Embankment GitHub parameters

In Figures 3.43-3.45 the settlement over time graph, the strain over stress with isotachs is shown, the stress over time and the strain over time and the stress and strain over time per loading step are shown for the GitHub set for a POP of 20 kPa.

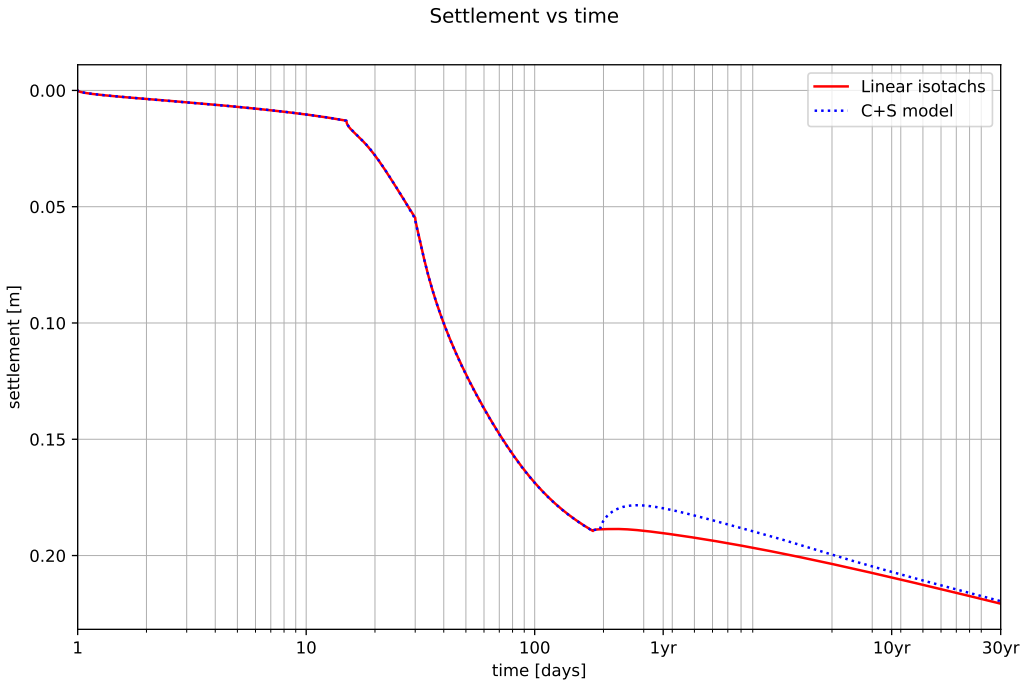

Figure 3.43: Settlement graph for GH POP 20 kPa

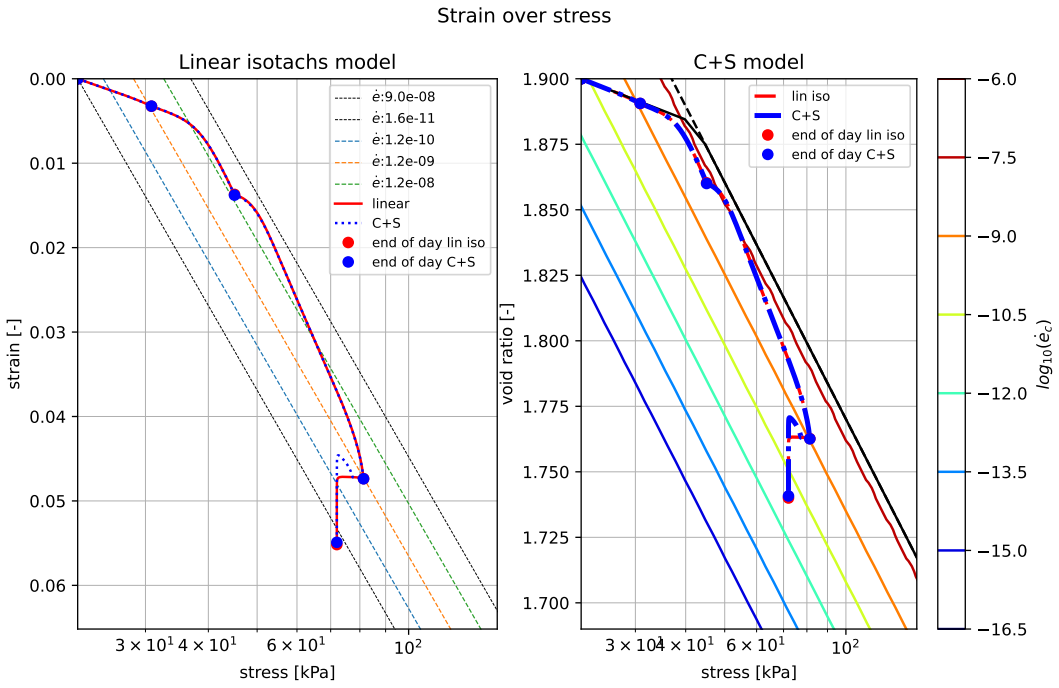

Figure 3.44: Isotachs for GH POP 20 kPa

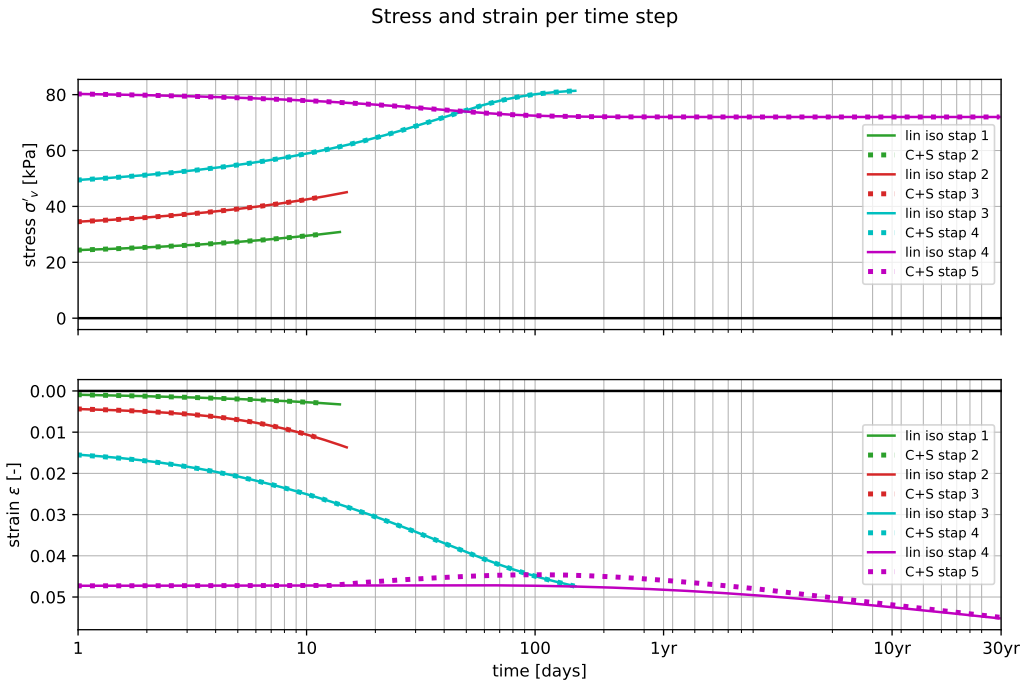

Figure 3.45: Strain and stress development per load increment for GH POP 20 kPa

In these figures it can be seen that upon loading the both models predict comparable results but when stress becomes constant the C+S model predicts less strain, this is due to the non-linearity. Next to that it can be seen that the C+S model predicts more swell. In Figure 3.46, the isotachs upon unloading are presented. They should be compared with the isotachs in 3.44, it can be seen that their spacing is constant. In Appendix A.4.2 the development of the strain rates is shown.

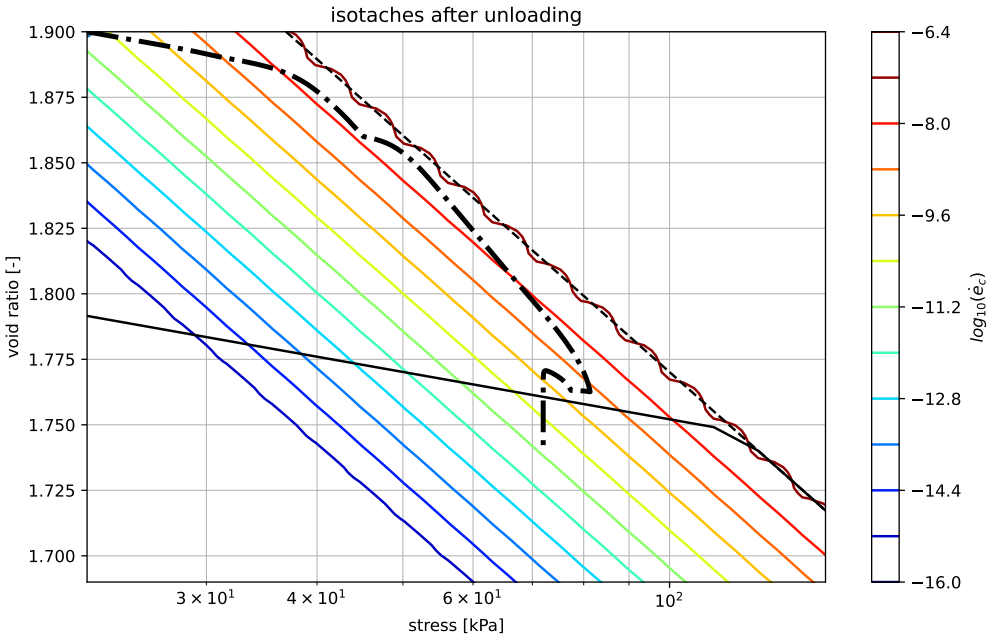

Figure 3.46: Isotachs after unloading for GH POP 20 kPa

Embankment Paper parameters

In Figures 3.47-3.49 the settlement over time graph, the strain over stress with isotachs is shown, the stress over time and the strain over time and the stress and strain over time per loading step are shown for the paper set for a POP of 20.

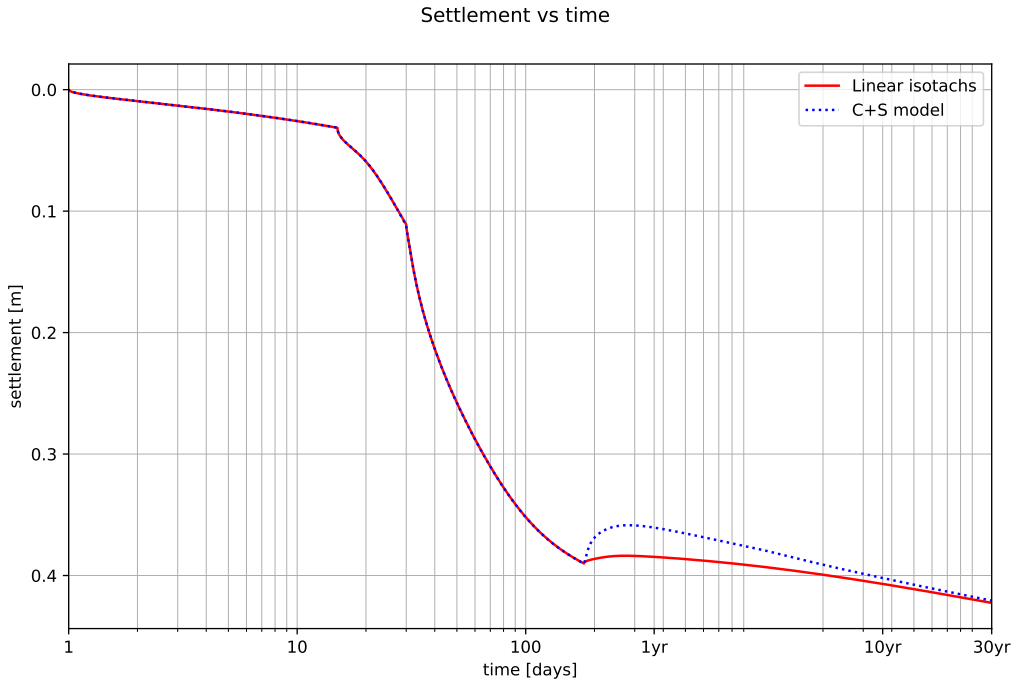

Figure 3.47: Settlement graph for paper POP 20 kPa

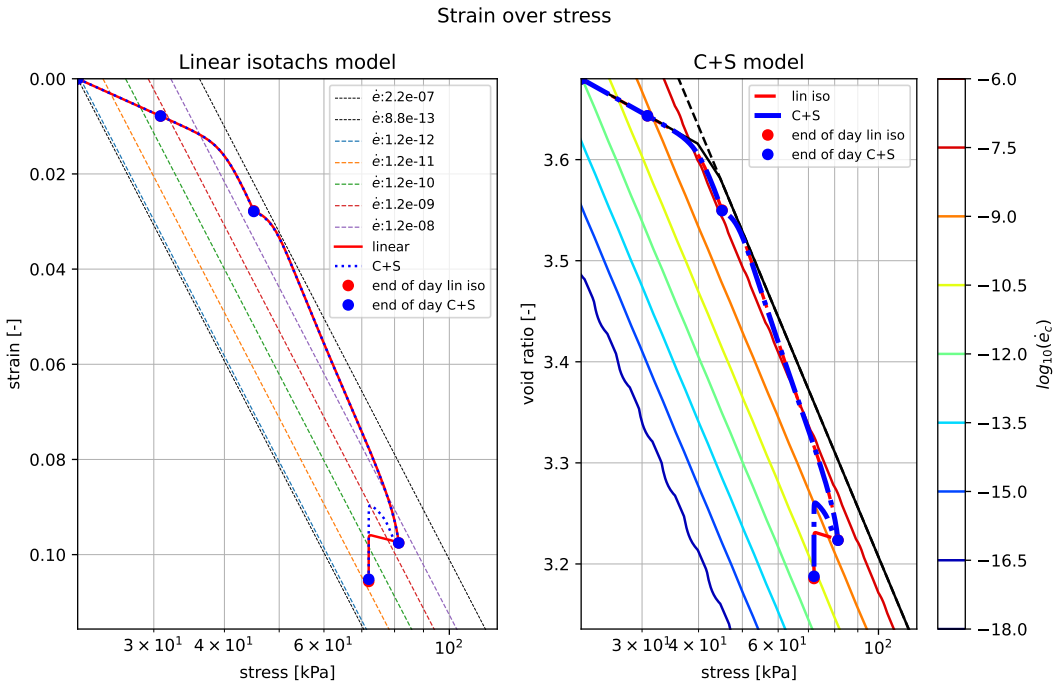

Figure 3.48: Isotachs for paper POP 20 kPa

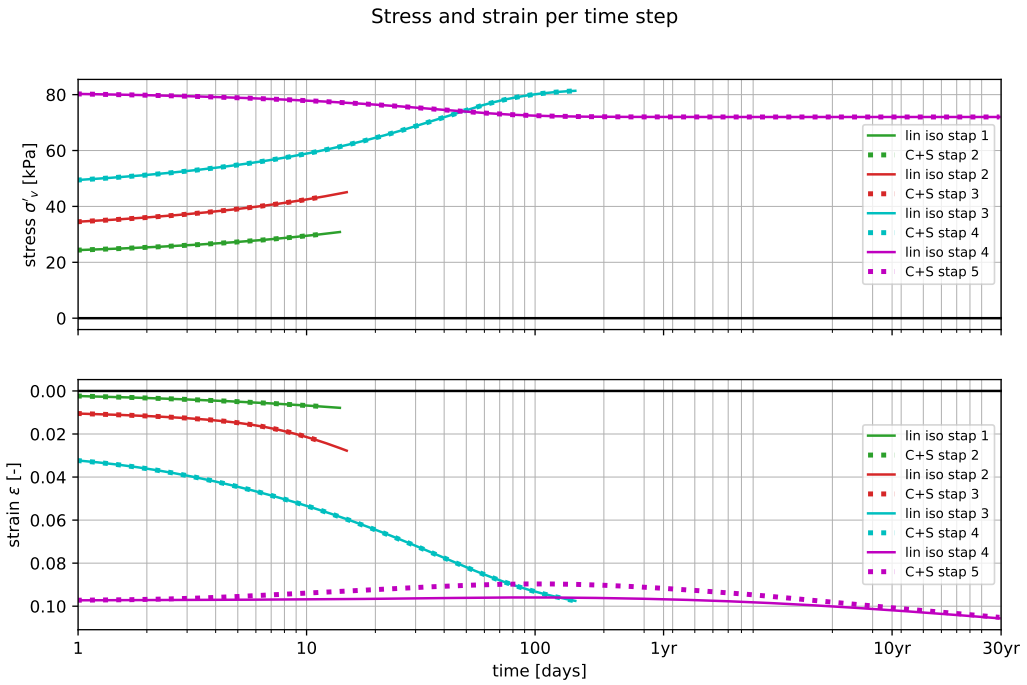

Figure 3.49: Strain and stress development per load increment for paper POP 20 kPa

In these figures it can be seen that upon loading the both models predict comparable results but when stress becomes constant the C+S model predicts less strain, this is due to the non-linearity. Next to that it can be seen that the C+S model predicts more swell. In Figure 3.42, the isotachs upon unloading are presented. They should be compared with the isotachs in 3.48, it can be seen that their spacing is constant. In Appendix A.4.2 the development of the strain rates is shown.

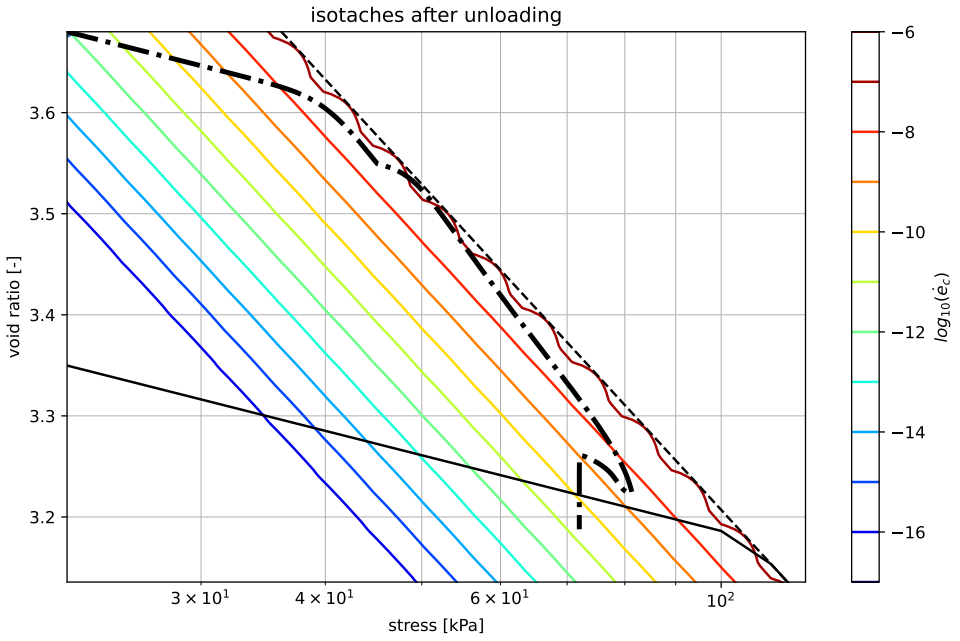

Figure 3.50: Isotachs after unloading for paper POP 20 kPa

3.4.3. Discussion

First of all, the influence of the yield stress (in terms of a POP) has been considered. As mentioned in Section 3.4.2 the yield stress does change the magnitude but not so much the shape of settlement behaviour over time. This was shown by Figures 3.33 and 3.34.

Secondly, the comparison is made between the linear isotach model and the C+S model with non-linear, distorted isotachs and viscoplastic swell included. For both parameter sets it can be observed that the settlement predicted by the C+S model is less than the linear isotach model over a period of 30 years. Next to that, the behaviour is different as well. This can be best seen in the Figure 3.37 and 3.41 where the stress and strain development are visualised per load increment. For the last load increment, removal of the pre-load, the predictions start to diverge. The swell period for the C+S model is longer and more uplift is found and the strain rate decreases faster as well. This longer swell period is in accordance with the findings on Mexico clay were after unloading a longer period of swell was found as well.

In the last comparison, where the C+S model was used with linear isotachs and viscoplastic swell, the settlement predictions over 30 years for both models converge. An explanation for this is that a higher creep strain rate is found for the C+S model after swell which makes it settle faster and therefor it compensates for the uplift (Figures 3.44 and 3.48).

4

Groundwater table fluctuations

4.1. Methodology

The groundwater table of a soil is important for the effective stress. To answer the second sub-question several scenarios will be run in which there is one base scenario in which the groundwater table will remain constant. By adding one component to equation 2.29, the groundwater fluctuation, it is possible to vary it over the time. The scenarios are presented in Table 4.1 and will all have the same soil parameters and loading scheme as the embankment with the parameter set of Mexico clay, which are given in Tables 3.4, 3.13. The POP is chosen as 40 kPa. The predictions are only made in the linear isotach model.

$$GWT = z(t) + f(t) \tag{4.1}$$

$$z(t) = H - dH(t) \tag{4.2}$$

$$f(t) = A \cdot sin(\frac{t}{T}) \tag{4.3}$$

Where:

GWT = groundwater table
$z(t)$ = hydraulic head over time
H = surface -0.5[m]
$f(t)$ = seasonal fluctuations
$dH(t)$ = the decrease of increase of hydraulic head over life time
A = magnitude of season fluctuation
t = time
T = period of seasonal fluctuations = 180 days

Table 4.1: Groundwater table fluctuations

Scenario	change(t) [m]	A [m]
Base	0	0
Constant flux	0	0.2
Constant flux + decrease	-0.5	0.2
Constant flux + increase	+0.5	0.2
Increasing flux	0	0.2 + 0.3/time
Increasing flux + decrease	-0.5	0.2 + 0.3/time
Increasing flux + increase	+0.5	0.2 + 0.3/time

From these scenarios it must become clear what influence temporal fluctuations have on settlement behaviour of an embankment. Next to the fluctuations a more permanent change in groundwater table can be observed in these scenarios. Lowering of the groundwater table would result in higher effective stresses while a higher groundwater table would result in lower effective stresses. To see if the magnitude of the fluctuations affect the settlement behaviour a constant fluctuation and an increasing fluctuation is simulated.

4.2. Results

In Figure 4.1 the settlement behaviour is shown for the scenario without any change in groundwater table. This is used as a reference to compare the other scenarios with.

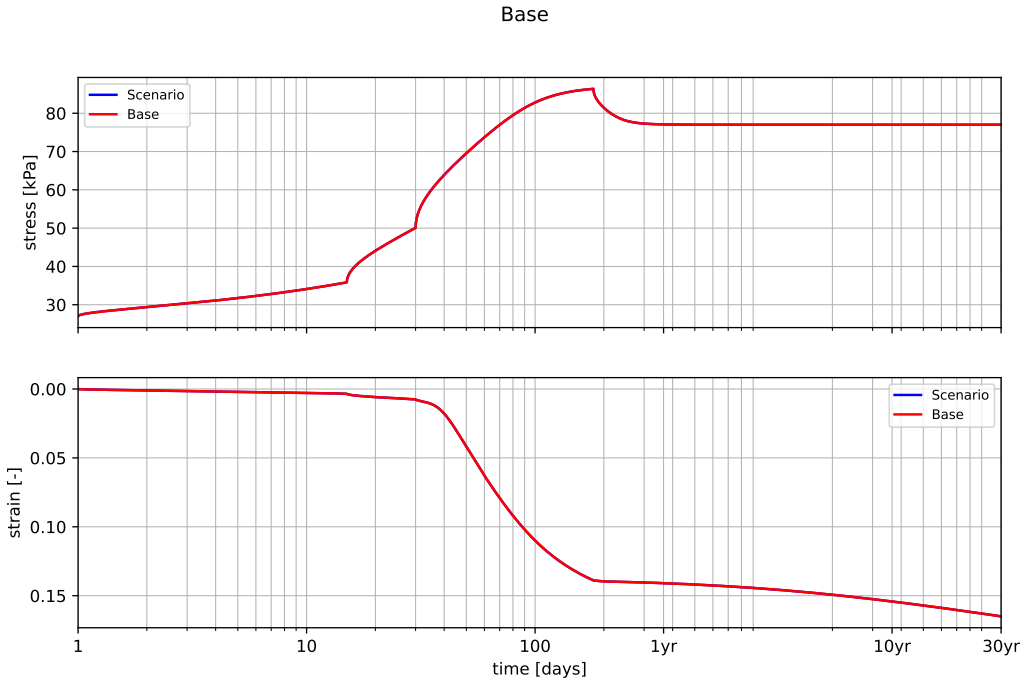

Figure 4.1: Stress and strain over time for base scenario

Constant fluctuation in groundwater table

In Figure 4.2 it can be seen that the total strain is not affected by the constant fluctuation of the groundwater table. However it can be seen that prior to the unloading step the stress level of the constant flux scenario is higher and more strain is obtained. This can be explained by a temporal dry period which results in higher effective stress. When a constant fluctuation is combined with an increase or decrease in hydraulic head it can be seen that this affects the stress resulting in either more or less strains than predicted by the base model (Figures 4.3 and 4.4).

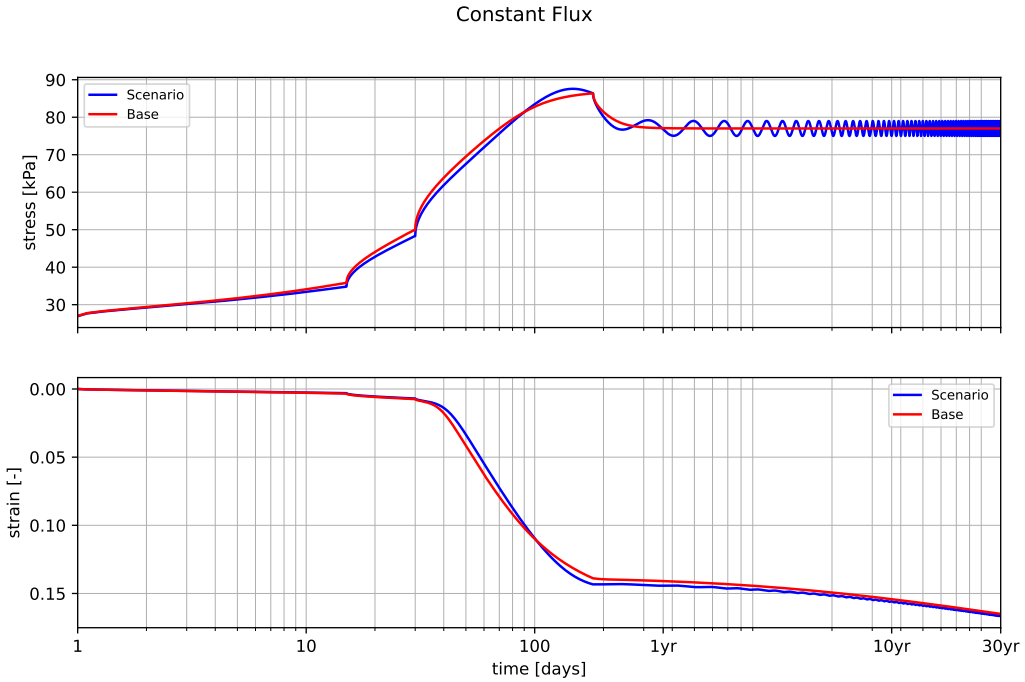

Figure 4.2: Stress and strain over time for Constant flux scenario

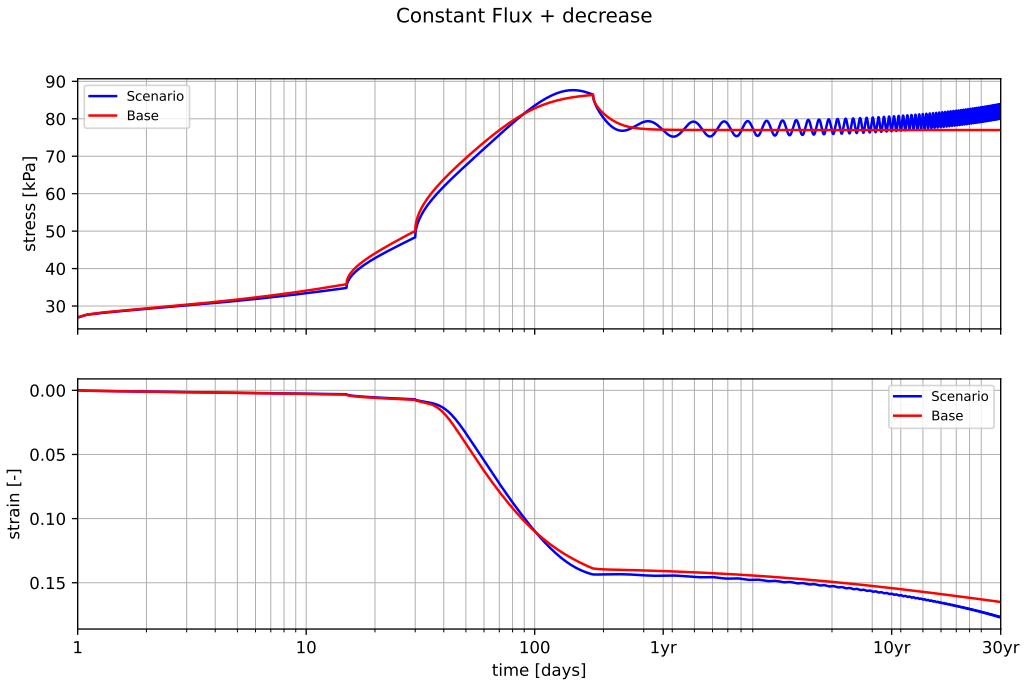

Figure 4.3: Stress and strain over time for Constant flux + decrease scenario

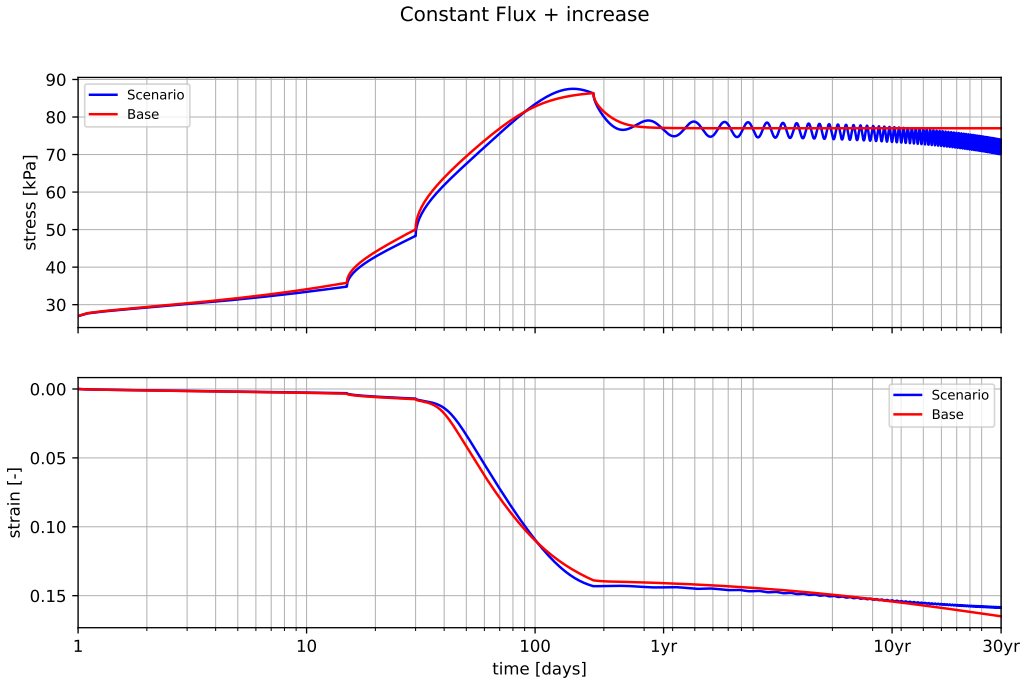

Figure 4.4: Stress and strain over time for Constant flux + increase scenario

Increasing fluctuation in groundwater table

Comparable to the constant fluctuation the final settlement does not change when an increasing fluctuation is simulated as can be seen in Figure 4.5. Furthermore it can be seen that the final strains predicted for an increase and decrease in groundwater table are comparable for the predictions with a constant fluctuation and an increasing fluctuation. In Appendix B, the strain versus stress and settlement over time graphs are also attached. There it can be seen that for the strain against stress graph a same oscillation around the average effective stress level is present.

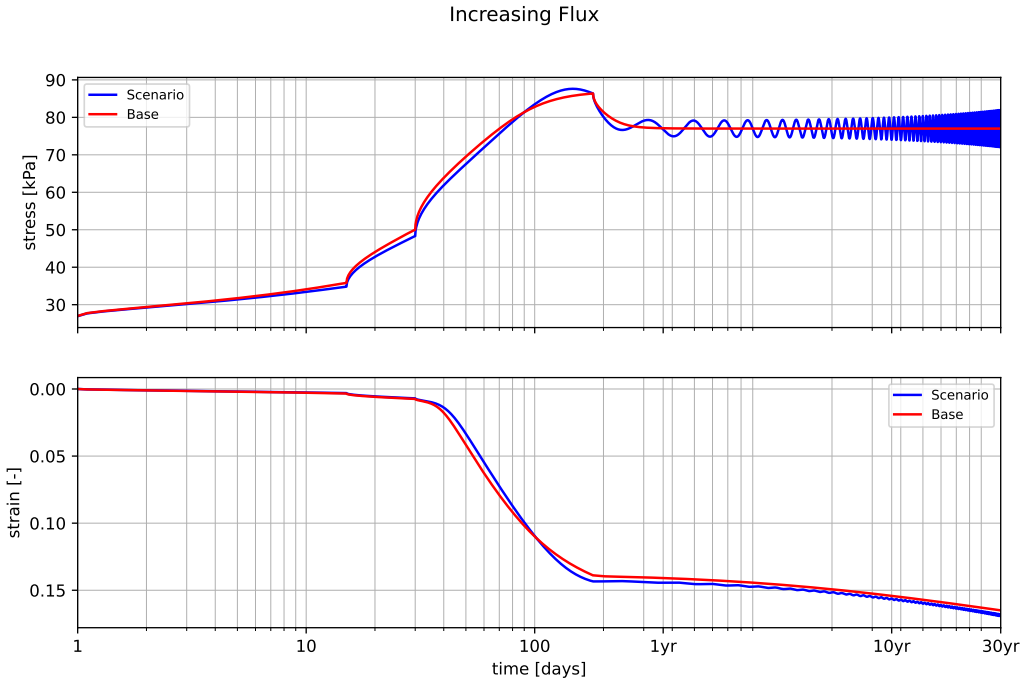

Figure 4.5: Stress and strain over time for Increasing flux scenario

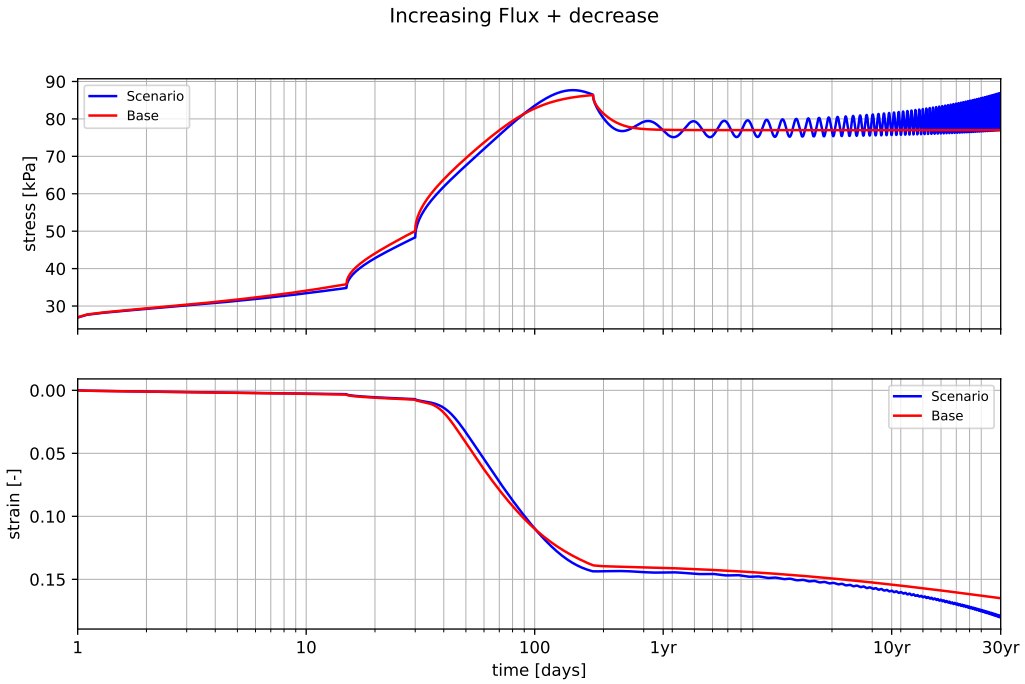

Figure 4.6: Stress and strain over time for Increasing flux + decrease scenario

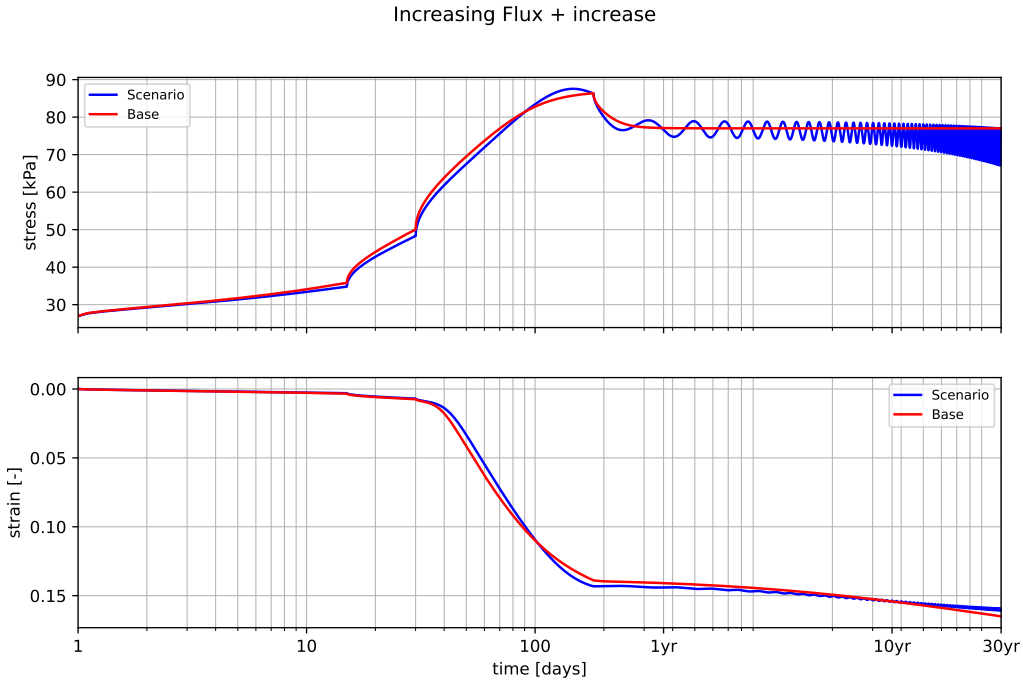

Figure 4.7: Stress and strain over time for Increasing flux +increase scenario

4.3. Discussion

The first observation based on Figures 4.1, 4.2 and 4.5 is that temporal fluctuations around a constant hydraulic do not affect the final settlement. However, it can be observed that temporal fluctuations do change the settlement behaviour and that small periods of compression and swell succeed one another. Furthermore it can be observed in Figures 4.4 and 4.7 that an increase in the groundwater table does result in a decrease of effective stress which is in accordance with equation 2.29. In terms of strain this results in lower final strains. Also in accordance to equation 2.29 a decrease in groundwater table increases the effective stress with an increase strain as result.

Even though the stress level oscillate with an amplitude up to 5 kPa (Figure 4.5), the oscillation in strain is limited. An explanations for this is that the elastic strains cancel each other out over time and the viscoplastic strain does not change much. The same hold when the decrease and increase in groundwater table is considered. But here it should be noted that an increase in groundwater table causes a shift in the isotach graph (See Appendix B) which results in lower strain rates and therefore a flatter curve in Figure 4.4 and 4.7 compared to the base scenario. Vice versa, a decrease in groundwater table causes in increase in stress and with it a shift in the isotach graph towards a higher isotach with a higher strain rate and therefore a steeper curve compared to the base scenario in Figures 4.3 and 4.6.

5

InSAR

With the use of InSAR two locations will be considered. The first location is the N3, a road between two highways (A15 and A16) through Dordrecht. Secondly the A2 highway between Amsterdam and Utrecht will be considered. Both locations are shown in Figure 5.1.

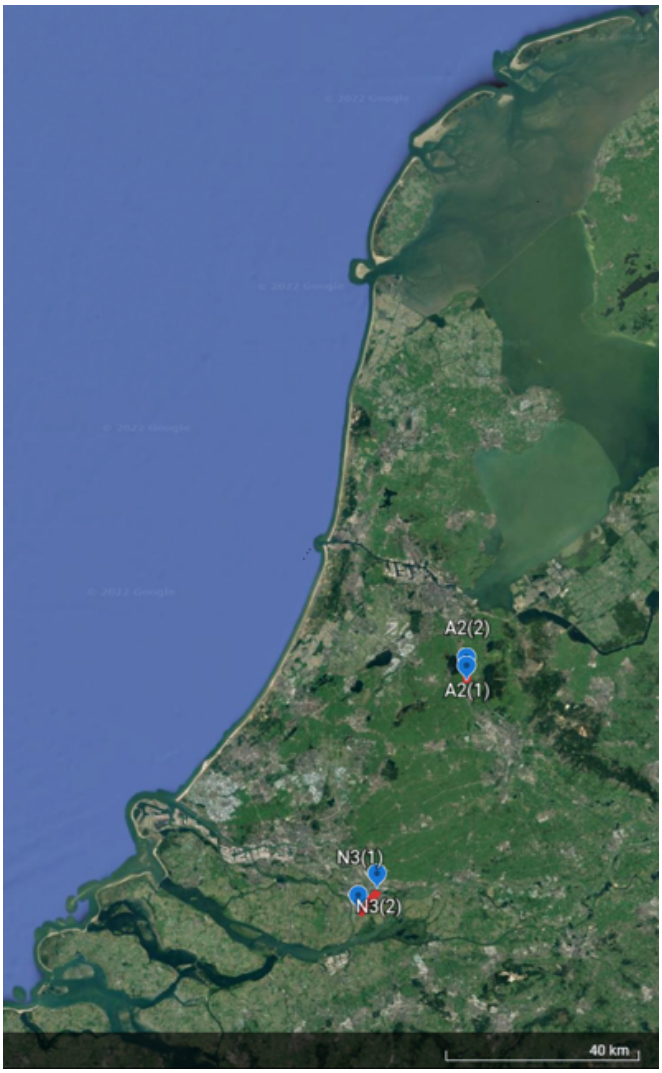

(a) Project locations in NL

(b) Zoom in on N3

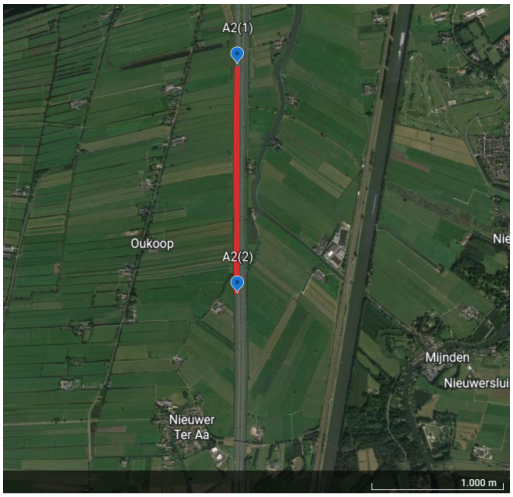

(c) Zoom in on A2 Westbaan

Figure 5.1: Overview of project locations for InSAR

5.1. N3: yield stress determination

5.1.1. Methodology

In the period of 2018-2021 maintenance of the foundation and asphalt took place which caused a small change in stress state which could cause a different settlement behaviour than before maintenance. As presented in Chapter 2 one of the parameters to make predictions is the yield stress (σ'_p). Since the yield stress is determined by the intersection between the reloading and compression lines (RR & CR), due to, for example, sample disturbance and unloading when taking a sample, there is uncertainty in this parameter. With the use of InSAR the yield stress can be derived based on the in situ situation. With the measured displacement rate (dz / dt) and a known layer thickness the strain rate can be calculated (equations 5.1). With this strain rate and soil parameter C_α the intrincisc time of the soil can be calculated (equation 5.2). By rewriting equations 5.2 and 5.3 for the intrinsic time, equation 5.4 is obtained which can be used for the calculation of the yield stress.

$$\frac{dz}{dt} = \dot{\varepsilon} \cdot H \tag{5.1}$$

$$\tau = \frac{C_\alpha}{ln(10)\dot{\varepsilon}} \tag{5.2}$$

$$\tau = (\frac{\sigma_p}{\sigma_v})^{\frac{CR-RR}{C_\alpha}} \tag{5.3}$$

$$\sigma'_p = \sigma'_v(\frac{C_\alpha}{\dot{\varepsilon} \cdot ln(10)})^{\frac{C_\alpha}{CR-RR}} \tag{5.4}$$

InSAR does not measure strain rates but a (relative) change in surface level, from a certain starting point settlement over time is taken as the displacement rate, which can be converted to strain rate. This is, since the surface displacement is considered, a strain rate for all the compressible layers together. By dividing the settlements with the initial layer thickness a time series of strain is obtained. From such a time series the strain rate can be determined and used in equations 5.4. As can be seen in Figure 5.1b the road covers multiple kilometres, for that reason there can be local difference in settlement behaviour and stress history, e.g. yield stress. The first step to take, is to determine regions of uniform motion (RUM) on the displacement map. Secondly these locations must be studied in more detail, elevations (based on Actuele Hoogtebestand Nederland (AHN, 2019)) and soil layering (based on bore hole logs and CPT's from Dinoloket (TNO, 2022)) must be considered. Finally the soil parameters are derived based on laboratory tests performed by Wiertsma & Partners (2018) and Table 2.b from NEN (2017). A first general elevation map is presented already in Figure 5.2 and a displacement rate map in Figure 5.3; more detailed maps based on the chosen locations will be presented in the results as will the displacements over time. The soil parameters for the different soil types are listed in Table 5.1. When a more detailed study is performed at the locations of interest, these parameters will be used to calculate the initial effective stress based on the layer thickness of the sand and the soft soil. Finally, with the parameters, the displacement rate and equation 5.4 the yield stress will be calculated.

(a) Elevation profile project area N3

(b) N3 area AHN

Figure 5.2: Elevation map N3

Table 5.1: Soil parameters (Wiertsma & Partners, 2018), (NEN, 2017), (TNO, 2022)

Parameter	Value
Sand	
$\gamma_{sand;sat}$	19 [kPa]
GWT	NAP - 1 [m]
γ_{water}	10 [kPa]
Clay	
RR	0.027 [-]
CR	0.24 [-]
C_{α}	0.0126 [-]
$\gamma_{clay;sat}$	14.3 [kPa]
Peat	
RR	0.056 [-]
CR	0.29 [-]
C_{α}	0.018 [-]
$\gamma_{peat;sat}$	11 [kPa]

(a) North part of N3

(b) Middle part of N3

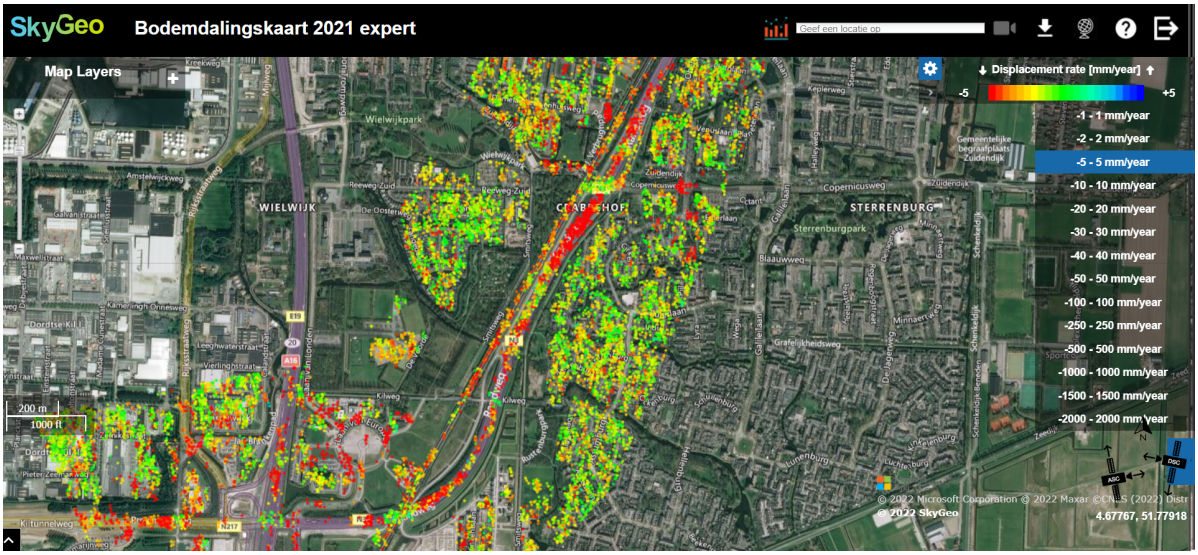

(c) South part of N3

Figure 5.3: Displacement rates measured between 2015 - 2020 by InSAR of the N3 Highway

5.1.2. Results

RUM locations

The first step was to determine so called RUMs (regions of uniform motion). For this purpose the scale on the settlement map was set on -5 to +5 mm / year. This made that only small displacement rates show up in green, these regions are all cross overs and bridges. In Figure 5.4a a first location of interest is shown and a more detailed scale (-10 to +10 mm / year) is used in Figure 5.4b. The location is close to a cross over where there is a clear distinction in settlement behaviour. The red dots indicate faster displacement rate while the green dots indicate a very small displacement rate. This location is chosen since the elevation is relatively constant as is the thickness and depth of the soft soil layer which makes that the initial stress state of this location is representative for the whole area. The location with the red dots in Figure 5.4a also shows a RUM but the road elevation is increasing which makes it harder to perform an analysis for the yield stress.

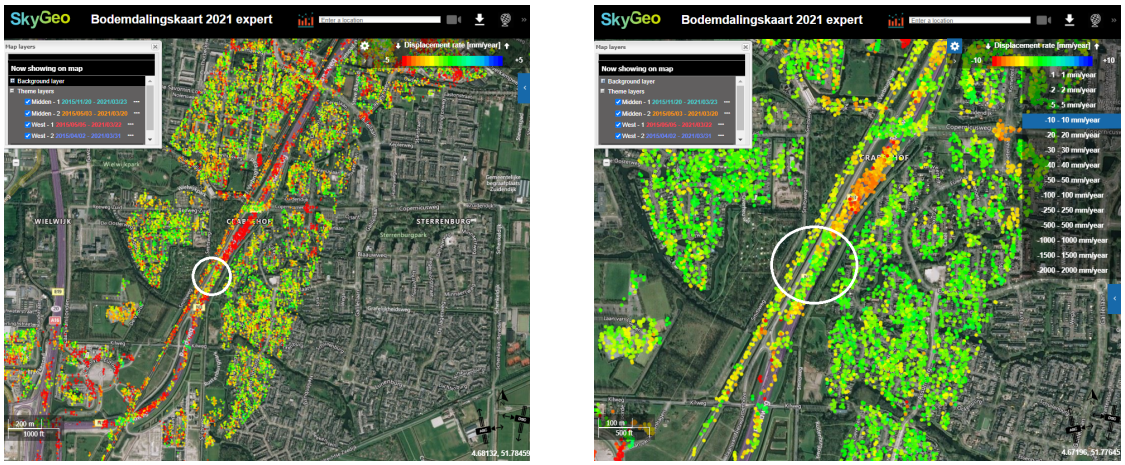

(a) RUM location 1

(b) RUM location 1 more detailed scale

Figure 5.4: First location of interest

The second location that will be considered has a higher displacement rate and is located north of the previous location. The location is white encircled in Figure 5.5. Just as for location 1, in Figure 5.5b a more detailed scale is used.

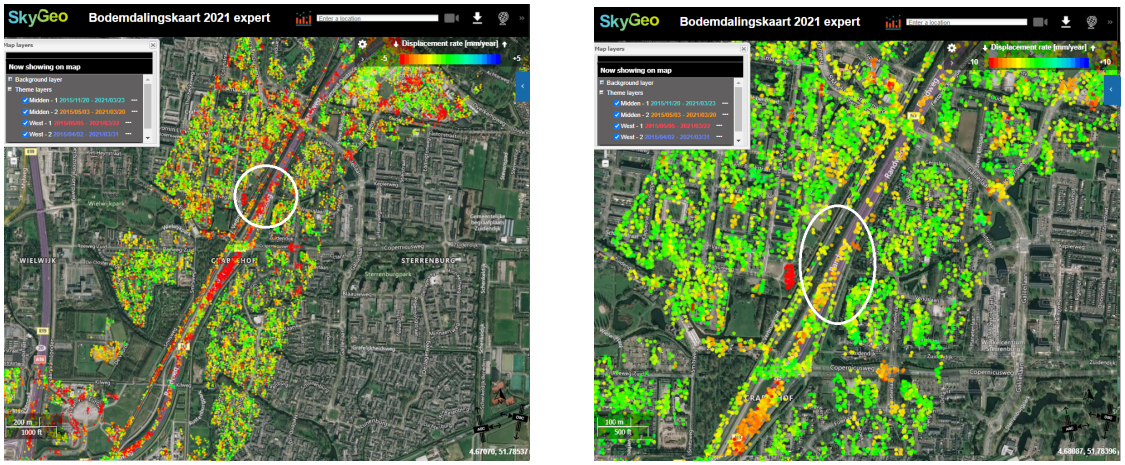

(a) RUM location 2

(b) RUM location 2 more detailed scale

Figure 5.5: Second location of interest

Soil profile and elevation

For the determination of the yield stress in this location, the subsurface profile must be considered and the height of the surface level to determine which part of the soil is dry and which part is below the

groundwater table. Figures 5.7 and 5.8 show these profiles for the two locations of interest. In Figure 5.6 the soil layers derived from multiple CPTs from DINOloket are shown, the used CPTs can be found in Appendix C.3.

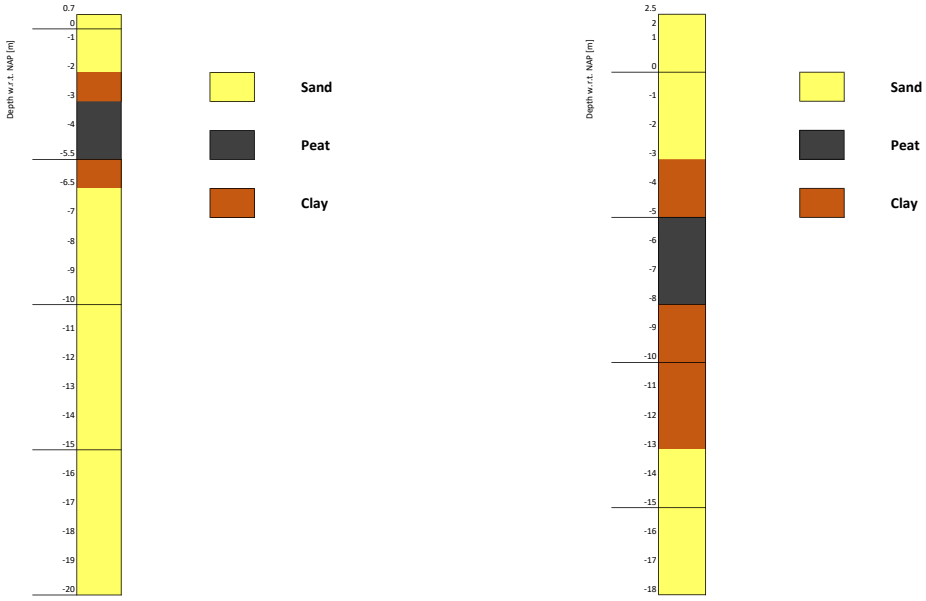

(a) Layering of the 1st location of interest

(b) Layering of the 2nd location of interest

Figure 5.6: Layering of subsurface at N3

Based on these soil profiles, the soil parameters of Table 5.1 to make one soft soil layer with soil parameters that are the weighted averages. This starting point for further analysis and is called the mixed soil layer scenario. An overview of these parameters is given in Table 5.2. Calculations of the weighted averages can be found in Appendix C.1.

Table 5.2: Soil parameters for mixed scenario for location 1 and 2

Parameter	Location 1	Location 2
CR	0.27 [-]	0.26 [-]
RR	0.044 [-]	0.035 [-]
C_α	0.016 [-]	0.014 [-]
γ_{soft}	12.1 [kPa]	13.3 [kPa]

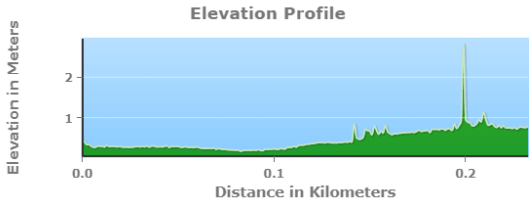

(a) Elevation of road

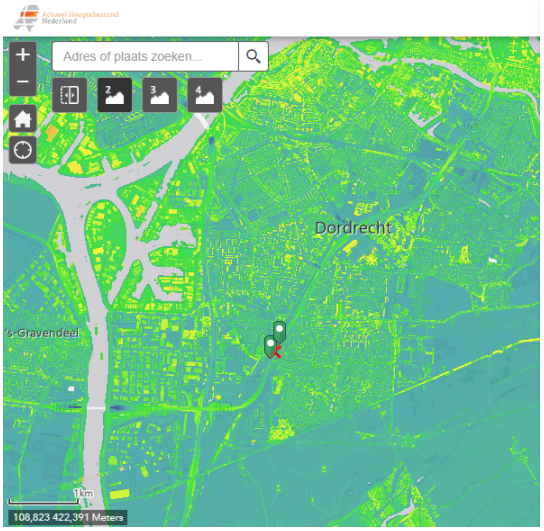

(b) Location elevation

Figure 5.7: AHN profile location 1

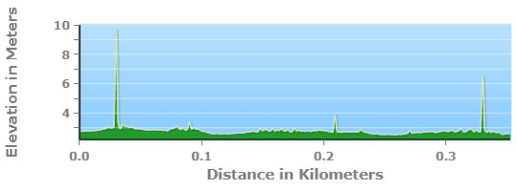

(a) Elevation of road

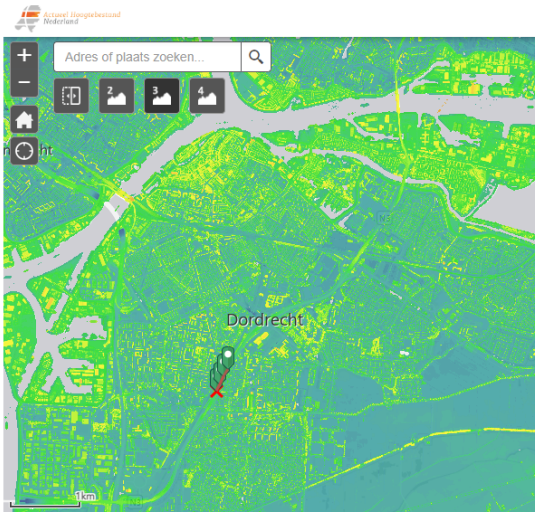

(b) Location elevation

Figure 5.8: AHN profile location 2

Displacement rate, yield stress and OCR

Based on the elevation and the soil layering as presented in figures 5.6 - 5.8, the initial effective stress can be determined. The next parameter necessary is the strain rate. For location 1, the displacement over the time is presented in Figure 5.9 and for location 2 the displacement over time can be found in Figure 5.10 a linear regression through these data points result in the displacement rates in millimetres per year, this is converted to strain rate with the soft soil layer thickness. Since the soft soil layer does not exist of 1 soil type, the determination of the yield stress has been done 3 times. First assuming all the soft soil is peat, in the second calculation the whole layer is assumed to be clay and in the last calculation a weighted average for the soil parameters is taken based upon the thickness of the different soils. For the latter one, the starting point for the calculation is presented in Table 5.2 and 5.3. For location 1, Figure 5.11a shows the yield stress with the influence of the different parameters. What can be seen is that the yield stress is very sensitive to the layer thicknesses and the volumetric weights but so is the initial stress state. Therefore, Figure 5.12a shows the over consolidation ratio and its sensitivity to the parameters. For the other two calculations (assuming the whole layer is either peat or clay) the yield stress for a clay layer is lower than for a mixed situation and for a peat layer the yield stress is higher and the same holds for the OCR's. The graphs of those scenarios can be found in Appendix C.2. For location two, the same calculations are done for the input parameters of the second location (Table 5.3). Figures 5.11b and 5.12b show the yield stress and OCR for the mixed soil layer and again for a full peat and clay layer the results can be found in Appendix C.2. As for the first location, the yield stress and OCR calculated for the second location for a full layer of peat are higher than for the mixed soil layer and lower for a full clay layer. The results for the strain rate, intrinsic time and OCR are listed in Table 5.4.

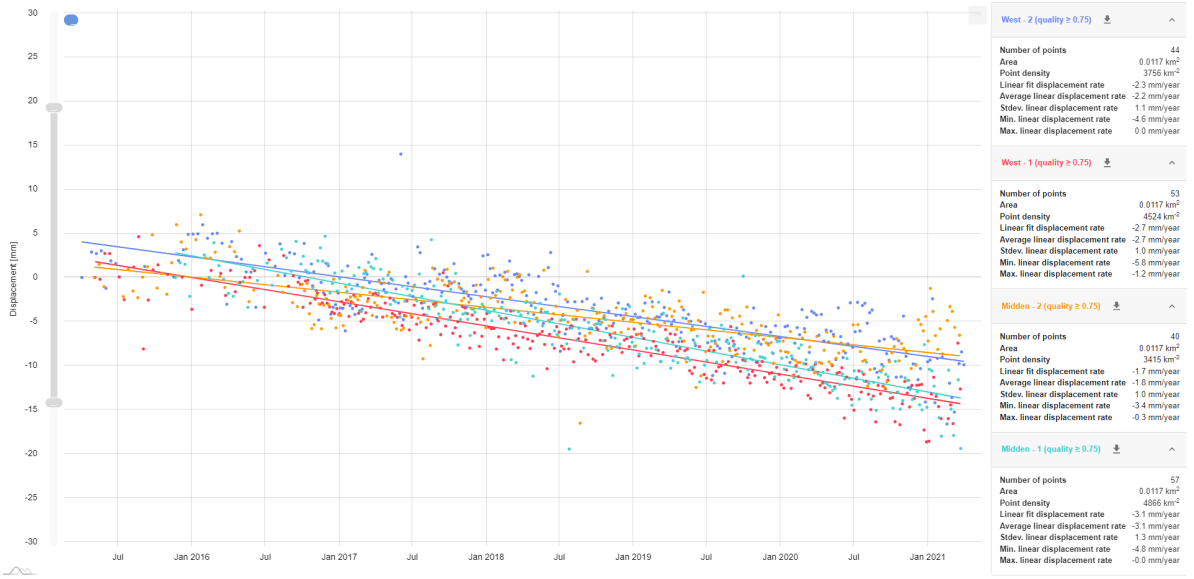

Figure 5.9: Displacement over time for location 1

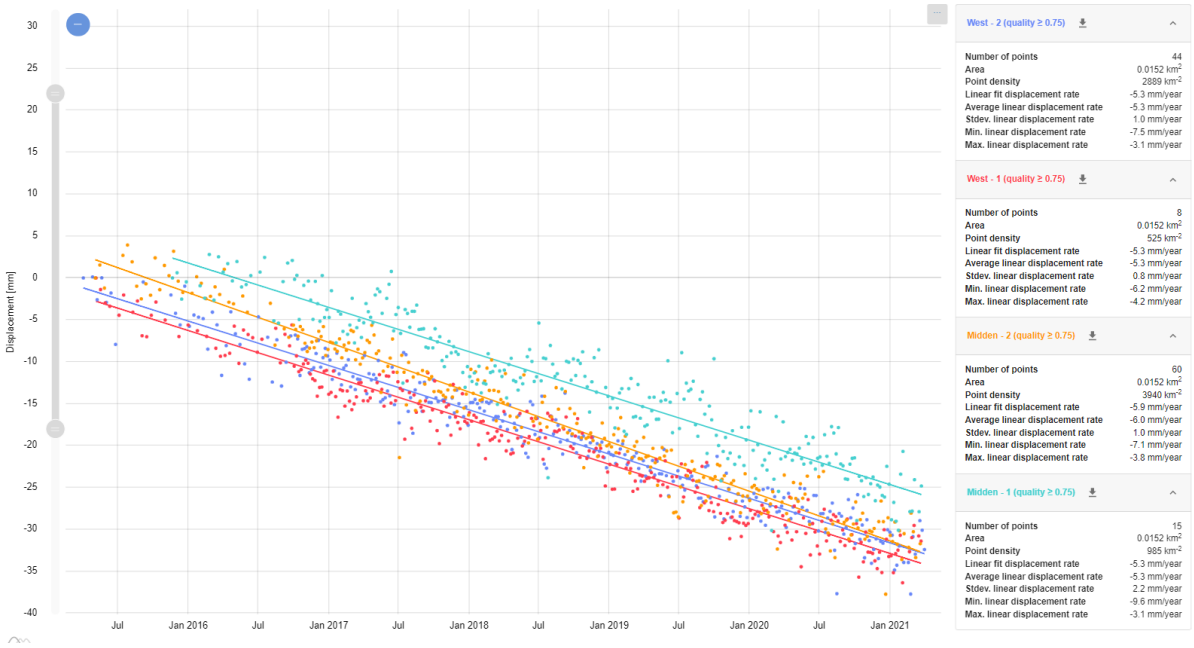

Figure 5.10: Displacement over time for location 2

Table 5.3: Soil properties

Parameter	Value location 1	Value location 2
H_{soft}	3.5 [m]	10 [m]
H_{sand}	2.5 [m]	5.5 [m]
$\frac{\delta z}{\delta t}$	-2.27 [mm/year]	-5.65 [mm/year]
$\sigma_{v;0}$	29 [kPa]	94 [kPa]

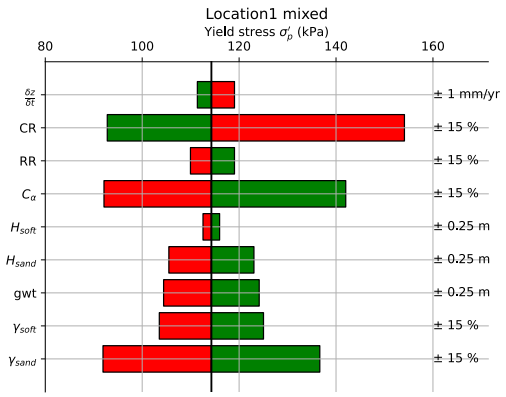

(a) Yield stress sensitivity for different parameters

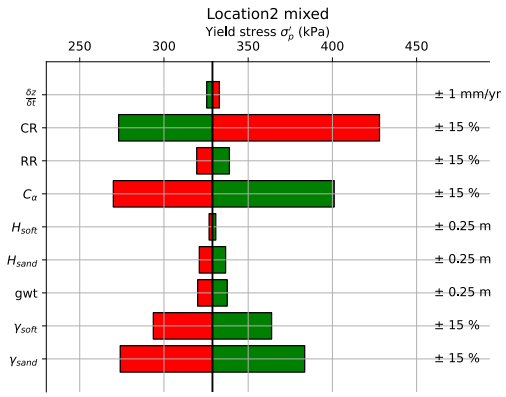

(b) Yield stress sensitivity for different parameters

Figure 5.11: Yield stresses for two locations . The green bar indicate that a parameter is bigger, the amount of variation is shown right.

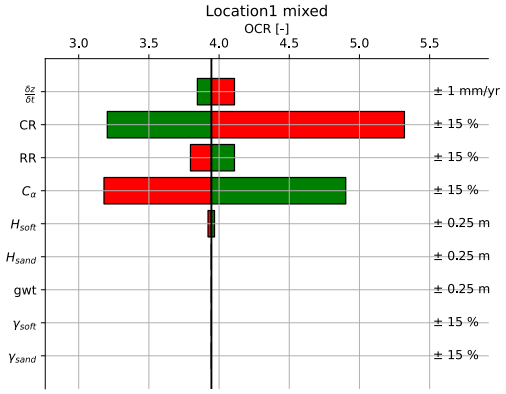

(a) OCR sensitivity for different parameters

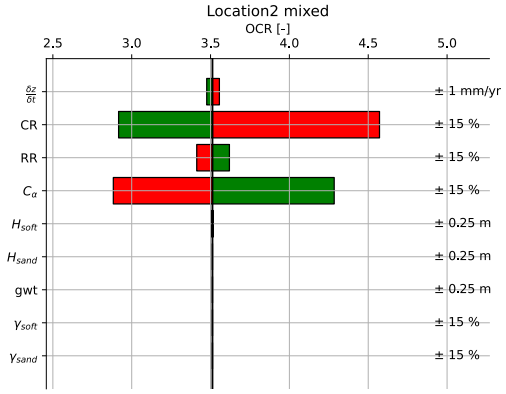

(b) OCR sensitivity for different parameters

Figure 5.12: OCR's for two locations. The green bar indicate that a parameter is bigger, the amount of variation is shown right.

(a) Intrinsic time sensitivity for different parameters

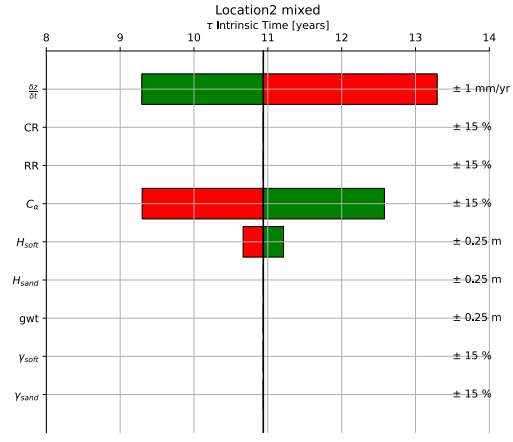

(b) Intrinsic time sensitivity for different parameters

Figure 5.13: Intrinsic time for two locations. The green bar indicate that a parameter is bigger, the amount of variation is shown right.

Table 5.4: InSAR results for strain rate, intrinsic time, yield stress and OCR

Parameter	Location 1	Location 2
$\dot{\varepsilon}$	2.07 e-6 [1/day]	1.54 e-6 [1/day]
τ	9.3 [year]	10.9 [year]
σ'_p	114 [kPa]	327 [kPa]
OCR	3.9 [-]	3.1 [-]

5.1.3. Discussion

This part of the study focused on the derivation of a yield stress based on InSAR measurements. It can be seen that over a period of multiple years, a clear trend was visible in the displacements over time for two separate locations (Figures 5.9 - 5.10). Together with available soil investigation, elevation maps and laboratory tests it was possible to derive a yield stress. Laboratory tests were conducted on bore hole samples located along the road in almost virgin soil. This implies that the compressibility parameters can be derived quit well except for the yield stress. It can be seen in Figures 5.11a - 5.12b that the settlement parameters affect the yield stress and the OCR more than the displacement rate. From the displacement rate, the strain rates and intrinsic times were calculated and what can be seen in Table 5.4 is that even though the calculated yield stress and OCR are high, the intrinsic time is only 9.3 and 10.9 years. Something else that can be seen in Figures 5.13a and 5.13b is that the intrinsic time is highly dependent on the measured displacement rate and that the standard deviation in the measurements (1 and 1.1 mm/year) causing a wide range for the intrinsic time.

An explanation for the high yield stress and OCR while the intrinsic time is not that high is that the intrinsic time is a linear function of the strain rate and C_α while the yield stress and OCR are dependent on the power of $(CR - RR)/C_\alpha$. The yield stress, intrinsic time and OCR are derived according to the linear isotach model (NEN-Bjerrum), this could be an explanation for the high yield stress. When a non-linear isotach model is used, the isotach spacing reduces over time and a smaller yield stress can be found. Figure 5.14 illustrates this principle. In the left figure a stress-strain space is drawn with linear isotachs, starting from a point with a fixed stress, strain and strain rate the RR line can be followed to determine the intersection with the CR line which is the yield stress. This distance is dependent on the spacing of the isotachs which for linear isotachs is constant. However when non-linear isotachs are considered as is the case in the right drawing, the same starting point is considered with the same stress, strain and strain rate and again the RR line must be followed until the intersection with the CR line to find the yield stress. It can be seen that when the spacing between isotachs reduces over time, e.g. further away from the 1-day isotach (CR-line), the distance between the starting point and the intersection is smaller. This leads to a lower yield stress than for the linear isotach models.

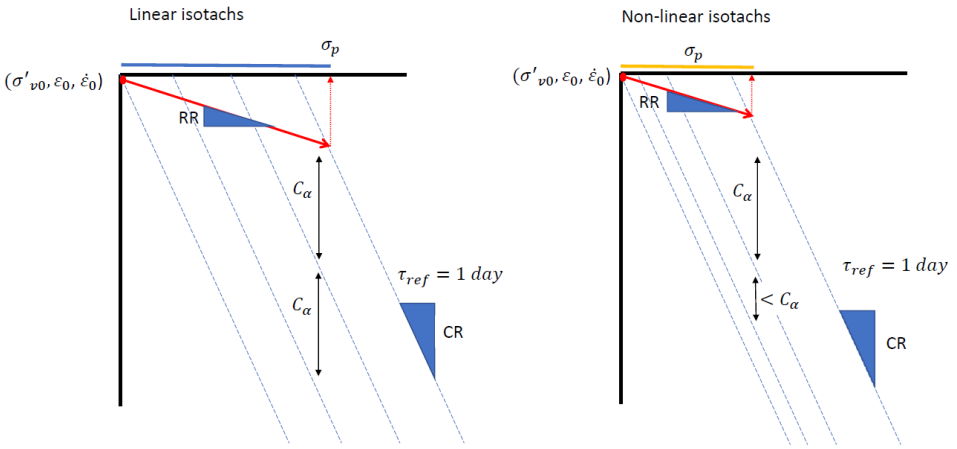

Figure 5.14: Yield stress for linear and non-linear isotachs

5.2. A2: post diction

5.2.1. Methodology

For the A2 project, a post diction of Visschedijk and Temmerman (2009) will be used and compared with displacement rates measured by InSAR. During construction of the embankment "Westbaan" several cross sections have been studied with settlement plates and these settlement measurements were used to fit the soil parameters in D-Settlement (fit for settlement plate). In Visschedijk and Temmerman (2009) the soil layering and load schemes for every cross section are given and those are implemented in D-Settlement. The soil profile for the whole project area is given by Figure 5.15 and the soil parameters can be found in Table 5.5. After fitting the linear isotach model to the D-Settlement calculations the strain rates will be compared with the measured displacement rates by InSAR. Figure 5.16 gives an overview of the displacement rates and it can be clearly seen that the newly constructed lane in the west settles faster than the already existing lane in the east.

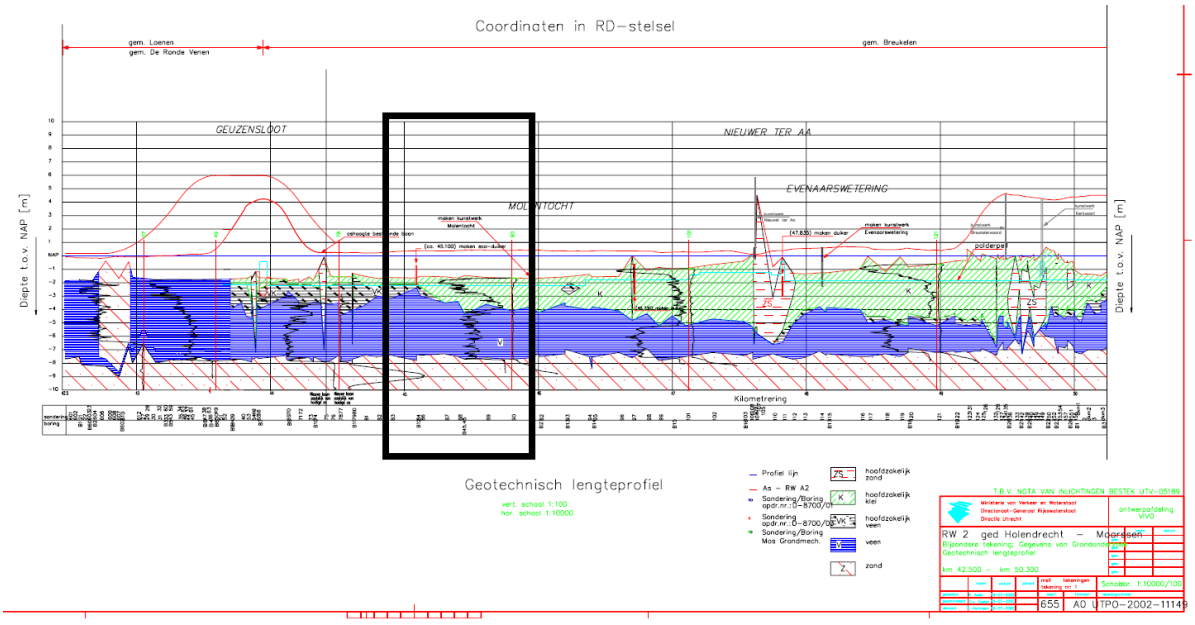

Figure 5.15: Soil profile A2, the area Westbaan is located in the black square Visschedijk and Temmerman, 2009

Figure 5.16: Displacement rates A2

Table 5.5: Soil parameters (Visschedijk & Temmerman, 2009)

Parameter	Value
Sand	
$\gamma_{sand;sat}$	19 [kPa]
GWT	NAP - 2.2 [m]
γ_{water}	10 [kPa]
Clay	
RR	0.132 [-]
CR	0.237 [-]
C_α	0.026 [-]
$\gamma_{clay;sat}$	14 [kPa]
H_{clay}	0.8 [m]
Peat	
RR	0.1896 [-]
CR	0.409 [-]
C_α	0.0312 [-]
$\gamma_{peat;sat}$	10.2 [kPa]
H_{peat}	5 [m]

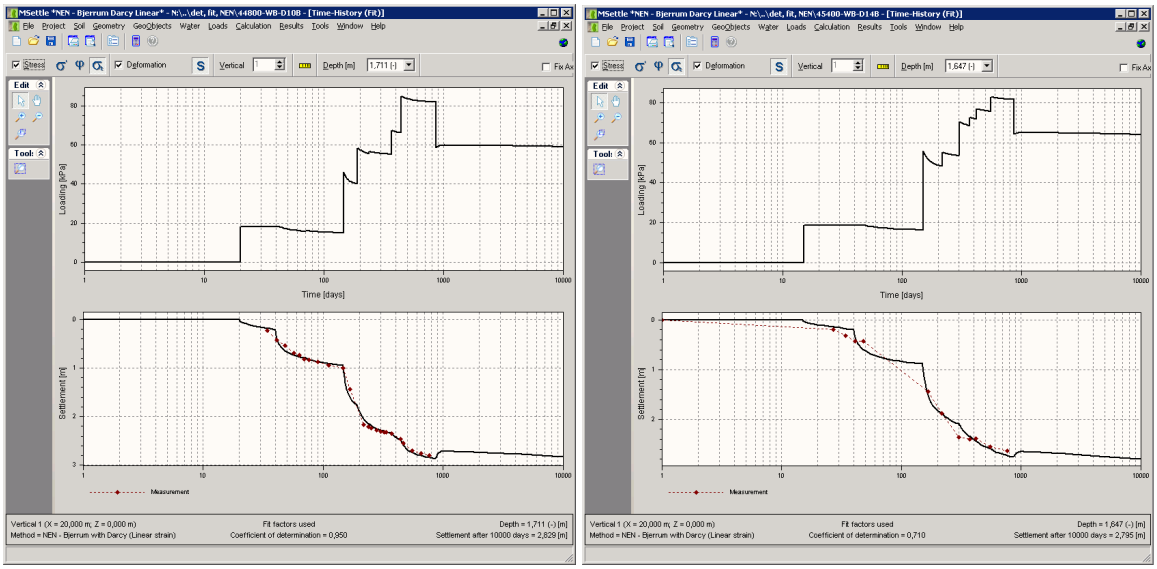

(a) D10B stress and settlement over time

(b) D14B stress and settlement over time

Figure 5.17: Results of Visschedijk and Temmerman (2009) after settlement plate fit

For the comparison, two cross sections are considered: D10 and D14. The loading schemes and the settlement predictions after settlement plate fit are shown in Figures 5.17a and 5.17b. These figures have been reproduced in D-Settlement, the used cross sections can be found in Appendix C.5. Based on the fitted D-Settlement measurements, the linear isotach model as presented in Chapter 3 is fitted on those predictions. For the python implementation of the linear isotach model to fit, soil parameters

must be adapted because of simplifications in the python implementation compared to the D-Settlement analysis. Simplifications in the python implementation are: no submerging, no vertical drainage and dimension limitations (the python implementation considers 1D compression only while the D-Settlement model uses a 2D cross section). Once the linear isotach model has been fitted to the D-Settlement results, the C+S model will be used to reach the displacement rate measured by InSAR. In this way the goal is to keep the settlement predictions before unloading close to the D-Settlement results, which are in accordance with settlement plates, and also be in accordance with the measured data from InSAR. The displacement rates according to InSAR measurements for the two cross sections D10 and D14 are shown in Figures 5.18a and 5.18b. The average displacement rate for D10 is 2.25 ±0.39 mm/year and for D14 it is 2.46 ±0.60 mm/year.

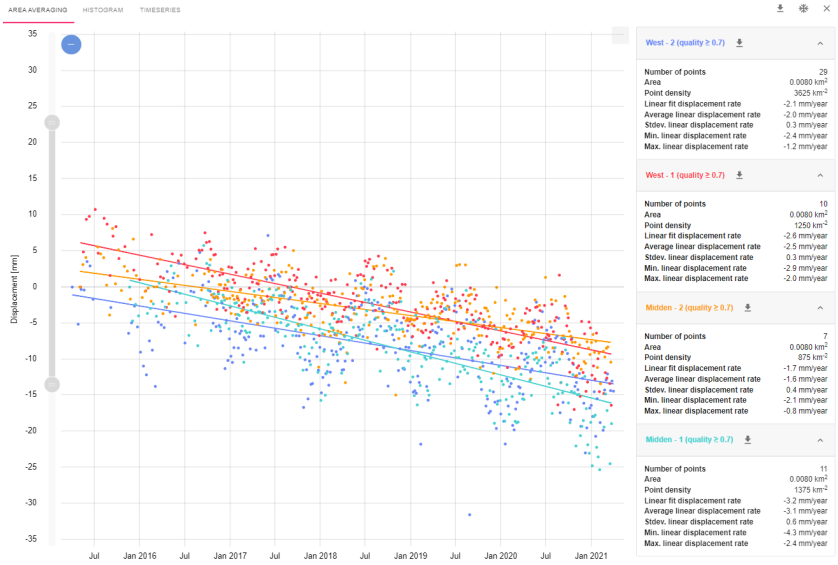

(a) D10 displacement rate (2.25 ±0.39 mm/year for 57 data points)

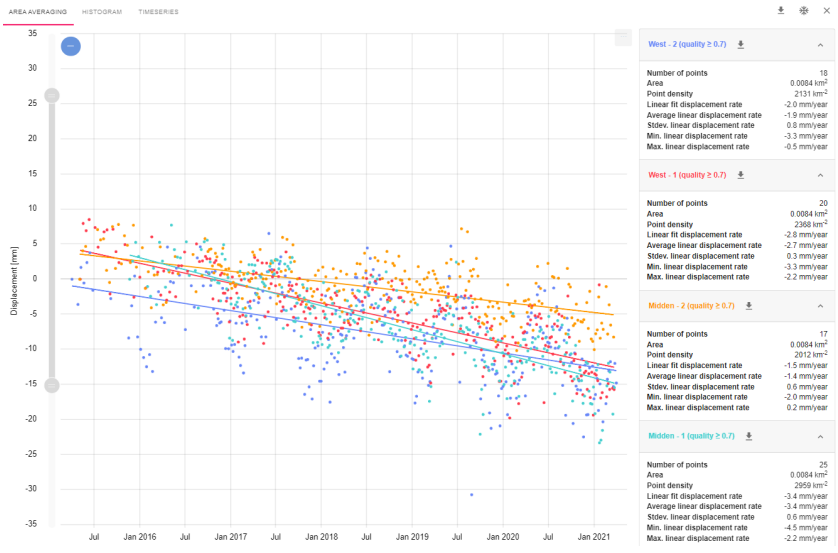

(b) D14 displacement rate (2.46 ±0.60 mm/year for 80 data points)

Figure 5.18: Displacement rate measurements by InSAR

5.2.2. Results

Cross section: D10

Figure 5.19 shows the results of the D-Settlement predictions for the stress over time and the stress development according to the python implementation. What can be seen in this figure is that the stress develops faster in the D-Settlement analysis, this could be due to the vertical drains that reduce the

consolidation period. Next, it is visible that submerging reduces the stress level over time for the D-Settlement calculation while in the python implementation stress levels remain constant. Figure 5.20 shows that in the first steps the D-Settlement calculations predict less settlement than the python implementation does. An explanation for this is submerging; lower stress levels reduce the development of strain and therefor settlement. Since this study is focusing on long-term behaviour this difference is neglected. For long-term behaviour it was necessary to match the final steps which match quit well when looking at Figure 5.21.

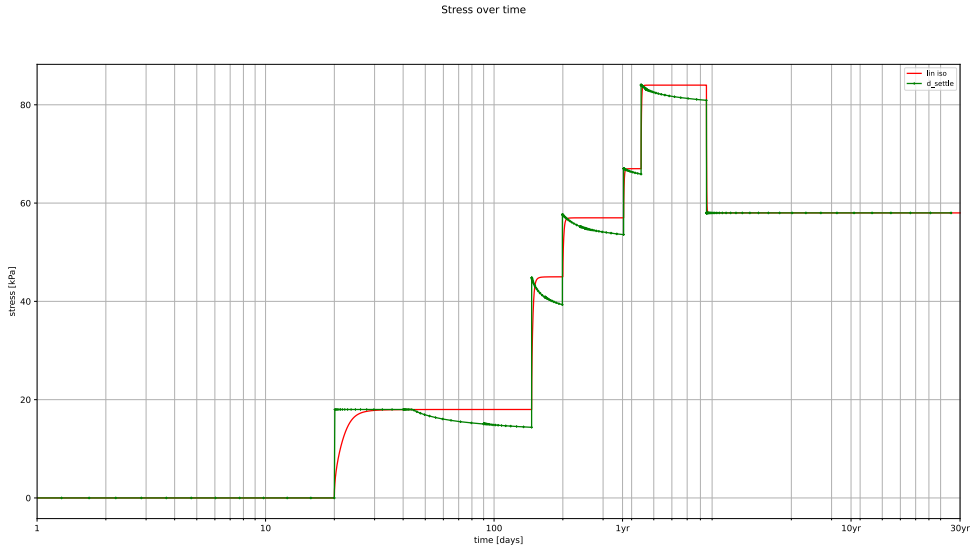

Figure 5.19: Stress over time for D10 for D-Settlement analysis and python implementation of the linear isotach model (similar to the C+S model)

Figures 5.20 and 5.21 show the development of settlement over time for the complete loading scheme (Figure 5.20) and from 1000 days after start of the construction (Figure 5.21), in this graph the settlement at day 1000 is set to zero so the development of the residual settlement can be seen.

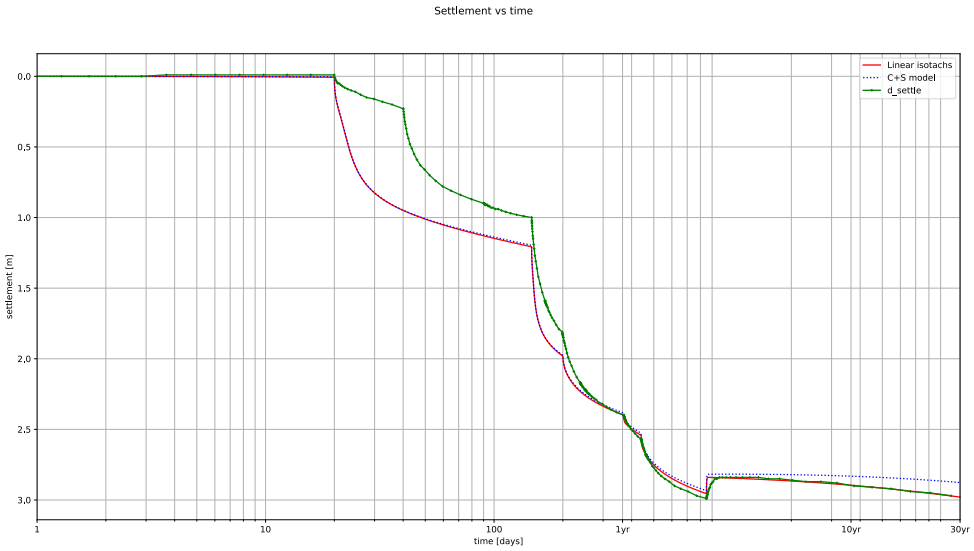

Figure 5.20: Settlement over time for D10 for calculation of D-Settlement, linear isotach model and the C+S model

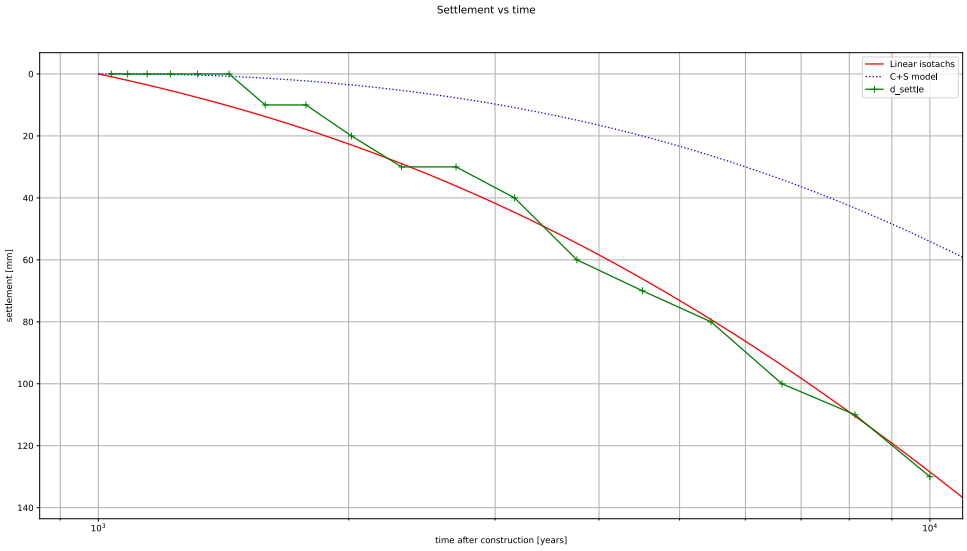

Figure 5.21: Settlement after 1000 days for D10 for calculation of D-Settlement, linear isotach model and the C+S model

To match the D-Settlement and python implementation of the linear isotach model, it was necessary to change the soil parameters. Table 5.6 present the factors that are applied on the weighted averages of RR, CR and C_α from Table 5.5. In Figures 5.20 and 5.21 the blue dotted line presents the implementation of the C+S model. For the C+S model the same values for RR, CR, C_α are used as for the linear isotach model and viscoplastic swell and non-linearity is added to match the displacement rate found by the InSAR measurements. It can be seen in Figure 5.20 that the C+S model predicts almost the same settlement upon loading, in Figure 5.21 it can be seen that after unloading the C+S model shows different settlement development.

Table 5.6: Soil parameter input for linear isotach implementation with fit factors

Parameter	Weighted average	fit factor
RR	0.18 [-]	0.8
CR	0.39 [-]	1.35
C_α	0.03 [-]	1.65
γ_{soft}	10.7 [kPa]	1

The comparison of the displacement rates based on the linear isotach model, the C+S model and the measurement by InSAR is presented in Figure 5.22. In the left graph of Figure 5.22 the displacement rates for the C+S are shown and it can be seen that due to the viscoplastic swell the swell period is longer and that the total displacement rate (black dotted line) is smaller than for the linear isotach model, right graph. Next to the viscoplastic swell this is also due to the non-linearity, due to non-linearity the creep strain rate (red line) is lower for the C+S model than for the linear isotach model. The linear isotach model predicts a displacement rate 5.95 mm/year after 10 years of unloading while the C+S model predicts a displacement rate of 2.50 mm/year. The measured displacement rate by InSAR is 2.25 ±0.39 mm/year. The used viscoplastic swell and non-linearity parameters are presented in Table 5.7.

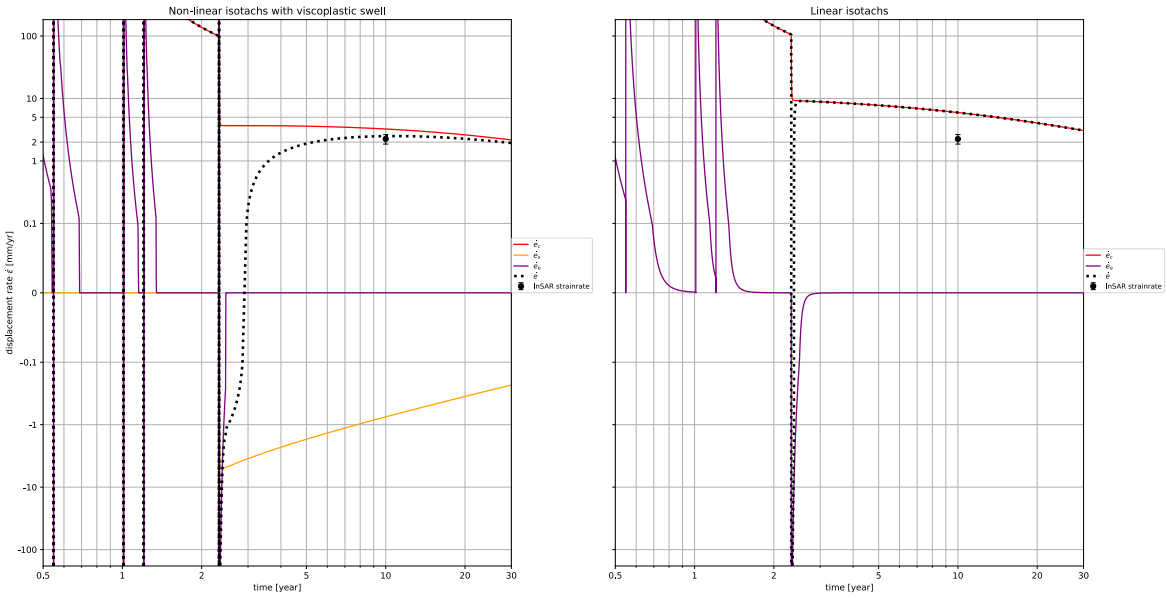

Figure 5.22: Displacement rates for D10. Left: C+S model; right: linear isotach model

Table 5.7: Parameters for viscoplastic swell and non-linearity for the C+S model to fit the InSAR measurements for D10 and D14

Parameter	D10	D14
β_2	0.2	0.2
β_3	7.5	8.55
b_1	-0.9	-0.4
m_1	0.9	0.9
b_2	-8	-7
m_2	4	4

Cross section: D14

For cross section D14, the same method as for D10 was applied with initially the same C+S model parameters (see column D10 in Table 5.7). Figure 5.23 shows the stress development and similar to the D10 cross section the development of stress according to D-Settlement shows a shorter consolidation period and a decrease after some time since submerging is included. In Figures 5.24 and 5.25 the settlement over time for the linear isotach model and the C+S model diverge in the last step, after unloading.

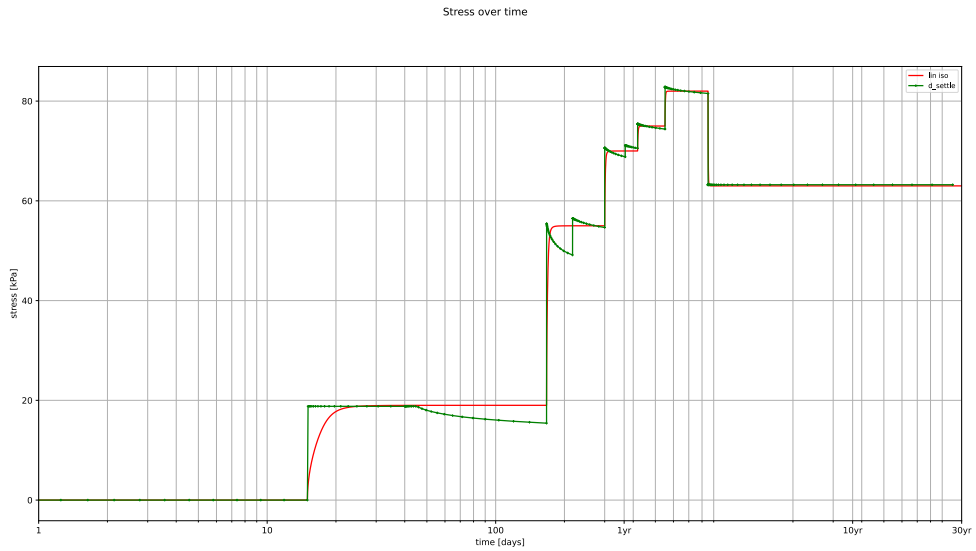

Figure 5.23: Stress over time for D14 for D-Settlement analysis and python implementation of the linear isotach model (similar to the C+S model)

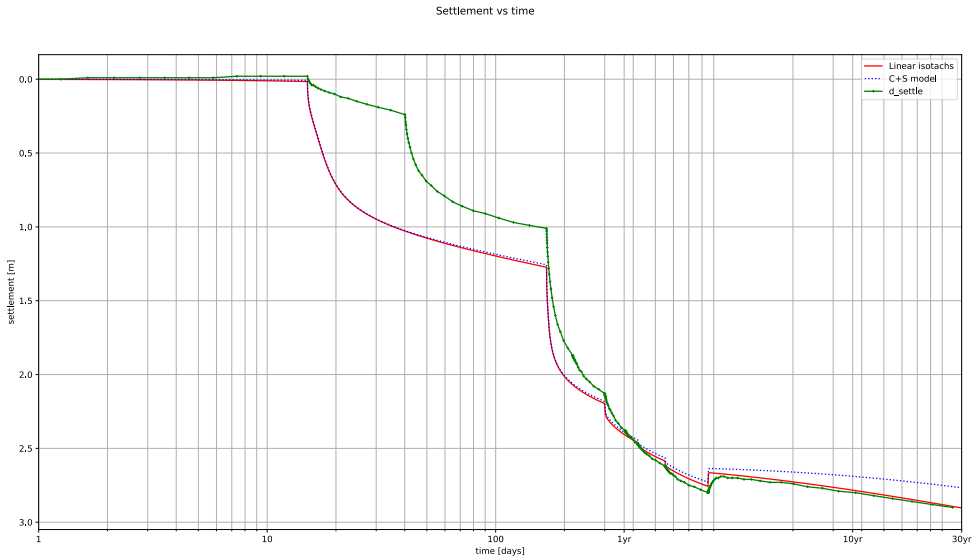

Figure 5.24: Settlement over time for D14 for calculation of D-Settlement, linear isotach model and the C+S model

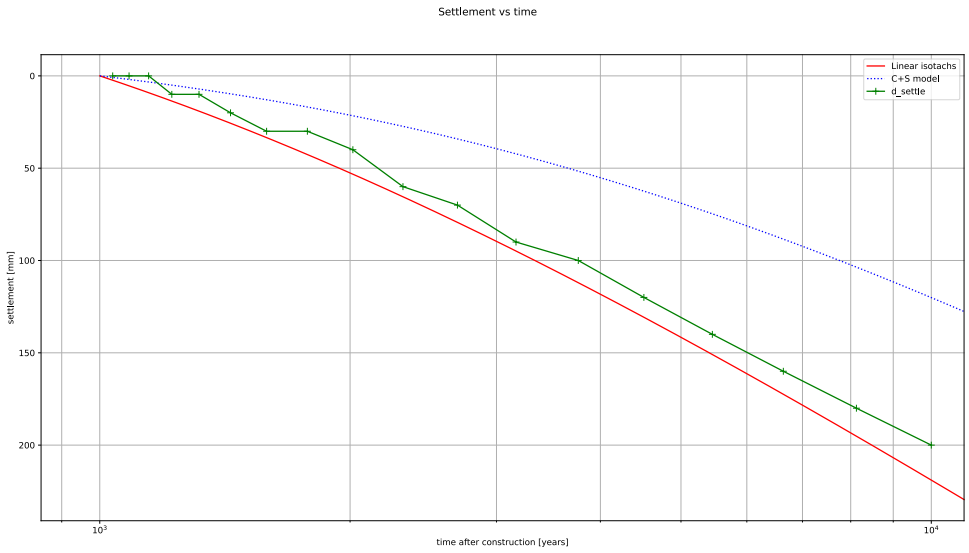

Figure 5.25: Settlement after 1000 days for D14 for calculation of D-Settlement, linear isotach model and the C+S model

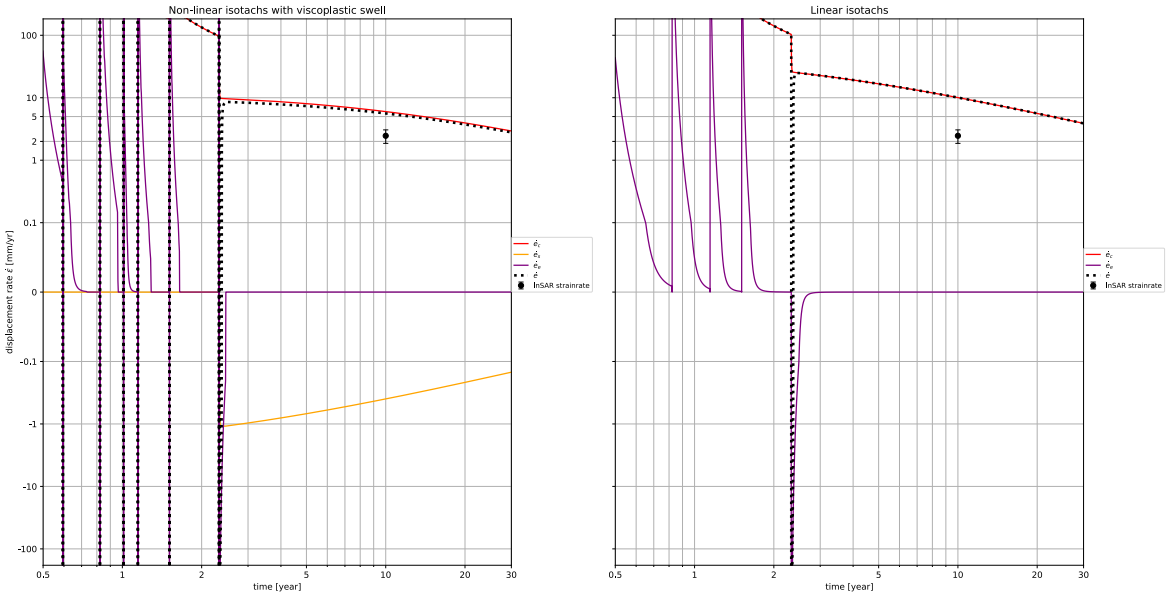

Figure 5.26: Displacement rates for D14. Left: C+S model; right: linear isotach model

Despite the less predicted settlement with the C+S model, Figure 5.26 shows that the displacement rate after 10 years is still higher than measured; 5.09 mm/year for the C+S model, 10.06 mm/year for the linear isotach model and 2.46±0.60 mm/year measured by InSAR. Different from D10, the viscoplastic swell strain rate (yellow line) in this cross section has a lower initial value and reduces faster. Next to that, the creep strain rate (red line) is higher after unloading. To get a better fit, the initial viscoplastic strain rate is increased by increasing b_2 from -8 to -7 and the reduction of the viscoplastic strain rate is slowed down by increasing b_1 from -0.9 to -0.4. This parameter b_1 controls the magnitude of $\hat{C}_{\alpha;s}$ which on its turn controls the rate of change in viscoplastic strain rate (see equations 2.26- 2.28). Next to the viscoplastic swell parameters the non-linearity parameter β_3 was also adapted in a way that the creep strain rate after unloading is lower. With a β_3 value of 8.55 the predicted displacement rate after 10 years is close to the InSAR measurement with a displacement rate of 3.41 mm/year. Figures 5.27 - 5.29 show the results for the C+S model with the adapted parameters for the settlement over time,

settlement after 1000 days and the displacement rate. A bigger change in the parameter β_3 would give an even better fit to the measured displacement rate but it would also give a worse fit upon loading and is therefor not used.

$$\ddot{e}_s = -\frac{\dot{e}_s^2 \cdot ln(10)}{\hat{C}_{\alpha;s}} \quad \text{(2.26 revisited)}$$

$$\frac{\hat{C}_{\alpha;s}}{C_{\alpha;NC}} = 10^{b_1}(OCR - 1)^{m_1} \quad \text{(2.27 revisited)}$$

$$\dot{e}_{s;init} = 10^{b_2}(OCR - 1)^{m_2} \quad \text{(2.28 revisited)}$$

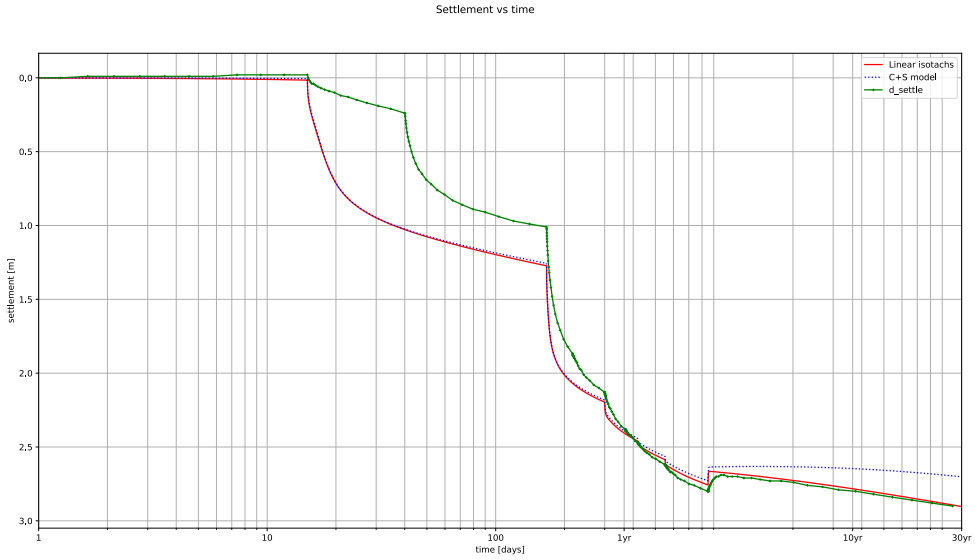

Figure 5.27: Settlement over time for D14 after fit for calculation of D-Settlement, linear isotach model and the C+S model

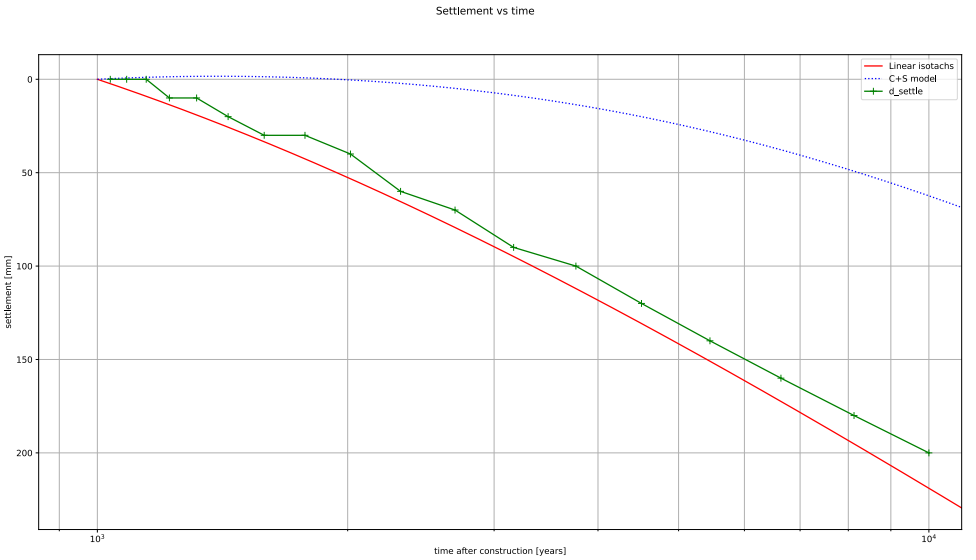

Figure 5.28: Settlement after 1000 days for D14 after fit for calculation of D-Settlement, linear isotach model and the C+S model

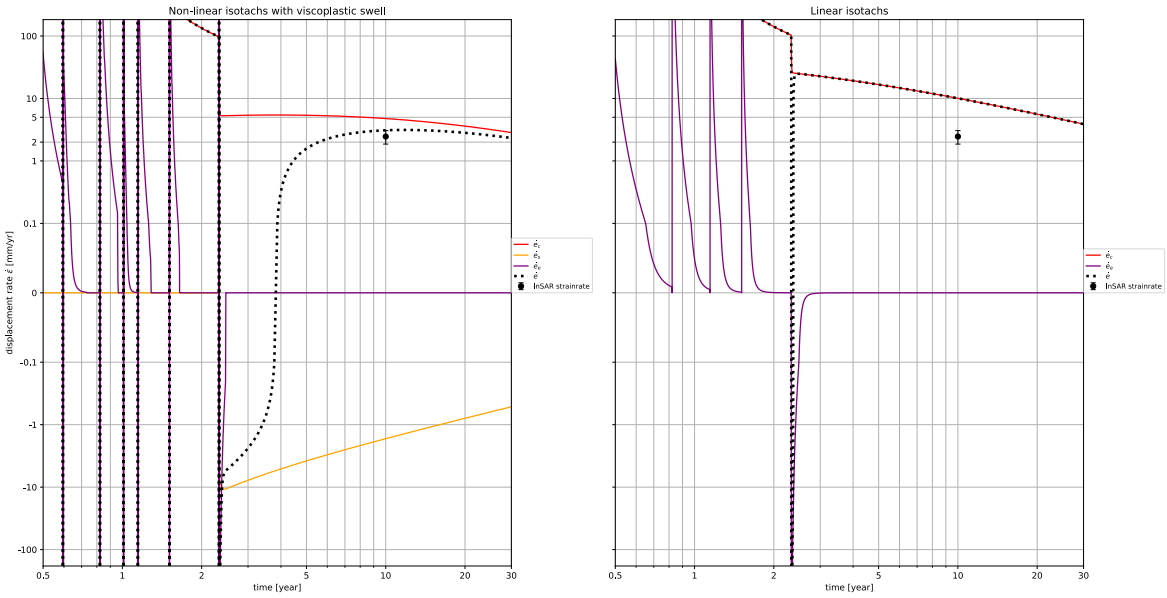

Figure 5.29: Displacement rates for D14 after fit. Left: C+S model; right: linear isotach model

Table 5.8: Sum up of displacement rates

Method	Displacement rate D10 [mm/year]	Displacement rate D14 [mm/year]
InSAR	2.25 ±0.39	2.46 ±0.60
Linear isotach model	5.95	10.06
C+S Model	2.50	3.41

5.2.3. Discussion

By comparing the displacement rates measured by InSAR with the predictions made by Visschedijk and Temmerman (2009) the first notable point is that the InSAR measurements show lower rates for both cross sections D10 and D14. Next, for the comparison of the linear isotach model and the C+S model with InSAR measurements it was necessary to fit the linear isotach model to the D-Settlement predictions. A difference between the two calculations is caused by the stress development. The influence of submerging is visible in all load increments and causes a decrease in stress and with that less settlement, this effect becomes smaller when stress levels become higher. These differences in the early load increments are neglected because in the last load increment, the unloading step, the stress is almost identical and the settlement development is as well for D-Settlement and the linear isotach model (Figures 5.21 and 5.25). This part is considered most important since this study focuses on long-term settlement behaviour. It can also be seen that the C+S model is able to predict almost the same settlement during loading as the linear isotach model but after unloading a different behaviour is found for both D10 and D14. The viscoplastic swell makes that compression starts later and that the total strain rate, and therefor displacement rate, is reduced compared to the linear isotach model where it is only dependent on the creep strain rate (after consolidation). Next to the viscoplastic swell, non-linearity also causes a better fit to the InSAR displacement rate. When β_3 is larger than $(C_c - C_r)/C_\alpha$ there is a stronger reduction in strain rate than in the linear isotach model due to a change in stress. The value of β_2 makes that the $\hat{C}_\alpha$ also reduces when there is a change in OCR. Based on these results it looks like the linear isotach model and the D-Settlement calculations give a conservative prediction with a higher displacement rate and therefor higher residual settlement than might be expected when looking at the InSAR measurements. It was shown that the C+S model is able to give a better fit to these measurements but this only based on measurements after 10 years.

6 Conclusion

6.1. Sub-Question 1

How can InSAR be used for settlement predictions done by isotach models?

In Chapter 2 different isotach models were introduced and one of the unknown parameters which could have been determined based on InSAR is the yield stress. Section 5.1 shows that is possible to determine a yield stress based on the measured displacement rate but soil layering, soil properties and topography must be known. By using linear isotachs with the measured strain rate and secondary compression parameter (C_α) the intrinsic time (τ) can be calculated. For the two locations at the N3 the resulting yield stress and OCR seems to be high but since no laboratory tests are performed on the soil below the road this can't be validated. The determined yield stress and OCR are the aged values so high values for yield stress and OCR are not necessarily wrong. When soil tests are performed on this soil and smaller values for the yield stress are found than calculated through InSAR, the non-linear isotach model could provide an explanation for this.

Section 5.2 was used for the validation of long-term settlement behaviour of two cross sections of a new embankment for a highway (A2). The results show that the predicted displacement rates based on linear isotach models are larger than the measured displacement rates. With the same soil parameters as for the linear isotach model it was possible to get a better fit by using the C+S model. The use of non-linear isotachs and viscoplastic swell made it possible to get a settlement development during loading in accordance with the prediction of D-Settlement after settlement plate fit and also be in accordance with the measured displacement rates by InSAR.

From this study it can be concluded that InSAR can be used to analyse the settlement behaviour after construction, something which is not possible with for example settlement plates. A disadvantage of InSAR is that the measured displacements are relative to the first measurement in time. However it could give a good insight in the behaviour the soil is experiencing.

6.2. Sub-Question 2

How do transient changes in pore pressures relate to extra settlement?

Temporal changes in the pore pressures affect the settlement behaviour. First mentioned in Section 2.2, a change in groundwater table will affect the degradation of organic matter if present in the soil. Next to that, in the simulations with changing groundwater table it can be seen that fluctuating groundwater tables barely change the long-term result of settlement predictions. However, the behaviour is different and an oscillating prediction is found around the average groundwater table. Besides the oscillation also the magnitude of the amplitude has been changed in the simulations. It has been found that an increasing amplitude does not affect the final settlement prediction either.

What does affect the outcome of the settlement prediction is the average groundwater table. By changing it over time it was shown that the effective stress level changes and so do the strain and settlement

predictions. In accordance with the calculation of effective stress, an increase in groundwater table causes more pore pressure and a lower effective stress which reduces the predicted strain. On the other hand, a decrease in average groundwater table would increase in the effective stress and it would predict larger settlements than with a constant groundwater table.

Based on the above it can be concluded that temporal fluctuations in pore pressure do not cause extra settlements calculated by isotach models. However, a more permanent change in water level will.

6.3. Sub-Question 3

How does degradation of organic matter cause extra settlement and is it quantifiable?

In Chapter 2 a literature review has shown that there are two different types of influence the organic matter has in soil settlement. The first discussed influence is the degradation of organic matter. Due to multiple causes a part of the organic remains in the soil can change into gas. This can be aerobic and anaerobe resulting in CO_2 and CH_4. It has been found that the organic matter can be used for quantifying a change in void ratio. However this equation uses the organic matter as in input parameter and it can not be predicted easily. Nevertheless this equation could be used to describe a change in void ratio due to decay of organic matter when organic matter content is determined at multiple time intervals. With this, extra settlement can be attributed to the decay of organic matter.

The second influence organic matter has on the settlement behaviour of a soil is found by an extension of the consolidation equation of Terzaghi. In the conventional consolidation equation of Terzaghi the change in volume is due to the flow of water and in addition the compressibility of water (or mixed with gas) can be changed. The new found model expands the equation by assigning a change of volume to flow of water, compression of gas and compression of organic matter. To do so, this new model considers soil as a three phase medium consisting of gas, water and solids and it splits the solid phase up into organic and mineral solids and states that organic solids are compressible. The results show that this new model follows the settlement and strain curves over time from laboratory results better than the conventional equation. What however should be concluded is that this only changes the settlement behaviour until the end of primary consolidation and does not change the final result significantly. This can also be seen in the results, the final settlements and strains are close for both models. This would mean that it does not necessarily improve the long-term settlement predictions. Besides it should be compared with a model that also takes secondary compression into account whilst the Terzaghi equation only calculates direct compression.

6.4. Sub-Question 4

How do adapted isotachs represent strain rate behaviour of soils compared to equally spaced isotachs

In Chapter 2 first the non-linear isotachs have been introduce to describe a different behaviour in which the strain rate over time decreases faster than for linear isotachs. Later this is combined with extra viscoplastic swell in the Creep + Swell model. In Section 3.1 one can see that with the C+S model a wider range of settlement predictions can be made, e.g. linear and non-linear isotachs can be used and viscoplastic swell can be added if preferred.

In Section 3.2 the results of the analysis on Mexico Clay show that the C+S model is able to predict the measured strain with the inclusion of viscoplastic swell even though not all parameters can be derived from laboratory results. When looking at the strains upon unloading the features of the viscoplastic swell become clear, after a period of consolidation the measured development of strain and the simulated development of strain overlap and are still increasing. This behaviour is not captured in the linear isotach model, in this linear isotach model the swell is only due to elastic deformation till the end of consolidation and afterwards creep strain dominate the strain. By the use of a smaller reloading and unloading ratio and the inclusion of viscoplastic swell, the strain prediction in the first loading steps, prior to the yield stress, are closer to the measurements than the linear isotach predictions while they do not deviate upon unloading either.

Furthermore in Section 3.3 simulations of incremental loading tests have been performed to get a better understanding of the difference between the two models. A first conclusion is that during the ”standard” incremental loading test simulations the predictions are only affect a very small amount when load exceeds the yield stress but final settlements are still comparable. However the influence of the viscoplastic swell is clearly visible in the results of the ”standard” incremental loading tests.

In the results of the ”unloading” incremental loading tests the two features of the C+S model are visible. First of all, just as for the ”standard” test, viscoplastic swell is found. Similar to the observations in the Mexico Clay analysis, it has been found that a higher value of OCR leads to an higher initial viscoplastic strain rate and also to more viscoplastic strain due to the larger values of respectively $\dot{e}_{s;init}$ & $C_{\alpha;s}$. Secondly the influence of the non-linearity is larger than it was in the ”standard” test. This is due to the fact that the time steps were larger and creep plays a more important role especially after the final step were a small unloading step is followed by 36 days with a constant load to detect the creep. It can be concluded from this comparison that non-linearity result leads to smaller strain and settlement predictions than linear isotachs.

After the comparison of both models in a laboratory situation, simulation of field situations in Section 3.4 show comparable results. The C+S model with non-linear isotachs predicts less creep and the the final settlements are less than predicted by the linear isotach model. When the C+S model is used and linear isotachs are used it can be seen that the final settlements are similar but that the settlement behaviour is different. The swell behaviour predicted by the C+S model not only results in a larger swell but also in higher strain rates after the swell period. After some time the strain rates converges for both models. Therefore, it can be concluded from these simulations that the C+S model, with the proposed non-linear parameters, predict less final settlement and when linear isotachs are used final settlements are the same but a different behaviour is found after unloading.

6.5. Main-Question

Are long-term settlements predicted well by current prediction models and if not, what adjustments should and can be made?

Long-term settlements have been analysed with the use of InSAR, the results show that the measured strain rates are smaller than predicted by the linear isotach model (NEN-Bjerrum). Adjustments that can be made are the use of non-linear isotachs and the inclusion of viscoplastic swell, for example by using the C+S model. This model, as shown by different simulations and comparison with incremental loading test on Mexico Clay, is able to predict unloading behaviour better than linear isotach models. Since this is often the case for embankments like at the A2, the C+S model should be further investigated and validation of settlement behaviour both on short and long-term should be considered. The short term behaviour is important to validate the viscoplastic swell theory used in the C+S model and to compare strain rates after the transition to creep where a higher strain rate with a faster decay could be found if linear isotachs are combined with viscoplastic swell or whether the strain rates are lower as will be the case with non-linear isotachs. This could result in predictions with less residual settlement. Next to that, the inclusion of volume loss due to degradation of organic matter can be important as well and further research should quantify its importance. If it turns out to play a significant role the degradation of organic matter must be made quantifiable and included in settlement models as well. Finally, if a long-term groundwater table prediction is present this must be included as well since it would change the stress state of the soil.

7

Recommendations

In this study the long-term settlement behaviour for small loading steps are considered and a new approach for prediction was compared with models that are currently used in engineering practice. Based on the results and conclusions presented throughout this thesis some recommendations for further research are listed below.

Organic Matter

- In peat areas it is unavoidable that organic matter decays. The focus for this study is that there can be a loss of volume due to the decay but for other study fields the accumulation of greenhouse gases like CO_2 and CH_4 can be interesting as well. For that reason more research on the degradation of organic matter should be done. For settlement related problems it is first of all interesting to monitor the amount of settlement which is caused by the degradation of organic matter and quantify its significance.
- For different purposes but especially when above mentioned research shows that the degradation of organic matter plays a significant role in settlement problems, a study should be performed on predicting the degradation and see if the degradation can be made quantifiable.
- With respect to the new found consolidation theory in which organic matter compression is taken into account, further research should focus on the comparison with settlement models. In the literature the new model has been compared with the Terzaghi equation which only predicts settlement during consolidation and this new model can also compress after the consolidation period. For that reason it should be compared with an isotach model.

InSAR

- It was shown that with the use of InSAR it was possible to derive the yield stress. However, this yield stress can not be validates as long as there is no soil investigation on soil below the road. Further research should focus on the validation of the yield stress based on InSAR.
- In this study only long-term settlement is observed. Another study could be set up to validate the whole lifespan, e.g. a more targeted study on a highway location that would measure the displacement during construction, just after construction and for a longer period after construction. In this way the measurements could be compared with settlement plates and also with the predicting models.

Groundwater Table

- With respect to the ground water table problem it is recommended to include long-term changes in the average water table. As was shown, transient changes do affect the predictions significantly by more permanent changes do so they should be taken into account.

Settlement Models

- As was shown in this study, the C+S model comes with some additional parameters. For validation of the C+S model new parameter sets must be conducted. This means that incremental loading tests must be designed with multiple unloading steps and with longer creep periods. In this way multiple sets of parameters can be used for comparison with the linear isotach models.
- In combination with engineering projects, parameter sets must be obtained for embankments that will be realised. With those parameter sets it should be possible to make predictions according to the current engineering practice (linear isotachs) but also with the new proposed model C+S model.
- In addition to the previous recommendation, more monitoring should be used for the validation of the C+S model. If, for a new project, a prediction is made with both linear isotachs and the C+S model monitoring data could be used for long- and short-term to see if the embankment indeed shows viscoplastic strain and non-linearity. This could for example be done by InSAR.

Bibliography

AHN. (2019). Actuele hoogtebestand nederland. https://www.ahn.nl/

Berry, P. L., & Vickers, B. (1975). Consolidation of fibrous peat. *Journal of the Geotechnical Engineering Division*, *101*(8), 741–753. https://doi.org/10.1061/AJGEB6.0000183

Bianchini Ciampoli, L., Gagliardi, V., Clementini, C., Latini, D., Del Frate, F., & Benedetto, A. (2020). Transport infrastructure monitoring by insar and gpr data fusion. *Surveys in Geophysics*, *41*, 371–394. https://doi.org/https://doi.org/10.1007/s10712-019-09563-7

Bjerrum, L. (1967). Engineering geology of norwegian normally-consolidated marine clays as related to settlements of buildings. *Géotechnique*, *17*(2), 83–118. https://doi.org/10.1680/geot.1967.17.2.83

Broers, D. (2021). Net opgeknapte wegen zijn aan het verzakken en gaan deurne veel geld kosten. *Eindhovens Dagblad*.

Çelik, S., & Tan, Ö. (2005). Determination of preconsolidation pressure with artificial neural network. *Civil Engineering and Environmental Systems*, *22*(4), 217–231. https://doi.org/10.1080/10286600500383923

CROW. (2010). *Standaard raw bepalingen 2010*.

CROW. (2022). Cur rapport 162: Construeren met grond.

Cuhel, J., Simek, M., Laughlin, R., Bru, D., Cheneby, D., Watson, C., & Philippot, L. (2010). Insights into the effect of soil ph on n2o and n2 emissions and denitrifier community size and activity. *Applied and Environmental Microbiology*, *76*(6), 1870–1878. https://doi.org/10.1128/AEM.02484-09

Dalal, R., & Allen, D. (2008). Turner review no. 18. greenhouse gas fluxes from natural ecosystems. *Australian Journal of Botany*, *56*(5), 369–407. https://doi.org/10.1071/BT07128

Deltares. (2021). D-settlement, user manual.

den Haan, E. (1992). The formulation of virgin compression of soils. *Geotechnique*, *42*, 465–483.

den Haan, E. (1996). A compression model for non-brittle soft clays and peat. *Géotechnique*, *46*(1), 1–16.

den Haan, E., Essen, H., Visschedijk, M., & Maccabiani, J. (2004). Isotachenmodellen: Help, hoe kom ik aan de parameters? *Geotechniek*, *1*, 62–69.

Hanssen, R. F. (2001). *Radar interferometry: Data interpretation and error analysis*. Kluwen Academic Publishers. https://doi.org/https://doi.org/10.1007/0-306-47633-9

Hoefsloot, F. J. M. (2022). Simulatie en verbetering interpretatie samendrukkingsproef. *Geotechniek*, 18–24.

Izaurralde, R. C., Lemke, R. L., Goddard, T. W., McConkey, B., & Zhang, Z. (2004). Nitrous oxide emissions from agricultural toposequences in alberta and saskatchewan. *Soil Science Society of America Journal*, *68*(4), 1285–1294. https://doi.org/https://doi.org/10.2136/sssaj2004.1285

Koster, K., Stafleu, J., Cohen, K. M., Stouthamer, E., Busschers, F. S., & Middelkoop, H. (2018). Three-dimensional distribution of organic matter in coastal-deltaic peat: Implications for subsidence and carbon dioxide emissions by human-induced peat oxidation. *Anthropocene*, *22*, 1–9. https://doi.org/10.1016/j.ancene.2018.03.001

Lade, P. V., & De Boer, R. (1997). The concept of effective stress for soil, concrete and rock. *Géotechnique*, *47*(1), 61–78. https://doi.org/10.1680/geot.1997.47.1.61

Liu, K., Xue, J., & Yang, M. (2016). Deformation behaviour of geotechnical materials with gas bubbles and time dependent compressible organic matter. *Engineering Geology*, *213*, 98–106. https://doi.org/https://doi.org/10.1016/j.enggeo.2016.09.003

Marée, K. (2021). Zachte bodem zorgt voor problemen met treindienstregeling. *NRC*.

Moein, F. (2016). *Investigating the consolidation behaviour of brown coal* (Doctoral dissertation). Monash University.

Moreira, A., Prats-Iraola, P., Younis, M., Krieger, G., Hajnsek, I., & Papathanassiou, K. P. (2013). A tutorial on synthetic aperture radar. *IEEE Geoscience and Remote Sensing Magazine*, *1*(1), 6–43. https://doi.org/10.1109/MGRS.2013.2248301

NEN. (2017). Nen 9997-1+c2 (nl) geotechnisch ontwerp van constructies - deel 1: Algemene regels.

Oertel, C., Matschullat, J., Zurba, K., Zimmermann, F., & Erasmi, S. (2016). Greenhouse gas emissions from soils—A review. *Chemie der Erde*, *76*(3), 327–352. https://doi.org/10.1016/j.chemer.2016.04.002

Polinder, H. B. (2019). Development of the Yield Stress due to Aging. http://resolver.tudelft.nl/uuid:9bbc14ef-dab5-4b78-ac09-fafaab12a90d

Reicosky, D., Gesch, R., Wagner, S., Gilbert, R., Wente, C., & Morris, D. (2008). Tillage and wind effects on soil co2 concentrations in muck soils. *Soil and Tillage Research*, *99*(2), 221–231. https://doi.org/https://doi.org/10.1016/j.still.2008.02.006

Reinders, K. J., Giardina, G., Zurfluh, F., Ryser, J., & Hanssen, R. F. (2022). Proving compliance of satellite insar technology with geotechnical design codes. *Transportation Geotechnics*, *33*, 100722. https://doi.org/https://doi.org/10.1016/j.trgeo.2022.100722

Schuurman, I. E. (1966). The compressibility of an air/water mixture and a theoretical relation between the air and water pressures. *Géotechnique*, *16*(4), 269–281. https://doi.org/10.1680/geot.1966.16.4.269

Stepniewska, Z., & Goraj, W. (2014). Transformation of methane in peatland environments. *Forest Research Papers*, *75*(1), 101–110. https://doi.org/10.2478/frp-2014-0010

Tieleman, J. (2020). Huizen verzakken sneller door droogte, schade loopt in de tientallen miljarden. *Volkskrant*.

TNO. (2022). Dinoloket. https://www.dinoloket.nl/

van den Akker, R., J.J.H. Hendriks. (2017). Diminishing peat oxidation of agricultural peat soils by infiltration via submerged drains. https://edepot.wur.nl/441644

van der Linden, T. (2021). Note / memo: Back-calculation of oedometer tests with the isotach model based on linear and natural strain.

Vergote, T. A. (2020). *Deformation of soils: Time and strain effects after unloading* (Doctoral dissertation). NATIONAL UNIVERSITY OF SINGAPORE.

Vergote, T. A. (2021). Evspy - 1d elasto-viscoplastic modelling of soils with swelling. https://github.com/thomasvergote/evspy

Vergote, T. A. (2022). Personal communication.

Vergote, T. A., Leung, C. F., & Chian, S. C. (2021). Elastoviscoplastic modelling with distorted isotaches and swelling for constant strain rate and incremental loading. *International Journal for Numerical and Analytical Methods in Geomechanics*, *45*(13), 1920–1933. https://doi.org/10.1002/nag.3248

Verruijt, A., & Broere, W. (2011). *Soil mechanics*. VSSD.

Visschedijk, M. (2010). Isotachen berekeningen op een sigarendoosje. *Geotechniek*, 30–33.

Visschedijk, M., & Temmerman, L. (2009). *Zetting door wegophoging, Casestudy: A2 Holendrecht Maarssen* (tech. rep.). Deltares.

Wageningen University and Research. (2006). https://www.wur.nl/nl/show/Grondsoortenkaart.htm

Wheeler, S. J. (1988). A conceptual model for soils containing large gas bubbles. *Géotechnique*, *38*(3), 389–397. https://doi.org/10.1680/geot.1988.38.3.389

Wiertsma & Partners. (2018). Geotechnisch laboratoriumonderzoek, reconstructie van de n3 te dordrecht.

Yang, M., & Liu, K. (2016). Deformation behaviors of peat with influence of organic matter. *SpringerPlus*, *5*. https://doi.org/https://doi.org/10.1186/s40064-016-2232-3

Yuan, Y. (2016). *A new elasto-viscoplastic model for rate-dependent behavior of clays* (Doctoral dissertation). Massachusetts Institute of Technology.

Yuan, Y., & Whittle, A. J. (2018). A novel elasto-viscoplastic formulation for compression behaviour of clays. *Géotechnique*, *68*(12), 1044–1055. https://doi.org/10.1680/jgeot.16.P.276

Yuan, Y. X., Whittle, A. J., & Nash, D. F. T. (2015). Model for Predicting and Controlling Creep Settlements with Surcharge Loading. *Deformation Characteristics of Geomaterials*, *6*(November), 931–938. https://doi.org/10.3233/978-1-61499-601-9-931

Yuan, Y., Whittle, A. J., & den Haan, E. J. (2021). A novel elasto-viscoplastic formulation for compression behaviour of clays. *Géotechnique*, *0*(0), 1–6. https://doi.org/10.1680/jgeot.20.D.014

Zanello, F., Teatini, P., Putti, M., & Gambolati, G. (2011). Long term peatland subsidence: Experimental study and modeling scenarios in the venice coastland. *JOURNAL OF GEOPHYSICAL RESEARCH*, *116*. https://doi.org/doi:10.1029/2011JF002010

Zwanenburg, C. (2021). Settlement prediction.

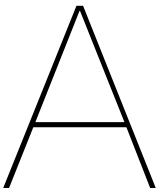

Settlement Models

A.1. Iteration part C+S model python code

```
while (running)&(t<self.dimt-1):
    next_load_step, running, load_step, reset_minimum_swelling_rate=self.initiate_new_load_step(load_step,t,running, reset_minimum_swelling_rate)
    if running:
        t+=1
    if self.load.type[load_step]=='CRS':
    elif self.load.type[load_step]=='IL':
        dt=self.time[t]-self.time[t-1]
        self.erate_e[t]= self.Cr*0.434*(self.sigma[t]-self.sigma[t-1])/dt/np.average([self.sigma[t],self.sigma[t-1]])
        self.ee[t]=self.ee[t-1]-self.erate_e[t]*dt

    self.OCR_real[t]=self.sigpref[t-1]/self.sigma[t]
    self.OCR[t]=np.clip(np.max(np.append(np.array([self.sigpref[0]]),self.sigma[:t]))/self.sigma[t],1.005,np.infty)
    self.OCRrate[t] = (self.OCR[t]-self.OCR[t-1])/dt

    sigmarate=(self.sigma[t-1]-self.sigma[t-2])/dt
    self.erates[t],self.Calphahats_real[t-1],reset_minimum_swelling_rate=swelling_law(self.erates[t-1],self.OCR[t],self.OCRrate[t],
                                                            self.Calphahats_real[t-1],dt,self.CalphaCc*self.Cc,
                                                            self.m1,self.b1,self.m2,self.b2,sigmarate,-self.erate_e[t],reset_minimum_swelling_rate)

    # Distortion occurs only during swelling and not during relaxation
    if ((self.sigma[t]<self.sigma[t-1]/1.000001)
            &(self.sigma[t-1]<self.sigma[t-2]/1.000001)
            &(np.abs(self.e[t]-self.e[t-1])>0)
            &(np.abs(self.e[t-2]-self.e[t-1])>0)):
        if (self.load.type[load_step]=='IL')&(np.round(self.load.load[load_step-1],1)==np.round(self.load.load[load_step],1)):
            self.sigp_update[t]=self.sigp_update[t-1]
        else:
            self.sigp_update[t]=np.max(self.sigpref[self.sigpref>0])
    else:
        self.sigp_update[t]=self.sigp_update[t-1]

    self.e[t]=self.e[t-1]+(self.eratec[t-1]+self.erates[t-1])*dt+(self.ee[t]-self.ee[t-1])
    self.sigpref[t] = self.get_sigpref(self.sigma[t-1:t+1],self.e[t-1:t+1],self.sigpref[t-1:t])
    self.eratec[t]=self.calc_pos_isotache(self.sigma[t],self.e[t],self.sigp_update[t],steps=20)
    self.eratec[t]=-self.eratec[t]

    if np.isnan(self.ee[t]):
        print(dt)
        print(self.Cr*0.434*(self.sigma[t]-self.sigma[t-1])/dt/np.average([self.sigma[t],self.sigma[t-1]]))
        print(str(self.sigma[t-1])+' '+str(self.sigma[t]))
        print('failure')
    if self.eratec[t]>1:
        print((self.sigma[t],self.e[t],self.beta2, self.beta3,self.Cc,self.Cr,self.CalphaNC,self.sigp_update[t],self.e0))
    self.erate[t]=(self.e[t]-self.e[t-1])/dt#

    self.Calphahats_real[t]=self.CalphaCc*self.Cc*10**self.b1*(np.clip(self.OCR[t]-1,0.005,np.infty))**self.m1

self.time = self.time[:t]
self.sigma = self.sigma[:t]
self.e = self.e[:t]
self.erate = self.erate[:t]
self.Calphahats_real = self.Calphahats_real[:t]
self.sigpref = self.sigpref[:t]
self.eratec = self.eratec[:t]
```

A.2. Mexico clay analysis

A.2.1. Equal c_v

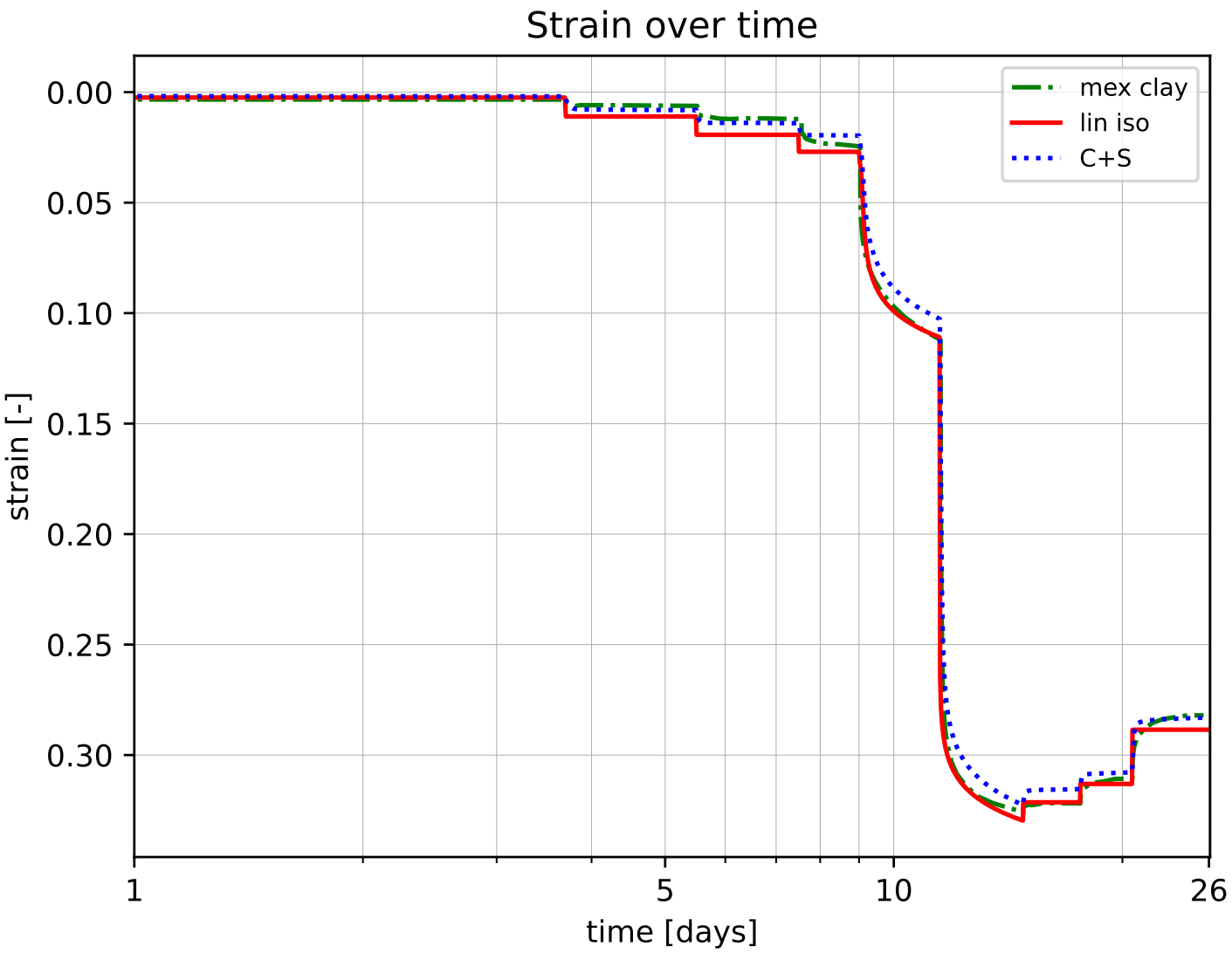
Strain over time
mex clay
lin iso
C+S
strain [-]
0.00
0.05
0.10
0.15
0.20
0.25
0.30
1
5
10
26
time [days]

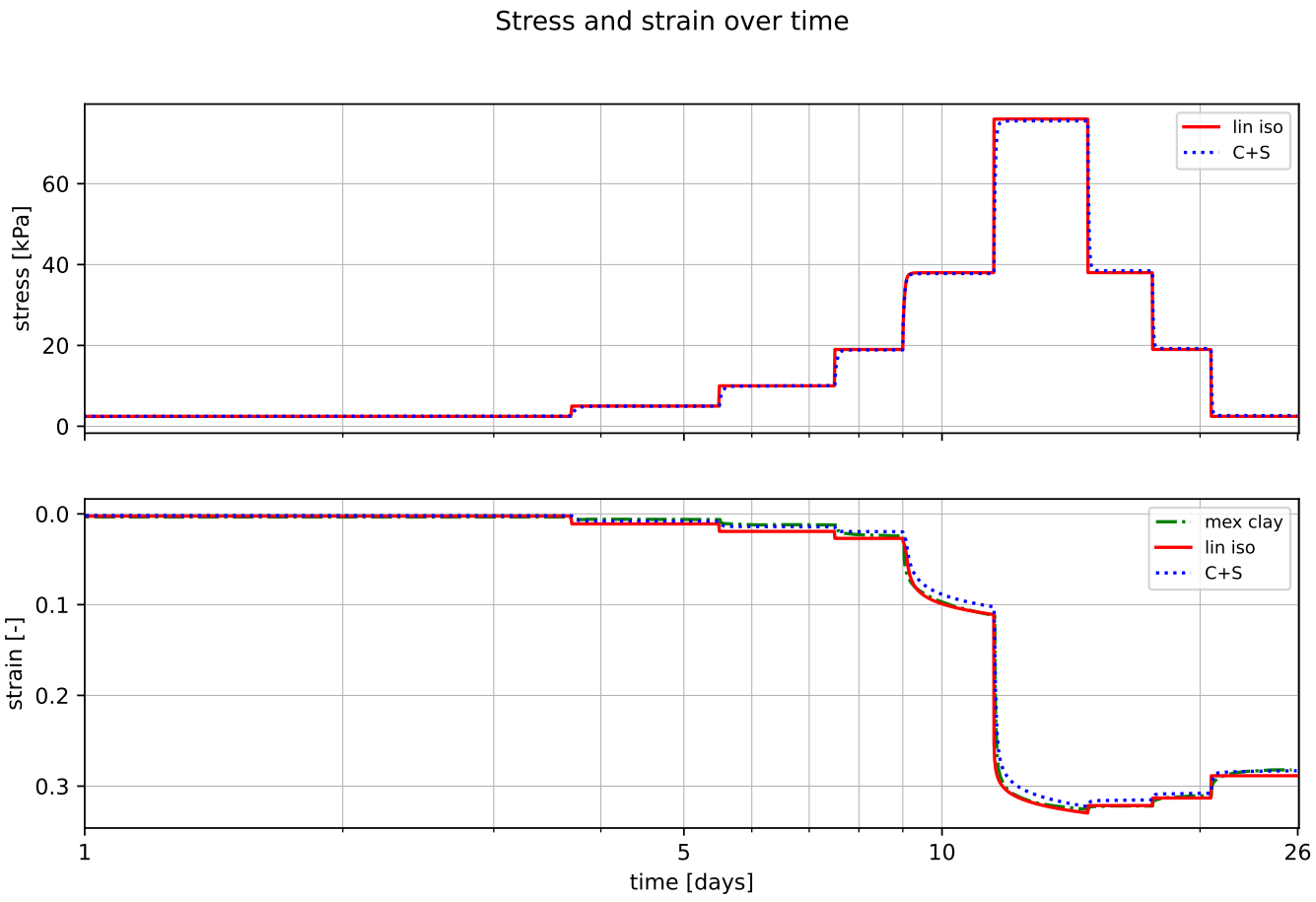
Stress and strain over time
stress [kPa]
0
20
40
60
lin iso
C+S
strain [-]
0.0
0.1
0.2
0.3
mex clay
lin iso
C+S
1
5
10
26
time [days]

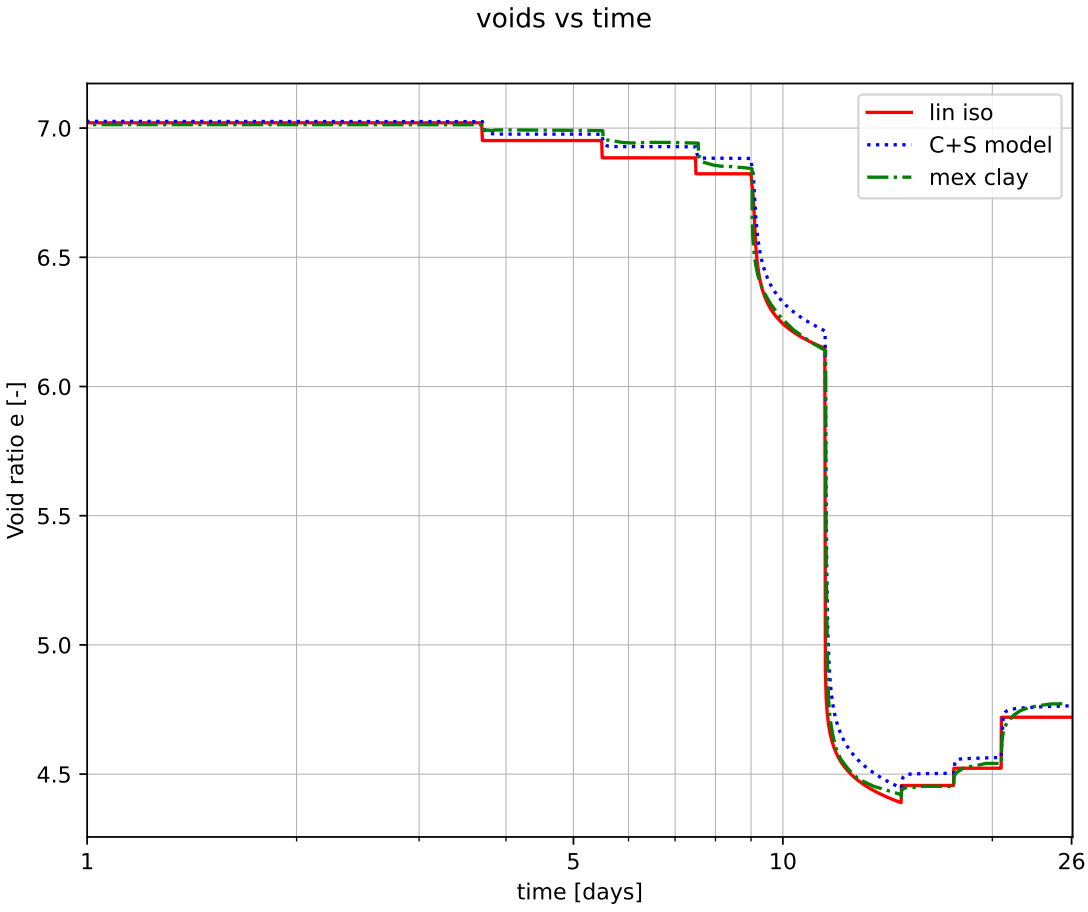
voids vs time
lin iso
C+S model
mex clay
7.0
6.5
6.0
5.5
5.0
4.5
Void ratio e [-]
1
5
10
26
time [days]

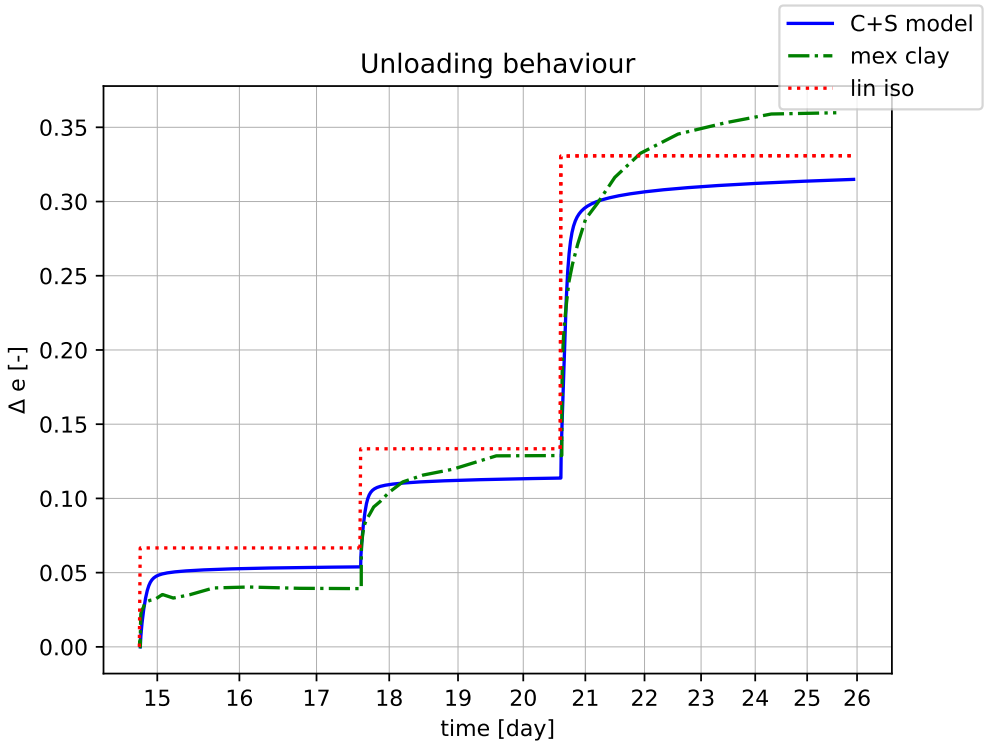
Unloading behaviour
C+S model
mex clay
lin iso
Δ e [-]
0.35
0.30
0.25
0.20
0.15
0.10
0.05
0.00
15
16
17
18
19
20
21
22
23
24
25
26
time [day]

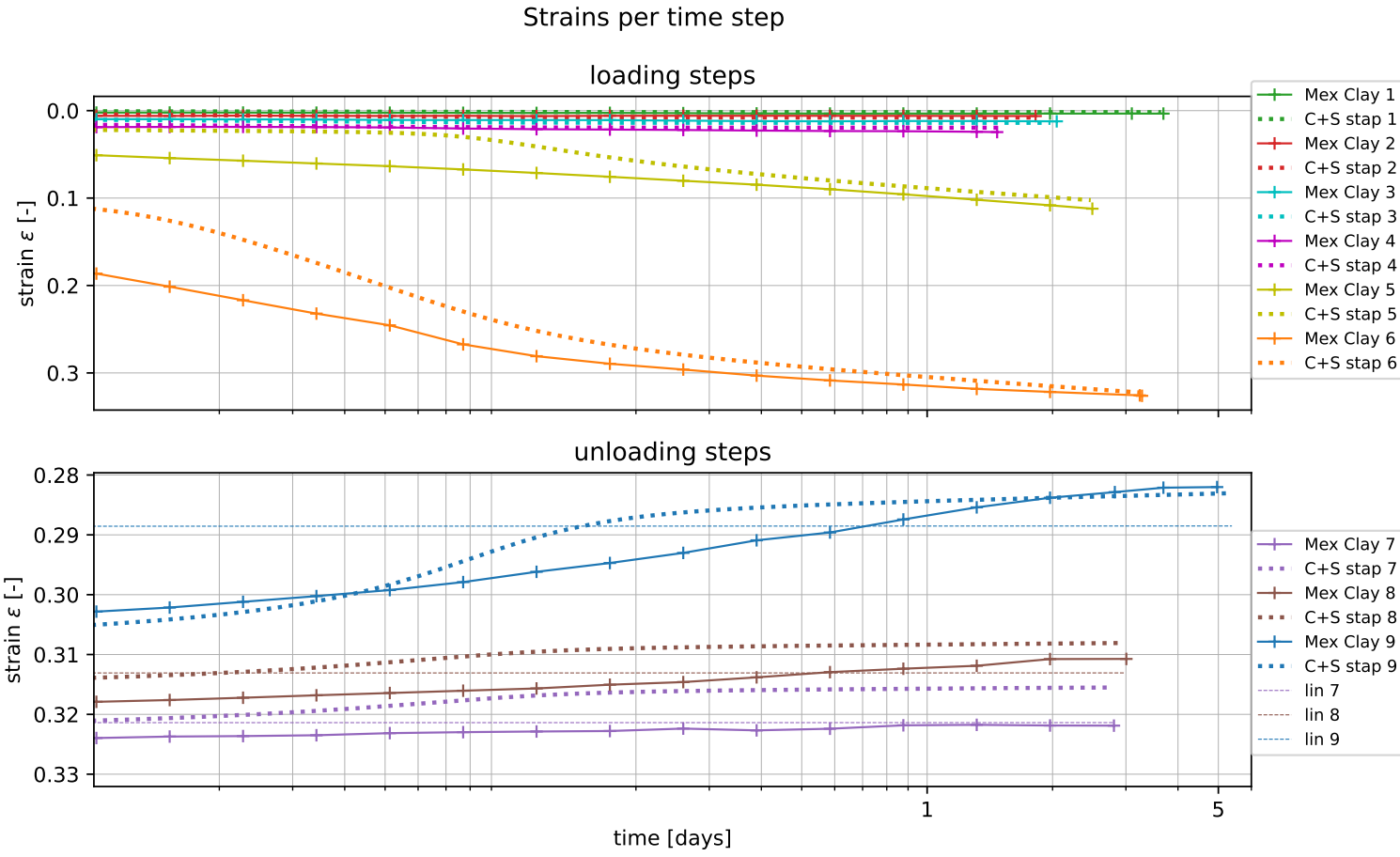
Strains per time step
loading steps
strain ε [-]
0.0
0.1
0.2
0.3
Mex Clay 1
C+S stap 1
Mex Clay 2
C+S stap 2
Mex Clay 3
C+S stap 3
Mex Clay 4
C+S stap 4
Mex Clay 5
C+S stap 5
Mex Clay 6
C+S stap 6
unloading steps
strain ε [-]
0.28
0.29
0.30
0.31
0.32
0.33
Mex Clay 7
C+S stap 7
Mex Clay 8
C+S stap 8
Mex Clay 9
C+S stap 9
lin 7
lin 8
lin 9
1
5
time [days]

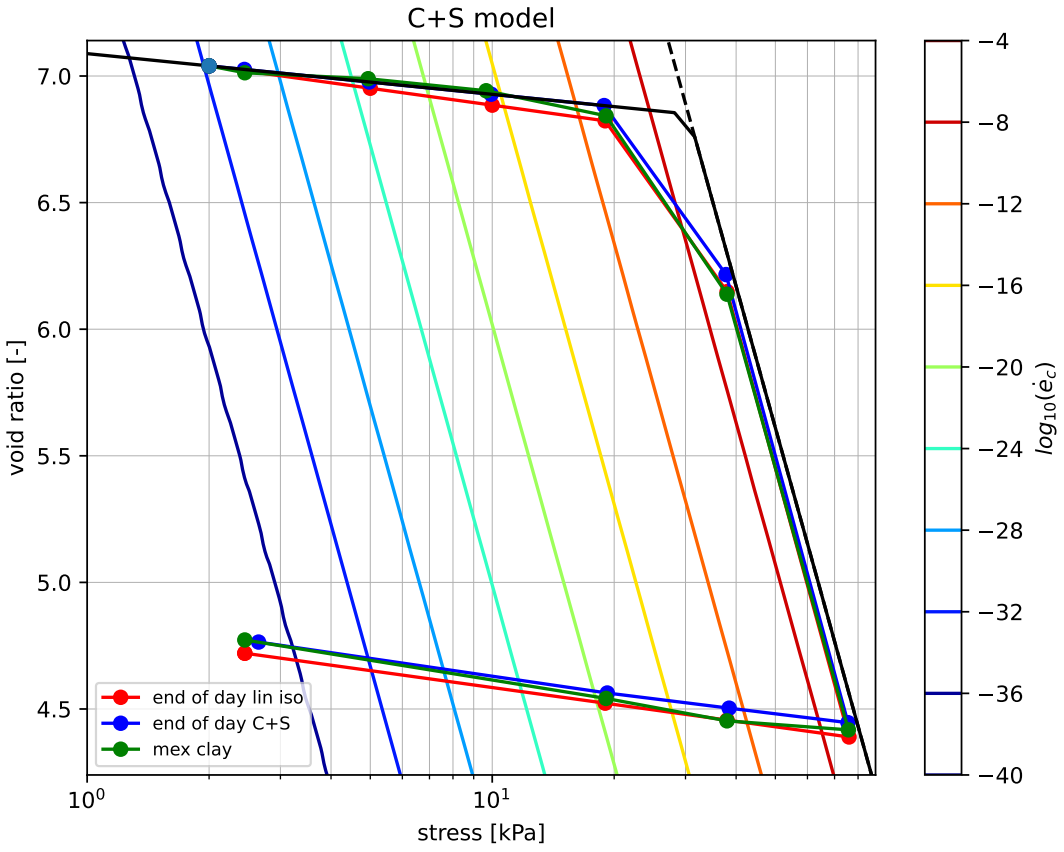
C+S model
void ratio [-]
stress [kPa]
end of day lin iso
end of day C+S
mex clay
$log_{10}(\dot{e}_c)$

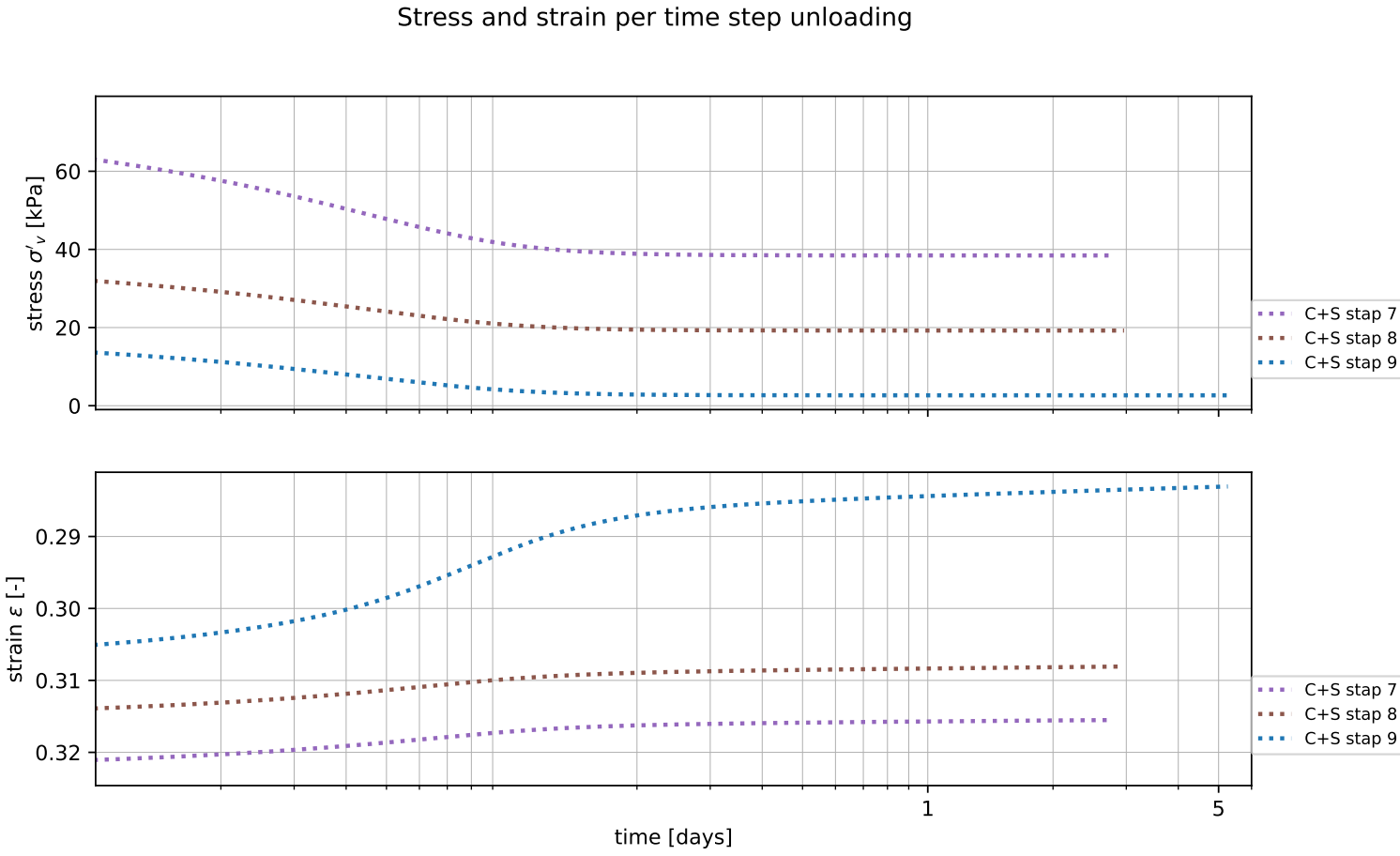
Stress and strain per time step unloading
stress σ'_v [kPa]
60
40
20
0
C+S stap 7
C+S stap 8
C+S stap 9
strain ε [-]
0.29
0.30
0.31
0.32
1
5
time [days]
C+S stap 7
C+S stap 8
C+S stap 9

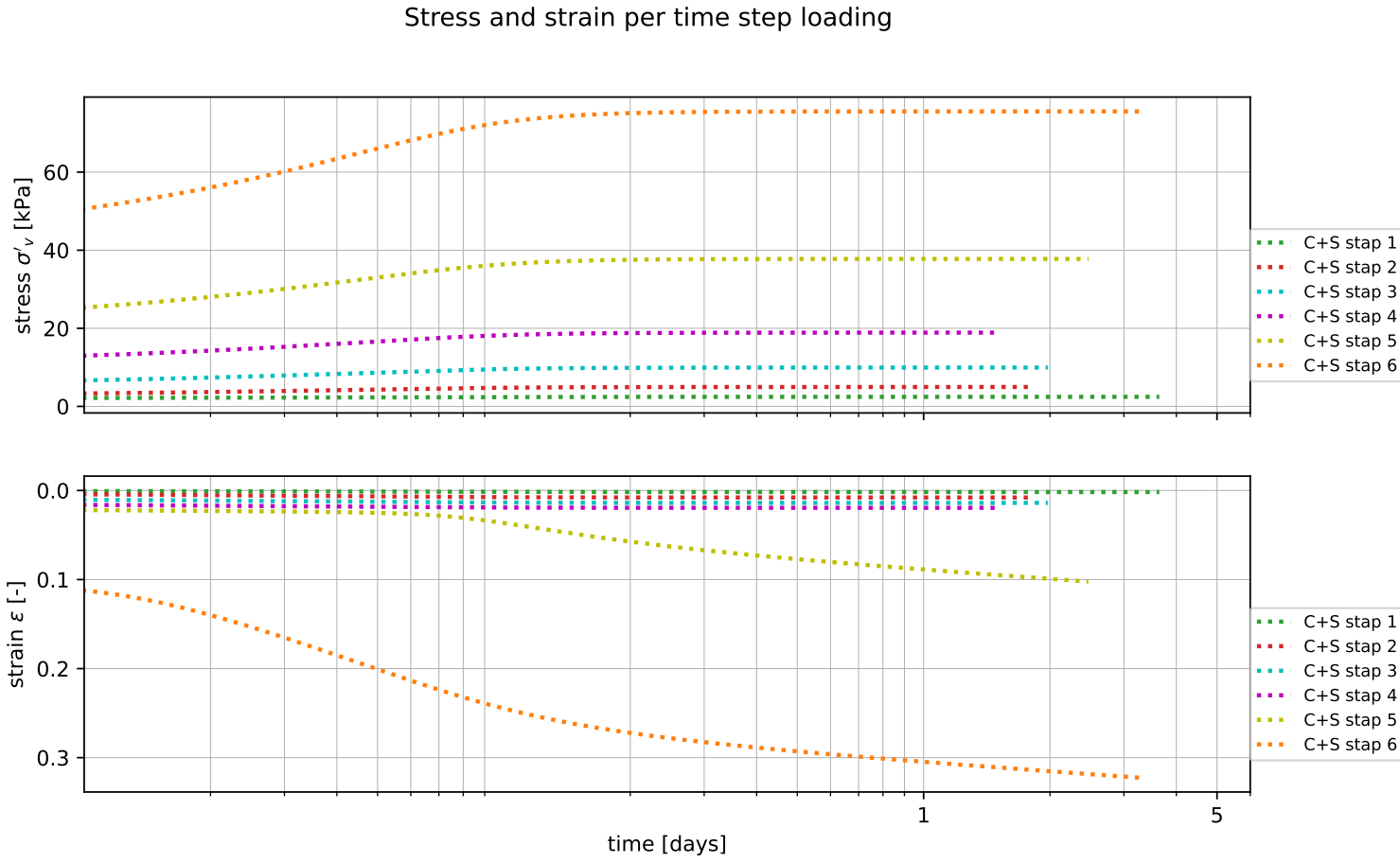
Stress and strain per time step loading
stress σ'_v [kPa]
0
20
40
60
strain ε [-]
0.0
0.1
0.2
0.3
1
5
time [days]
C+S stap 1
C+S stap 2
C+S stap 3
C+S stap 4
C+S stap 5
C+S stap 6

A.2.2. Changed c_v for unloading

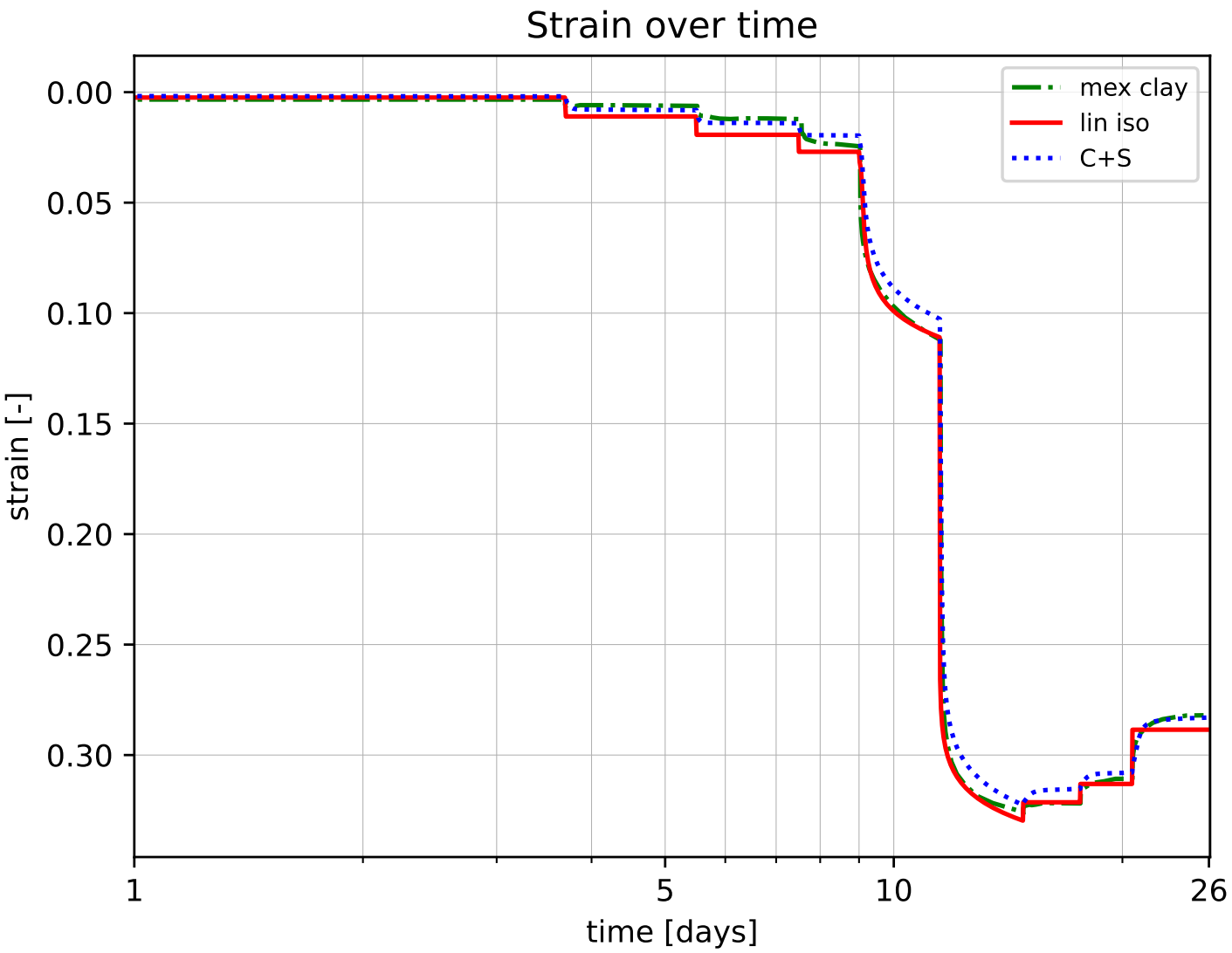

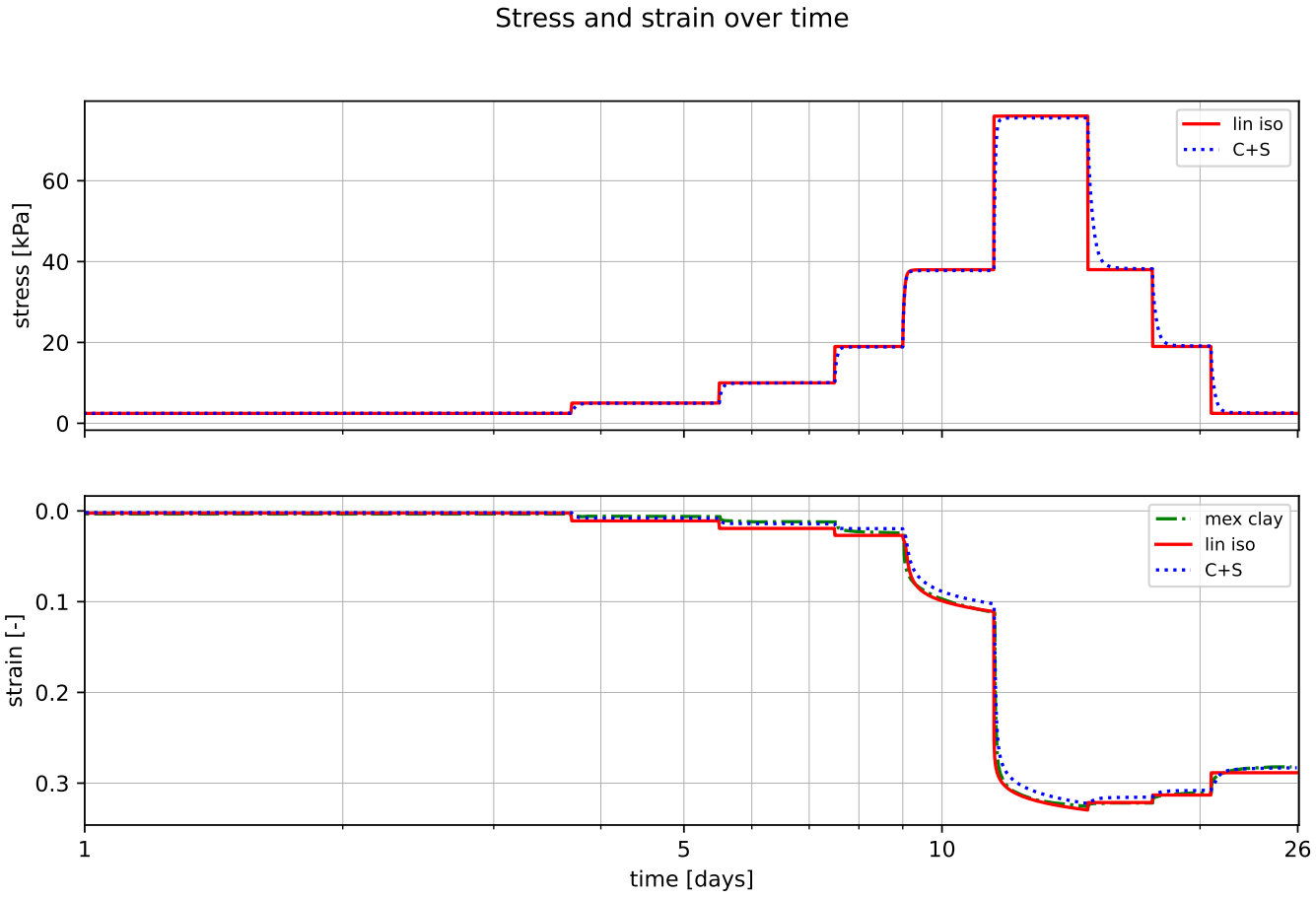
Stress and strain over time
stress [kPa]
0
20
40
60
lin iso
C+S
strain [-]
0.0
0.1
0.2
0.3
mex clay
lin iso
C+S
1
5
10
26
time [days]

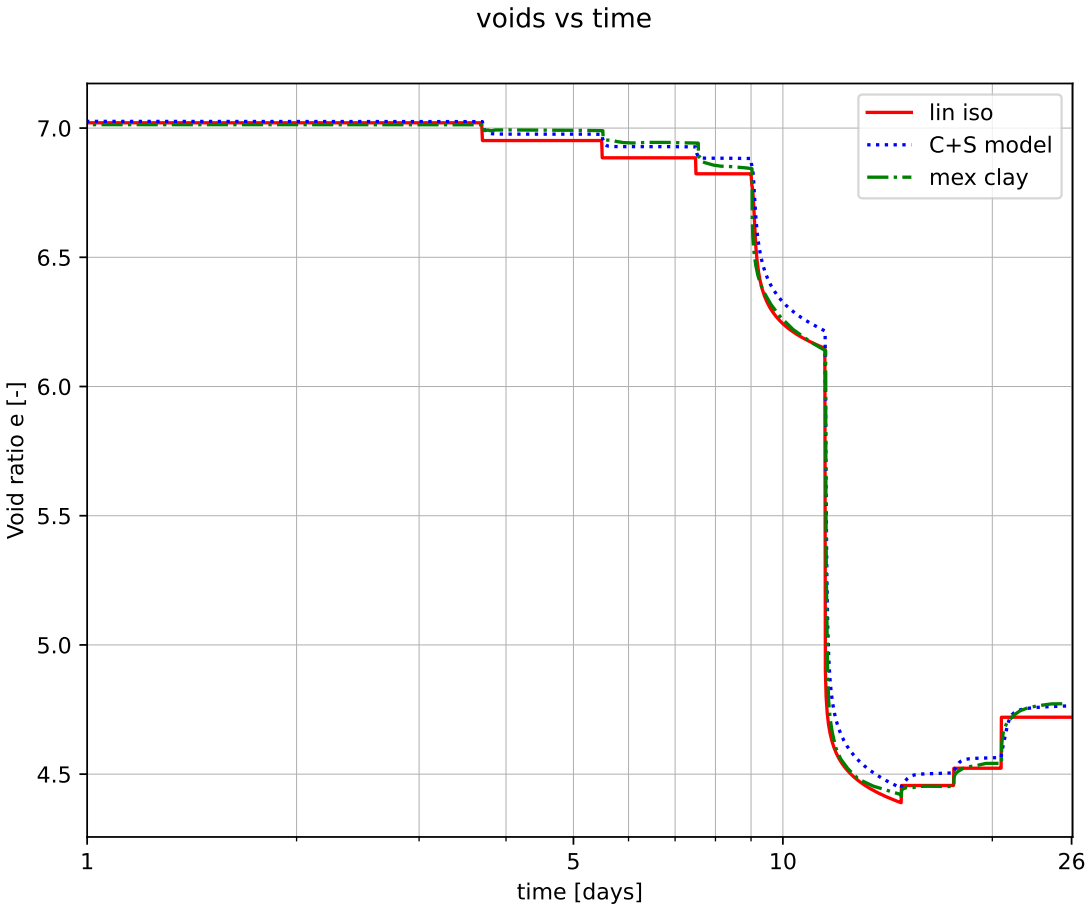
voids vs time
lin iso
C+S model
mex clay
7.0
6.5
6.0
5.5
5.0
4.5
Void ratio e [-]
1
5
10
26
time [days]

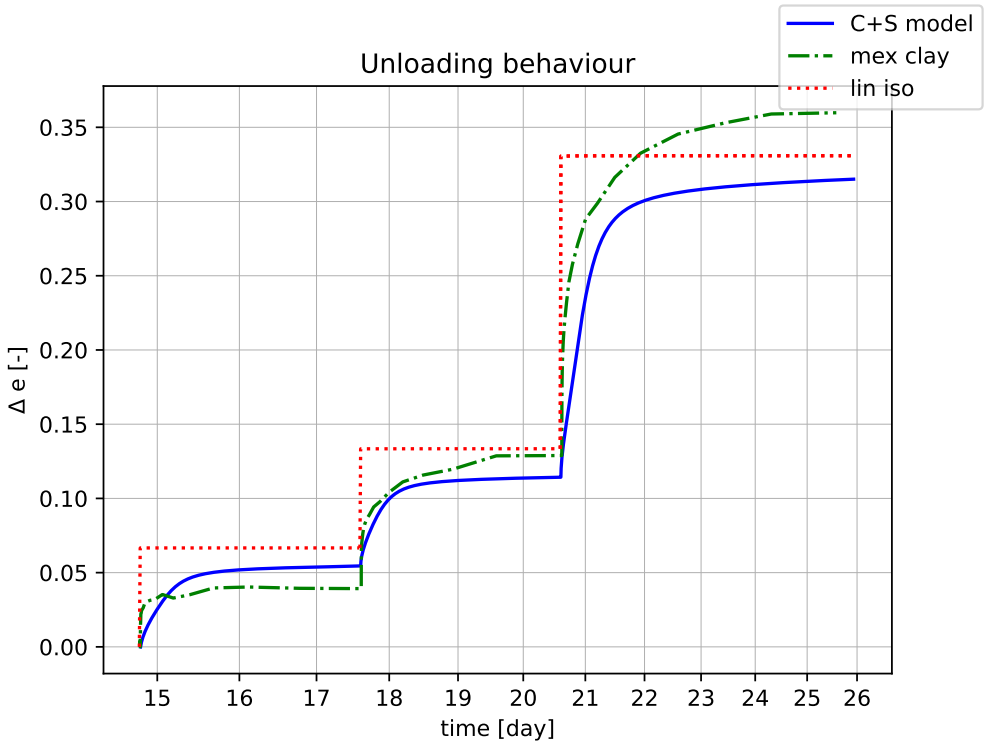
Unloading behaviour
C+S model
mex clay
lin iso
Δ e [-]
0.35
0.30
0.25
0.20
0.15
0.10
0.05
0.00
15
16
17
18
19
20
21
22
23
24
25
26
time [day]

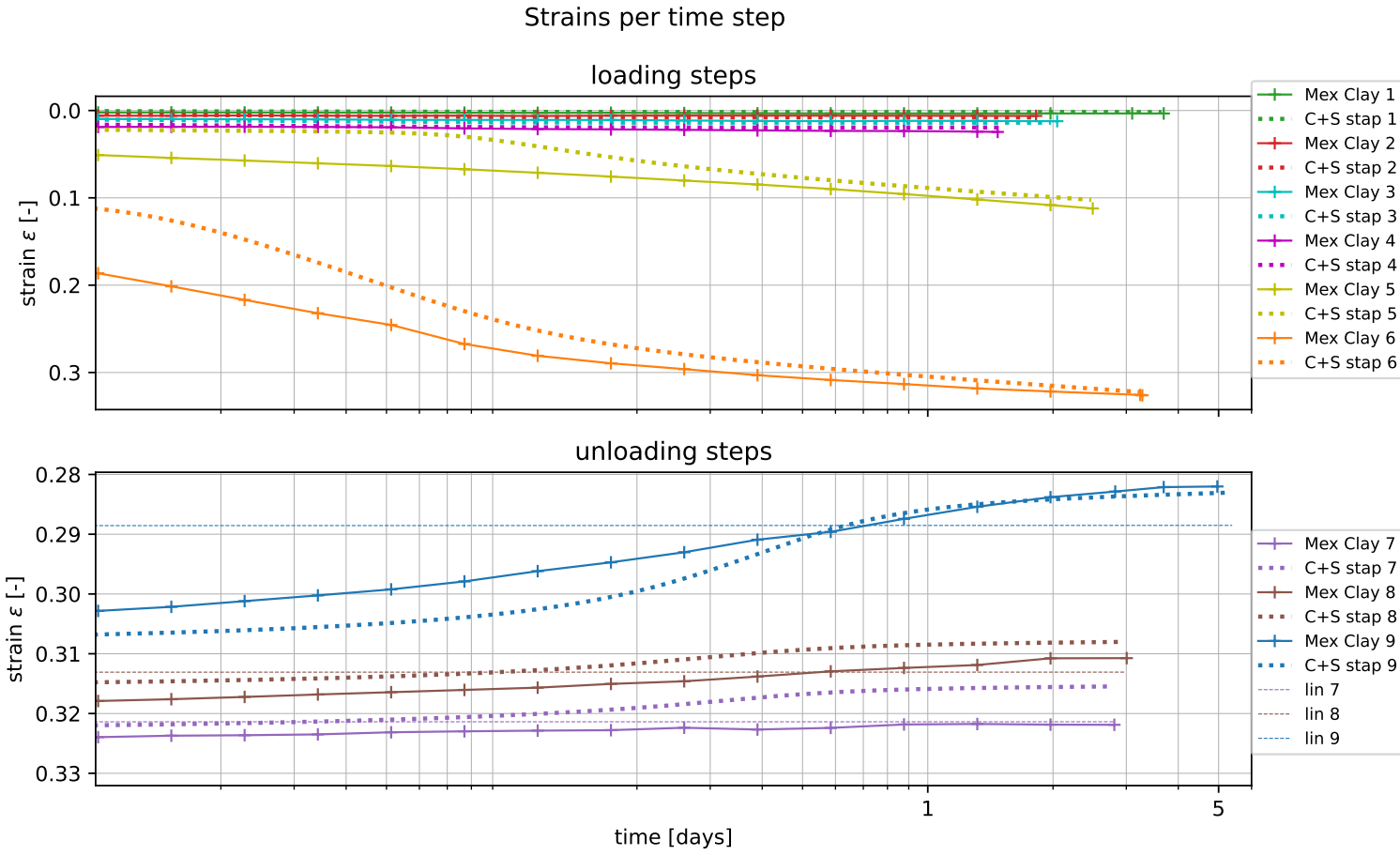
Strains per time step
loading steps
strain ε [-]
0.0
0.1
0.2
0.3
Mex Clay 1
C+S stap 1
Mex Clay 2
C+S stap 2
Mex Clay 3
C+S stap 3
Mex Clay 4
C+S stap 4
Mex Clay 5
C+S stap 5
Mex Clay 6
C+S stap 6
unloading steps
strain ε [-]
0.28
0.29
0.30
0.31
0.32
0.33
Mex Clay 7
C+S stap 7
Mex Clay 8
C+S stap 8
Mex Clay 9
C+S stap 9
lin 7
lin 8
lin 9
1
5
time [days]

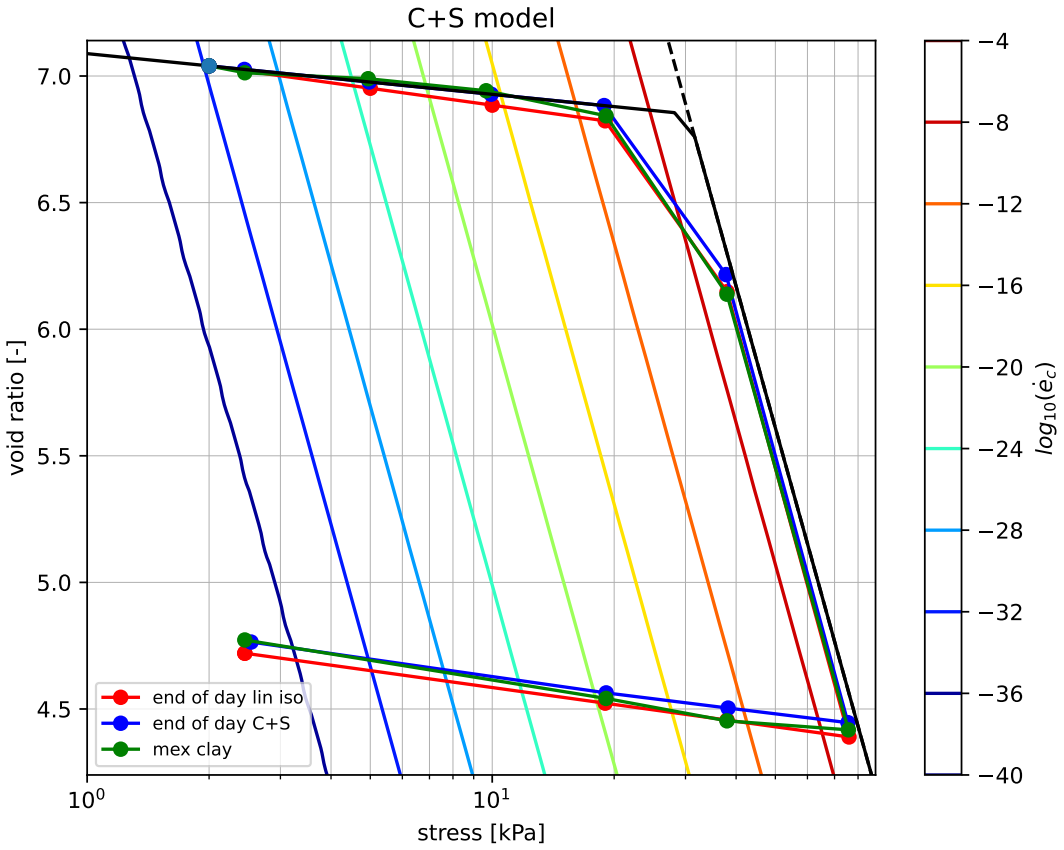
C+S model
void ratio [-]
stress [kPa]
end of day lin iso
end of day C+S
mex clay
$log_{10}(\dot{e}_c)$

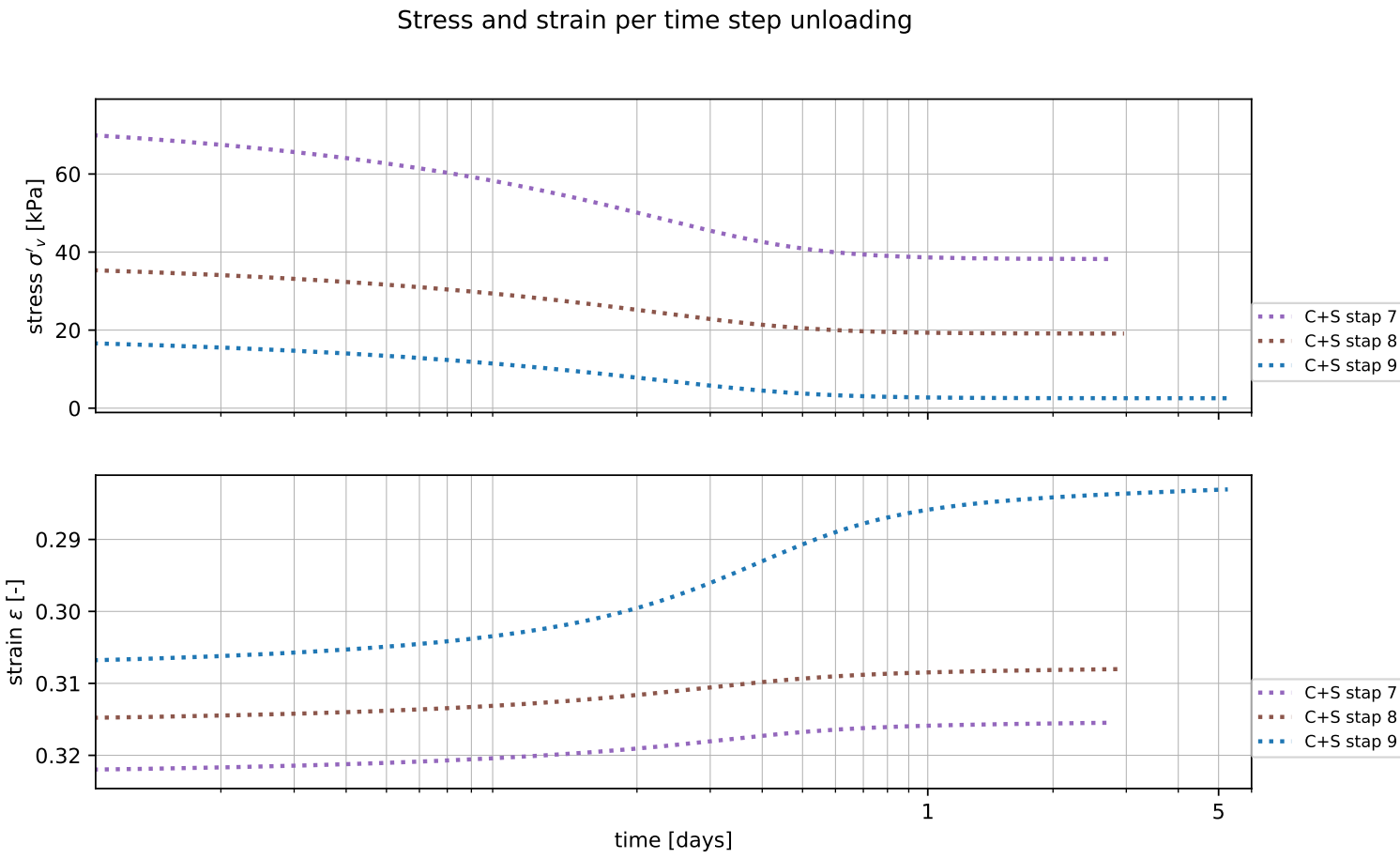
Stress and strain per time step unloading
stress σ'_v [kPa]
0
20
40
60
strain ε [-]
0.29
0.30
0.31
0.32
1
5
time [days]
C+S stap 7
C+S stap 8
C+S stap 9
C+S stap 7
C+S stap 8
C+S stap 9

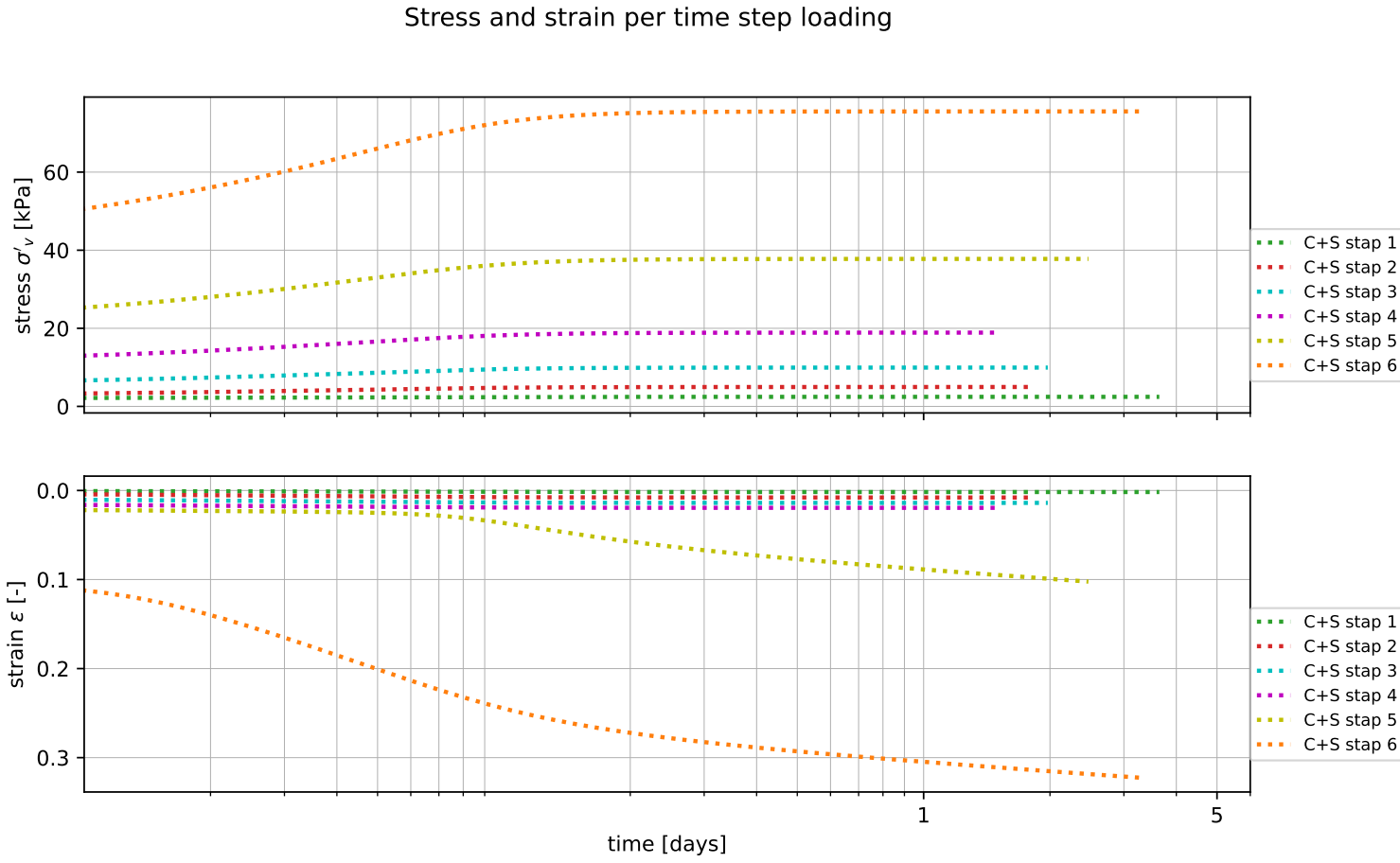
Stress and strain per time step loading
stress σ'_v [kPa]
0
20
40
60
strain ε [-]
0.0
0.1
0.2
0.3
1
5
time [days]
C+S stap 1
C+S stap 2
C+S stap 3
C+S stap 4
C+S stap 5
C+S stap 6

A.3. Incremental loading test plots

A.3.1. C+S model with swell and non-linearity

In this Appendix all the generated graphs are presented for the incremental loading tests in which the C+S model has both swell and distorted isotachs. The GitHub and Paper parameter set are presented for both the standard and unloading scenarios.

Standard IL test GH non-linear isotachs

Standard IL test GH non-linear isotachs

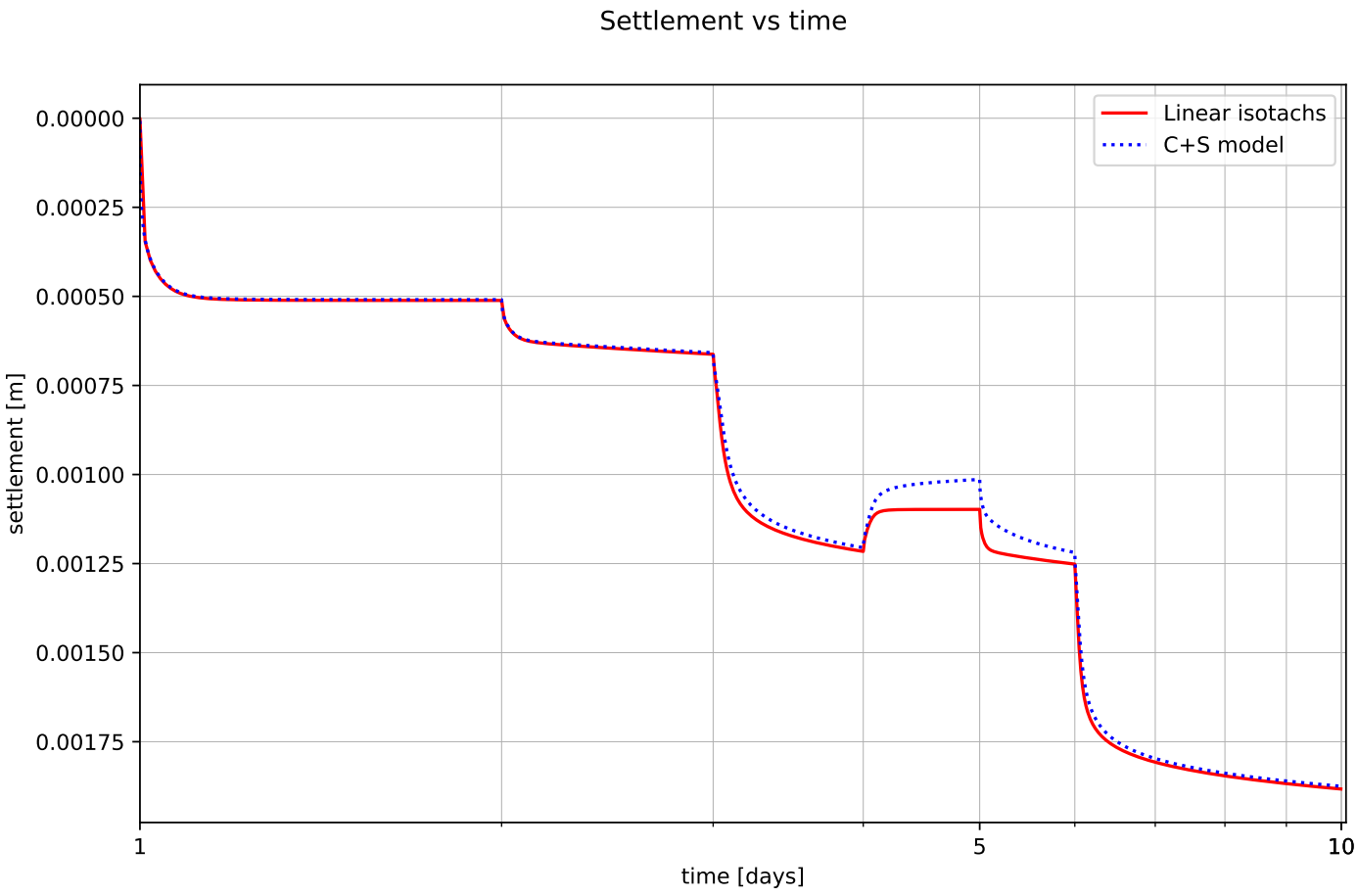

Standard IL test GH non-linear isotachs

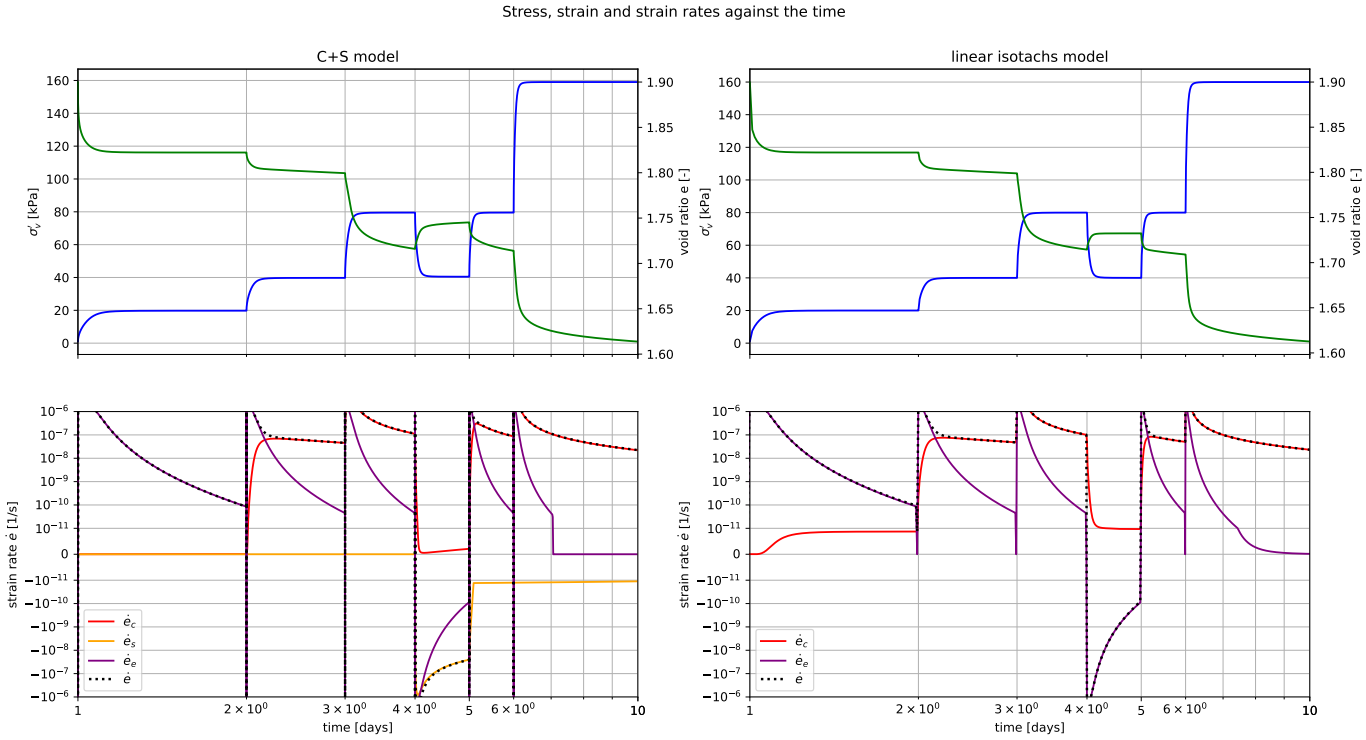

Standard IL test GH non-linear isotachs

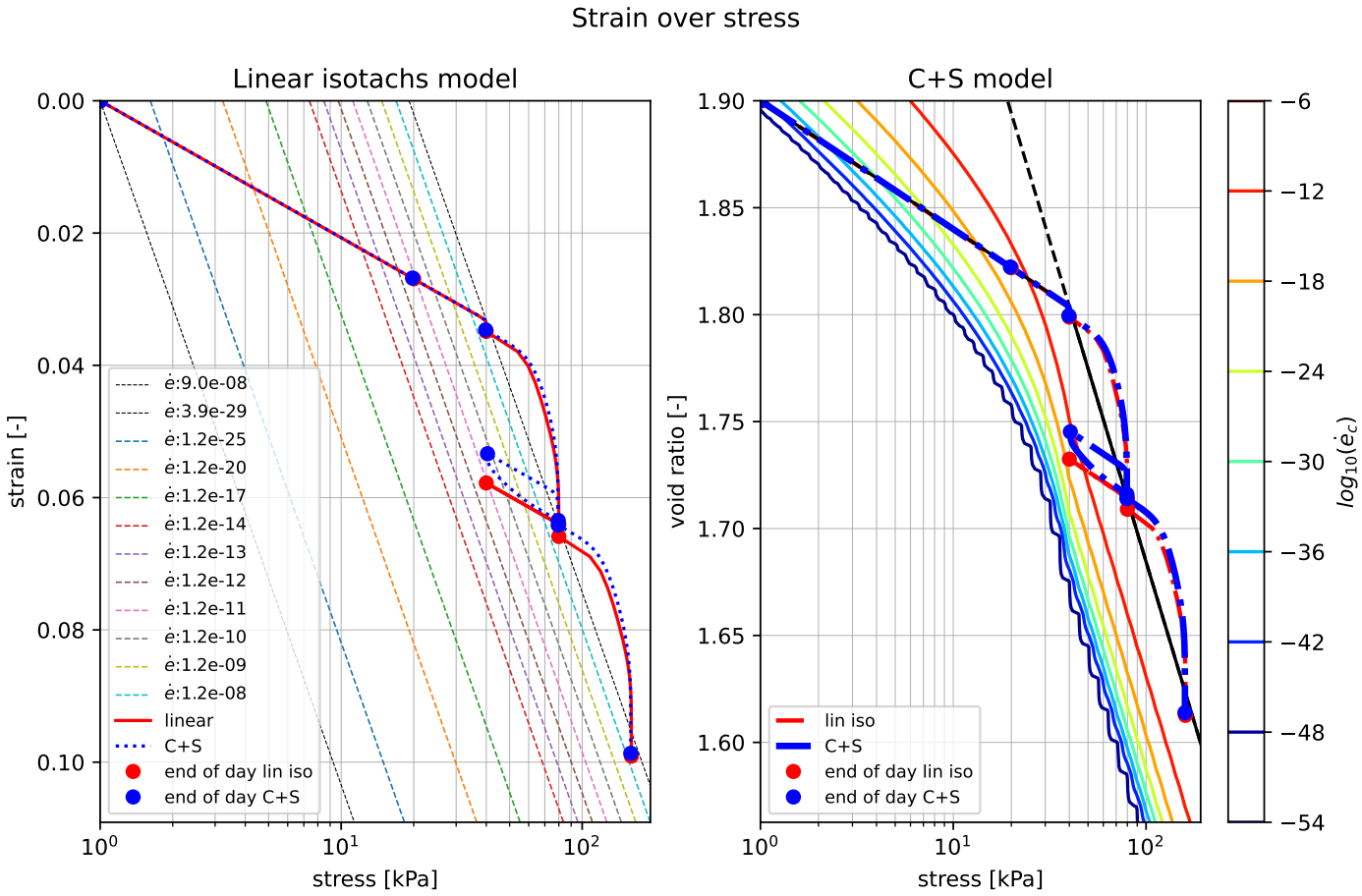

Standard IL test GH non-linear isotachs

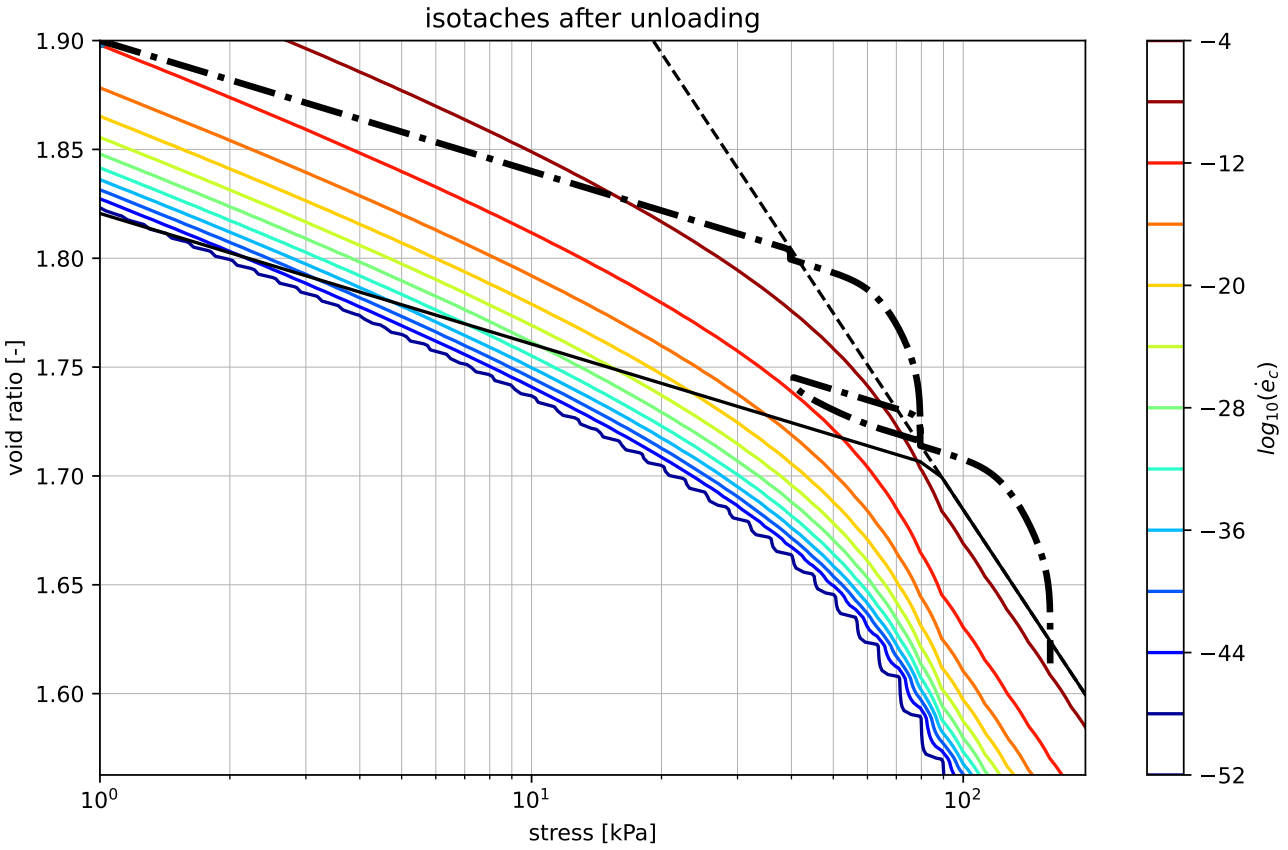

Standard IL test GH non-linear isotachs

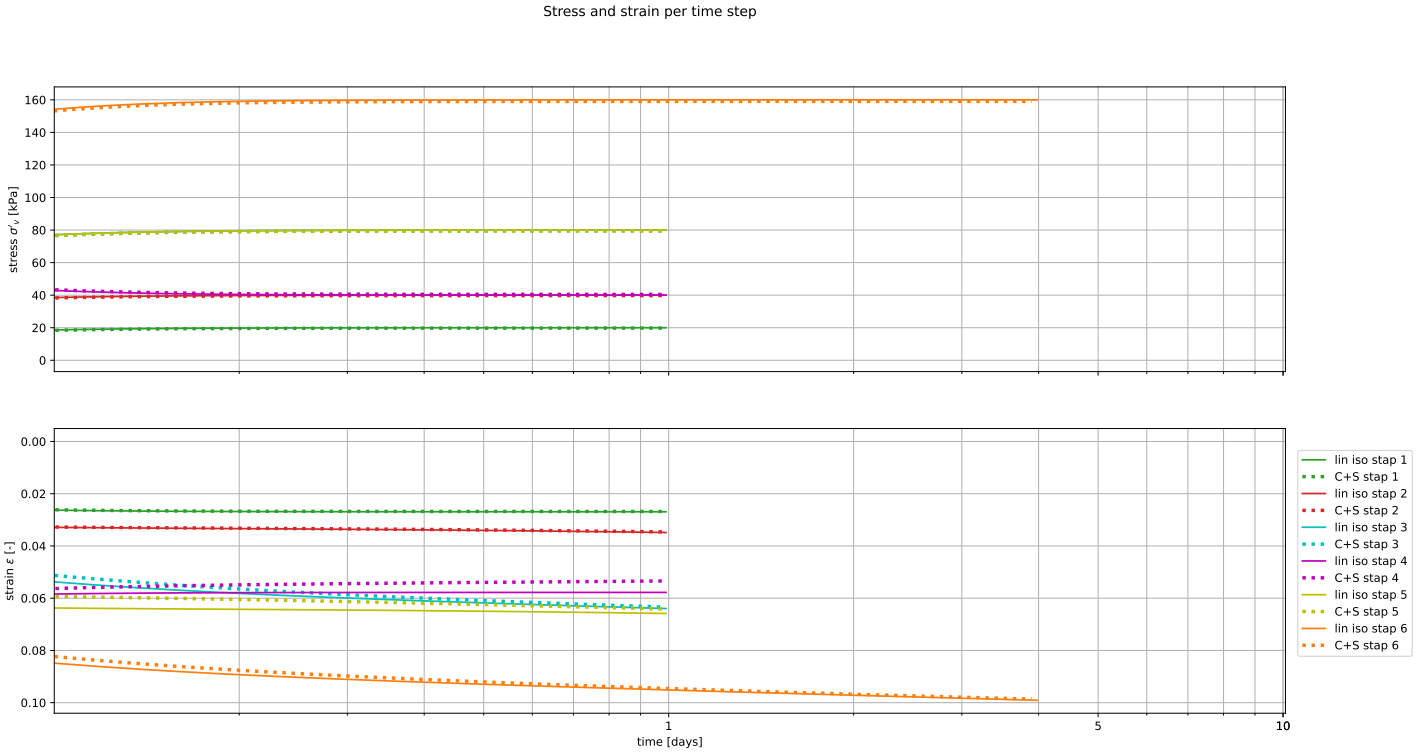

Unloading IL test GH non-linear isotachs

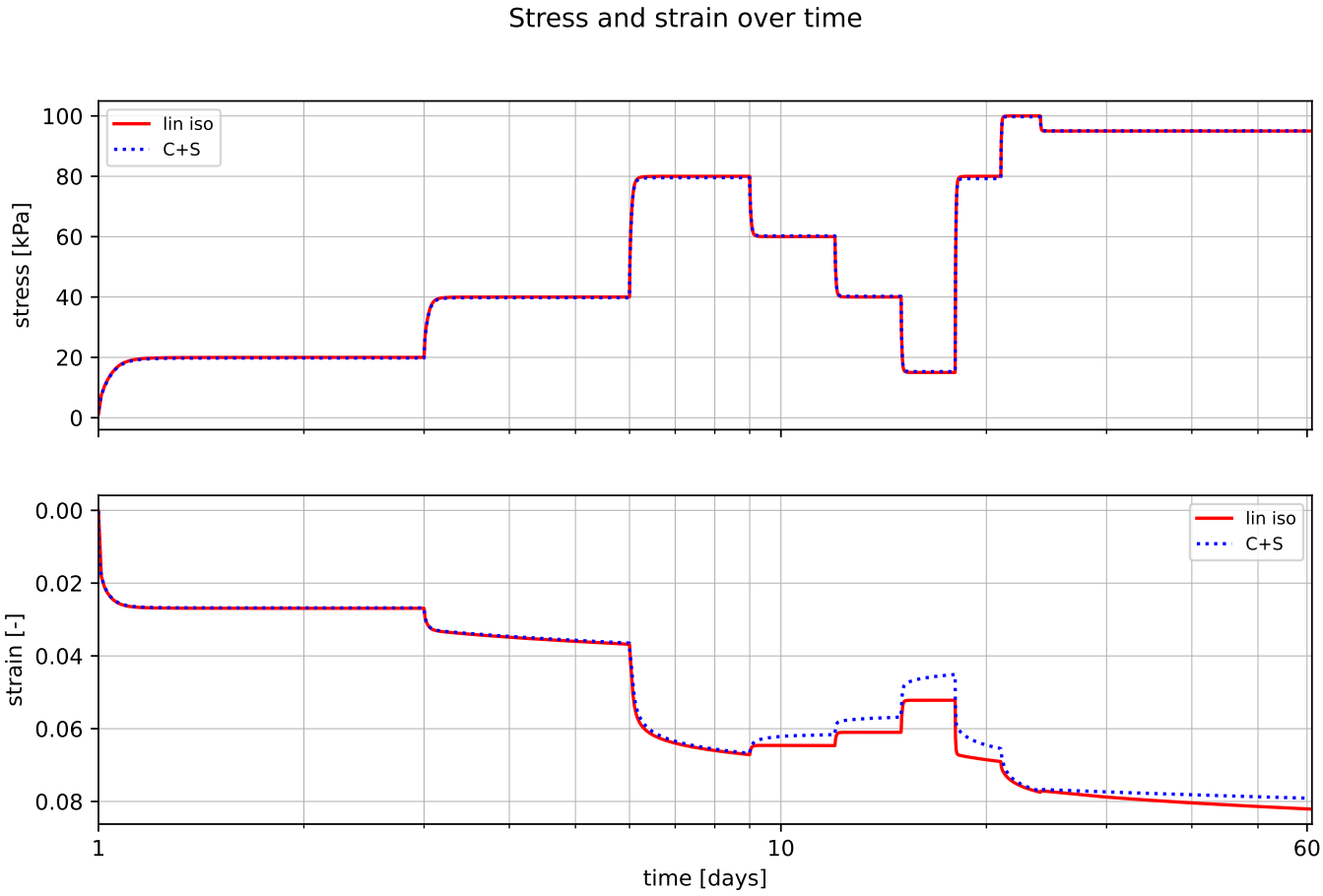

Unloading IL test GH non-linear isotachs

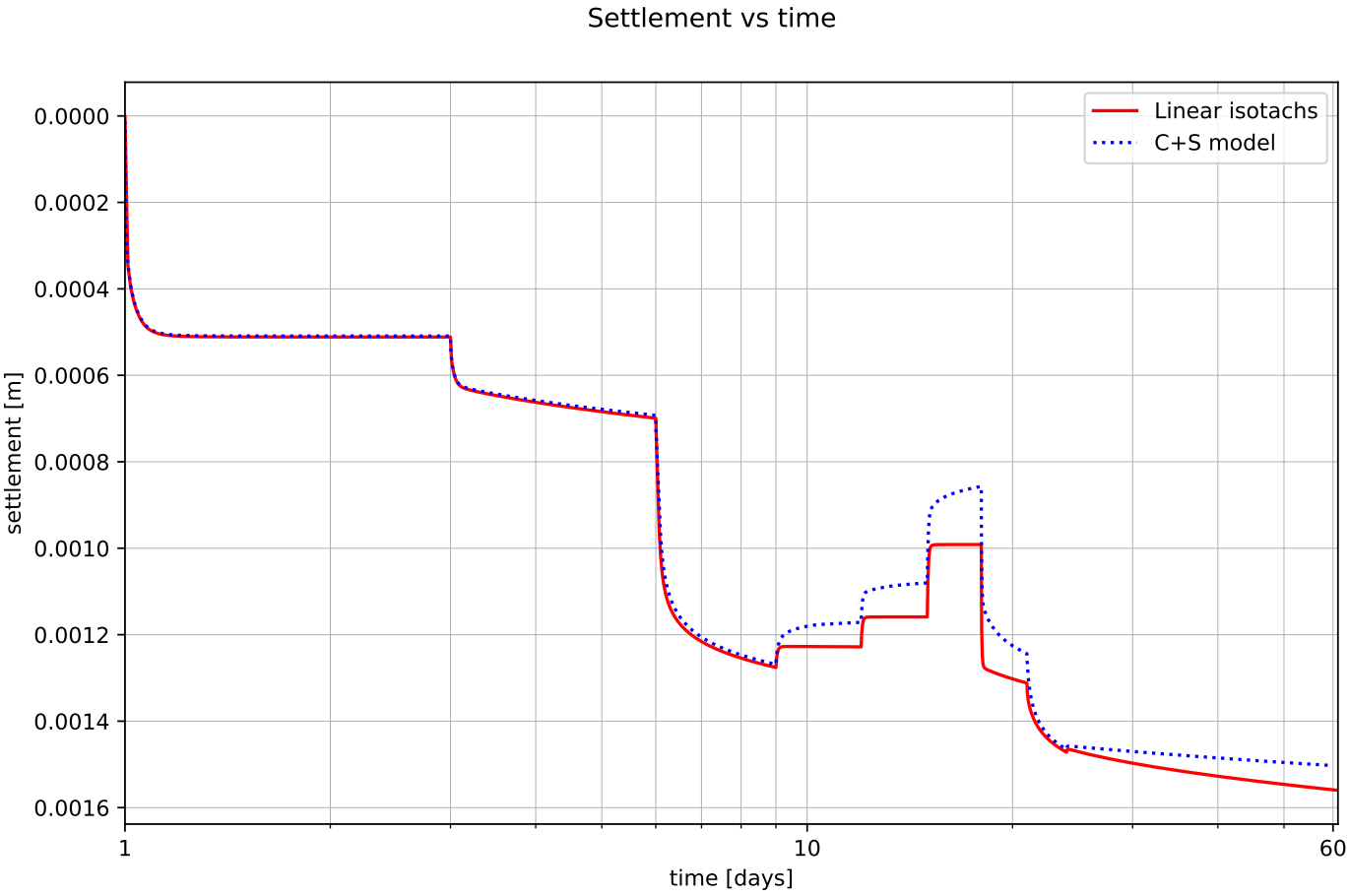

Unloading IL test GH non-linear isotachs

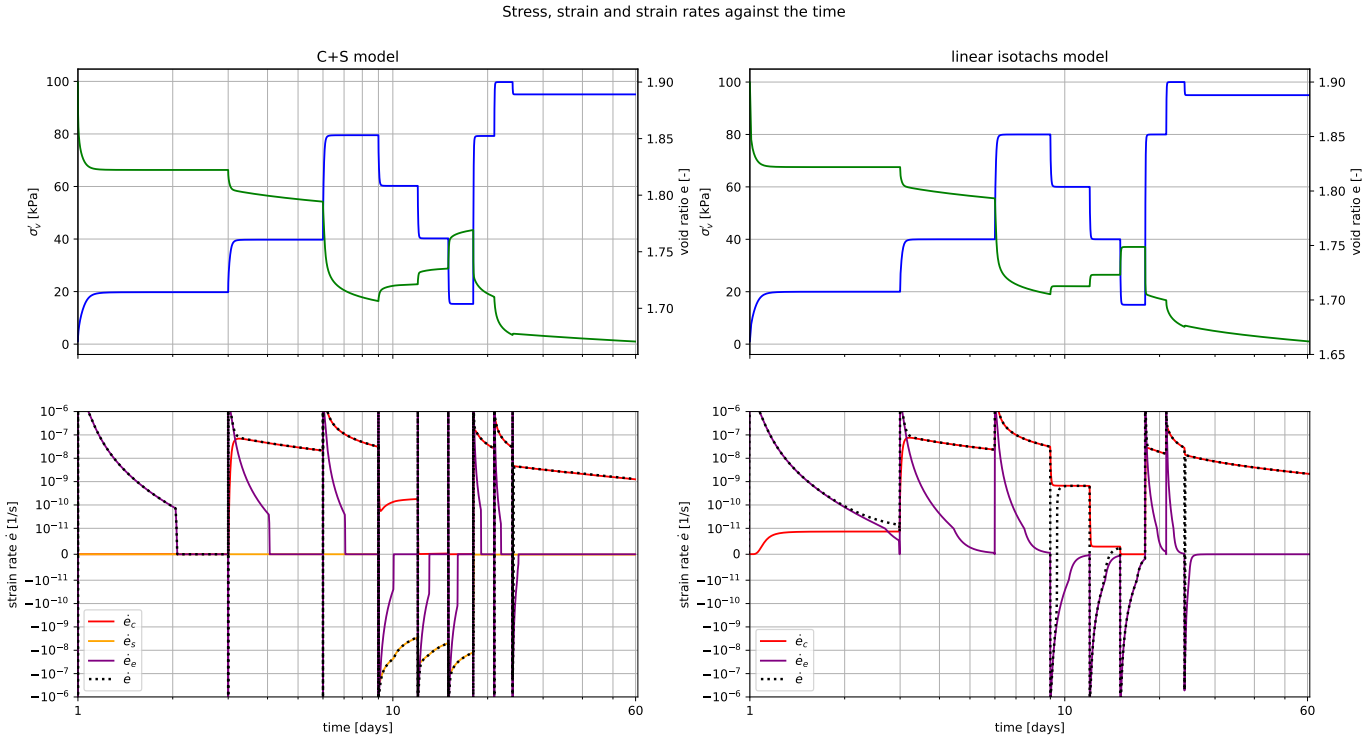

Unloading IL test GH non-linear isotachs

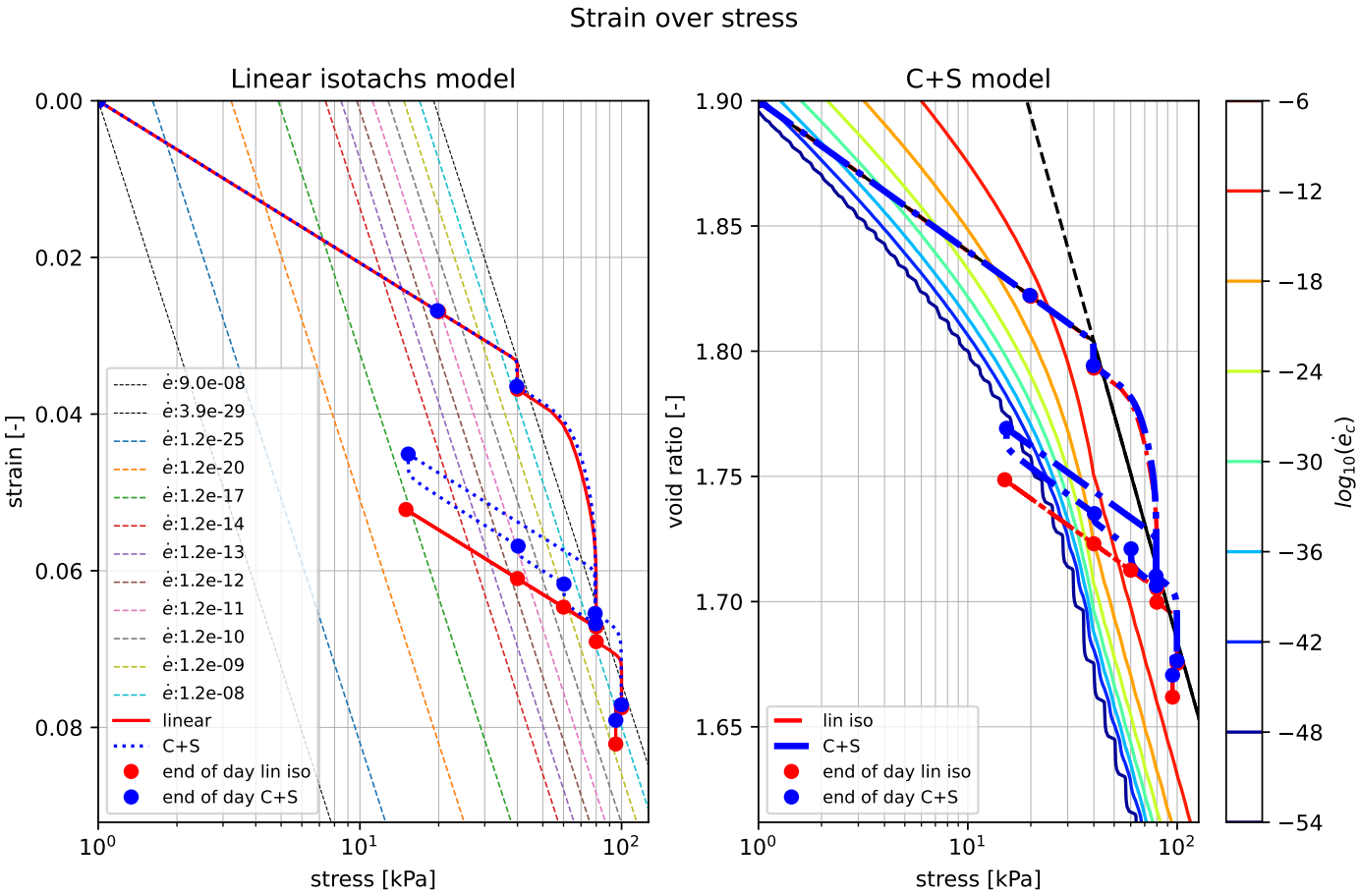

Unloading IL test GH non-linear isotachs

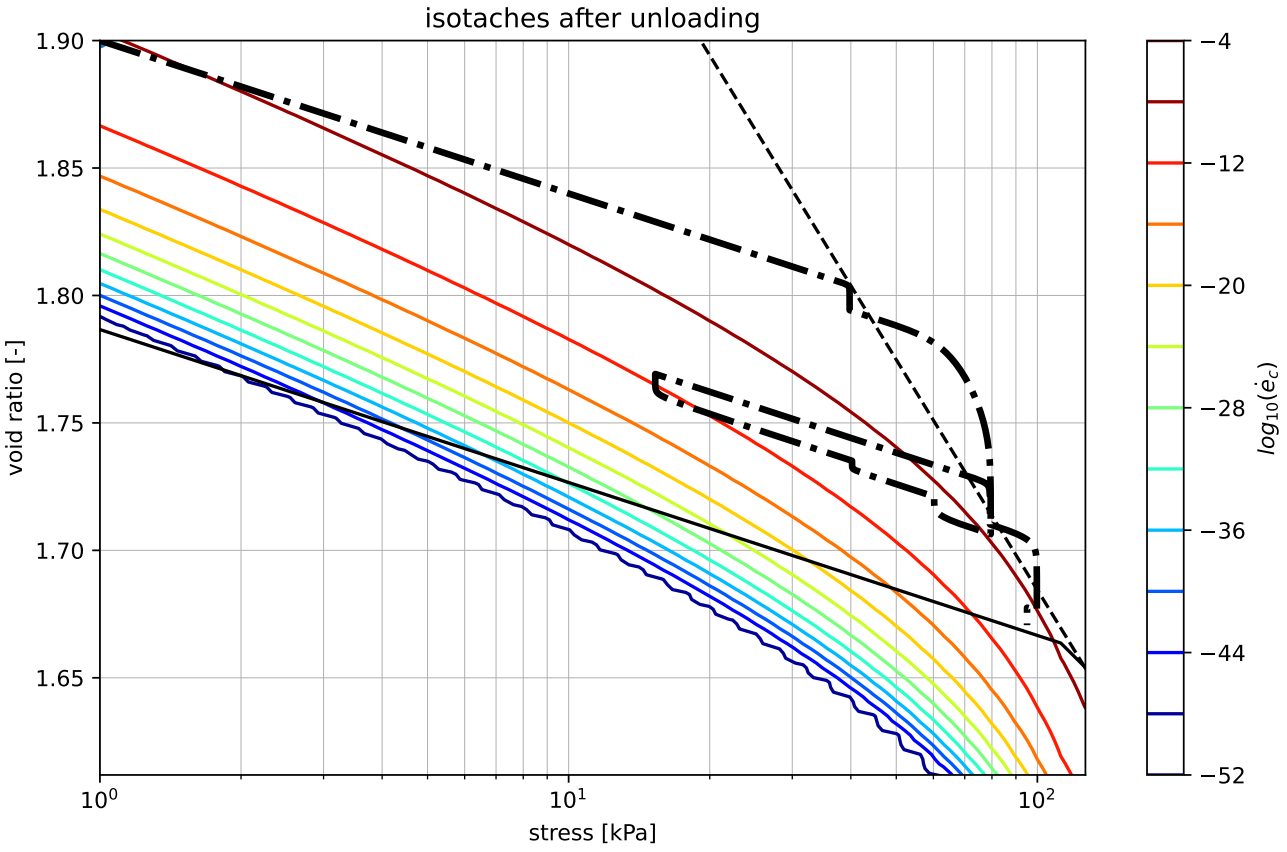

Unloading IL test GH non-linear isotachs

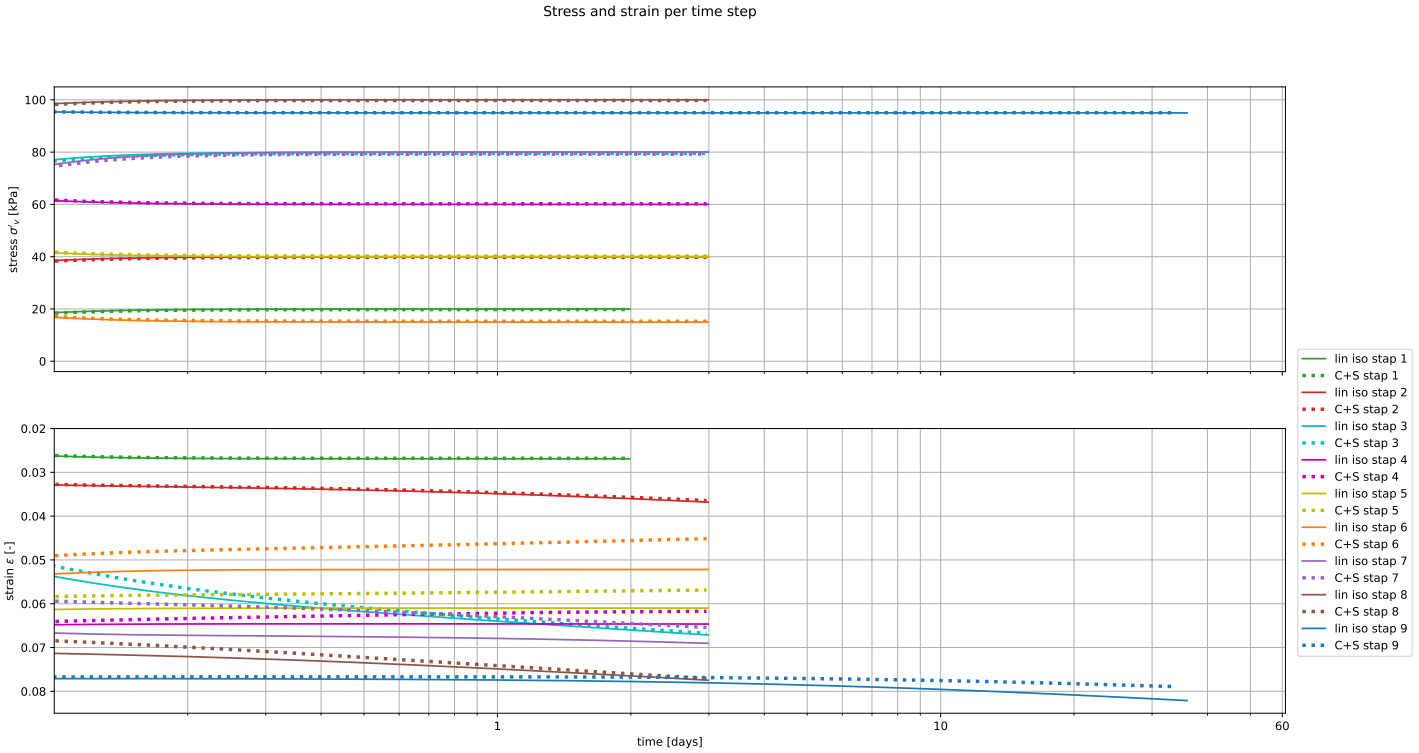

Standard IL test Paper non-linear isotachs

Standard IL test Paper non-linear isotachs

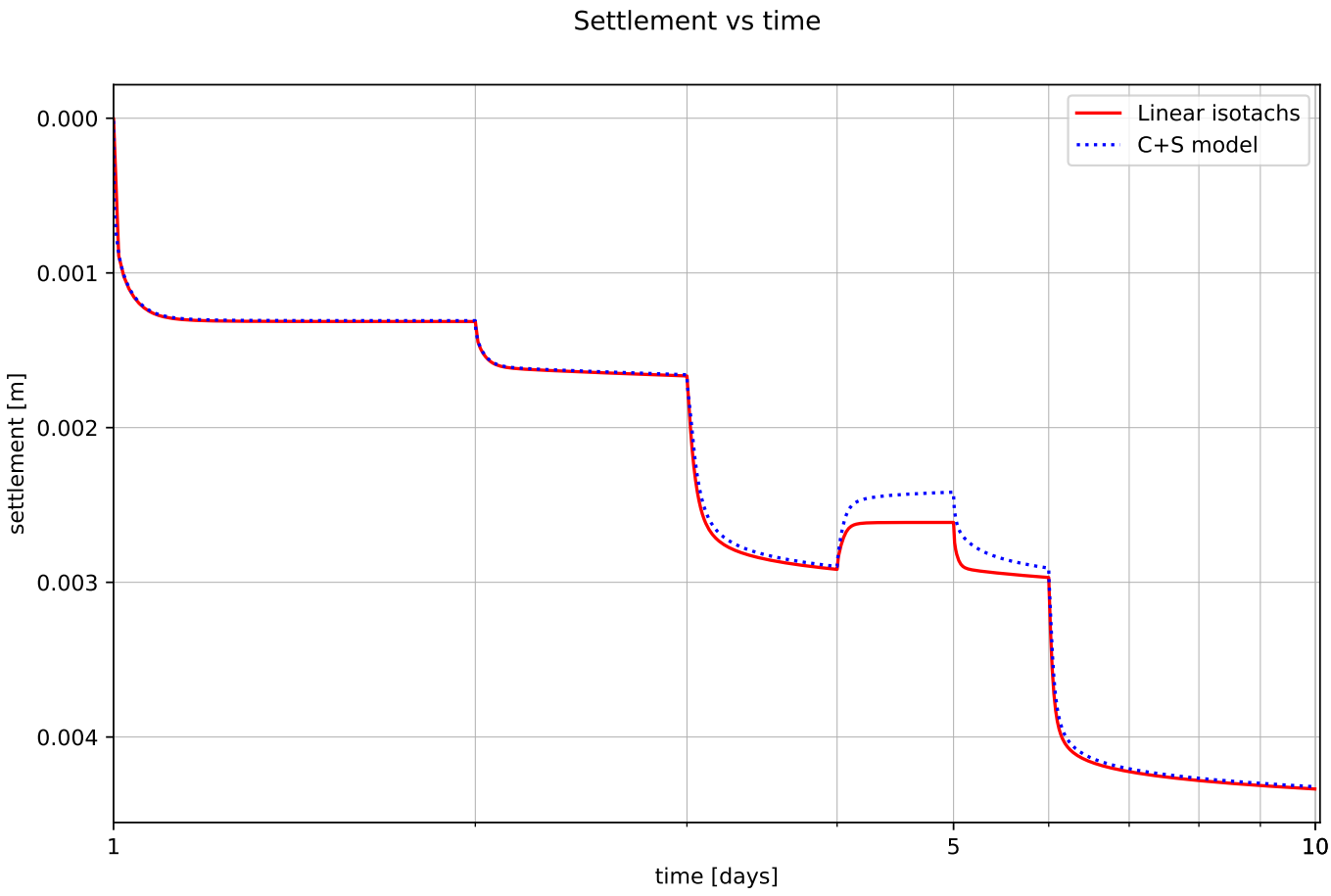

Standard IL test Paper non-linear isotachs

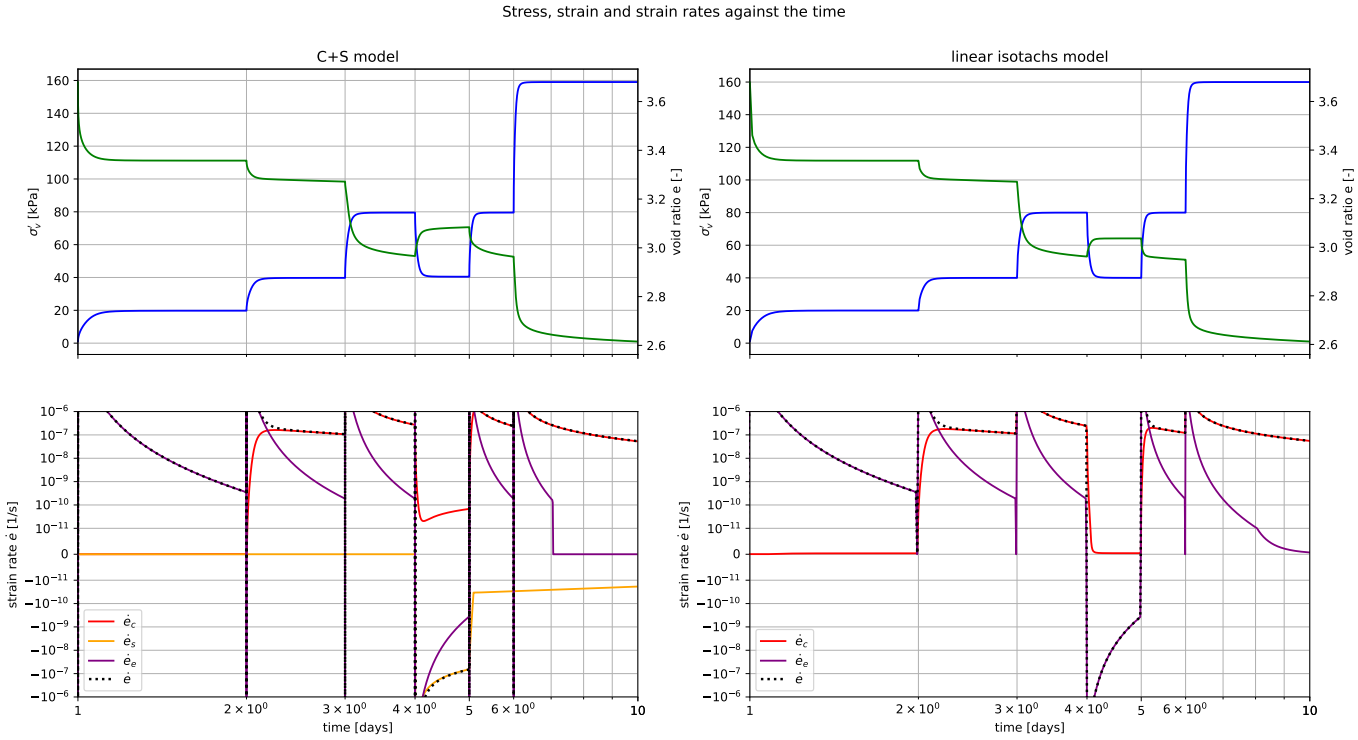

Standard IL test Paper non-linear isotachs

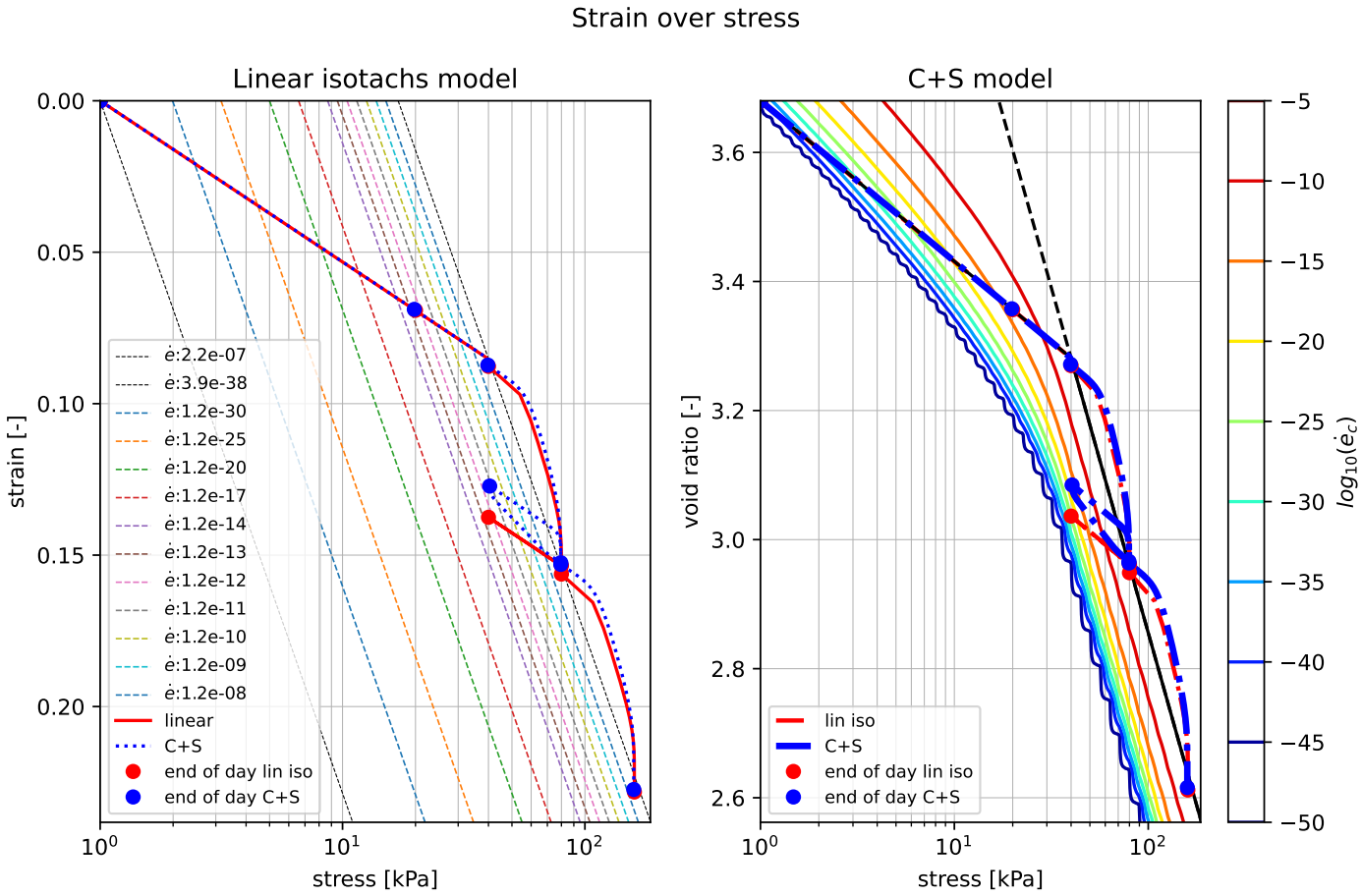

Standard IL test Paper non-linear isotachs

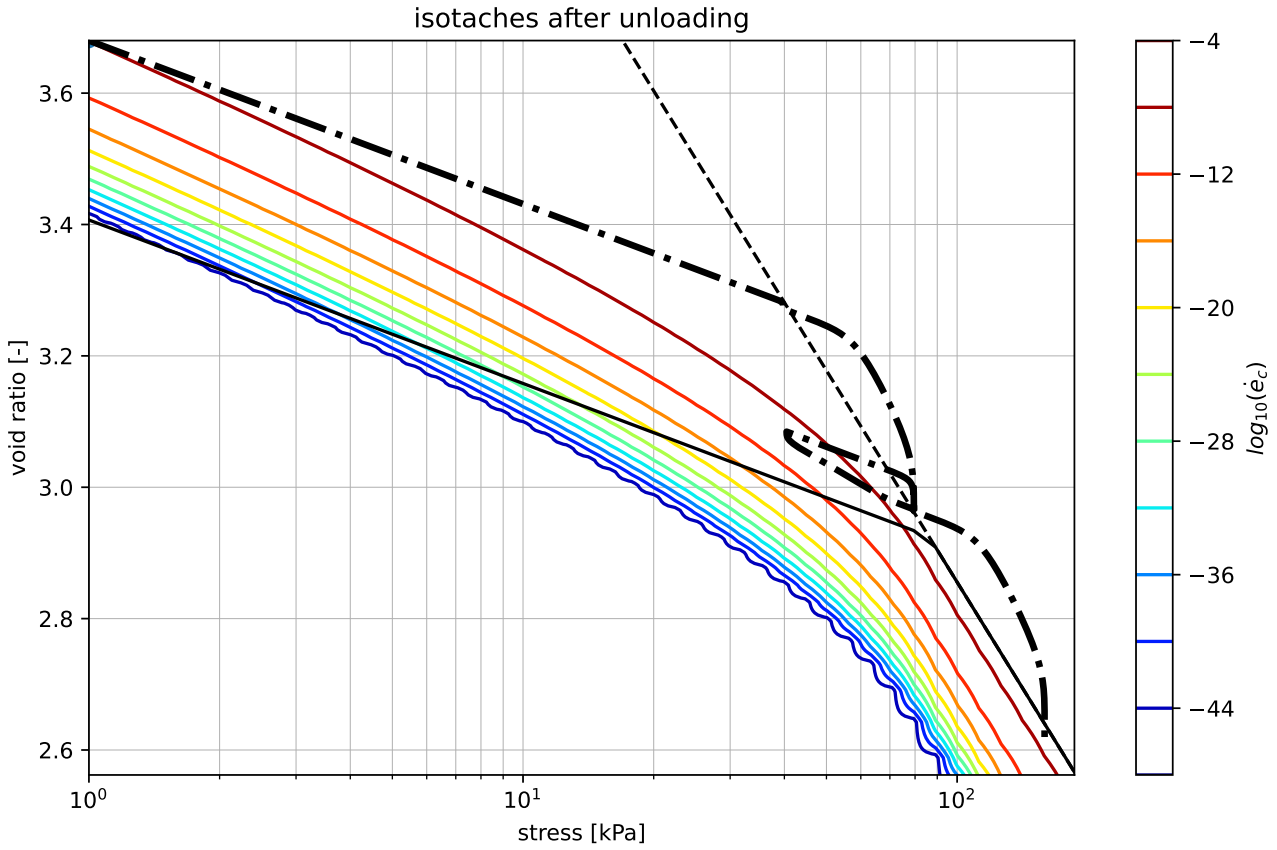

Standard IL test Paper non-linear isotachs

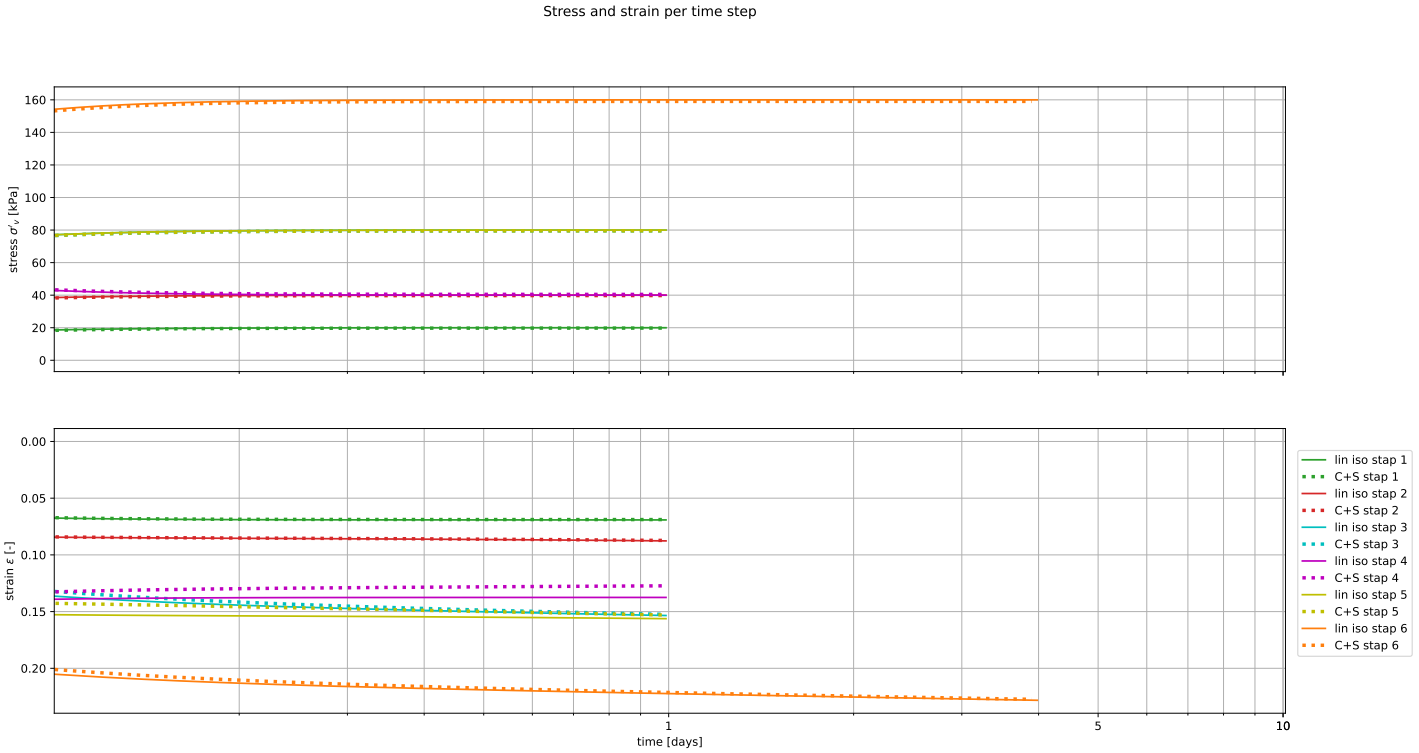

Unloading IL test Paper non-linear isotachs

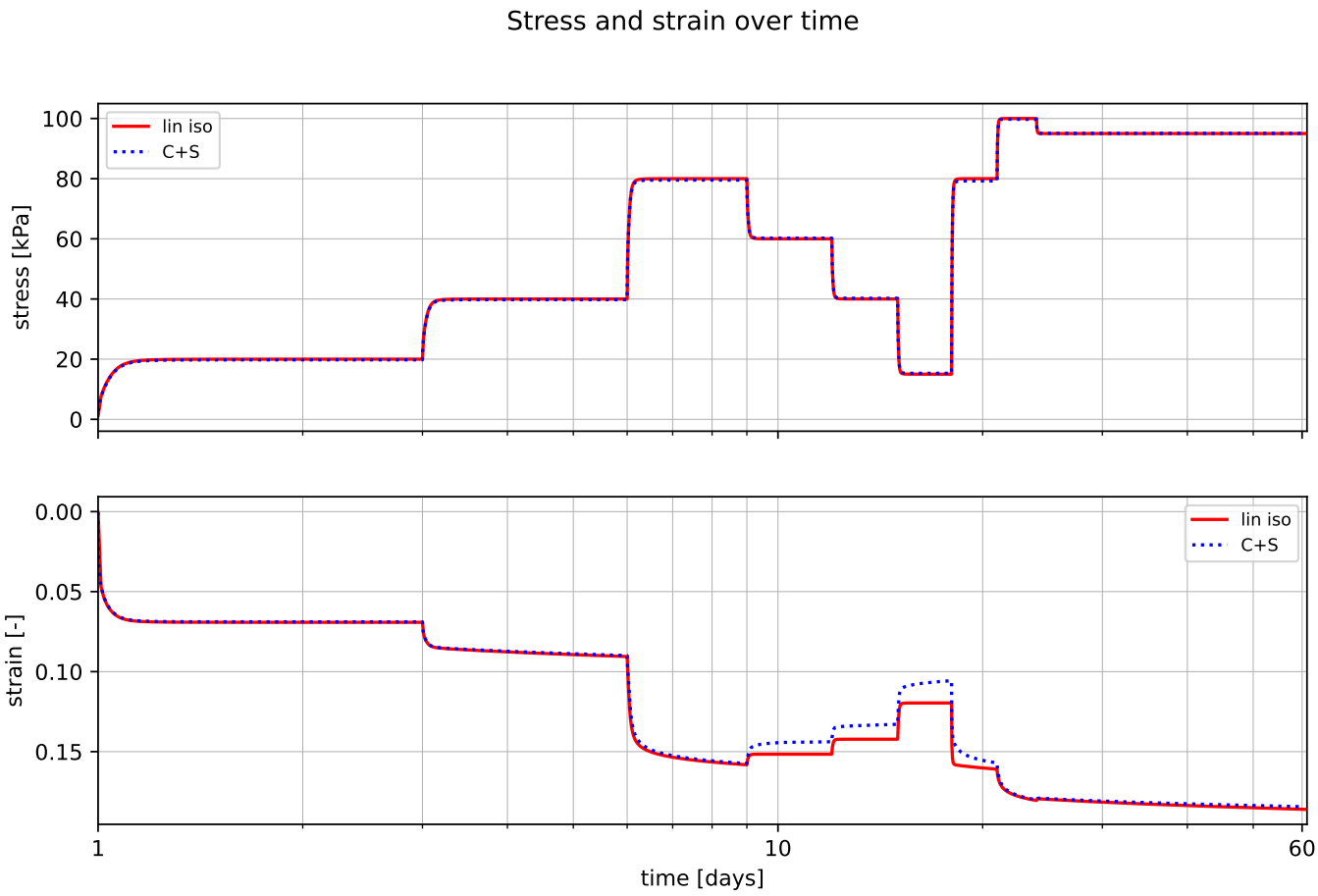

Unloading IL test Paper non-linear isotachs

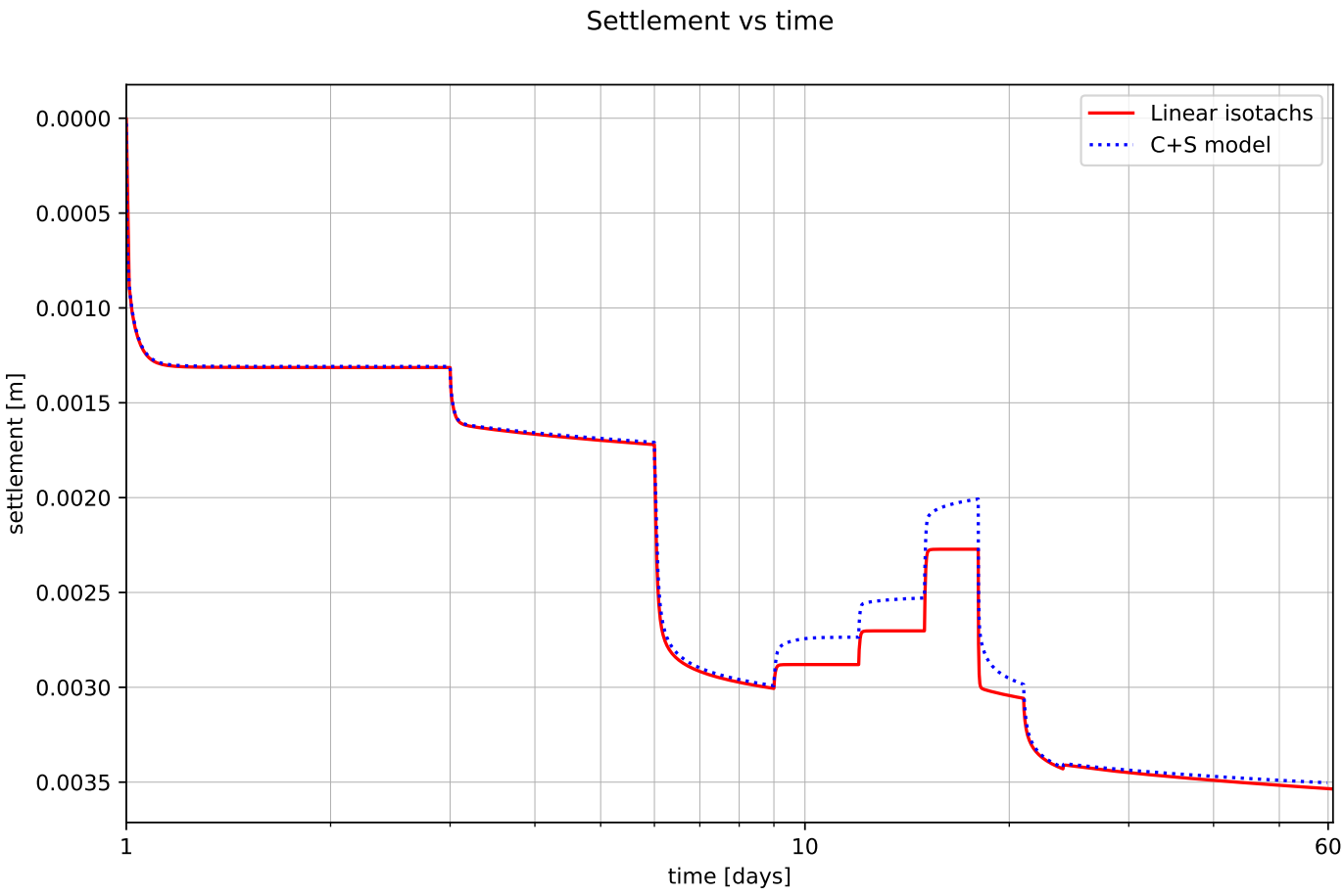

Unloading IL test Paper non-linear isotachs

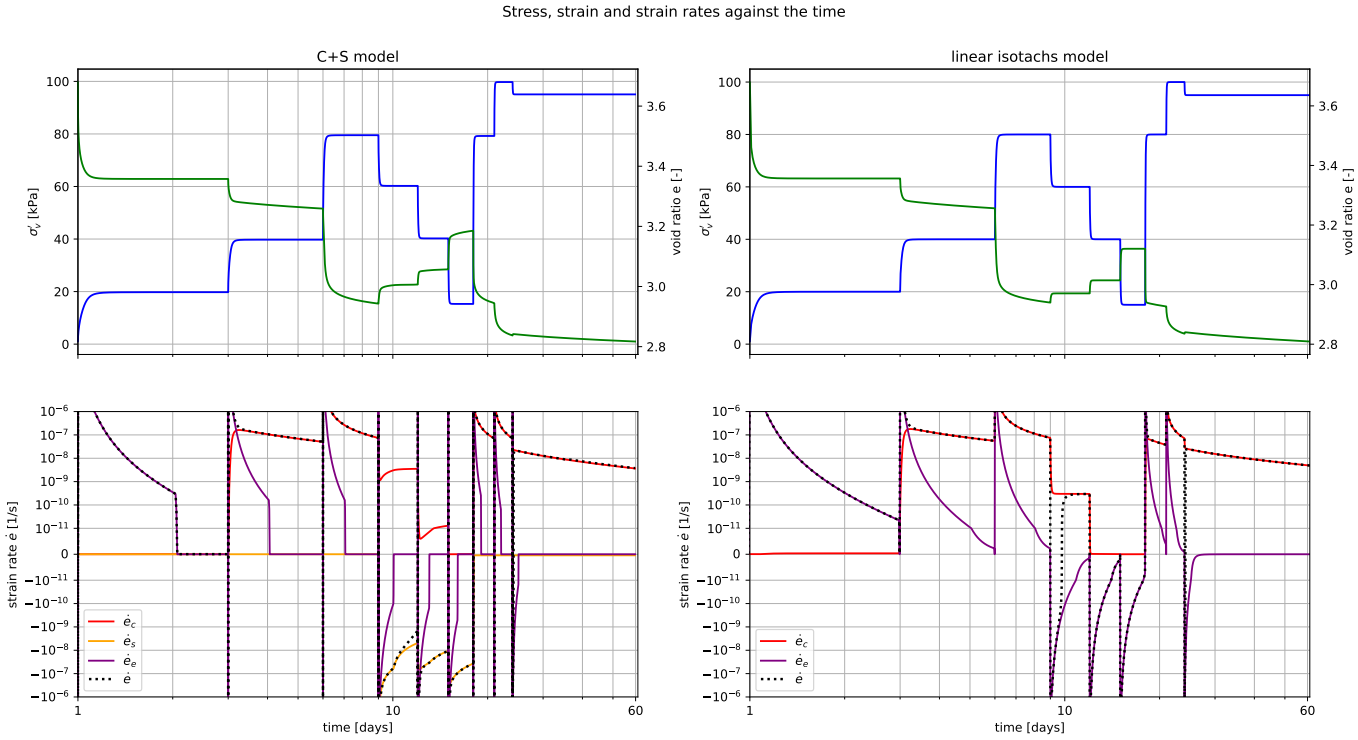

Unloading IL test Paper non-linear isotachs

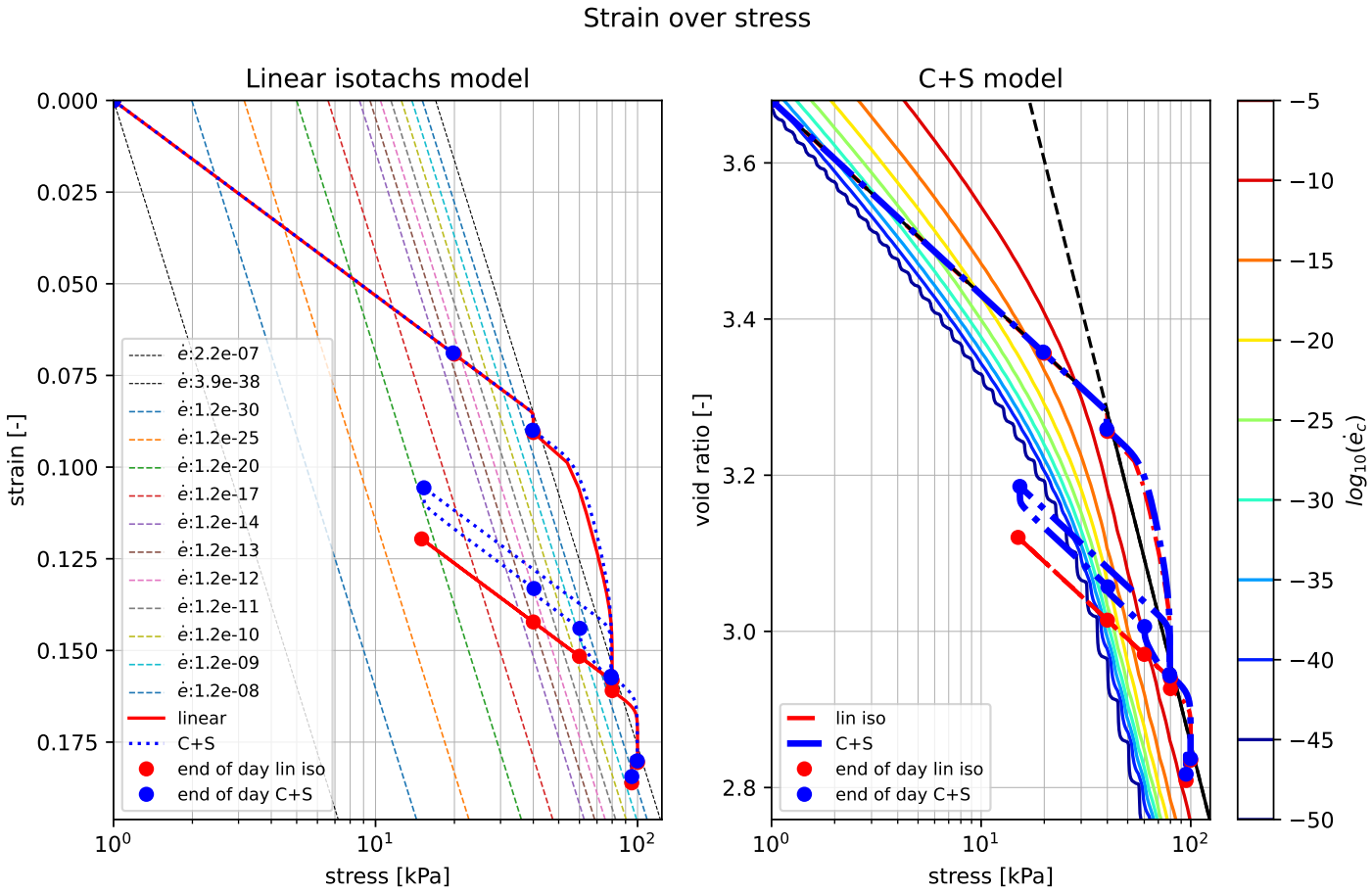

Unloading IL test Paper non-linear isotachs

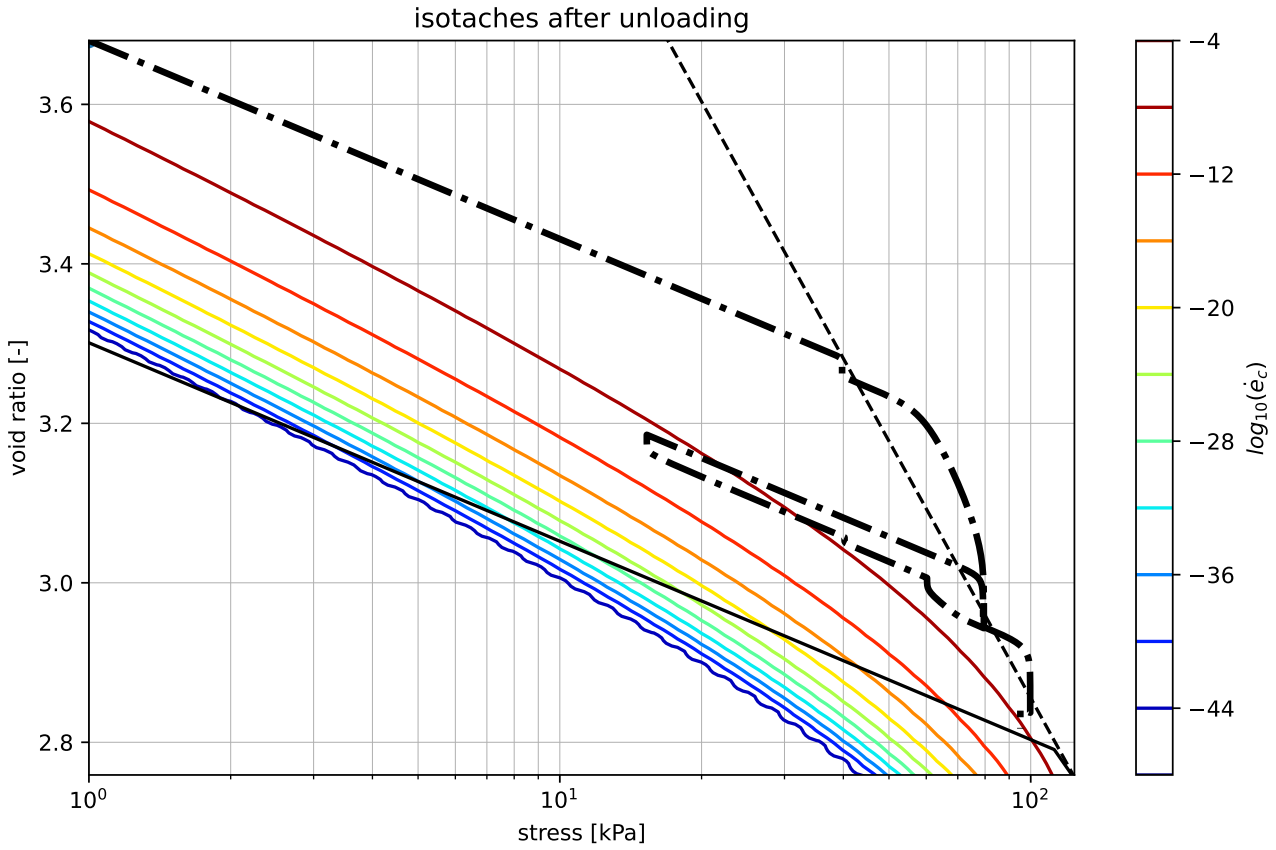

Unloading IL test Paper non-linear isotachs

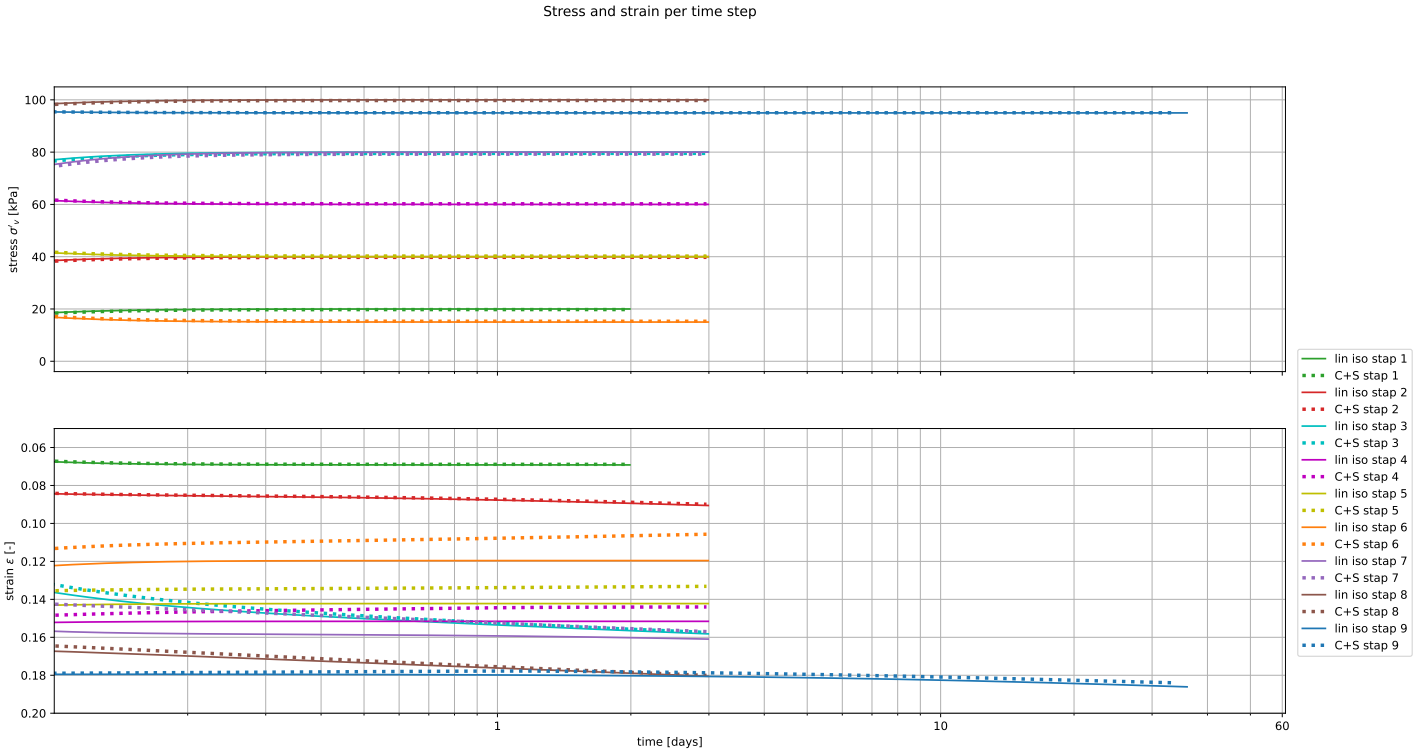

A.3.2. C+S model with swell and linearity

In this Appendix all the generated graphs are presented for the incremental loading tests in which the C+S model has swell and linear isotachs. The GitHub and Paper parameter set are presented for both the standard and unloading scenarios.

Standard IL test GH linear isotachs

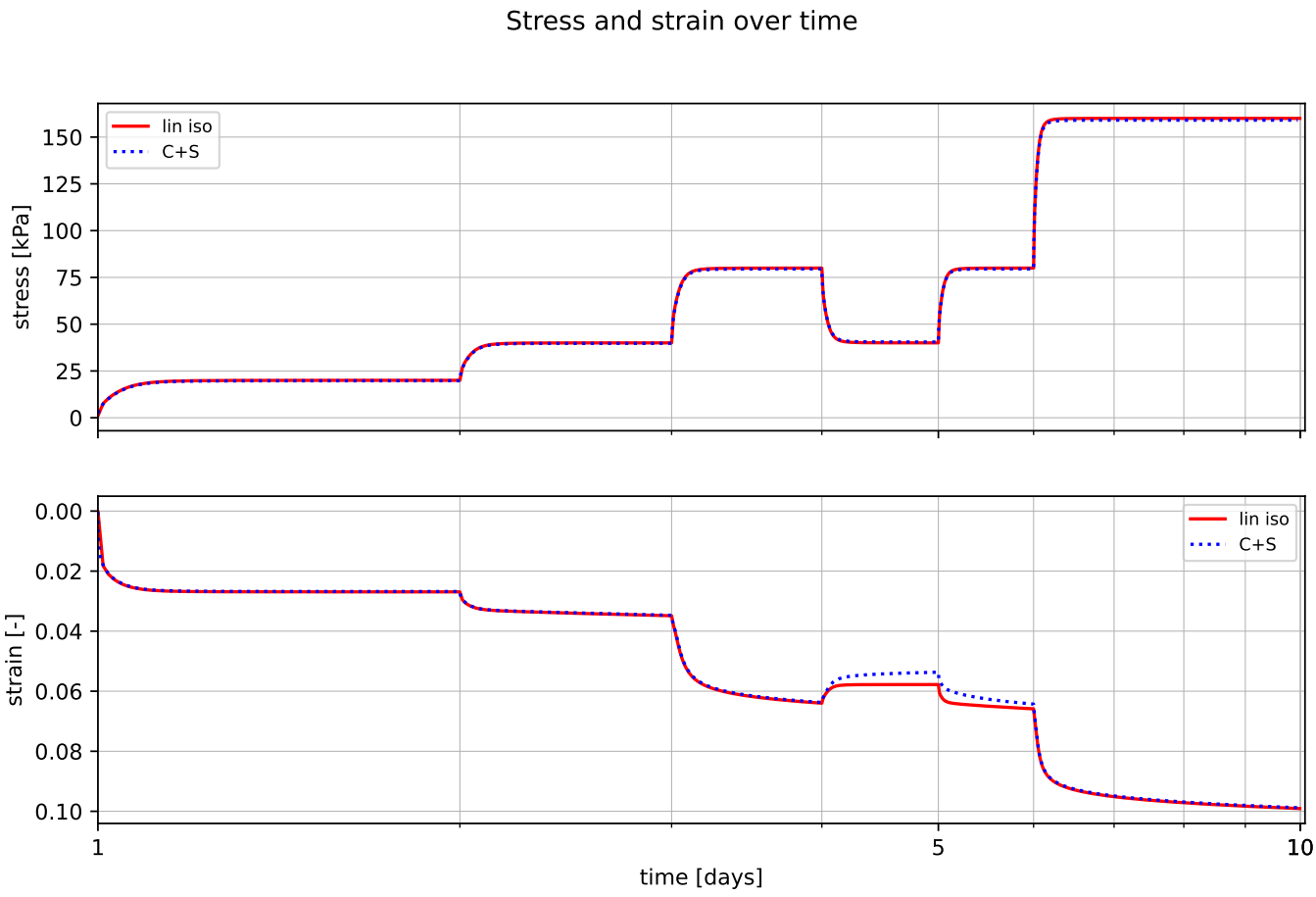

Standard IL test GH linear isotachs

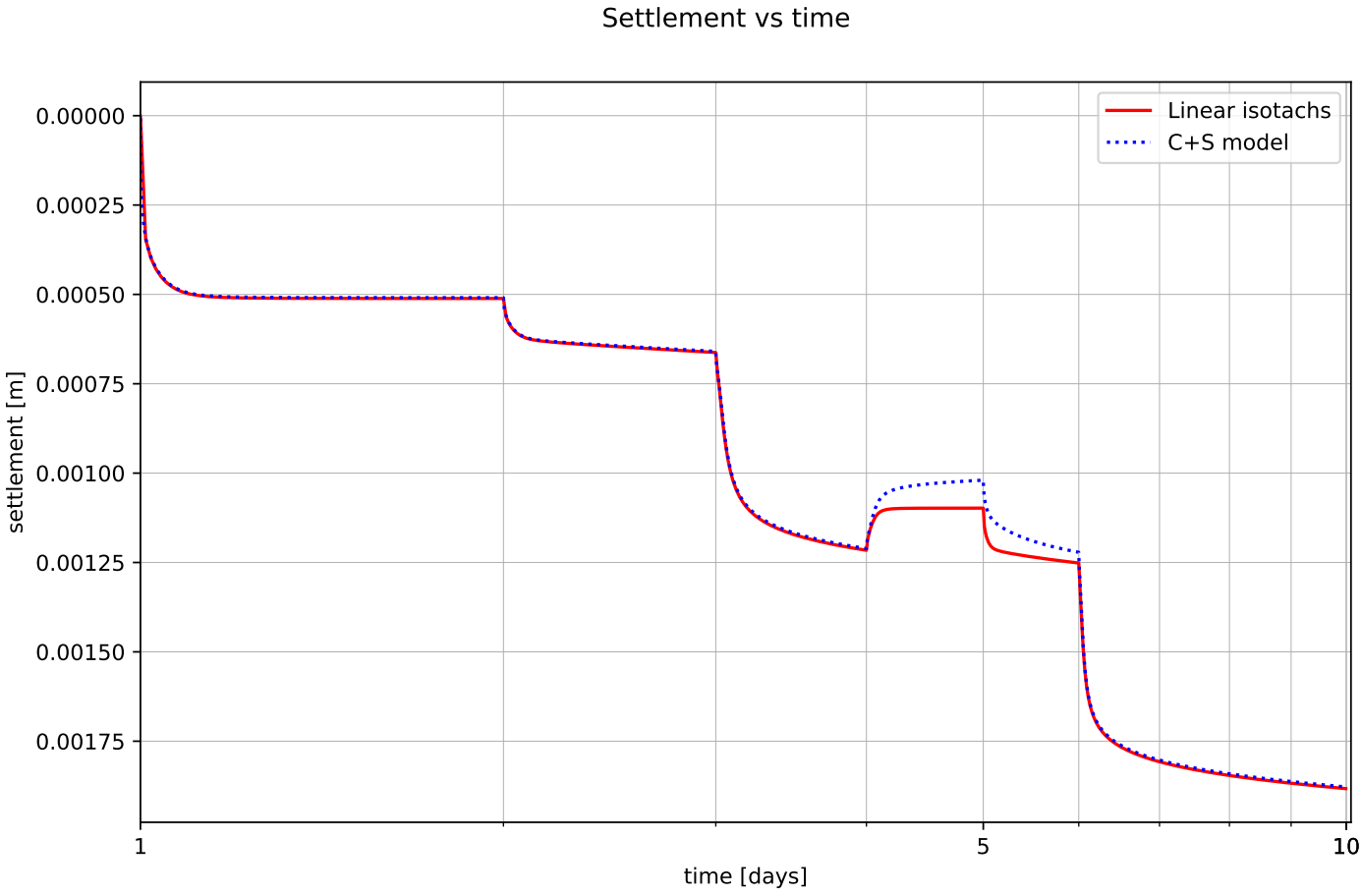

Standard IL test GH linear isotachs

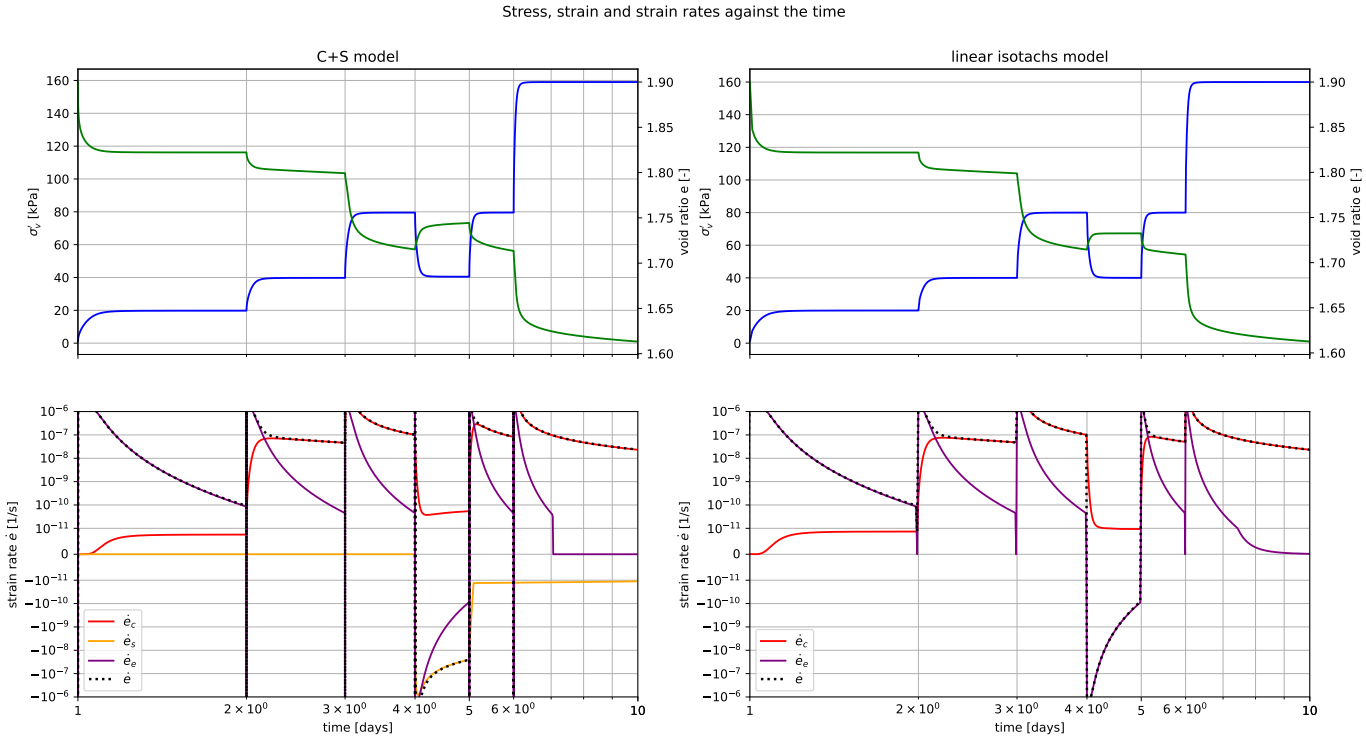

Standard IL test GH linear isotachs

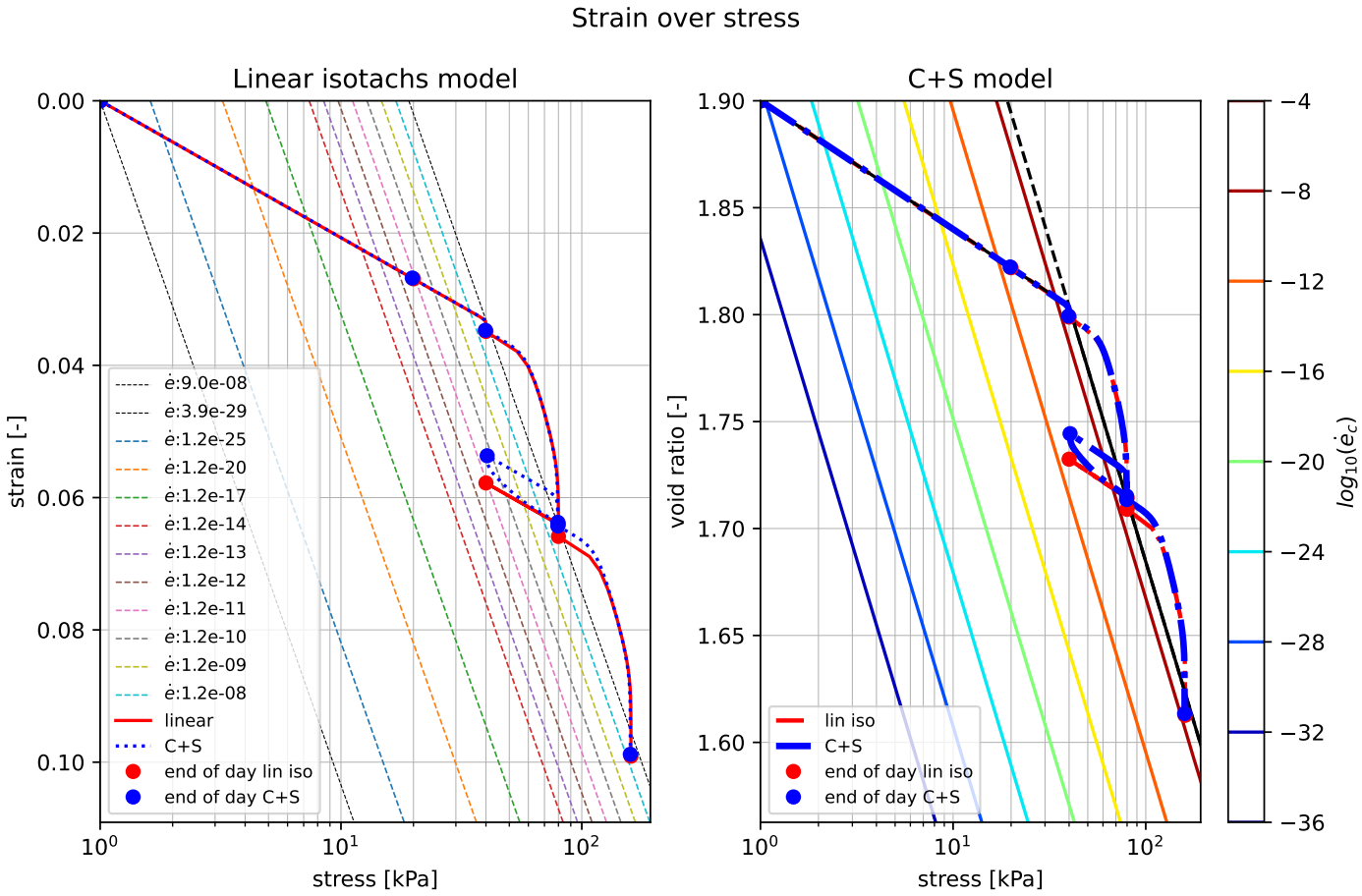

Standard IL test GH linear isotachs

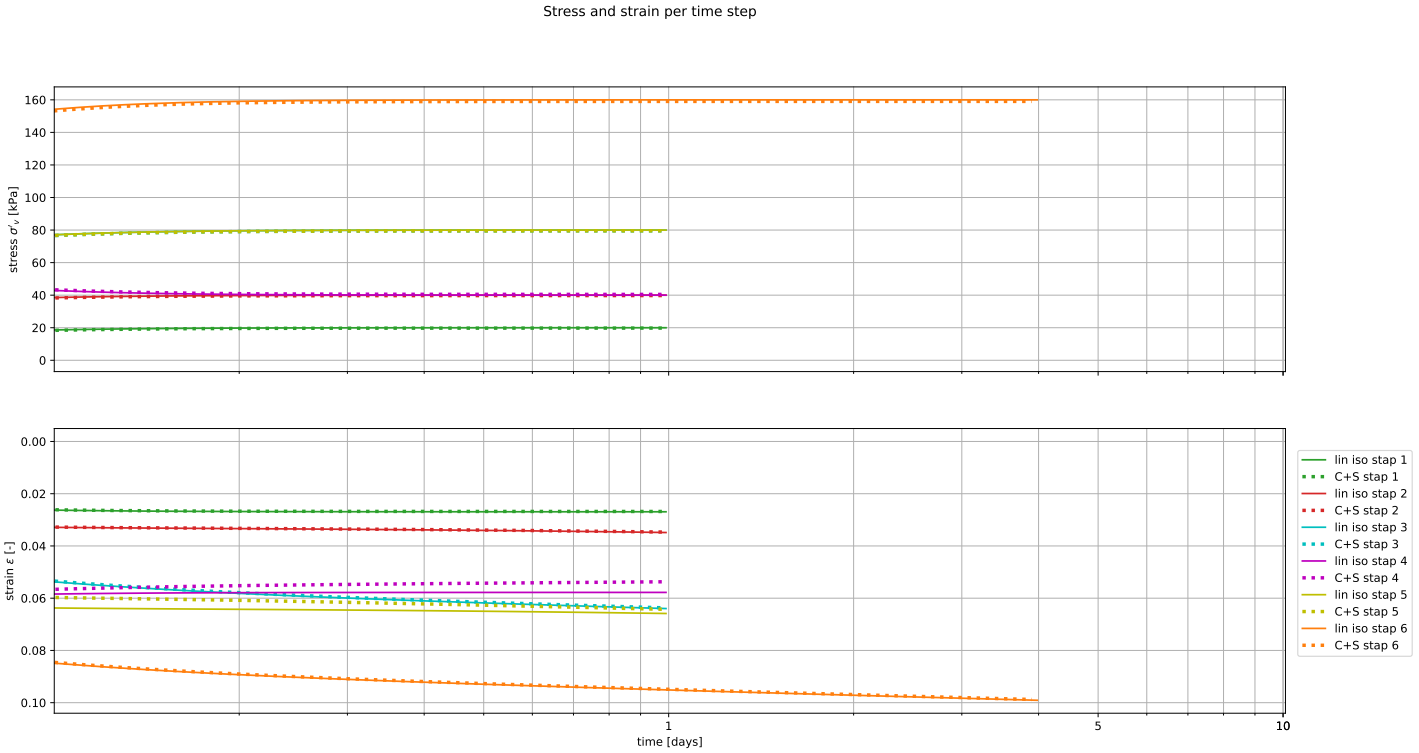

Unloading IL test GH linear isotachs

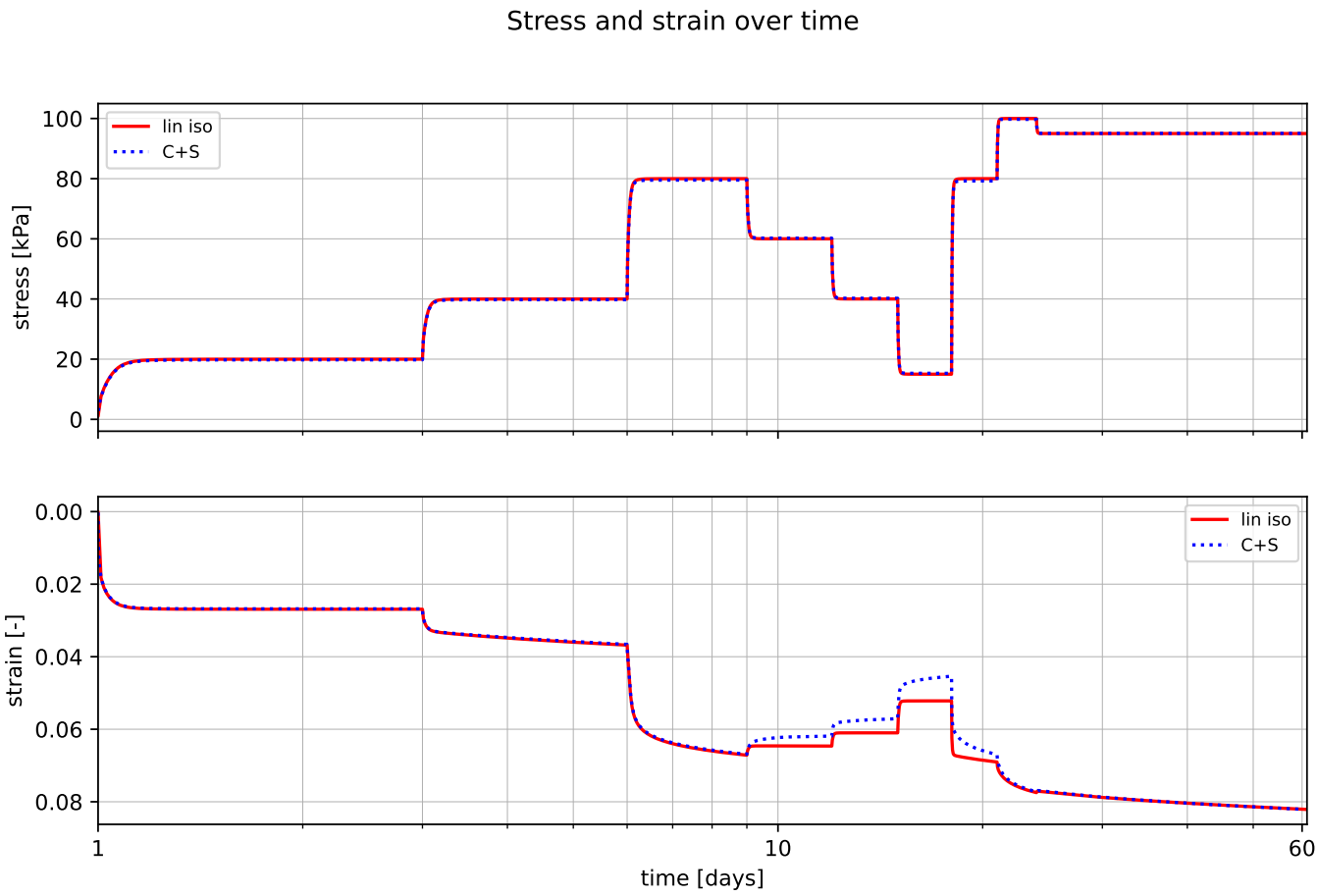

Unloading IL test GH linear isotachs

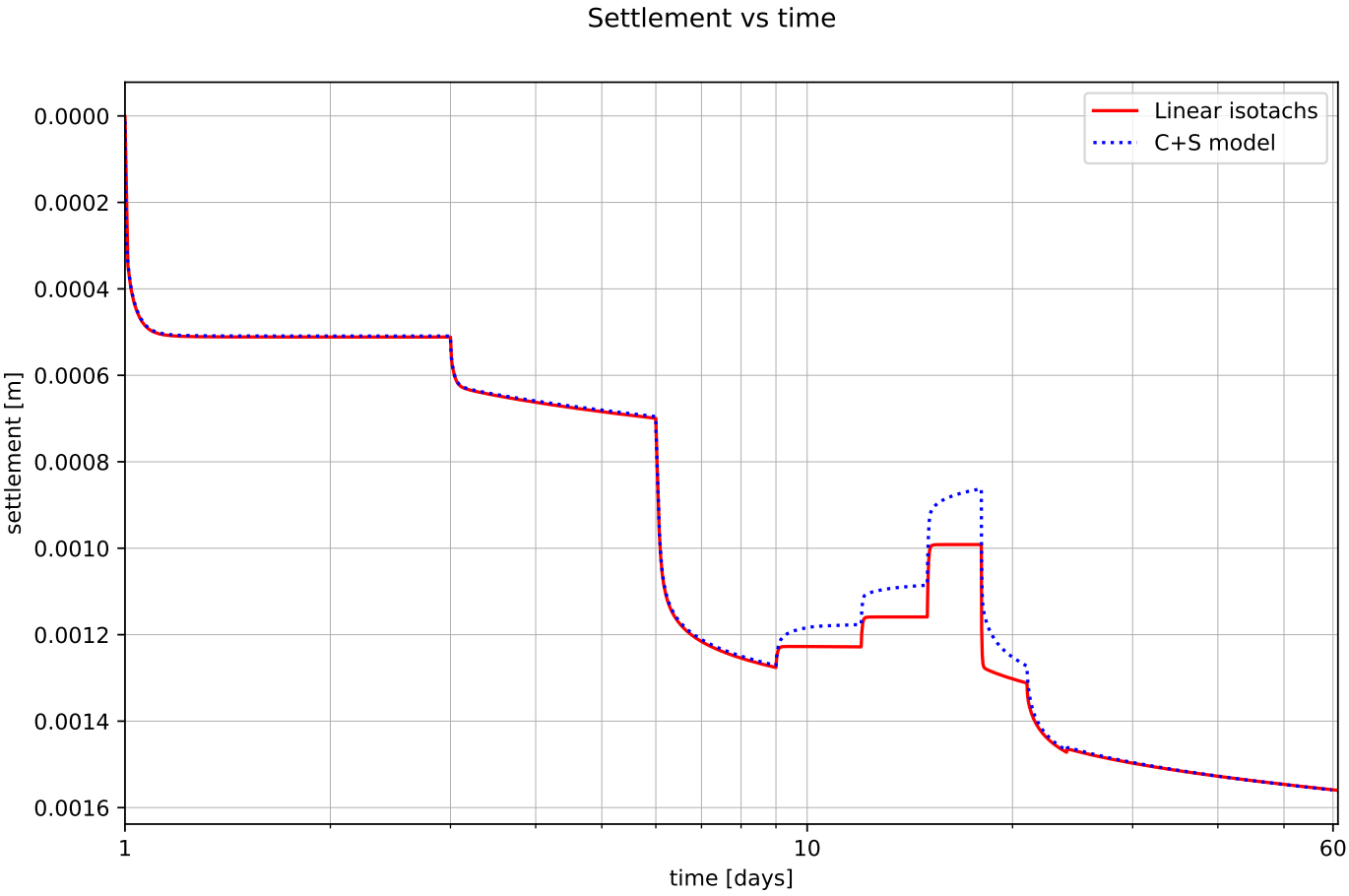

Unloading IL test GH linear isotachs

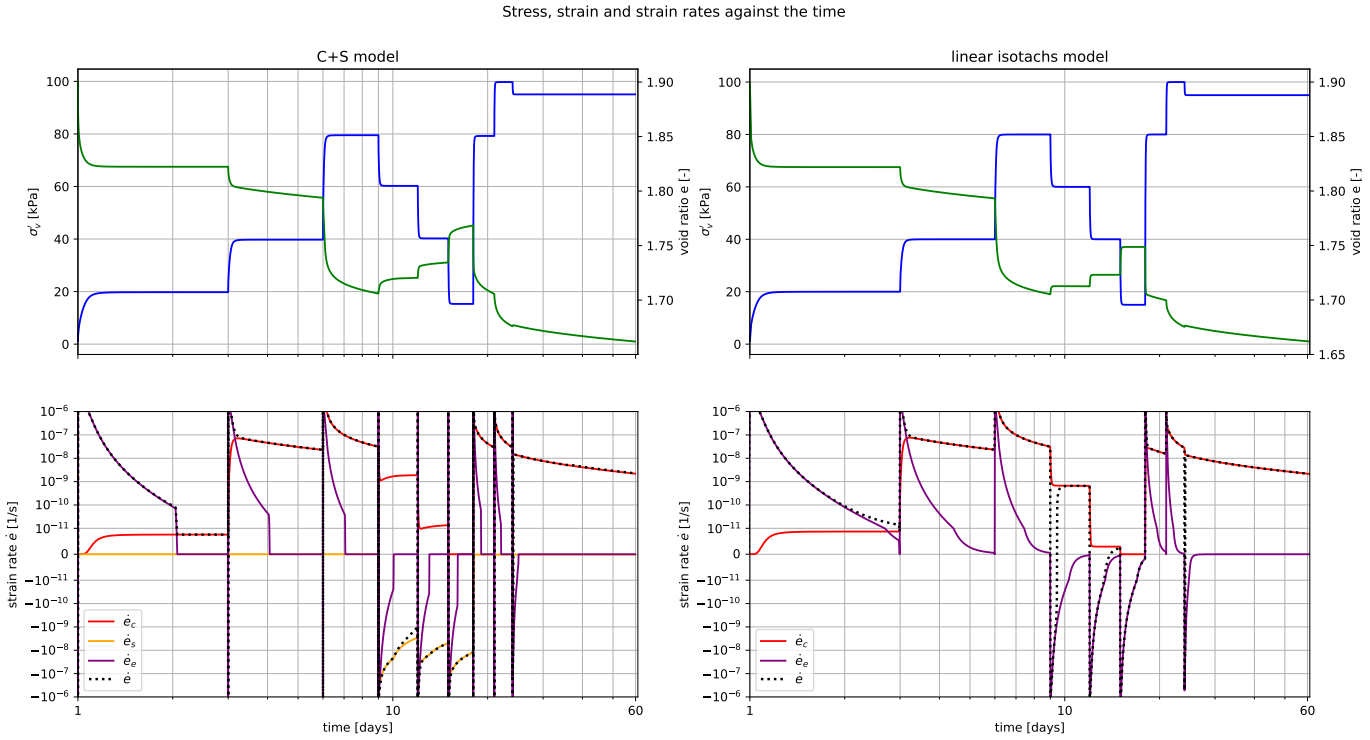

Unloading IL test GH linear isotachs

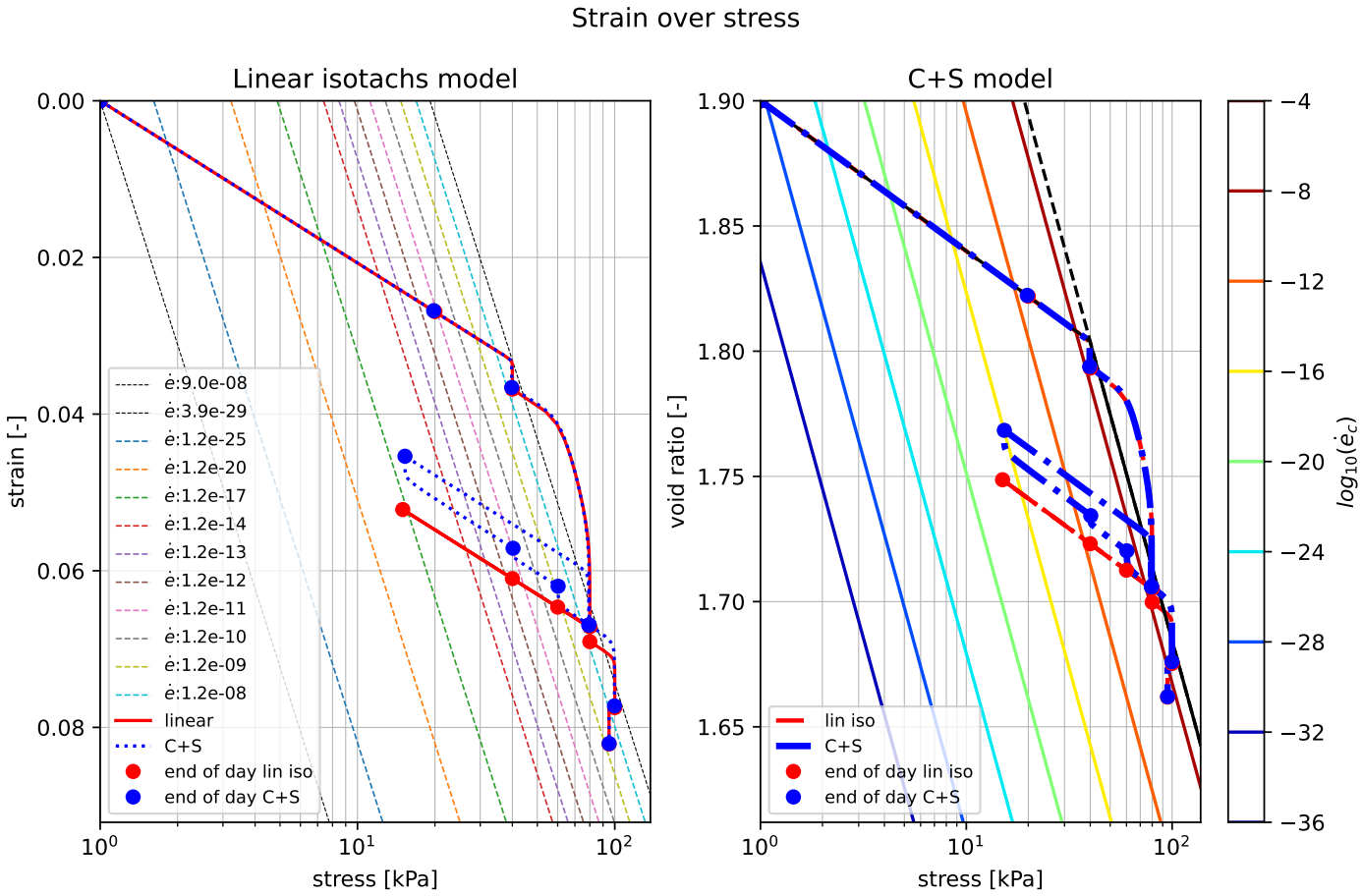

Unloading IL test GH linear isotachs

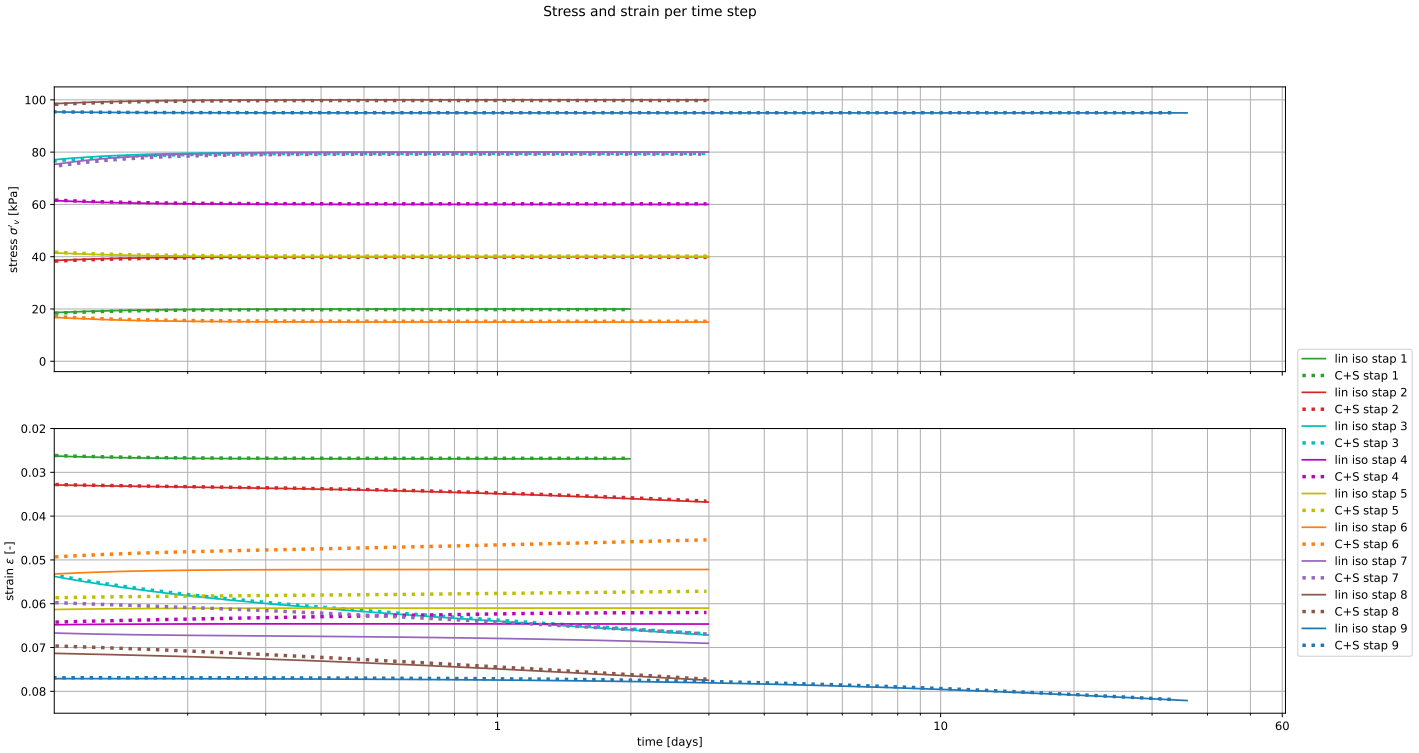

Standard IL test Paper linear isotachs

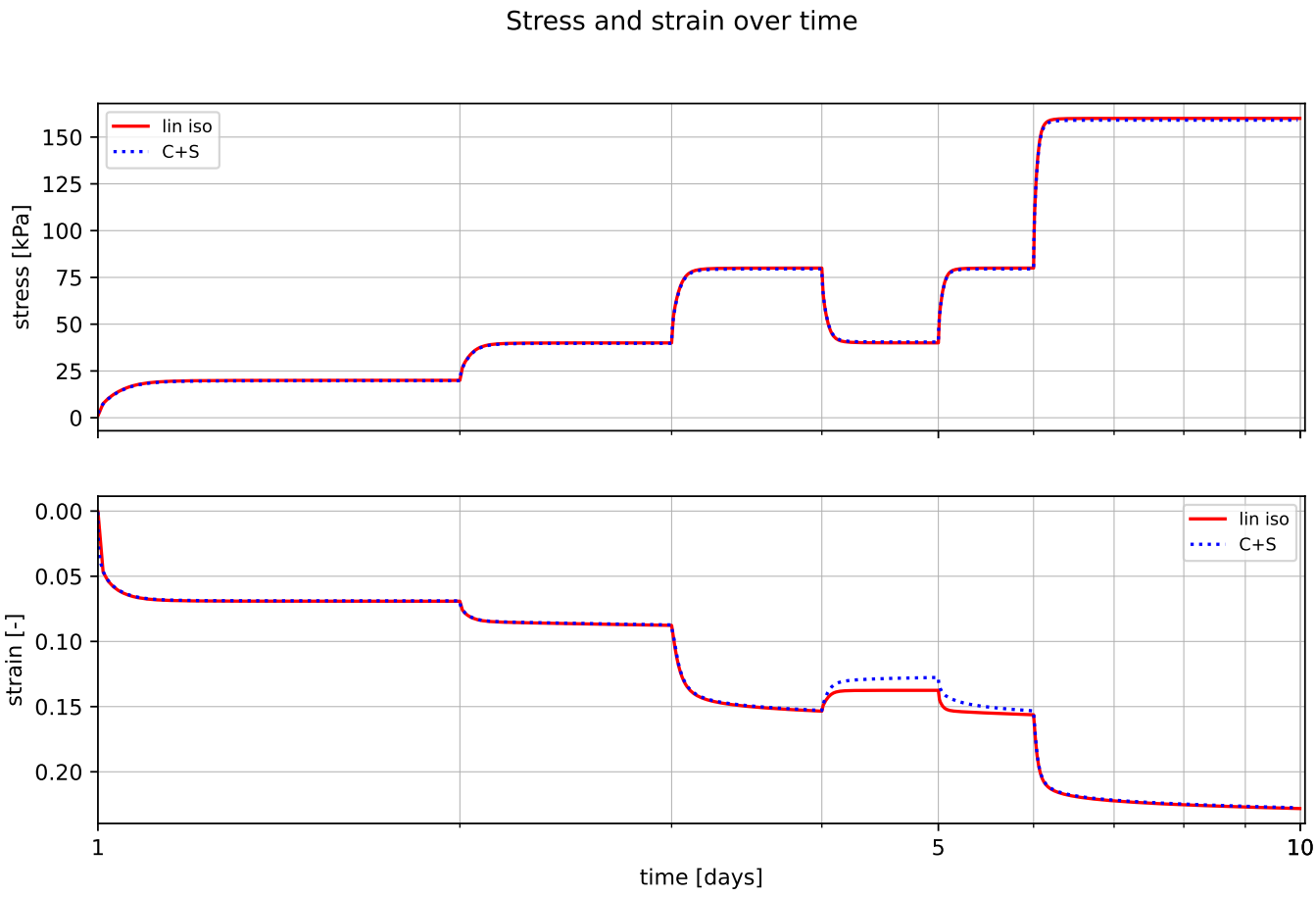

Standard IL test Paper linear isotachs

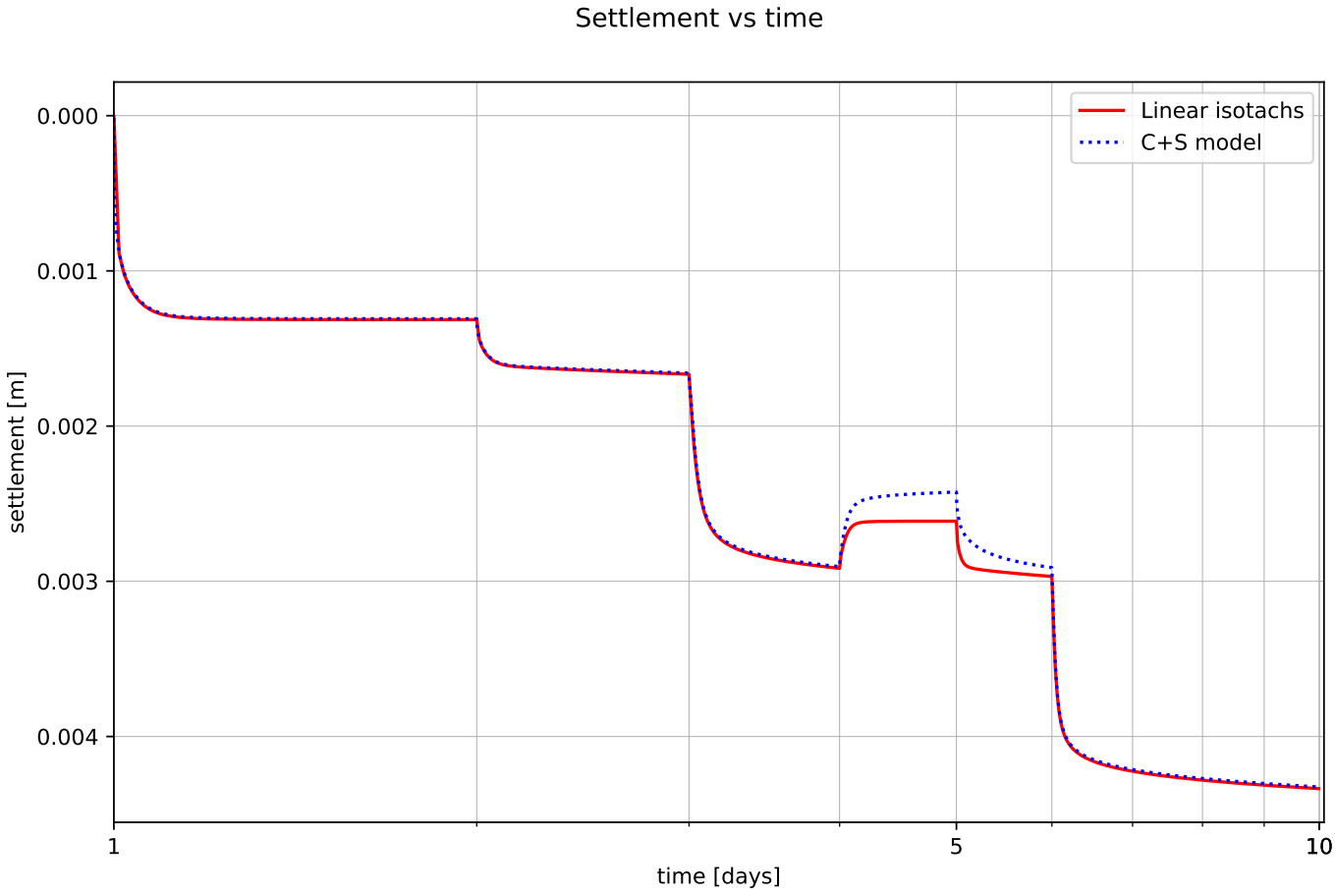

Standard IL test Paper linear isotachs

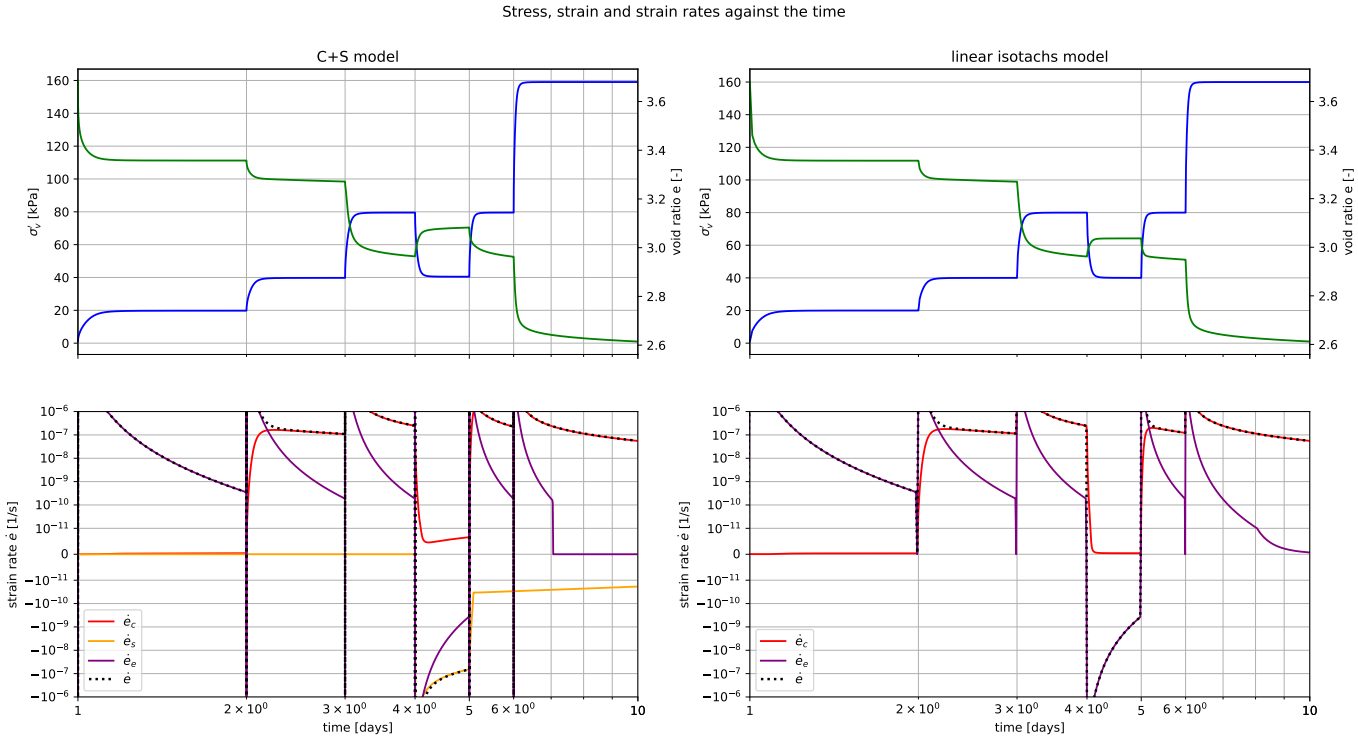

Standard IL test Paper linear isotachs

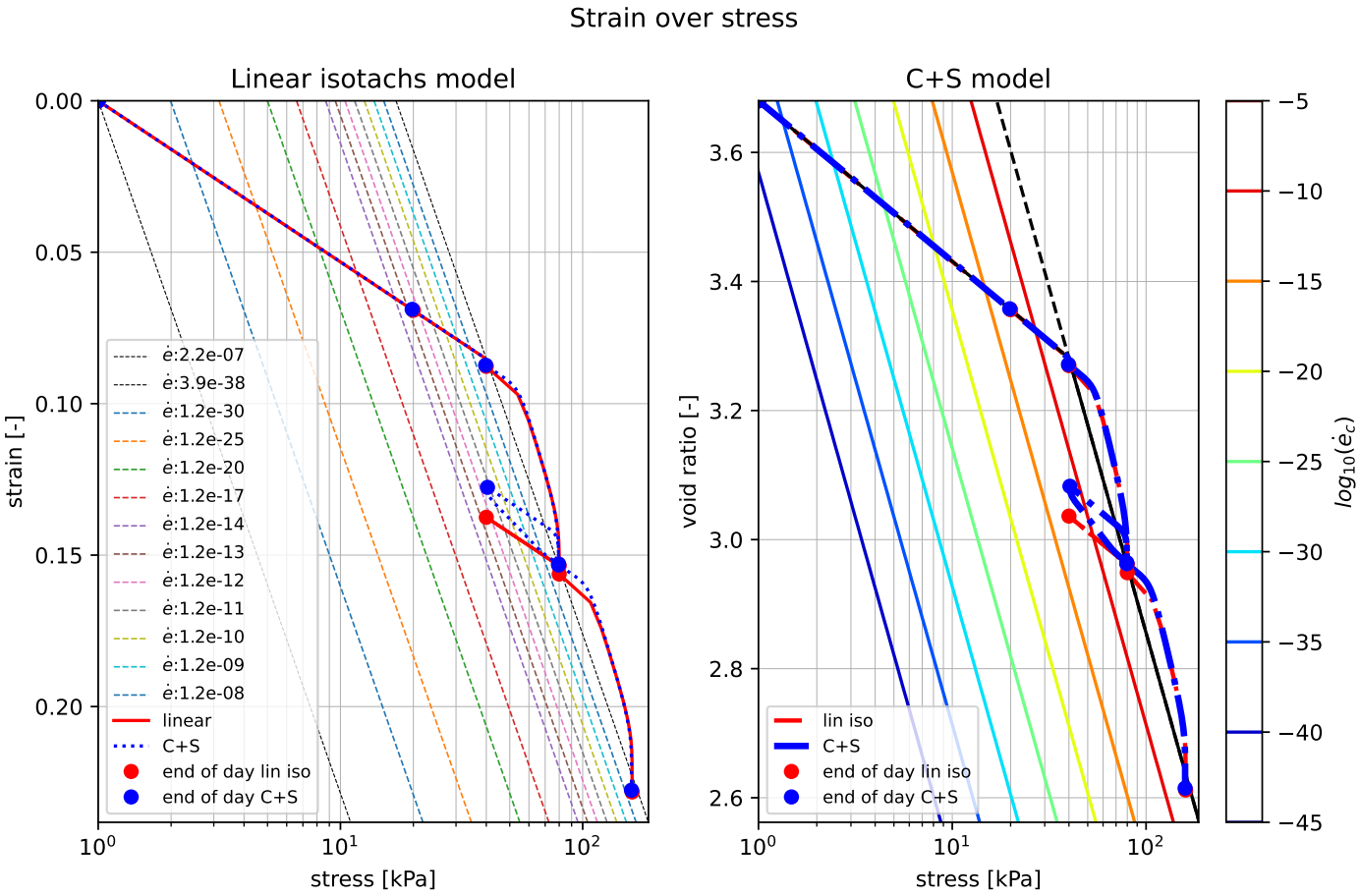

Standard IL test Paper linear isotachs

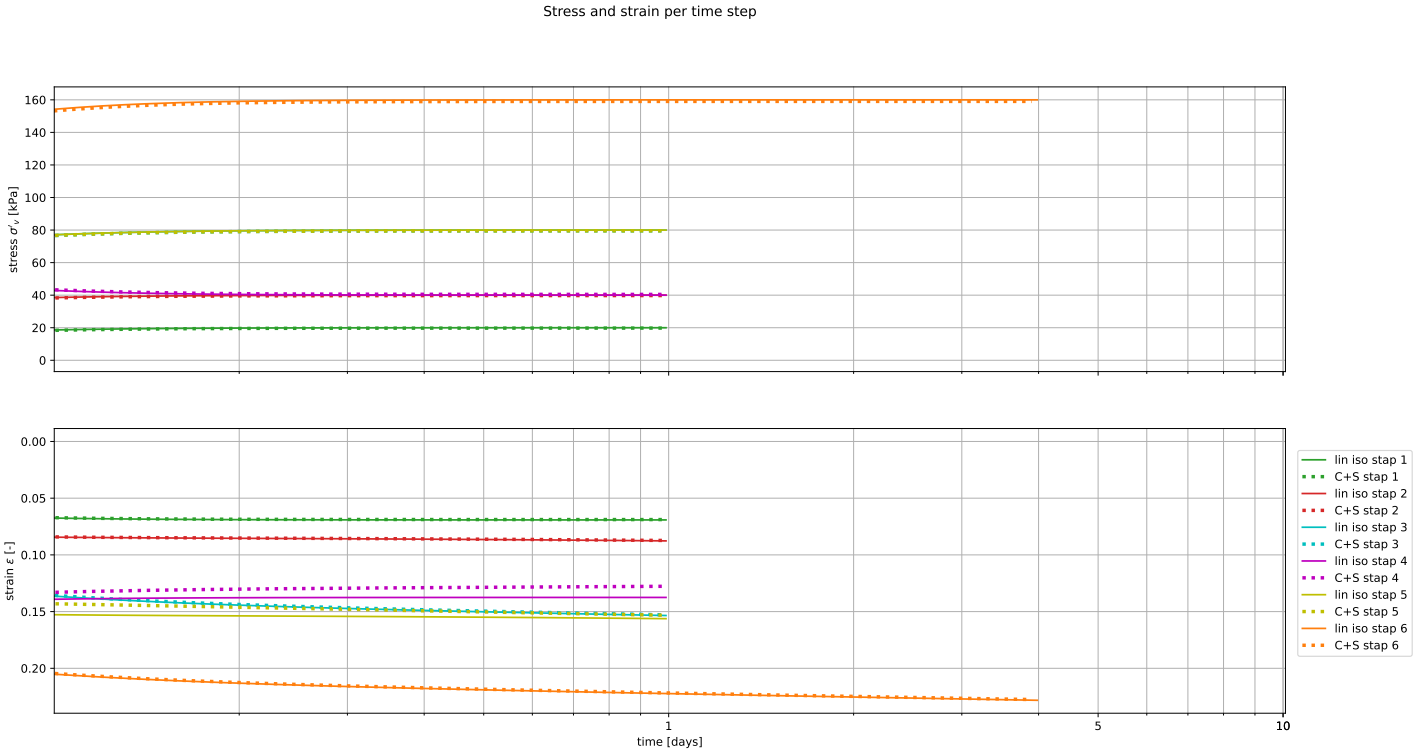

Unloading IL test Paper linear isotachs

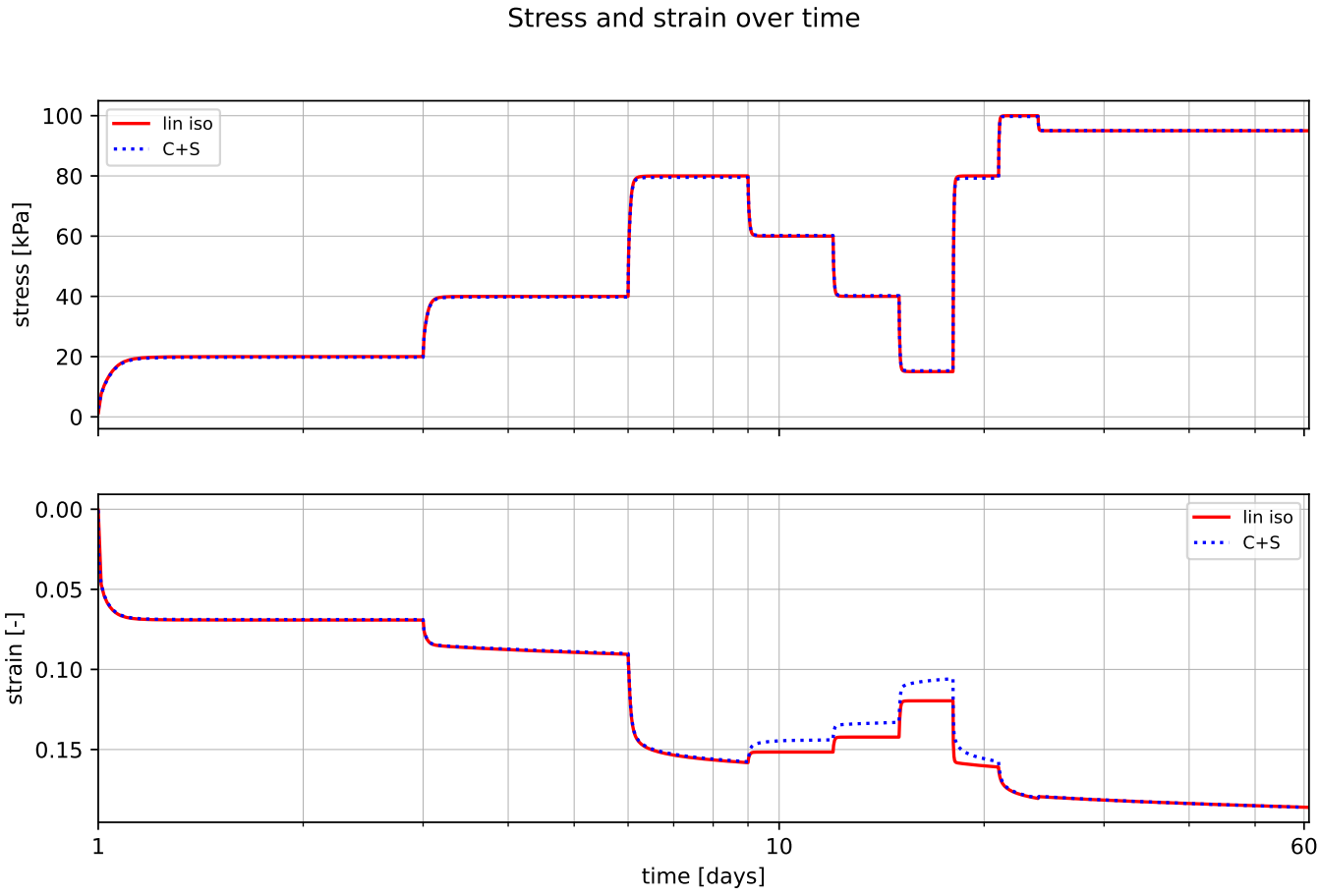

Unloading IL test Paper linear isotachs

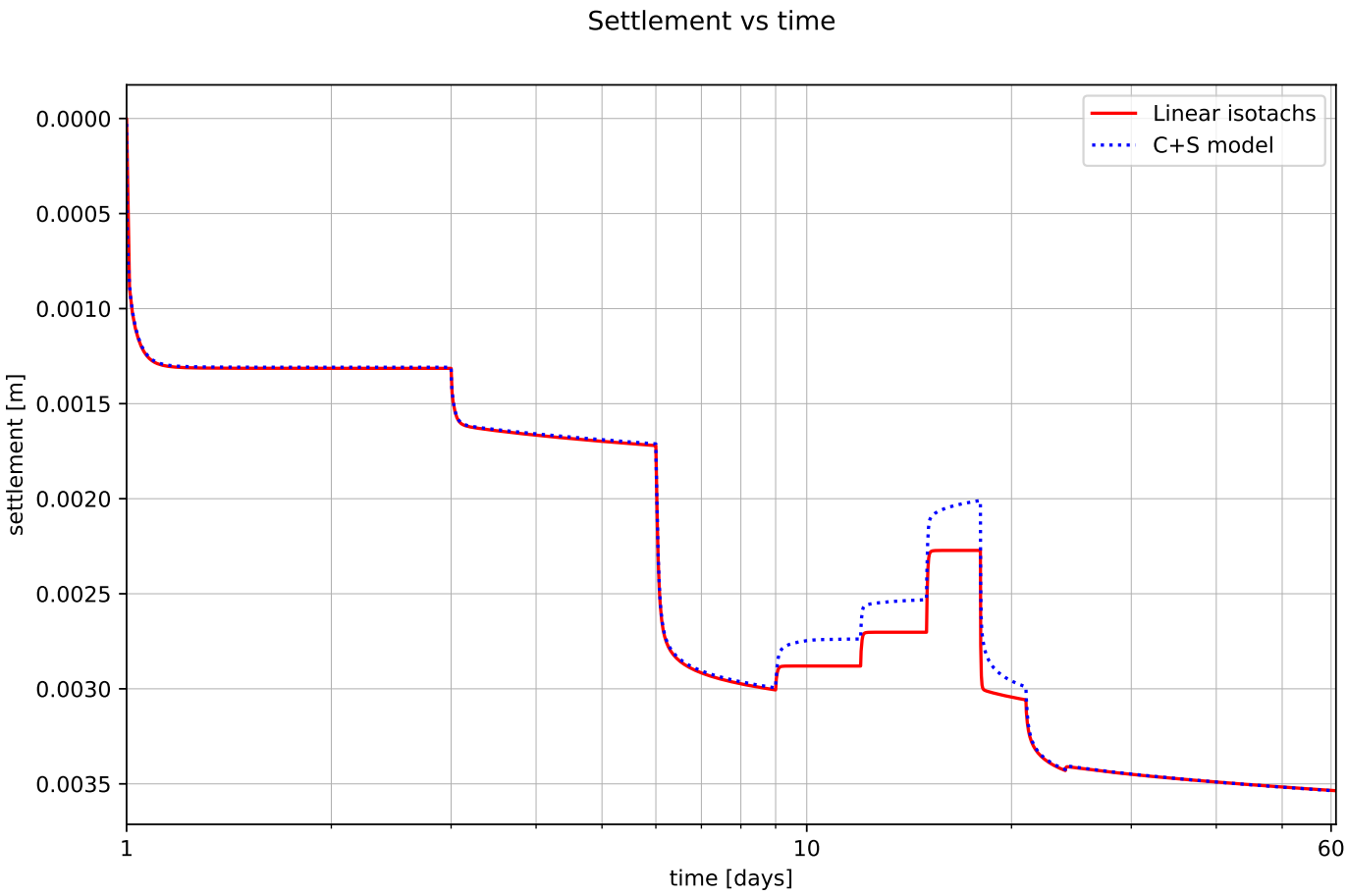

Unloading IL test Paper linear isotachs

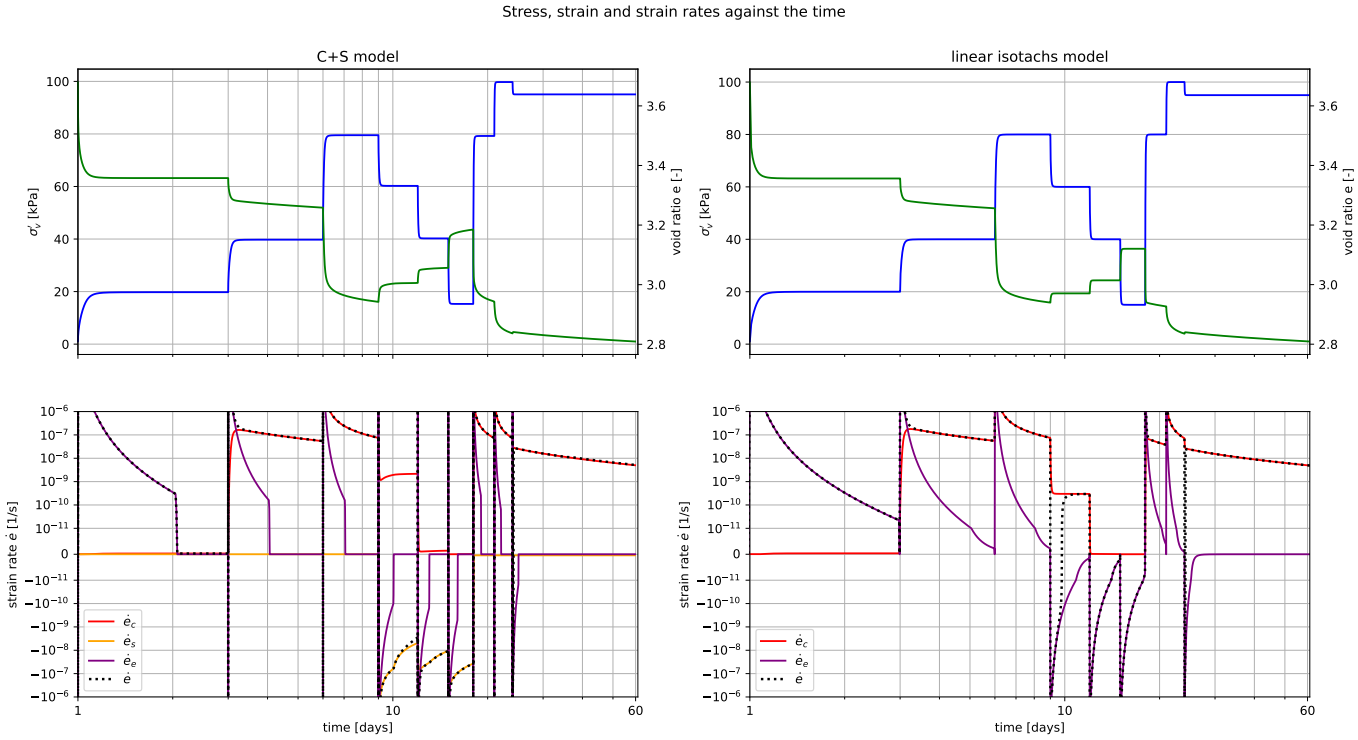

Unloading IL test Paper linear isotachs

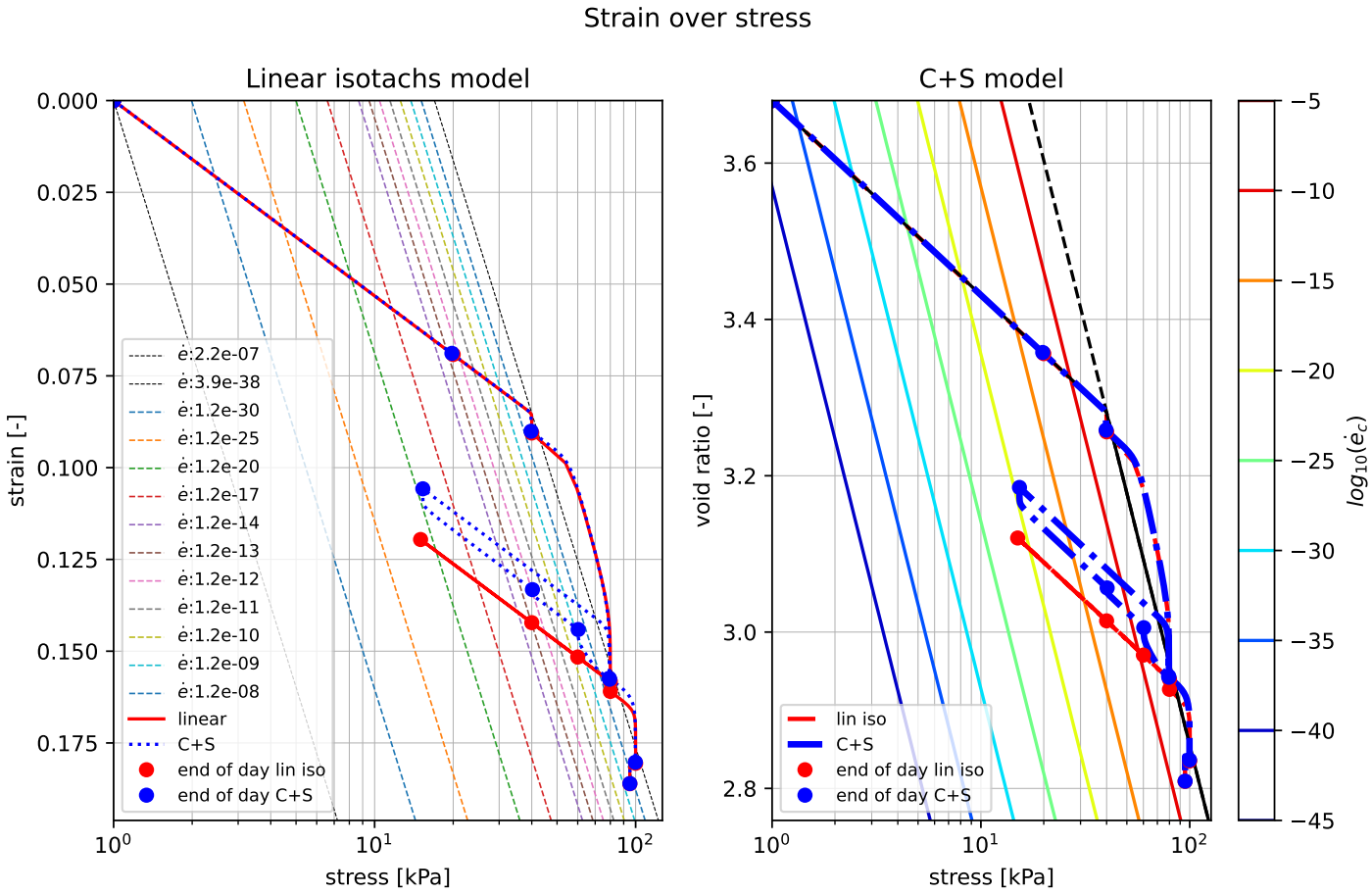

Unloading IL test Paper linear isotachs

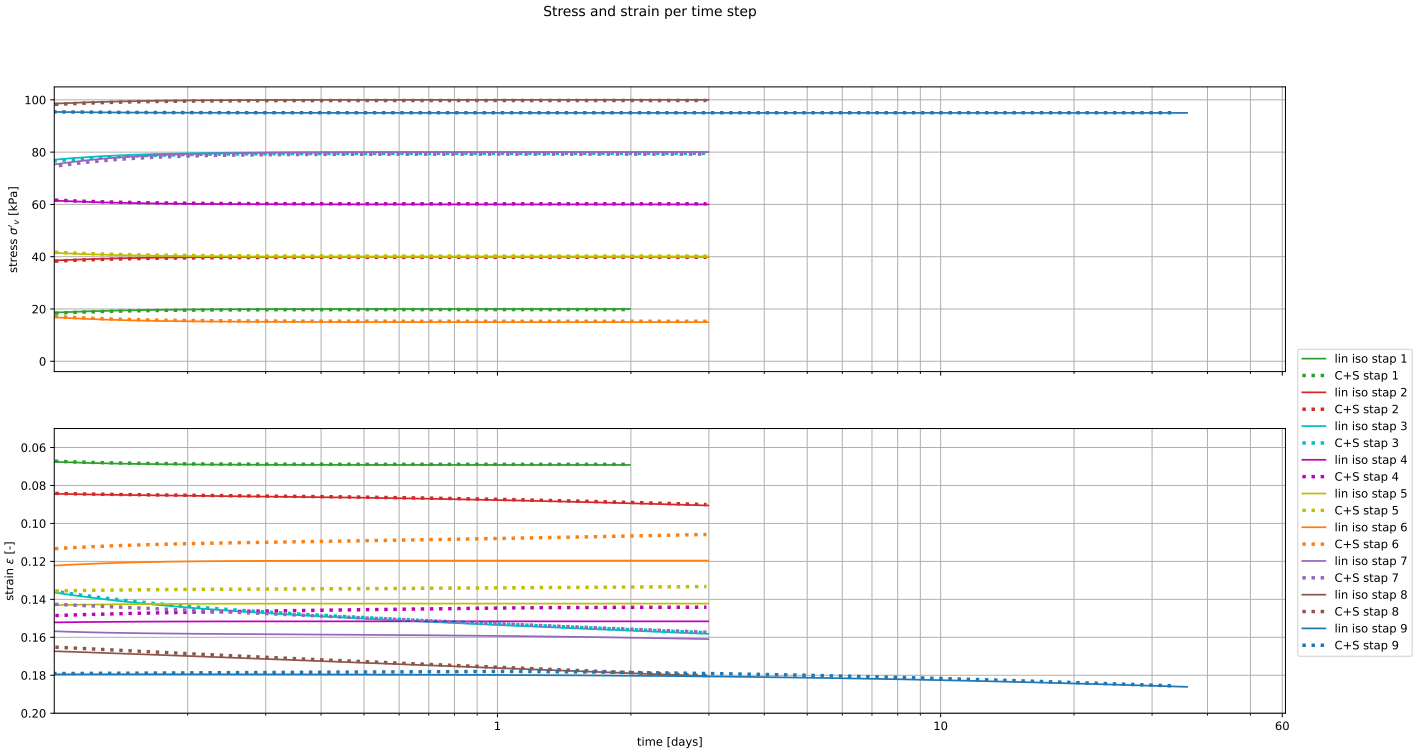

A.4. Embankment plots

A.4.1. C+S model with swell and non linearity

Below all graphs are presented for the C+S model for an embankment simulation with both the GitHub parameter set and the parameter set from the paper.

Graphs for GitHub with POP 20

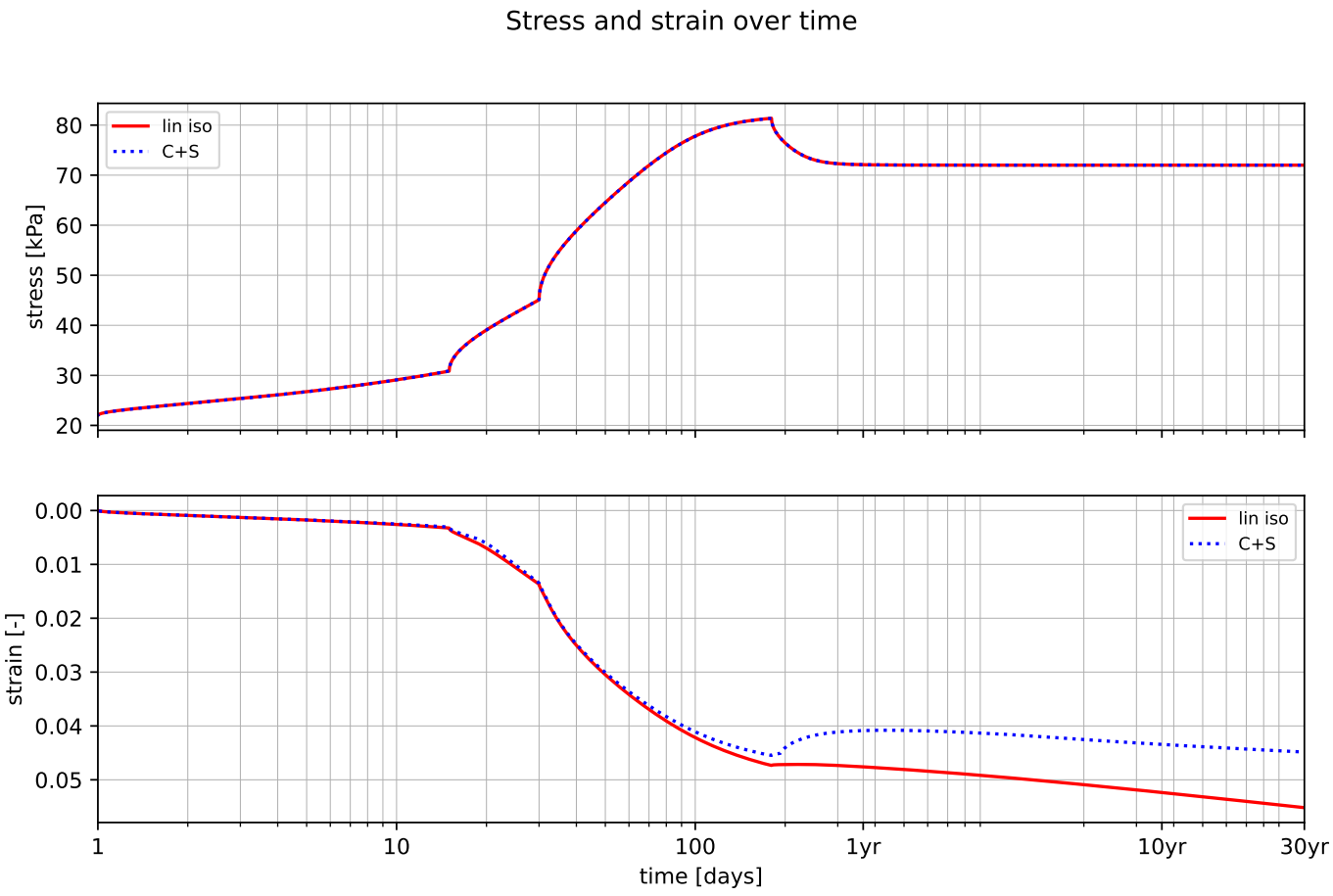

Graphs for GitHub with POP 20

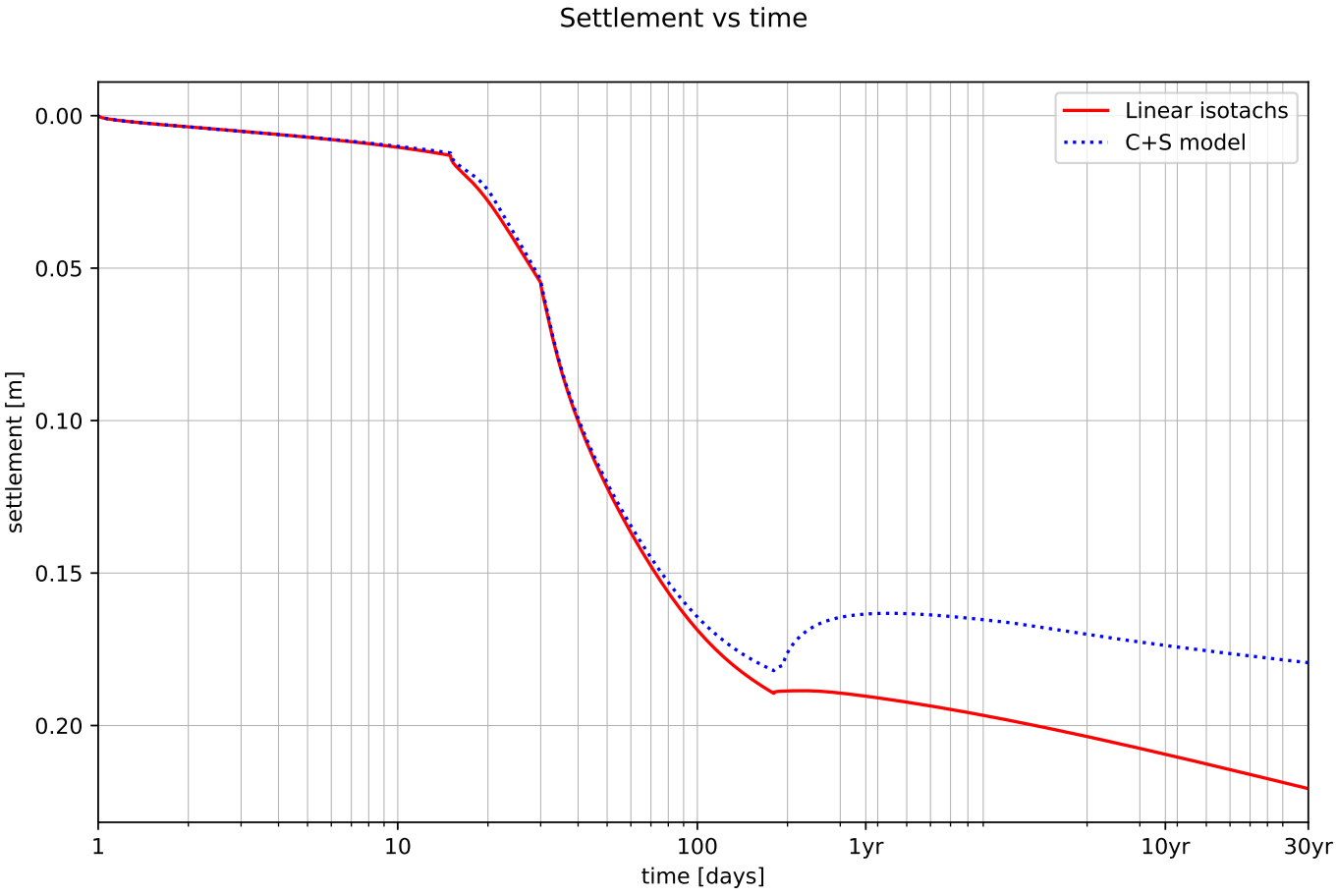

Graphs for GitHub with POP 20

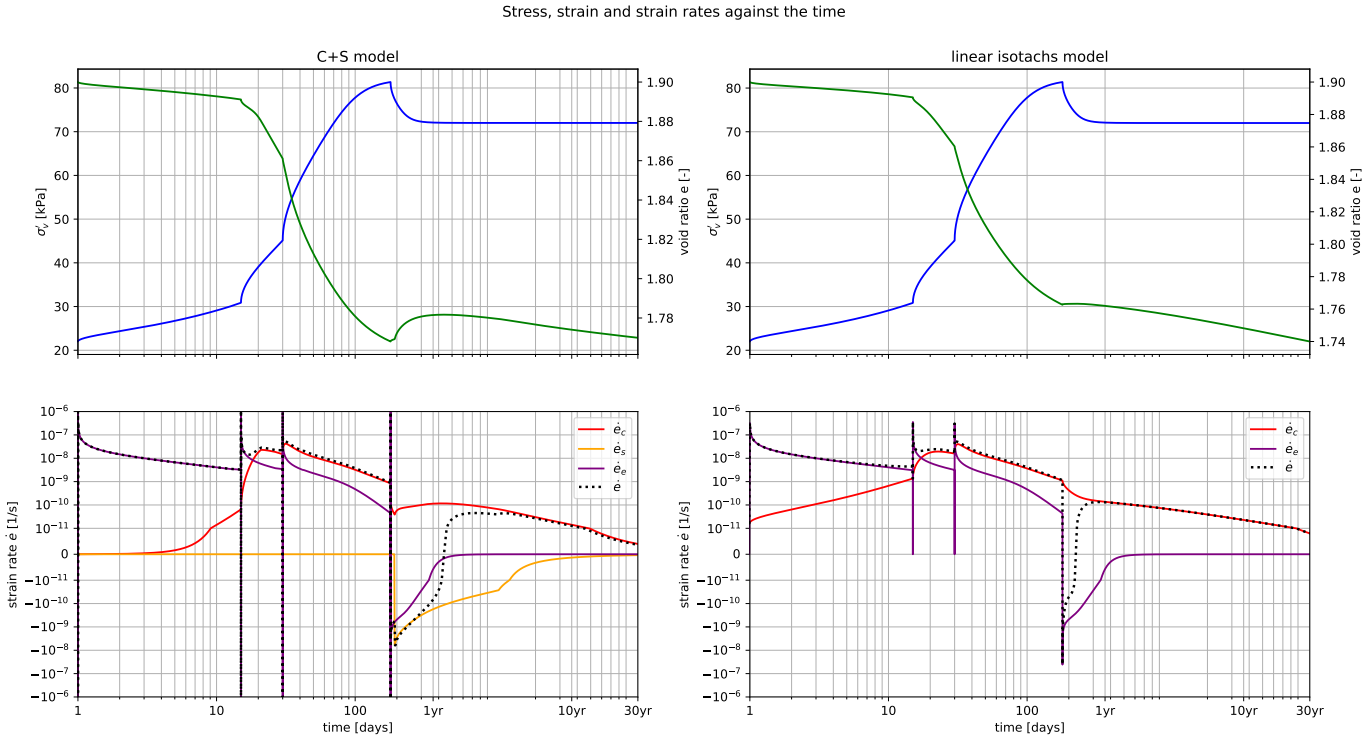

Graphs for GitHub with POP 20

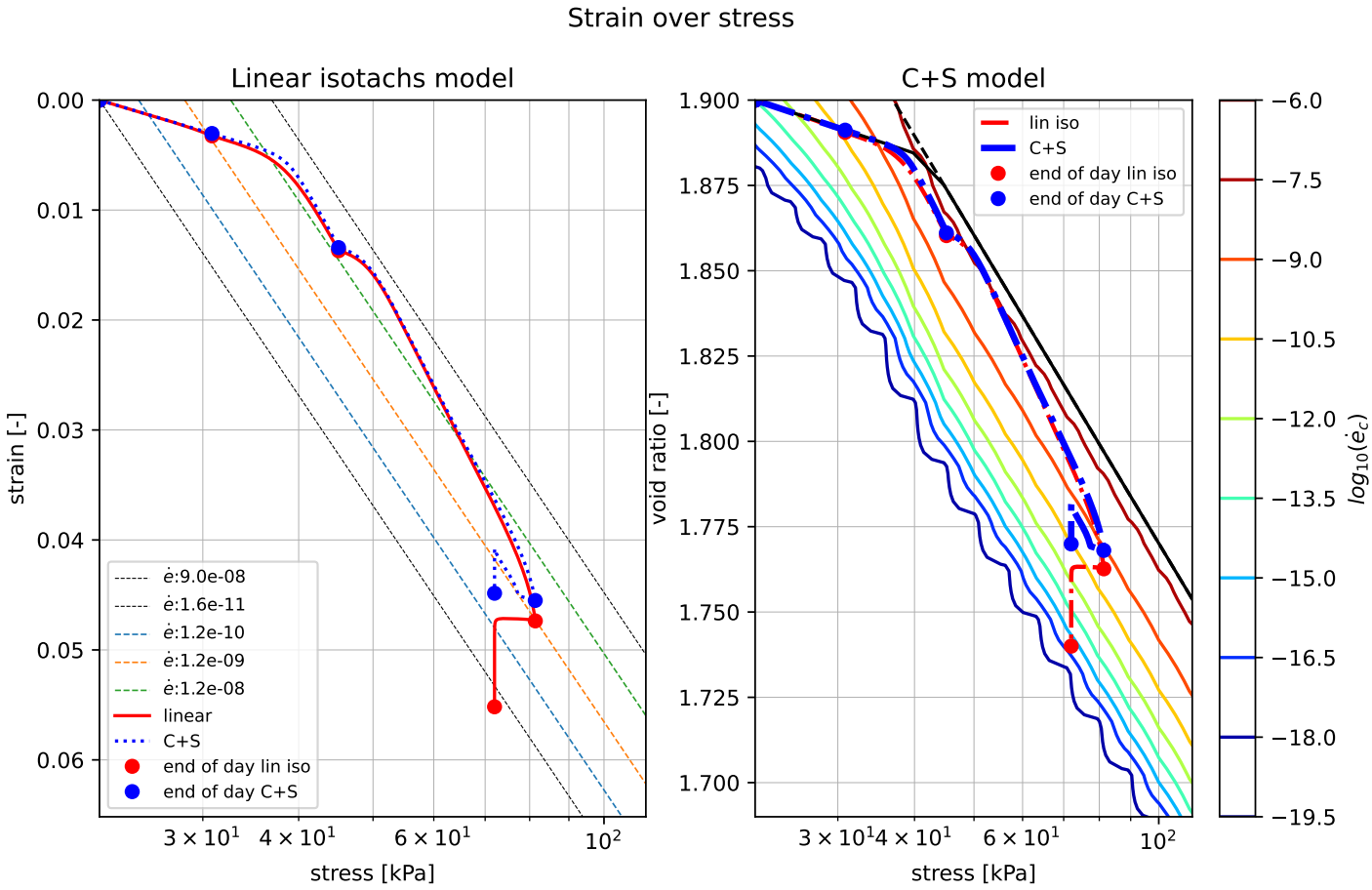

Graphs for GitHub with POP 20

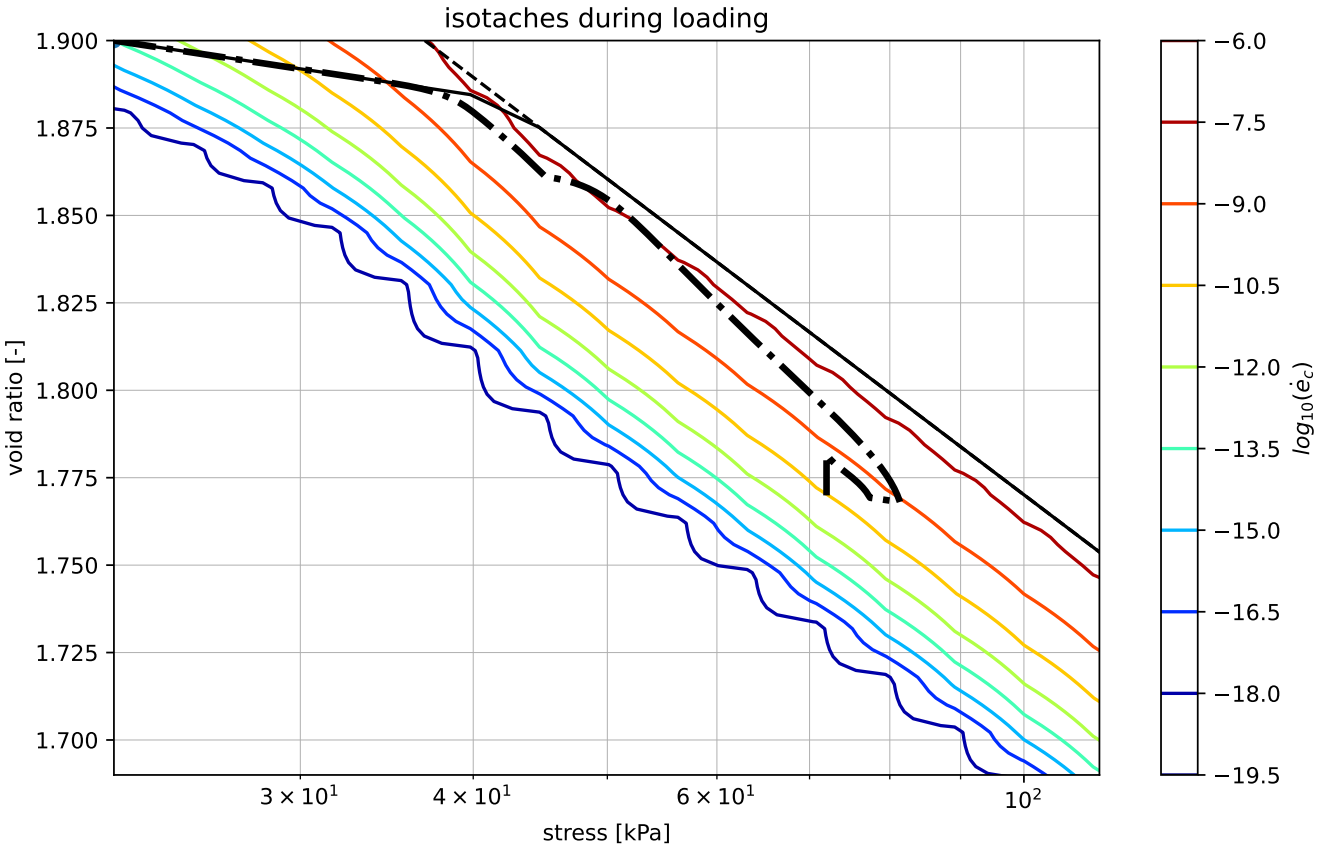

Graphs for GitHub with POP 20

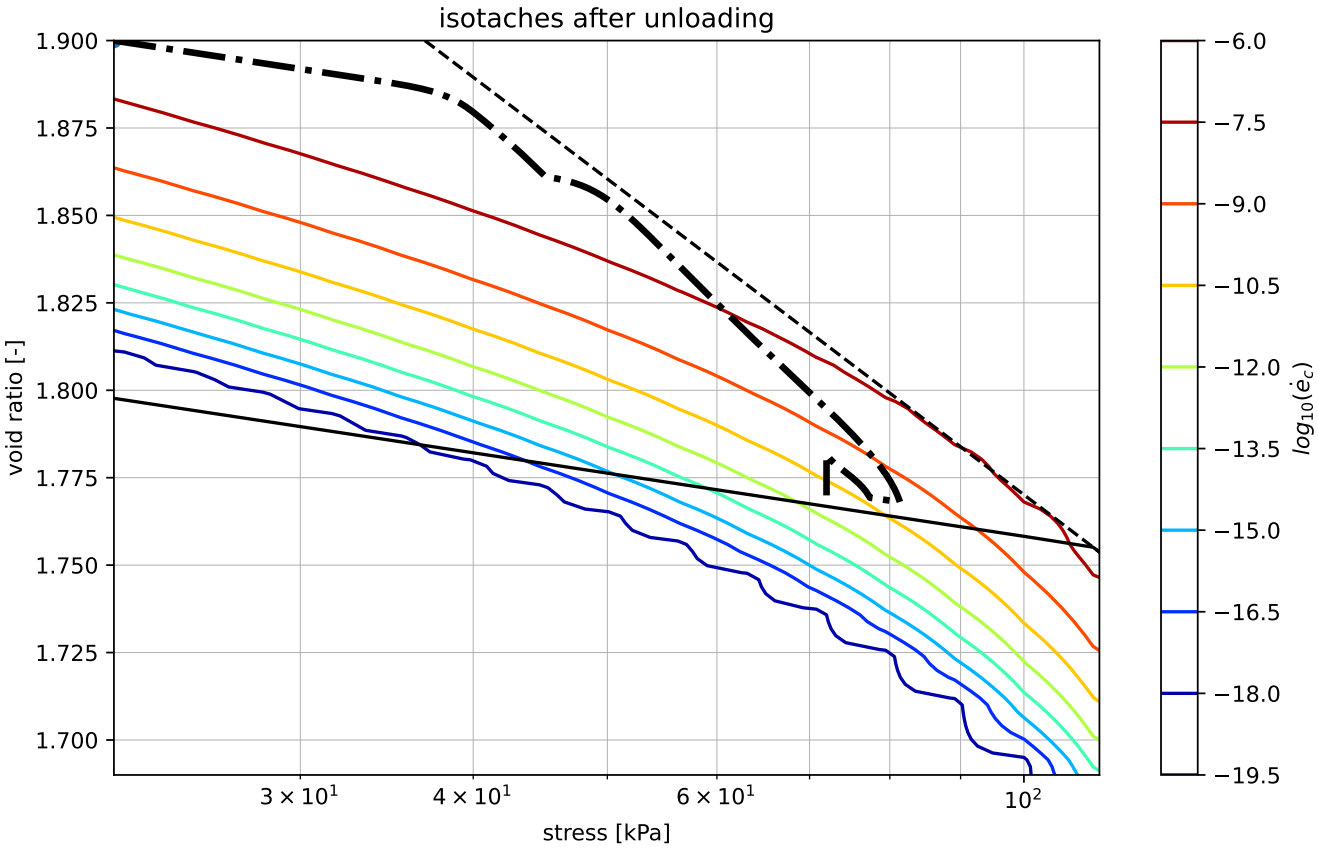

Graphs for GitHub with POP 40

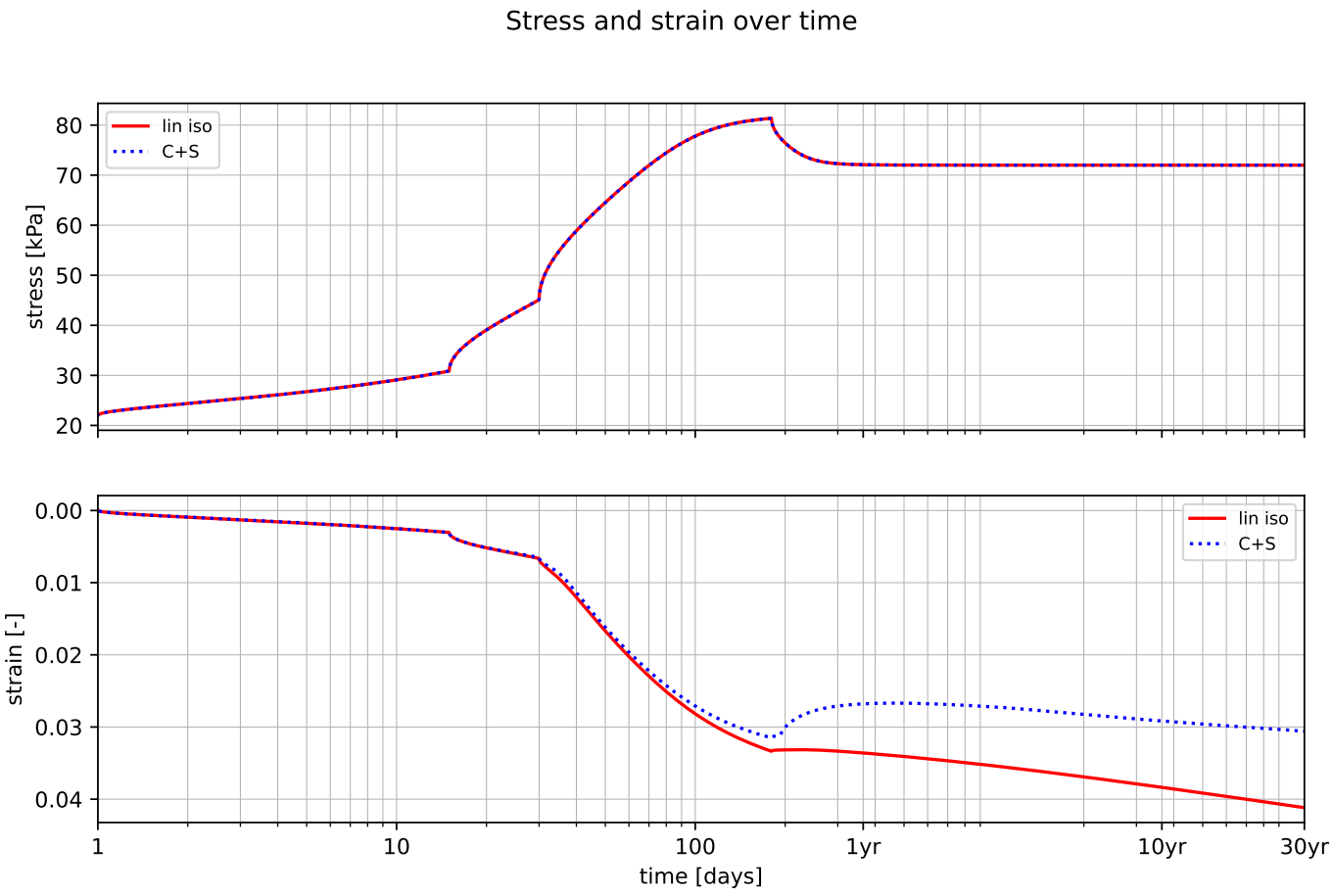

Graphs for GitHub with POP 40

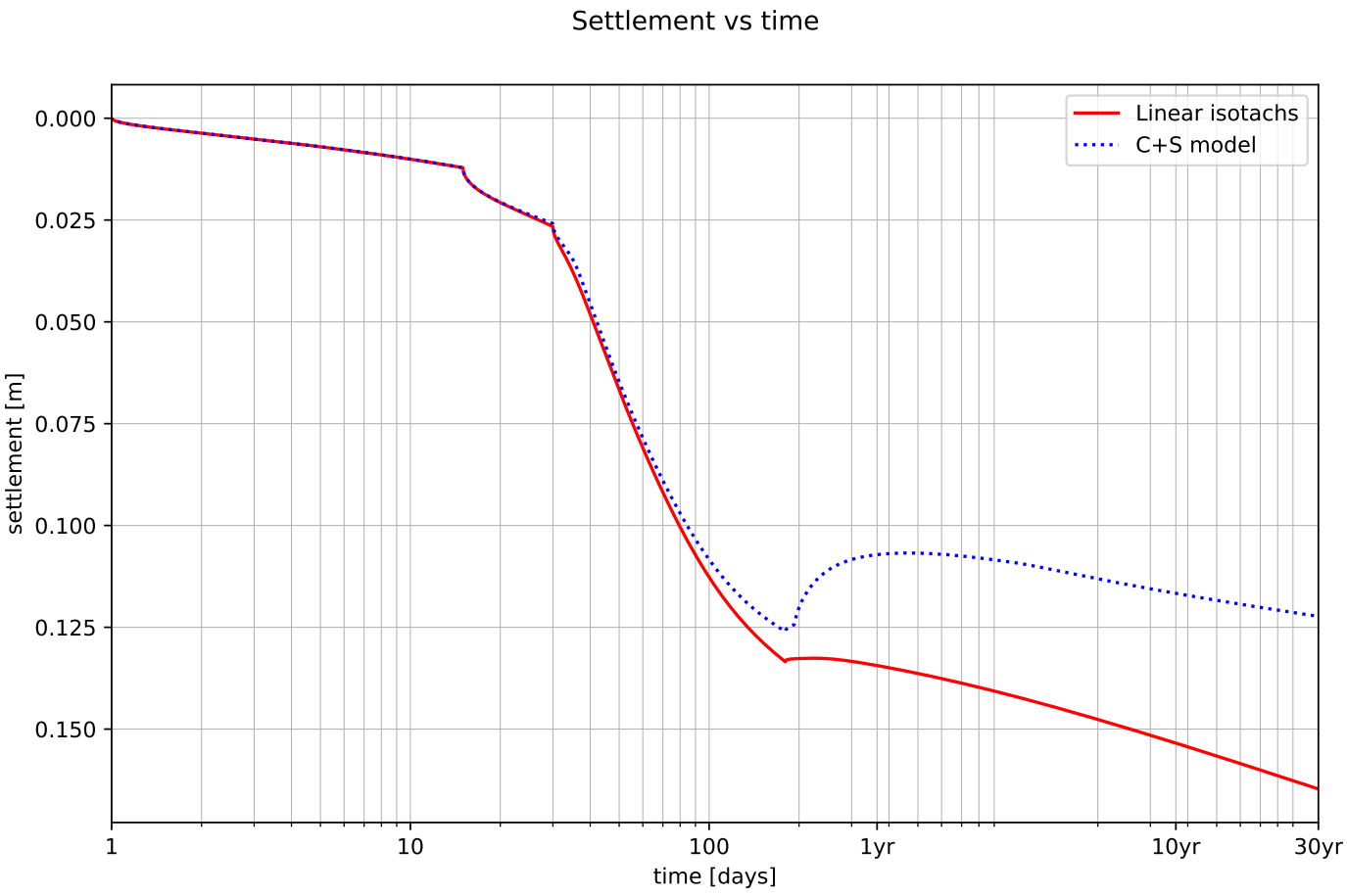

Graphs for GitHub with POP 40

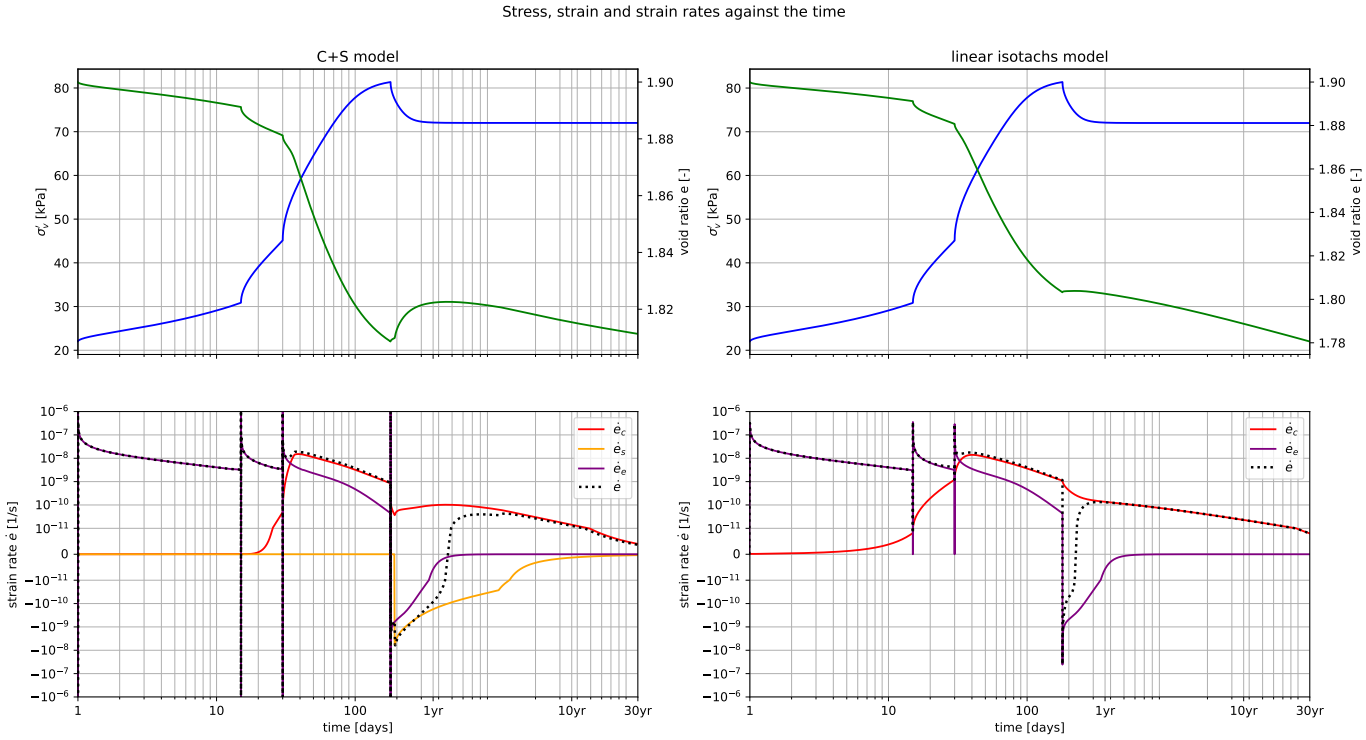

Graphs for GitHub with POP 40

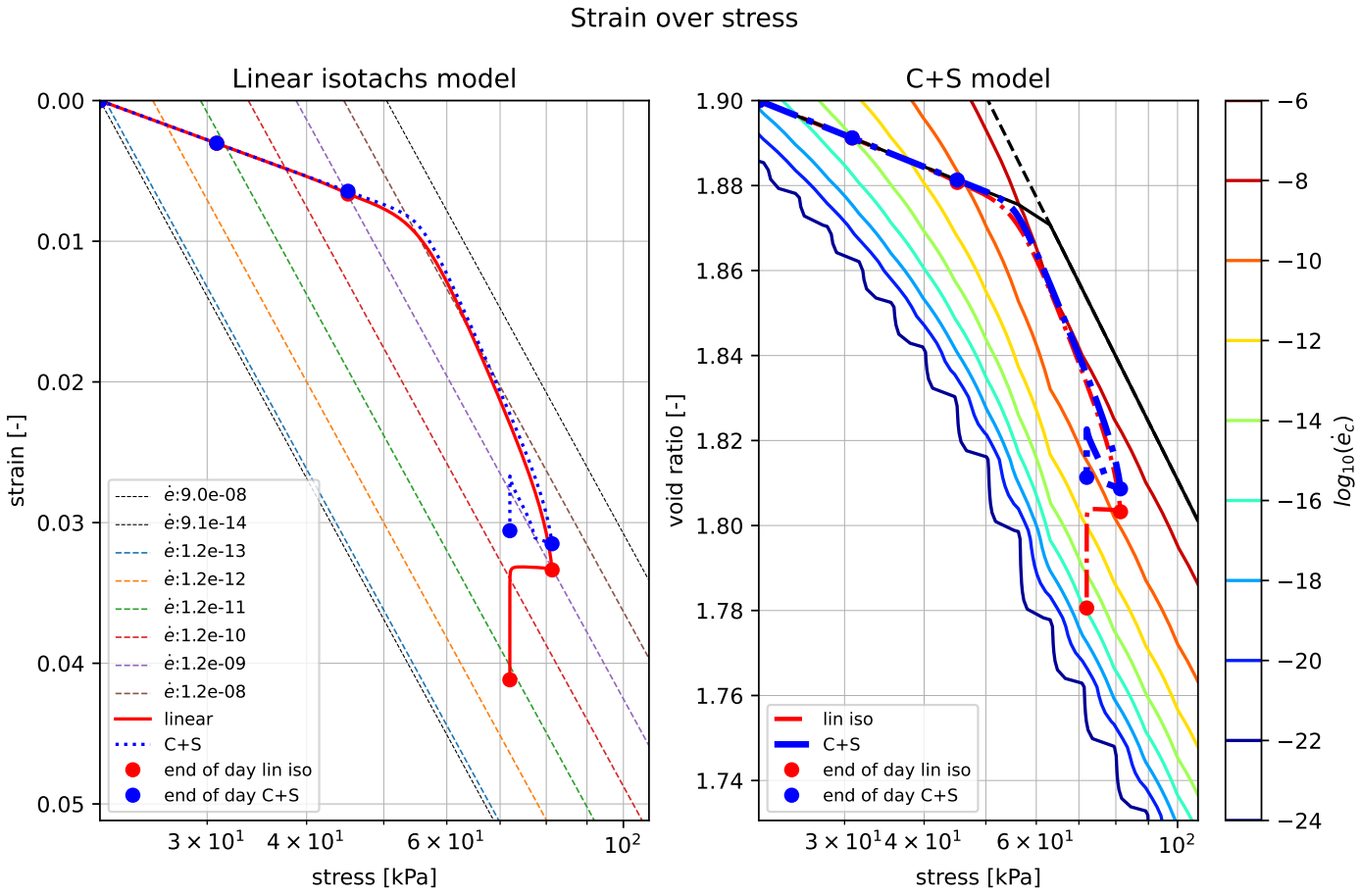

Graphs for GitHub with POP 40

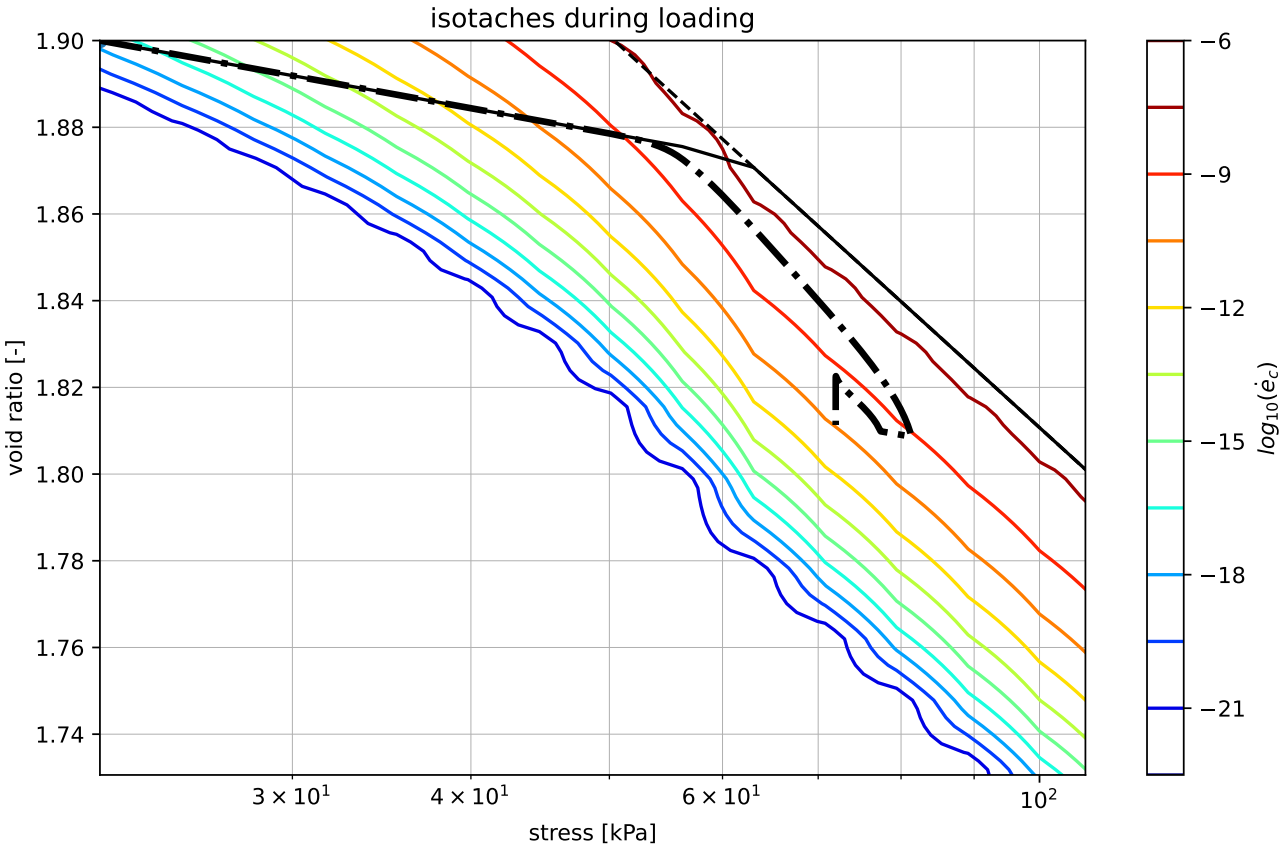

Graphs for GitHub with POP 40

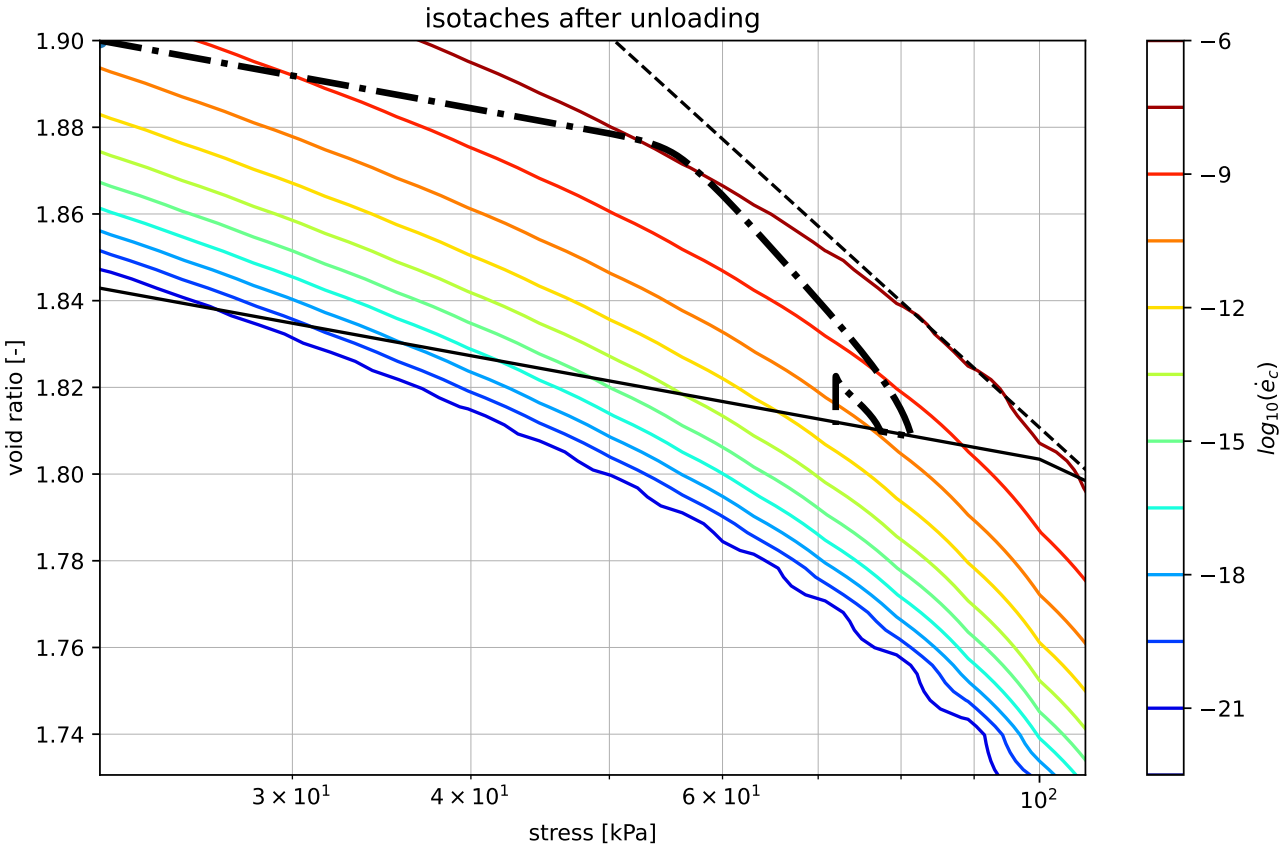

Graphs for Paper with POP 20

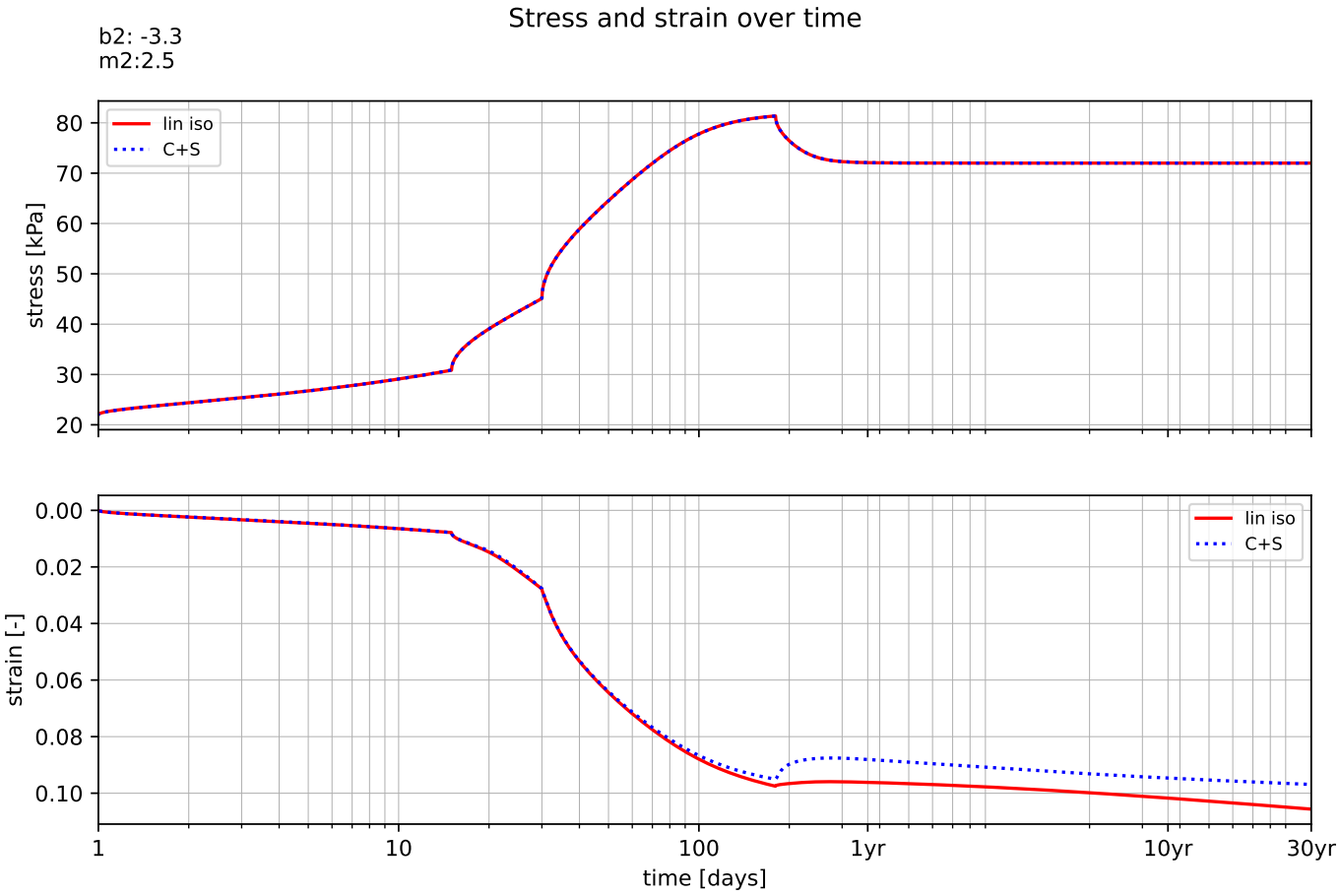

Graphs for Paper with POP 20

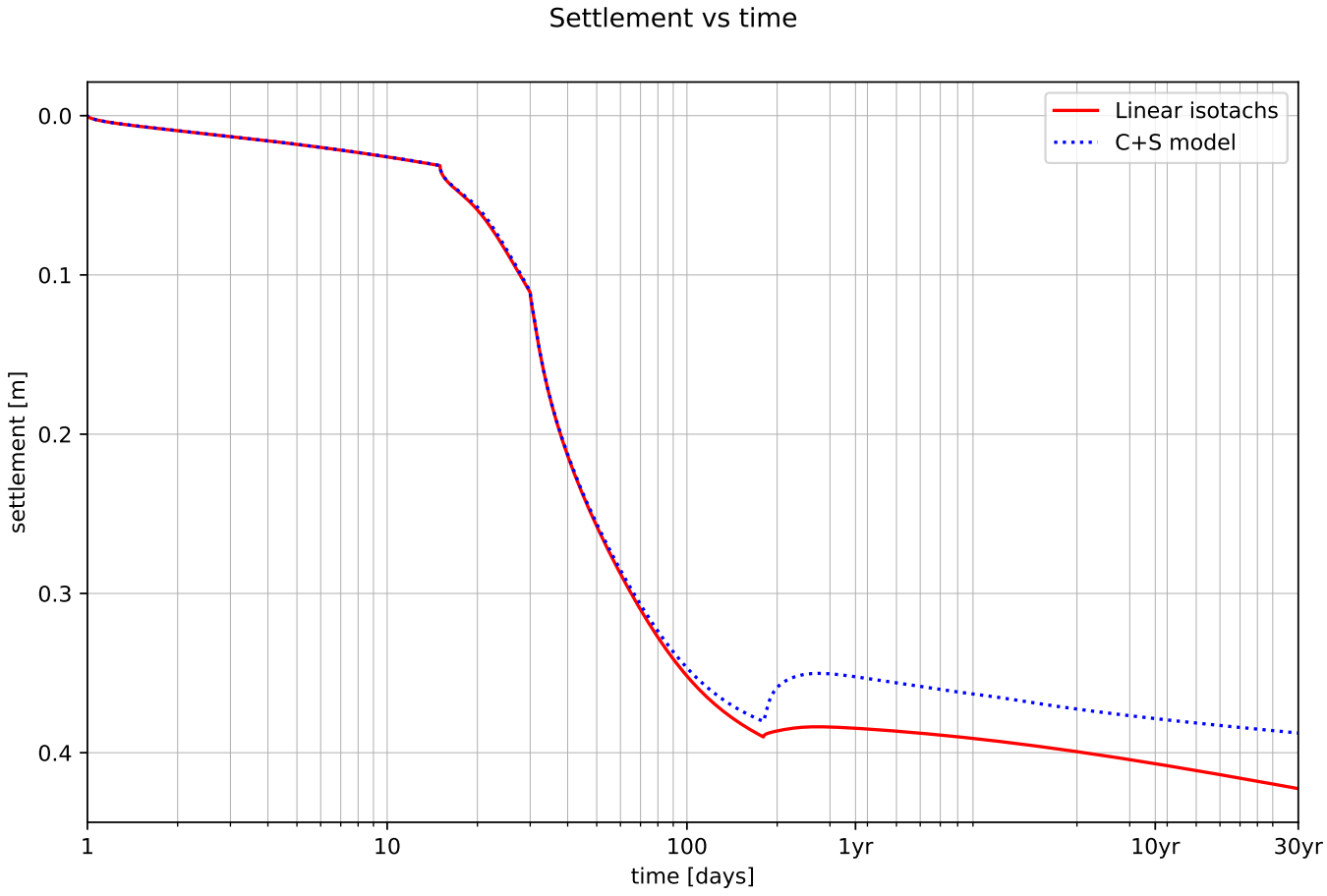

Graphs for Paper with POP 20

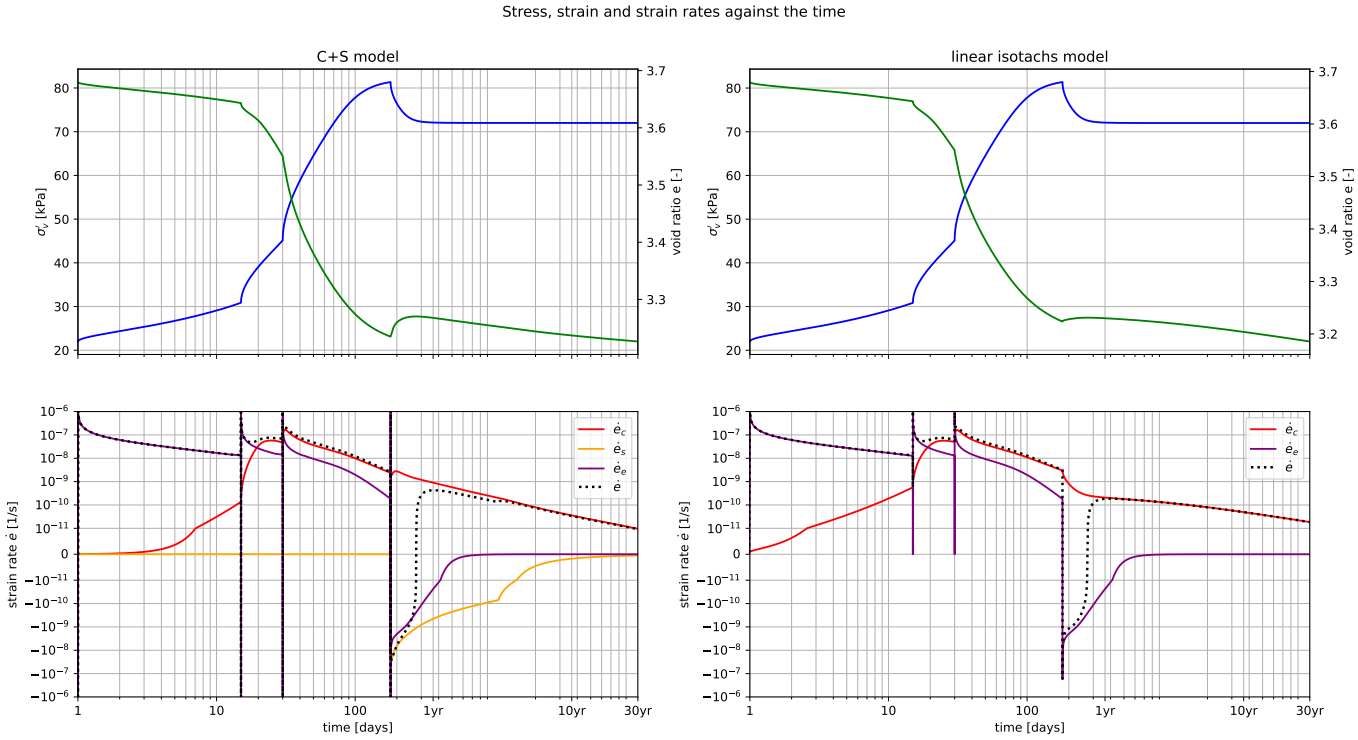

Graphs for Paper with POP 20

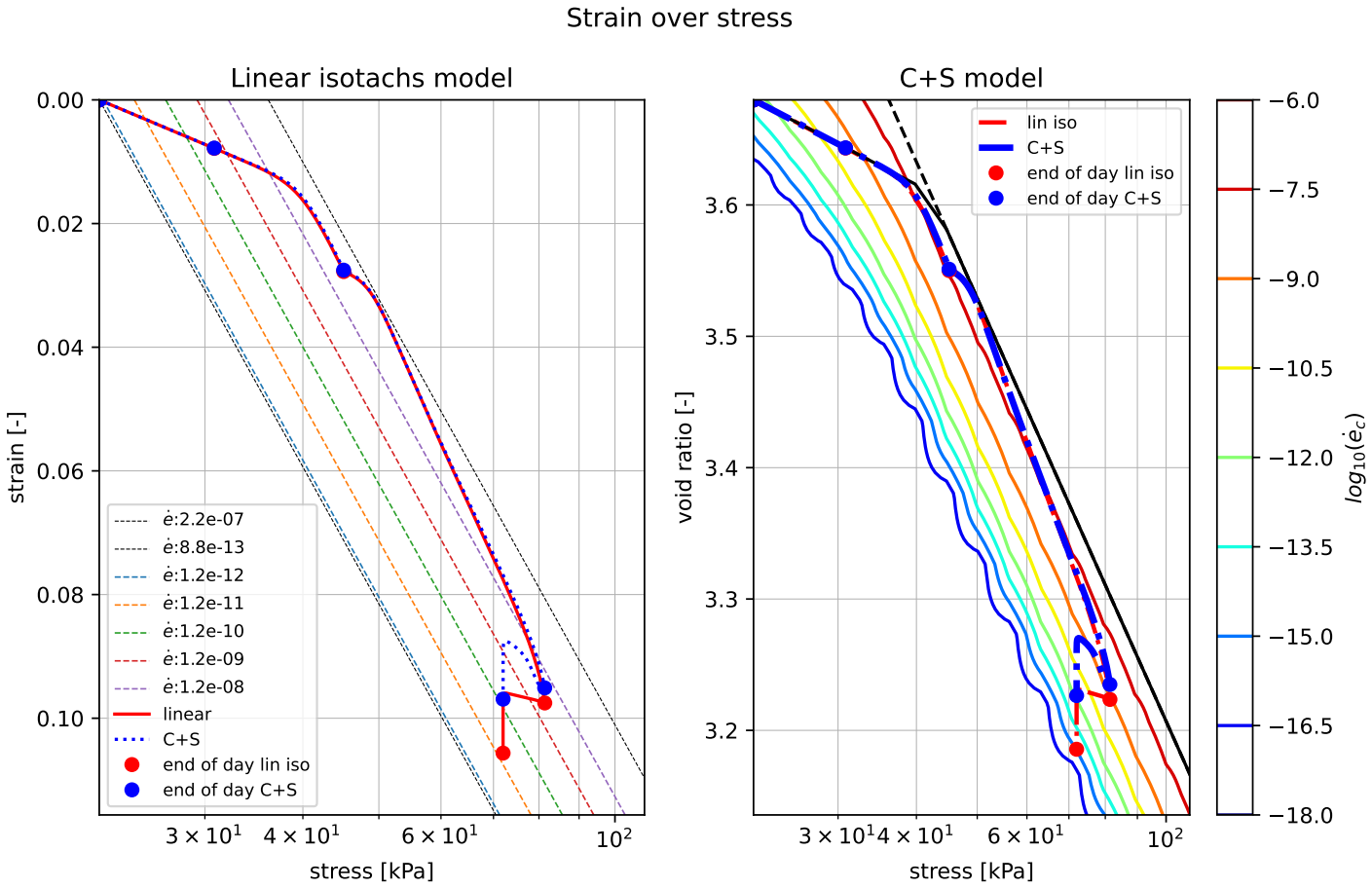

Graphs for Paper with POP 20

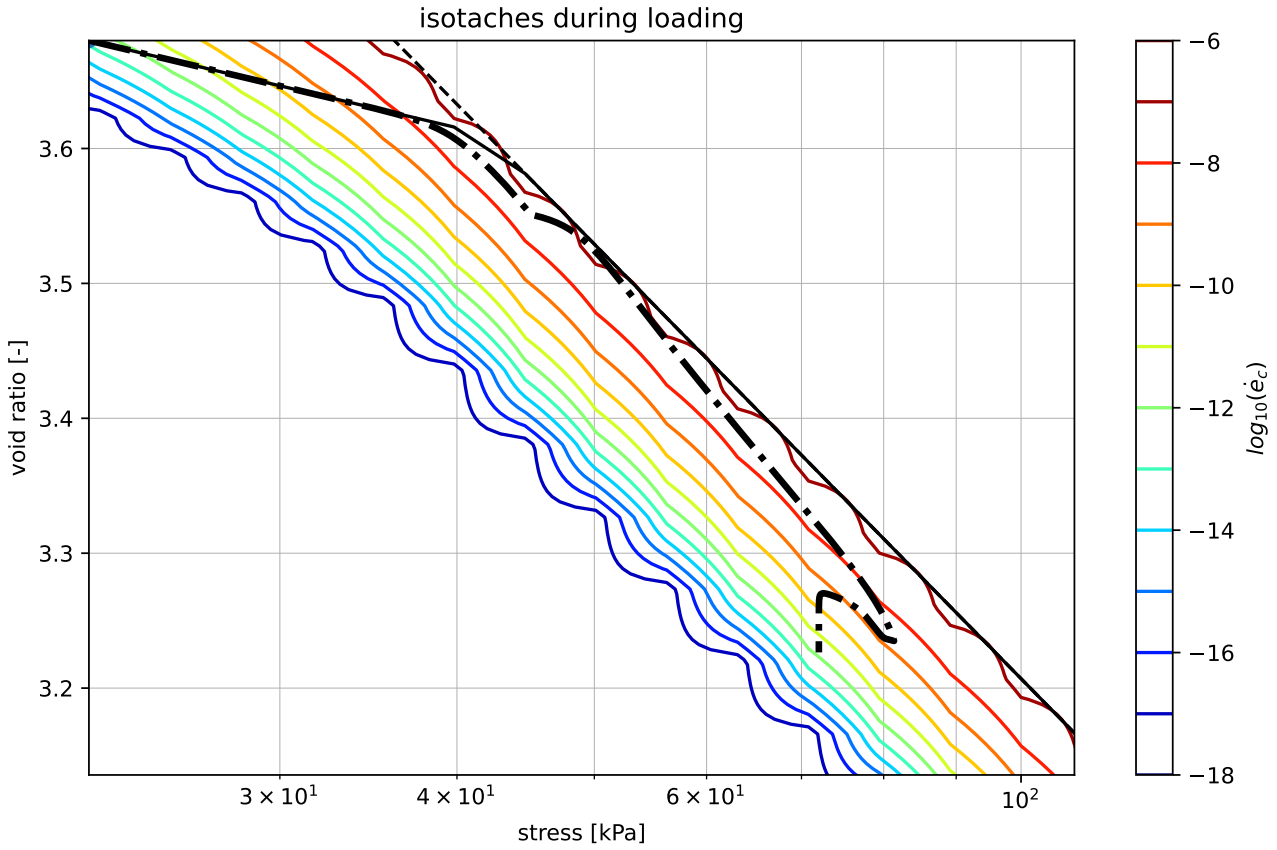

Graphs for Paper with POP 20

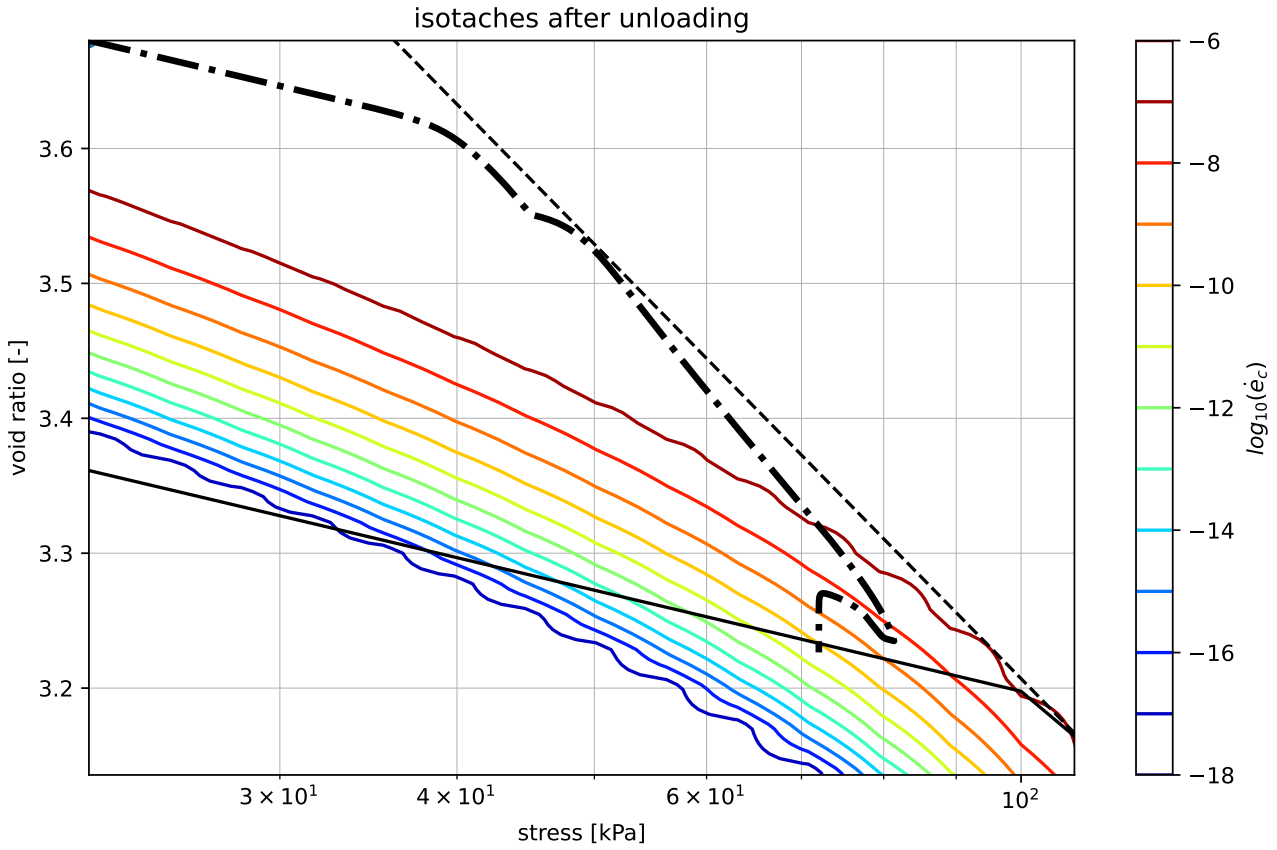

Graphs for Paper with POP 40

Graphs for Paper with POP 40

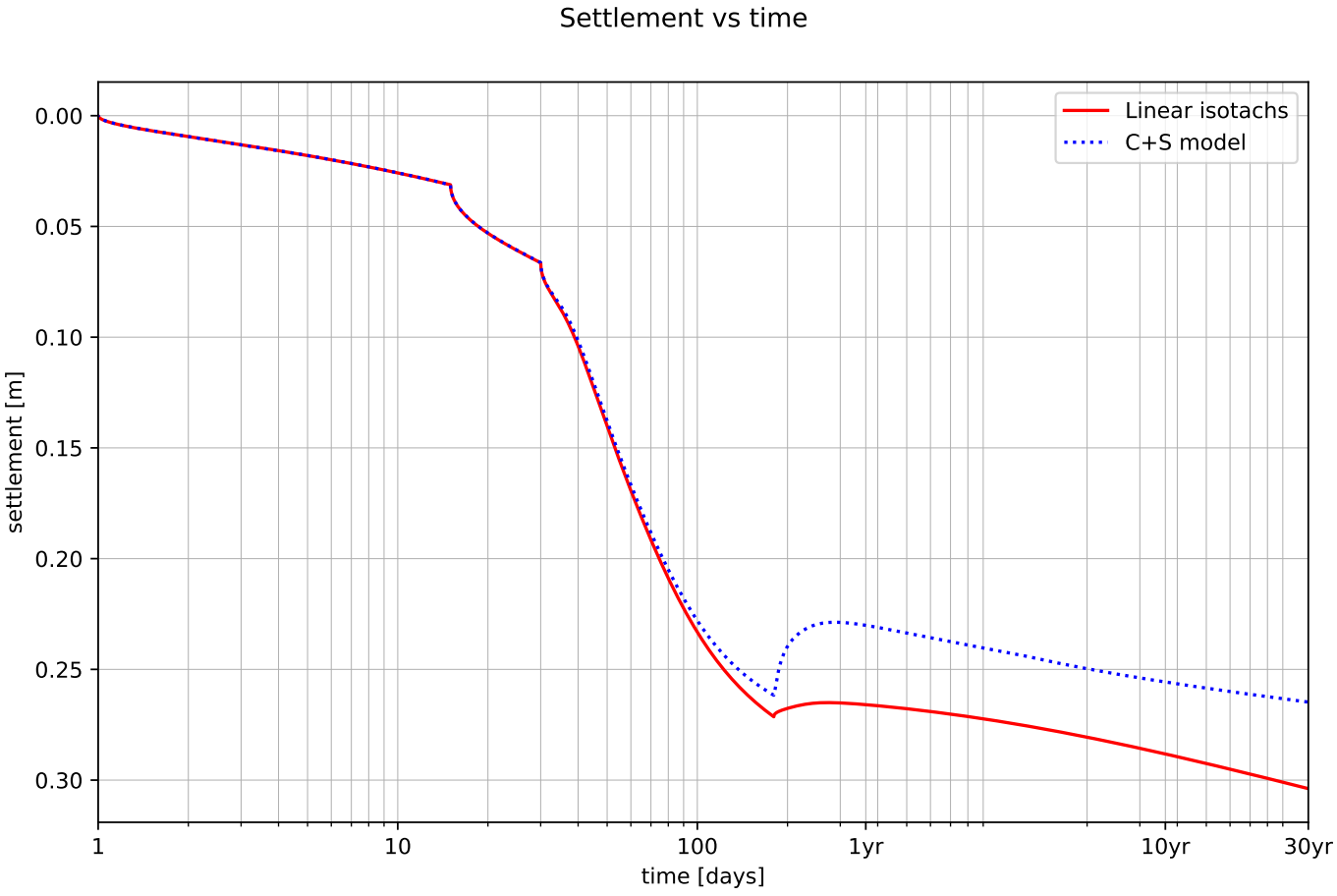

Graphs for Paper with POP 40

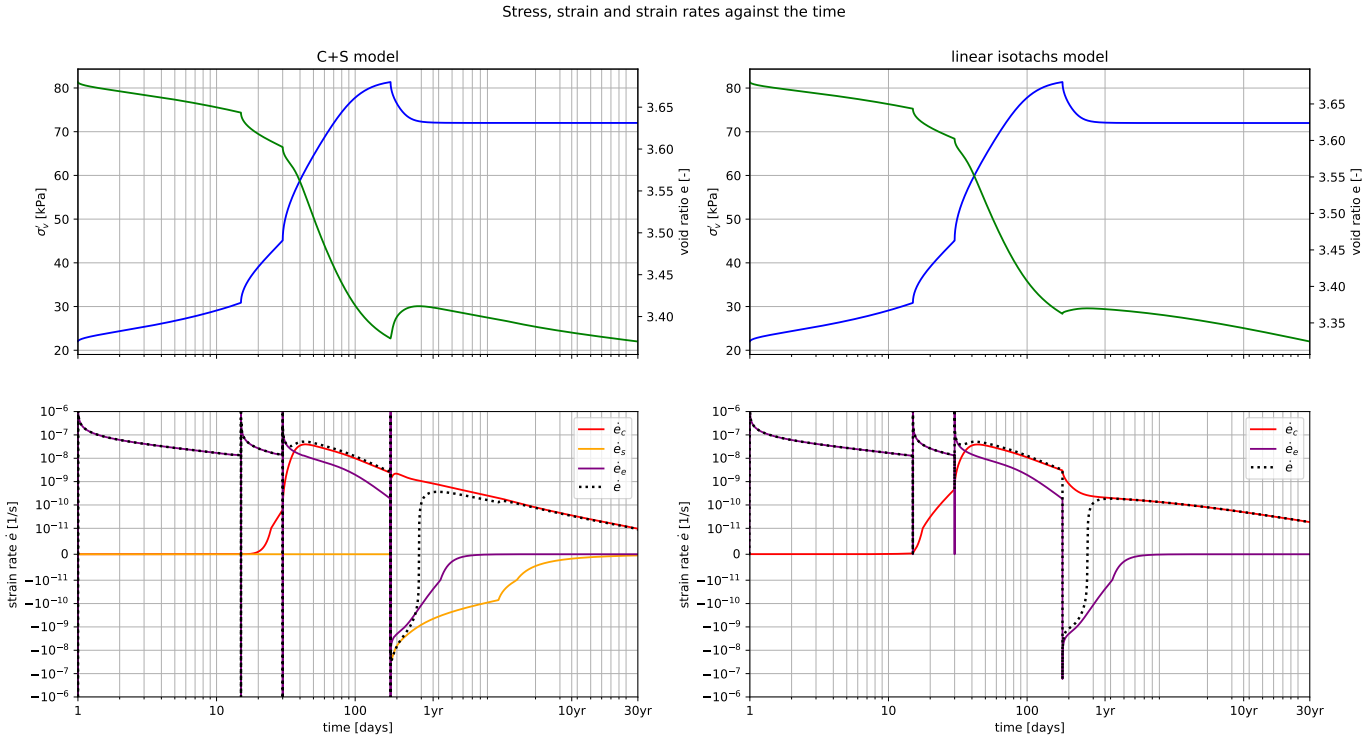

Graphs for Paper with POP 40

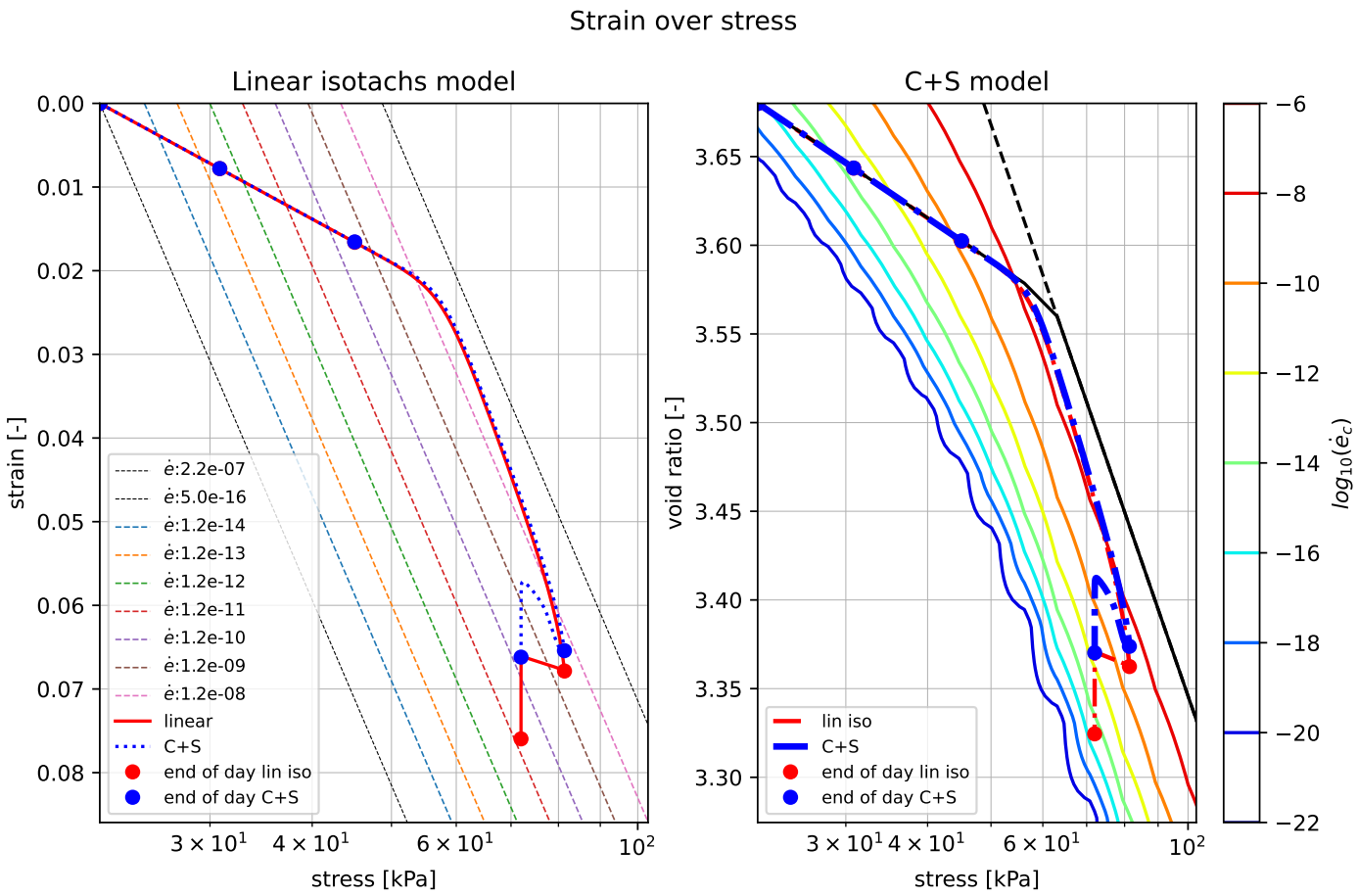

Graphs for Paper with POP 40

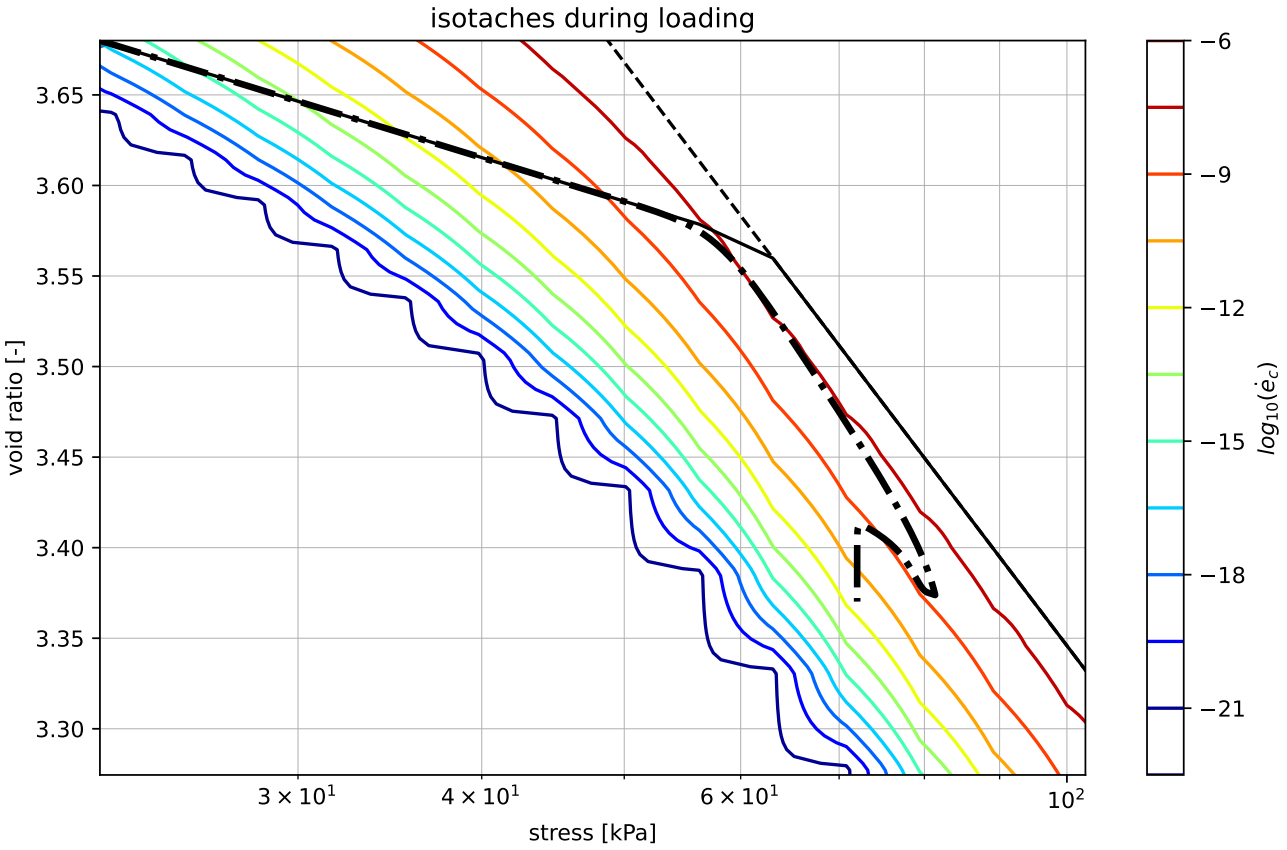

Graphs for Paper with POP 40

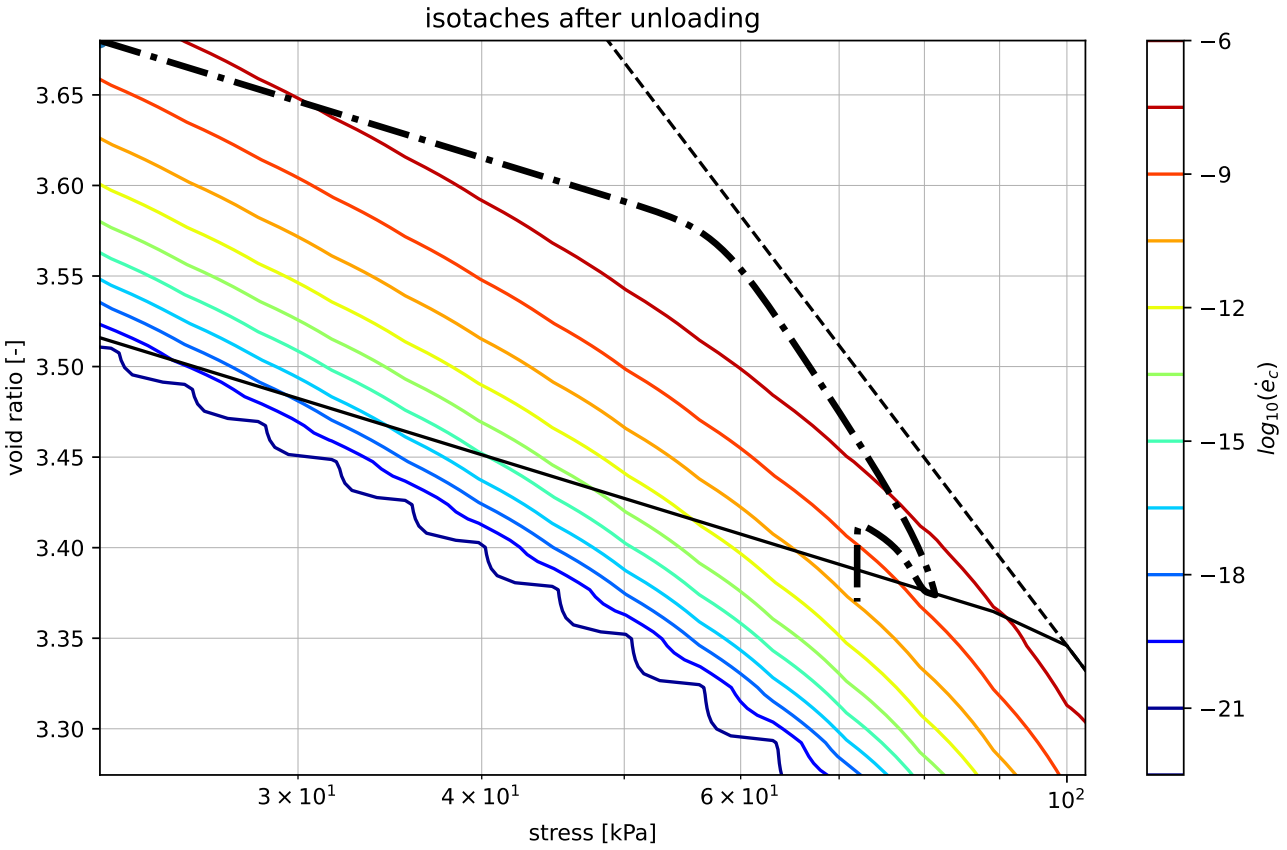

A.4.2. C+S model with swell and linearity

Graphs for GitHub with POP 20

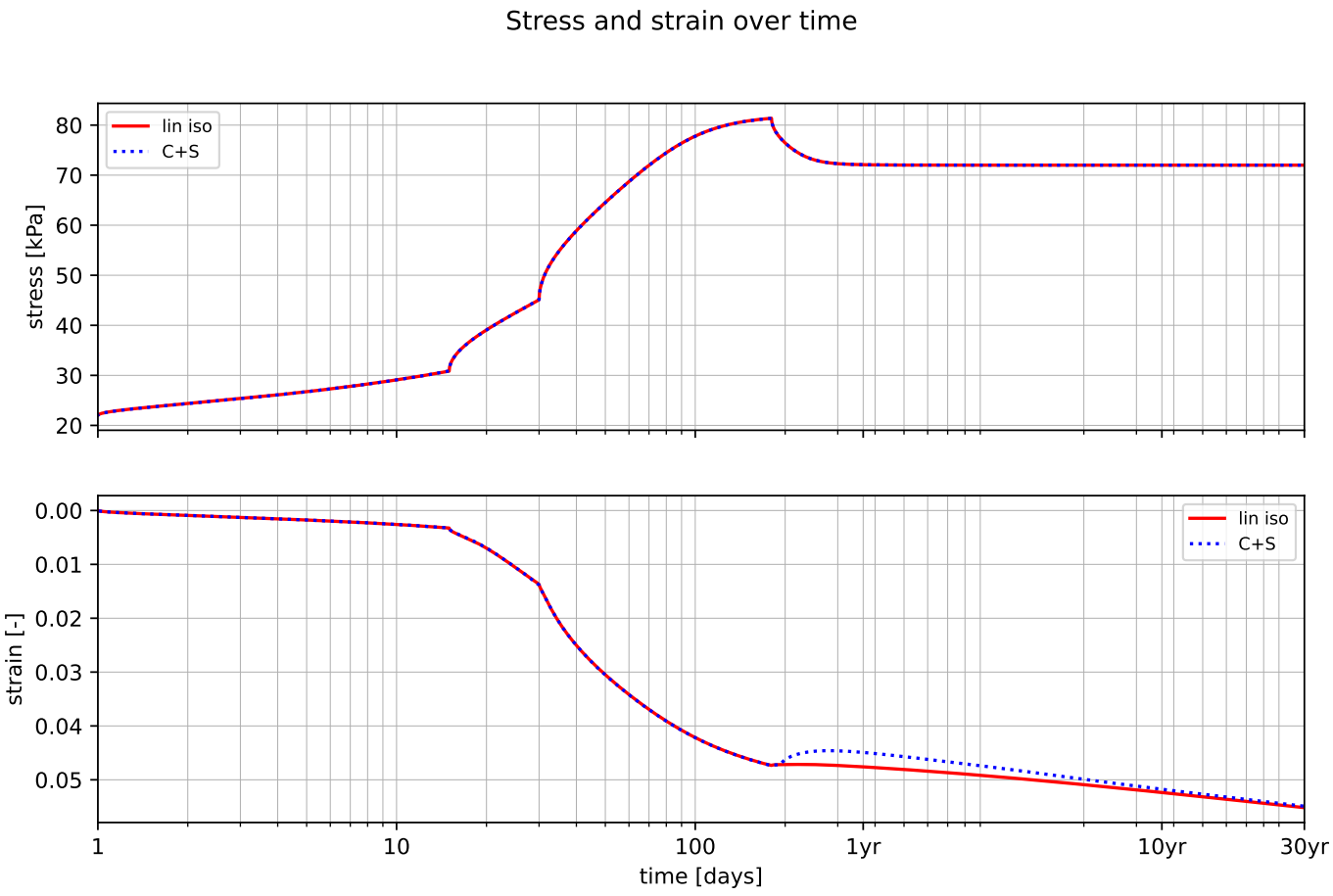

Graphs for GitHub with POP 20

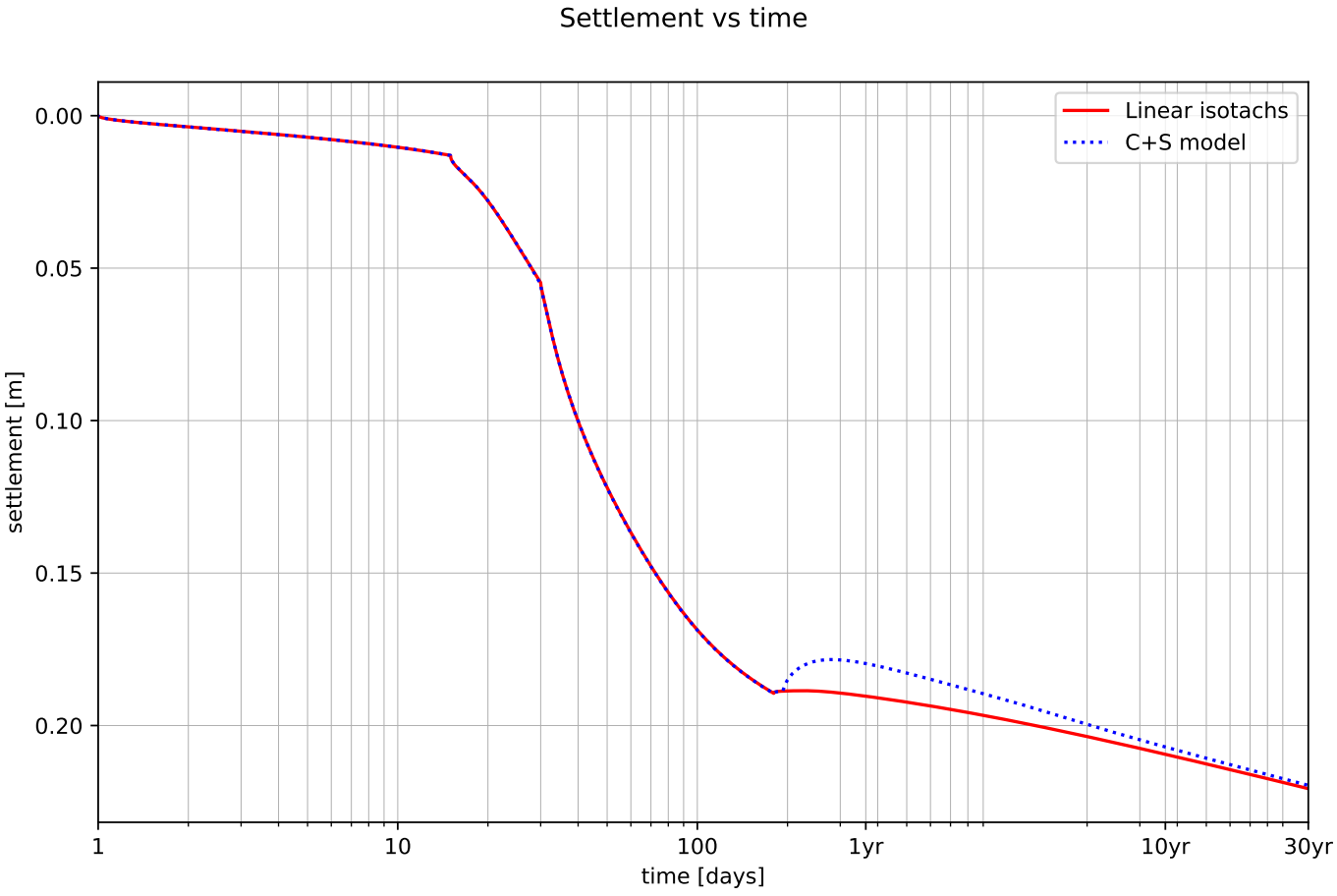

Graphs for GitHub with POP 20

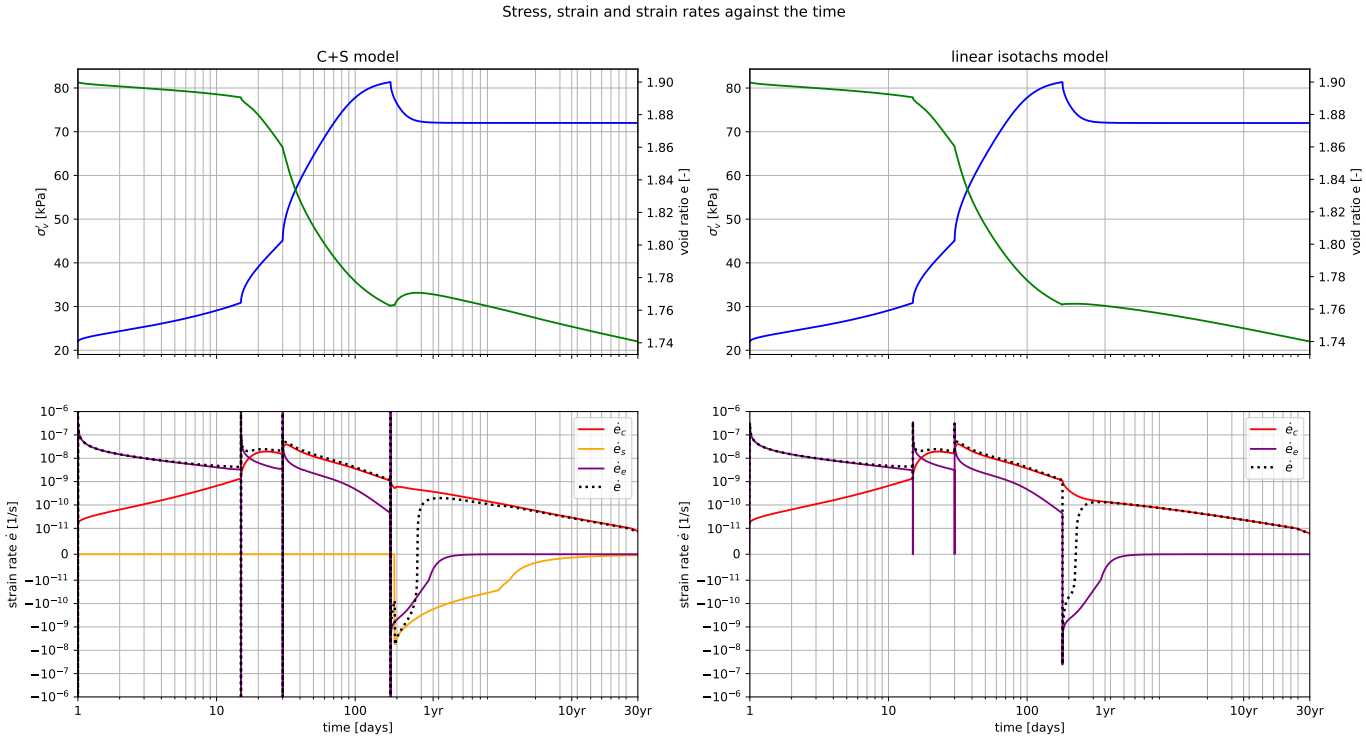

Graphs for GitHub with POP 20

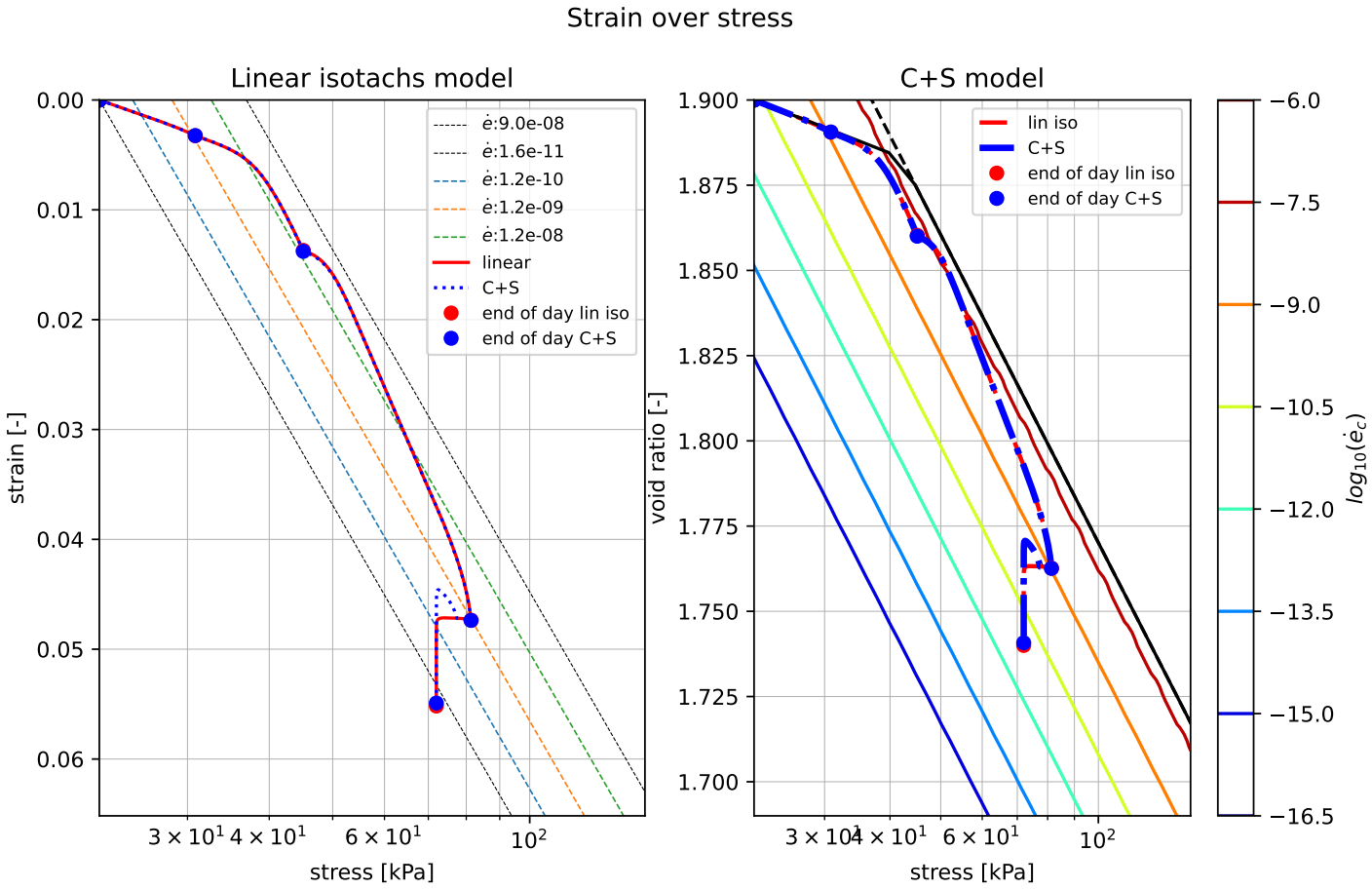

Graphs for GitHub with POP 20

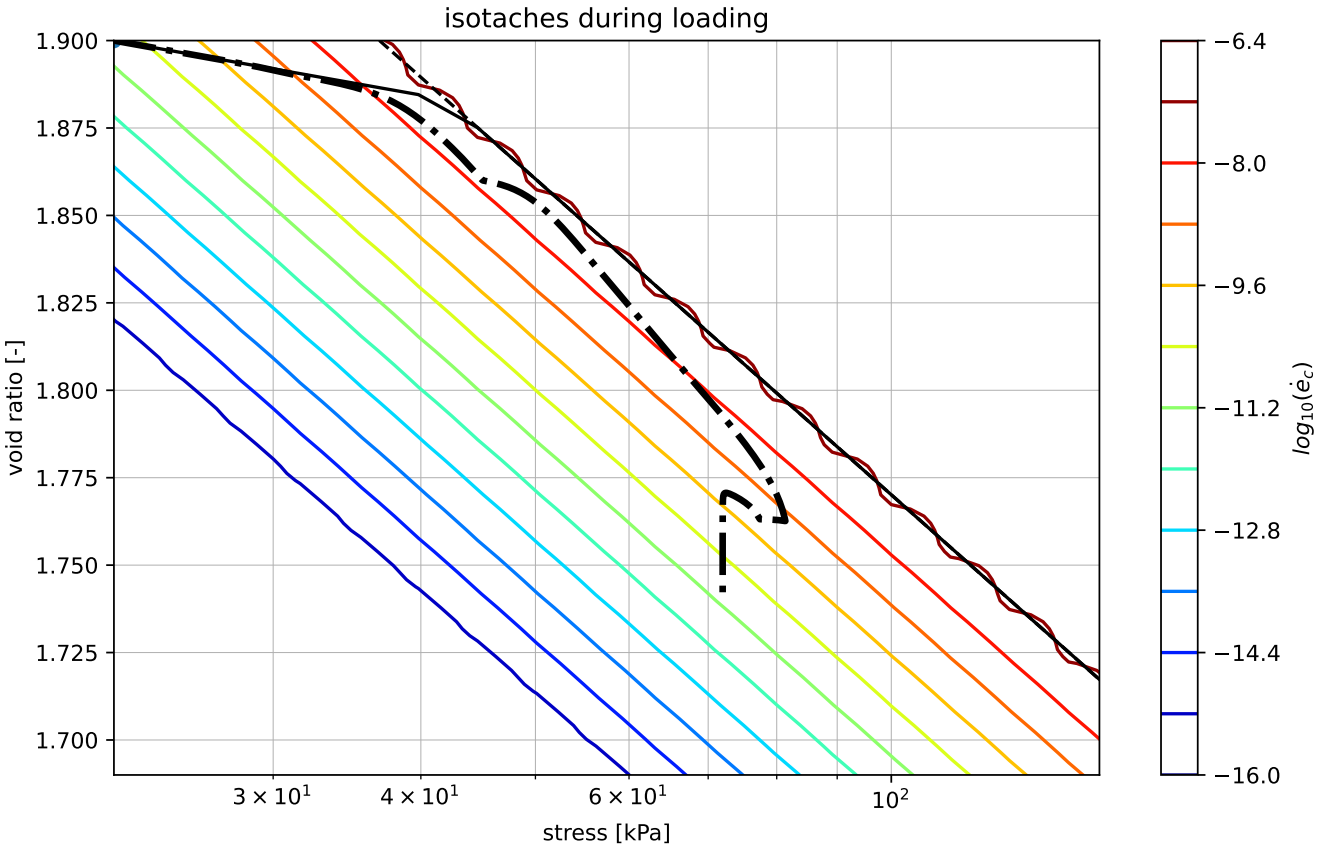

Graphs for GitHub with POP 20

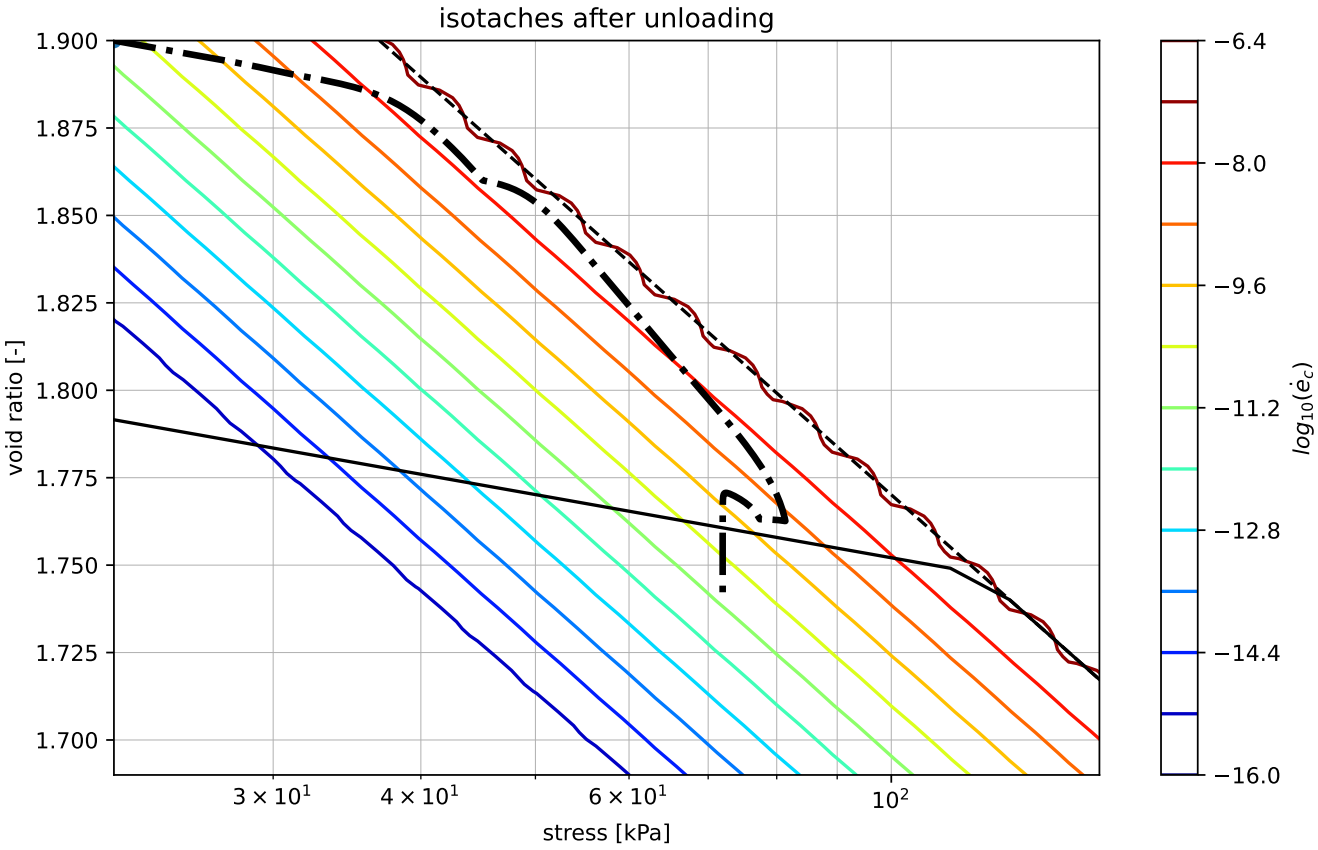

Graphs for GitHub with POP 40

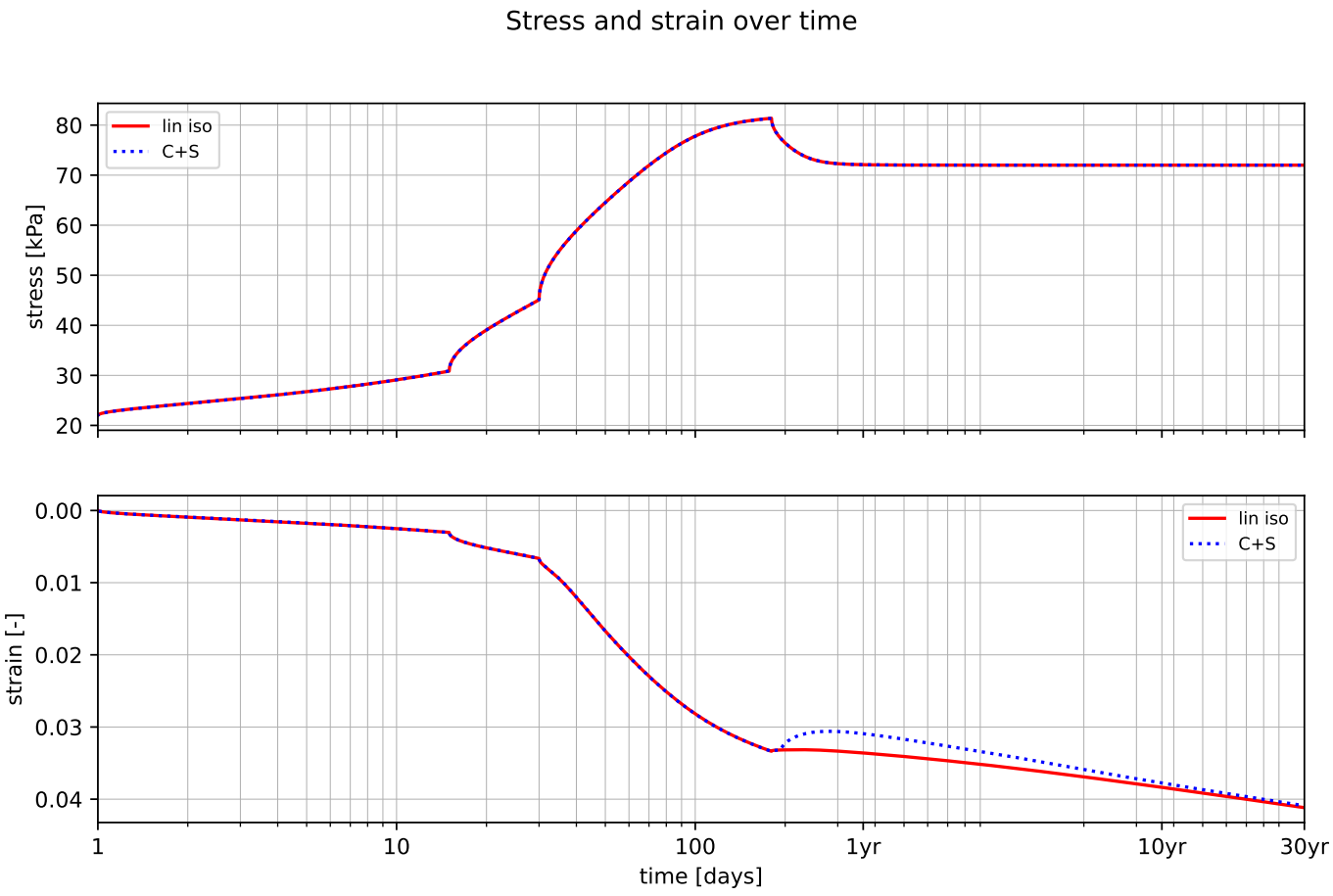

Graphs for GitHub with POP 40

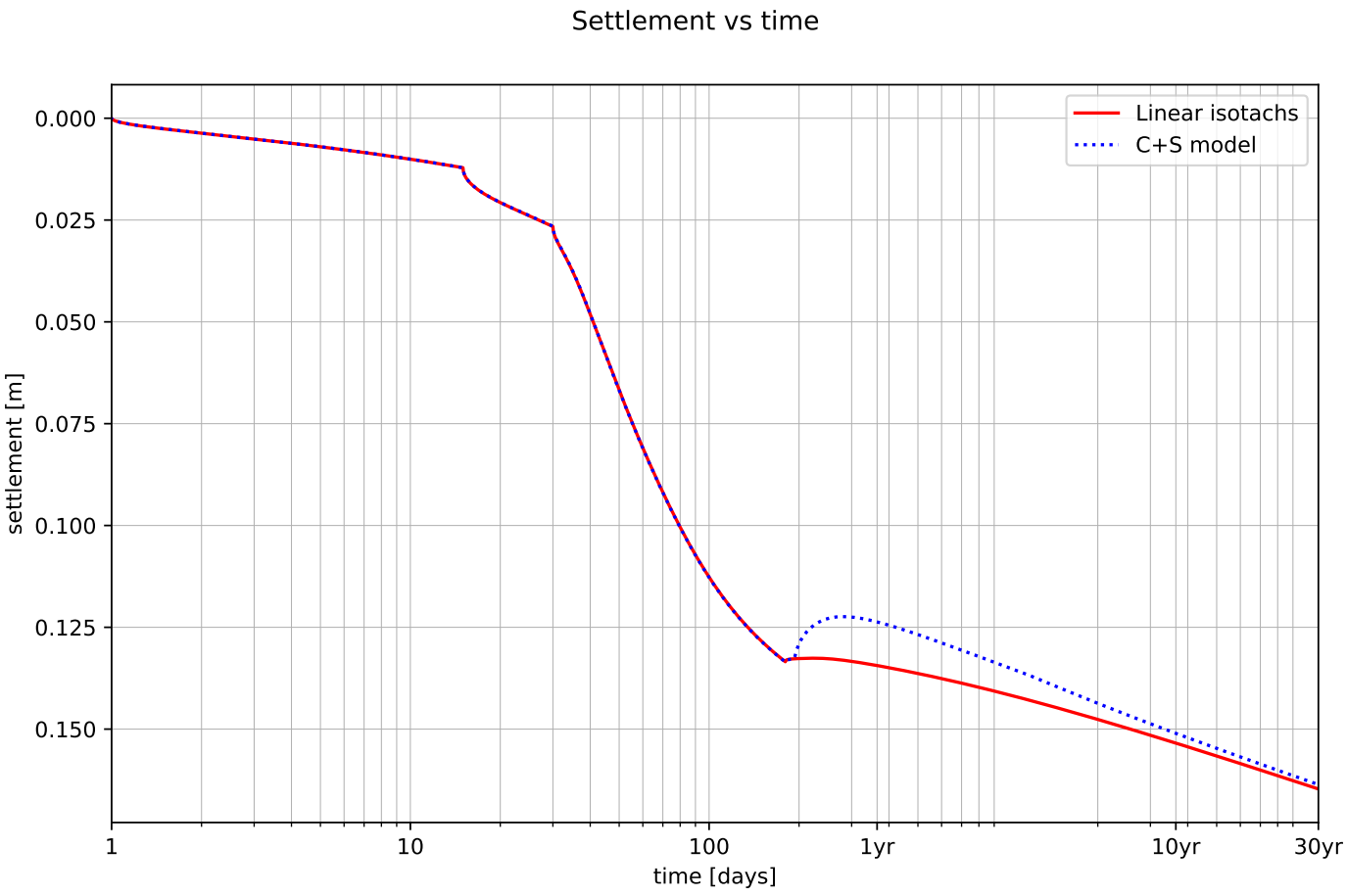

Graphs for GitHub with POP 40

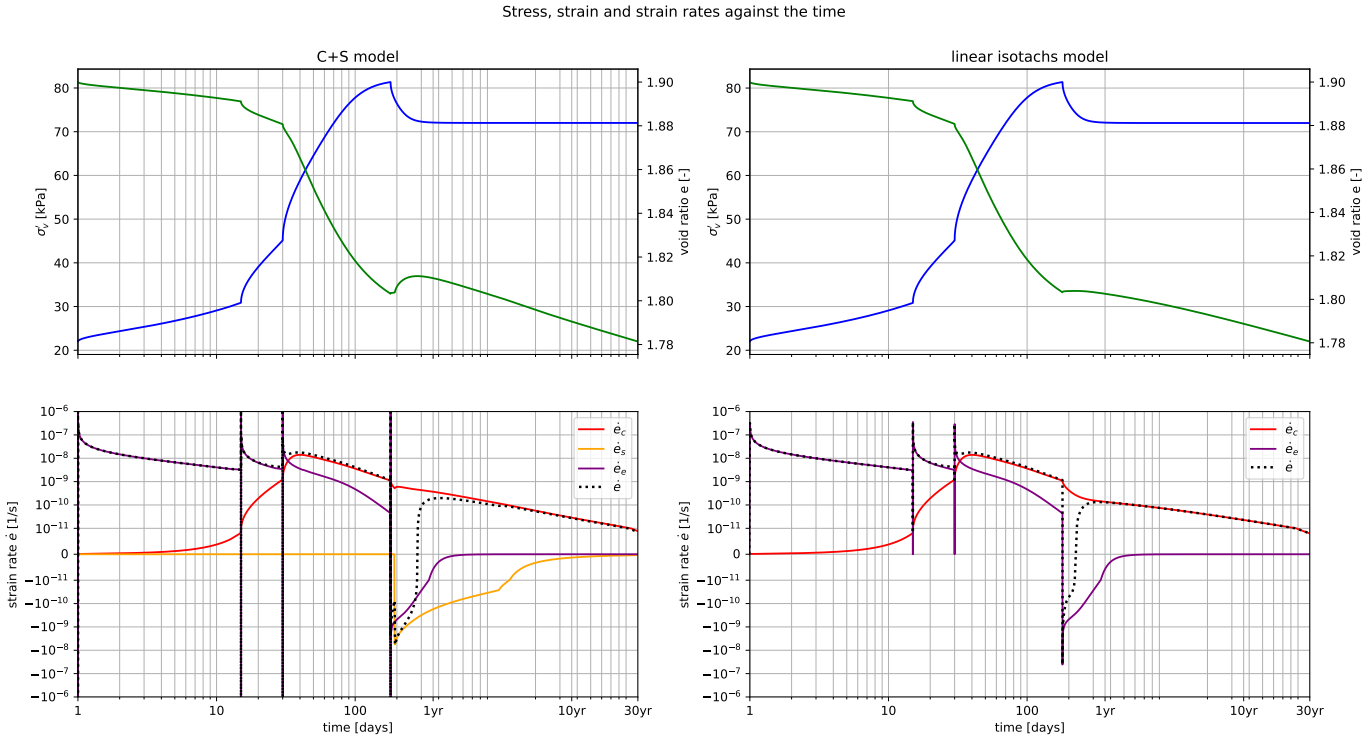

Graphs for GitHub with POP 40

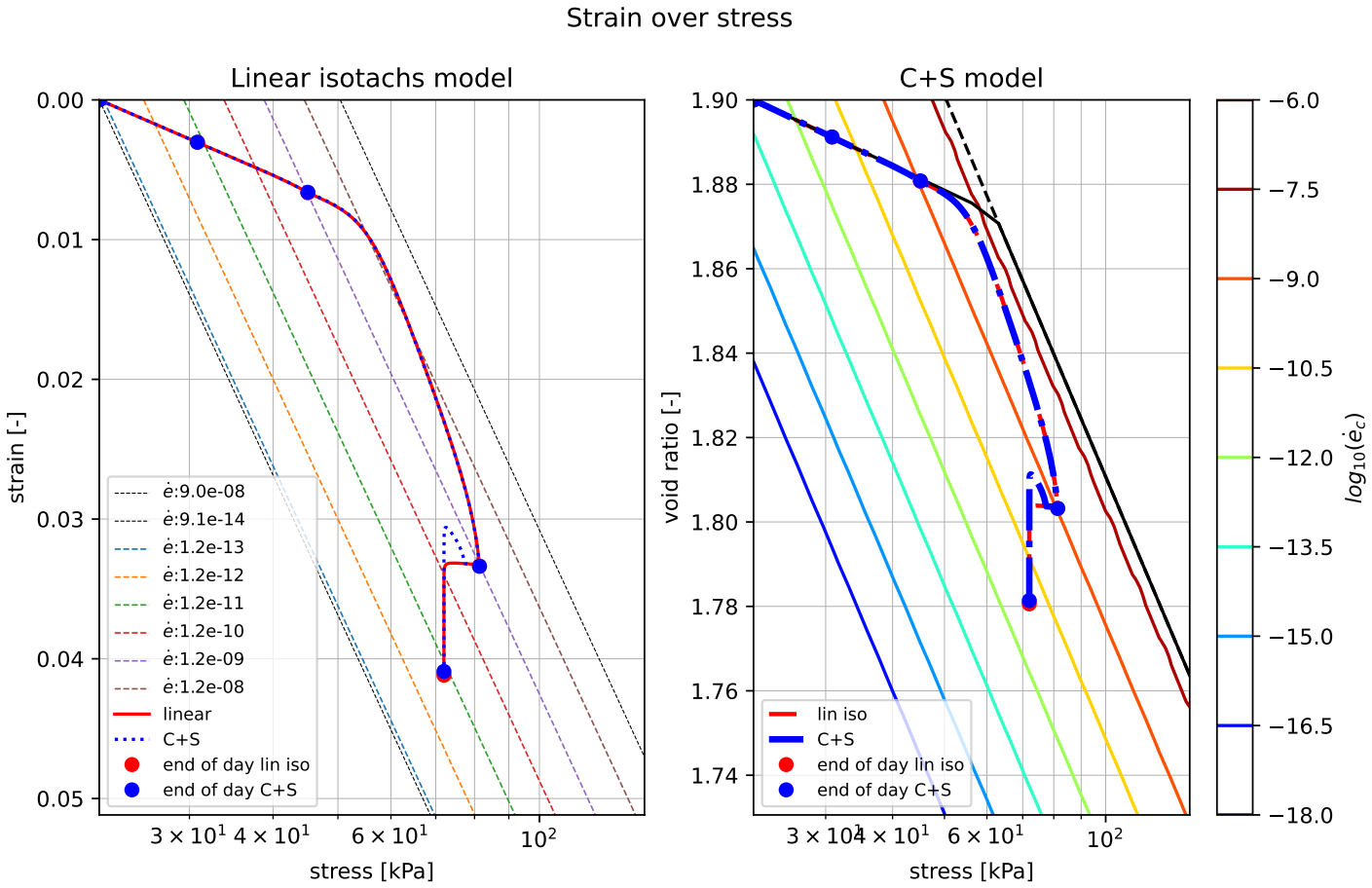

Graphs for GitHub with POP 40

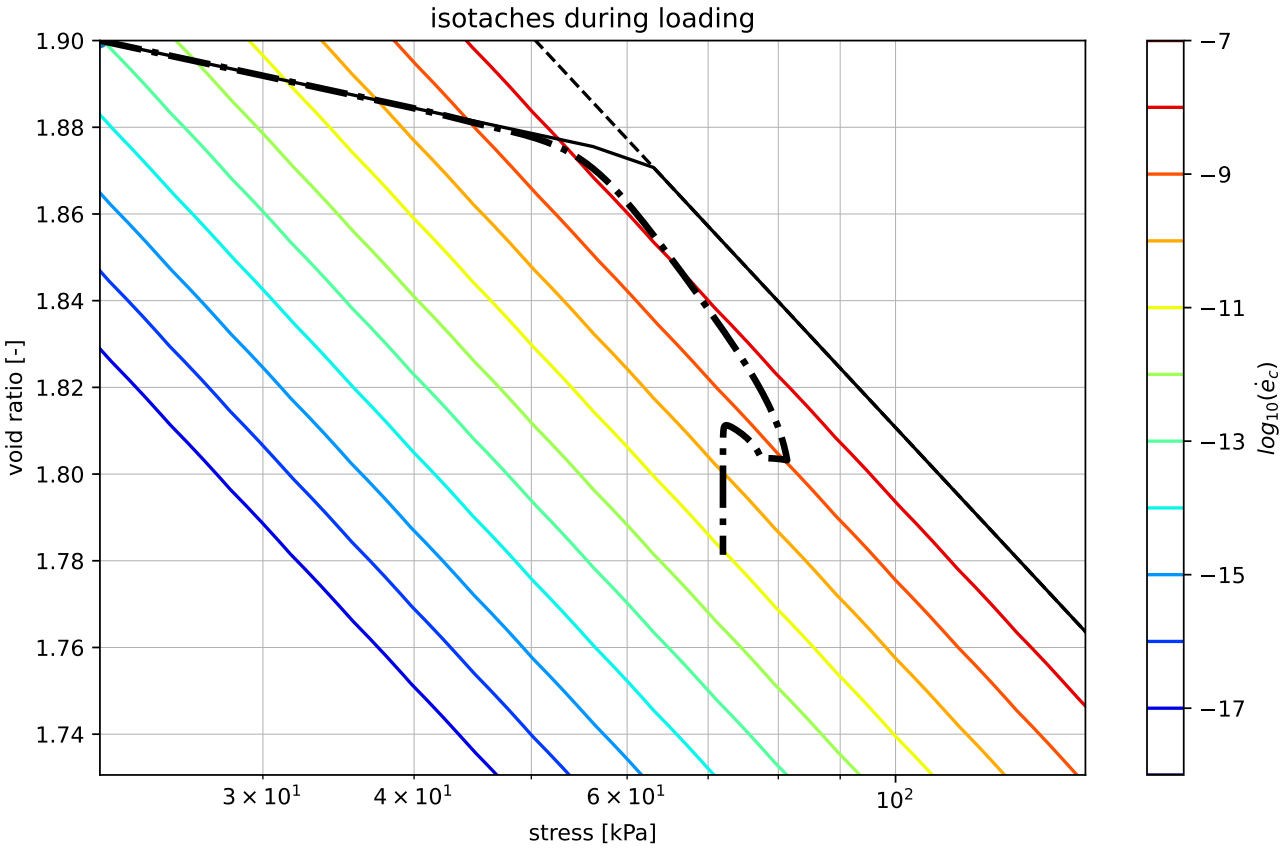

Graphs for GitHub with POP 40

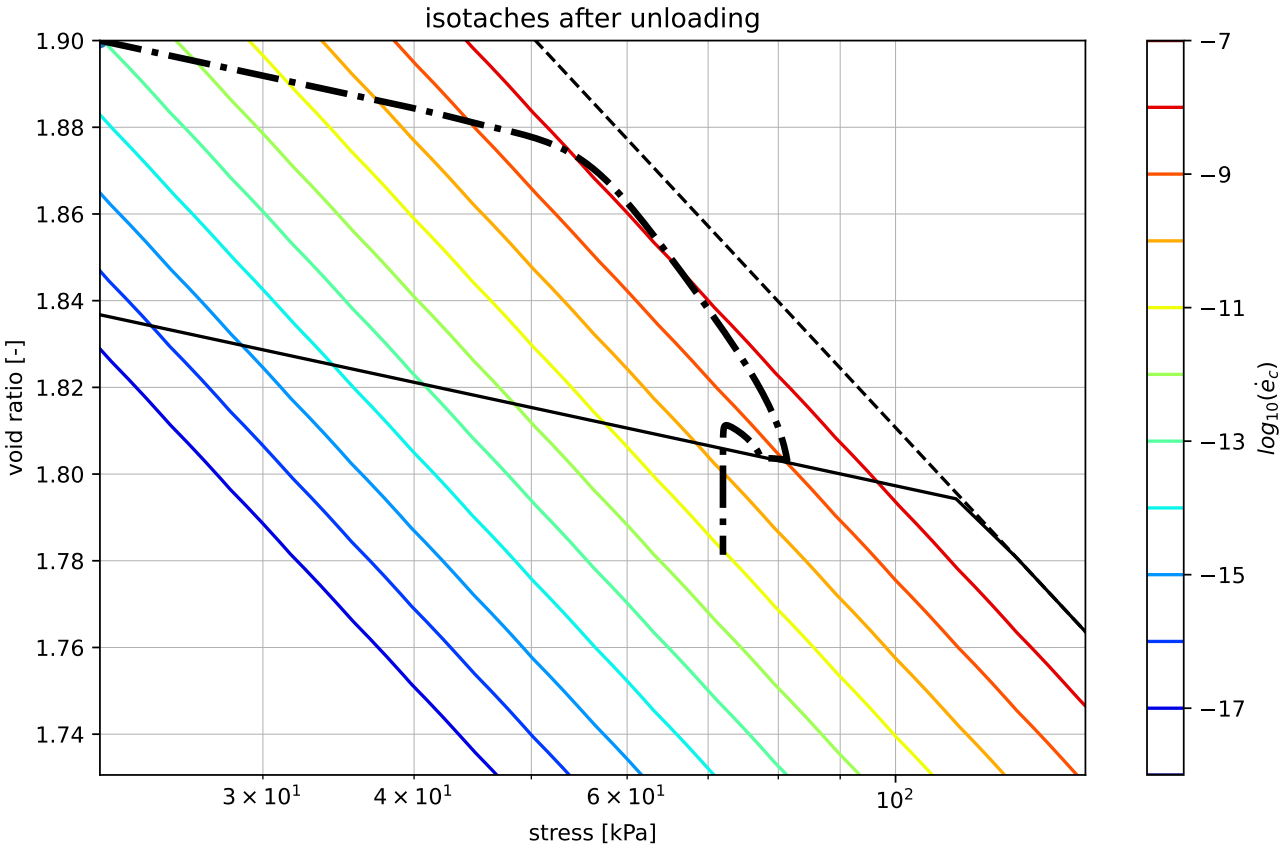

Graphs for Paper with POP 20

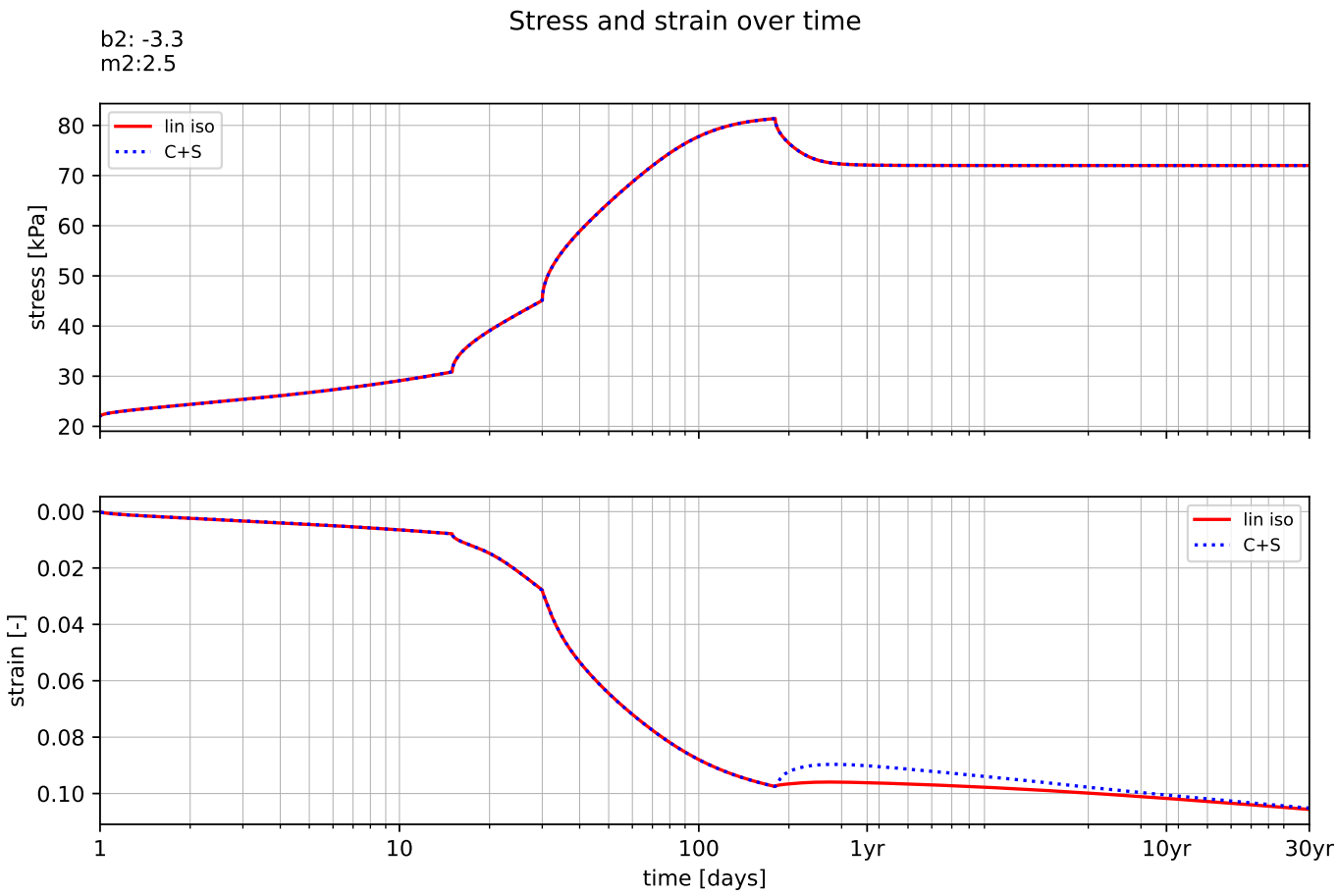

Graphs for Paper with POP 20

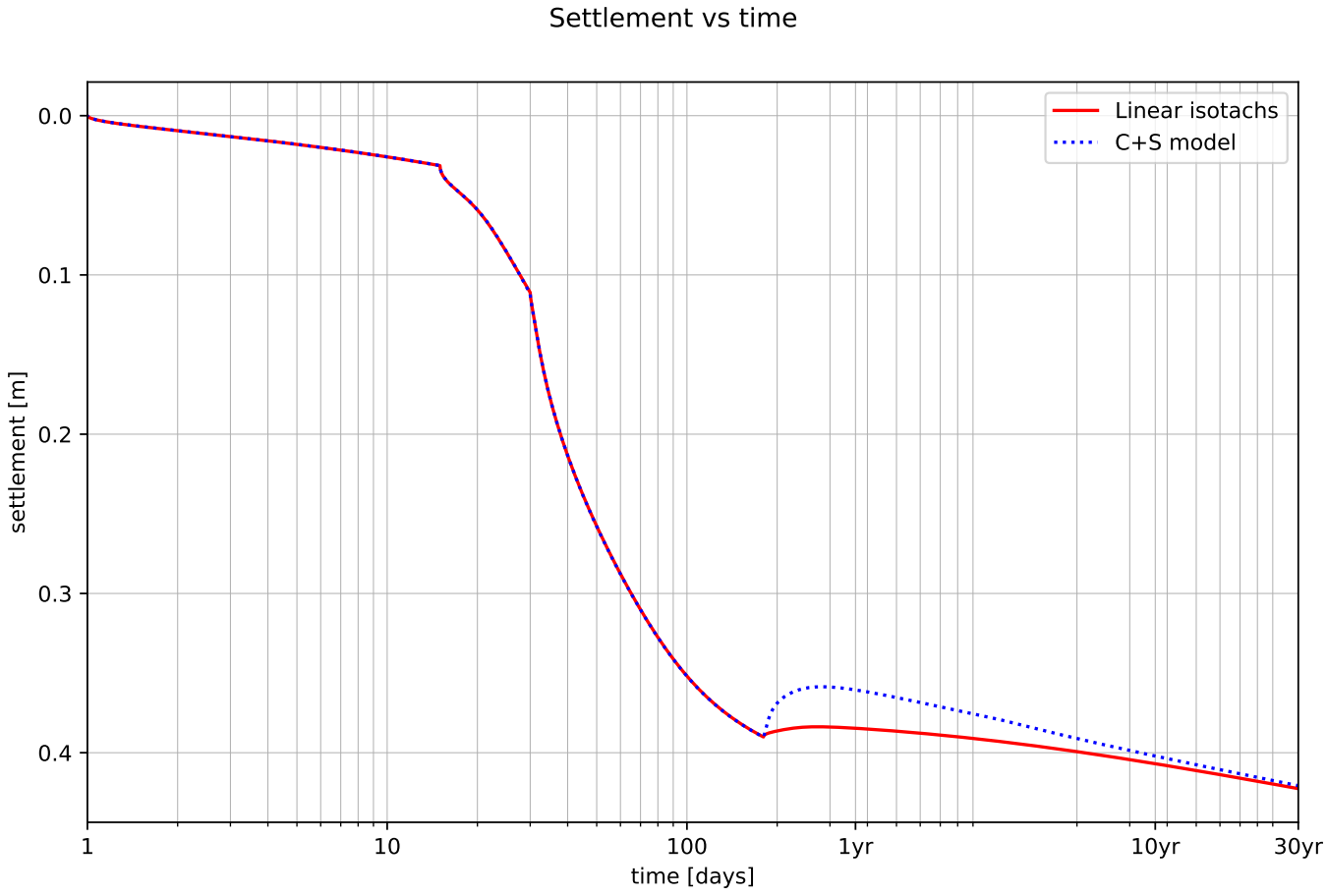

Graphs for Paper with POP 20

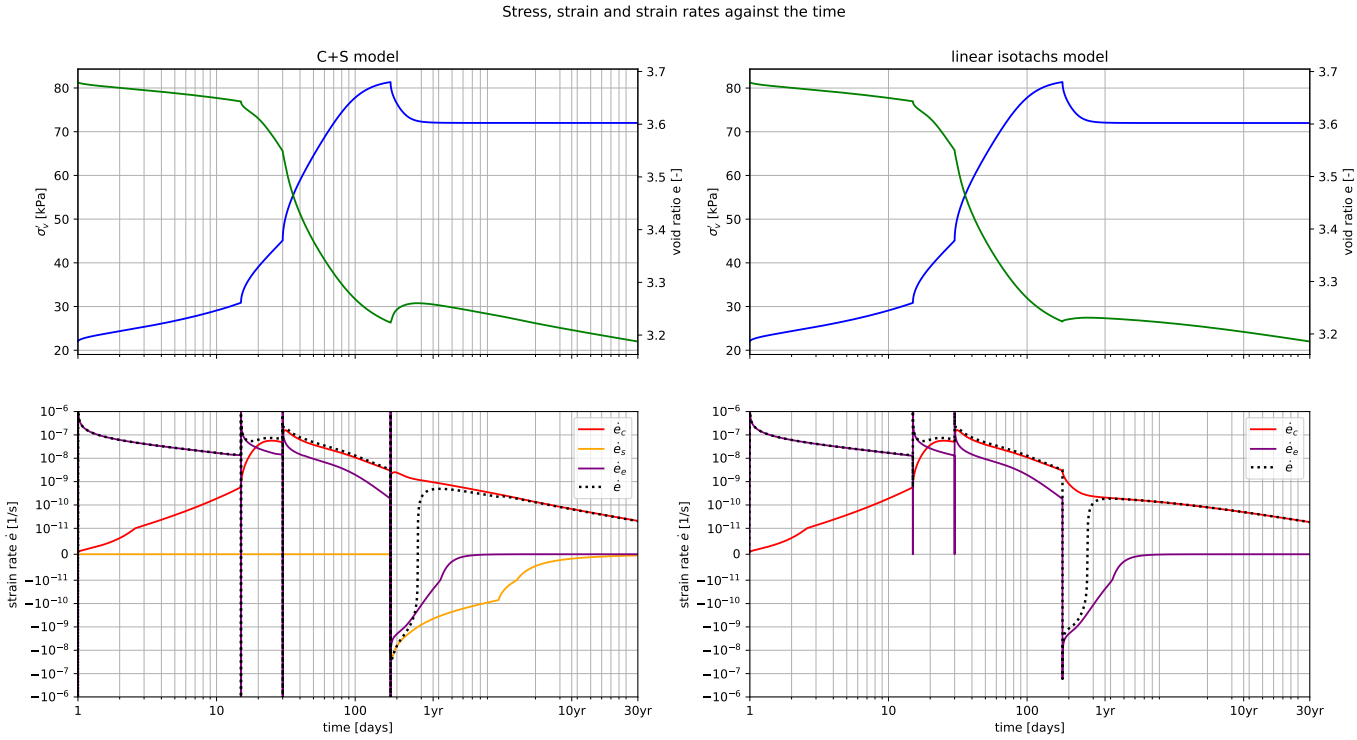

Graphs for Paper with POP 20

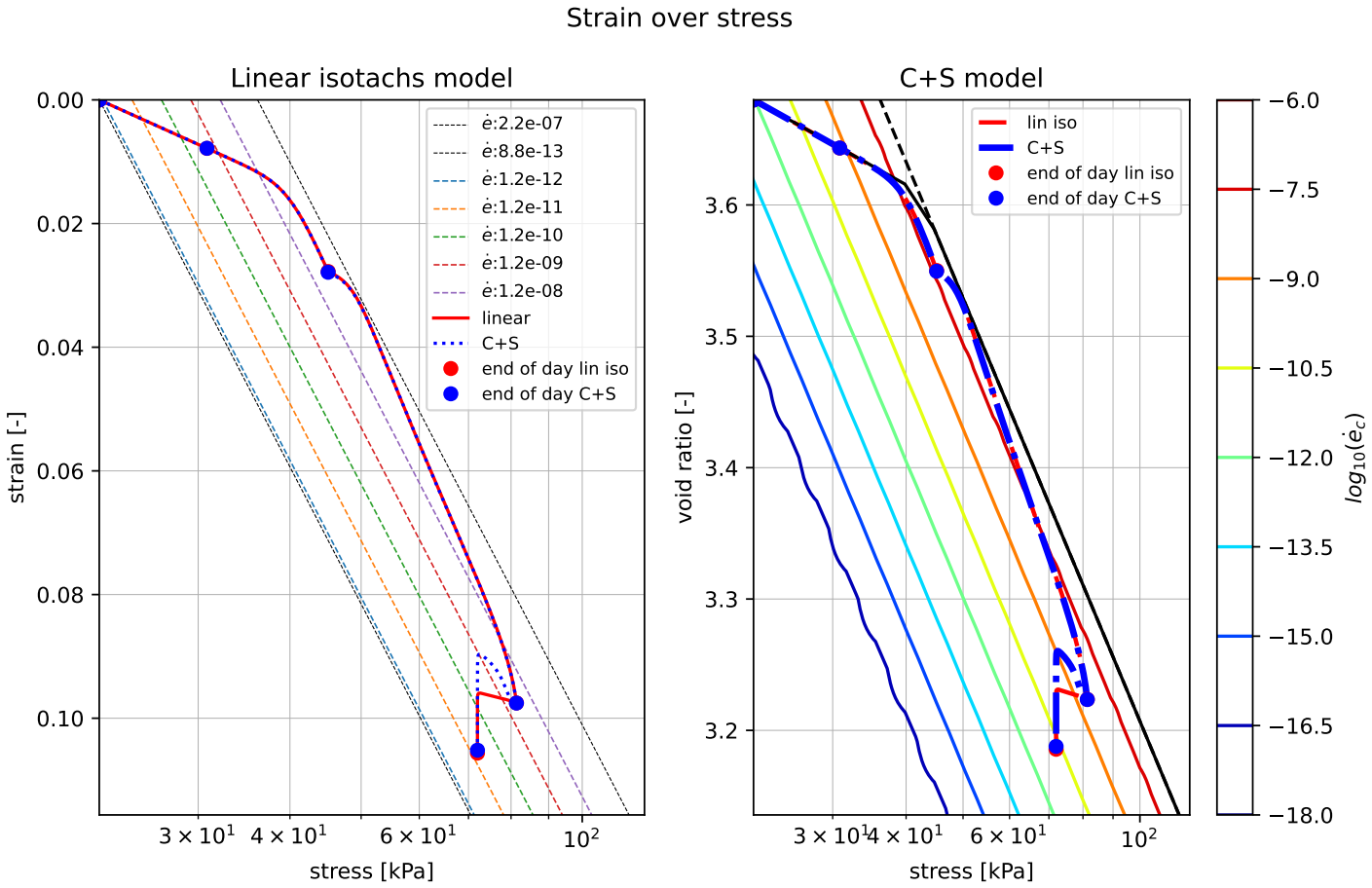

Graphs for Paper with POP 20

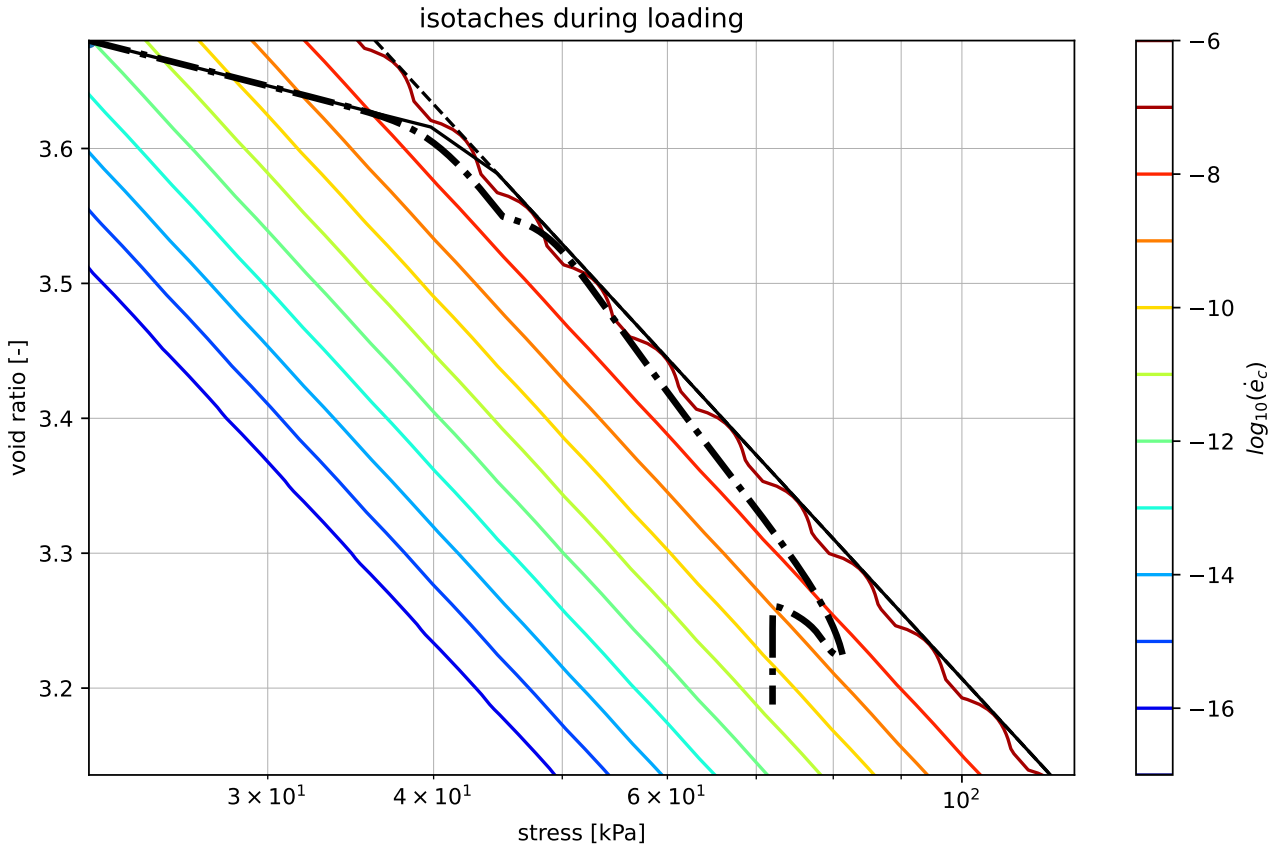

Graphs for Paper with POP 20

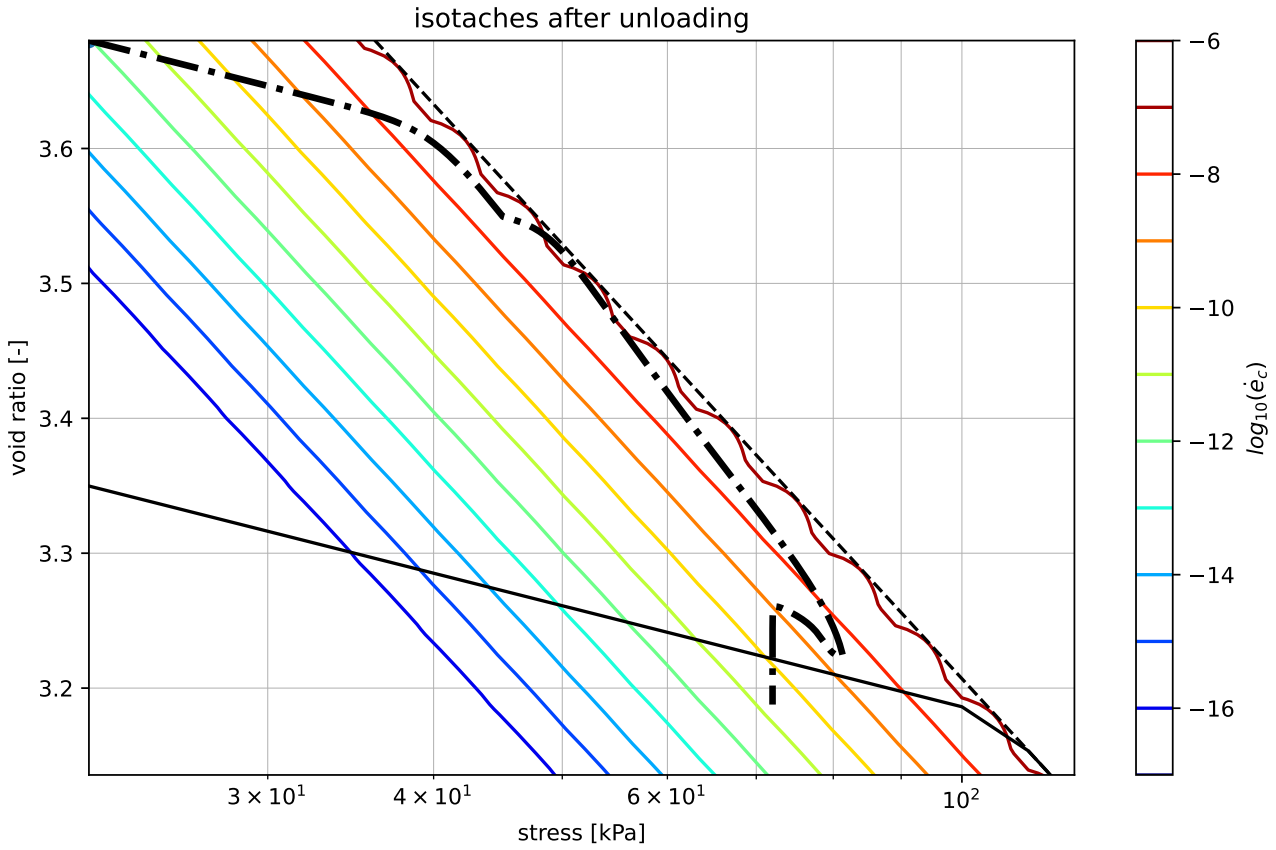

Graphs for Paper with POP 40

Graphs for Paper with POP 40

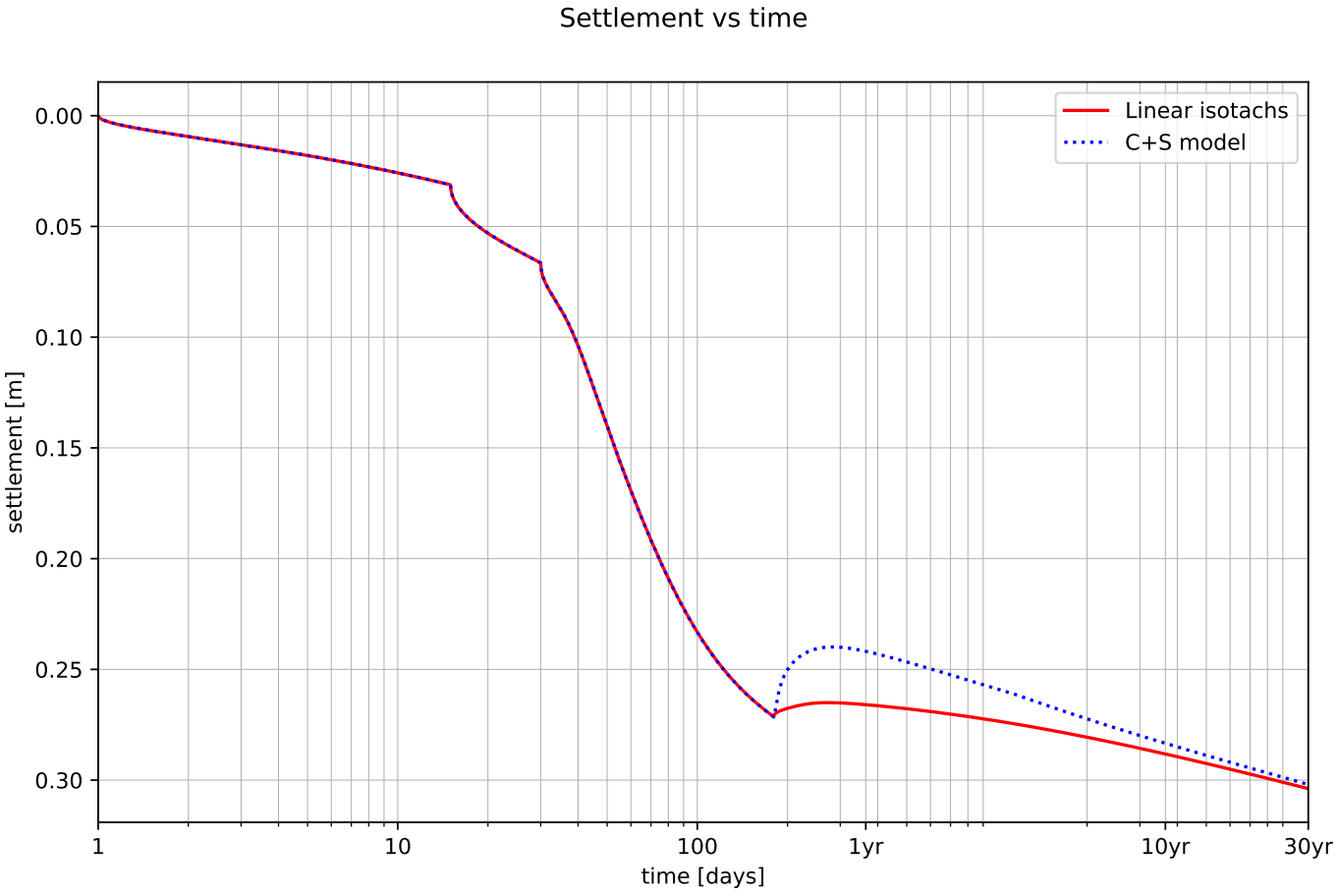

Graphs for Paper with POP 40

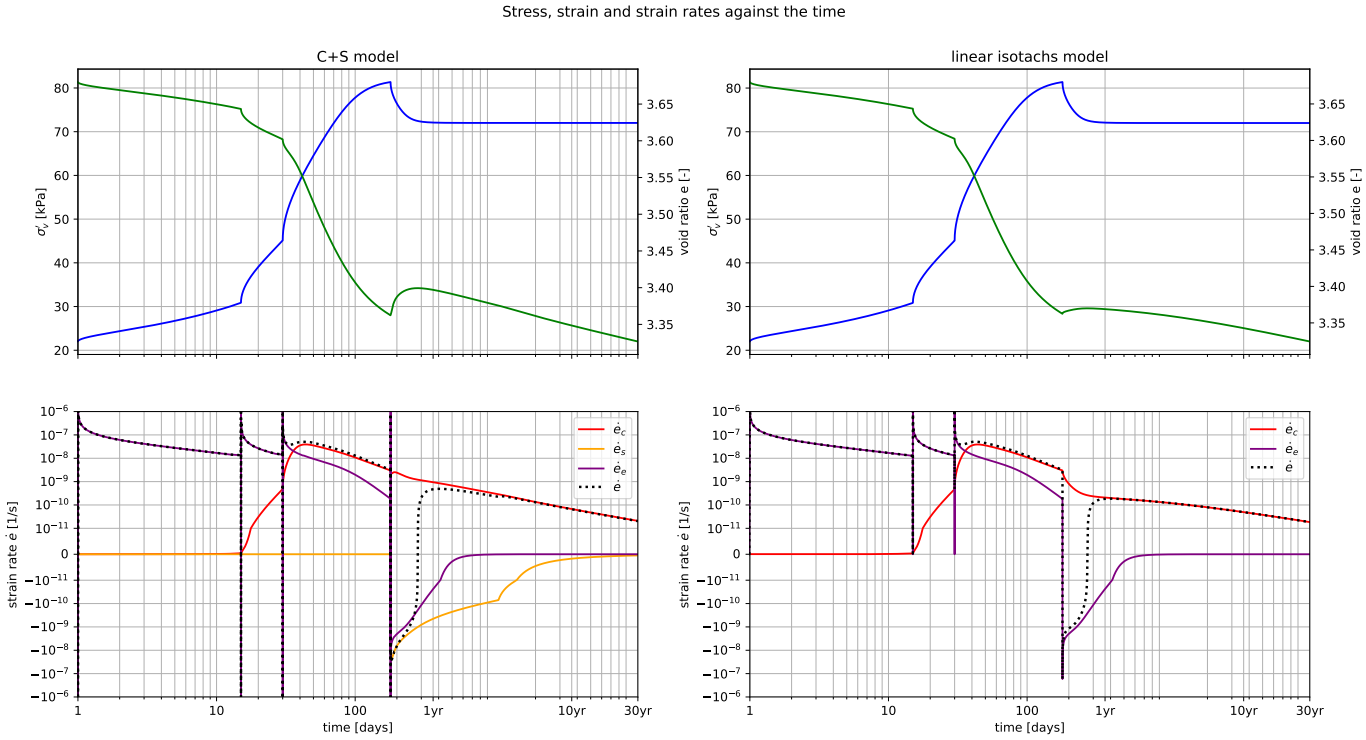

Graphs for Paper with POP 40

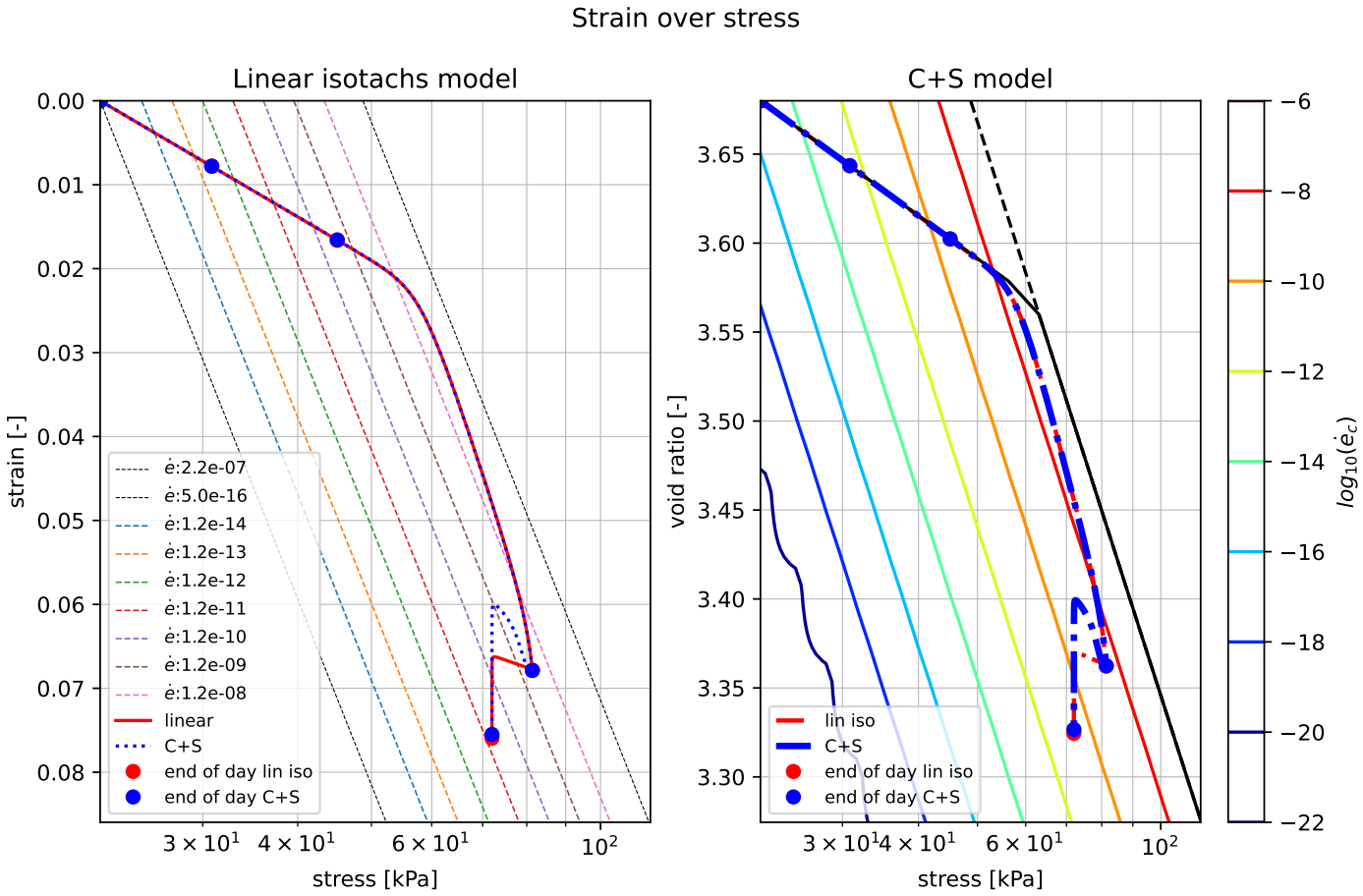

Graphs for Paper with POP 40

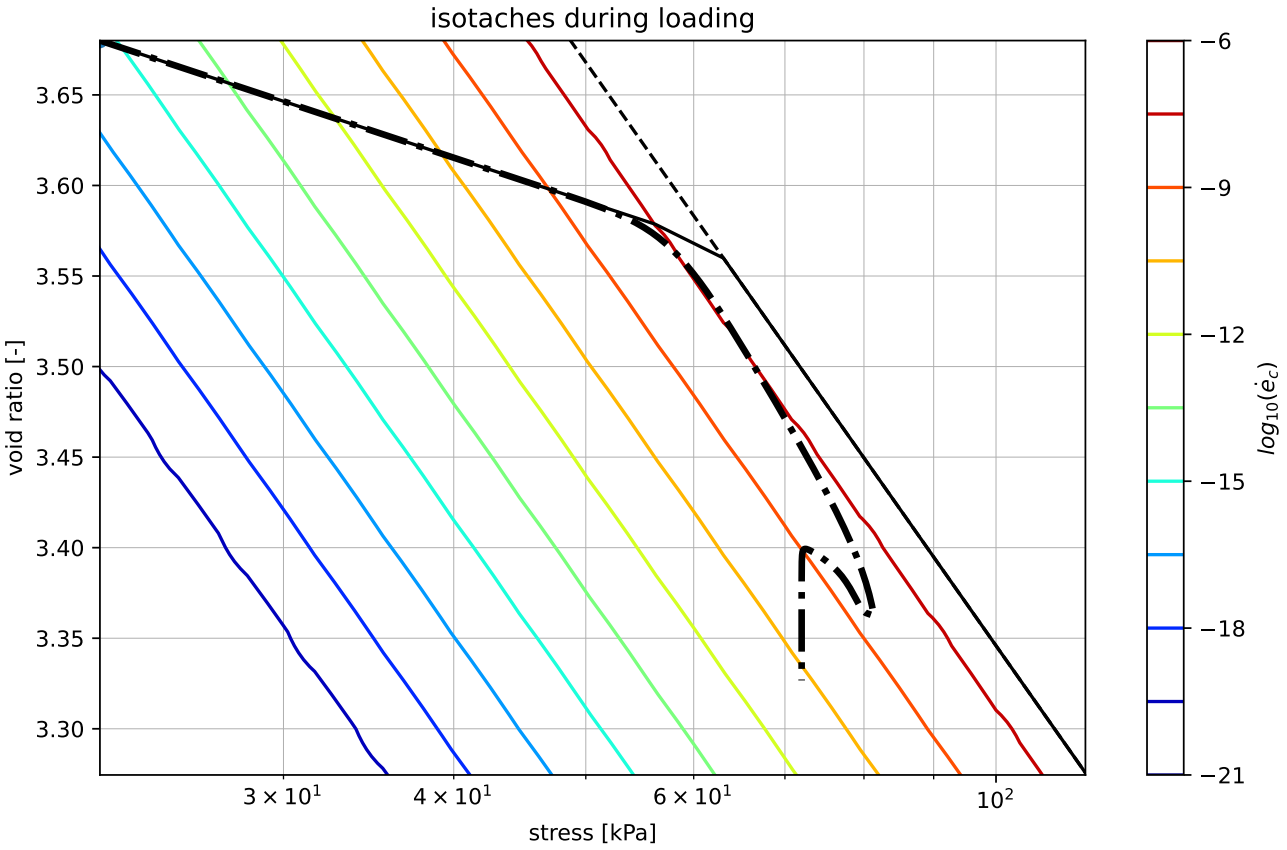

Graphs for Paper with POP 40

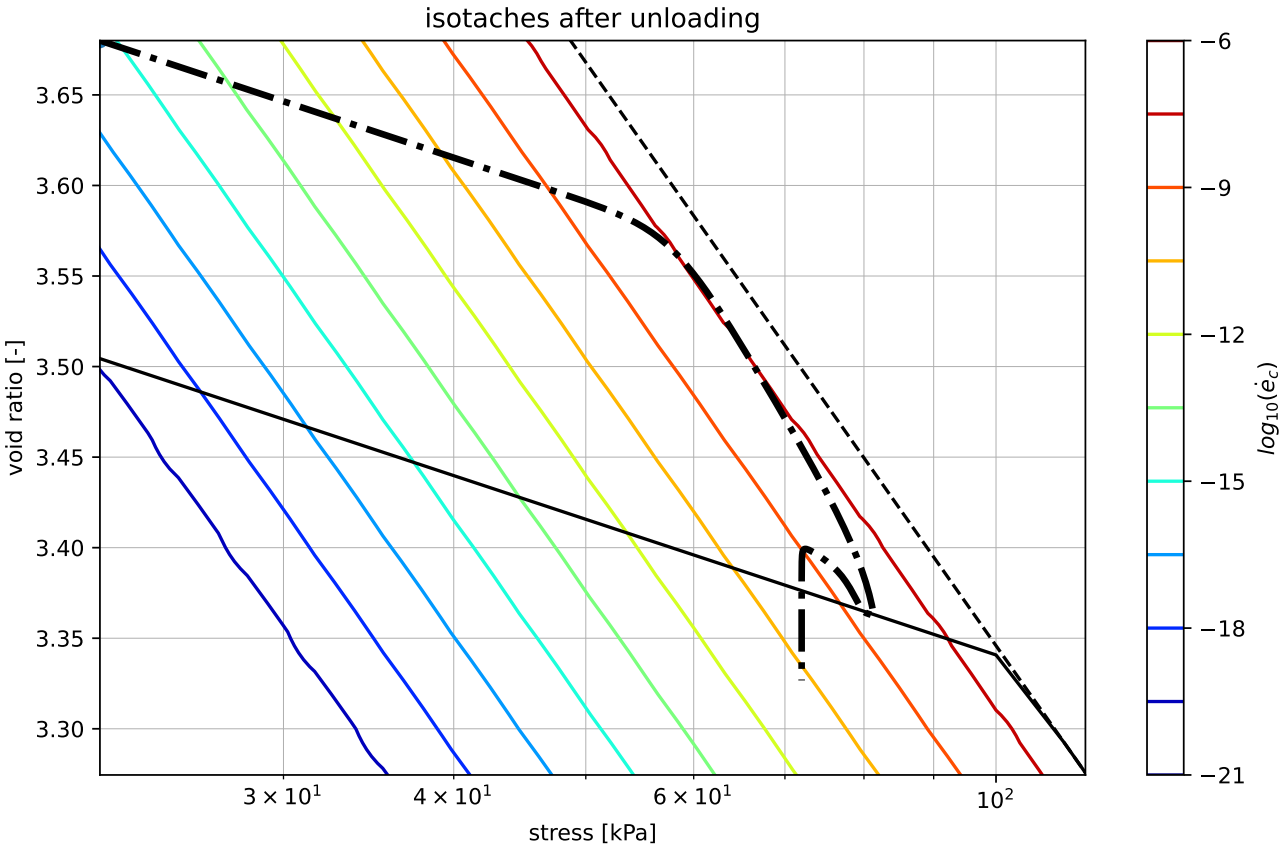

B

Groundwater table plots

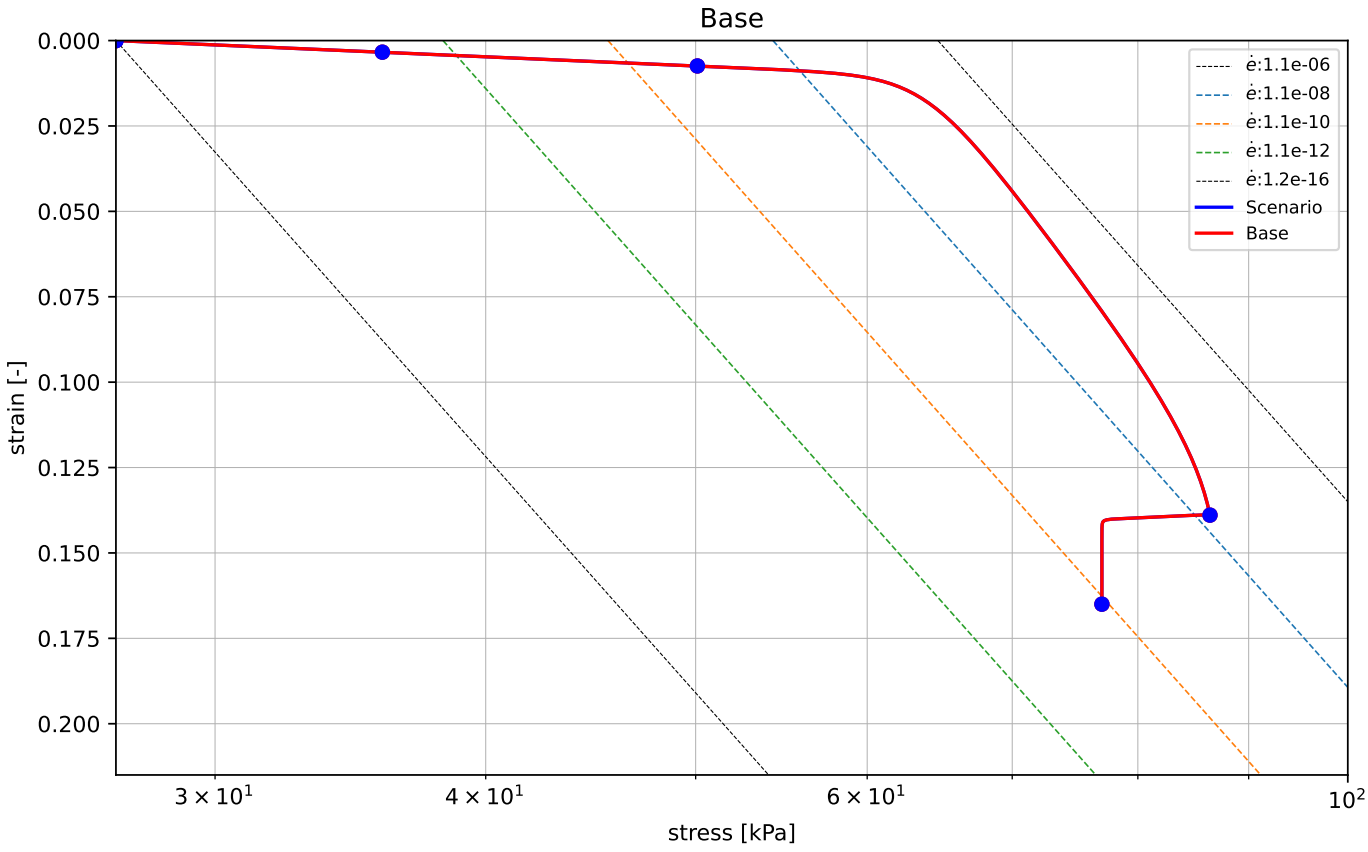
Base
0.000
0.025
0.050
0.075
0.100
0.125
0.150
0.175
0.200
strain [-]
3×10^1
4×10^1
6×10^1
10^2
stress [kPa]
ė:1.1e-06
ė:1.1e-08
ė:1.1e-10
ė:1.1e-12
ė:1.2e-16
Scenario
Base

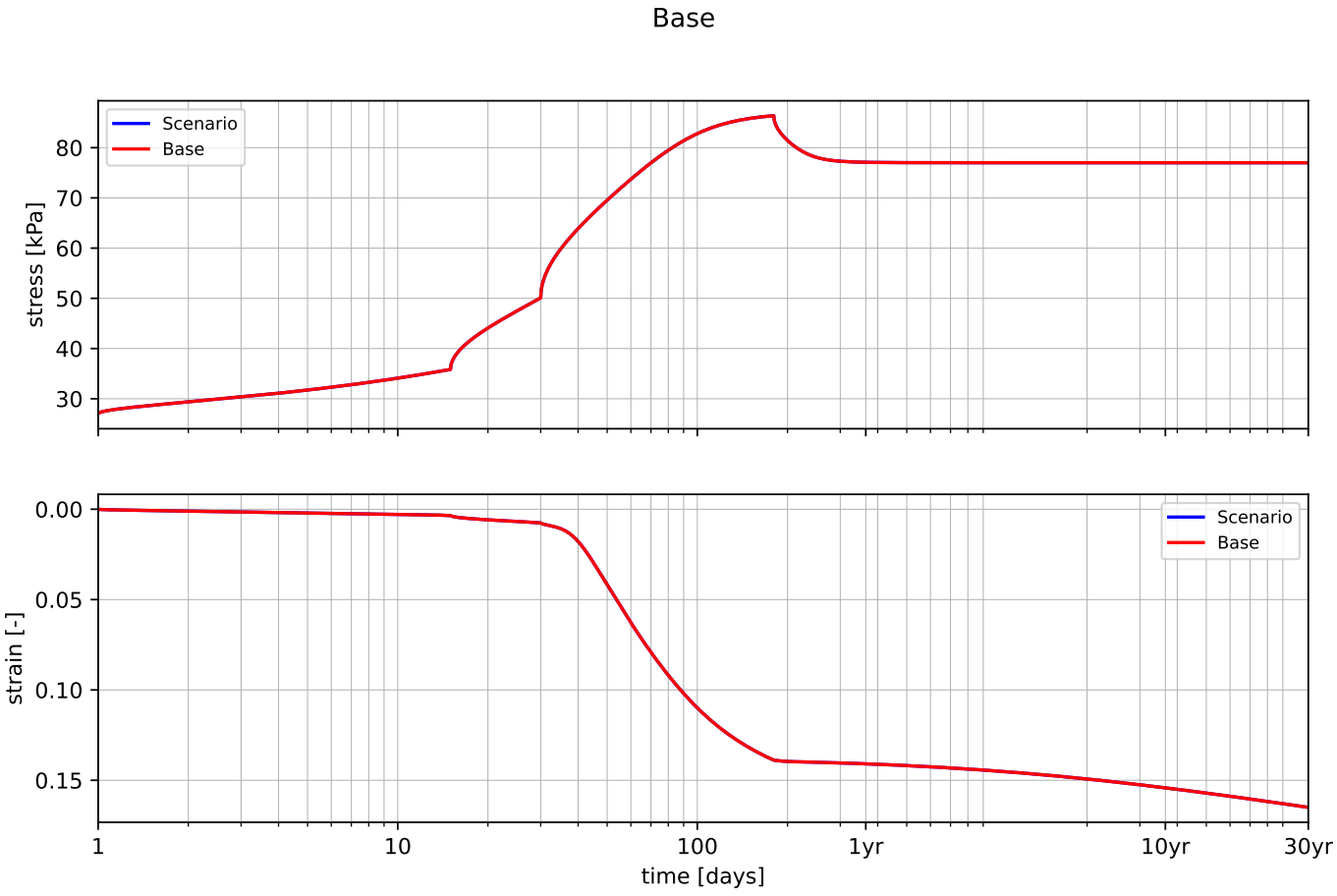
Base
Scenario
Base
stress [kPa]
80
70
60
50
40
30
Scenario
Base
strain [-]
0.00
0.05
0.10
0.15
1
10
100
1yr
10yr
30yr
time [days]

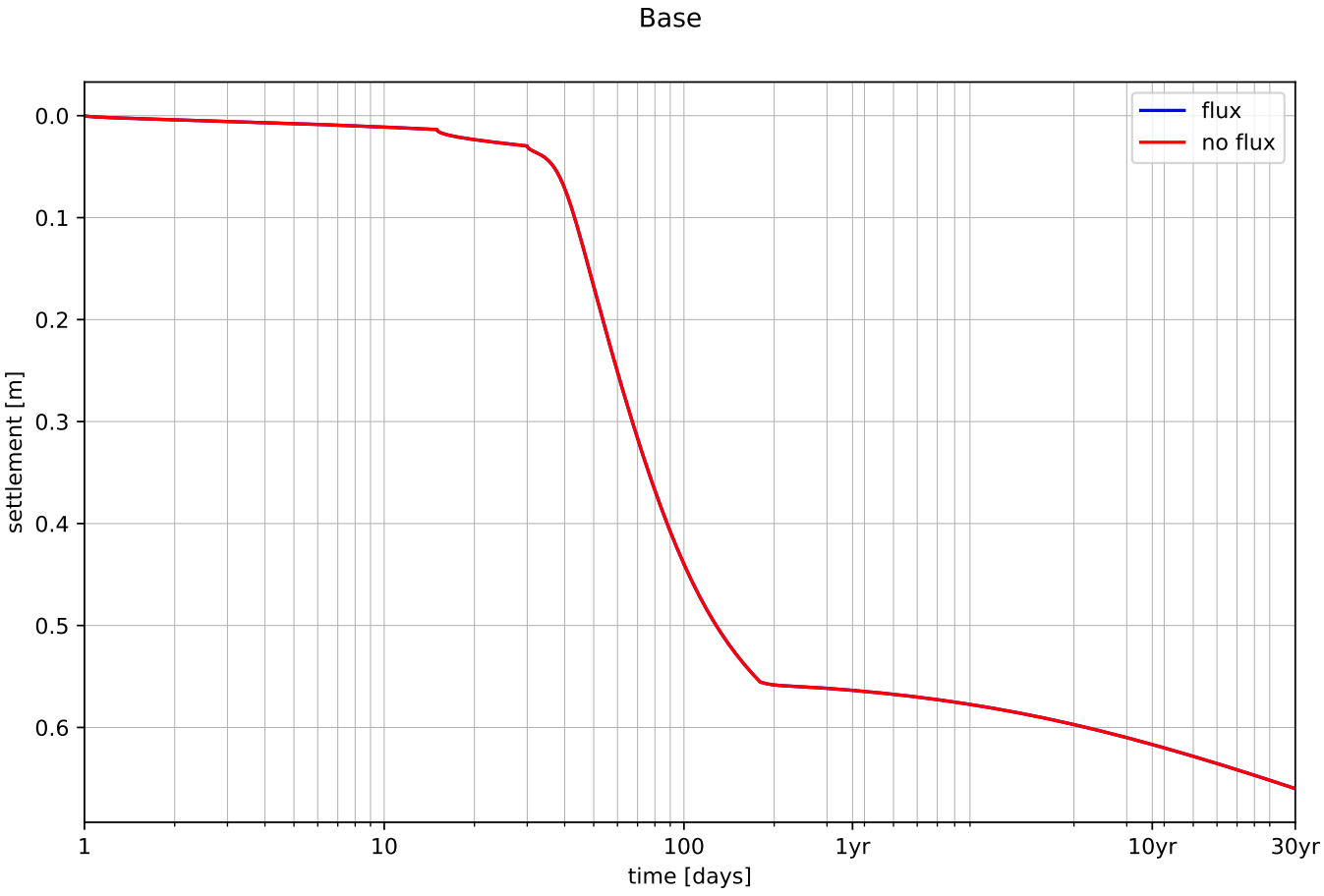
Base
flux
no flux
0.0
0.1
0.2
0.3
0.4
0.5
0.6
settlement [m]
1
10
100
1yr
10yr
30yr
time [days]

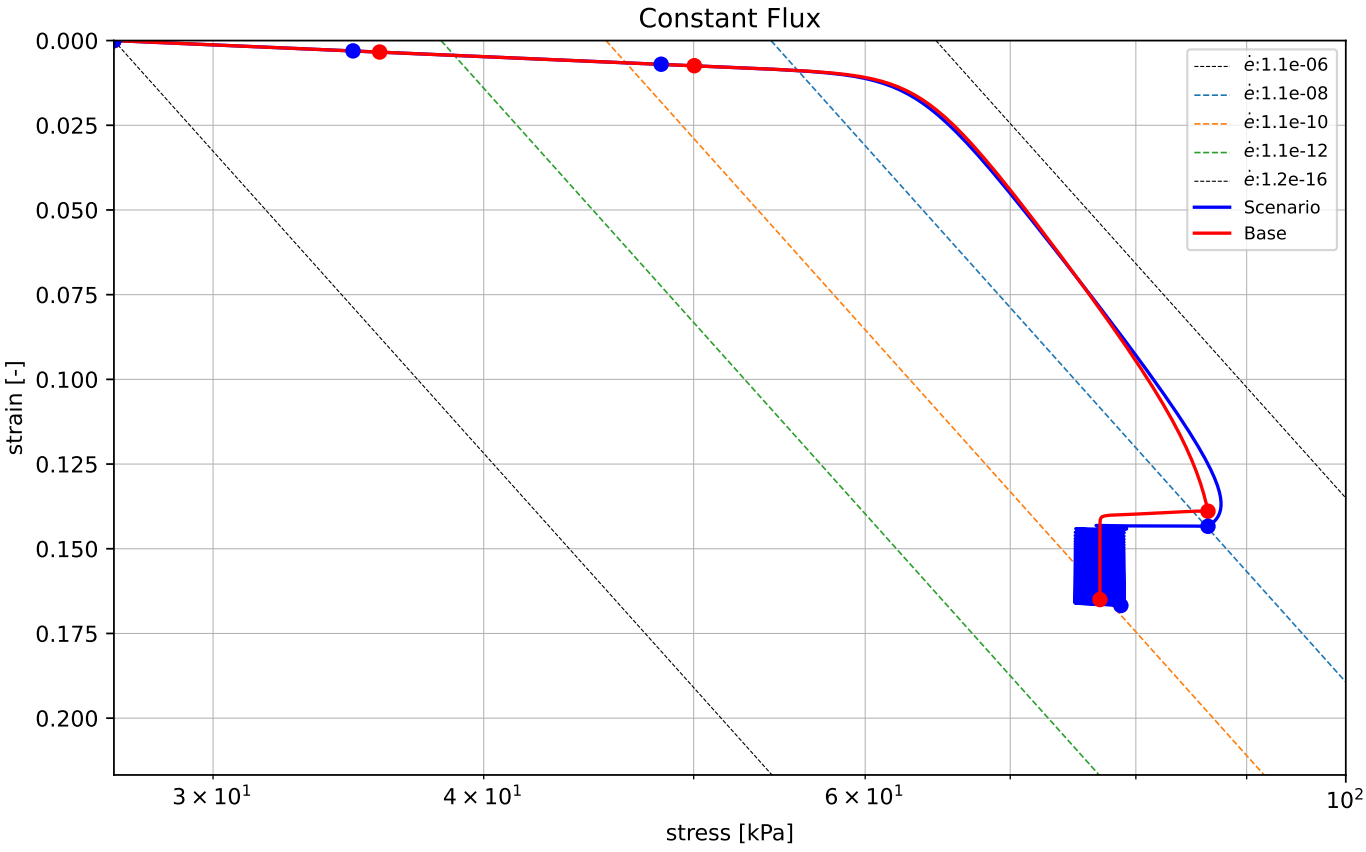
Constant Flux
0.000
0.025
0.050
0.075
0.100
0.125
0.150
0.175
0.200
strain [-]
3×10^1
4×10^1
6×10^1
10^2
stress [kPa]
ė:1.1e-06
ė:1.1e-08
ė:1.1e-10
ė:1.1e-12
ė:1.2e-16
Scenario
Base

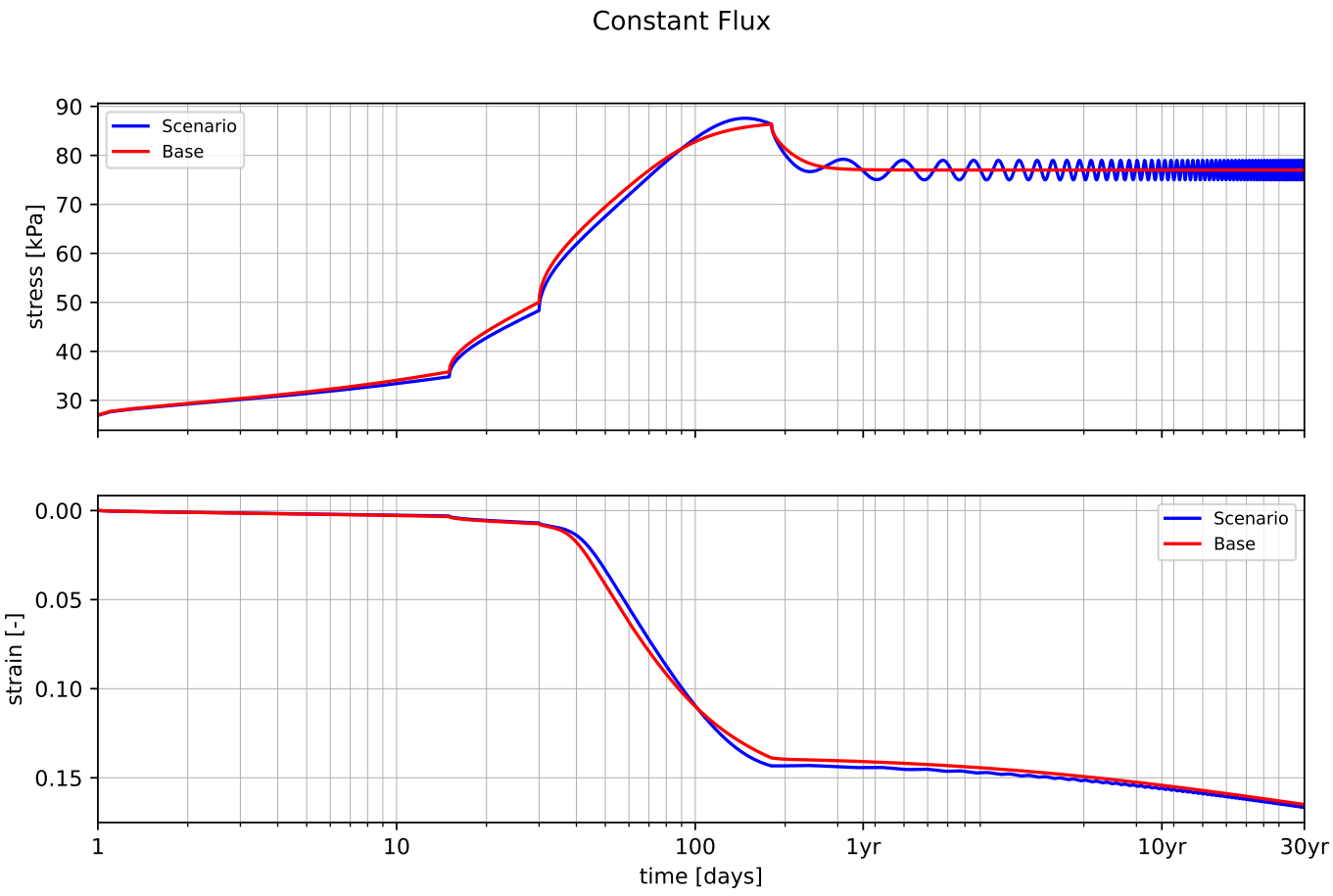
Constant Flux
Scenario
Base
stress [kPa]
90
80
70
60
50
40
30
Scenario
Base
strain [-]
0.00
0.05
0.10
0.15
1
10
100
1yr
10yr
30yr
time [days]

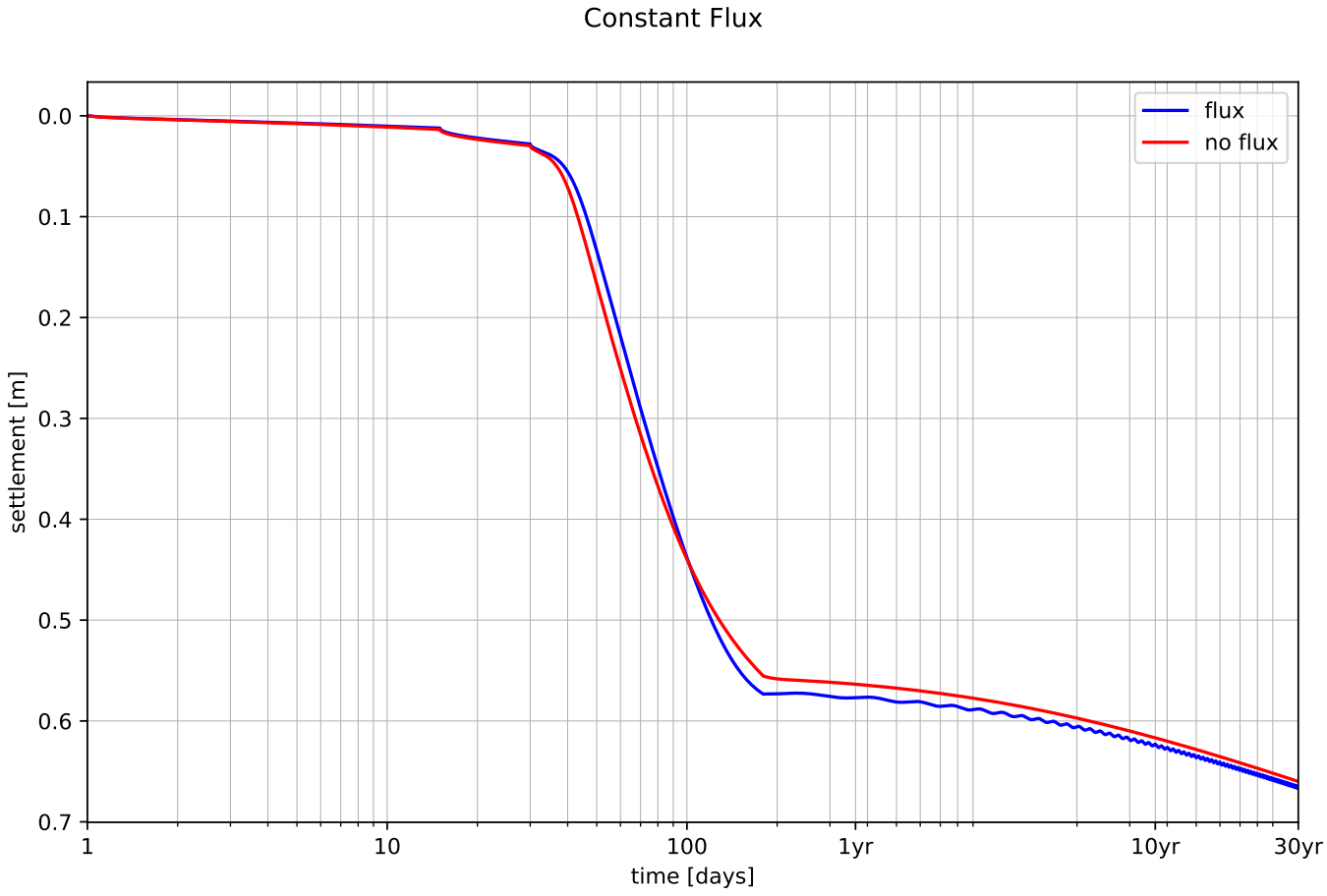
Constant Flux
flux
no flux
settlement [m]
0.0
0.1
0.2
0.3
0.4
0.5
0.6
0.7
1
10
100
1yr
10yr
30yr
time [days]

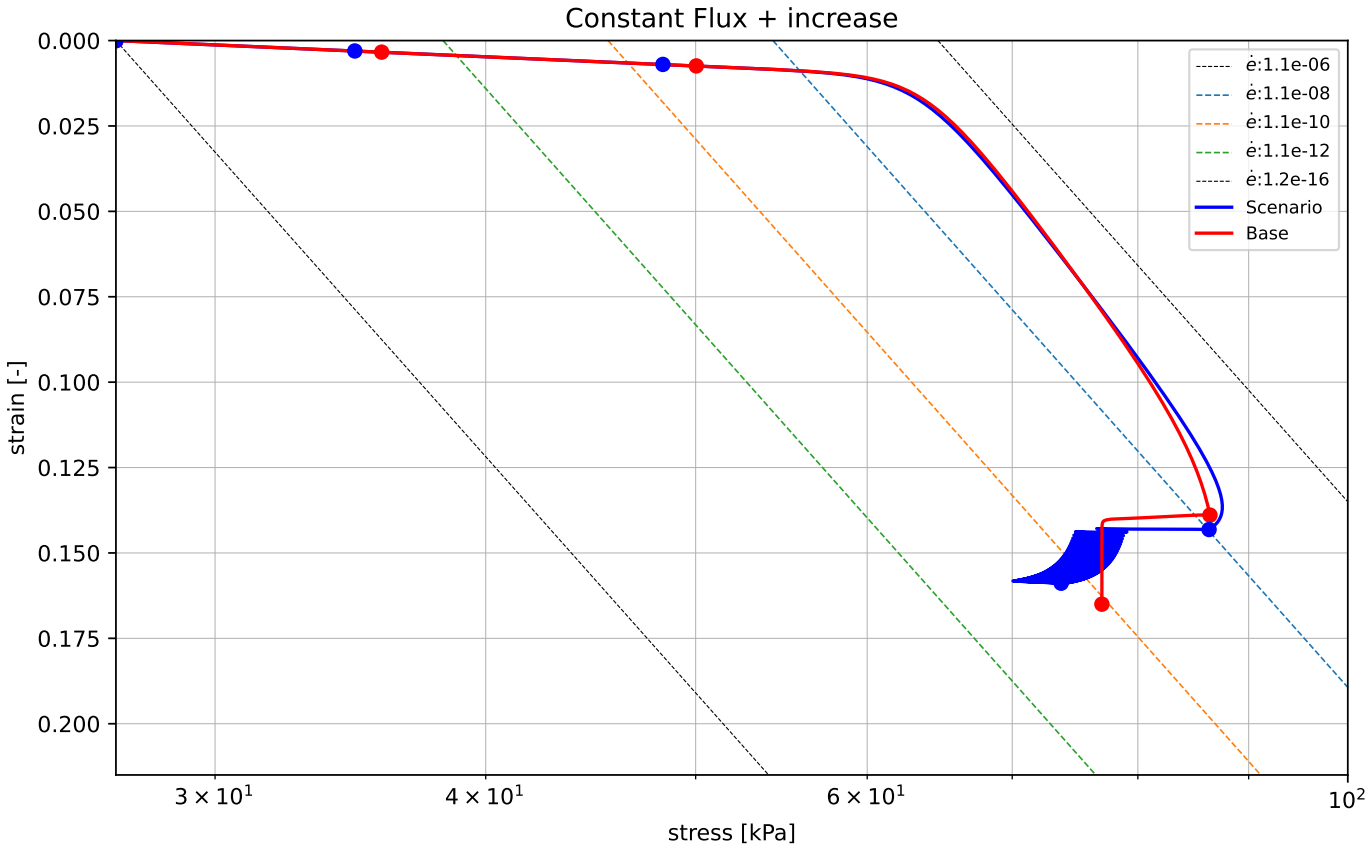
Constant Flux + increase
0.000
0.025
0.050
0.075
0.100
0.125
0.150
0.175
0.200
strain [-]
3×10^1
4×10^1
6×10^1
10^2
stress [kPa]
ė:1.1e-06
ė:1.1e-08
ė:1.1e-10
ė:1.1e-12
ė:1.2e-16
Scenario
Base

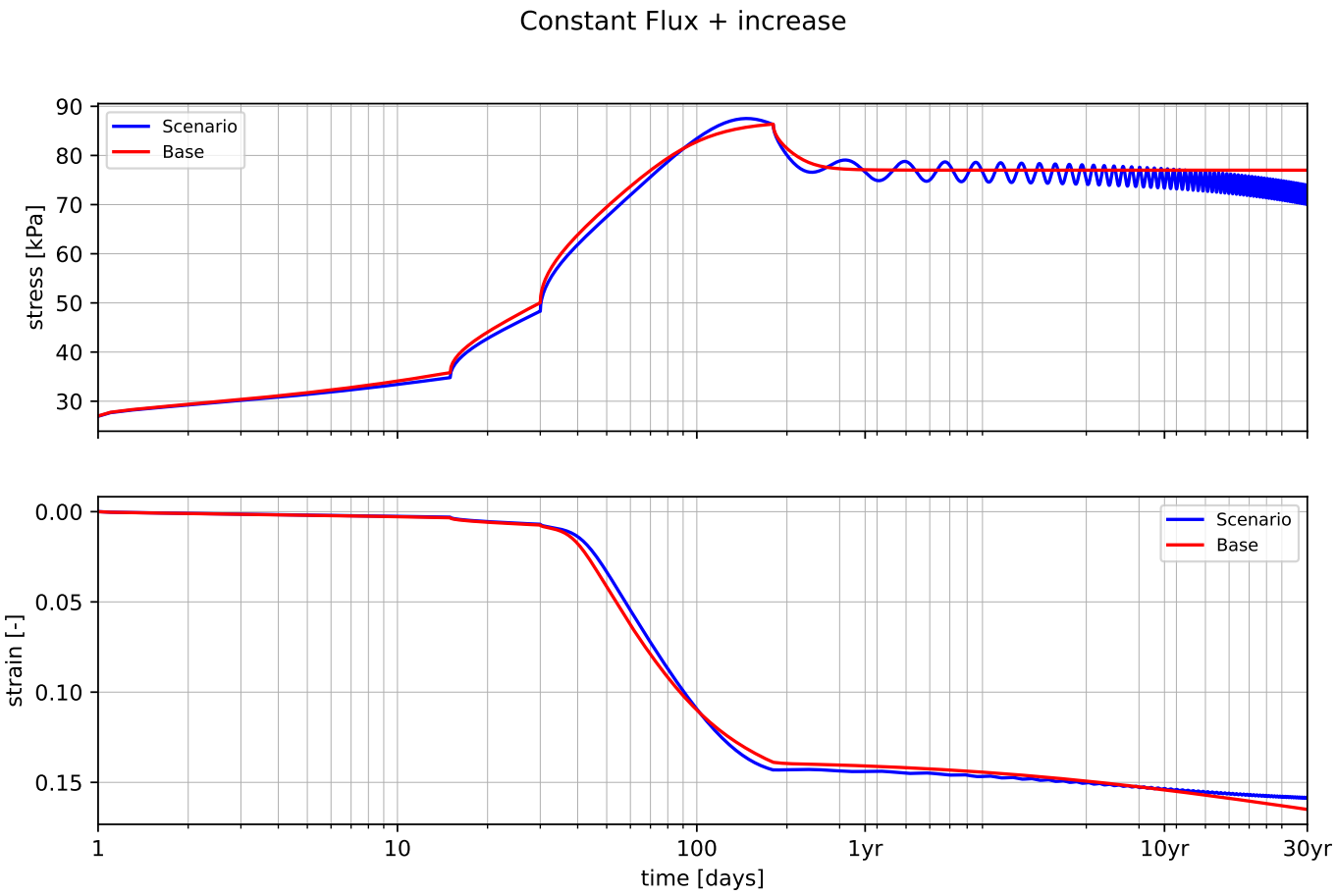
Constant Flux + increase
stress [kPa]
90
80
70
60
50
40
30
Scenario
Base
strain [-]
0.00
0.05
0.10
0.15
Scenario
Base
1
10
100
1yr
10yr
30yr
time [days]

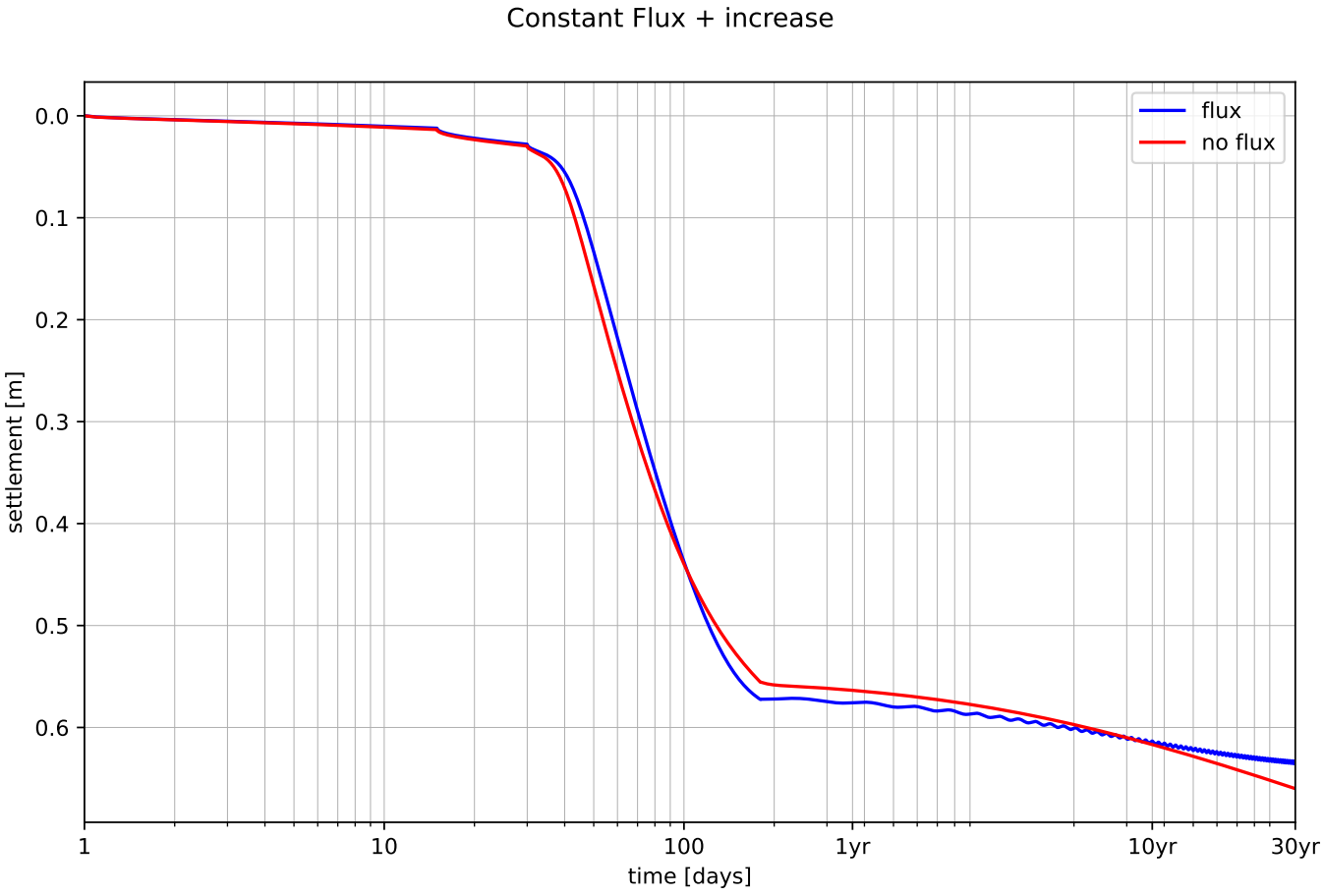
Constant Flux + increase
flux
no flux
0.0
0.1
0.2
0.3
0.4
0.5
0.6
settlement [m]
1
10
100
1yr
10yr
30yr
time [days]

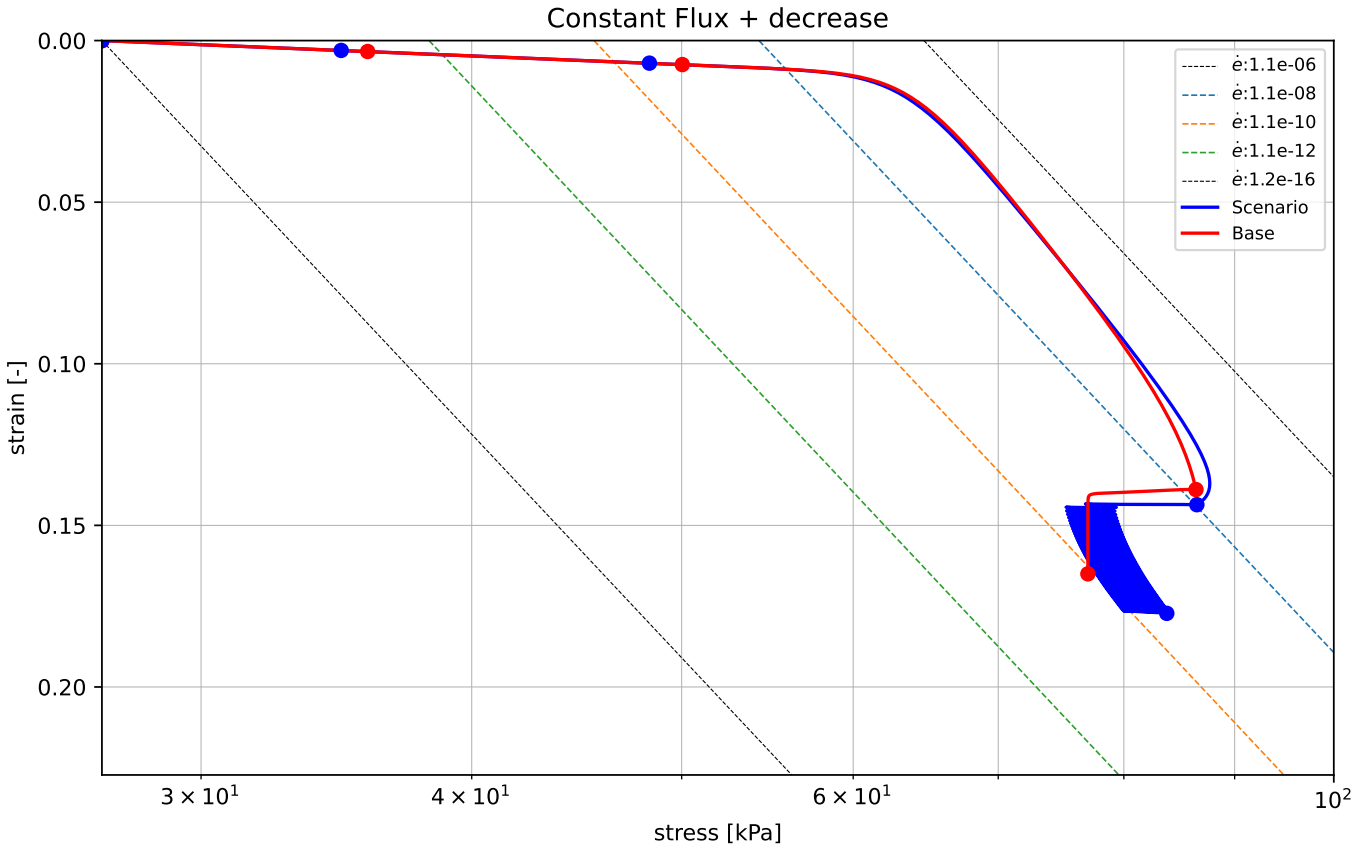
Constant Flux + decrease
0.00
0.05
0.10
0.15
0.20
strain [-]
3×10^1
4×10^1
6×10^1
10^2
stress [kPa]
ė:1.1e-06
ė:1.1e-08
ė:1.1e-10
ė:1.1e-12
ė:1.2e-16
Scenario
Base

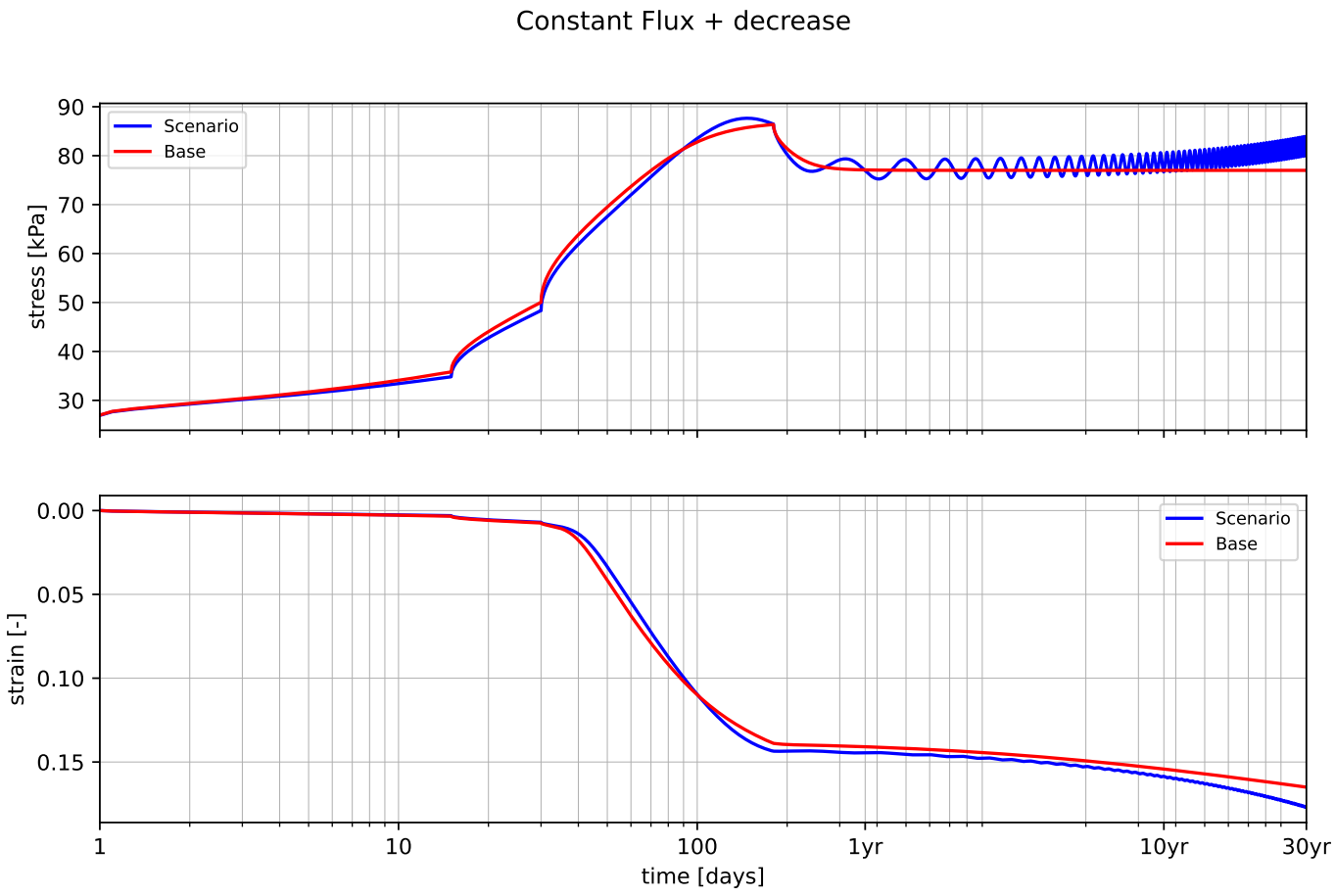
Constant Flux + decrease
stress [kPa]
90
80
70
60
50
40
30
Scenario
Base
strain [-]
0.00
0.05
0.10
0.15
Scenario
Base
1
10
100
1yr
10yr
30yr
time [days]

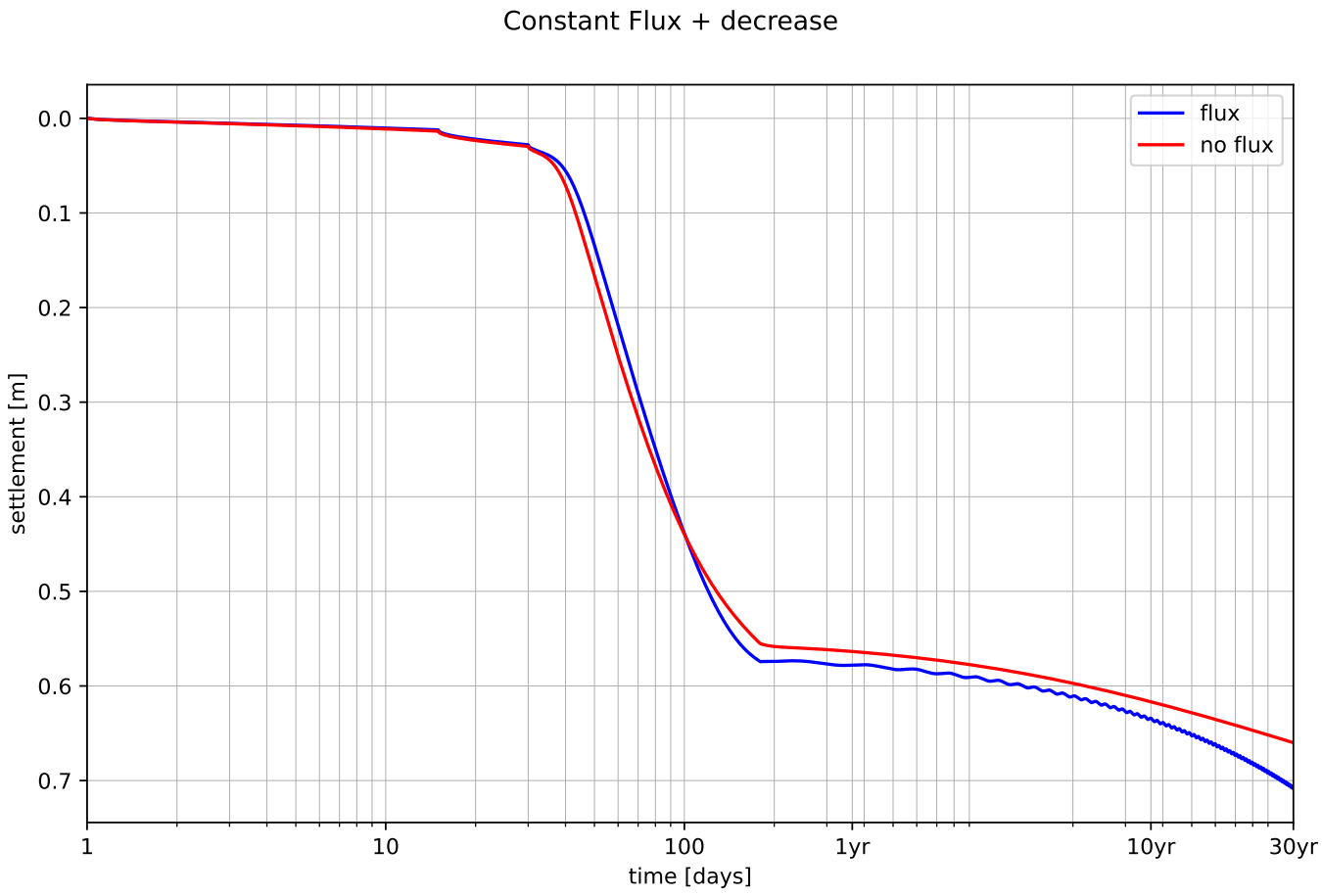
Constant Flux + decrease
flux
no flux
settlement [m]
0.0
0.1
0.2
0.3
0.4
0.5
0.6
0.7
1
10
100
1yr
10yr
30yr
time [days]

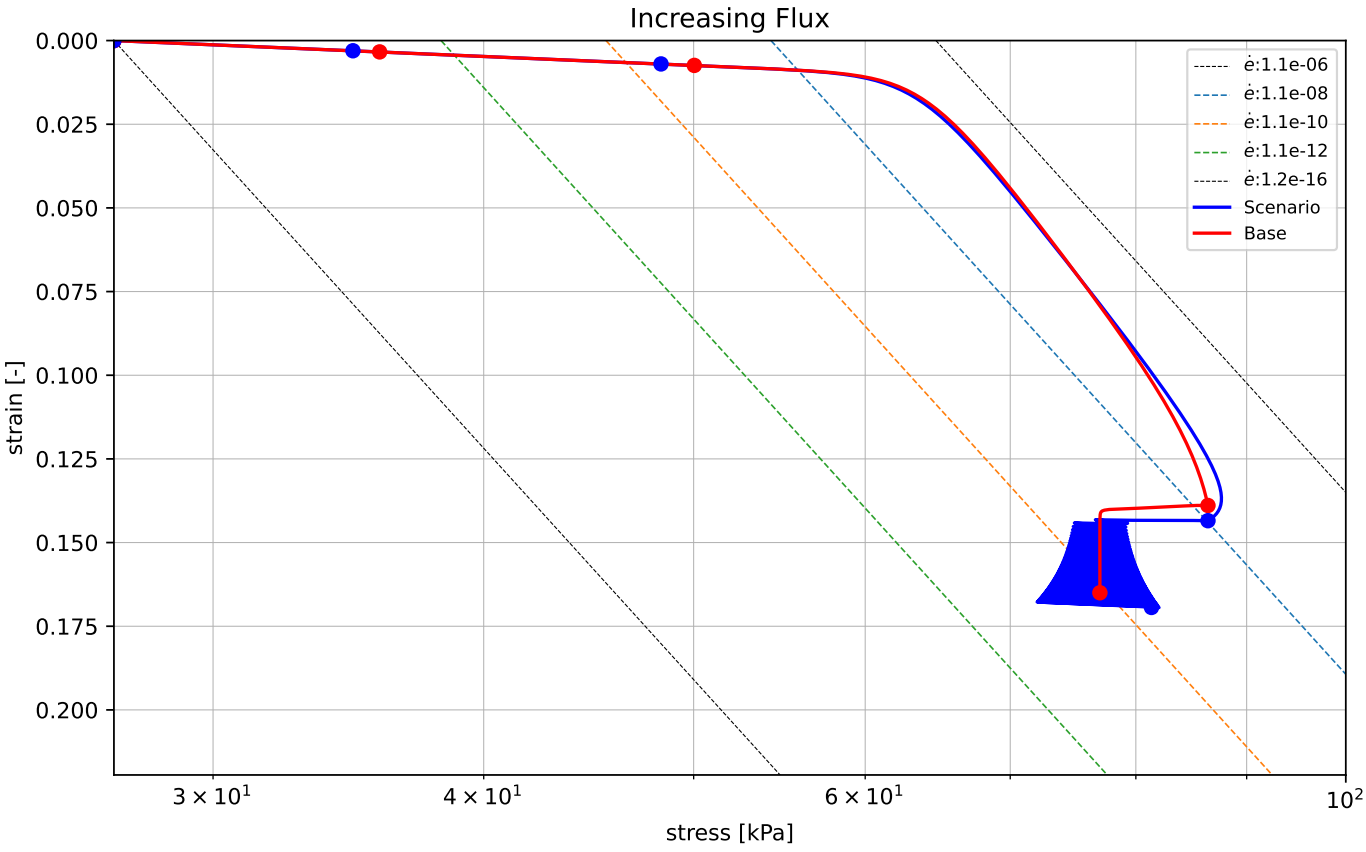
Increasing Flux
0.000
0.025
0.050
0.075
0.100
0.125
0.150
0.175
0.200
strain [-]
3×10^1
4×10^1
6×10^1
10^2
stress [kPa]
ė:1.1e-06
ė:1.1e-08
ė:1.1e-10
ė:1.1e-12
ė:1.2e-16
Scenario
Base

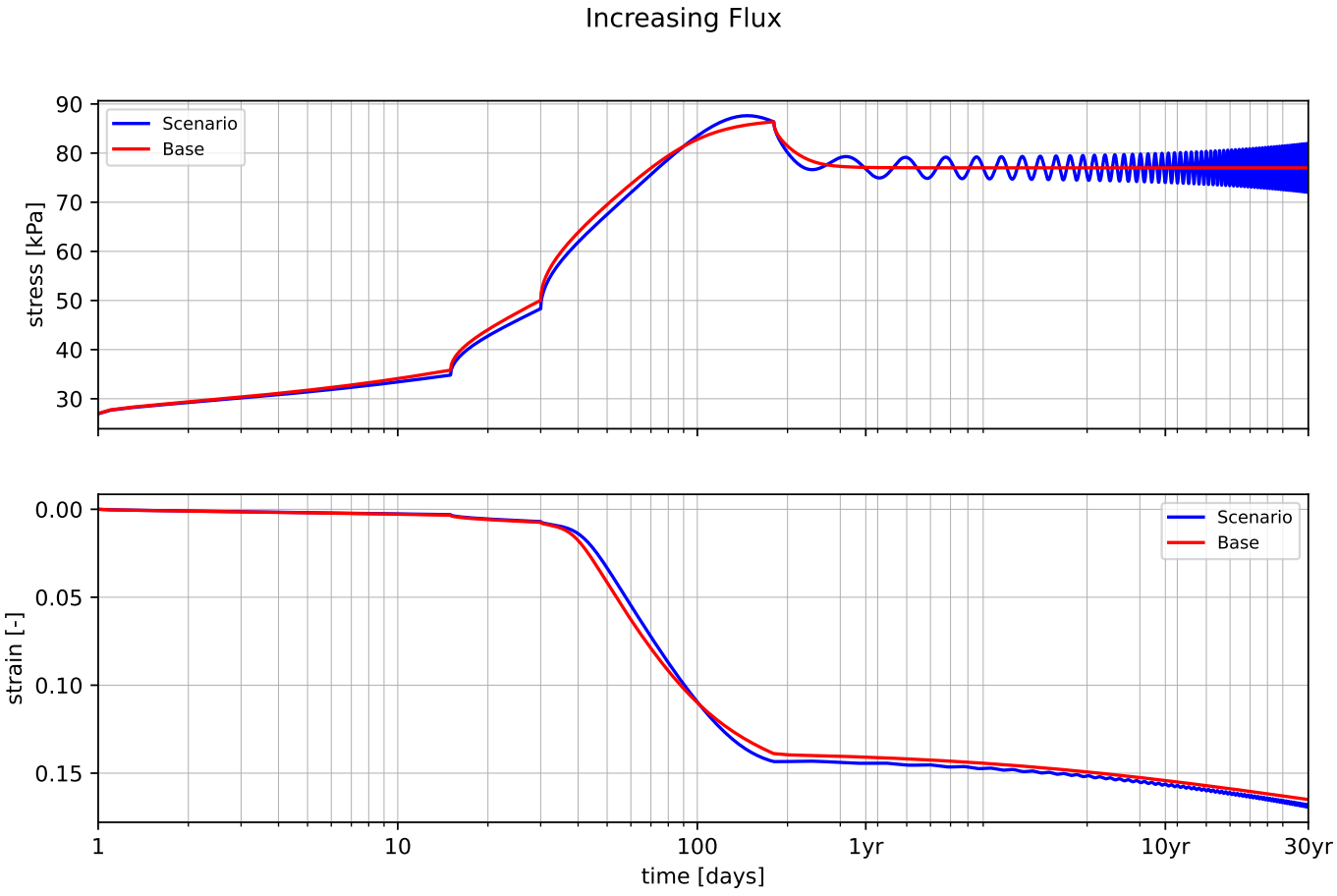
Increasing Flux
Scenario
Base
stress [kPa]
90
80
70
60
50
40
30
Scenario
Base
strain [-]
0.00
0.05
0.10
0.15
1
10
100
1yr
10yr
30yr
time [days]

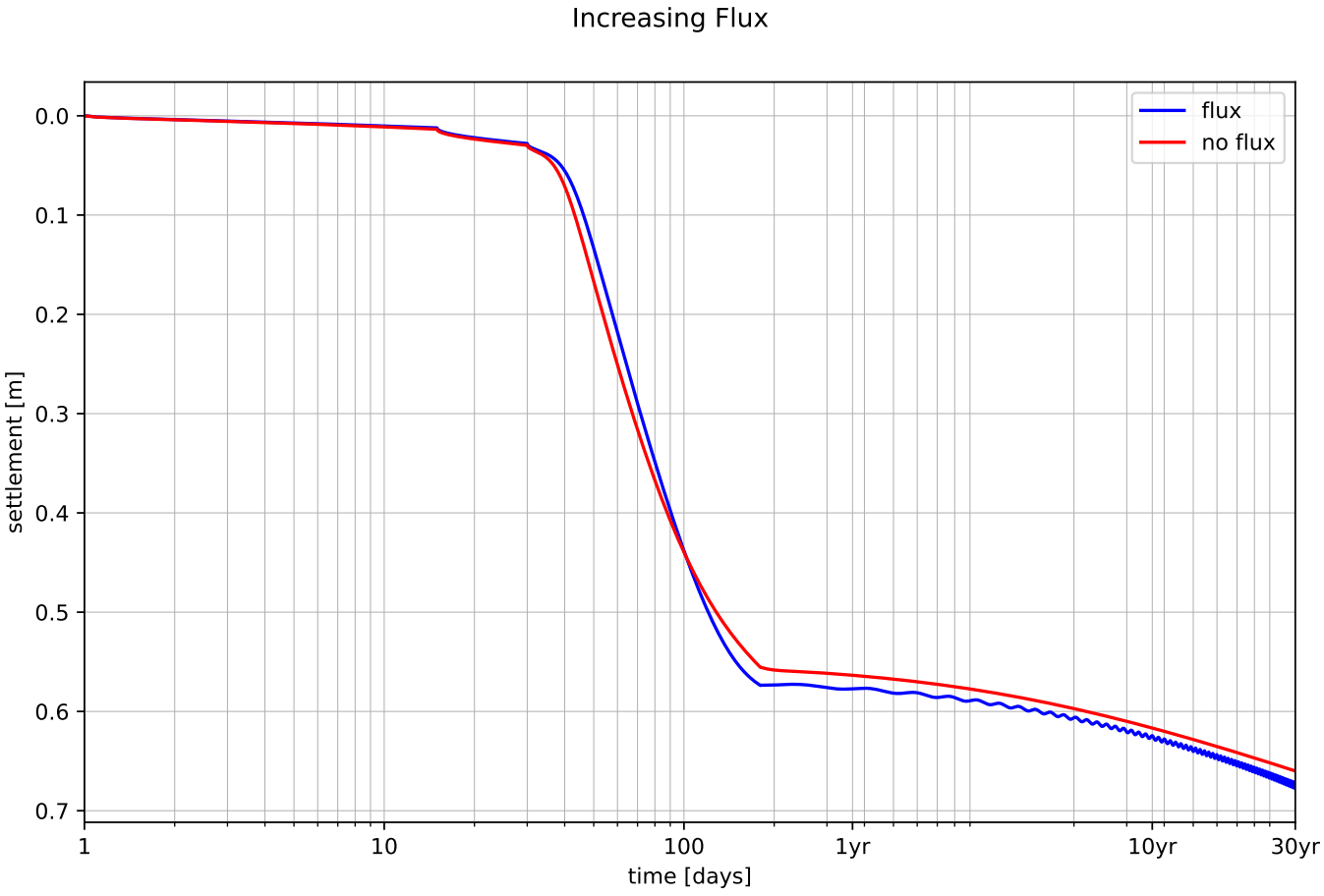
Increasing Flux
flux
no flux
settlement [m]
0.0
0.1
0.2
0.3
0.4
0.5
0.6
0.7
1
10
100
1yr
10yr
30yr
time [days]

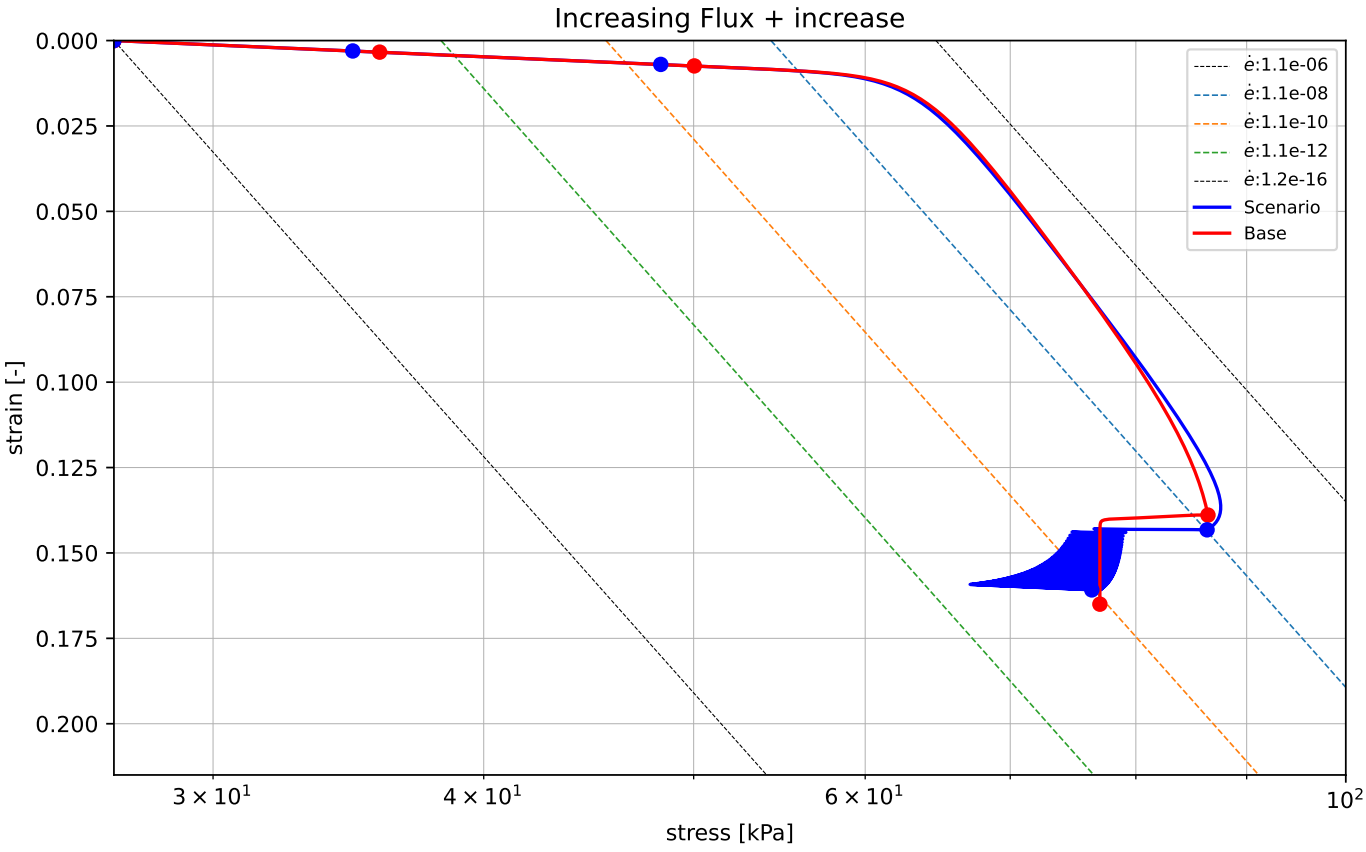
Increasing Flux + increase
0.000
0.025
0.050
0.075
0.100
0.125
0.150
0.175
0.200
strain [-]
3×10^1
4×10^1
6×10^1
10^2
stress [kPa]
ė:1.1e-06
ė:1.1e-08
ė:1.1e-10
ė:1.1e-12
ė:1.2e-16
Scenario
Base

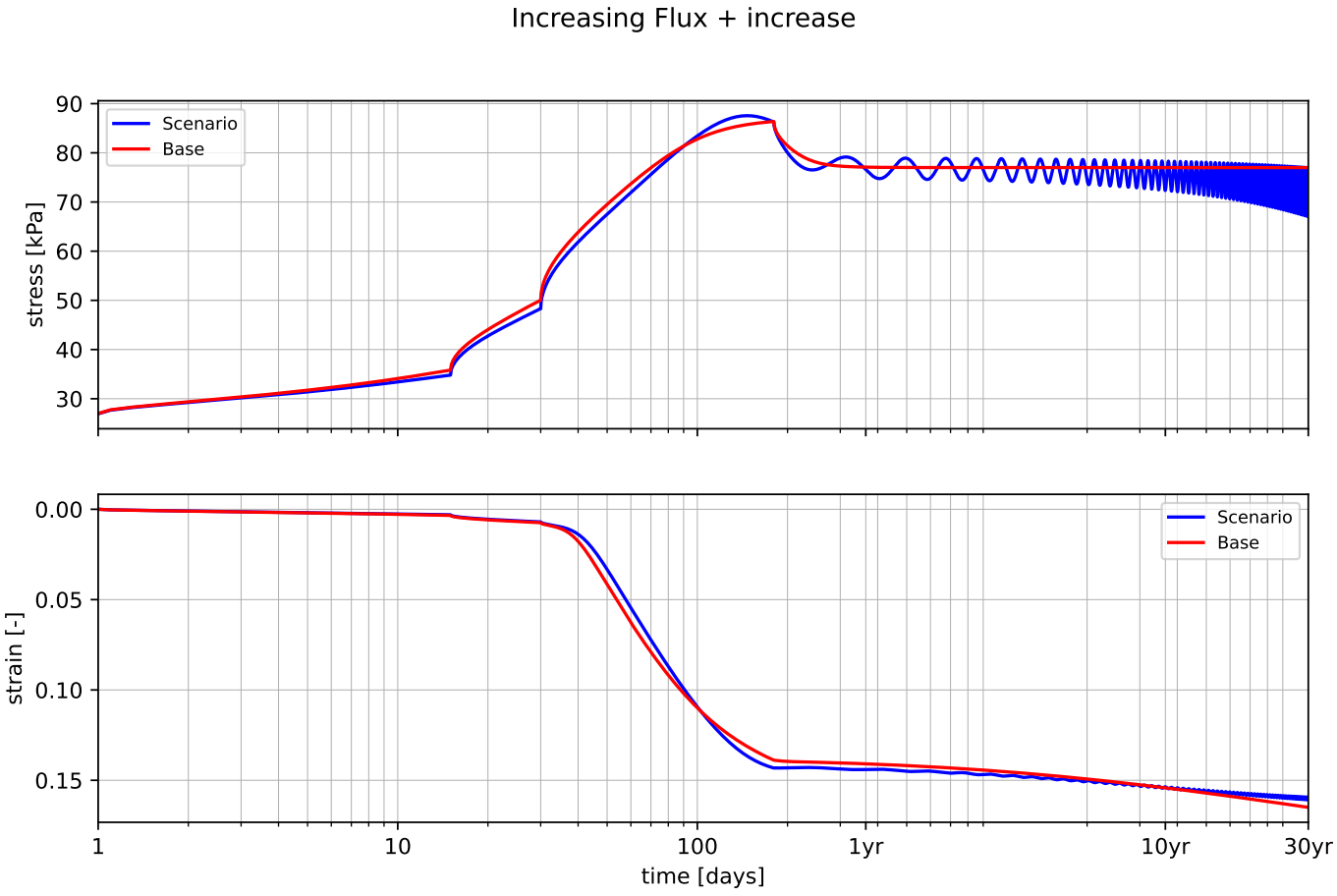
Increasing Flux + increase
Scenario
Base
stress [kPa]
90
80
70
60
50
40
30
Scenario
Base
strain [-]
0.00
0.05
0.10
0.15
1
10
100
1yr
10yr
30yr
time [days]

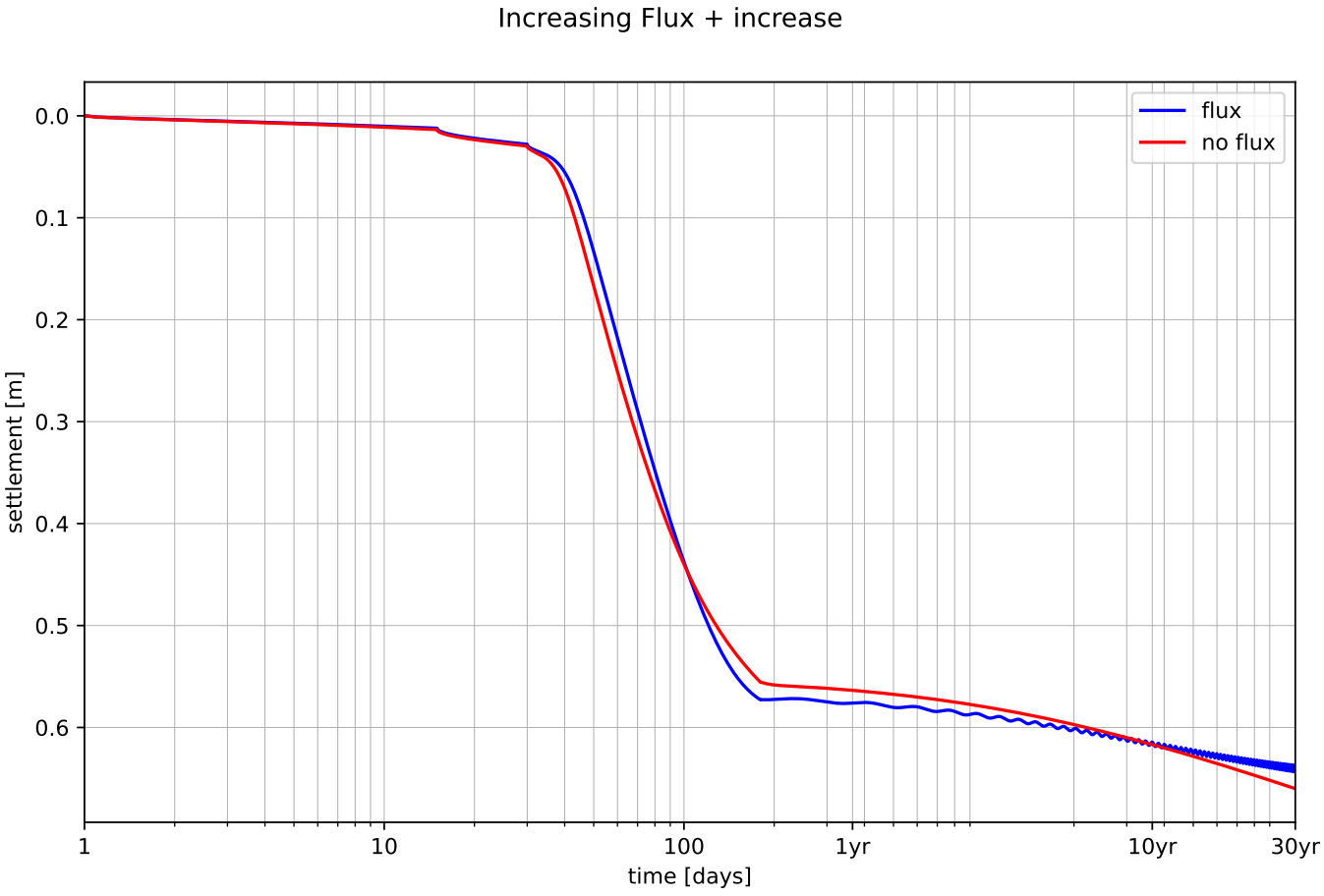
Increasing Flux + increase
flux
no flux
settlement [m]
0.0
0.1
0.2
0.3
0.4
0.5
0.6
1
10
100
1yr
10yr
30yr
time [days]

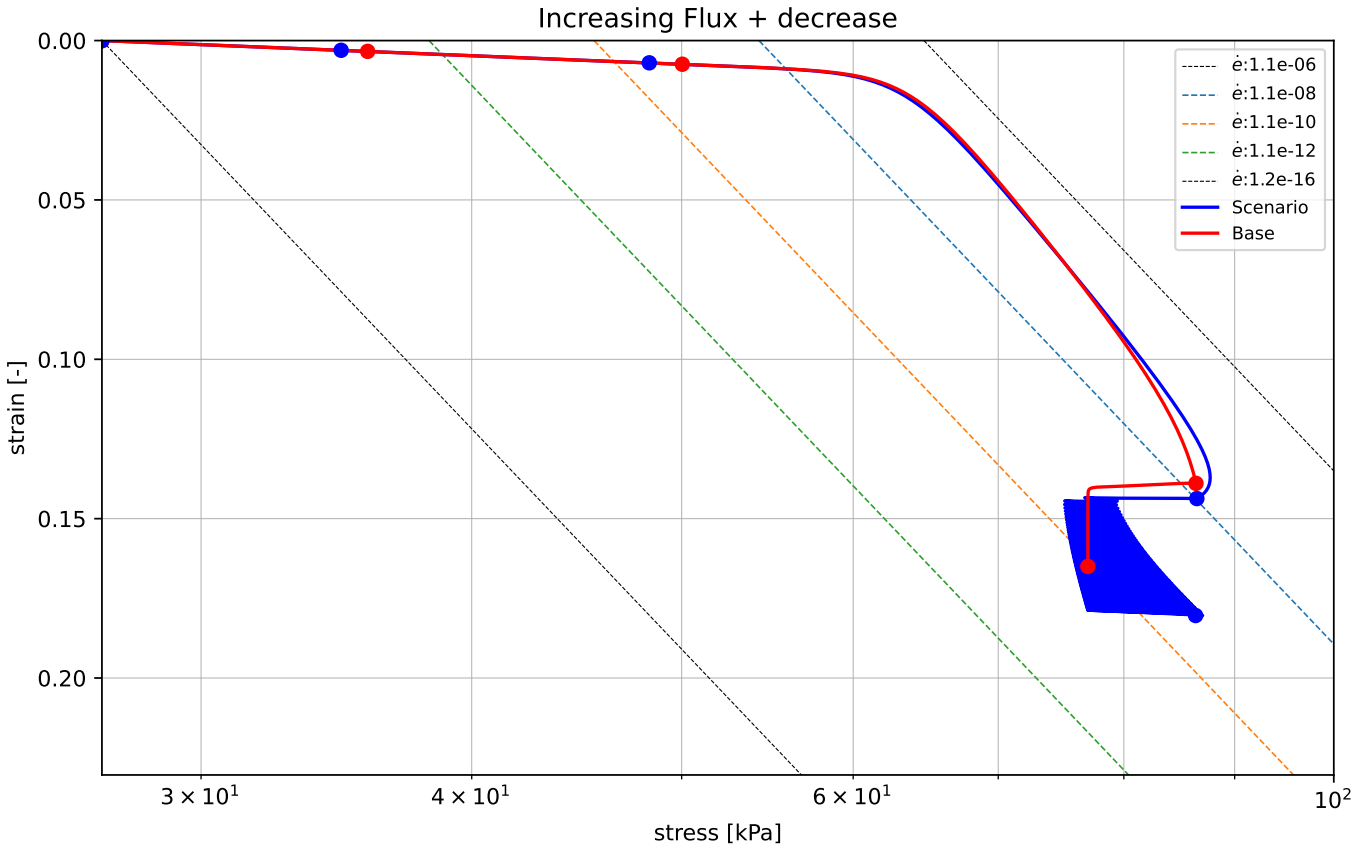
Increasing Flux + decrease
0.00
0.05
0.10
0.15
0.20
strain [-]
3×10^1
4×10^1
6×10^1
10^2
stress [kPa]
ė:1.1e-06
ė:1.1e-08
ė:1.1e-10
ė:1.1e-12
ė:1.2e-16
Scenario
Base

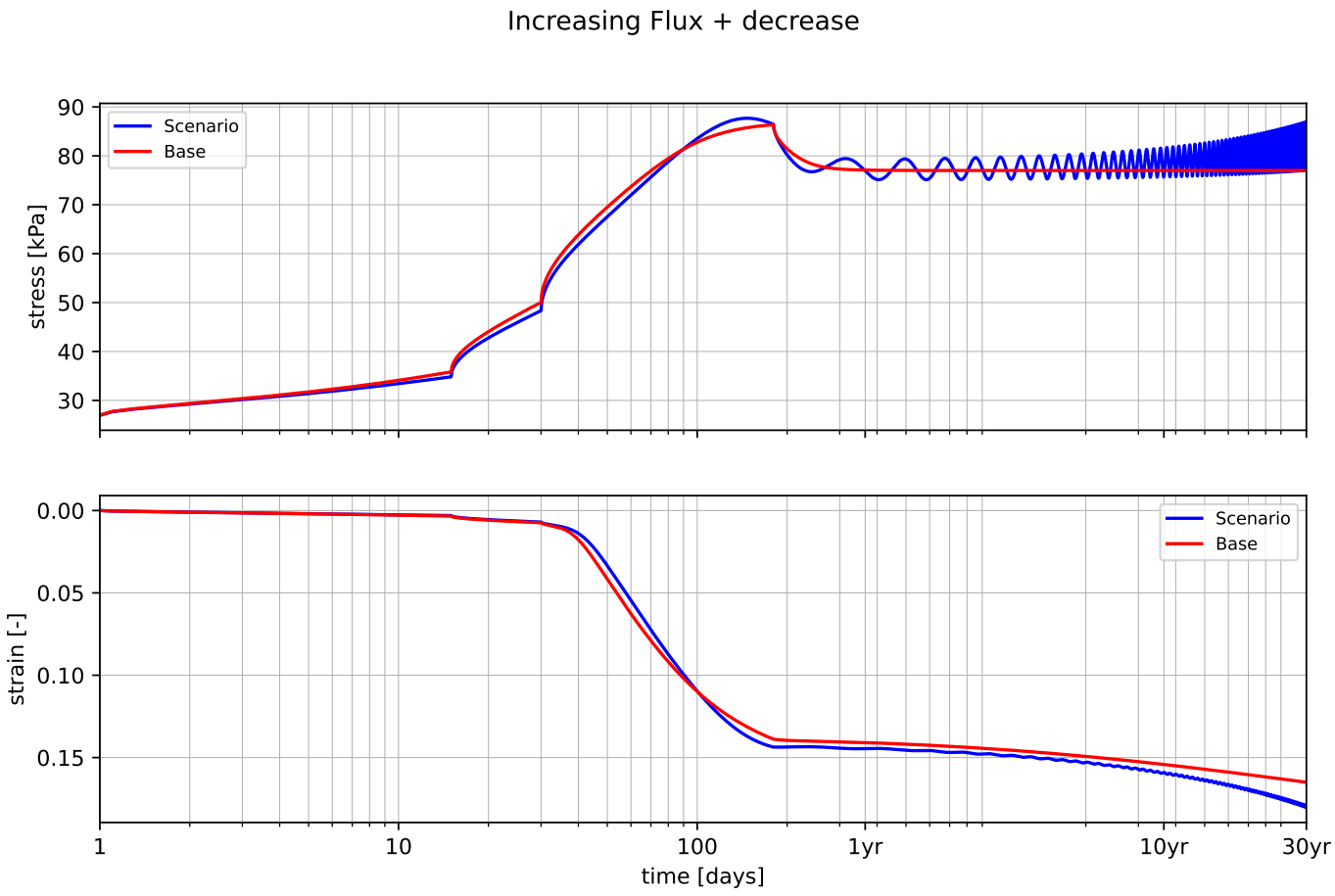
Increasing Flux + decrease
Scenario
Base
stress [kPa]
90
80
70
60
50
40
30
Scenario
Base
strain [-]
0.00
0.05
0.10
0.15
1
10
100
1yr
10yr
30yr
time [days]

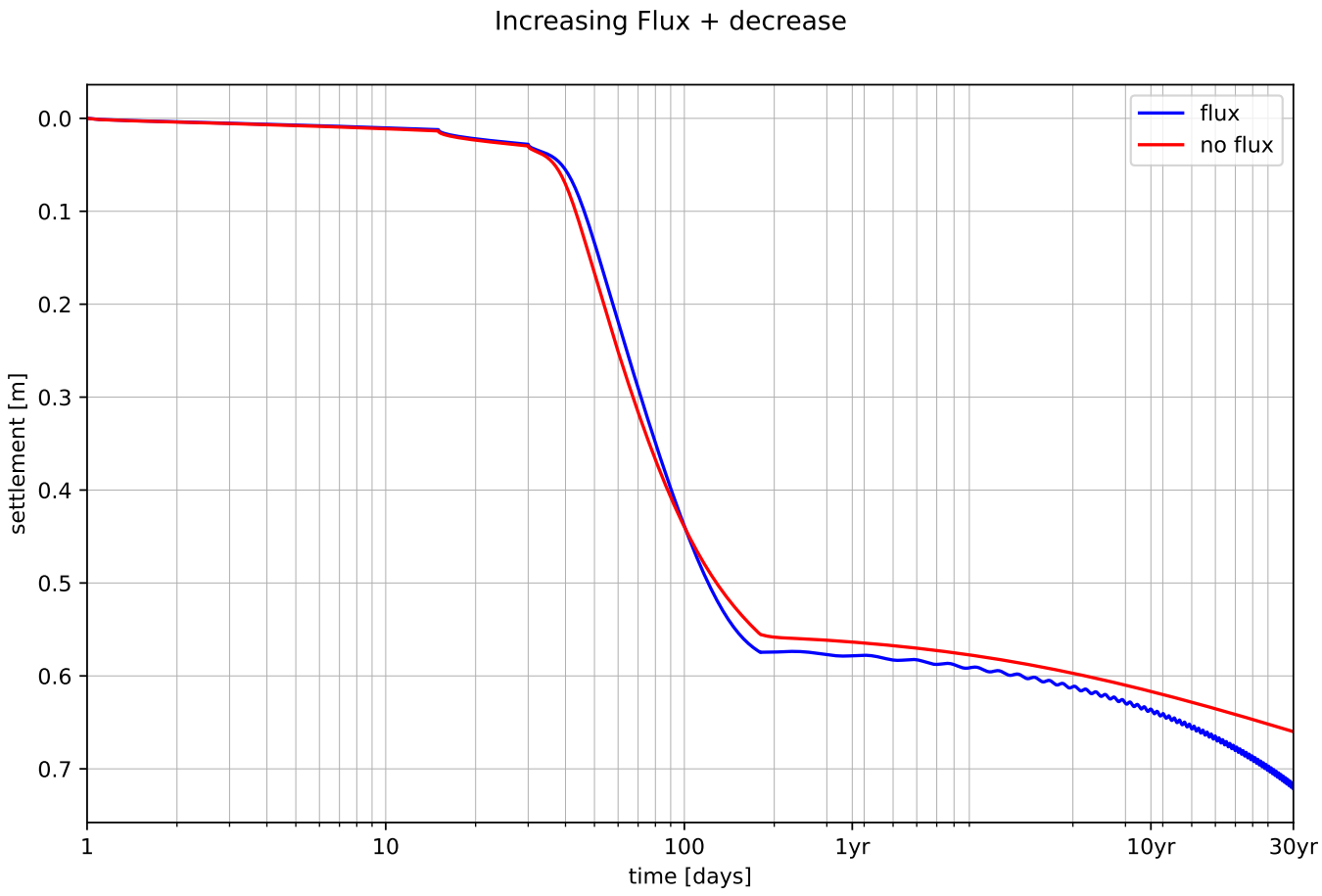
Increasing Flux + decrease
flux
no flux
settlement [m]
0.0
0.1
0.2
0.3
0.4
0.5
0.6
0.7
1
10
100
1yr
10yr
30yr
time [days]

C

InSAR

C.1. Parameter calculation

In general:

$$CR_{weighted} = \frac{CR_{clay} \cdot H_{clay} + CR_{peat} \cdot H_{peat}}{H_{clay} + H_{peat}}$$

$$RR_{weighted} = \frac{RR_{clay} \cdot H_{clay} + RR_{peat} \cdot H_{peat}}{H_{clay} + H_{peat}}$$

$$C_{\alpha weighted} = \frac{C_{\alpha clay} \cdot H_{clay} + C_{\alpha peat} \cdot H_{peat}}{H_{clay} + H_{peat}}$$

$$\gamma_{weighted} = \frac{\gamma clay \cdot H_{clay} + \gamma \cdot H_{peat}}{H_{clay} + H_{peat}}$$

For location 1 at the N3:

$$CR_{weighted} = \frac{0.24 \cdot 1 + 0.29 \cdot 2}{3} = 0.27$$

$$RR_{weighted} = \frac{0.027 \cdot 1 + 0.056 \cdot 2}{3} = 0.044$$

$$C_{\alpha weighted} = \frac{0.0126 \cdot 1 + 0.018 \cdot 2}{3} = 0.016$$

$$\gamma_{weighted} = \frac{14.3 \cdot 1 + 11 \cdot 2}{3} = 12.1$$

For location 2 at the N3:

$$CR_{weighted} = \frac{0.24 \cdot 7 + 0.29 \cdot 3}{10} = 0.26$$

$$RR_{weighted} = \frac{0.027 \cdot 7 + 0.056 \cdot 3}{10} = 0.035$$

$$C_{\alpha weighted} = \frac{0.0126 \cdot 7 + 0.018 \cdot 3}{10} = 0.014$$

$$\gamma_{weighted} = \frac{14.3 \cdot 7 + 11 \cdot 3}{10} = 13.3$$

C.2. Yield stress and OCR sensitivity

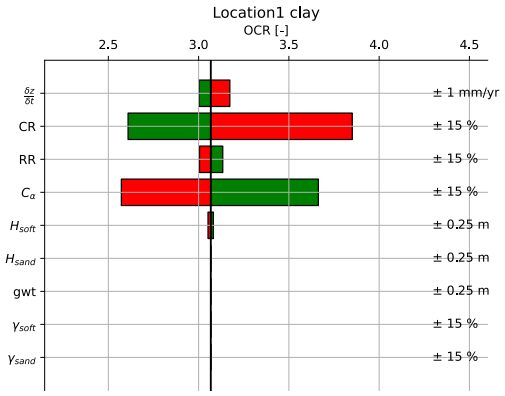

(a) OCR

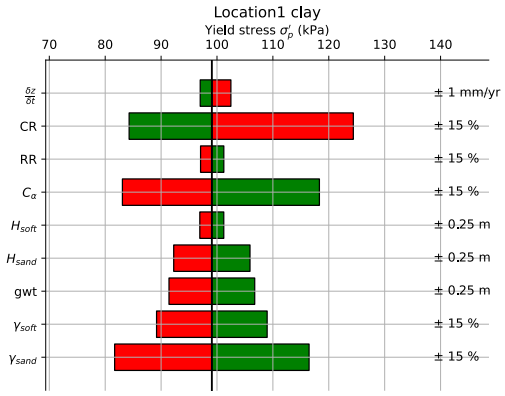

(b) σ_p

Figure C.1: Location 1, all clay

(a) OCR

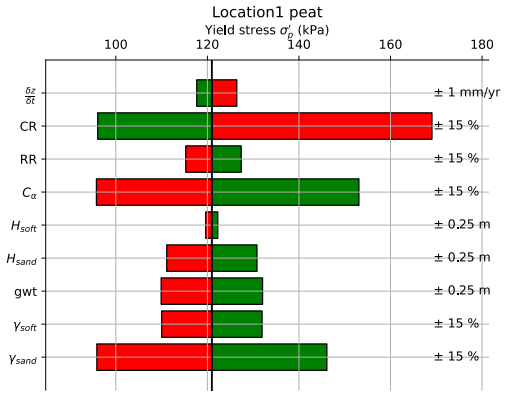

(b) σ_p

Figure C.2: Location 1, all peat

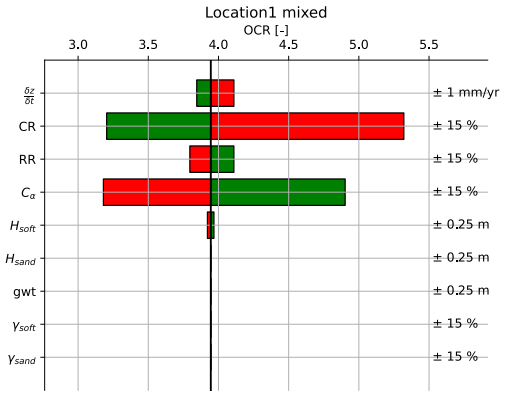

(a) OCR

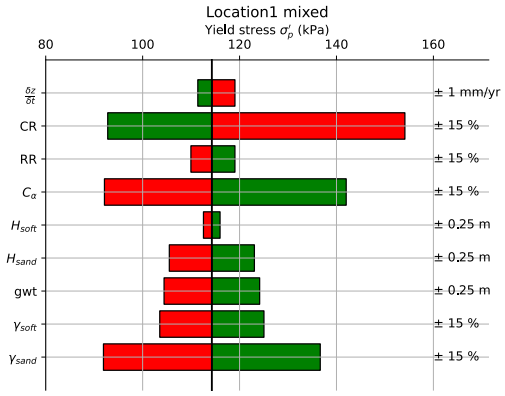

(b) σ_p

Figure C.3: Location 1, mixed layer

(a) OCR

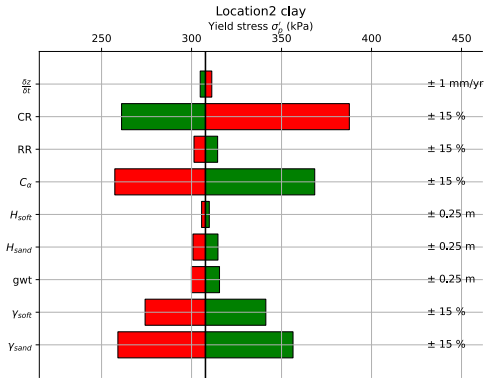

(b) σ_p

Figure C.4: Location 2, all clay

(a) OCR

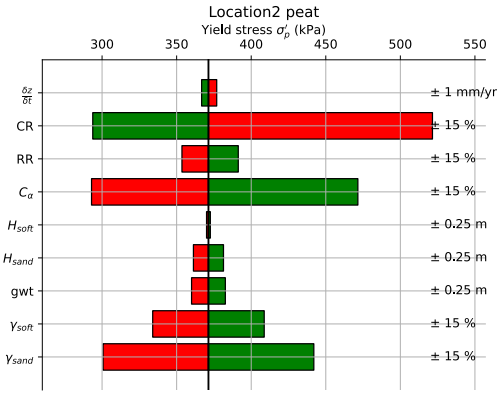

(b) σ_p

Figure C.5: Location 2, all peat

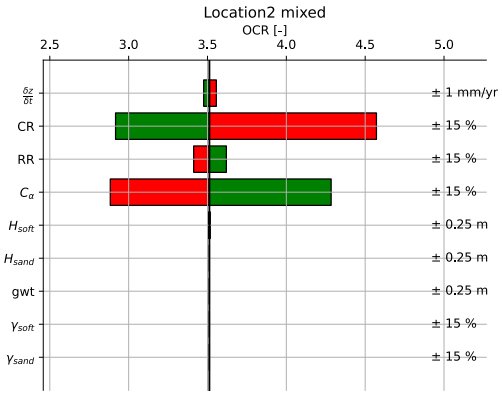

(a) OCR

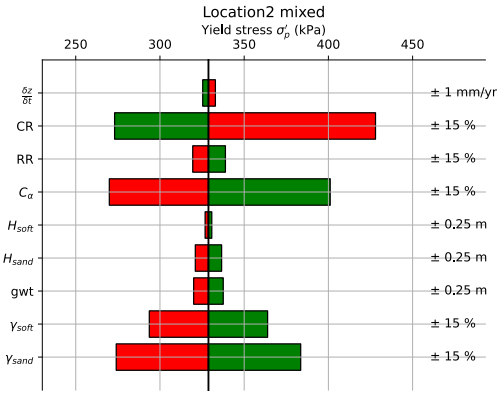

(b) σ_p

Figure C.6: Location 2, mixed layer

C.3. CPTs

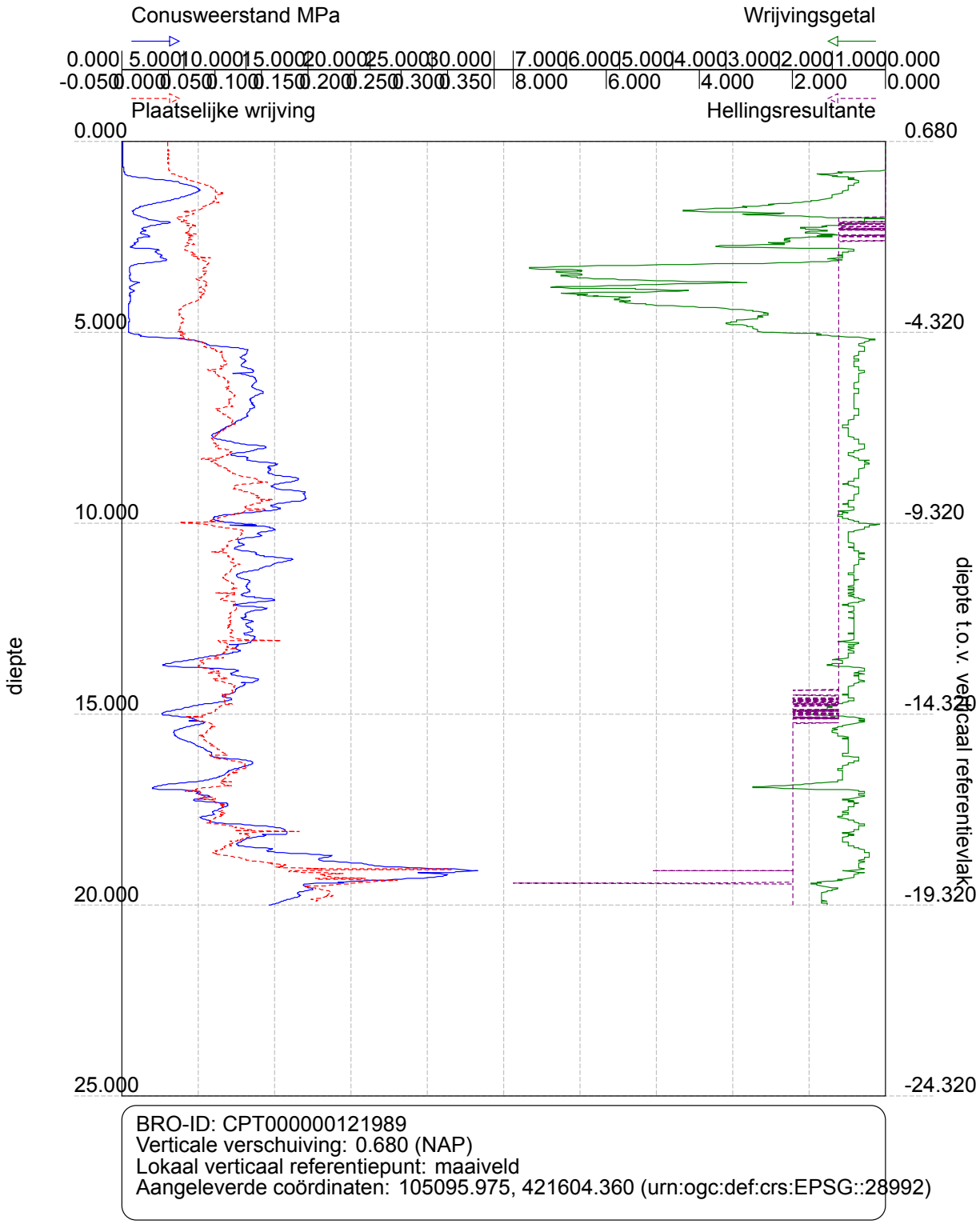

Figure C.7: N3 location 1: CPT 1

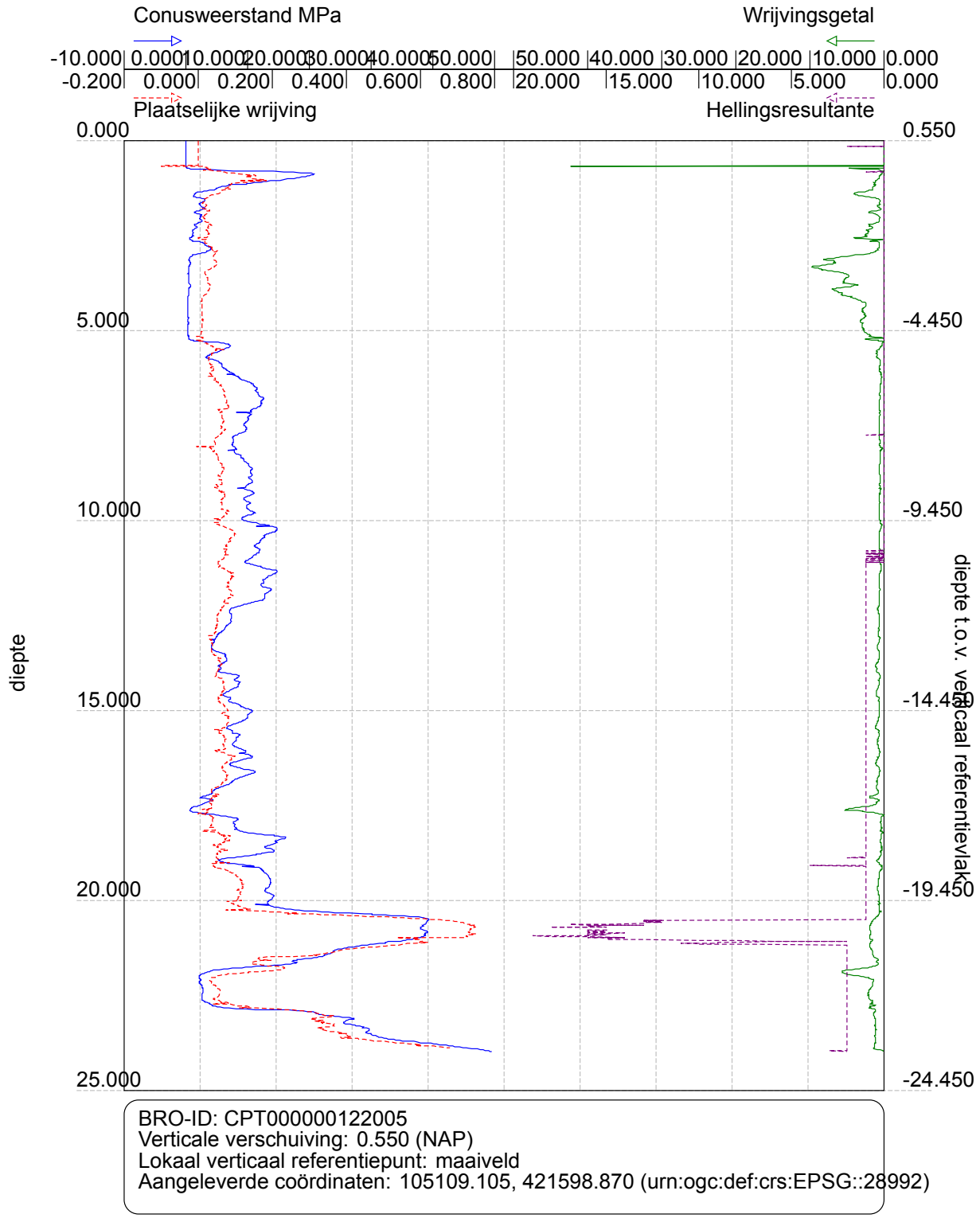

Figure C.8: N3 location 1: CPT 2

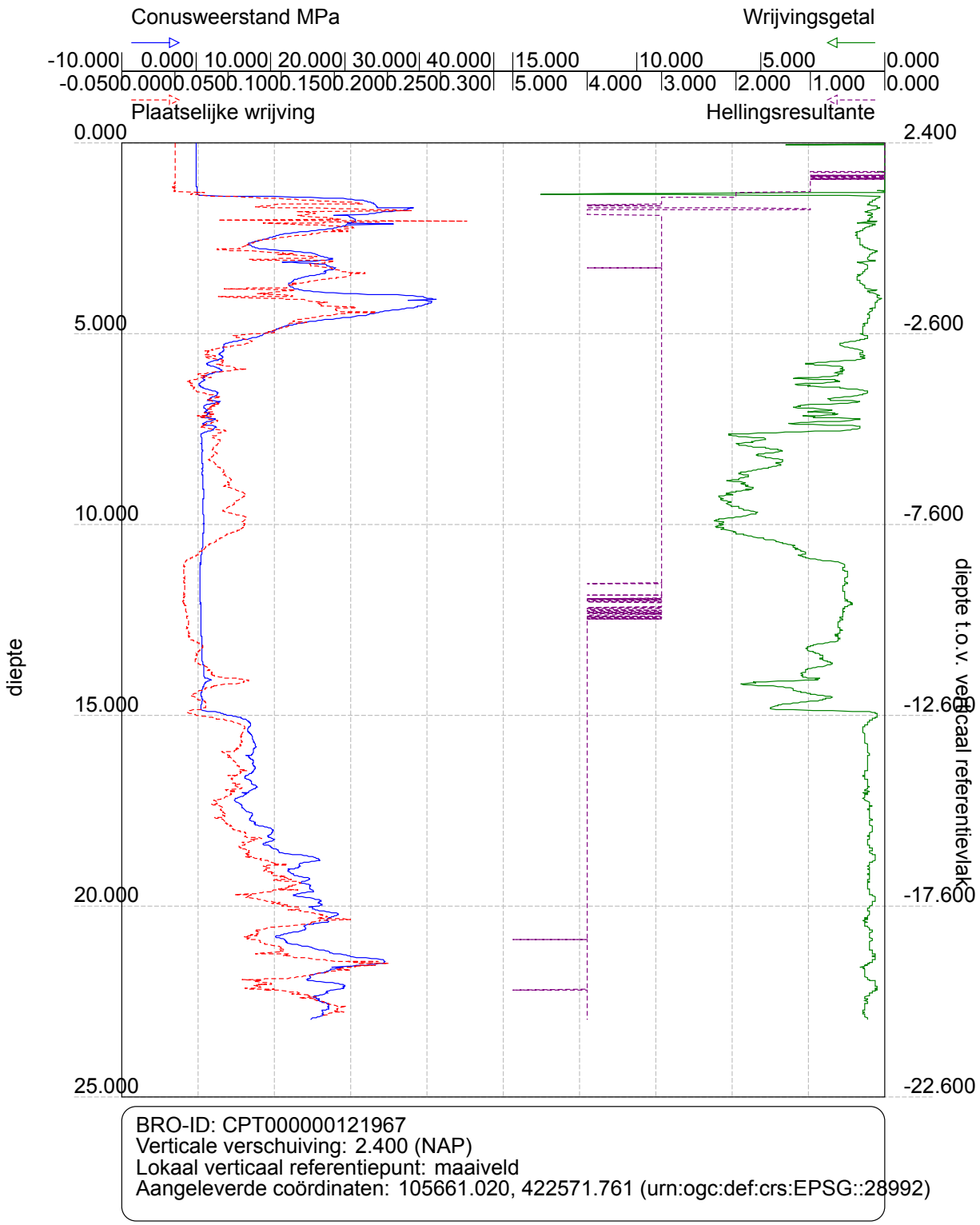

Figure C.9: N3 location 2: CPT 1

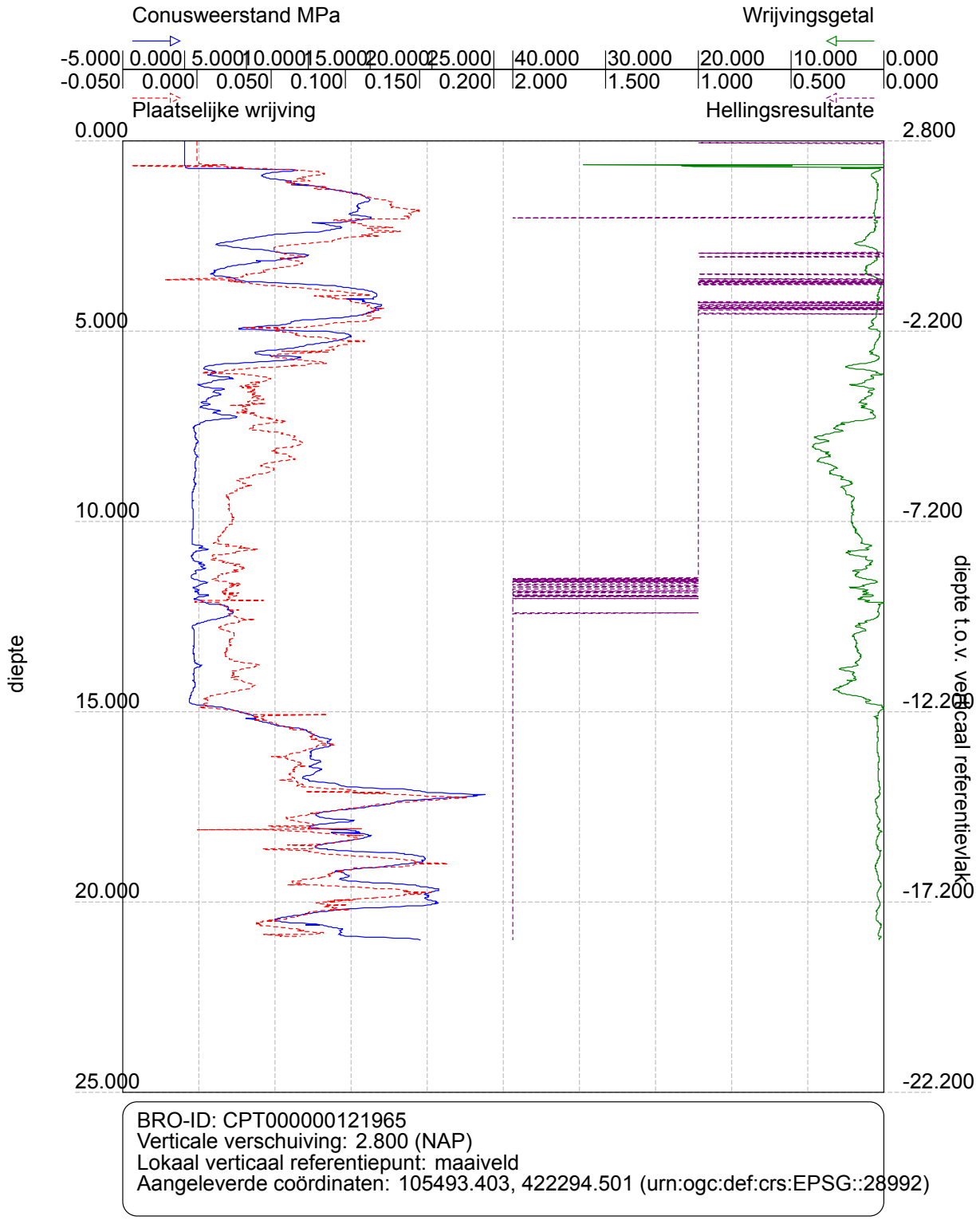

Figure C.10: N3 location 2: CPT 2

C.4. A2 settlement plots

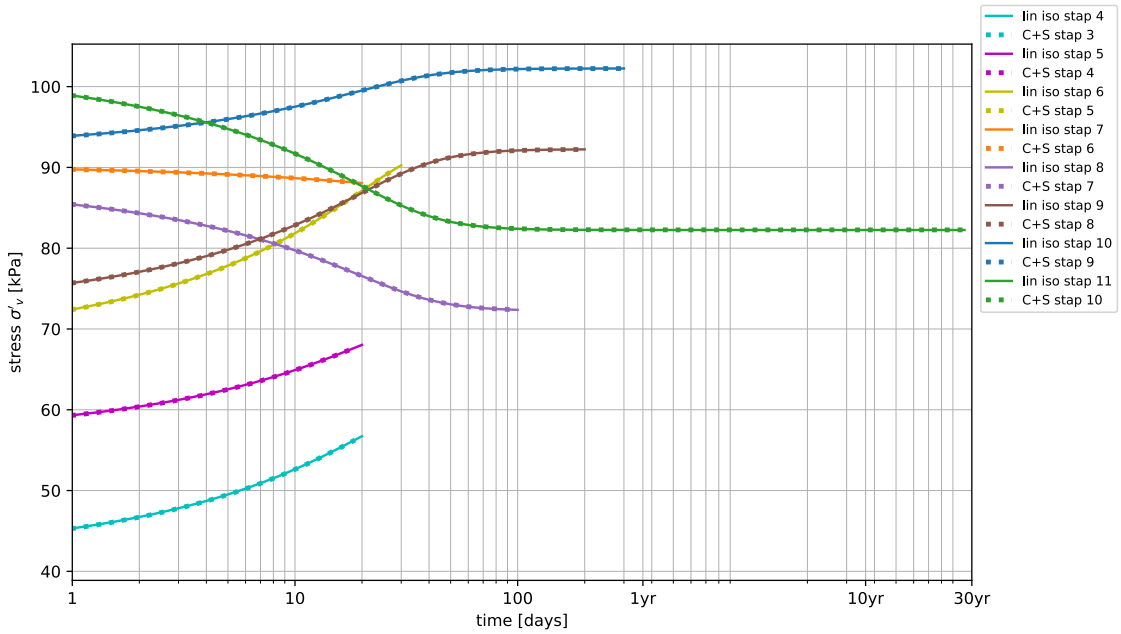

Figure C.11: Stress development per time step for all isotach model variations for the A2

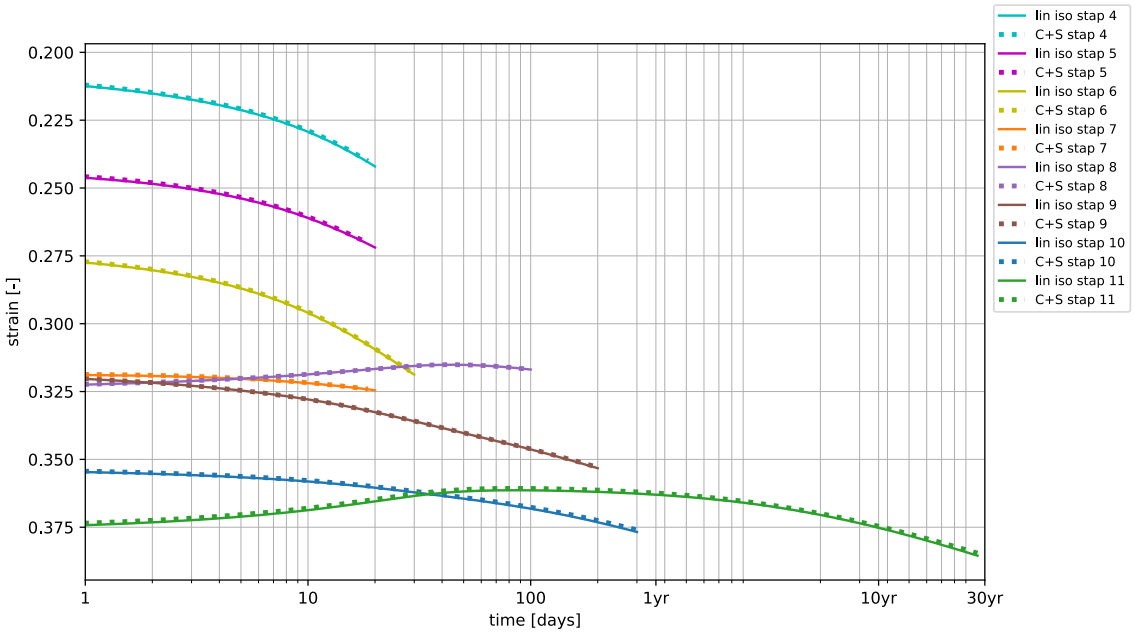

Figure C.12: Strain development per time step for linear isotachs for the A2

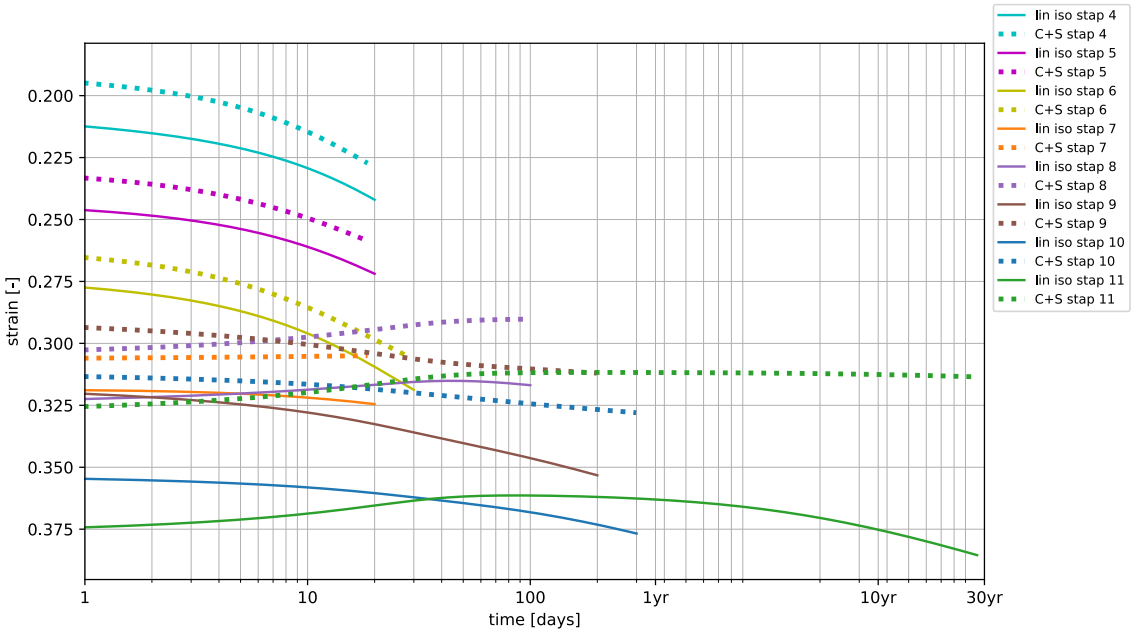

Figure C.13: Strain development per time step for non-linear isotachs for the A2

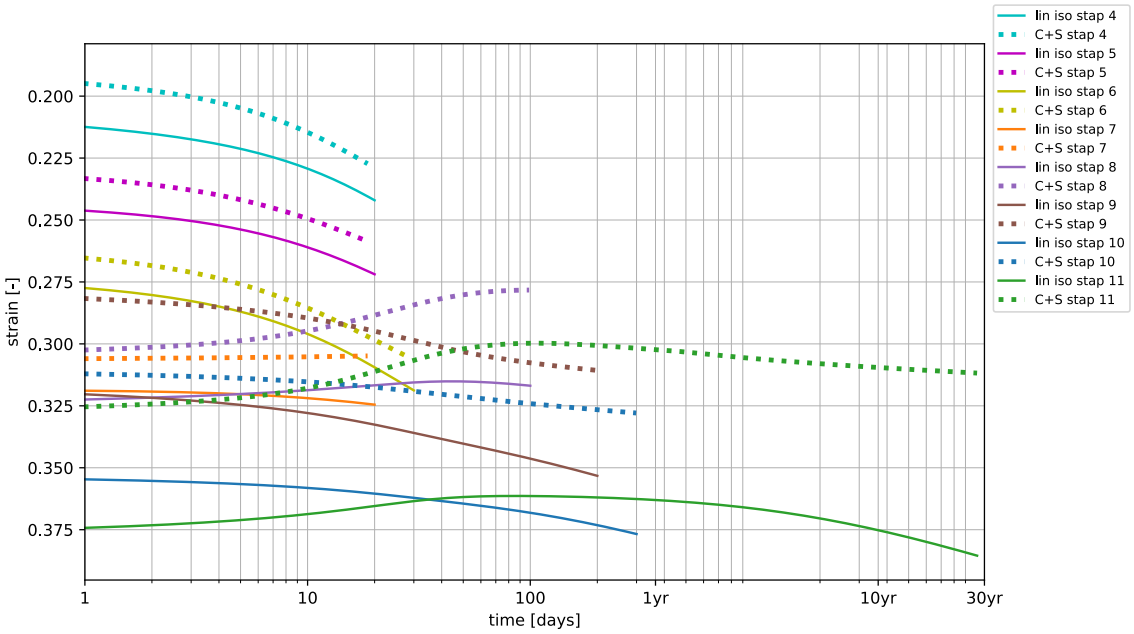

Figure C.14: Strain development per time step for non-linear isotachs with viscoplastic swell for the A2

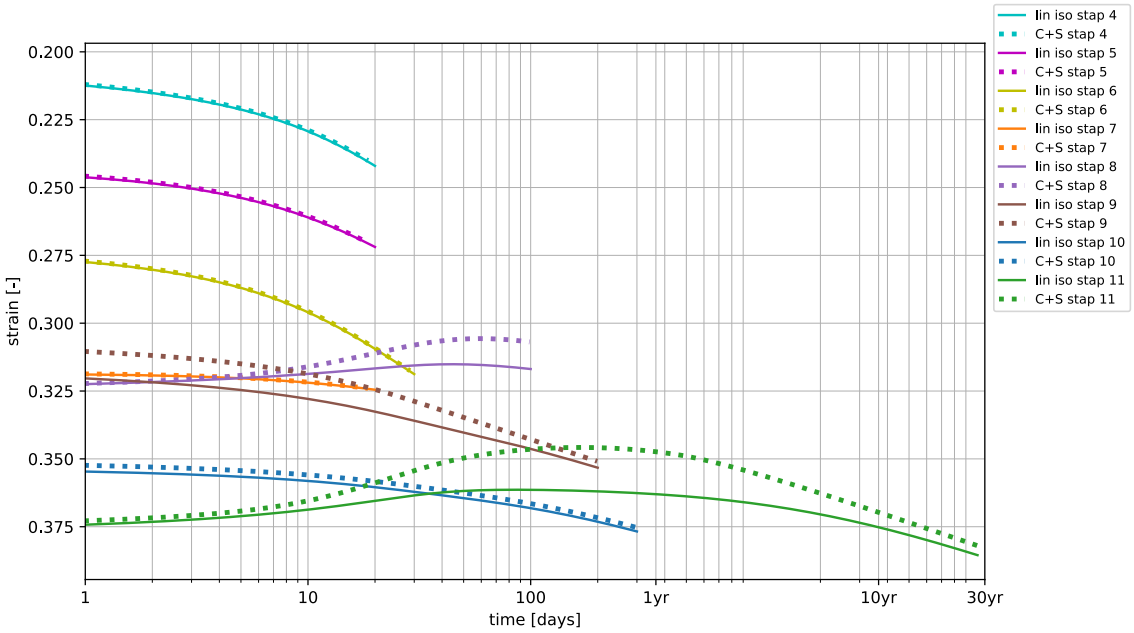

Figure C.15: Strain development per time step for linear isotachs with viscoplastic swell for the A2

C.5. D-Settlement A2

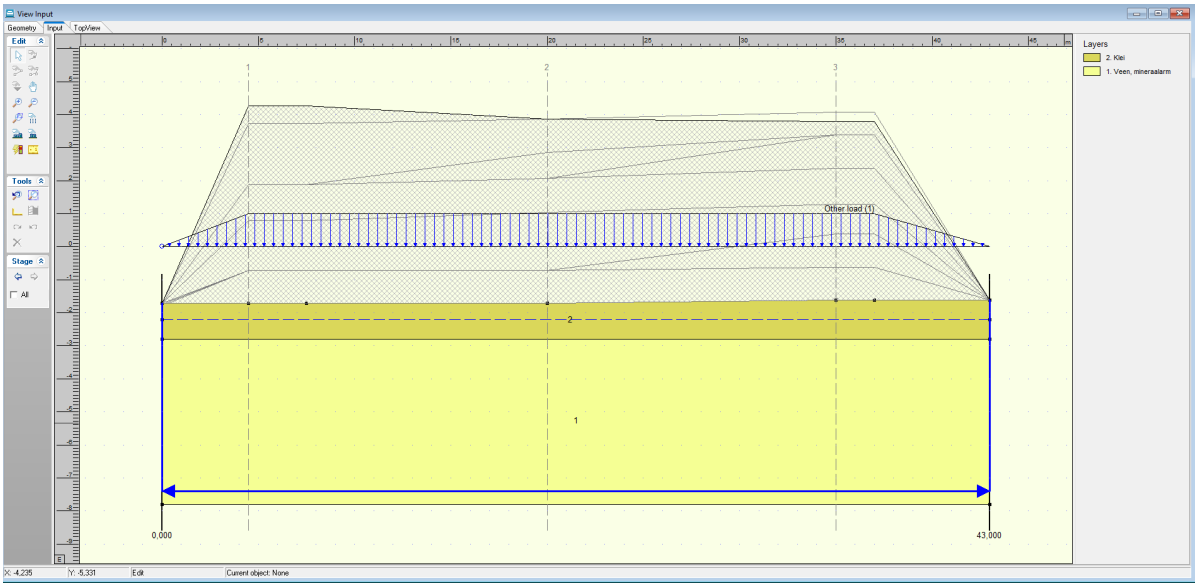

Figure C.16: Cross section D10

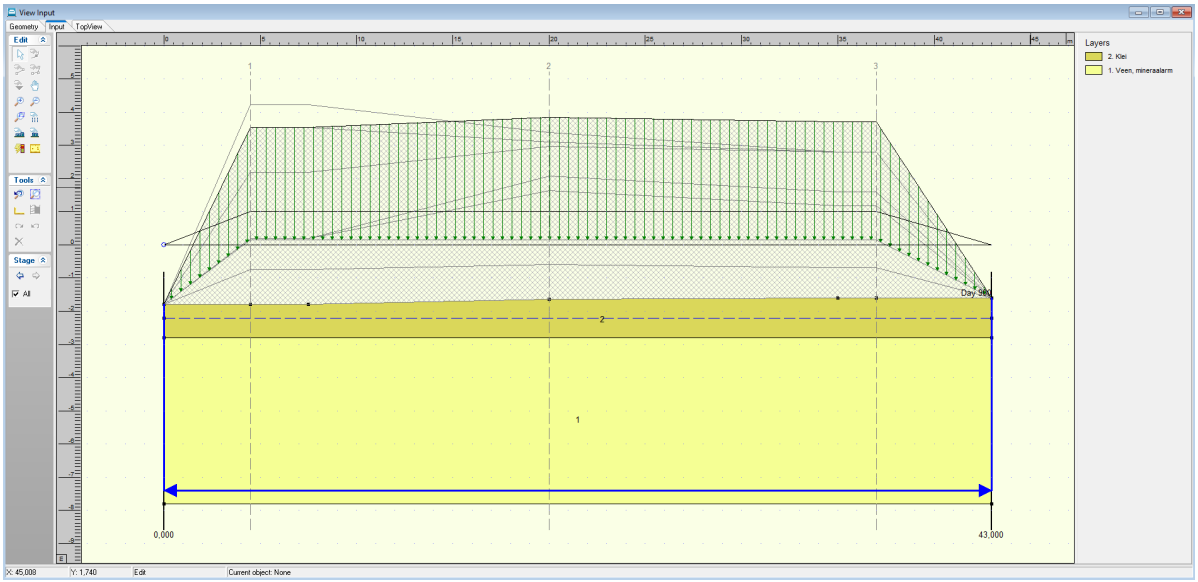

Figure C.17: Cross section D14